REMEMBERING SAMUEL KRINSKY

L.H. Yu, BNL, Upton, NY 11973, USA

Abstract

This year, we lost our colleague Samuel Krinsky. Sam has made many important contributions to very broad field of accelerator physics. In remembrance of his life and achievements, we will review his contributions to the field of free electron lasers. In particular, we will concentrate on his contributions to the foundation of the theory of high gain FELs, and his managerial and experimental contributions to pioneer work on x-ray FEL development.

Figure 1: Sam Krinsky January 14, 1945 - April 26, 2014.

SAM'S CONTRIBUTIONS

Sam has made contributions in accelerator physics covering very broad areas. Among many of these contributions to accelerator physics, we focus on the following:

- NSLS X-ray ring (1978) design and commissioning
- First short-period in-vacuum undulator at NSLS (1987)
- First global orbit feedback system at NSLS
- Design NSLS-II storage ring (2014)
- Important contributions to studies of impedances and collective effects including the theory on coherent synchrotron radiation and micro-bunching in electron beams.
- Founded Source Development Laboratory at BNL

We will not be able to cover such broad areas of research works in these proceedings. Instead, we shall concentrate on his contributions to free electron laser physics.

Among many other contributions made by Sam, we would like to highlight his most important seminal contributions to the FEL community. We shall categrize these contributions in two aspects: theoretical basis for high gain FEL, and leading experimental and managerial roles.

Among Sam's many contributions to the theoretical basis of high gain FEL physics:

- Universal gain scaling function [1]
- 3-D SASE start-up noise [2]
- Effect of wiggler errors [3]
- Average spacing of peaks in SASE spectrum [4]

We also recognize among many of his leading experimental and managerial roles:

With his managerial skill and foresight, Sam contributed decisively to the formation of FEL team. This led to the creation and successful execution of FEL projects at Brookhaven National Laboratory during his tenure as deputy chairman of the NSLS department, paving the way toward many accomplishments with important impacts on the worldwide short wavelength FEL development. Here we highlight some of the most significant of these:

- Facilitated the 1990 Sag Harbor "Prospects for a 1 Å Free Electron Laser" Workshop with R. Palmer.
- 1997-1999 ATF HGHG Experiment at 5 μm:
Sam was instrumental in getting the NSLS to provide resources to the BNL Accelerator Test Facility to complete R&D on the photo-injector and to carry out the HGHG proof-of-principle experiment in the infrared.
- Leading role in the construction of the DUVFEL at the SDL for 2000 -2003 HGHG Experiment at 266 nm.

SCALING FUNCTION OF GAIN

In 1990, collaborating with L. H.Yu and R. Gluckstern, Sam derived an FEL integral differential equation describing evolution of the electric field strength E in an undulator, taking into account of diffraction, optical guiding, energy spread, emittance, detuning, focusing and betatron oscillation [1]:

$$(\Delta_\perp^2 + \Omega)E(\vec{r}) = \frac{i}{2}(2\rho\gamma_0)^3 \int \frac{d\gamma}{\gamma^2} h'(\gamma) \int d^2p \int_{-\infty}^{0} ds e^{-i\alpha s} u(p^2 + \kappa^2 r^2) E[\vec{r}\cos(\kappa s) + \frac{\vec{p}}{\kappa}\sin(\kappa s)]. \quad (1)$$

This equation has many eigen-solutions, each representing an eigen-mode of the optical guiding, giving the gain of the

ISBN 978-3-95450-133-5

FIRST LASING AT FLASH2

S. Schreiber*, B. Faatz, DESY, Hamburg, Germany†

Abstract

FLASH, the free-electron laser user facility at DESY (Hamburg, Germany), has been upgraded with a second undulator beamline FLASH2. The installation of the FLASH2 electron beamline, including twelve variable gap undulators, was finalized early 2014, and beam commissioning of the new beamline started in March 2014. We announce first lasing at FLASH2 achieved at a wavelength of 40 nm on August 20, 2014.

INTRODUCTION

FLASH [1–5], the free-electron laser (FEL) user facility at DESY (Hamburg), delivers high brilliance XUV and soft X-ray FEL radiation for photon experiments. FLASH is a user facility since 2005.

FLASH is a linear accelerator with a photoinjector followed by a superconducting linac. The maximum electron beam energy is 1.25 GeV, allowing lasing down to 4.1 nm with its fixed gap undulators. This undulator beamline (FLASH1) is in operation since 2004. More details on the FLASH facility and its present status can be found in these proceedings [5].

As FLASH, all high gain FEL's in the soft and hard X-ray range are driven by a linear accelerator. Therefore, beam can only be delivered to one experiment at a given time. FLASH has five experimental beamlines, so that usually two or sometimes three experiments can be set-up in parallel. But, they usually receive beam by a day to day basis, not at the same time.

Fortunately, the superconducting accelerating technology of FLASH allows to accelerate several thousand electron bunches per second. The bunches come in bursts with a repetition rate of 10 Hz. The maximal burst length is 0.8 ms, the smallest distance between single bunches is 1 µs allowing a maximum number of 800 bunches per burst.

Since years, beam time for users is overbooked by a factor of about four. Therefore, a second undulator beamline FLASH2 has been constructed in 2011-14. The burst of electron bunches is now shared between two undulator beamlines, such that two experiments receive beam simultaneously with 10 Hz each. Sharing is possible for pairs of experiments requiring together at maximum the full burst duration of 0.8 ms, minus a transition time of 30 µs for the kicker-septum system to divide the pulse train burst.

An additional important and unique feature is, that beam parameters and bunch pattern can vary for the two undulator beamlines, so that two experiments with different wavelengths, pulse durations, and pulse pattern are possible at the same time. The flexibility is realized with three main features. Firstly, variable gap undulators allow to adjust the wavelength for FLASH2 experiments, while the beam energy is determined by the wavelength required for FLASH1. Secondly, two different laser systems operated in parallel at the photoinjector allow different charges, different pulse pattern, and to create a variable gap between the sub-bursts for FLASH1 and FLASH2. Thirdly, the low-level RF control of the accelerating structures are able to adjust phases and amplitudes – to a certain extend – independently for both beamlines, thus making different compression schemes possible.

For details on FLASH2 photon beam parameters the reader is referred to [6].

* siegfried.schreiber@desy.de
† for the FLASH team

COMMISSIONING AND FIRST LASING

Mounting the FLASH2 electron beamline, including 12 undulator modules (Fig. 1), was finished in January 2014. The official permission of FLASH2 beam operation was given in early February, and the beam commissioning started in March.

Figure 1: FLASH2 undulator beamline with twelve variable gap undulators.

Due to FLASH1 user operation, dedicated beam time for FLASH2 had been restricted to a few days only until simultaneously operation was established end of May. Starting with June, the FLASH2 beam commissioning has taken place, whenever possible, parallel to FLASH1 user operation. This increased significantly the time available for FLASH2 commissioning with beam.

The first electron beam was transported into the FLASH2 extraction beamline on March 4, 2014, and beam transport up to the dump was achieved on May 23, 2014. In order to avoid radiation damage on the permanent undulator magnets, the first beam operation has been carried out with open undulator gaps.

ISBN 978-3-95450-133-5

PULSE CONTROL IN A FREE ELECTRON LASER AMPLIFIER

Luca Giannessi, ENEA C. R. Frascati and Elettra-Sincrotrone Trieste, Italy

Abstract

A significant progress has been made in controlling the properties of the radiation emitted by a FEL amplifier. Experiments have demonstrated the possibility both to increase the temporal coherence and to reduce the amplifier length to reach saturation, by seeding it with an external source. This may be a solid state, short pulse, laser (Ti:Sa,OPA..), doubled or tripled in a crystal, or a high order harmonic pulse generated in gas. The coherence improvement and the increased compactness of the source are only the first beneficial offspring of this marriage between the optical laser world and that of FELs. Non-linear effects in the seeded FEL dynamics may be exploited to shorten the pulse length beyond that allowed by the FEL natural gain bandwidth. Multiple seed pulses can be used to generate pulses whose temporal distance and properties are also controlled. Similarly, the FEL gain can be adapted to match the seed properties by tailoring the electrons phase space to generate ultra-short output pulses at unparalleled intensities.

INTRODUCTION

The free electron laser is a very special laser amplifier relying on a quasi "medium-free" amplification mechanism. The active medium is indeed constituted by electrons interacting with the ponderomotive potential made by the undulator and the laser field itself. This fact allows great control on the resonances coming into play and the amplification process may be designed in an extremely wide spectral range. Single pass FELs operate in mirrorless configurations where the radiative interaction of electrons is mainly that with the laser optical electromagnetic wave at the resonant frequency, permitting the lasing process down to the VUV or X-ray spectral range. FEL light sources dedicated to user experiments are fully functional both in the hard X-rays, such as LCLS and SACLA [1, 2], and in the soft X-rays, as FLASH and FERMI [3–5]. After a first phase where the main scientific and technical challenge was that of achieving sufficient gain to reach saturation, the problem shifted to that of gaining full control of the properties of the emitted radiation. We are now learning how to influence the amplification process and modify the properties of radiation according to the needs of experiments where the FEL light is the investigation tool. Several experiments have demonstrated the possibility of both increasing the temporal coherence and reducing the amplifier length required to reach saturation, by seeding the amplifier with an external source. The electron beam, can be shaped to influence the gain spectrum and effectively modify the gain frequency bandwidth to generate ultrashort pulses, even beyond the limit posed by the intrinsic gain bandwidth of the FEL process. Other experiments have shown the ability of the FEL to act as harmonic converter, extending to very high order the emission of harmonics. In this contribution we have reviewed some of the experiments carried out at SPARC and FERMI, that were done within this specific scientific framework.

SEEDING AND HARMONIC GENERATION

The FEL conversion from electron kinetic energy to energy of the optical wave has the typical behavior of an instability, with an exponental growth regime followed by a saturation process [6–9]. The gain of the instability, as resulting from the one-dimensional theory and in the cold beam limit, is described by the universal scaling parameter ρ_{fel} [9], related to the power e-folding (gain) length L_G by the relation $L_G = \lambda_u/(4\pi\sqrt{3}\rho_{fel})$. When the process starts from the electronic noise, after an exponential growth over a distance $L_{sat} \sim 20\, L_G$ the signal saturates at a power $P_{sat} \sim \rho_{fel} P_{beam}$ where $P_{beam} = I_{peak}\gamma\, m_0 c^2/e_0$ is the power carried by the electron beam. The natural line width of the output radiation from the SASE process in the classical regime is of the order of the parameter ρ_{fel}. The frequency spectrum of the emitted radiation corresponds to the white noise associated to the initial electron random distribution, filtered by the FEL gain bandwidth. Self amplified spontaneous emission output usually has poor longitudinal coherence, with a temporal and spectral structure consisting of a series of spikes uncorrelated in phase or amplitude [10–12].

This natural evolution of the FEL process may be influenced at startup by seeding the amplifier with an external source. The coherence properties of the seed are transferred to the electron modulation, leading to coherent emission at the undulator resonance and at its harmonics. The input seed, in order to be effective, must be intense enough to dominate the beam shot noise associated intensity, which may be derived according to the model in [13] and is given by $I_{sn} \approx 3\,\omega\,\gamma\, m_0 c^2 \rho_{fel}^2$, where ω is the FEL resonant frequency.

Harmonic generation in gas [14] is one of the most promising methods to generate radiation in the VUV region of the spectrum, and this method was used at different facilities to seed directly an FEL amplifier at wavelengths ranging from 160 nm down to 38 nm [15–19]. Seeding at the shortest wavelengths has pointed out the increasing difficulty in overcoming the electron beam associated shot noise power, which is linearly proportional to the photon energy. An alternative is to seed the FEL at longer wavelengths and exploit the harmonic generation mechanism to reach the desired spectral range. The first idea on implementing an FEL as an harmonic converter appeared in [20]. Afterwards different schemes involving higher order harmonic bunching and harmonic generation were proposed and studied both theoretically and experimentally by several authors [21–27]. Harmonic generation combined with a high gain FEL am-

ISBN 978-3-95450-133-5

SMALL-SCALE ACCELERATOR-BASED RADIATION SOURCES AND THEIR APPLICATIONS

Young Uk Jeong, KAERI, Daejeon, Korea

Abstract

Small-scale accelerator-based radiation sources can be used more widely for developing advanced technologies and exploring new science with high convenience and low cost. Sometimes they are competitive comparing with giant facilities like X-ray free-electron lasers (X-FELs). We have developed a table-top terahertz (THz) FEL for substituting X-ray or millimeter-wave-based security imaging technologies (body scanners) and a laboratory-scale ultrashort electron accelerator for investigating femtosecond dynamics of atoms or molecules with pump-probe experiments. I will present on the status of the development of the small-scale radiation sources and plans for the pump-probe experiments. Additionally recent research results on biological study with the operating KAERI (Korea Atomic Energy Research Institute) THz FEL will be given with the information of the references.

THZ FREE-ELECTRON LASER DRIVEN BY MAGNETRON-BASED MICROTRON

We have developed a laboratory-scale terahertz (THz) free-electron laser by using a compact conventional microtron with a magnetron RF generator. The brief history and references of the developments are listed as follows.

- FIR FEL Development (1995-1998) [1-3]
  - Target wavelength of 30-40 μm with a 12.5-mm-period undulator
  - Failed in FEL lasing
- THz FEL Development (1998-2007) [4-16]
  - Target wavelength of 100-300 μm with a 25-mm-period period
  - First lasing at the end of 1999 (λ=100-170 μm)
  - FEL & beam dynamics study
  - System stabilization & upgrade (λ=100-300 μm)
- THz Applications (2004-present) [17-23]
  - THz imaging, spectroscopy, meta-material study, THz-bio interaction, & so on
- Table-top THz FEL Development (2008-present) [24-27]
  - Rack-type FEL for security inspection (dimensions of 1.5 x 2.5 m^2)
  - Target wavelength of 300-600 μm with the average power of 0.1-1 W

ULTRAFAST ELECTRON DIFFRACTION FACILITIES

An RF-photogun-based linear accelerator for ultrafast pump-probe research is under construction [28]. The layout of the KAERI ultrashort accelerator is shown in Fig. 1. This system has four beamlines. Two of them are for ultrafast electron diffraction (UED) experiments on solid and gas targets. The main target parameters of the UED beamlines are listed on the Table 1. The electron bunch duration and timing jitter of the UED beamlines are designed to be less than 50 fs in FWHM and 30 fs in rms. The UED beamlines can perform single-shot measurement with a temporal accuracy less than 100 fs. This small-scale facility can be used for investigating time-resolved diffraction experiments with samples of gas, liquid, solid, and surface. The performance of the UED for those samples can compete with that of the X-FEL facilities. The details on the facility will be shown in these Proceedings [29].

The application experiments of the UED beamlines will be performed by the collaboration with universities in Korea. We are planning to investigate the reaction dynamics of gas-phase samples of pyridine and cyclohexadiene (CHD) with higher temporal resolutions than those of previous studies.

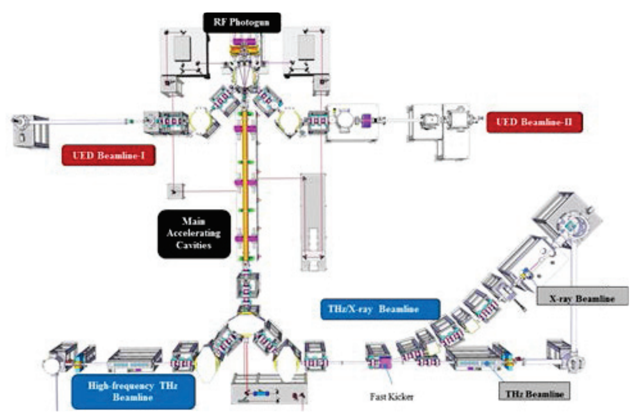

Figure 1: Layout of the KAERI ultrashort accelerator for femtosecond pump-probe experiments.

Table 1: Simulated Beam Parameters of The KAERI UED

Bunch Charge	1 pC
Beam Energy	2.6 MeV
Bunch Length (FWHM)	< 50 fs
Norm. Emittance	0.3 mm mrad
Energy Spread (r.m.s.)	0.3%

ACKNOWLEDGMENT

This work was supported by the World Class Institute program (WCI 2011-001) of the National Research Foundation of Korea funded by the Ministry of Science, ICT and Future Planning.

ISBN 978-3-95450-133-5

PHASE SPACE MANIPULATIONS IN MODERN ACCELERATORS*

Dao Xiang†, Shanghai Jiao Tong University, Shanghai, China

Abstract

Beam manipulation is a process to rearrange beam's distribution in 6-D phase space. In many cases, a simple phase space manipulation may lead to significant enhancement in the performance of accelerator based facilities. In this paper, I will discuss various beam manipulation techniques for tailoring beam distribution in modern accelerators to meet the requirements of various applications. These techniques become a new focus of accelerator physics R&D and hold great promise in opening up new opportunities in accelerator based scientific facilities.

INTRODUCTION

The ability to tailor a beam's 6-D phase space to meet the demands of various applications is of fundamental interest in accelerator physics. For instance, the electron bunch length typically needs to be reduced in FELs to drive the exponential growth process while it may need to be increased in storage rings to increase beam life time. Beam manipulations include a wide array of techniques that use rf cavities, dispersive elements, lasers, etc. to rearrange beam distribution in 6-D phase spaces. On the one hand, one has the freedom to use many elements to design a beam for a specific application (see. e.g. [1]); on the other hand, beam manipulation has to obey some basic rules (e.g. the emittances of the subspaces cannot be partially transferred from one plane to another if the beam is uncoupled before and after the transformation [2]). Here I will discuss a few representative beam manipulation techniques and show how they may enhance the capabilities of modern accelerators.

GENERAL DISCUSSIONS

In transverse plane, dipoles are used to bend the beam and quadrupoles are used to focus the beam. When they are integrated in a suitable way, they can form a closed loop (an electron storage ring) which allows the beam to circulate for millions of thousands turns. While it appears trivial to control the transverse beam size with quadrupoles, focusing the beam to extremely small size requires special efforts. For instance, a ~500 m final focus beam line is needed to focus the electron beam to nanometer (nm) level in linear colliders [3]; another extreme is electron microscope where the spherical aberration is corrected up to the 5th order to provide sub-50 pm resolution which allows one to see individual Hydrogen atom [4].

In longitudinal plane, beam phase space manipulation typically requires an element to change beam energy and a dispersive element to change beam path length. This is because relativistic electrons travel more or less with the speed of light (e.g., for 1 GeV electron, $1 - v/c \approx 1.3 \cdot 10^{-7}$. As a result, for modern beams with typical small energy spreads, the relative longitudinal velocities of electrons are so small that they do not change their relative positions when the beam travels along a straight line in a drift. With a dispersive element, one can force the particles to follow different paths and the beam longitudinal distribution can be readily shaped.

BEAM MANIPULATION FOR FELS

So far most of the high-gain FELs in the short wavelength (VUV to hard x-ray regime) have operated in the SASE mode in which radiation from the electron beam shot noise is exponentially amplified to the GW level. While a SASE FEL has excellent transverse coherence, its temporal coherence is rather limited (noisy in temporal profile and spectrum). In this section we discuss several beam manipulation techniques that may improve temporal coherence of FELs by providing coherent bunching to seed the FEL amplification process.

To provide bunching at short wavelength, fine structures in beam current distribution have to be created. The creation of a charge density modulation at sub-optical wavelengths in an electron beam with lasers is analogous to the manipulation of the electron bunch length in a magnetic bunch compressor. The difference is that the energy chirp (correlation between a particle's energy and its longitudinal position) is imprinted by lasers rather than RF cavities. The process of longitudinal bunch compression, to the first order, can be described as a linear transformation where the bunch length is reduced while the energy spread (conservation of phase space area) and peak current (conservation of charge) are both increased. This is achieved by first accelerating the beam off-crest in RF cavities to establish a correlated energy chirp (e.g. with bunch head having a slightly lower energy than the bunch tail), and then sending the beam through a dispersive chicane. The particles with lower energy are bent more in the chicane and therefore tra-

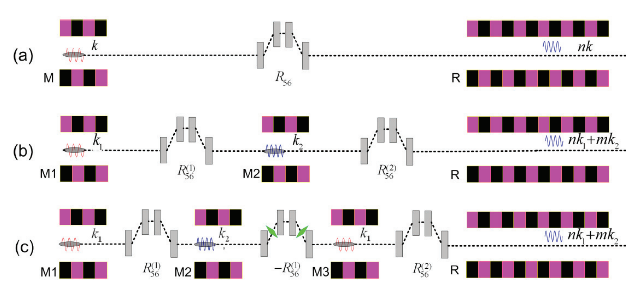

Figure 1: Various harmonic generation schemes for seeding FELs.

* Work supported by the National Natural Science Foundation of China under Grants No. 11327902.

† dxiang@sjtu.edu.cn

ISBN 978-3-95450-133-5

PARTICLE TRACKING SIMULATIONS FOR EXFEL COMPLEX SHAPE COLLIMATORS

V.G. Khachatryan*, V.H. Petrosyan, T.L. Vardanyan, CANDLE SRI, Yerevan 0040, Armenia

Abstract

The study sets the objective to investigate through numerical simulation the produced secondary radiation properties when the electron beam particles hit collimator walls. Using particle tracking simulation code FLUKA, the European XFEL electron beam as well as beam halo interaction with the collimator were simulated [1,2]. The complex geometrical shape and material composition of the collimator have been taken into account. Absorbed dose spatial distribution in the material of the collimators and particle fluencies from the downstream surface of the collimator were simulated for the total secondary radiation and its main components.

INTRODUCTION

The beam halo consists of particles per bunch with large betatron or energy amplitudes. Evaluation of the number of large-amplitude particles which can be expected due to the scattering processes, wakefields, and magnet nonlinearities is a difficult task. The beam collimation systems are applied to get rid of beam halo. description of collimators with the picture of general view and the photo of "Collimators Block" unit is provided Nina Golubeva [3] The XFEL main collimator CL.COLM (4 collimators) is a sytem consisting of 4 Titanium alloy tubes (diameters are 4, 6, 8 and 20 mm) distributed vertically, internal pure Al block and outer Copper block (length=50cm) with brazed cooling tubes[4]. Collimator with its movers will be located inside the steel housing (length=1m), in vacuum. In numerical calculations with FLUKA only the main characteristics of geometry has been taken into account. Therefore, somewhat simplified geometry was used in calculations which includes only main collimator block, steel housing and beam pipe (with 40.5mm diameters). The thickness of the titanium tubes and beam pipe wall is 2 mm. All tubes (0.5m long) are not tapered. Vertical direction movers enable the usage of any of four aperture of the collimator. The general view does not correspond to the exact final design. EXFEL linear accelerator beam main parameters are specified in Table 1 [2].

Table 1: Beam Parameters at Undulators

Energy	17.5 GeV
Emittance (normalized)	≤ 1.4 mm-mrad
Beta function	≈ 220 m
Spot size	9 x 10^{-5} m

*Khachatryan@asls.candle.am

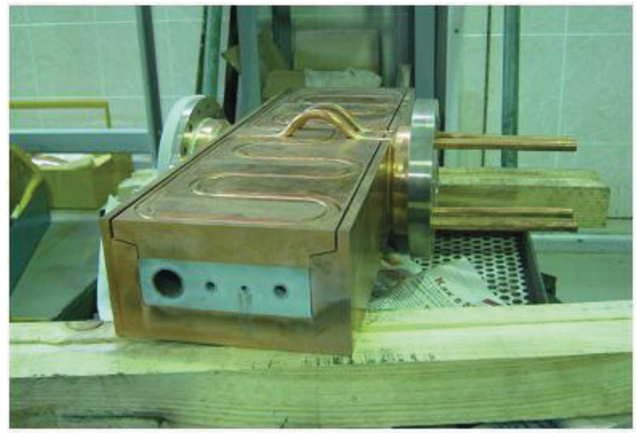

Figure 1: The photo of "Collimators Block" unit (The photo is provided by N. Golubeva) [3].

BEAM IMPACT ON COLLIMATOR WALL

At the undulator the beam size corresponds to the beta function value 220 m [3]. We took 17.5 GeV for the beam energy and 1.4 mm-mrad for the beam normalized emittance.

Bending or corrector magnets supply current values deviations from the stationary ones deflect the beam to the collimator wall. The simulation of the beam impact on the collimator is important from the radiation protection point of view, since high rate of the radiation produced can be harmful for both humans and sensitive equipment. Spatial distribution of the radiation field downstream collimator may indicate where an additional shielding would be useful. We assume that miss-stirred beam hits the front wall of the titanium tube at the coordinates x=0, y=0.4 cm. Electromagnetic cascade has been developed in the body of the titanium tube and then the shower spreads out to the neighbouring volumes (Figure 2). All the plots shown in Figures 2 and 3 are normalized to one of the primary particle. One can see that downstream to collimator outside beam pipe dose rate (Dose-Equivalent) reaches to a few Pico Sievert (≤10 pSv) per primary electron. That corresponds to 0.06 Sieverts per 1nC. Plots in the Figure 2 (right column) depict dose distribution [pSv] along the channel with maximum value. A full scale electromagnetic shower developments starts at the middle of the collimator. Figure 3 shows particle fluencies from the downstream surface of the collimator [GeV^{-1} cm^{-2}]. Note that the Fluence from the surface of the housing flange prevails in the low energy region while at higher energies most radiation passes through the beam pipe cross sectional area.

ISBN 978-3-95450-133-5

HELICAL UNDULATOR RADIATION IN INTERNALLY COATED METALLIC PIPE*

T. Vardanyan#, A. Grigoryan, L. Hovakimyan, M. Ivanyan, A. Tsakanian, V. Tsakanov, CANDLE SRI, Yerevan, Armenia

Abstract

The vacuum chambers of many advanced undulator sources are coated internally in order to reduce the impedance of the vacuum chamber or improve the vacuum performance. Although the impedances and radiation properties of the internally coated metallic pipes for straightforward moving charge are well studied, the peculiarities of the particles wiggling motion on the radiation characteristics in such structure are missed. In this paper we obtain exact expressions for the fields of a particle moving along a spiral path, as in the single-layer resistive as well as in the two-layer metallic waveguides, modelling NEG coating of the waveguide walls. Based on these results, it will be possible to obtain the necessary characteristics of the radiation of helical undulators, very close to reality. The solution is obtained as a superposition of a particular solution of inhomogeneous Maxwell's equations in a waveguide with perfectly conducting walls, and the solutions of the homogeneous Maxwell equations in the single-layer and double-layer resistive waveguides. Solution in the form of the multipole expansion for inhomogeneous Maxwell's equations for a waveguide with perfectly conducting walls, are also obtained in this study.

INTRODUCTION

We consider the spiral motion of a point charge in a resistive circular waveguide, modeling the charge motion in the vacuum chamber of a helical undulator. Helical undulator radiation, which has a number of important specific properties (axial symmetry of the distribution of the radiation power and its narrow directional and narrow band character) is widely used in modern synchrotron radiation sources [1,2].

The problem was considered earlier in the approximation of the spiral motion of the bunch in the free space [3] and in the presence of cylindrical [3-5] or rectangular [6] vacuum chamber with perfectly conducting walls. Limitation on the transverse dimensions of the vacuum chamber by the magnet poles causes a significant impact on the character of the chamber wall radiation. In connection with this it is necessary to take into account the finite conductivity of vacuum chamber walls, which is made in this paper. In this paper we consider also the case of a two-layer metal vacuum chamber, the presence of which, under certain conditions, causes the presence of narrow-band resonance of wakefield radiation in case of rectilinear motion of a particle [7].

In this paper, the method of expansion of the field in multipoles [8,9] is used, in contrast to the method of eigenfunction expansion of the waveguide, used previously to solve similar problems. The work examines the particle radiation, moving along a spiral trajectory in perfectly conducting cylindrical waveguide, in the resistive cylindrical waveguide and in the two-layer metal waveguide.

RADIATION IN A PERFECTLY CONDUCTING CIRCULAR WAVEGUIDE

Density distribution of charge and current in a cylindrical coordinate system in time domain are represented as follows:

$$\rho(z,r,\varphi,t)=\frac{1}{\sqrt{ra}}\delta(r-a)\delta(\varphi-\omega_b)\delta(z-vt),$$
$$j(z,r,\varphi,t)=\left(v\vec{e}_z+\omega_b a\,\vec{e}_\varphi\right)\rho(z,r,\varphi,t) \qquad (1)$$

and in frequency domain:

$$\tilde{\rho}(\omega,r,\varphi,t)=\frac{1}{2\pi\sqrt{ra}}\delta(r-a)\exp\{j(z-vt+\varphi-jn\omega_b t)\} \qquad (2)$$
$$\tilde{\tilde{j}}(\omega,r,\varphi,t)=\left(v\vec{e}_z+\omega_b a\,\vec{e}_\varphi\right)\rho(\omega,r,\varphi,t),\ n=1,2,3,\dots .$$

Here a is the radius of the helical curve, ω_b the gyroscopic rotation frequency, v the longitudinal velocity of the particle, $\vec{e}_z,\vec{e}_\varphi$ the unit vectors of cylindrical coordinate system. Solutions for the radiation fields are searched using the pair of combinations of vector-valued functions [8,9]:

$$\vec{e}_{I,K}(\alpha)=\exp\{j(z-vt+\varphi-jn\omega_b t)\}\begin{Bmatrix} nI_n(\alpha r)/\alpha r,\ \ jI_n'(\alpha r),\ 0\\ nK_n(\alpha r)/\alpha r,\ \ jK_n(\alpha r),\ 0\end{Bmatrix} \qquad (3)$$

Here I_n, K_n are the modified Bessel functions of the first and second kind, respectively and $\alpha=k/\gamma$, where γ is a Lorentz factor and $k=\omega/v$ with frequency ω.

With the help of these functions solutions of the inhomogeneous Maxwell's equations for the radiation fields in the waveguide with a perfectly-conducting walls can be constructed. The result is a combination of TM $(H_z\equiv 0)$ and TE $(E_z\equiv 0)$ waves:

$$\vec{E}^i=\vec{E}^{TM}+\vec{E}^{TE} \qquad (4)$$

with

*This work was supported by State Committee of Science MES RA, in frame of the research project № SCS 13YR-1C0056

#tvardanyan@asls.candle.am

ISBN 978-3-95450-133-5

HIGH ACCURACY SHIMMING TECHNIQUE FOR THE PHASE SHIFTERS OF THE EUROPEAN XFEL

Yuhui Li, Joachim Pflueger, The European XFEL, Notkestr 85, 22607 Hamburg, Germany

Abstract

For the European XFEL 91 phase shifters are needed, which have to fulfil stringent field integral specifications: There should be no observable beam deflection when the strength, i.e. the magnetic gap is changed

In order to facilitate the mass production of 91 phase shifters within the tough XFEL schedule a shimming technique was developed. It is based on measured shim signatures and is straight forward and fast to apply. The method is described and results are presented demonstrating that all requirements can be fulfilled.

INTRODUCTION

The undulator systems of the European XFEL need a total of 91 phase shifters. They should be transparent to the electron beam: This means that there should be no detectable effect by changing their strength i.e. their magnetic gap. As a consequence the gap dependent first field integrals error of a phase shifter must not exceed 0.004Tmm (4Gcm) for phase shifter gaps > 16mm. For smaller gaps tolerances can be relaxed as shown in table 1. In addition these requirements must be fulfilled in a good field region in the horizontal plane ±0.5mm around the device axis limiting allowed integrated gradient to below 0.004T. A summary is given in table 1.

These tolerances are tight. The magnetic design has a high magnetic symmetry to eliminate any systematic gap dependency due to geometry [1]. Nevertheless small effects may arise due to imperfections in the magnetic material and errors in the pole contours. From observations made on the first prototype [1] it became clear that the gap dependence cannot be compensated by the pole height tuning as applied to the XFEL undulators [2]. By placing shims on poles and/or magnets gap dependent effects can be compensated. Moreover a smart strategy can also provide a good field region of ±0.5mm in the horizontal plane to facilitate alignment. Therefore a systematic method was developed which allows the determination of shim parameters to compensate any measurable gap dependency and to provide a sufficient good field region.

Table 1: Gap dependent Tolerance Specifications

Gap (mm)	>16	15	14	13	12	10.5
Spec (Gcm)	±4	±7	±10	±13	±16	±18
Good field range (mm)	±0.5					

On the other hand, a fast and effective tuning procedure is a key issue for an economic and timely production of a large number of phase shifters. This paper explains a fast and systematic shimming technique to obtain the required gap dependent field integral specification and simultaneously a small enough gradient to have the required good field range. Measured results are presented.

MAGNETIC MOMENT IN SHIMS

A shim is made from highly permeable such as low carbon iron. When placed on a pole or magnet the external magnetic field induces a magnetic moment in the shim. Its effects are similar but not identical to that of an additional small permanent magnet.

Fig. 1 explains the effect and shows a schematic cut through a hybrid type magnet structure as are used for the Phase Shifters [1]. The magnetization of the magnets is parallel/antiparallel to the beam axis. The flux is redirected perpendicular to the axis by the poles. If a shim is placed on a magnet besides a pole the magnetic moment vector in the shim is mainly parallel to axis and only a small contribution is perpendicular to the axis. In contrast a shim on a pole mainly induces a perpendicular contribution and acts similar to a pole shift.

The magnetic field $\vec{B}$ of a magnetic moment $\vec{m}$ at position $\vec{r}$ is given by:

$$\vec{B}(\vec{r}) = \frac{\mu_0}{4\pi}\left[\frac{3\vec{r}\,(\vec{m}\cdot\vec{r})}{r^5} - \frac{\vec{m}}{r^3}\right]. \tag{1}$$

Therefore the field integral caused by $\vec{m}$ perpendicular to the axis is given by:

$$\begin{aligned}\int_{-\infty}^{+\infty} B_\perp dz &= \int_0^\pi \frac{m_\perp(3\sin^2\theta - 1) + 3m_{//}\sin\theta\cos\theta}{r^3}\,d\theta\,. \\ &= \frac{28\,m_\perp}{15\,d^3}\end{aligned} \tag{2}$$

Where $m_\parallel$ and $m_\perp$ represent the magnet moment parallel and perpendicular to phase shifter axis, respectively. d is the distance from the magnetic moment to the axis as shown in Fig. 1. According to Eq. 2 only $m_\perp$ contributes to the vertical field integral and $m_\parallel$ does not. The induced magnetic moment of shims on poles is mainly $m_\perp$ and by shims on magnet is predominantly $m_\parallel$. So shims on poles are clearly more efficient. Unfortunately they eat up the effective phase shifter gap and are not self-adhesive by magnetic forces and therefore need to be restrained (glued). In contrast shims on magnet don't narrow the gap due to a 0.5mm pole overhang with respect to magnets. Experimental tests have demonstrated that in contrast to Eq. 2 magnet shims still give a small strength suitable for weak corrections. They stay on magnets firmly. They are a convenient choice Phase Shifters shimming.

ISBN 978-3-95450-133-5

TEMPERATURE EFFECTS OF THE FLASH2 UNDULATORS

M. Tischer*, A. Schöps, P. Vagin, DESY, Hamburg, Germany

Abstract

FELs are very sensitive to small changes in the resonance condition of the emitted radiation. As a consequence, permanent magnet undulators in FELs usually require extensive temperature control in order to assure stable operation conditions. In principle, the temperature dependence of permanent magnet material is well known but more things need to be considered like different thermal expansion of various mechanical parts or thermally induced deformation which do not only affect the K parameter but also the field quality. We have performed temperature dependent magnetic measurements in a range from 19 to 28 degrees Celsius and have analyzed the magnetic performance of the undulator. The results of this case study can be transferred to all FLASH2 undulators and shall allow for a simple temperature dependent gap correction in order to make the spectral properties insensitive to temperature changes of the insertion devices.

MAGNET MATERIAL REMANENCE

The temperature coefficient for the remanent magnetization of the magnet material VACODYM 776AP used for the FLASH2 undulators is -1100ppm/K [1]. For determining the effects of changes in the remanence on the magnetic field amplitude in a complex structure like a hybrid undulator, also the geometry and the saturation of the poles have to be taken into account.

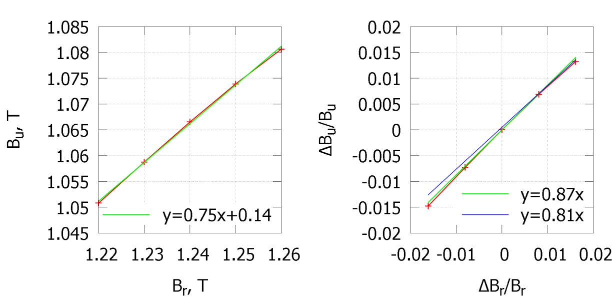

Figure 1: Calculated undulator magnetic field amplitude B_u versus magnet material remanence B_r (left) and $\Delta B_u/B_u$ versus $\Delta B_r/B_r$ normalized for B_r = 1.24...1.26T (right).

The dependence of the magnetic field B_u on the remanence of the magnet material B_r was calculated using Radia [2]. For the FLASH2 pole and magnet geometry, it can be described as: $B_u(B_r) = 0.75 \cdot B_r + 0.14$T (Fig. 1). Therefore the expected relative change in magnetic field $\Delta B_u/B_u$ due to the temperature-induced change in the remanent magnetization B_r, normalized for B_r = 1.24..1.26T, is $\Delta B_u/B_u$ = -1100ppm/K · 0.87..0.81 = -960..-890ppm/K.

MAGNETIC MEASUREMENTS

Recently temperature effects have also been studied for XFEL undulators [3]. For the FLASH2 undulators, magnetic field maps were measured with different methods for crosschecking that the temperature dependence of the field sensors is properly compensated. The field was measured by a Hall probe, a pick-up coil and a stretched wire. The Hall probe and coil gain were calibrated by an NMR magnetometer in a 0.4T permanent magnet at each temperature change. This single point calibration was used for the Hall probe as mainly its gain and offset change with temperature, and changes of a higher order nonlinearity could be neglected. For the coil, the gain of the whole measurement system was calibrated, not just the coil area, as the coil and the integrator input resistances are also temperature dependent.

The alignment of the bench scan axis with respect to undulator magnetic axis was performed at each temperature change by magnetic measurements, in order to compensate probe displacement caused by thermal expansion of the undulator and the measurement bench.

In contrast to the Hall probe which has a small sensitive area with a width of 100μm, the coil measures a field which is averaged over its size of 3mm. For a sinusoidal magnetic field of an undulator with a period of 31.4mm, such an averaging reduces the measured field amplitude by up to 1% [4]. This gain error for the sensitivity of the coil would be the same for different temperatures, and the relative temperature dependence of the field amplitude could still be measured with a such sensor even without any gain compensation.

The stretched wire for the field integral measurements was installed transversely to the magnet structure, instead of the usual orientation along the undulator. This way, by moving the wire along the magnet structure, it measures the vertical field, averaged transversely over the whole pole width. Therefore the measured field could not be compared directly to the Hall probe and coil measurements on the beam axis. However, the temperature dependence of the average field should be the same as the temperature dependence of the field on beam axis. Also, only a small part of the magnet structure could be measured due to the limited range the moving stages of 100mm, covering only few undulator periods. The stretched wire setup was not calibrated. With 1mm wire step size, its gain is defined by the mechanical accuracy and temperature stability of the linear stages.

The measured temperature dependence for the magnetic field amplitude shows a linear behaviour with a temperature coefficient of -885±3ppm/K (Fig. 2). The 3 different measurement methods obtain this value in almost perfect agreement. The measured value compares very well to the calculated value of the B_r-induced temperature dependence. This indicates that other effects like thermal expansion of the support structure should be smaller than 80ppm/K.

* markus.tischer@desy.de

ISBN 978-3-95450-133-5

THE PHOTON BEAM LOSS MONITORS AS A PART OF EQUIPMENT PROTECTION SYSTEM AT EUROPEAN XFEL

N. Gerasimova#, H. Sinn, European XFEL GmbH, Hamburg, Germany
S. Dziarzhytski, R. Treusch, DESY, Hamburg, Germany

Abstract

For the X-ray beam transport systems, the problem of potential damage to the equipment by mis-steered photon beam emerged with advent of powerful X-ray Free-Electron-Lasers (FELs). In particular high repetition rate machines as European XFEL, where not only focused beam can produce ablation, but even unfocused beam can melt the beamline components while machine operates in multibunch mode, demand for implementation of equipment protection. Here we report on development of photon beam loss monitors at European XFEL facility. The photon beam loss monitors will react on the mis-steered photon beam and interface the machine protection system. The prototype comprises the vacuum chamber with fluorescence crystals positioned outside the photon beampath. The fast sub-hundred ns fluorescence induced by mis-steered beam can be detected by photomultiplier tube allowing for intra-train reaction of machine protection system. First tests have been carried out at FLASH and shown the feasibility of detection based on PMT-detected fluorescence. In addition to the efficient YAG:Ce crystal, the robust low-Z material as CVD microcrystalline diamonds has shown a potential to be used as fluorescence crystals.

INTRODUCTION

The high energy and high intensity accelerator facilities use the beam loss detection systems to react on losses of the particle beam and prevent radiation damage to the equipment. Different types of such beam loss monitors exist (see, for instance, [1]). The beam loss detection becomes an essential part of the machine protection system in case of superconducting linacs.

In case of photon beam transport systems, the problem of potential damage to the equipment was not considered till very recently. The total energy of a particle beam is usually much higher than the energy of produced by it photon beam. However with advent of highly brilliant X-ray Free-Electron-Lasers the potential danger of damage to the photon beam transport systems has been realised. Focused X-rays can ablate components of the beam transport systems. And in case of high repetition rate machines as European XFEL, trains of photon pulses capable to melt the beamline components even in case of unfocused beam [2]. In order to prevent such damage, we propose to introduce photon beam loss monitors reacting on mis-steered beams and interfacing the machine protection system in a way similar to electron (particle) beam loss monitors. To our knowledge the development presented in this paper is the first attempt to introduce a protection system for the photon beamlines.

#natalia.gerasimova@xfel.eu

DETECTION SCHEME

The kind of potential damage to the photon beam transport system differs from those in case of a particle beam. While highly energetic particles escape the vacuum chamber of the accelerator, and beam losses are usually detected outside the vacuum, the X-ray beam, in particular of low photon energies, is potentially capable to produce highly localized damage to the vacuum chamber itself or to the components inside the vacuum. This leads to necessity of introducing a detection system reacting on losses of photon beam into the vacuum of the beamline. The possible realization of such detection will be presented in following subsections. As for electronics and interface to machine protection system, this part of beam loss detection system can be in high degree adopted from the beam loss monitors for the particle beam. In our case, the systems developed for the electron beam loss detection at European XFEL [3] will be used.

Conceptual Scheme

The conceptual scheme of proposed photon beam loss monitors is presented in Fig. 1. As discussed above, the main task of the photon beam loss monitors is to prevent hitting of the beamline components by the photon beam. To react on mis-steering of the photon beam, some 'screen' can be introduced into vacuum vessel around the nominal beam path (represented in yellow in Fig. 1). This 'screen' converts the X-rays into visible light. The conversion of photons into visible range enables relatively easy detection, since many types of detectors are available

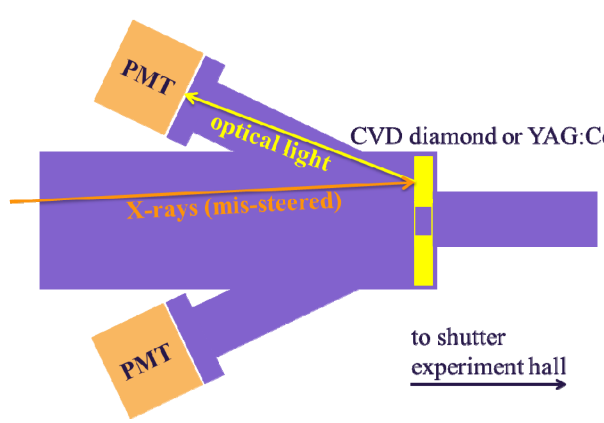

Figure 1: Conceptual scheme of the photon beam loss monitor (see text).

ISBN 978-3-95450-133-5

IMPLEMENTATION PHASE OF THE EUROPEAN XFEL PHOTON DIAGNOSTICS

Jan Grünert, Jens Buck, Wolfgang Freund, Andreas Koch, Marc Planas, Florian Dietrich, European XFEL GmbH, Hamburg, Germany

Abstract

The European XFEL facility with 3 undulators and initially 6 experimental end-stations requires an extensive set of photon beam diagnostics for commissioning and user operation, capable of handling the extreme brilliance and its inherent damage potential, and the high intra bunch train repetition rate of 4.5 MHz, potentially causing additional damage by high heat loads and making shot-to-shot diagnostics very demanding [1].

After extensive design [2-5] and prototype studies, in 2014 the installation of the photon beam devices starts with the equipment in the first photon tunnel XTD2 which is where the SASE1 hard X-ray undulator is located. This contribution reports on the device construction progress by focusing on the XTD2 tunnel devices and their implementation into the tunnel environment.

OVERVIEW

The photon part of the European XFEL facility is here defined as starting from the undulators, followed by the photon transport system leading into the experimental hall with the experimental endstations. The photon transport system contains beam transporting and shaping X-ray optics as well as X-ray photon diagnostics and is located in the photon tunnels XTD1 through XTD10. The hard X-ray undulator SASE1 is located in tunnel XTD2 which is also the first tunnel in the installation sequence to be equipped with the machine. As an example of the photon diagnostics devices in the overall facility, in this article we will describe the devices in XTD2 and their current implementation.

After definition of the overall diagnostics layout [1], long design phases of the individual devices, prototyping and production, most devices for XTD2 are ready for installation. Their implementation into the tunnel is prepared, which means that their design was accommodated to the space restrictions at their particular tunnel position, possible collisions were checked, infrastructure interfaces defined, and where required special infrastructure such as the rare-gas supply was designed.

Implementation

A particular feature of the XTD1 and XTD2 tunnels and an example of the tunnel implementation difficulties is that here the photon beamline is at a different and varying height – up to 2.65 m above the tunnel floor, whereas in all other tunnels there is a standard beamline height of 1.4 m. These two tunnels containing the undulators SASE2 and SASE1 respectively have downward slopes towards their ends in order to allow for transport paths crossing underneath the photon and electron beamlines when approaching the shaft buildings which are the branching points of tunnels and connect the incoming tunnel to the subsequent two outgoing tunnels. Due to this feature it was decided to build concrete platforms for the devices bringing the floor up so that the devices and their mounts can be built for the standard beamline height, avoiding special versions of the devices which are present in all tunnels. One such platform can be seen in Fig. 7.

Installation Sequence

The sequence of tunnel installations of infrastructure and also photon transport and diagnostics was fixed in the same order as the future commissioning sequence: first SASE1, then SASE3, and finally SASE2 will be installed. SASE1 is the hard X-ray beamline with a directly linear transport of the electron beam into the undulator - in SASE2 the electrons need to pass a bend before entering into the undulator which is an additional complication. Once electrons are transported through SASE1 they necessarily pass through the soft X-ray undulator SASE3 on their way to one of the two available main dumps, which is why the SASE3 area is installed next after SASE1.

DEVICES

This proceedings paper focuses on the photon diagnostics devices in XTD2 which is a representative subset of all diagnostics. In this conference the temporal diagnostics will be presented in another contribution (MOP014), as well as more details on the undulator commissioning spectrometer (MOP009) and details about the imagers (MOP013).

The photon diagnostics devices in XTD2 are all downstream of the separation point where the electron beam is separated from the photon beam. The first device, pushed as far as spatially possible towards the source, towards this separation, is a filter chamber and the transmissive imager. The space is very limited since the electron beamline is still very close, branching off at only a small angle.

The **Filter chamber**, see Fig. 1, is the most upstream photon diagnostics component and allows for initial spectroscopy by selecting and inserting X-ray filters, using characteristic K-lines of metals, and it contains absorbers for synchrotron radiation during undulator commissioning.

*corresponding author, contact jan.gruenert@xfel.eu

ISBN 978-3-95450-133-5

X-RAY PHOTON TEMPORAL DIAGNOSTICS FOR THE EUROPEAN XFEL

Jia Liu*, Jens Buck, Florian Dietrich, Wolfgang Freund, Jan Grünert, Michael Meyer,
European XFEL GmbH, Hamburg, Germany

Abstract

The European XFEL facility (XFEL.EU), which will be commissioned starting 2016 shows exceptional features with its high delivery rate of light pulses and extremely high average brilliance. Characterizing the temporal properties of the FEL pulses on a shot-to-shot basis is important and challenging. Here we report about the concept and recent progress concerning temporal diagnostics for XFEL.EU. Spectral encoding and THz-streaking are the techniques which will be implemented to deliver arrival time and pulse duration monitoring while coping with the high repetition rate and high brilliance of XFEL.EU.

INTRODUCTION

European XFEL (XFEL.EU) will be commissioned in 2016 and become operational in 2017. Its most prominent advantages will be its extremely high number of light pulses per second (27000 p/s) and two or three orders higher average brilliance than other FEL facilities. The FEL pulses in XFEL.EU are produced in 10 Hz bunch trains that contain up to 2700 individual pulses within the 600 μs time of one bunch train, corresponding to a pulse separation of 220 ns between individual light pulses or a 4.5 MHz repetition rate, as illustrated in the conceptual (CDR) and technical design reports (TDR) [1-5].

When choosing and designing the timing tools for XFEL.EU, the extremely high peak brilliance and high repetition rate must be addressed. A universal independent shot-to-shot temporal tool shall be developed, which is expected to be applicable in a broad range of x-ray photon energies and with various x-ray pulse lengths under different operation modes.

Adapted from attosecond (as) metrology, where the as XUV pulses generated via high harmonic generation (HHG) are characterized by using a few-cycle near Infrared laser pulse [6-8], the x-ray THz streaking technique was experimentally successfully employed for single shot soft x-ray temporal diagnostic [9-12], utilizing THz radiation from a THz undulator or an external laser based THz source. Very recently, hard x-ray streaking was successfully demonstrated as an arrival time monitor and pulse length monitor in SACLA across a broad photon energy range of 5 to 12 keV.

Independent photon arrival time monitoring based on spectral encoding was first demonstrated by LCLS and is also planned for XFEL.EU. It needs to be shot-to-shot burst mode compatible, and ideally permit extraction of a veto signal. Since spectral encoding was demonstrated so far only for repetition rates of 10 Hz to 120 Hz, an extension to MHz repetition rates for XFEL.EU has yet to be studied and developed.

*corresponding author, contact jia.liu@xfel.eu

STREAKING ELECTRONS WITH THZ RADIATION

The energy distribution of photoelectrons ejected from noble gases ionized by x-ray pulses can be broadened and shifted by an external optical field depending on its ionization time instant, and the temporal properties of the x-ray pulse are then mapped onto the kinetic energies of the photoelectrons. One can thus uniquely determine the relative time delay between x-ray and external field as well as the pulse length of the x-ray pulse by comparing the photoelectron energy with and without external streaking field.

Long wavelength THz pulses are chosen to get rid of the intrinsic time jitter of the x-rays since longer wavelength streaking fields give rise to a larger linear streaking region which is less sensitive to the x-ray time jitter.

A single-cycle THz pulse, generated by tilted pulse front pulses in a Lithium Niobate (LN) crystal, with zero crossing temporal duration of ~600 fs to 1 ps, will be implemented [13]. An example of a THz pulse, generated from 2.5 mJ, 1 kHz, 800 nm is illustrated in Fig. 1. The THz radiation has a central frequency of 0.65 THz and extends up to 3 THz, with the electric field strength of 130 kV/cm. More effect will be studied and further optimizations to the THz pulse shape and field strength will be done, e.g. by cooling down the LN crystal or using organic crystals like DAST for higher frequency and higher field strength THz generation [14].

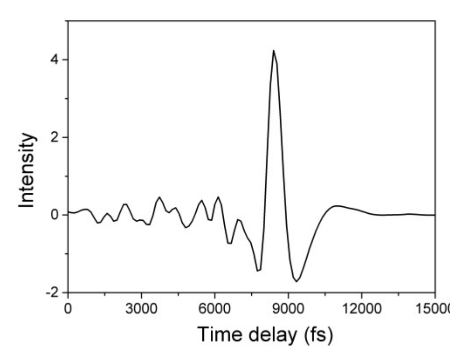

Figure 1: Typical single-cycle THz pulse from LN using the tilted pulse front method.

It should be pointed out that the temporal resolution of THz streaking is related to the THz field strength and the initial photoelectron energies and is limited to the bandwidth of the x-ray pulse, the energy resolution of the electron time of flight (eTOF) spectrometer and shot-to-

ISBN 978-3-95450-133-5

A POWER SWITCHING IONIZATION PROFILE MONITOR (3D-IPM)

H. Breede, L. V. Vu, M. Sachwitz, H. Grabosch, DESY, Zeuthen, Germany

Abstract

FLASH at DESY in Hamburg is a linear accelerator to produce soft x-ray laser light ranging from 4.1 to 45 nm. To ensure the operation stability of FLASH, monitoring of the beam is mandatory. Two Ionization Profile Monitors (IPM) detect the lateral x and y position and profile changes of the beam. The functional principle of the IPM is based on the detection of particles, generated by interaction of the beam with the residual gas in the beam line. The newly designed IPM enables the combined evaluation of the horizontal and vertical position as well as the profile. A compact monitor, consisting of two micro-channel plates (MCP) is assembled on a conducting cage along with toggled electric fields in a rectangular vacuum chamber. The particles created by the photon beam, drift in the homogenous electrical field towards the respective MCP, which produces an image of the beam profile on an attached phosphor screen. A camera for each MCP is used for assessment. This indirect detection scheme operates over a wide dynamic range and allows the live detection of the clear position and the shape of the beam. The final design is presented.

INTRODUCTION

To ensure a smooth operation of the free electron laser FLASH at DESY Hamburg, numerous detectors for the precise measurement of the electron and laser beam are necessary. The great advantage of the here described Ionization Profile Monitor (IPM) is an undisturbed determination of the position and intensity distribution of the laser beam.

MEASURING PRINCIPLE OF AN IONIZING PROFILE MONITOR (IPM)

The FLASH laser beam with a variable wavelength from 4.1 to 45 nm is located in an Ultra High Vacuum (UHV) beam pipe. Despite the vacuum a certain amount of residual gases still exist. If the laser beam hits a residual gas atom, it becomes ionized and charged electrons and ions are created. By means of a homogeneous electric field, these electrons and ions can be deflected in a rectilinear way towards the micro-channel plate (MCP). Here, the impacting particles create an avalanche of secondary electrons in the micro tubes of the MCP and are being visualized on the phosphor-screen see Figure 1). These results in an image of the intensity-dependent laser beam profile (see Figure 2).

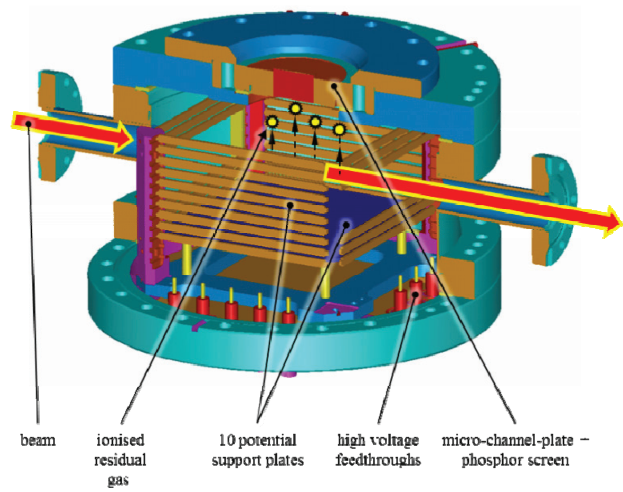

Figure 1: Conventional set up [1].

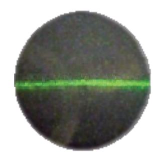

Figure 2: Image of the FLASH laser beam [1] [2].

CONVENTIONAL SET UP

Figure 2 shows an IPM module for the laser beam position measurement as implemented in FLASH [1] [2]. Problems and disadvantages of this design are the following:

- The large size of the monitor (approx. 400 mm x 300 mm x 200 mm) results in an insufficient homogeneity of the electrical field applied. Therefore the exact path of the electrons or ions from the origin of creation to the MCP is unknown and the spatial resolution is in the order of about ±50 microns.
- The size makes the IPM harder to manufacture and more expensive due to the high number of high voltage feedthroughs.
- To detect the horizontal and vertical parameters of the laser beam (3D) two consecutive detectors have to be implemented with perpendicular orientation to each other demanding large space.
- To take a look at the single bunches rather than just examining the whole train, the IPM needs a time resolution of at least 100 ns, the conventional set is not capable of.

A NEW DESIGN OF THE IONIZATION PROFILE MONITOR

In order to tackle the challenges described above the following design is proposed:

ISBN 978-3-95450-133-5

MEASUREMENT OF THE OUTPUT POWER IN MILLIMETER WAVE FREE ELECTRON LASER USING THE ELECTRO OPTIC SAMPLING METHOD

A. Klein#, A. Abramovich, D. Borodin, A .Friedman, H. Marks,
Department of Electrical and Electronic Engineering, Ariel University, Ariel, Israel

Abstract

In this experimental work an electro optic (EO) sampling method was demonstrated as a method to measure the output power of an Electrostatic Accelerator Free Electron Laser (EA-FEL). This 1.4 MeV EA-FEL was designed to operate at the millimeter wavelengths and it utilizes a corrugated waveguide and two Talbot effect quasi-optical reflectors with internal losses of ~30%. Millimeter wave radiation pulses of 10 µs at a frequency of about 100 GHz with peak power values of 1-2 kW were measured using conventional methods with an RF diode. Here we show the employment of an electro-optic sampling method using a ZnTe nonlinear crystal. A special quasi optical design directs the EA-FEL power towards the ZnTe nonlinear crystal, placed in the middle of a cross polarized configuration, coaxially with a polarized HeNe laser beam. The differences in the ZnTe optical axis due to the EA-FEL power affects the power levels of the HeNe laser transmission. This was measured using a polarizer and a balanced amplifier detector. We succeeded in obtaining a signal which corresponds to the theoretical calculation.

INTRODUCTION

Continue Wave (CW) and pulsed millimeter wavelength (MMW) and Terahertz (THz) radiation have many applications in medicine, industry, military and security [1]. In order to realize those applications, knowledge of the MMW or THz beam properties such as beam power, beam diameter and beam cross section pattern are required. For the MMW Electrostatic Accelerator-Free Electron Laser (EA-FEL) operating at 100 GHz we used heterodyne detection and received good results [2]. For higher frequenc radiation and pulsed sources, photoconductive antennas and far-infrared interferometric techniques are used [3, 4]. Photoconductive antennas have higher responsivity, and their signal-to-noise ratios are better than liquid helium cooled bolometers. Their detection bandwidth with a short dipole length can exceed 1-3 THz. The drawback of those photoconductive antennae is the resonant behavior and the limited operating bandwidth. Interferometric techniques provide an autocorrelation of terahertz pulses but important parameters of the beam are lost and it is complicated to realize. In this study, we report the use of an alternative optoelectronic method, free-space electro-optic sampling [5], to characterize freely propagating terahertz bandwidth CW or pulsed electromagnetic radiation. The advantages of this method are the sensitivity and speed of response allowing the identification of a short pulse envelope. Also this method can detect the cross-section of the THz beam radiation. In this work we demonstrated power measurements of single pulses and in-the future we intend-to image the cross sectional pattern of MMW and THz pulses. Our detection is independent of the source of MMW and we use inexpensive components, which include a HeNe CW laser, detector, optical components and two off-axis parabolic mirrors (OPM) to focus the MMW beam onto the ZnTe Elecro-Optic (EO) crystal cross section (see Fig. 1).

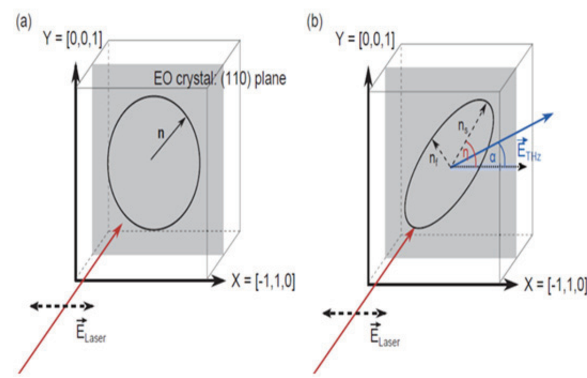

Figure 1: Refractive index ellipsoid of ZnTe Electro Optic crystal (a) Symmetric ellipsoid, without electric field and (b) The directions and the magnitudes of the main axes are changed, when an electric field is applied.

THEORY

Electro-Optic Effect in ZnTe [6, 7]

The EO crystal ZnTe exhibits a birefringence, which means a different refractive index property along the propagating direction of a laser beam. Each refractive index is linear dependent on the electric field's strength. This effect is called Pockels effect.

The direction of the axes and the dependency of each refractive index can be calculated by considering the constant energy surface of the electric displacement vector space and the impermeable tensor which is linear in the electric field. The main refractive indices can be known from the refractive index ellipsoid equation by a principal-axis transformation. For a ZnTe crystal cut in the 110 plane, polarized laser light enters the crystal with amplitude equal to the two main axis, the different refractive index in each one cause to different phase between them [3].

#klenavi1@gmail.co.il

ISBN 978-3-95450-133-5

CONCEPTUAL STUDY OF A SELF-SEEDING SCHEME AT FLASH2

T. Plath, L. L. Lazzarino, Universität Hamburg, Hamburg, Germany
K. E. Hacker, T.U. Dortmund, Dortmund, Germany

Abstract

We present a conceptual study of a self-seeding installation at the new FEL beamline, FLASH2, at the free-electron laser at DESY, Hamburg. For self-seeding, light from a first set of undulators is filtered by a monochromator and thus acts as a seed for the gain process in the main undulator. This scheme has been tested at LCLS at SLAC with a diamond monochromator for hard X-rays and with a grating monochromator for soft X-rays covering energies between 700 and 1000 eV. For such a design to offer benefits at FLASH2, it must be modified to work with X-rays with wavelength of about 5 nm (248 eV) where the damage threshold of the monochromator in the setup and the divergence at longer wavelengths become an issue. An analysis of the potential performance and limitations of this setup is performed using GENESIS 1.3 and a method developed for the soft X-ray self-seeding experiment at the European XFEL.

With a total of 9 undulators in the first stage and 8 undulators after the monochromator, a pulse energy contrast ratio of 3.3 was simulated with an initial peak current of 2.5 kA.

INTRODUCTION

Starting the lasing process in Free-Electron Lasers (FELs) from noise limits the longitudinal coherence and shot-to-shot wavelength stability of the FEL radiation. To overcome the limitations of self amplified spontaneous emission (SASE) operation, the FEL process can be initiated by an external light field from either a tabletop laser or from an upstream FEL. When the seed light comes from an upstream FEL, the process is called self-seeding.

Self-seeding, originally proposed by [1], describes a seeding scheme in which the light from a first set of radiators is sent through a monochromator and used to seed a second set of radiators. It has been experimentally demonstrated at LCLS for hard X-rays [2] and soft X-rays with energies from 500-1000 eV [3, 4].

This is a study of a soft X-ray self-seeding design for FLASH2 [5]. An FEL energy of 248 eV was chosen because this is close to the high energy limit of operation. Our design is based on the one used at LCLS [4]. The simulation methods are adapted from the ones used for the European XFEL [6].

Our studies show that tolerances on the electron bunch are very tight due to the space constrains of FLASH2. To generate sufficient pulse energies in both, the first and the second undulator stage, the electron peak current has to be about 2.5 kA with an emittance of 1.5 mm mrad and a slice energy spread of 200 keV at an electron bunch energy of 1.1 GeV. These conditions are estimated through simulation alone and are not based on past performance at FLASH2. Achieving a slice energy spread of 200 keV with 2.5 kA peak current would be challenging. A larger energy spread would decrease the performance and self-seeding operation under the given space constraints would no longer be possible.

While losses in the monochromator are comparable to the LCLS and European XFEL designs, the divergence of the beam is larger due to the longer wavelength operation regime, leading to lower intensity and a best predicted pulse energy contrast between the seed and SASE background of 3.3.

Hardware Setup at FLASH2

FLASH2 is the second FEL beamline at FLASH, the Free-Eectron Laser at DESY in Hamburg. In this paper we describe a rearrangement of the 12 existing undulator modules as well as the addition of 7 further modules and a 3 m long chicane for self-seeding and study the performance given the space constrains.

Altogether there are 21 open spaces for the self-seeding undulators and chicane, 18 of which are filled in this design.

MONOCHROMATOR AND CHICANE

Monochromator Design

The monochromator shown in Fig. 1 consists of a variable line spacing (VLS) toroidal grating followed by a plane mirror (M1), a cylindrical mirror (M2) and another plane mirror (M3). Between the first and the second mirror, a slit is located: it allows for the selection of the transmitted bandwidth, stray light reduction and much easier alignment of the optics. The VLS grating focuses the dispersed wavelengths into lines at the slit position, while the grating sagittal curvature and M2 tangential curvature focus them in the middle of the first undulator module of the seeded undulator stage.

The monochromator parameters can be found in table 1 for a minimum of 200 eV (6.2 nm) and a maximum of 350 eV (3.5 nm) photons. The working point for the FEL simulations in this paper lies at 248 eV (5 nm).

Chicane Design

The chicane delay and the monochromator delay need to be approximately equal so that the longitudinal overlap with the radiation is preserved. The chicane additionally destroys the micro-bunching from the first undulator stage leaving a smeared out longitudinal charge density to be seeded in the main undulator.

The chicane as shown in Fig. 1 consists of 4 steering dipoles with 300 mm yoke length. The magnetic length of each magnet is given by 330 mm with a maximum possible magnetic field of 0.25 T. The FODO structure of FLASH2 limits the overall chicane length to about 3.2 m. The chicane parameters can be found in table 2 for the minimum and

ISBN 978-3-95450-133-5

DOUBLE-GRATING MONOCHROMATOR FOR ULTRAFAST FREE-ELECTRON-LASER BEAMLINES

F. Frassetto, L. Poletto#, CNR-IFN, Padova, Italy
E. Ploenjes, M. Kuhlmann, DESY, Hamburg, Germany

Abstract

We present the design of an ultrafast monochromator explicitly designed for extreme-ultraviolet FEL sources, in particular the upcoming FLASH II at DESY. The design originates from the variable-line-spaced (VLS) grating monochromator by adding a second grating to compensate for the pulse-front tilt given by the first grating after the diffraction. The covered spectral range is 6-60 nm, the spectral resolution is in the range 1000–2000, while the residual temporal broadening is lower than 15 fs. The proposed design minimizes the number of optical elements, since just one grating is added with respect to a standard VLS monochromator and requires simple mechanical movements, since only rotations are needed to perform the spectral scan.

INTRODUCTION

One of the most demanded features for free-electron-laser beamlines is the possibility to monochromatize the FEL beam even beyond the intrinsic FEL resolution. Grating monochromators are used both at FLASH [1, 2] and LCLS [3, 4]. Unfortunately, especially for operation in the extreme-ultraviolet region of FLASH, the monochromator temporal response strongly affects the pulse duration, because of the pulse-front tilt introduced by the grating after the diffraction [5]. The full exploitation of the ultrashort temporal characteristics of a FEL source requires the use of a grating monochromator that compensates for the pulse-front tilt, that we define Compensated Monochromator (CM). The design consists in using two gratings in compensated configuration, i.e., the second grating compensates for the pulse-front tilt introduced by the first one [6–10]. CMs have been realized and used in high-order laser harmonics ultrafast beamlines, giving at the output pulses as short as 8 to 10 fs in the 20-45 nm region [11-14]. A CM for FEL has to be designed taking into account the peculiar parameters of the source, particularly the peak intensity, and the different requirements, particularly the definitely larger size of the optics.

Here we present the design of a CM explicitly tailored for extreme-ultraviolet FEL sources, in particular the upcoming FLASH II. The driving parameters for the design are: a) spectral range 6–60 nm; b) spectral resolution in the 1000–2000 range; c) time response shorter than 50 fs; d) minimum lateral displacement to let space to adjacent beamlines; e) minimum vertical displacement to reduce the change of the beam height; f) mirror length shorter than 500 mm; g) grating length shorter than 300 mm.

The monochromator design originates from the variable-line-spaced (VLS) grating monochromator that is already used at LCLS (see Ref. 2) by adding a second grating to compensate for the pulse-front tilt.

BEAMLINE DESIGN

The design originates from the variable-line-spaced (VLS) grating monochromator, that has been adopted for synchrotron radiation beamlines [15], high-order laser harmonics [16] and FELs (see Ref.s 3 and 4). The light coming from the source is focused by a concave mirror, that produces a converging beam. This is intercepted by a VLS plane grating, that diffracts the radiation onto the exit slit. The variable groove spacing of the grating provides the additional free parameters to keep the focal distance almost constant as a function of the wavelength and to compensate for high-order aberrations. The VLS monochromator is also rather simple mechanically in that only two optical elements are required and the photon energy is scanned by a single rotation of the grating around an axis passing through its center.

The CM is realized by adding a second section with an identical VLS plane grating illuminated by the diverging monochromatic light coming out from the slit and mounted in a compensated geometry with respect to the first grating, i.e., internal and external diffraction orders are splitted between the two gratings.

The design has been specialized to the requirements of FLASH II:

a) The monochromator works without an entrance slit, being the FEL itself the source point (as the case of the monochromator at LCLS).
b) An additional plane mirror is inserted between the two gratings to fold the beam and give very low displacement of the output beam with respect to the input.
c) Horizontal and vertical foci are kept separated to reduce the radiation density on the slit blades, due to high peak intensity. In particular, the first mirror, that is demanded to illuminate the grating in converging light, is a plane-elliptical one, therefore the focus on the intermediate slit is astigmatic, i.e., the beam is focused only in the spectral direction.

The optical layout is shown in Fig. 1. The FEL beam is focused by the plane-elliptical mirror M1 toward the plane VLS grating G1. The latter diffracts the radiation toward the intermediate slit, where the beam is

#luca.poletto@ifn.cnr.it, National Research Council of Italy, Institute of Photonics and Nanotechnologies, via Trasea 7, I-35131 Padova (Italy)

ISBN 978-3-95450-133-5

COMPACT SPECTROMETER FOR SINGLE SHOT X-RAY EMISSION AND PHOTON DIAGNOSTICS

L. Poletto#, F. Frassetto, P. Miotti, CNR-IFN, Padova, Italy
P. Finetti, E. Giangrisostomi, R. Mincigrucci, E. Principi, Sincrotrone Elettra, Trieste, Italy
C. Grazioli, Department of Chemical and Pharmaceutical Sciences, Trieste, Italy
A. Kivimäki, CNR-IOM, Trieste, Italy
A. Di Cicco, F. Iesari,
University of Camerino, School of Science and Technology, Camerino (MC), Italy
S. Stagira, Department of Physics, Politecnico di Milano, Milano, Italy
M. Coreno, CNR-ISM, Trieste, Italy

Abstract

The design and characterization of a compact spectrometer realized for photon in-photon out experiments (in particular X-Ray Emission Spectroscopy), conceived to be used at the FERMI free-electron-laser (FEL) at ELETTRA (Italy) is here presented. The instrument can be easily installed on different end stations at variable distances from the target area both at synchrotron and FEL beamlines. Different input sections can be accommodated in order to fit the experimental requests. The design is compact in order to realize a portable instrument within an overall size of less than one square meter. The spectrometer covers the 25-800 eV spectral range, with spectral resolution better than 0.2%. The characterization on Gas Phase @ ELETTRA as instrument for XES and some experimental data of the FEL emission acquired at EIS-TIMEX @ FERMI, where the instrument has been used for photon beam diagnostics, are introduced.

INTRODUCTION

X-ray emission spectroscopy (XES) is a well-established method in surface and solid-state investigations at third generation synchrotron radiation sources [1-2]. The instrument presented here is designed for photon in-photon out experiments, in particular XES, at synchrotron and FEL beamlines. The equipment is intended to be used at the LDM (Low-Density-Matter) [3] and EIS-TIMEX (Elastic and Inelastic Scattering - TIme-resolved studies of Matter under EXtreme and metastable conditions) [4] beamlines of FERMI. Additionally, it can be used as a diagnostic tool for the real-time shot-to-shot acquisition of the FERMI spectral content (both fundamental and high-harmonics) and of the shot-to-shot fluctuations beam characteristics, especially at energies above 250 eV, where it could be complementary to the existing spectrometer used as a diagnostic of FERMI [5]. Two selectable gratings are used to cover the 25-800 eV energy range with a spectral resolution higher than 0.2% and an acceptance angle as high as 1.7×10^{-4} rad. Different input sections, with/without an entrance slit and with/without an additional relay mirror can be attached to the spectrometer to adapt it to the size of the experimental chamber.

INSTRUMENT DESIGN

The optical design of the instrument is well established both for FELs [6] and high-order laser harmonics [7,8] and has been presented elsewhere [9]. It consists of an entrance slit, a grazing-incidence spherical diffraction grating with variable groove spacing and a detector. The 25-800 eV range is covered by gratings (Hitachi cod. 001-0437, 1200 gr/mm and cod. 001-0450, 2400 gr/mm). An EUV-enhanced back-illuminated CCD camera (Princeton Instruments PIXIS-XO 400B, 1340 × 400 pixel, 20-um pixel size), is mounted on a motorized linear translation stage and is connected to the grating stage by a bellows. Since the length of his focal curve is longer than the detector size, the latter is moved by means of a motorized stage to cover the whole spectral region. Three configurations have been realized by connecting three different input stages to the grating block. Configuration A is shown in Fig. 1. It has a variable-width entrance slit. Configuration B, shown in Fig. 2, has an additional cylindrical mirror acting as a relay section between the slit and the grating. In this way, the distance between the input and the grating is increased. Configurations A and B were tailored to the needs of the experimental chambers of the Gas Phase beamline of Elettra and the LDM beamline of FERMI and were designed for measurements on gas samples. Configuration C, shown in Fig. 3, is mainly planned to be used in chambers for measurements on solid targets. It is operated without an entrance slit, since the FEL focal spot on the sample acts as point-like source of the instrument. Again, a cylindrical mirror was added to the configuration, acting as a relay section between the source and the grating to adapt the envelope of the instrument to the size of the TIMEX experimental chamber. To maintain the pressure gradient between the inner and outer parts of the shield that contains the instrument, a pumping system is connected via a dedicated pumping flange to the spectrometer.

The spectral resolving element of the instrument, defined as the energy dispersion on the 20-µm detector pixel, is shown in Fig. 4. The global response of the

#luca.poletto@ifn.cnr.it, National Research Council of Italy, Institute of Photonics and Nanotechnologies

ISBN 978-3-95450-133-5

COMMISSIONING OF A DUAL-SWEEP STREAK CAMERA WITH APPLICATIONS TO THE ASTA PHOTOINJECTOR DRIVE LASER*

A. H. Lumpkin#, D. Edstrom, J. Ruan, and J. Santucci
Fermi National Accelerator Laboratory, Batavia, IL 60510, USA

Abstract

Following re-commissioning of the dual-sweep streak camera with a Gig-E readout CCD camera, a comprehensive set of measurements has been performed on the ASTA drive laser beam components with respect to bunch length, phase stability, and multiplicity of peaks. The multi-pass amplifier was identified as the primary source of the longer UV component bunch length at 4 ps and peak multiplicity. This amplifier was replaced with three single-pass amplification stages and tests indicate clean micropulses and bunch lengths of about 3.6 ps sigma.

INTRODUCTION

The high-power electron beams for the Advanced Superconducting Test Accelerator (ASTA) facility [1] will be generated in a photoinjector based on a UV drive laser and the L-band rf photocathode (PC) gun cavity. Initially, the laser was composed of a Calmar Yb fiber oscillator and amplifier, a multi-pass YLF-based amplifier (MPA), three single-pass YLF-based amplification stages, and two frequency-doubling stages that result in a UV component at 263 nm with a 3 MHz micropulse repetition rate [2]. The initial objectives of these studies were: 1) to evaluate the amplified UV component's bunch length and phase stability and 2) to commission the laser room Hamamatsu C5680 streak camera system. A Prosilica GC1380 digital CCD with Gig-E readout was used for streak camera readout as it was compatible with our image processing tools. In the following sections, the process of characterizing the UV beam using the streak camera is described. This includes identification of a UV micropulse length longer than expected, multiplicity within the bunch structure, steps taken to mitigate these issues, and UV beam characterizations following these steps. We have systematically investigated the issues of whether the multiplicity was with each micropulse of the 3 MHz train (using the gated MCP), if any multiplicity is on different cycles of the 81.25 MHz rf (using dual-sweep streak images), and the origin in the laser system of the longer bunch length and the multiplicity. We describe our extensive investigations that indicated both issues originated in the multi-pass amplifier.

EXPERIMENTAL ASPECTS

A request to have the streak camera readout camera be compatible with the Gig-E vision protocol has been addressed by selection of the Prosilica 1.3 Mpixel camera with 2/3" format. We have then used both the online Java-based ImageTool and the offline MATLAB-based ImageTool processing programs [3,4] in the commissioning of the system. Initial measurements of the UV component indicated the bunch length Gaussian fit sigma was closer to 4 ps, and there was evidence of more-than-expected peak multiplicity near the 3 MHz main peaks with spacing of 65-70 ps. Initially timing effects between the controls group 3 MHz source and that derived from the master oscillator were detected, but these were ultimately ruled out as the source of the peak multiplicity through a process of selection of individual pulses by gating the streak camera MCP and employing the dual-sweep synchroscan functions of the streak camera. Unless noted otherwise, the streak camera's synchroscan unit was phase locked to the master oscillator, which operationally provides the rf sync for the linac and rf gun. We provide a description of the commissioning of the streak camera system and image acquisition tools and the application to the drive laser.

The Drive Laser

The drive laser (Fig. 1) was based on an Yb fiber laser oscillator running at 1.3 GHz that was then divided down to 81.25 MHz and amplified. The four-stage origination and amplification was a set of commercial components from Calmar collectively referred to as the seed laser in the context of ASTA. The 81.25 MHz packets of infrared (IR) laser, at a wavelength of 1054 nm was initially directed into a YLF-based multi-pass amplifier (MPA), at 3MHz, selected by a Pockels cell referred to as the pulse picker. A number of pulses was selected using two pulse cleaner Pockels cells, while three YLF-based single-pass amplifiers (SPA) and a Northrup-Grumman SPA (NGA) boost the intensity as high as 50 µJ per pulse before the two doubling crystal stages generate the green and then the UV components at 3 MHz [2]. The UV component was transported from the laser lab through the UV transport line to the photocathode of the gun for generation of the photoelectron beams for use in the SC rf accelerator [2].

The multi-pass amplifier is a cavity that allows the amplification of the IR macropulse dependent on the timing of a fourth Pockel's cell (Conoptics 350-105) referred to as the Q-Switch. In combination with a Brewster plate, the IR beam is injected into the MPA cavity and is amplified using an YLF solid state amplifier, similar to those used in the single-pass amplification stages, until the Q Switch triggers, directing the amplified beam back out by means of the same Brewster plate, collinear with its injection trajectory. The round trip time for laser within the cavity is 12 ns, and several roundtrips-

*Work supported under Contract No. DE-AC02-07CH11359 with the United States Department of Energy.
#lumpkin@fnal.gov

ISBN 978-3-95450-133-5

PULSE BY PULSE ELECTRON BEAM DISTRIBUTION FOR MULTI-BEAMLINE OPERATION AT SACLA

Toru Hara*, Hideki Takebe, Takahiro Inagaki, Chikara Kondo, Yuji Otake, Hitoshi Tanaka,
RIKEN SPring-8 Center, Sayo-cho, Hyogo 679-5198, Japan
Kenji Fukami,
JASRI, Sayo-cho, Hyogo 679-5149, Japan

Abstract

In SACLA, the second undulator beamline (BL2) is installed during the 2014 summer shutdown. The beamlines are initially switched by a DC switching magnet for the commissioning. Then the DC switching magnet will be replaced by a kicker and a DC twin-septum magnet and the pulse by pulse operation will start in January 2015. The kicker magnet is driven by a 60 Hz trapezoidal current waveform. In the pulse by pulse multi-beamline operation of XFEL, the electron beam energy should be optimized for the laser wavelengths of each beamline from bunch to bunch. To control the beam energy of the electron bunches, the multi-energy operation of the linac has been proposed and demonstrated at SACLA. The pulse by pulse operation will be also applied for the beam injection to the upgraded low-emittance ring of SPring-8 (SPring-8-II) in future. Since the SPring-8-II storage ring has a small dynamic aperture, low emittance is required for the injection beam. In addition, the use of SACLA as a low-emittance injector enables to save the running cost of the injector system during top-up operation.

INTRODUCTION

In order to meet the increasing demand for XFEL user operation, the second undulator beamline (BL2) is installed during the 2014 summer shutdown at SACLA. Different from the storage ring based synchrotron radiation facilities, the linac of XFEL can not simultaneously operate plural beamlines. However, quai-simultaneous pulse by pulse operation by distributing the electron beam to the beamlines on a bunch-to-bunch basis improves efficiency and usability of the facility.

The undulator hall of SACLA is designed to accommodate five XFEL beamlines, and a DC switching magnet located at the end of the linac currently switches the beamlines (see Fig. 1) [1]. For the pulse by pulse operation, this DC switching magnet will be replaced by a kicker magnet and a DC twin-septum magnet in January 2015. The electron beam is deflected into three directions at 60 Hz by the kicker, which is the maximum beam repetition at SACLA, and then the DC twin-septum magnet augments the deflection angles. Since the stability of the electron beam orbit is crucially important for XFEL, high stability is required, particularly, for the kicker magnet power supply.

In the XFEL operation, the electron beam energy is normally optimized for the laser wavelength requested from the user. But in case of the multi-beamline operation, the wavelengths can be different between the beamlines. Although the wavelength can be adjusted by changing the undulator gap, the tuning range is limited and small K-values result in drop of laser intensity. In order to avoid these limitations on the user experiments, it is necessary to control the beam energy from bunch to bunch in the multi-beamline operation.

The method to control the electron bunch energy in the linac has been proposed and demonstrated at SACLA by changing the repetition of a certain number of RF units [2]. In the pulse by pulse multi-beamline operation of SACLA, the multi-energy operation of the linac is planned to be used in combination with the electron bunch distribution to provide the electron beam having the optimized energy to the laser wavelength of each beamline.

ELECTRON BUNCH DISTRIBUTION

Although the maximum beam repetition of SACLA is 60 Hz, lower repetitions are sometimes used for user experiments due to the time necessary to exchanging samples. Also to save the time for preparation and removal of experimental instruments, the multi-beamline operation contributes to improve the efficiency and usability of the facility.

The schematic of SACLA is shown in Fig. 1. After the acceleration and longitudinal compression of the electron bunches in the linac, the DC switching magnet currently switches the beamlines by deflecting the beam orbit by ±3 degrees (±52 mrad). For the electron bunch distribution, this DC switching magnet will be replaced by the kicker magnet and the DC twin-septum magnet as shown in Fig. 2. In order to minimize the orbit fluctuation of the deflected beam by the kicker magnet, the deflection angle of the kicker is kept small as ±9 mrad and the rest of the angle is given by the DC twin-septum magnet (±43 mrad).

The yoke of the kicker is 0.4 m long made of laminated silicon steel plates with 0.35 mm thickness and 20 mm gap, and its maximum field is 0.67 T (see Fig. 3). The power supply of the kicker is a PWM (Pulse Width Modulation) type using 8 FET units connected in parallel. The power supply generates a 60 Hz trapezoidal current waveform and its amplitude and polarity can be arbitrarily changed according to the beam energy and an electron bunch distribution pattern.

Figure 4 is an example of the distribution pattern of the electron bunches. The arrival timing of the electron

*toru@spring8.or.jp

ISBN 978-3-95450-133-5

DEVELOPMENT OF A MAGNET SYSTEM TO CANCEL THE ATTRACTIVE FORCE TOWARD STRUCTUAL REFORM OF UNDULATORS

R. Kinjo and T. Tanaka, RIKEN SPring-8 Center, Sayo, Hyogo, Japan
T. Seike and A. Kagamihata, JASRI, Sayo, Hyogo, Japan
S. Yamamoto, KEK Photon Factory, Tsukuba, Ibaraki, Japan

Abstract

Toward realization of a new undulator concept based on a much more compact and lightweight structure than conventional ones, cancellation of a magnetic attractive force is being studied, which significantly relaxes the requirements for the undulator mechanical design and reduces the cost and lead time of construction and installation. We have proposed to add periodically-magnetized monolithic magnets beside the main magnets generating the undulator field and attractive force, which are expected to generate a repulsive force having the same gap-dependency as the attractive force in a cost-effective way. The present status of the development of the force cancellation system is presented, with a focus on the result of preliminary experiments using the periodically-magnetized magnets. Also introduced is a development plan for the compact and lightweight undulator based on the cancellation system.

INTRODUCTION

It is well known that a large attractive force is generated between the top and bottom magnetic arrays of undulators, if the gap in between is relatively narrow. For example, a typical undulator in SPring-8 having the Halbach configuration with the period of 32 mm and the total length of 4.5 m has the attractive force of about 3 tons at the gap of 8 mm. The undulator in SACLA having the hybrid configuration with the period of 18 mm and the total length of 5 m has the attractive force of around 9 tons at the gap of 3 mm. To control the magnet gap precisely against the large attractive force, the undulators usually require rigid mechanical components and frames. Moreover, a large number of components are necessary to distribute the mechanical load along the undulator axis and avoid deformation of the magnetic arrays. Such a conventional undulator design gives rise to structural issues that most of the weight, dimension and cost of the undulator are attributable to the auxiliary apparatus but not to the core part, i.e. the magnetic arrays.

The above discussion in turn gives us a new concept of undulator design; if the attractive force is cancelled out, the heavy and large base frame is no longer required, and then the undulator can be much more lightweight and compact. As a result, the cost and lead time of construction, transportation and installation are significantly reduced.

Up to now, two different methods have been developed to cancel the attractive force. One is the mechanical system composed of a number of springs having different lengths and coefficients attached to the both sides of the main magnets, which was applied to an in-vacuum wiggler developed at Synchrotron SOLEIL [1]. The other is the magnetic system composed of two rows of magnet array generating a repulsive force attached to the both sides of the main magnets, which is applied to the in-vacuum revolver undulator (IVRU) developed at SPring-8 [2]. Although both systems worked well for their own purposes, they may not be applicable to the new undulator concept.

In the former method, the precise magnetic measurement indispensable for undulator field correction is not possible with the conventional instrument, and the gap-dependency of the repulsive force generated by the springs is somewhat different from that of the attractive force. In the latter method, the number of magnets and magnet holders is three times as large as that of the main magnetic array, which increases the cost and time and effort for manufacturing.

As an alternative to the above two methods, R&Ds are under progress in SPring-8, toward realization of a cost-effective force cancellation system, which are reported in this paper.

BASIC CONCEPT

The cancellation system under development is based on the magnetic system applied to IVRU, which is schematically illustrated in Fig. 1. The point is that to generate repulsive force the magnets arrays which has the same structure with the main magnets are used in IVRU, while multipole monolithic magnets (MMMs) are discussed in this paper, which may be more cost-effective and easier fabricable than the IVRU type.

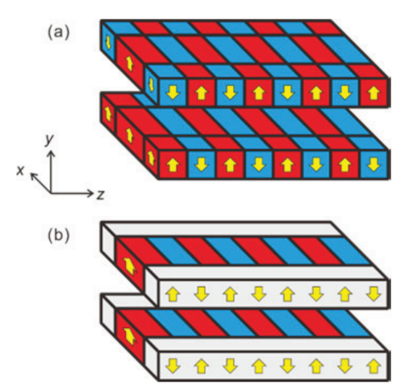

Figure 1: Conceptual drawing of force cancellation system (a) by normal magnets applied to IVRU and (b) by MMMs discussed in this paper.

ISBN 978-3-95450-133-5

FIELD INTEGRAL MEASUREMENT SYSTEM AND OPTICAL ALIGNMENT SYSTEM FOR HUST THz-FEL

B. Qin, K.F. Liu, X.L. Liu, Y.B. Wang, X. Lei, X. Liu, Q.S. Chen, Z. Ouyang, Q. Fu, L. Yang, T.N. Hu, J. Yang, P. Tan, Y.Q. Xiong, M.W. Fan, HUST, Wuhan 430074, China
Y.J. Pei, USTC/NSRL, Hefei 230026 , China

Abstract

A Free Electron Laser oscillator with radiation wavelength 50–100 µm is under construction in Huazhong University of Science and Technology (HUST). The linear polarization undulator with K=1.0-1.25 has been designed and manufactured by Kyma s.r.l., by using a pure permanent magnet scheme. Acceptance test bas been performed in Kyma factory with well controlled phase error and field integrals for all gaps. This paper introduces the development of an online field integrals measurement system for the undulator, using the stretched wire method. The design and considerations of the optical alignment system is described as well.

INTRODUCTION

High average power and continuous tunable terahertz (THz) sources based on low gain FEL oscillator scenario have widely applications covering materials, security inspection, molecule imaging etc.

A compact THz FEL oscillator for prototype study was proposed by Huazhong University of Science and Technology (HUST) and National Synchrotron radiation Laboratory (NSRL/USTC), which is designed to generate 50–100 µm coherent radiation with Watt level average power at initial stage [1, 2]. The general view is shown in Fig. 1, with the main parameters listed in Table 1. For the injector, a thermionic electron gun with an independently tunable cell (ITC) was chosen as the electron beam source for simplicity, and a S-band linac with traveling wave structure will accelerate the beam to range of 6 MeV to 14 MeV [3]. The macro pulse duration 5 µs is long enough for the power build up process which is around 1 µs. A 2.93m symmetrical near-concentric optical cavity is formed by two gold-coated copper toroid mirrors and a rectangular partial waveguide installed with the range covering the undulator, with estimated 15% total round trip loss [4]. The schematic view of this facility is shown in Fig. 1, with main specifications in Table 1.

STATUS OF THE PLANAR UNDULATOR

A pure permanent planar undulator with a moderate K is adopted, and design considerations were described in Ref. [2]. We signed contract with Kyma s.r.l. for design and manufacturing of the undulator, and the assembly was accomplished in November 2013, as shown in Fig. 2.

Main characteristics of this undulator are:

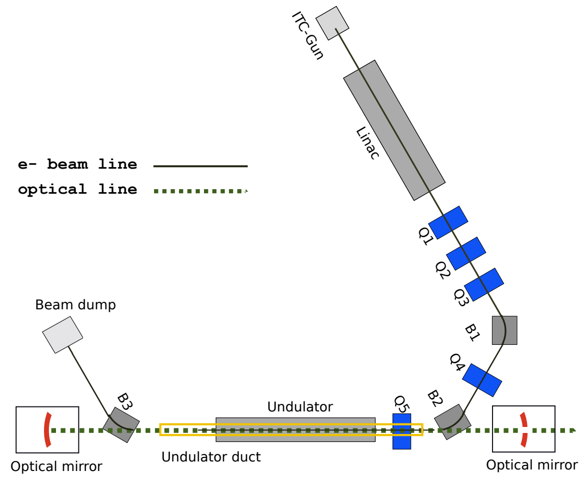

Figure 1: Schematic view of HUST THz-FEL oscillator.

Table 1: Parameters of HUST THz FEL Oscillator

Beam energy	8–12 MeV
Radiation wavelength, λ_r	50–100 µm
Bunch charge	≥ 200 pC
Bunch length (FWHM), σ_s	5-10 ps
Energy spread (FWHM)	0.3%
Macro pulse duration	4-6 µs
Repetition rate	10–200 Hz
Number of the full strength period, N_u	30
Undulator period, λ_u	32 mm
Undulator parameter, K	1.0–1.25
Optical cavity length	2.9 3m
Peak power	0.5–1 MW

- Total length 1.03 m, with $N_u = 30$, $L_u = 32mm$; Nu is optimized by balancing the single pass gain and the natural extraction efficiency ($\approx 1/4N_u$)
- Pure permanent magnet (PPM) structure was chosen, and some techniques such as pre-sorting in block modules and "virtual shimming" [5] are used for controlling the field homogeneity and phase error. To achieve designed K for short period, high coercivity grades ($H_{cj} > 20kOe$) of NdFeB material was chosen; and the deviation of polarization and spread of the remanent field B_r were controlled within 1% level (rms)
- $K = 1.0 - 1.35$, by varying the gap from 19mm to 16mm, and two pair of independent controlled correction coils are installed in the transverse side of the undulator end, to correct the first and second field integrals both in vertical and horizontal directions

ISBN 978-3-95450-133-5

PERFORMANCE ANALYSIS OF VARIABLE-PERIOD HELICAL UNDULATOR WITH PERMANENT MAGNET FOR A KAERI THz FEL

Jungho Mun[1, 2], Young Uk Jeong[1,#], Nikolay Vinokurov[1], Kitae Lee[1], Seong Hee Park[1], Kyu-Ha Jang[1], Min Yong Jeon[2]
[1]WCI Center for Quantum-Beam-based Radiation Research, Korea Atomic Energy Research Institute,1045 Daedeok, Yuseong-gu, Daejeon, 305-353, Korea
[2]Department of Physics, Chungnam National University, 99 Daehak-ro, Yuseong-gu, Deajeon, 305-764, Korea

Abstract

We could realize a variable-period (V-P) permanent-magnet helical undulator, which shows strong (~ 1 T) and constant field for the whole range of undulator period-length from 23 to 26 mm. This new compact and strong undulator will be used for developing a table-top high-power terahertz (THz) free-electron laser (FEL).

INTRODUCTION

A common way of tuning the undulator radiation wavelength is by varying the magnetic field of the undulator, which changes the *K* value. For a permanent-magnet undulator, the magnetic field strength is adjustable by changing the gap between the parts of the undulator. Another solution for wavelength tuning is variation of the undulator period-length [1, 2]. Recently, a V-P undulator was proposed with a planar structure using a split-pole structure of a hybrid permanent-magnet undulator [3]. The V-P undulator gives almost constant field strength at different periods, which results in less variations of a gain and radiation power for a given wavelength tuning range as compared with those for variable-gap undulators. The V-P undulator has a far less stringent dimensional tolerance and less driving force as compared to those for the variable-gap undulator, as it is shown in Ref. 3.

DESIGN AND FABRICATION

The concept of the design is based on the structure of the hybrid permanent-magnet planar undulator.

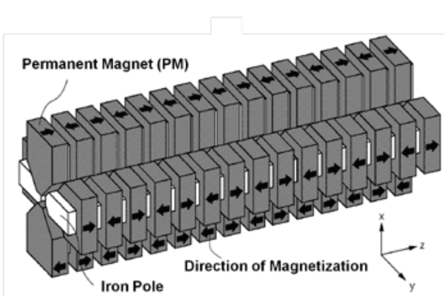

Figure 1: Magnetic design of the V-P helical permanent-magnet undulator [4].

yujung@kaeri.re.kr

Table 1: Main Parameters of the V-P Helical Permanent Magnet Undulator for a Compact THz FEL [4].

Gap	5 mm
Number of periods	30
Length of period	23-26 mm
Peak magnetic field	1 T

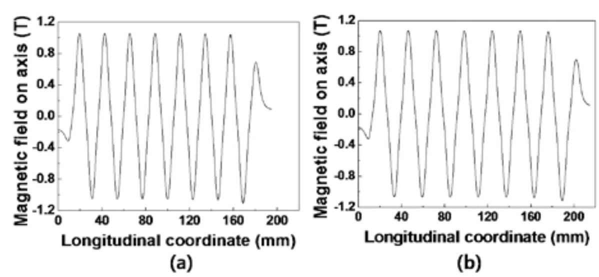

Figure 2: Calculated vertical component of the on-axis magnetic field of the V-P helical undulator. (a) λ_w = 23 mm and (b) λ_w = 26 mm. The calculated peak magnetic field is about 1 T [4].

This helical undulator is a combination of two planar undulators. A three-dimensional (3-D) simulation of the V-P helical undulator using the CST code [5] for different undulator period lengths was carried out. Table 1 shows the main parameters of our V-P helical undulator for a compact THz FEL. Figure 1 shows the structure of the V-P helical undulator, consisting of permanent magnets and iron poles. A short undulator with seven periods was then simulated for λ_w = 23 mm and 26 mm, where λ_w is the undulator period-length. In this simulation, the sizes of the magnets and poles were fixed. Only the period length of the undulator was varied. Figure 2 shows the simulated vertical component of magnetic field on the axis of the V-P helical undulator. According to the results of the simulation, the peak magnetic field on the undulator axis almost does not depend on the period length. Thus, the V-P helical undulator enables us to tune FEL wavelength without significant degrading the FEL gain.

ISBN 978-3-95450-133-5

PAL-XFEL MAGNET POWER SUPPLY SYSTEM

Seong Hun Jeong#, Ki-Hyeon Park, Hyung Suck Suh, Sang-Bong Lee, Bongi Oh, Young-Gyu Jung, Hong-Gi Lee, Dong Eon Kim, Heung-Sik Kang and In Soo Ko
PAL, Pohang, Republic of Korea

Abstract

This paper presents an overview of the magnet power supply (MPS) for the PAL-XFEL. The number of total MPS is up to 624 and they will be installed along the accelerator and the undulator sections. The power capacity of the MPS was ranging from about 1 A to 300 A. These MPSs were required to meet the high stability that was subjected from the beam dynamics specifications. This paper described the overall MPS requirements, MPS assembling, test process, control scheme, installation plan and so on.

INTRODUCTION

The PAL-XFEL is the 4th-generation light source, base on a single pass FEL, under constructing at Pohang Accelerator Laboratory in Korea. This project aims at the generation of X-ray FEL radiation in the range of 0.1 to 10 nm for users. The machine consists of 10 GeV linear accelerator and hard and soft X-ray undulator beamlines. The accelerator will operate at a 60 Hz and will be extended to 120 Hz [1]. Total 624 set of MPS are used for beam orbit correction and maintained for the beam trajectory. To reach the best performances expected from a 4th-generation source, very demanding specifications have been targeted notably on magnetic field stability and reproducibility of the various magnets, hence on the currents delivered by the power supplies. The power supplies have ratings which range from about 1 A to 300 A. The topologies of the MPSs are buck and H-bridge chopper type. This paper describes the MPS developing status and installing plan and so on.

MAGNET POWER SUPPLY SPECIFICATIONS

Table 1 describes the specifications of the three kinds - quadrupole, dipole and corrector - magnet power supplies for the PAL-XFEL.

Table 1: Total MPSs Number for PAL-XFEL

Magnet	MPS type	Qty	Stability(ppm)
Corrector	Digital	283	10 & 50
	Analog	108	50
Quadrupole	Unipolar	122	100
	Bipolar	86	
Dipole	Unipolar	20	20
	Bipolar	2	
Solenoid	Bipolar	3	20

*Work supported by Ministry of Science, ICT & Future Planning of Korea, #jsh@postech.ac.kr

Based on the maximum operating current and voltage, 213 quadrupole magnets are divided into 11 families, 48 dipole magnets are 7 families. The 391 corrector magnets are grouped 3 families base on the current rating and stability. The power supplies can be categorized as unipolar and bipolar power supplies.

HARDWARE STRUCTURE AND CONTROL SCHEME

The basic structure of a power supply with controller, ADC and interface to the control system is shown in figure 1. The topologies of the converters are either buck or H-bridge. It is based for the unipolar of dipole and quadrupole MPS on the following chain of elements: 12-phase transformer, rectifier, input filter, energy storage, switching device and output filter.

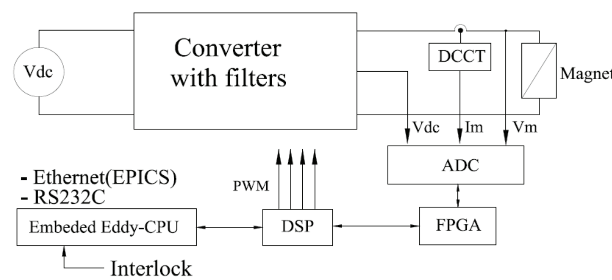

Figure 1: PS control structure overview.

The transformers adapted to the higher power capacity have two secondary windings, one delta-connected and the other wye-connected to configure the 12 phase rectifier in order to reduce the AC ripple on the DC link of the power supply. The bandwidth of the input filter should be less than 30 Hz to have a good output performance. A freewheeling diode and an L-C filter are put across the output stage. The cut-off frequency of output L-C filter is about 5 kHz. It gives a good dynamic control performance. A soft charge circuit on the rectifier limits the inrush current during power on.

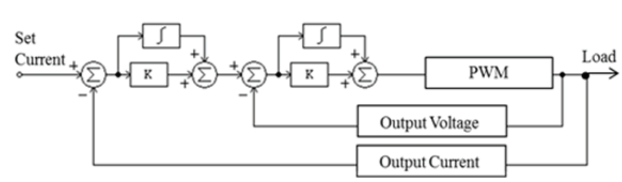

Figure 2: Control loop structure.

Figure 2 shows the control loop structure of MPS. The control loops for the switching mode power supply are consisted of a cascaded current and voltage feedbacks, the inner loop controls the output voltage, and outer loop

ISBN 978-3-95450-133-5

DESIGN, FABRICATION, AND PERFORMANCE TESTS OF DIPOLE AND QUADRUPOLE MAGNETS FOR PAL-XFEL*

Hyung Suck Suh#, Bongi Oh, Dong Eon Kim, Heung-Sik Kang, Hong-Gi Lee, In Soo Ko, Ki-Hyeon Park, Moo Hyun Cho, Sang-Bong Lee, Seong Hun Jeong, Young-Gyu Jung
PAL, Pohang, Republic of Korea

Abstract

PAL(Pohang Accelerator Laboratory)-XFEL is now being constructed in Pohang, Korea. This facility will consist of a 10 GeV linac and five undulator beamlines. As the first phase we will construct one hard X-ray and one soft X-ray beamlines which require 6 different families of dipole magnets, and 11 families of quadrupole magnets. We have designed these magnets with considering the efficient production and the proper power supplies. In this presentation, we describe the design features of the magnets, the manufacturing, and the thermal analysis with the test results.

INTRODUCTION

The PAL-XFEL is a 0.1-nm hard X-ray FEL project starting from 2011. Three hard X-ray and two soft X-ray branches are planned. As the first phase of this project, one hard X-ray (HX1) and one soft X-ray (SX1) which consist of 51 dipole and 208 quadrupole magnets will be constructed [1].

We have designed all magnets on our own by using OPERA and ANSYS codes [2, 3]. We tried to reduce the number of coil types and the number of the power supply types for the convenient production. Every magnet is designed to maintain the maximum temperature rise of coils below 20 K for about 120% of the rated currents. In the process of the design, it was helpful to parameterize the main figures of the magnets in a spread sheet for easy estimation by changing some parameter often. Now we are manufacturing them and testing the prototype magnets.

DIPOLE MAGNETS

The dipole magnets were classified into 6 kinds according to the pole gap, the effective magnetic length, and the maximum magnetic field. The results of the classification are listed in Table 1.

Dipole magnets have the same pole gaps of 30 mm except D6 of 15 mm for the self-seeding. D1, D2, and D4 have H-type core shape, and D3, D6, and D7 have C-type. All dipole magnets of D1~D6 for the bunch compressor, the chicane, and the self-seeding have the trim coils with 1% of the main field.

The pole profiles of magnets are optimized by the small bumps at the tip of the pole for the field uniformity. The requirements for the field uniformity are different from each magnet, e.g. in the case of H-type dipole magnet D1, $\Delta B/B_0 < 1.0\text{E-}4$ for ±17mm, $\Delta B/B_0 < 5.0\text{E-}4$ for ±41mm in 3D calculation.

Table 1: The Families of Dipole Magnets (D5 was Replaced with D2)

Family	Magnetic length [m]	Max. field [T]	Qty	Position
D1	0.20	0.80	6	BC1
D2	0.70	1.00	18	BC2,BC3, BAS1
D3	1.50	1.30	11	BAS2,3,4
D4	0.17	0.30	4	Laser Heater
D6	0.30	0.485	4	Self seeding
D7	0.75	1.164	2	Tune-up dump

So the pole contour of D1 is made like Fig. 1 where the a-b line has a slight slope. The 2D/3D field uniformities of the calculation results are shown in Fig. 2.

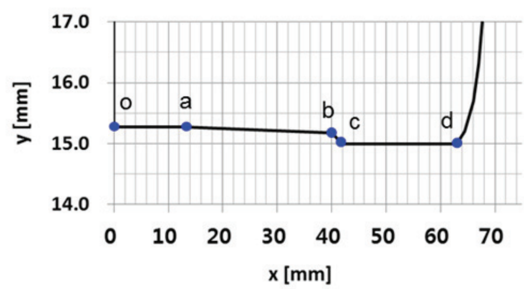

Figure 1: Pole contour of H-type dipole magnet D1.

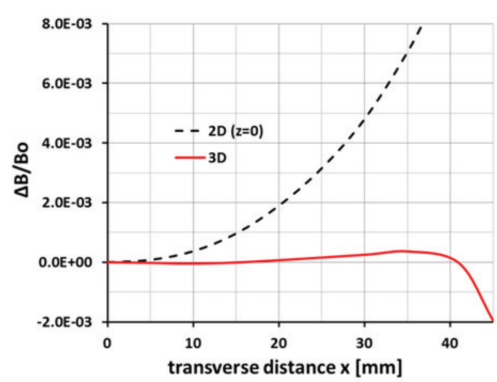

Figure 2: Calculated 2D/3D field uniformities of dipole magnet D1.

The laminated cores are used for the magnets D2 and D3 which quantities are more than 10 magnets, and the solid cores are used for the rest of the dipole magnets.

*Work supported by Ministry of Science, ICT and Future Planning of Korea, #suhhs@postech.ac.kr

ESTIMATING EFFECT OF UNDULATOR FIELD ERRORS USING THE RADIATION HODOGRAPH METHODH

N.A. Sokolov[#], Budker INP, Novosibirsk, Russia
N. Vinokurov, Russia, and KAERI, Daejeon, Rep. of Korea

Abstract

Spatially-periodic magnetic structures are widely used for generation of high-brilliance radiation in storage rings, sources of synchrotron radiation and free electron lasers. In 1947, V.L. Ginzburg suggested the first undulator scheme.

An alternating magnetic field created by a planar undulator makes electrons oscillate in the transverse direction, with interference of radiation emitted from separate parts of the trajectory. The spectrum of the forward emitted radiation is enchanced due to constructive interference.

The ondulator is made of the magnetized bars that are not perfect and their magnetization differs. Therefore, the electron trajectory is not purely sinusoidal and, as a result, the spectral intensity fades. The task was to find out if the precision of magnet manufacturing is sufficient.

This paper presents modelling of electron motion in the measured magnetic field of the new (third) free electron laser at the Siberian Synchrotron Radiation Centre. We have managed to estimate the effect of the field errors through comparison of the resulting emitted field amplitude with the amplitude from ideal magnet bars using the hodograph method.

CALCULATING MAGNETIC FIELD OF UNDULATOR

The undulator under study consists of two rows of magnetized bricks with 1.5×1.5 cm^2 square cross-section, a width w of 9 cm and alternating magnetization directions as shown in Fig. 1. A brick is characterized by homogeneous magnetization M and the brick shorter side b. The vertical component of the field of a break, centered at the origin is given by two expressions for contributions of vertical My and horizontal Mz components of of magnetizations. Now the undulator field can be calculated as the sum of the fields of all its bricks (Eq. 1):

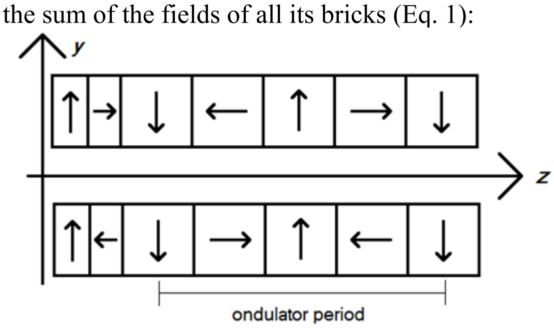

Figure 1: Scheme of permanent magnet undulator.

$$B_y(z) = 2\sum_n \Big[B_v(0,g,z-nb)\cos\frac{\pi n}{2} + B_h(0,g,z-nb)\sin\frac{\pi n}{2}\Big], \tag{1}$$

where g is the distance between the undulator axis and the brick centres, and $M_y = M_z = M$. It should be taken into account that the undulator begins and ends with two pairs of halved bricks for the average angle of particle trajectory and the transverse coordinate to be the same at the undulator ends. The fields of these termination bricks were calculated with formula, similar to Eqs. 2 and 3. The contribution of termination bricks is skipped in Eq. 1, but was taken into account in field and trajectory calculations. Bricks with vertical (along the OY axis) magnetization change the particle transverse angle, while bricks magnetized horizontally along the OZ axis change the transverse coordinate of particle.

This results, for a magnetic field of ideal bricks, in an electron trajectory which is close to the ondulator axis and has close-to-zero transverse angle and coordinate (see Fig. 2).

Since the average magnetization of brick M is not known precisely, let select it such that the ideal ondulator field is close to the measured undulator field, shown in Fig. 3. We obtained an average magnetization of 1.076 kG using the method of standard deviations. The field errors, shown in Fig. 4, apparently do not exceed 5 % of the field maximum.

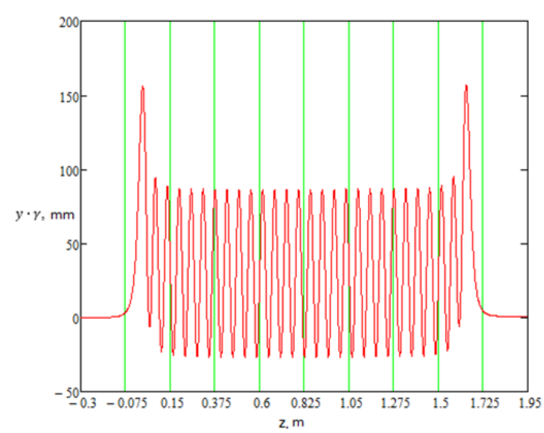

Figure 2: Electron trajectory in the field of the ideal undulator.

#faucct@gmail.com

ISBN 978-3-95450-133-5

MODELING AND DESIGN OF THE VARIABLE PERIOD AND POLE NUMBER UNDULATOR FOR THE SECOND STAGE OF THE NOVOSIBIRSK FEL*

O.A. Shevchenko, V.G. Tcheskidov, N.A. Vinokurov, BINP, Novosibirsk, Russia
I. Davidyuk#, Novosibirsk State University, Novosibirsk, Russia

Abstract

The concept of the permanent magnet variable period undulator (VPU) has been proposed just several years ago and there are few examples of its implementation yet. The VPUs have several advantages compared to conventional undulators. One of them is wider radiation wavelength tunability range and another one is an option to increase the number of poles for shorter periods. Both these advantages will be realized in VPU which is being developed now at Budker INP. In this paper, we present the 2-D and 3-D magnetic field simulation results and discuss the design features of this VPU.

INTRODUCTION

Tuning of the radiation wavelength is one of the basic FEL advantages which differs them from conventional lasers. Wide tunability range is desirable for many applications. Therefore its increasing is important goal of the FEL design optimization. As the wavelength in FEL depends on several parameters it can be tuned several ways. Each of them has its own advantages and disadvantages. But from the point of view of the maximum tunability range the best way of wavelength tuning is based on the varying of the undulator period.

The concept of the variable period undulator (VPU) has been proposed just recently [1] and it has very few implementations yet. There are several types of the VPU design. One of them proposed in [2] is similar to conventional hybrid undulator in which the iron poles are divided in two halves. This type of VPU is composed from separate magnet blocks which can move freely along longitudinal axis. Each block includes one permanent magnet and two iron plates. At fixed positions of the outer blocks the inner blocks distribute evenly in longitudinal direction due to the repulsive forces and the period of this distribution can be adjusted by moving of the outer blocks. This design allows to change number of blocks so, that at fixed space allocated for undulator one can have larger number of periods for shorter wavelength.

The variable period undulator for the NovoFEL is being developed now at Budker INP. It will replace electromagnetic undulator of the second stage FEL which is installed on the bypass of the second horizontal track [3]. The tunability range of the existing FEL is 35 - 80 microns. Application of VPU will allow to shift the short wavelength boundary to 15 microns (see simulation results below). By now design of the VPU magnetic block has been already developed and small prototype which has only six blocks is being manufactured now. In this paper we discuss undulator design and its magnetic field properties.

UNDULATOR GEOMETRY AND FIELD SIMULATION RESULTS

To find the optimal undulator geometry and investigate the magnetic field properties 2-D and 3-D simulations were carried out. For 2-D simulations we used code FEMM [4] which runs quite fast therefore we could calculate magnetic field for the total number of undulator periods (about 50). The final 3-D geometry is presented in Fig. 1. It was simulated by CST Studio [5].

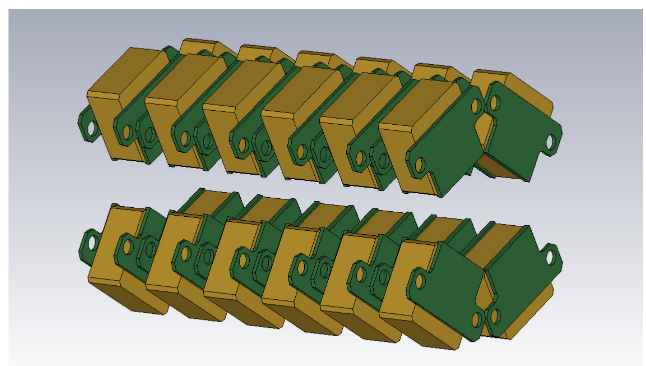

Figure 1: Undulator geometry used in 3-D simulations. Yellow blocks – permanent magnets, green plates – iron poles.

The undulator transverse aperture was chosen to be 50 mm. This value cannot be significantly reduced because of electron and optical beam losses. The minimal undulator period 48 mm is limited by the aperture. For the smaller periods the undulator deflection parameter and consequently the FEL gain become too small (see Fig. 6,8).

Each undulator block consists of one permanent magnet and two iron plates. The opposite plates of two blocks adjacent in longitudinal direction form one pole. Two blocks at the top as well as two blocks at the bottom are combined in one unit which moves as a whole. Top and bottom units are not connected. The blocks in one unit are tilted with respect to each other. This configuration provides the growth of the field amplitude with the distance from the central axis in all directions. As the

*Work supported by Russian Science Foundation (project 14-12-00480).
#daveduke@outlook.com

ISBN 978-3-95450-133-5

CHARACTERIZATION OF THE UNDULATOR MAGNETIC FIELD QUALITY BY THE ANGLE AVERAGED RADIATION SPECTRUM*

O. A. Shevchenko#, Budker INP SB RAS, Novosibirsk, Russia
N. Vinokurov, Budker INP SB RAS, Novosibirsk, Russia, and KAERI, Daejon, Rep. of Korea

Abstract

The real undulator magnetic field always contains errors which influence undulator performance. The effect of these errors is usually characterized by broadening of the spontaneous emission spectrum at zero angle and corresponding reduction of the spectral intensity. This approach works very well for the phase errors while it does not take into account transversal trajectory displacements. The integrated over the angles radiation spectrum contains more complete information about the undulator field quality but its calculation requires more effort. Therefore the spectral density of emitted radiation (the total number of emitted photons with given energy) can be considered as a figure of merit for an undulator. In this paper we derive analytical formula for this spectrum suitable for doing efficient numerical calculations and demonstrate its application to the case of some typical undulator field errors.

INTRODUCTION

Real undulators differ from ideal ones. The common way of the characterization of this difference is comparison of calculated spectral intensities of their radiation in forward direction and trajectories (see, e. g., [1]). For good undulator the reduction of spectral intensity is small and the trajectory deviation is less than the radius of first Fresnel zone divided by 2π, $\sqrt{\lambda L}/(4\pi)$, where L is the undulator length, and λ is the radiation wavelength. These two conditions are independent. Indeed, let us consider an undulator with parallel shift of electron trajectory in the middle (see below). The reduction of the forward-direction spectral intensity can be fully compensated by proper phase shift of radiation from the second half of the undulator (for example, by proper longitudinal shift of the second half). In this case we return constructive interference of the radiation from the undulator halves. But, in other but forward directions the path difference differs and spectral intensity will remain less than an ideal one. Therefore the total (integrated by angles) spectral power of radiation in this example is reduced. In this paper we consider the use of the spectral density of emitted radiation (the total number of emitted photons with given energy) as a figure of merit for an undulator. We derive analytical formula for this spectrum suitable for doing efficient numerical calculations and demonstrate its application for simple examples.

*Work supported by Russian Science Foundation (project 14-12-00480).
#O.A.Shevchenkoe@inp.nsk.su

SPECTRUM FORMULA

Let electron with charge e and coordinate $\mathbf{r}_0$ moves at velocity $\mathbf{v} = d\mathbf{r}_0/dt$. The Fourier harmonics of the radiation vector potential is [2]

$$\mathbf{A}_\omega(\mathbf{r}) = e\frac{e^{ikr}}{cr}\int_{-\infty}^{\infty}\mathbf{v}(t)e^{i\omega t-i\mathbf{k}\mathbf{r}_0(t)}dt\,, \quad (1)$$

where $k = \omega/c$, $\mathbf{r} = \mathbf{n}r$, $\mathbf{k} = \mathbf{n}k$. The spectral intensity (energy, radiated to the solid angle do and frequency interval $d\omega/(2\pi)$) is

$$dE_\omega = \frac{ck^2}{2\pi}\left|\mathbf{n}\times\mathbf{A}_\omega\right|^2 r^2 do\frac{d\omega}{2\pi} = \frac{e^2k^2}{2\pi c}\int_{-\infty}^{\infty}\int_{-\infty}^{\infty}\left[\mathbf{v}(t_1)\cdot\mathbf{v}(t_2) - \mathbf{n}\cdot\mathbf{v}(t_1)\mathbf{n}\cdot\mathbf{v}(t_2)\right]\cdot e^{i\omega(t_1-t_2)-i\mathbf{k}\left[\mathbf{r}_0(t_1)-\mathbf{r}_0(t_2)\right]}dt_1dt_2do\frac{d\omega}{2\pi} \quad (2)$$

Integration over the angles gives the total energy, radiated to the frequency interval $d\omega/(2\pi)$, or the spectral power,

$$dW_\omega = \int_{4\pi} dE_\omega = 2\frac{e^2k^2}{c}\int_{-\infty}^{\infty}\int_{-\infty}^{\infty}e^{i\omega(t_1-t_2)}\left[\mathbf{v}(t_1)\cdot\mathbf{v}(t_2)\left\langle e^{-ik\mathbf{n}\left[\mathbf{r}_0(t_1)-\mathbf{r}_0(t_2)\right]}\right\rangle - v_p(t_1)v_q(t_2)\left\langle n_pn_qe^{-ik\mathbf{n}\left[\mathbf{r}_0(t_1)-\mathbf{r}_0(t_2)\right]}\right\rangle\right]dt_1dt_2\frac{d\omega}{2\pi}, \quad (3)$$

where

$$\left\langle e^{-i\mathbf{n}\mathbf{a}}\right\rangle = \frac{1}{4\pi}\int_{4\pi}e^{-i\mathbf{n}\mathbf{a}}do = \frac{1}{4\pi}\int_0^\pi e^{-ia\cos\theta}2\pi\sin\theta\, d\theta = \frac{\sin a}{a}, \quad (4)$$

$$\left\langle n_pn_qe^{-i\mathbf{n}\mathbf{a}}\right\rangle = \left(\frac{\sin a}{a^3} - \frac{\cos a}{a^2}\right)\delta_{pq} + \left(\frac{\sin a}{a} - 3\frac{\sin a}{a^3} + 3\frac{\cos a}{a^2}\right)\frac{a_pa_q}{a^2}, \quad (5)$$

and $\mathbf{a} = k\left[\mathbf{r}_0(t_1) - \mathbf{r}_0(t_2)\right]$.

Taking into account that

ISBN 978-3-95450-133-5

HIGH STABILITY RESONANT KICKER DEVELOPMENT FOR THE SwissFEL SWITCH YARD

M. Paraliev#, C. Gough, S. Dordevic, H. Braun,
Paul Scherrer Institut, Villigen PSI, Switzerland

Abstract

The SwissFEL is a linac-based X-ray free electron laser facility under construction at the Paul Scherrer Institute. The facility will provide femtosecond, high brightness X-ray pulses for fundamental and applied science research. To increase facility efficiency, a double bunch operation is planned to serve simultaneously two experimental stations at the full linac repetition rate. The main linac will accelerate two electron bunches spaced 28 ns apart and a fast and stable deflecting system will be used to separate the two bunches into two different undulator lines. The deflecting system uses a novel concept based on resonant kicker magnets. A prototype kicker magnet and its control system were designed and built. Since stability is crucial, the stability performance of the prototype was studied. The peak to peak amplitude stability of ±11 ppm (3.5 ppm rms) was achieved, which is well within the FEL tolerance of ±80 ppm. The layout of the deflecting system and the key design parameters are also presented.

INTRODUCTION

The Swiss X-ray Free Electron Laser (SwissFEL) [1] is a 4th generation light source under construction at Paul Scherrer Institute (Switzerland). It is based on a linear electron accelerator with maximum energy of 5.8 GeV and will be a user operated facility. It will produce short (2 to 20 fs) and high brightness (up to $6 \cdot 10^{35}$ photons$\cdot$mm$^{-2}\cdot$mrad$^{-2}\cdot$s^{-1}) X-ray pulses covering the spectral range from 1 to 70 Å [2]. In order to make the facility more efficient the main linac operates in two electron bunch mode. Each RF pulse will accelerate two electron bunches, separated in time by 28 ns. At 3.0 GeV beam energy a high stability deflector system separates them and sends them to two additional linacs and respectively to two undulator lines. This allows simultaneous operation of two experimental stations at the full repetition rate of the machine (100 Hz). The SwissFEL layout is schematically presented in Fig. 1.

RESONANT KICKER SCHEME

A novel approach using fast high Q-factor resonant deflecting magnets is being used for high stability, reliable and fast bunch separation. The main component of the deflecting system is the composite kicker magnet. It consists of two vertical resonant kicker magnets (kickers) and three compensating vertical DC dipole magnets (dipoles). The two kickers are high Q-factor LC resonators tuned to frequency with half period equal to the bunch separation time (17.857 MHz). They are synchronously excited and after they reach their nominal current amplitude (500 A peak-to-peak) the two electron bunches arrive and are deflected up and down (~±1 mrad) by the positive and negative maximum of the magnetic field created by the oscillating magnet current. This process is illustrated in Fig. 2. The three compensating dipoles steer the “down deflected” beam (straight beam) back to the machine axis. After some drift distance (with quadrupole magnets) the “up deflected” beam (deflected beam) enters a DC septum magnet 10 mm off axis [3]. The DC septum is a Lambertson type dipole magnet that bends the deflected beam 2° in the horizontal plane and creates the final angular separation between them. A system of DC dipole magnets brings the deflected beam back into the machine horizontal plane and steer it parallel to the machine axis at 3.75 m distance.

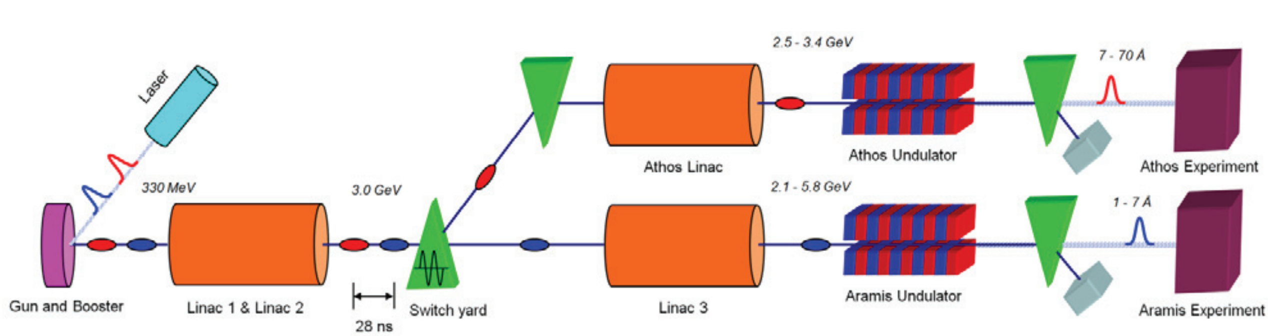

Figure 1: Schematic representation of SwissFEL double bunch operation scheme.

#martin.paraliev@psi.ch

ISBN 978-3-95450-133-5

GENERAL STRATEGY FOR THE COMMISSIONING OF THE ARAMIS UNDULATORS WITH A 3 GeV ELECTRON BEAM

M. Calvi, M. Aiba, M. Brügger, S. Danner, Th. Schmidt, R. Ganter, L. Patthey, Th. Schietinger, R. Ischebeck, PSI, Villigen, Switzerland

Abstract

The commissioning of the first SwissFEL undulator line (Aramis) is planned for the beginning of 2017. Each undulator is equipped with a 5-axis camshaft system to remotely adjust its position in the micrometer range and a gap drive system to set K-values between 0.1 and 1.8. In the following paper the beam-based alignment of the undulator with respect to the golden orbit, the definition of look-up tables for the local correction strategy (minimization of undulator field errors), the fine-tuning of the K-values as well as the setting of the phase shifters are addressed. When applicable both electron beam and light based methods are presented and compared.

INTRODUCTION

The large number of undulator modules required in a free electron laser (FEL) makes the commissioning of a beamline more involved than in a synchrotron where the light source consists (regularly) of a single device. Thirteen U15 modules (assuming to use also the spare unit), each 4 m long, will be operated together in the first SwissFEL hard X-ray line (called Aramis). It requires a precise control of the K-value of each unit within 100 ppm, a steering of the electron beam trajectory better than 2 μm RMS and a phase error of less than 5° RMS over a 4 m long unit.

All the SwissFEL undulators will be tested and optimized in the PSI magnetic measurement laboratory before the installation in the accelerator tunnel, see [1]. Nevertheless residual field errors together with the tight tolerances indicate the need of commissioning individual undulator modules directly with the beam as already experienced in comparable facilities [2]. Additional correction magnets are installed between undulator units and procedures are defined to improve the performance of the FEL during the commissioning and operation time.

In the following the different measurements together with the correction strategy are presented in the preliminary sequence planned for the commissioning of the beamline at the starting electron energy of 3.0 GeV.

UNDULATOR E-BEAM BASED ALIGNMENT

When the electron beam energy of at least 3 GeV (5.8 GeV is the nominal energy) is attained in the linac and transported to the undulators, the commissioning of the line can technically start. During the beam-based alignment (BBA) the undulators are set at open gap where the low magnetic field should minimize the orbit errors. An alternative candidate for the BBA is the nominal gap where the undulator is magnetically optimized.

Definition of the Reference Orbit

The first step is the definition of a reference orbit using BBA technique. For the SwissFEL a novel approach has been developed, as described in details in [3]. The proposed algorithm is based on the minimization of the deviation of the correction required to steer the beam to BPMs (beam position monitors) centers.

The BBA method in operation at the LCLS [4] is considered a valuable back up in case the baseline solution will not give satisfactory results. It is established on the BPMs reading at different beam energies (dispersion measurements) but the algorithm is rather complex and the full procedure is time consuming [5].

Once this phase is completed the undulators have to be aligned to the reference orbit as described in the following.

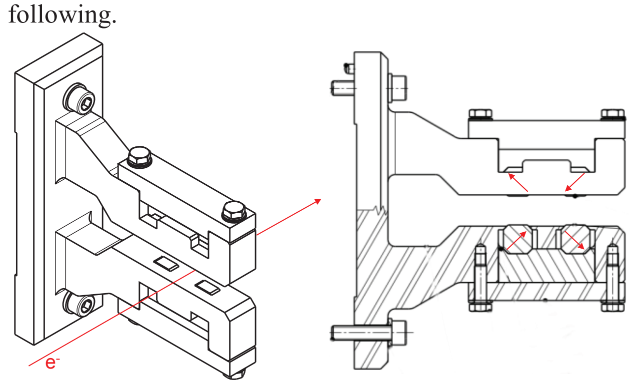

Figure 1: Alignment quadrupoles, on the left the 3D drawing with the detail of the beam axis, on the right the front view with the details of the magnets and magnetization directions.

Alignment Quadrupoles Technique

The axis of a planar undulator (light linear horizontal polarized) is the region where the vertical field (By) is minimum and where the longitudinal field (Bs) is zero. This definition identifies clearly the axis on the vertical plane while leaves some margin in the horizontal where a mechanical reference is used.

Taking the axis as a reference has the advantage to reduce the requirements on the alignment accuracy (dBy/dy=0) and to minimize the kicks due to the natural focusing on the vertical plane. Choosing a reference injection orbit with specific magnetic properties simplifies the challenging task of matching the field of different undulator modules which shall work together as a single device to make the FEL lasing.

ISBN 978-3-95450-133-5

SUMMARY OF THE U15 PROTOTYPE MAGNETIC PERFORMANCE

M. Calvi, M. Aiba, M. Brügger, S. Danner, R. Ganter, C. Ozkan, Th. Schmidt,
PSI, Villigen, Switzerland

Abstract

The first undulator prototype for SwissFEL (U15) was assembled and magnetically tested. The measurement instrumentations and the algorithms developed for the undulator optimization are presented and a comparison among different approaches is reviewed. The magnetic measurement results before and after the installation of the vacuum components are discussed. The summary of the undulator test with 100 MeV electron beam is presented and the impact of the radiation on the magnetics is addressed.

INTRODUCTION

The U15 design has been developed specifically for the SwissFEL project. Both the hard and the soft X-ray lines will be equipped with undulators built with the same frame and gap drive system.

To optimize the undulator stiffness and its dimensions a close frame has been implemented. This feature makes the undulator more compact but it required the development of a new magnetic measurement bench to optimize the structure.

Two new benches were developed based on SAFALI system [1]: the first is used without the vacuum chamber during the optimization phase and the second one with the vacuum chamber for phase adjustment and final checks before the installation in the tunnel.

The large number of undulator modules required per beamline (12 for Aramis I) increases substantially the effort associated with the magnetic shimming compared to a synchrotron where a beamline consists usually of a single module. To mitigate this issue and the cost associated, the support of the magnetics has been designed more flexible. It is now possible to precisely adjust the pole heights in the range of micrometers by means of a flexor driven by a wedge-screw system.

Before the series production a prototype was built to validate the new design approach. It was extensively tested and magnetically optimized before the installation into the SwissFEL Injector Test Facility of PSI. This last activity aimed to a better integration of the undulator hardware within the rest of the accelerator components as well as to test the field quality directly with the electron beam. The impact of the radiation on both the magnetics and electronics was monitored. In the following all these activities are discussed in view of the series production.

MAGNETIC MEASUREMENT INTRUMENTATION

There are two main systems used for the magnetic measurements of the undulators, the Hall sensors and the moving wire. The first is used to estimate the field profile and to calculate the trajectory and the phase error; the second is needed to measure the field integrals and the earth field in the laboratory (this measurement is performed before installing the undulator). The first field integral and the earth field are also used to calibrate the data measured with the Hall sensors. A zero Gauss chamber is planned for a systematic cross check during the production phase. A third system, the so-called pulsed wire, is also available but it is not planned to be used on a regular basis and it is not discussed in the following.

Hall Sensor Measurement Benches

A Hall probe is used to measure the magnetic field profile along or parallel to the undulator axis. The probe is built of three Hall sensors to measure the three components of the field. They are embedded in a ceramic support and aligned to the direction of the measurement axis and spaced of 2 mm.

To precisely follow the undulator axis the probe is guided with lasers. The two beams pass through two pinholes attached to the probe. The transmitted light carries the information about its position. This information is detected by two position sensitive diodes (PSD) and used to correct the trajectory of the probe. This logic is implemented in a feedback loop and optimized to decrease the measurement noise produced by the vibrations.

As already previously mentioned there are two different Hall sensor benches with two specific applications.

The one used for the optimization (bench A) is not constrained by the vacuum chamber and its implementation is more comfortable. A linear motor is used to displace the probe and the electronics. This last feature has the advantage to reduce the cable length and to have a fix connection between the probe and the ADC.

The measurements after the installation of the vacuum chamber (bench B) require more integration efforts. A piezoelectric-motor has been implemented in place of the linear motor because of the reduced dimensions. These actuators are usually made for travel shorter than a meter and the ceramic supports where the two piezoelectric legs actually “walk” are produced only for short length. Custom manufacture is possible but expensive and fragile. The solution implemented consists of several ceramic supports glued along the measuring bench and a piezoelectric motor with four legs to easily overcome the junction region between ceramic modules.

Moving Wire Bench

The moving wire bench has been modified and improved with respect to the system available at the SLS. A set of servomotors has been implemented in place of the steppers used previously to move the stages. This

ISBN 978-3-95450-133-5

MAGNETIC DESIGN OF AN APPLE III UNDULATOR FOR SWISSFEL

Th. Schmidt, A. Anghel, P. Böhler, M. Brügger, M. Calvi, S. Danner, P. Huber, A. Keller, M. Locher, PSI, Villigen, Switzerland

Abstract

For the SwissFEL at PSI beside the hard x-ray beamline to start with a soft x-ray line is planned to cover the wavelength between 0.7 and 7.0nm. For full control of the polarization of the FEL light, APPLE undulators are forseen. In this paper the design of these devices is introduced and the preliminary magnetic configuration together with the optimization strategy is presented in details.

INTRODUCTION

The SwissFEL free-electron laser currently under construction is designed with two beamlines: the hard x-ray beamline Aramis will be driven by the in-vacuum undulator U15 and will start operation with commissioning in summer 2016 being ready for user operation in 2017. The soft x-ray beamline Athos will be constructed in a second phase from 2017 to 2020. Both beamlines will have a self-seeding option [1].

While the U15 is trimmed to shortes period length, the focus on the soft x-ray undulator lies on a full polarization control by the users, that is circular, elliptical and linear polarizations to be rotatable from 0° to 180°.

The 5.8GeV SwissFEL shall accelerate two successive bunches in any of the rf – buckets coming with up to 100Hz. At an electron energy of 3 GeV the second bunch is extracted and sent into the Athos beamline where another linac can accelerate or decelerate the electrons by another 400MeV, so that the electron energy can be varied independently from the hard x-ray line within 2.6 – 3.4GeV. The wavelength range for the soft x-ray beamline shall be 0.7nm – 7nm (177eV – 1800eV). To reach with the 3.4GeV electron energy the minimum wavelength with a minimum K-value of 1 the period length is determined to 40mm. Accordingly to reach the 7nm with 2.6GeV a K-value of 4 is required.

The self-seeding chicane divides the undulator into two stages which allows to use planar devices before and for full flexibility APPLE type undulators in all modules of the second stage. The position of the self-seeding chicane has been optimized to be after 4 modules [2], which will result in 4 planar U40 and 8 APPLE type UE40 undulator modules.

The undulator design for SwissFEL is based on a modular support structure. One single frame is designed to support all kind of undulator types, planar in and out of vacuum [3] as well as APPLE undulator with their more complex forces. So for the UE40 only the shiftable magnet arrays, the magnets and their keeper have to be designed. The support structure with gap drive, the mover, the transport infrastructure and cabling etc. remains the same (see Fig. 1).

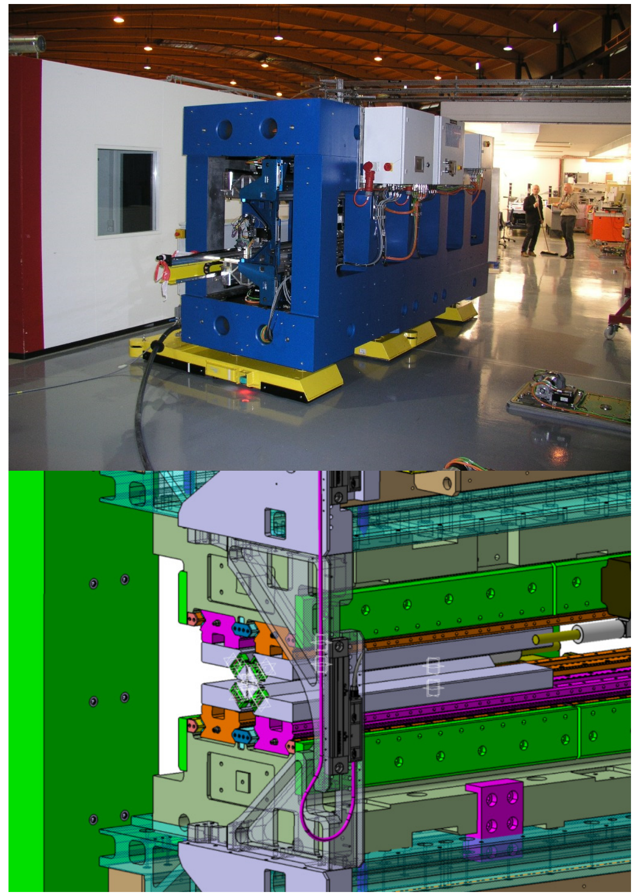

Figure 1: Modular support structure of the SwissFEL undulator series. This support structure out of cast mineral with a wedge based gap drive system can be equipped with planar in and out of vacuum magnet structures or APPLE magnet arrays.

As the APPLE undulators have to be properly aligned in vertical and horizontal direction, the mover system is a camshaft design with 5 degrees of freedom. Based on a SLAC design [4] these movers have already been used at PSI for the SLS girder and in-vacuum undulators. The movers have been reinforced and the drive system has been optimized so that they now allow the remote alignment of the undulator with µm precision. The alignment will be done by beam-based alignment with dedicated alignment quadrupoles. These are fixed quadrupoles made of permanent magnets, which are moved in and out by a simple pneumatic system. The system has been successfully tested with the prototype U15 undulator in the SwissFEL test injector [3].

Following the concept of the U15 the magnetic optimization of the UE40 shall also be based on adjustable keeper with a flexor design. Therefore the

ISBN 978-3-95450-133-5

A STRIPLINE KICKER DRIVER FOR THE NEXT GENERATION LIGHT SOURCE*

Fred Niell, Dr. Neal Butler, Dr. Marcel P.J. Gaudreau, PE, Michael Kempkes,
Diversified Technologies, Inc., Bedford, MA 01730, USA

Abstract

Diversified Technologies, Inc. (DTI) has designed, built, and demonstrated a prototype stripline kicker driver capable of less than 10 ns rise and fall time, ~40 ns pulse length, and peak power greater than 1.7 MW/pulse.

INTRODUCTION

Diversified Technologies, Inc. (DTI), under an SBIR grant from the U.S. Department of Energy, assembled a prototype pulse generator capable of meeting the original specifications for the Next Generation Light Source (NGLS) fast deflector. The ultimate NGLS kicker driver must drive a 50 © load (a 50 © terminated Transverse Electromagnetic (TEM) deflector blade) at 10 kV, with flat-topped pulses according to the NGLS pulsing protocol and a sustained repetition rate of 100 kHz. Additional requirements of the specification include a 2 ns rise time (10 to 90%), a highly repeatable flattop with pulse width from 5 – 40 ns, and a fall time (90% to .01%) less than 1 µs. The driver must also effectively absorb high-order mode signals emerging from the deflector itself.

STRIPLINE KICKER DRIVERS

The ultimate size, and hence cost, of any damping ring strongly depends on the speed of the kickers. It is envisioned that a scintilla of deflection will be imparted by a symmetric pair of shaped parallel deflection blades, pulsed in opposition at 10 kV. Within the guide, comprised of the two deflector blades and their environment, each TEM wave produced by the two pulse generators traverses the guide synchronously with the selected (relativistic) charge packet. Various system designs were explored for producing the desired pulse wave forms. The options included a direct series high voltage switch, solid-state Marx bank, inductive adder, or more conventional pulse transformers and transmission-line adders, several of which were considered in detail. The inductive adder was ultimately selected as the preferred development path for the remainder of the program.

The DTI team has designed and demonstrated the key elements of a solid-state kicker driver capable of meeting the NGLS requirements, with possible extension to a wide range of fast-pulse applications. The current iteration employs compensated-silicon MOSFETs with a charge-

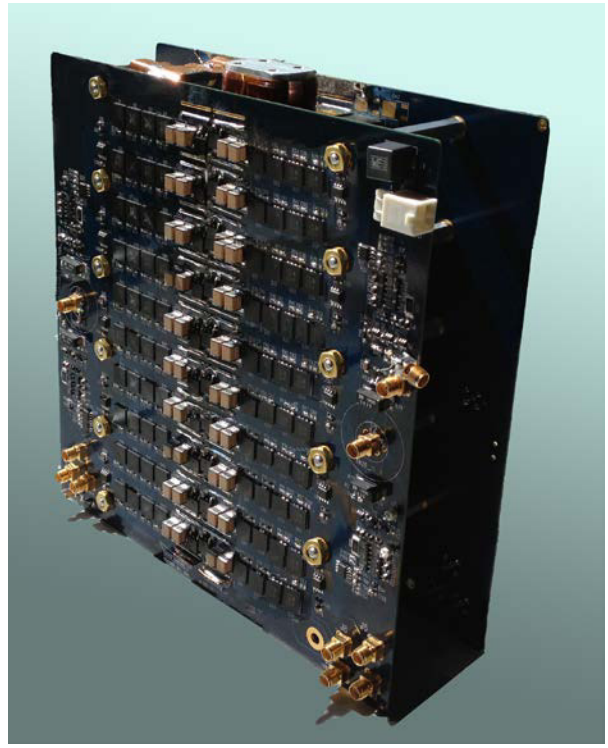

Figure 1: The dual-board pulser, displaying top and bottom boards with central output busbar.

pump gate drive arrangement (Figure 1). Two of these transistor-gate driver modules are used to drive opposite ends of the primary winding of an inductive adder transformer in a Marx-derived topology, achieving 1 kV per stage with transistors rated for 650 V. The high voltage gate-drive technique speeds up switching by quickly charging the power transistor gate capacitance in spite of significant internal gate resistance and package inductance. This can be considered a Marx generator-type circuit because two capacitors are charged from the prime power in parallel and discharged in series.

HYBRID MARX-INDUCTIVE ADDER

The inductive adder functions by applying several separately-powered primary circuits, each with its own ferrite coupling transformer core, to a single shared secondary circuit. In this manner, the voltages of all the primaries add together, creating one large output pulse. The output pulse voltage is simply the applied voltage, minus any forward drop in the switching circuitry, across the "T" model of the output transformer. The current

*Work supported by U.S. Department of Energy SBIR Award DE-SC0004255

ISBN 978-3-95450-133-5

PHASE SHIFTER DESIGN FOR ISASE

S.D. Chen, K. Fang, L.Zhu, H.-D. Nuhn, C. Pellegrini, J. Wu, SLAC, CA 94025, USA
S.D. Chen, C.S. Hwang, NCTU, Hsinchu 30076, Taiwan
C.S. Hwang, NSRRC, Hsinchu 30076, Taiwan

Abstract

A phase shifter to generate an additional phase advance of the spontaneous light versus the electron beam was designed for the iSASE scheme. The iSASE mechanism is for reducing the bandwidth further from SASE FEL process. A large phase advance about 1600*2Pi as the FEL operating at wavelength 0.8 nm was needed according to the simulation of iSASE process. Since the iSASE is thought to implement into LCLS II project, the space limitation causing by LCLS II should be considered when designing the phase shifter. An optimized three-pole electric phase shifter with 7.3 mm gap has the center field of 1.8 T . The vanadium steel was considered as pole material and the magnet physical length is 260 mm, meanwhile the water-cooling type copper coil was adopted. The temperature increment, force analysis, low field operation mode concept, and preliminary tolerance study were discussed.

INTRODUCTION

Improved SASE (iSASE) [1,2] was proposed to reduce the SASE bandwidth. In iSASE scheme, several phase shifters with large phase delay are inserted to increase the coherence length. In this scheme, the phase shifters should be placed in linear growth region, for example in our layout: five phase shifter was inserted into LCLS-II lattice, and the phase shifter for phase matching at local place [3, 4] will be replaced.

In our case, five phase shifters divide the linear growth region into six sections. Looking into the details of how the mechanism works: as electron beam passing through the first section, the electric field (light field) grows up and contains the informations of structure of local electron beam; after going through the first phase shifter, the electric field got a further phase advance and located at a new position inside the electron bunch; in the second section, the electric field can stimulate the new local electrons as a seed; in the following sections, same thing happens that the electric field will be placed at a new position by large phase delay caused by phase shifter and works as a seeding stimulating local electrons at new position. The coherence length was hence increased.

The scheme was first studied by a fundamental set up of five phase shifter with 100, 200, 400, 800, 1600*2pi phase delay, at wavelength 0.8 nm. The largest phase shifter, 1600*2pi, which is the hardest one to be achieved, was first designed and presented in this paper. Restricted by the space limitation from LCLS-II undulator hall, the length of phase shifter should be less than 260 mm, which forces the magnetic field high as 1.8 T to generate such a large phase delay. A permanent magnet can not afford the requirement; an electric magnet with pole material of the vanadium steel, which has a high saturation field of 2.4 T, was chosen. Meanwhile the water-cooling type copper coil was adopted to eliminate the Joule heat from copper wire.

This paper was organized as following: the specifications of magnet were first presented, then the water cooling system and evaluation of phase delay were described; the requirement of fringe field and remanence field were also discussed; the preliminary tolerance study was mentioned; the conclusion was in the end.

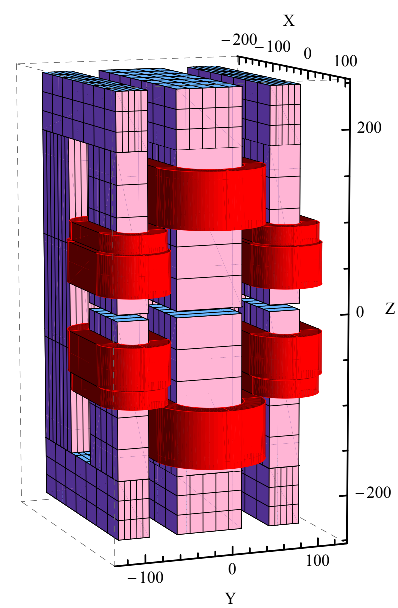

Figure 1: Magnet model plotted by Radia.

DESIGN OF THE MAGNET

The model displayed herein is a preliminary design, but can be the proof of the feasibility of producing 1600*2pi phase delay under space limitation, which is that physical length is less than 260 mm, gap is 7.3 mm, and physical height is less than 500 mm. To make the model practical, the details of manufacturing of the magnet and the effects on neighber magnets as inserting into undulator hall were integrally considered. The model was designed by Radia associated with Mathematica; the diagram of model is in Figure 1 and the specifications were in Table 1. The pole will be sliced and glued to prevent strong eddy current and reduce the charging time. The minimum bending radius of copper wire is considered. The transverse good filed region is now 10 times larger than requirement, however the saturation

ISBN 978-3-95450-133-5

UNDULATOR RADIATION DAMAGE EXPERIENCE AT LCLS*

H.-D. Nuhn[#], R.C. Field, S. Mao, Y. Levashov, M. Santana, J.N. Welch, Z. Wolf
SLAC National Accelerator Laboratory, Menlo Park, CA 94025, U.S.A

Abstract

The SLAC National Accelerator Laboratory has been running the Linac Coherent Light Source (LCLS), the first x-ray Free Electron Laser since 2009. Undulator magnet damage from radiation, produced by the electron beam traveling through the 133-m long straight vacuum tube, has been and is a concern. A damage measurement experiment has been performed in 2007 in order to obtain dose versus damage calibrations. Radiation reduction and detection devices have been integrated into the LCLS undulator system. The accumulated radiation dose rate was continuously monitored and recorded. In addition, undulator segments have been routinely removed from the beamline to be checked for magnetic (50 ppm, rms) and mechanic (about 0.25 µm, rms) changes. A reduction in strength of the undulator segments is being observed, at a level, which is now clearly above the noise. Recently, potential sources for the observed integrated radiation levels have been investigated. The paper discusses the results of these investigation as well as comparison between observed damage and measured dose accumulations and discusses, briefly, strategies for the new LCLS-II upgrade, which will be operating at more than 300 times larger beam rate.

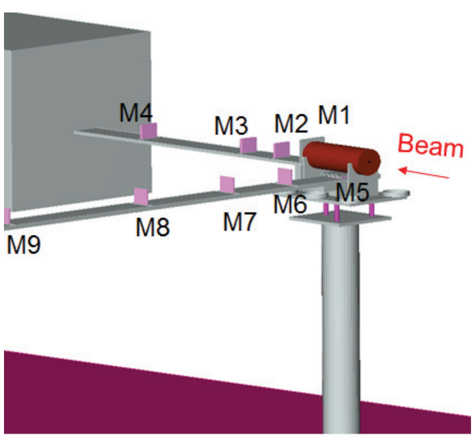

Figure 1: Layout of the SLAC End-Station A (ESA) undulator magnet block damage experiment. M1 to M9 indicate the placement of the individual magnet blocks relative to the copper cylinder. M5 is located underneath the copper cylinder.

INTRODUCTION

The Linac Coherent Light Source (LCLS) has been delivering intense ultra-short x-ray beams to international users at the SLAC National Accelerator Laboratory (SLAC) since 2009 [1]. These x-ray beams are generated with fixed, canted gap hybrid ($Nd_2Fe_{14}B$) permanent magnet undulators [2].

* Work was supported by U.S. Department of Energy, Office of Basic Energy Sciences, under Contract DE-AC02-76SF00515.
# nuhn@slac.stanford.edu

MAGNET DAMAGE CALIBRATION

In July 2007, a radiation damage experiment was conducted on nine LCLS-I type ($Nd_2Fe_{14}B$) permanent magnet blocks, mounted well separated from one another, behind a solid Cu cylinder, which was bombarded with a 13.6-GeV electron beam (see Figure 1). The experiment was located inside SLAC's ESA (End-Station A) enclosure. During the 12 days of irradiation the magnet blocks stayed at a temperature of 23.8°C±0.8°C. The estimated accumulated maximum radiation doses in each block, based on a FLUKA [3,4] model, ranged from about 1500 kGy to less than 1 kGy and the corresponding measured reduction in total magnetic moment from about 9.6% to less than 0.1%. In fact, the two magnet blocks with the lowest amount of accumulated radiation dose showed a slight increase in total magnetic moment. Linear fitting resulted in a scaling factor of 70 kGy/%. This simple scaling seems not to describe the low-dose behaviour with sufficient detail. Other radiation damage studies and experiments have been conducted in other laboratories around the world, answering a wider range of questions with more detail [5,6,7].

LCLS UNDULATOR RADIATION DOSE MEASUREMENTS

A record of the integrated radiation dose, as actually received by the LCLS undulator magnets, has been kept over the entire operational period with the help of thermo-luminescent dosimeters (TLDs). The TLDs have been shielded in small Pb-casings and were mounted in front of each undulator segment with the sensitive element about 25 mm above and horizontally centered on the beam axis. The Pb-casings were added in order to filter out the low energy and non-damaging radiation background coming from synchrotron radiation during the FEL process. Each TLD is left in place for some time (originally several weeks, now several months), before it is replaced by a fresh TLD. Some of the readings are shown in Figure 2 versus the total amount of beam energy that passed through the beam pipe during the same time period. Beam energy is the integral of the product of particle energy, number of particle per bunch and bunch repetition rate. The figure shows a fairly consistent loss rate over about a 3-year period. Three different regions along the undulator line (girder numbers) can be distinguished. The higher levels in the front end (girders 1-10) come from LTU scattering events from inserted wires, screens or the tune-up stopper (TDUND). The higher levels at the back end of the undulator line (girders 17-33) come from events within the undulator vacuum chamber, especially from a

ISBN 978-3-95450-133-5

A 200 µm-PERIOD LASER-DRIVEN UNDULATOR*

F. Toufexis, T. Tang, S.G. Tantawi, SLAC, Menlo Park, CA 94025, USA

Abstract

To reduce the linac energy required for a given synchrotron radiation wavelength, and hence the size of the device, a smaller undulator period with sufficient field strength is needed. In this work, a microfabricated, laser-driven undulator with 200 µm undulator period is proposed. A transverse electric (TE) wave that co-propagates with the electron beam is excited between two polysilicon thin films, having a gap of 16.5 µm. The mode that is excited is a deflecting mode and causes the electron beam to wiggle. The device is fabricated on a silicon wafer, using conventional silicon micromachining techniques. A single polysilicon thin film is supported on a silicon chip, which has a slit from the back to allow delivery of the laser beam. Two such chips are bonded together to form a 16.5 µm gap, within which the electron beam passes through. The final device has dimensions 1cm x 1cm x 1.1mm and has approximately 35 undulator periods. In this paper, the model, design, fabrication, and cold measurements of the device are reported.

INTRODUCTION

Traditionally, coherent emission of short wavelength electromagnetic radiation employed undulators – devices that generate a periodic magnetic field – made of permanent magnets. Such undulators present several limitations on how short their period can be, while maintaining reasonable field strength and beam aperture. These limitations, along with the resonance condition between the electrons' oscillatory motion, including relativistic and Doppler effects, and the wavelength of the emitted light, require very high-energy beams, making a tabletop free electron laser (FEL) prohibitive. In order to shrink an FEL, a smaller linac and therefore lower beam energy is required. A smaller undulator period is therefore required, while maintaining sufficient field strength. However, the undulator wavelength cannot be too small – for example using directly a laser beam – because the emittance requirements make it infeasible to operate as a laser [1]. Alternatives to traditional undulators are superconducting magnet-based undulators [2], photonic crystal undulators [3], and microwave undulators [4]. Recently laser driven undulators have been developed [5–8].

In this work, a novel laser–driven undulator is proposed. Figure 1a outlines the principle of operation of the proposed device. A parallel plate dielectric waveguide is used as the interaction region. A TE wave is excited with a 10.6 µm silicon dioxide (CO2) laser. The angle of incidence is chosen so that a specific undulator wavelength is produced. The electron bunch co–propagates with the TE wave, producing an effective undulator wavelength that is larger than the excitation wavelength. The waveguide is formed by two thin polycrystalline silicon (p-Si) films, supported on two single crystal silicon (SCS) dies that are bonded together, as shown in Figure 1b. A thicker epitaxially grown polycrystalline silicon (epi p-Si) layer, along with sacrificial silicon oxide (SiO2) layers are used to define the gap between the two plates of the waveguide, as well as assist in etching the backside trench, without affecting the plates of the waveguide. Figure 1c shows the two sides of a single die before assembly. Note that in Figure 1c, the SiO2 has not been etched, and the thin film covering the trench has been removed, for better visibility. The devices were fabricated in the Stanford Nanofabrication Facility (SNF) [9].

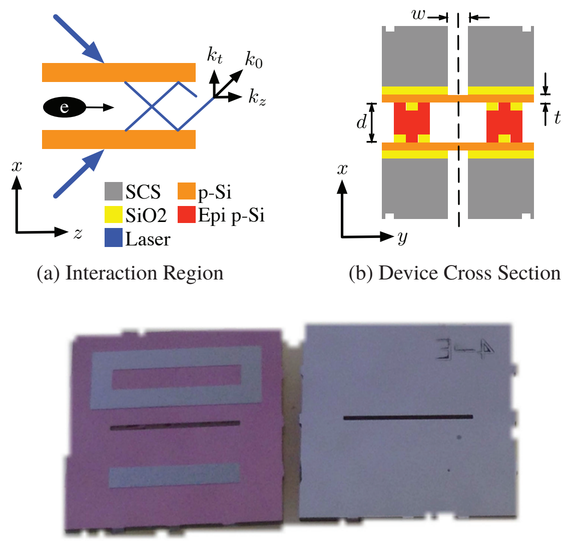

(a) Interaction Region (b) Device Cross Section

(c) Fabricated Die before Assembly

Figure 1: Proposed Device Overview.

ANALYTICAL MODEL & DESIGN

Eigen Modes in Infinite Metallic Parallel Plate Waveguide

In this section, solutions to the Time Harmonic Maxwell's equations are sought for the case of the infinite parallel metallic plate waveguide. Analysis starts with this structure, since it is a very good approximation of the fields inside the interaction region of the undulator. The structure has a finite height d in the x–direction, is infinite in y and z–directions, and waves travel along the z direction. Fields are assumed to vary with time as $e^{-j\omega t}$, and therefore, a field propagating in the positive z direction has a z–dependence of the form $e^{jk_z z}$, where $\omega = \frac{2\pi c}{\lambda_0}$ is the field angular frequency, $k_0 = \frac{2\pi}{\lambda_0}$ is the free space propagation constant, $k_z = \frac{2\pi}{\lambda_G}$ is the propagation

* This project was funded by U.S. Department of Energy under Contract No. DE-AC02-76SF00515 and the DARPA AXiS program.

ISBN 978-3-95450-133-5

OXYGEN SCINTILLATION IN THE LCLS*

J.L. Turner, R.C. Field, SLAC NAL, Menlo Park, CA 94025, U.S.A.

Abstract

Oxygen was tested as a replacement for nitrogen in the Gas Detector system in the Linac Coherent Light Source (LCLS) X-ray Free Electron Laser (FEL) at the SLAC National Accelerator Center. The attenuation and pulse-to-pulse intensity monitors for LCLS use nitrogen, but for experiments at the nitrogen K 1S energy of about 410eV this functionality is gone due to energy fluctuations above and below the K-edge. Oxygen was tested as a scintillating gas at 400 eV and 8.3 keV.

INTRODUCTION

In the LCLS X-ray beam, a length of the beam transport line is filled with low pressure nitrogen. One use of the gas is to attenuate the X-ray intensity as needed [1]. The gas pressure in a 4 meter section is controlled at pressures of up to 20 Torr to implement this, and it is useful up to X-ray energies of about 1.5 keV. Additional short sections before and after the attenuator section have independent pressure controls for up to 2 Torr, and are used to monitor the X-ray laser beam intensity. They function by making use of the excitation of the nitrogen molecules by the X-ray beam. As the nitrogen de-excites, a fraction of the energy is emitted in spectral lines in the range 300 to 430 nm, corresponding to both excited and ionized molecular transitions. Some of this light is detected through sapphire beam windows by photomultiplier tubes.

THE BEAMLINE AND NITROGEN

The beam chamber for these devices contains a series of 4 mm diameter beam apertures with differential pumping between them, to reach the base level at E-8 Torr beyond the device. Ion-pumps, turbo-pumps backed by scroll-pumps and Roots pumps are used.

The nitrogen K-edge occurs at about 410 eV (Fig. 1). When the LCLS is tuned to operate at this energy, the nitrogen gas systems are not useful because their response varies wildly as the beam energy fluctuates within its intrinsic width.

For the occasions when users need X-ray energies in the nitrogen K-edge range, a solution is to use an alternative gas. The practical requirements are that the pumping system can maintain the upstream and downstream base pressures, while delivering a useful range of pressures for the attenuator and detectors (Fig. 2), and that the de-excitation light should be detectable with the present vacuum windows and photomultiplier system.

Light noble gases would be considerably more difficult to pump, and, with the exception of helium, their reported light emission wavelengths are too deep in the ultraviolet. Oxygen is the nearest analogue to nitrogen as far as gas handling and pumping is concerned.

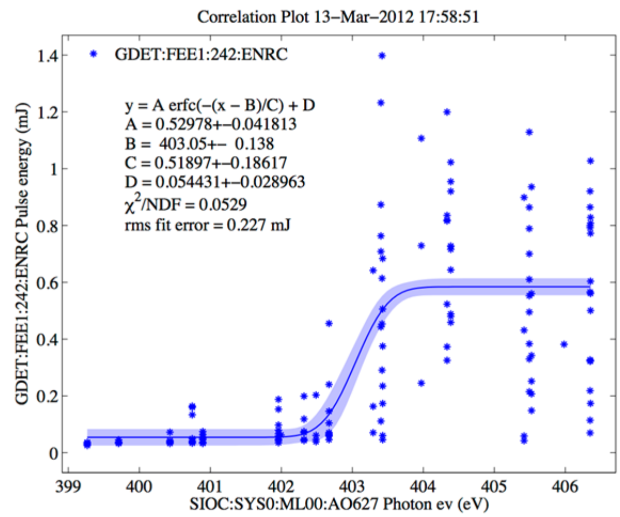

Figure 1: X-ray energy on the horizontal axis, vertical is nitrogen response as a function of the energy fluctuating under and over and spanning the K 1S edge.

THE BEAMLINE AND OXYGEN

Oxygen Concerns

With oxygen, no changes to the pumps are needed, and the switch over from one gas to the other is fairly simple. Since it is used at very low pressures, there is no significant combustion safety issue, except for normal oxygen precautions for the source and regulator. The chemical activity of atomic oxygen and ozone generated in the beam pipe has been considered. Most of it is, of course, intercepted by the walls and aperture plates, and the concentration downstream is too small to be of concern. B4C, which is often used as an absorber for X-rays, is known to be etched by ozone in the presence of strong UV illumination. Based on this, an upper limit on the etching rate on B4C components in the ~10 Torr oxygen environment shows surface loss too small to be significant.

Oxygen Utility

The oxygen K-edge is at 530 eV, and so, used at near 409 eV, its absorption would be relatively low, comparable to that of nitrogen at 1095 eV. This improves resolution, and operability at low pressure, of the controls of the gas system. For example, a pressure of 0.05 Torr used in nitrogen at 415 eV would be matched by 0.6 Torr using oxygen.

* This work was supported by U.S. Department of Energy, Office of Basic Energy Sciences, under Contract DE-AC02-76SF00515

ISBN 978-3-95450-133-5

UPDATE ON FEL PERFORMANCE FOR SWISSFEL

E. Prat and S. Reiche, PSI, Villigen, Switzerland

Abstract

The SwissFEL project under construction at the Paul Scherrer Institute foresees for 2017 the realization of an X-ray FEL with a photon wavelength down to 1 Å. In this paper we present the expected SASE performance for SwissFEL based on input distributions obtained from detailed start-to-end simulation results. The effects of the longitudinal wakefields due to resistive wall and surface roughness in the undulator beamline have been taken into account. We have studied and optimized the impact on the FEL performance of different factors like the electron focusing or the undulator tapering. Results for the standard cases with 200 pC and 10 pC electron bunch charge are shown.

INTRODUCTION

The SwissFEL facility, presently under construction at the Paul Scherrer Institute, will provide SASE and self-seeded FEL radiation at a hard (1-7 Å) and soft (7-70 Å) X-ray FEL beamlines [1]. SwissFEL will operate with electron beam charges varying between 10 and 200 pC and beam energies from 2.1 to 5.8 GeV. Two standard operational modes are foreseen: 1) the long-pulse (LP) mode to maximize the FEL output energy, with an electron beam charge of 200 pC and a rms bunch length of 18.4 fs; and 2) the short-pulse (SP) mode with 10 pC beam charge and 2.5 fs pulse duration.

In this document we present the SASE simulation results for the hard X-ray beamline and the two described operational modes. We have done the calculations for the shortest and longest radiation wavelengths, i.e. 1 Å and 7 Å. We have optimized the average β-function along the undulator beamline as well as the undulator tapering. We present the effects of the wakefields in the undulator beamline, showing that tapering can be employed to reduce the wakefields impact to a negligible level.

LAYOUT AND SIMULATIONS SETUP

The present design lattice for the hard X-ray beamline consists of 12 undulator modules. Each of them is 4 m long, has a period length of 15 mm and a variable gap with a nominal value of 4.2 mm. The distance between modules is 0.75 m. In addition we have reserved the space corresponding to an undulator module to place a magnetic chicane and a Bragg crystal to be used for self-seeding [2]. The facility is able to accommodate up to seven more modules for potential future upgrades such as long post-saturation tapering. A quadrupole magnet in the middle of each section between undulators is employed for beam focusing.

Figure 1 shows the properties of the electron beam distributions that we used as input for the FEL simulations for 1 Å. The distributions have been obtained by tracking with the simulation codes *ASTRA* [3] and *elegant* [4].

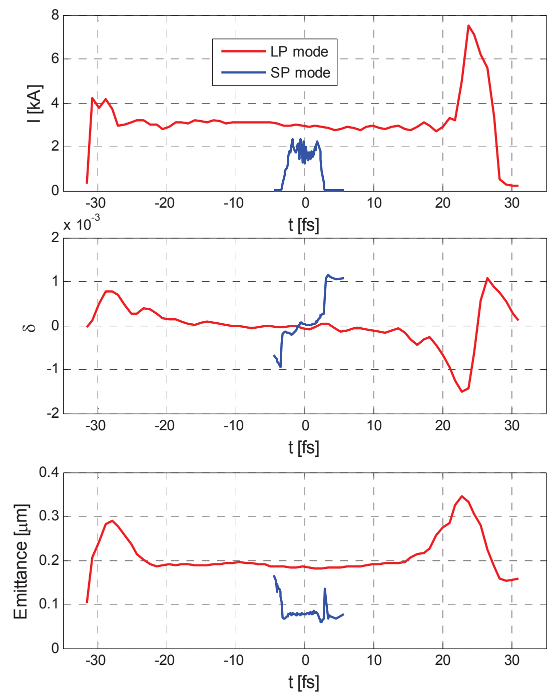

Figure 1: Electron beam slice properties at the undulator entrance for the LP mode (red) and SP mode (blue). Current profile (top), relative energy deviation (center) and normalized emittance (bottom).The emittance is defined as the geometrical average of the horizontal and vertical emittances.

The lasing at a radiation wavelength of 1 Å is obtained when the electron beam has a maximum energy of 5.8 GeV, which corresponds to an undulator parameter K of about 1.2. For the long wavelength (7 Å) we choose the undulator parameter as large as possible to maximize the beam energy and, as a consequence, to enhance the FEL output power. The maximum K is about 1.5, which corresponds to a beam energy of about 2.4 GeV. The particle distributions for 7 Å are obtained simply by scaling the distributions at 1 Å. This scaling is valid since the difference between the two configurations is only the energy provided by the last part of the linac, while keeping the same compression setup. The FEL interaction is simulated with *Genesis* [5].

FOCUSING OPTIMIZATION

We have analyzed how the FEL performance varies as a function of the focusing along the undulator for the LP mode. Figure 2 shows the relative FEL power at saturation as a function of the β-function for the two

ISBN 978-3-95450-133-5

SASE FEL PERFORMANCE AT THE SWISSFEL INJECTOR TEST FACILITY

S. Reiche *on behalf of the SwissFEL Team* – Paul Scherrer Institut, Villigen, Switzerland

Abstract

A 4 m long prototype of the SwissFEL undulator module with an undulator period length of 15 mm was installed at the SwissFEL Injector Test Facility and tested with a 200 MeV electron beam in the beginning of 2014. We observed FEL lasing in SASE mode in the wavelength range from 70 to 800 nm, tuning the wavelength by energy and gap. The measurements of the FEL performance are reported.

INTRODUCTION

Hard X-ray FEL facilities rely very heavily on cutting-edge technology for RF, diagnostics, insertion devices, and X-ray optics such that building these facilities would represent a high risk without a prior test of the key components. This was the main purpose of various test facilities around the world, such as GTF [1] for LCLS, PITZ [2] for the European XFEL, or SCSS [3] for SACLA. The SwissFEL [4], currently under construction at the Paul Scherrer Institute (PSI), is based on the results of the SwissFEL Injector Test Facility [5], also hosted by the PSI. The test facility has been in operation since August 2010 and will be decommissioned in fall 2014 to move parts over to the SwissFEL building for installation. The start of commissioning of SwissFEL is foreseen for 2015 with a duration of two years.

Like SACLA, SwissFEL will utilize in-vacuum undulators to minimize the undulator period and thus the required electron energy to reach one Angstrom as the resonant wavelength of the FEL. Due to the technical challenge to construct 12 modules of 4 m each a test with an electron beam is highly beneficial to discover possible limitations in the performance of the undulator prototype module. For that an undulator module was installed at the test facility in the early months of 2014. Demonstrating SASE performance was one of the goals for this measurement series and the results are reported in this paper.

THE SWISSFEL INJECTOR TEST FACILITY

The SwissFEL Injector Test Facility (SITF) is a platform to test key components for SwissFEL as well as to demonstrate the beam parameters of the electron beam to successfully operate SwissFEL at its shortest wavelength of 1 Angstrom.

The RF gun is a 2.5 cell photo RF gun [6], operating at European S-band frequency of 2.998 GHz, which has recently replaced the 3rd generation CLIC Test Facility (CTF3) Gun in spring 2014. The former CTF3 gun was sufficient to demonstrate the key beam parameters for a 200 pC beam and a slice emittance of about 200 nm [7]. The gun is followed by two 4 m long S-band traveling wave accelerating structures, boosting the electron energy up to 130 MeV. They are enclosed by focusing solenoids to keep the beam size and Twiss parameter within reasonable limits. An additional S-band RF station feeds two S-Band structures to increase the energy up to 250 MeV and to apply a chirp for compression. However running off-crest to generate the chirp yields less beam energy at a level of about 220 MeV. An X-band RF structure linearizes the energy chirp for a better control on the current profile after compression.

The 11 m long bunch compressor is movable to have variable R_{56} from 0 to 70 mm while keeping the vacuum chamber small. This allows for precise BPM readings in the dispersive section of the bunch compressor as well as the installation of quadrupoles and skew quadrupoles to correct for linear tilts in the electron beam distribution in both transverse planes [8].

A diagnostic section follows the bunch compressor for current profile, projected and slice emittance, and longitudinal phase space measurements (the last in the dispersive part of the beam dump). The key component is a S-band transverse deflecting cavity, streaking the beam in the vertical direction. Initially a FODO section was foreseen to measure the beam size at various positions along several cells of the FODO lattice and reconstruct the beam emittance values from it. In practice quad scans and multi-knob measurements with a dedicated high resolution YAG screen at the end of the beam line were more robust and easier to use [9]. The center part of the FODO section could therefore be modified for other tests.

One important test involved the in-vacuum undulator prototype: a 4 m long undulator with a period length of 15 mm and a tunable undulator parameter K between 1.0 and 1.7. The main study was the entrance and exit kick of the undulator on the electron beam and the alignment strategy of the module by means of alignment quadrupoles [10]. The orbit within the undulator is checked with the spontaneous radiation (or FEL beam) on various screens after the undulator and compared to the electron BPM reading.

With the installation of an undulator the expectation for a SASE signal comes naturally. In particular the narrow opening angle of the FEL signal would yield better resolution in the angle between light cone and electron beam than the rather broad and weak signal of the spontaneous undulator radiation.

The general layout of the SwissFEL Injector Test Facility is shown in Fig. 1.

ISBN 978-3-95450-133-5

HARMONIC LASING OPTIONS FOR LCLS-II

G. Marcus, Y. Ding, Z. Huang, T. Raubenheimer, SLAC, Menlo Park, CA 94025, USA
G. Penn, LBNL, Berkeley, CA 94720, USA

Abstract

Harmonic lasing can be a cheap and relatively efficient way to extend the photon energy range of a particular FEL beamline. Furthermore, in comparison to nonlinear harmonics, harmonic lasing can provide a beam that is more intense, stable, and narrow-band. This paper explores the application of the harmonic lasing concept at LCLS-II using various combinations of phase shifters and attenuators. In addition, a scheme by which individual undulator modules are tuned to amplify either the third or fifth harmonic in different configurations is presented in detail.

INTRODUCTION

Harmonic lasing in FELs, where the collective electron beam/radiation instability of odd harmonics in a planar undulator evolve independently of the fundamental resonant radiation, has generated much recent interest and potentially offers many benefits over nonlinear harmonic generation [1–3]. Some of these benefits include a more intense, stable, and narrow-band radiation pulse. Harmonic lasing can also be a relatively efficient way of extending the photon energy range of a particular FEL beamline.

The performance of harmonic lasing schemes is contingent on the successful suppression of the fundamental radiation. In this way, incoherent energy spread that is associated with the growth of the fundamental does not interrupt linear growth of the target harmonic, allowing it to reach full saturation. A variety of methods have been proposed to suppress the fundamental radiation including, but not limited to: introducing periodic phase shifts between the field and the electron beam such that the fundamental experiences a non-integer 2π phase shift while the desired harmonic experiences an integer 2π shift; periodically filtering the fundamental with a spectral attenuator while allowing the desired harmonic to pass and simultaneously debunching the electron beam in a bypass chicane; using a combination of detuned/retuned undulators such that the desired harmonic is resonant at different harmonic numbers (third, fifth, etc.) for contiguous undulator sections. This paper explores the application of each of these methods (and combinations thereof) in the case of the LCLS-II design study to not only extend the tuning range of individual beamlines, but to also increase the performance of the hard x-ray (HXR) and soft x-ray (SXR) beamlines at the high end of the tuning range [4]. The performance is illustrated through numerical particle simulations using the FEL code `GENESIS` [5] where we focus primarily on lasing at the third harmonic.

PARAMETERIZATION

The eigenvalue equation for a high-gain FEL with all of the relevant three-dimentional effects included was was first generalized to the case of harmonics in [6]. More recently [2], Ming Xie fitting formulas for the power gain length [7,8] were also generalized to harmonic lasing:

$$\frac{L_{1d}^{(h)}}{L_g^{(h)}} = \frac{1}{1+\Lambda\left(\eta_d^{(h)},\eta_\epsilon^{(h)},\eta_\gamma^{(h)}\right)}$$

$$L_{1d}^{(h)} = \left(\frac{A_{JJ1}^2}{hA_{JJh}^2}\right)^{1/3} L_{1d}$$

$$\eta_d^{(h)} = \left(\frac{A_{JJ1}^2}{hA_{JJh}^2}\right)^{1/3} \frac{\eta_d}{h} \tag{1}$$

$$\eta_\epsilon^{(h)} = \left(\frac{A_{JJ1}^2}{hA_{JJh}^2}\right)^{1/3} h\eta_\epsilon \tag{2}$$

$$\eta_\gamma^{(h)} = \left(\frac{A_{JJ1}^2}{hA_{JJh}^2}\right)^{1/3} h\eta_\gamma$$

The Xie approach to parameterizing the power gain length is useful for quickly estimating three-dimensional effects using scaled parameters that represent essential system features. Using this formalism, it is possible to quickly estimate electron beam and undulator parameters that are suitable for optimizing harmonic lasing. For instance, it offers a quick estimate on the distance between phase shifters necessary to effectively suppress the fundamental. It is also useful for determining if harmonic lasing is viable for given electron beam and undulator parameters. The harmonics can be extremely sensitive to the slice energy spread and emittance. The Xie formalism quickly quantifies this sensitivity and can illuminate how high in harmonics (and photon energy) the harmonic lasing concept can be pushed.

Table 1: Nominal Electron Beam and Undulator Parameters for the Baseline LCLS-II Scenario

Paramter	Symbol	Value SXR(HXR)	Unit
e-beam energy	E	4.0	GeV
emittance	ϵ	0.45	μm
current	I	1000	A
energy spread	σ_E	500	keV
beta	$\langle\beta\rangle$	12(13)	m
undulator period	λ_u	39(26)	mm
segment length	L_u	3.4	m
break length	L_b	1.0	m
# segments	N_u	21(32)	-
total length	L_{tot}	96(149)	m

ISBN 978-3-95450-133-5

START-TO-END SIMULATIONS FOR IR/THZ UNDULATOR RADIATION AT PITZ

P. Boonpornprasert*, M. Khojoyan, M. Krasilnikov, F. Stephan, DESY, Zeuthen, Germany
B. Marchetti, E. Schneidmiller, M. Yurkov, DESY, Hamburg, Germany
S. Rimjaem, Chiang Mai University, Chiang Mai, Thailand

Abstract

High brightness electron sources for modern linac-based Free-Electron Lasers (FELs) have been characterized and optimized at the Photo Injector Test facility at DESY, Zeuthen site (PITZ). Since the time structure of the electron bunches at PITZ is identical to those at the European XFEL, the PITZ accelerator is being considered as a proper machine for the development of an IR/THz source prototype for pump and probe experiments planned at the European XFEL. Tunable IR/THz radiation sources using synchrotron radiation from a dipole magnet, transition radiation, high gain FELs and coherent radiation of tailored or premodulated beams are currently under consideration. This work describes start-to-end simulations for generating the FEL radiation using an APPLE-II undulator with electron beams produced by the PITZ accelerator. Analysis of the physical parameter space has been performed with tools of the FAST program code package. Electron Beam dynamics simulations were performed by using the ASTRA code, while the GENESIS 1.3 code was used to study the SASE process. The results of these studies are presented and discussed in this paper.

INTRODUCTION

The concept of generating IR/THz radiation by electron bunches from a linear accelerator for pump and probe experiments at the European XFEL was presented in Ref. [1]. One of the important requirements for the IR/THz pulse is the possibility for a precise synchronization with the x-ray pulse. A way to meet this requirement is generating the IR/THz pulse from the same type of electron source which serves the European XFEL and therefore can provide the same time structure and repetition rate as those of the x-ray pulses.

The Photo Injector Test facility at DESY, Zeuthen site (PITZ) has been established to develop, study and optimize high brightness electron sources for modern linac-based short-wavelength Free-Electron Lasers (FELs) like FLASH [2] and the European XFEL [3]. The photocathode laser system at PITZ has the essential feature to be able to produce various temporal pulse shapes [4]. The flat-top temporal profile with a FWHM length of 20-22 ps and ~2 ps rise/fall times is usually used for the operation. The electron bunch charge can be varied from a few pC to 4 nC and the beam can be accelerated up to ~22 MeV/c.

Since PITZ serves as the facility for commissioning and optimizing RF guns for the European XFEL [5, 6] the same characteristics (time structure and beam quality) of the electron beam from the RF gun at PITZ is available as it will be at the European XFEL. In addition, the site of a PITZ-like setup is small enough to fit in the experimental hall for the European XFEL users so that the transport of the IR/THz radiation to the user experiments is very short. From these advantages, PITZ can be considered as an ideal machine for the development of a prototype IR/THz source for pump-probe experiments at the European XFEL.

With the current techniques for the production of electron beam at PITZ and different means for radiation generation (dipole magnet, transition radiation, high gain FELs, coherent radiation of tailored or premodulated beams, etc), it will be possible to cover wavelengths in the whole radiation spectrum from IR (μm) to THz (cm) wavelengths with a variety of field patterns (from single-cycled to narrow-band), and with a high level of the peak and average radiation power [1].

As the PITZ beamline has limited possibilities to install additional components, a preliminary layout for the IR/THz radiation source was developed and is presented in Fig. 1. Preliminary studies by using this layout have been done in order to get benchmark results for actual beamline modifications and further studies. The layout consists of a 1.6-cell L-band photo RF gun surrounded by main and bucking solenoids, a cut disk structure (CDS) booster, a c-shape chicane bunch compressor (D1 to D4), quadrupole magnets (Q1 to Q11), screen stations (S1 to S5) and an APPLE-II type undulator [7]. The components and their positions in this layout from the RF gun to the screen S1 are similar to those of the current PITZ layout. With this preliminary layout, we plan to study the radiation generation with 2 procedures: (i) Self-Amplification of Spontaneous Emission Free-Electron Lasers (SASE FELs) in the undulator using an uncompressed, high charge electron bunch and (ii) Coherent Transition Radiation (CTR) using an ultra-short electron bunch which is compressed by the chicane bunch compressor. The SASE radiation is anticipated to cover radiation wavelengths of 20-100 μm while radiation wavelengths above 100 μm are expected from the CTR.

This paper presents start-to-end (S2E) numerical simulations for the SASE FEL radiation in the wavelength range of 20-100 μm. An uncompressed electron beam with 4 nC bunch charge and the APPLE-II type undulator were used in the simulations. Calculation of the saturation characteristics has been performed with tools of the FAST program code package [8–10]. Beam dynamics simulations were performed by using A Space charge TRacking Algorithm (ASTRA) code [11], while the GENESIS1.3 code [12] was used to study the SASE process.

* prach.boonpornprasert@desy.de

ISBN 978-3-95450-133-5

SASE CHARACTERISTICS FROM BASELINE EUROPEAN XFEL UNDULATORS IN THE TAPERING REGIME

I. Agapov*, G. Geloni, European XFEL GmbH, Hamburg, Germany
G. Feng, V. Kocharyan, E. Saldin, S. Serkez, I. Zagorodnov, DESY, Hamburg, Germany

Abstract

The output SASE characteristics of the baseline European XFEL, recently used in the TDRs of scientific instruments and X-ray optics, have been previously optimized assuming uniform undulators without considering the potential of undulator tapering in the SASE regime. Here we demonstrate that the performance of European XFEL sources can be significantly improved without additional hardware. The procedure consists in the optimization of the undulator gap configuration for each X-ray beamline. Here we provide a comprehensive description of the X-ray photon beam properties as a function of wavelength and bunch charge. Based on nominal parameters for the electron beam, we demonstrate that undulator tapering allows one to achieve up to a tenfold increase in peak power and photon spectral density in the conventional SASE regime.

INTRODUCTION

The output SASE characteristics of the baseline European XFEL have been previously optimized assuming uniform undulator settings and used in the design of scientific instruments [2–4]. In order to enable experiments over a continuous photon energy range, European XFEL undulators have adjustable gap [1]. The availability of very long tunable gap undulators provides a unique opportunity for an up to tenfold increase in spectral density and peak output power (up to the TW-level) for nominal electron beam parameter sets. [5] provides an overview of the design considerations and the general layout of the X-ray instrumentation of the European XFEL sources, beam transport systems and instruments. Baseline parameters for the electron beam have been defined and presented in [6, 7]. These parameters have been used for simulating FEL radiation characteristics and saturation lengths relevant to the European XFEL SASE undulators [8]. A well-known way to enhance the SASE efficiency is to properly configure undulators with variable gap [9–12]. In [13] it has been studied on an example of a particular working point how a tapering procedure, i.e. a slow reduction of the field strength of the undulator in order to preserve the resonance wavelength, while the kinetic energy of the electrons decreases due to the FEL process, can be used to significantly improve performance of the European XFEL sources without additional hardware. In present article we demonstrate that tapering allows one to achieve up to a tenfold increase in output for all achievable photon energies and all nominal electron bunch charges. A new set of baseline parameters of the electron beam for the European XFEL has been recently updated [6, 7] and was used in present work.

In the following we assume that SASE1 operates at the photon energy of 12 keV, and the FEL process is switched off for dedicated SASE3 operation with the help of a betatron switcher [14]. The energy spread due to spontateous radiation emission in SASE1 is accounted for. We highlight operation of SASE3 for the electron energy of 14 GeV as the most probable working energy. Optimal tapering is found by numerical optimization using a piecewise-quadratic law. The Genesis 1.3 code [15] has been used for our FEL studies. Benchmarks have been performed with another FEL code ALICE [13, 16]. More details on the simulation procedure can be found in [17] and up-to-date parameters will be maintained on the XFEL.EU photon beam parameter web page [18].

PHOTON BEAM PROPERTIES

At the European XFEL facility three photon beamlines will be delivering X-ray pulses to six experimental stations. For fixed electron and photon energy, five working points are foreseen, corresponding to bunch charges of 0.02 nC, 0.1 nC, 0.25 nC, 0.5 nC, 1 nC, and resulting in pulse durations of roughly 2 fs, 8 fs, 20 fs, 40 fs and 80 fs. The hard X-ray undulators SASE1/2 are 250m long producing 4keV-25keV photons, and the soft X-ray undulator SASE3 is 120 m with photon energy range of 0.25-3 keV. We will focus on a more comprehensive description of SASE3 parameters, with the performance of SASE1 discussed more shortly. The improvement in SASE1 performance is comparable to that of SASE3. Moreover, a self-seeding setup [19] is foreseen for SASE1 from the beginning, which makes the high power extraction in the SASE mode more attractive in the soft X-ray range.

The source properties: size, divergence, radiation pulse energy, and maximum photon spectral density depend on photon energy, bunch charge, and electron energy. The pulse energies and the number of photons per pulse are shown in Fig. 1 for the tapered mode and in Fig. 2 for the saturation mode as functions of photon energy and bunch charge. In the tapered mode, pulse energy (or, equivalently, number of photons) increases by up to ten times compared to saturation, depending on the bunch charge and radiation wavelength. For short bunches (e.g. corresponding to 0.02 nC) the tapering efficiency drops since the radiation slips forward relative to the electron bunch and stops being amplified.

Figures 3 and 4 show comparisons of peak power and photon spectral density produced in the standard SASE mode

* ilya.agapov@xfel.eu

ISBN 978-3-95450-133-5

PROPOSAL TO GENERATE 10 TW LEVEL FEMTOSECOND X-RAY PULSES FROM A BASELINE UNDULATOR IN CONVENTIONAL SASE REGIME AT THE EUROPEAN XFEL

Svitozar Serkez, Vitali Kocharyan, Evgeni Saldin, Igor Zagorodnov
Deutsches Elektronen-Synchrotron (DESY), Hamburg, Germany
Gianluca Geloni
European XFEL GmbH, Hamburg, Germany

Abstract

Output characteristics of the European XFEL have been previously studied assuming an operation point at 5 kA peak current. Here we explore the possibility to go well beyond such nominal peak current level. We consider a bunch with 0.25 nC charge, compressed up to a peak current of 45 kA. An advantage of operating at such high peak current is the increase of the x-ray output peak power without any modification to the baseline design. Based on start-to-end simulations, we demonstrate that such high peak current, combined with undulator tapering, allows one to achieve up to a 100-fold increase in a peak power in the conventional SASE regime, compared to the nominal mode of operation. In particular, we find that 10 TW-power level, femtosecond x-ray pulses can be generated in the photon energy range between 3 keV and 5 keV, which is optimal for single biomolecule imaging. Our simulations are based on the exploitation of all the 21 cells foreseen for the SASE3 undulator beamline, and indicate that one can achieve diffraction to the desired resolution with 15 mJ (corresponding to about $3 \cdot 10^{13}$ photons) in pulses of about 3 fs, in the case of a 100 nm focus at the photon energy of 3.5 keV.

INTRODUCTION

Imaging of single molecules at atomic resolution using radiation from the European XFEL facility would enable a significant advance in structural biology, because it would provide means to obtain structural information of large macromolecular assemblies that cannot crystallize, for example membrane proteins. The imaging method “diffraction before destruction” [1]- [5] requires pulses containing enough photons to produce measurable diffraction patterns, and short enough to outrun radiation damage. The highest signals are achieved at the longest wavelength that supports a given resolution, which should be better than 0.3 nm. These considerations suggest that the ideal energy range for single biomolecule imaging spans between 3 keV and 5 keV [6]. The key metric for optimizing a photon source for single biomolecule imaging is the peak power. Ideally, the peak power should be of the order of 10 TW [7].

The baseline SASE undulator sources at the European XFEL will saturate at about 50 GW [8]. While this limit is very far from the 10 TW-level required for imaging single biomolecules, a proposal exists to improve the output power at the European XFEL by combining self-seeding [9]- [28], emittance spoiler foil [29]- [31], and undulator tapering techniques [32]- [42]. However, the realization of such proposal requires installing additional hardware in the undulator system and in the bunch compressor [7]. Here we explore a simpler method to reach practically the same result without additional hardware. This solution is based on the advantages of the European XFEL accelerator complex, which allows one to go well beyond the nominal 5 kA peak current.

The generation of x-ray SASE pulses at the European XFEL using strongly compressed electron bunches has many advantages, primarily because of the very high peak power, and very short pulse duration that can be achieved in this way [43]. Considering the baseline configuration of the European XFEL [8], and based on start-to-end simulations, we demonstrate here that it is possible to achieve a 100-fold increase in peak power by strongly compressing electron bunches with nominal charge. In this way we show that 10 TW power level, 3 fs-long pulses at photon energies around 4 keV can be achieved in the SASE regime. This example illustrates the potential for improving the performance of the European XFEL without additional hardware.

The solution to generate 10 TW power level proposed in this article is not without complexities. The price for using a very high peak-current is a large energy chirp within the electron bunch, yielding in its turn a large (about 1%) SASE radiation bandwidth. However, there are very important applications like bio-imaging, where such extra-pink x-ray beam has a sufficiently narrow bandwidth to be used as a source for experiments without further monochromatization.

In order to enable high focus efficiency with commercially available mirrors (80 cm-long) at photon energies around 4 keV, the undulator source needs to be located as close as possible to the bio-imaging instrument. With this in mind we performed simulations for the baseline SASE3 undulator of the European XFEL at a nominal electron beam energy of 17.5 GeV. We optimized our setup based on start-to-end simulations for an electron beam with 0.25 nC charge, compressed up to 45 kA peak current [44]. In this way, the SASE saturation power could be increased to about 0.5 TW.

In order to generate high-power x-ray pulses we exploit undulator tapering. Tapering consists in a slow reduction of the field strength of the undulator in order to preserve the resonance wavelength, while the kinetic energy of the electrons decreases due to the FEL process. The undulator taper can be simply implemented as discrete steps from one undulator segment to the next, by changing the undulator

ISBN 978-3-95450-133-5

PURIFIED SASE UNDULATOR CONFIGURATION TO ENHANCE THE PERFORMANCE OF THE SOFT X-RAY BEAMLINE AT THE EUROPEAN XFEL

Svitozar Serkez, Vitali Kocharyan, Evgeni Saldin, Igor Zagorodnov
Deutsches Elektronen-Synchrotron (DESY), Hamburg, Germany
Ilya Agapov, Gianluca Geloni
European XFEL GmbH, Hamburg, Germany

Abstract

The purified SASE (pSASE) undulator configuration recently proposed at SLAC promises an increase in the output spectral density of XFELs. In this article we study a straightforward implementation of this configuration for the soft x-ray beamline at the European XFEL. A few undulator cells, resonant at a subharmonic of the FEL radiation, are used in the middle of the exponential regime to amplify the radiation, while simultaneously reducing the FEL bandwidth. Based on start- to-end simulations, we show that with the proposed configuration the spectral density in the photon energy range between 1.3 keV and 3 keV can be enhanced of an order of magnitude compared to the baseline mode of operation. This option can be implemented into the tunable-gap SASE3 baseline undulator without additional hardware, and it is complementary to the self-seeding option with grating monochromator proposed for the same undulator line, which can cover the photon energy range between about 0.26 keV and 1 keV.

INTRODUCTION

The SASE3 beamline at the European XFEL will be operated in the photon energy range between 0.26 keV and at least 3 keV. A high level of longitudinal coherence is the key to upgrade the baseline performance. Self-seeding is a promising approach to significantly narrow the SASE bandwidth and to produce nearly transform-limited pulses [1]-[20]. The implementation of this method in the soft x-ray wavelength range necessarily involves gratings as dispersive elements, which may be installed in the SASE3 undulator without perturbing the electron focusing system and could cover the spectral range between about 0.26 keV and 1 keV [18]- [19]. In order to provide a high level of longitudinal coherence in the photon energy range between 1 keV and 3 keV, proposals exist to narrow the SASE bandwidth at the European XFEL by combining self-seeding and fresh bunch techniques. However, this requires installing additional hardware in the undulator system [21, 22]. Here we explore a simpler method to reach practically the same result without further changes in the undulator system. The solution is based in essence on the purified SASE (pSASE) technique proposed at SLAC [23], and naturally exploits the gap tunability of the SASE3 undulator. In the pSASE configuration, a few undulator cells resonant at a subharmonic of the FEL radiation, called altogether the "slippage-boosted

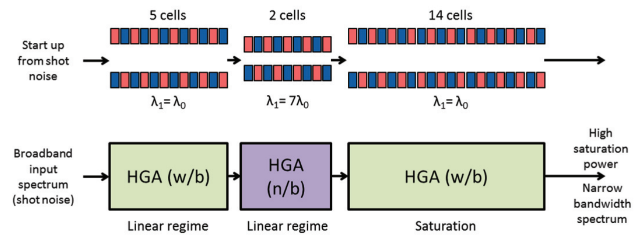

Figure 1: The pSASE undulator configuration proposed for the SASE3 beamline, which is expected to operate in the photon energy range between 1.3 keV and 3 keV.

section", are used in the high-gain linear regime to reduce the SASE bandwidth. The final characteristics of a pSASE source are a compromise between high output power, which can be reached with a conventional SASE undulator source resonant at the target wavelength, and narrow bandwidth, which can be reached with harmonic lasing [24]- [28]. We demonstrate that it is possible to cover the energy range between 1.3 keV and 3 keV using the nominal European XFEL electron beam parameters, and to reduce the SASE bandwidth by a factor 5, still having the same output power as in the baseline SASE regime. Note that the slippage-boosted section is tuned to a subharmonic (the fifth, or the seventh) of the FEL radiation. Therefore, the choice of the lowest pSASE photon energy considered in this article, 1.3 keV, is dictated by the minimal photon energy (0.26 keV) that can be reached in the conventional SASE regime.

A more detailed treatment can be found in [29].

FEL STUDIES

A schematic layout of the proposed pSASE configuration for the SASE3 undulator at the European XFEL is illustrated in Fig. 1 and consists of three parts which will be called U1 (5 cells), U2 (2 cells) and U3 (14 cells). We performed a feasibility study of the pSASE setup with the help of the FEL code Genesis 1.3 [30] running on a parallel machine. Results are presented for the SASE3 FEL line of the European XFEL, based on a statistical analysis consisting of 100 runs. The overall beam parameters used in the simulations are presented in Table 1.

The nominal beam parameters at the entrance of the SASE3 undulator, and the resistive wake inside the undulator are shown in Fig. 2, see also [31]. The evolution of the transverse electron bunch dimensions is plotted in Fig. 3.

ISBN 978-3-95450-133-5

BEAM DYNAMIC SIMULATIONS FOR SINGLE SPIKE RADIATION WITH SHORT-PULSE INJECTOR LASER AT FLASH*

M. Rehders†, J. Roensch-Schulenburg, Hamburg University and CFEL, Hamburg, Germany
J. Rossbach, Hamburg University, Hamburg, Germany
S. Schreiber, DESY, Hamburg, Germany

Abstract

This paper discusses the generation of single spike SASE pulses at soft x-ray wavelength at the free-electron laser FLASH by using very short electron bunches of only a few micrometer bunch length. In order to achieve these extremely short bunch lengths, very low bunch charges (in the order of 20 pC) and short electron bunches exiting the photo-injector are required. For this, a new short-pulse injector laser with adjustable rms pulse duration in the range of 0.7 ps to 1.6 ps and bunch charges up to 200 pC was installed, extending the electron beam parameter range before bunch compression in magnetic chicanes. Beam dynamic studies have been performed to optimize the injection and compression of low-charge electron bunches by controlling the effect of coherent synchrotron radiation and space-charge induced bunch lengthening and emittance growth. Optimization includes the pulse parameters of the injector laser. The simulation codes ASTRA, CSRtrack and Genesis 1.3 were employed.

MOTIVATION

The Free-Electron Laser in Hamburg (FLASH) is a high-gain SASE FEL user facility offering highly brilliant radiation pulses in the XUV- to soft x-ray range with a typical pulse duration between <50 and 200 fs (FWHM) [1]. Amongst the variety of user experiments that are performed at FLASH there are many pump-probe experiments where the time resolution is limited by the XUV pulse duration. These experiments would greatly benefit from being provided with shorter SASE pulses. In principle, the shorter the SASE pulses that can be offered to the users, the shorter the time scales that can be studied and the better the time resolution for a given process to be investigated. FEL facilities around the world are investigating on the generation of extremely short SASE pulses. A relatively straight-forward method is the generation of SASE pulses from very short electron bunches (see e.g. [2–4]).

Due to the relatively low energies of only a few mega electron volt, space charge forces still play a major role at the injector. Therefore the high peak current and short bunch duration required for the production of short SASE pulses cannot be created at the injector. Instead bunch compression is achieved at higher energies, typically in magnetic chicanes. Strong compression in magnetic chicanes requires very tight RF tolerances in the accelerating structure used to apply the required energy chirp on the bunch. The main challenge for the generation of very short electron bunches is therefore the tolerance of the accelerating RF fields.

At FLASH an additional injector laser has been installed to produce shorter bunches already at the injector. This short pulse injector laser reduces the bunch compression required in the magnetic chicanes for low charge electron bunches, relaxing the RF tolerances for short pulse SASE operation [5].

SASE pulses typically consist of many longitudinal optical modes in the power distribution and spectrum. These individual spikes are typically separated by the cooperation length L_{coop} [6]. The shortest possible SASE pulse consists of only a single mode. This single spike operation constitutes a special mode of operation for FELs. For single spike radiation the bunch length σ_z has to approximately obey $\sigma_z \leq 2\pi L_{\text{coop}}$ [2, 6]. At FLASH this means that the bunch length has to be in the order of only a few micrometers.

Beam dynamic simulations have been performed to achieve a detailed understanding of single spike operation at FLASH. A start-to-end simulation for single spike radiation with the short-pulse injector laser is presented that is very close to machine settings used for standard short pulse operation at FLASH.

SHORT PULSE OPERATION AT FLASH

FLASH has an RF photo-injector consisting of a 1.5 cell L-band gun and two solenoids for emittance compensation. Seven superconducting accelerating modules accelerate the bunch to energies of up to 1.25 GeV. Four third harmonic cavities upstream of the first bunch compressor are used to linearize the longitudinal phase space distribution. Two magnetic bunch compressors situated at 150 MeV and at 450 MeV are used to longitudinally compress the bunch to peak currents and bunch lengths required for SASE operation. Recently FLASH has been upgraded to have a second undulator beamline (FLASH2) that is currently being commissioned [1]. A schematic overview of FLASH is given in Fig. 1. The simulations presented in this paper have been performed for the original undulator beamline, FLASH1.

In order to adjust the SASE pulse duration to the needs of each specific user experiment, the bunch length at the undulator section is set accordingly. This is done by a combination of two methods. First, the bunch length can be scaled by adjusting the bunch compression applied in the magnetic chicanes. Second, especially for the shortest SASE pulses, the bunch length is additionally reduced already at the injector. This is done be scaling of the bunch charge

* The project has been supported by the Federal Ministry of Education and Research of Germany (BMBF) under contract No. 05K10GU2 and FSP301

† Marie.Rehders@desy.de

ISBN 978-3-95450-133-5

DEMONSTRATION OF SASE SUPPRESSION THROUGH A SEEDED MICROBUNCHING INSTABILITY*

C. Lechner†, A. Azima, M. Drescher, L.L. Lazzarino, Th. Maltezopoulos, V. Miltchev, T. Plath, J. Rönsch-Schulenburg, J. Rossbach, University of Hamburg, Hamburg, Germany
K. E. Hacker, S. Khan, R. Molo, DELTA, TU Dortmund University, Dortmund, Germany
S. Ackermann, J. Bödewadt, G. Brenner, M. Dohlus, N. Ekanayake, T. Golz, E. Hass, K. Honkavaara, T. Laarmann, T. Limberg, E. Schneidmiller, N. Stojanovic, M. Yurkov, DESY, Hamburg, Germany

Abstract

Collective effects and instabilities due to longitudinal space charge and coherent synchrotron radiation can degrade the quality of the ultra-relativistic, high-brightness electron bunches needed for the operation of free-electron lasers. In this contribution, we demonstrate the application of a laser-induced microbunching instability to selectively suppress the SASE process. A significant decrease of photon pulse energies was observed at the free-electron laser FLASH in coincidence with overlap of 800 nm laser pulses and electron bunches within a modulator located approximately 40 meters upstream of the undulators. We discuss the underlying mechanisms based on longitudinal space charge amplification (LSCA) [1] and present measurements.

INTRODUCTION

Microbunching instabilities driven by longitudinal space charge (LSC) forces occurring in linear accelerators driving free-electron lasers (FELs) affect electron beam diagnostics as well as FEL operation. For instance, emission of coherent optical transition radiation (COTR) was observed at several facilities and it has to be mitigated for accurate measurements of the transverse beam profile [2–5]. The concept to use these instabilities for short-wavelength radiation production was proposed as longitudinal space charge amplifier (LSCA) in [1]. As illustrated in Fig. 1, an LSCA comprises multiple amplification "cascades", each one consisting of a focusing channel (an electron beamline with quadrupole magnets) followed by a dedicated dispersive element. In the focusing channel, the electrons in the higher-density regions expand longitudinally introducing an energy change. The R_{56} value of the dispersive element (we consider chicanes here) converts these energy changes into a density modulation. Starting from shot noise, a strong density modulation can be achieved in two to four cascades.

* Work supported by Federal Ministry of Education and Research of Germany under contract No. 05K10PE1, 05K10PE3, 05K13GU4, and 05K13PE3 and the German Research Foundation programme graduate school 1355.
† christoph.lechner@desy.de

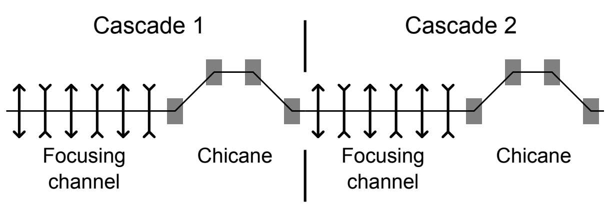

Figure 1: Schematic layout of an LSCA configuration with two cascades [1].

LSCA effects were studied experimentally at the Next Linear Collider Test Accelerator (NLCTA) at SLAC, where the impact of compression changes on spontaneous undulator radiation was measured [6]. At the National Synchrotron Light Source Source Development Laboratory (SDL) at Brookhaven National Laboratory (BNL), a modulated current profile was generated at the photoinjector with a modulated laser pulse. Microbunching gain was observed at wavelengths suitable for THz generation [7]. In [8] it is proposed to use longitudinal space charge effects to reduce the slice energy spread in HGHG seeding applications.

In this contribution, we give an overview of LSCA studies at FLASH in which the amplification process was initiated by modulating the electron bunch by means of an external laser pulse. The amplified energy modulation is shown to suppress the lasing process.

EXPERIMENTAL SETUP

The measurements presented in this contribution were performed at the FEL user facility FLASH at DESY, Hamburg [9]. The schematic layout of the facility is shown in Fig. 2. The superconducting linear accelerator (linac) driving the FEL delivers high-brightness electron bunches with energies up to 1.25 GeV. At a repetition rate of 10 Hz, bunch trains consisting of up to 800 bunches at a 1 MHz repetition rate can be produced. The facility has been upgraded by a second undulator beamline FLASH2, which is currently under commissioning. The hardware (fast kickers and a septum) needed for the distribution of electron bunches into the two undulator beamlines has been installed downstream of the linear accelerator.

The hardware used in the measurements is located in the FLASH1 electron beamline between the collimation section and the undulator system, compare Fig. 3. The electron bunches arriving from the collimation section of FLASH1 are modulated in an electromagnetic undulator (5 periods of 20 cm, $K_{max} = 10.8$) by the $\lambda = 800$ nm laser pulses arriving from the seeding laser system. After the modulator, chicane C_1 with variable R_{56} is installed. For studies of the LSCA, we use a combination of a transverse-deflecting structure (TDS) and a dipole spectrometer installed about

ISBN 978-3-95450-133-5

ELECTRON BEAM DELAYS FOR IMPROVED TEMPORAL COHERENCE AND SHORT PULSE GENERATION AT SWISSFEL

N.R. Thompson, ASTeC, STFC Daresbury Laboratory, UK
S. Reiche, PSI, Villigen, Switzerland

Abstract

Proposals have been made for the introduction of magnetic electron beam delays in between the undulator modules of a long sectional FEL undulator - these can be used for the generation of trains of FEL pulses which can individually be shorter than the FEL cooperation time [1] or to greatly improve the temporal coherence of the FEL output compared to the nominal SASE configuration [2–4]. This paper comprises a feasibility study of the application of these techniques to a future SwissFEL hard X-Ray beamline. Three-dimensional simulations are used to investigate the potential photon output.

INTRODUCTION

SwissFEL, the X-ray free electron laser at the Paul Scherrer Institut, is currently under construction with planned operation from the end of 2016. The facility comprises a FEL named Aramis operating from 1–7Å and a second FEL named Athos operating from 7–70Å. Both FELs will operate in SASE and self-seeding modes. Space is reserved in the undulator hall for the future addition of a second hard X-ray FEL. In this paper we investigate the potential performance of two proposed novel FEL schemes, the Mode-Locked Amplifier FEL [1] and the High-Brightness SASE FEL [2–4] if implemented on this future beamline. The two schemes are considered together because they utilise common hardware.

The Mode-Locked Amplifier FEL

In the Mode-Locked Amplifier FEL electron beam delay chicanes are introduced between the modules of a long FEL undulator. By delaying the electrons, the emission from each undulator module is delayed with respect to the emission from the previous undulator module. If the undulator modules are relatively short, such that the electron bunch microstructure does not evolve much from one undulator module to the next, the total field builds up as a series of delayed, overlapped, fields of similar phase and amplitude leading to interference. In the frequency domain the field comprises a spectral comb centred on the resonant wavelength $\lambda_r = \lambda_w(1+\bar{a}_w^2)/2\gamma^2$ with an overall envelope given by the spontaneous emission spectrum of a single undulator module with FWHM bandwidth $\Delta\lambda/\lambda \approx 1/N_w$. Here λ_w is the undulator period, $\bar{a}_w$ is the rms undulator deflection parameter, γ is the electron relativistic factor and N_w is the number of periods in one undulator module. The wavelength spacing between the sideband modes is given by $\Delta\lambda = \lambda_r^2/s$ where $s = \delta + N_w\lambda_r$ is the total slippage between radiation and electrons in one combined undulator+delay module with δ the applied delay in the chicane and $N_w\lambda_r$ the slippage in one undulator module. The spectrum is equivalent to that of a laser ring cavity of length s—in effect a very short laser cavity has been synthesised via the use of the macroscopic electron beam delays. Viewed in the temporal domain the radiation intensity builds up into a sequence of non-identical spikes of separation s modulated by the normal SASE envelope, which due to the increased slippage itself becomes stretched temporally by the slippage enhancement factor $S_e = s/N_w\lambda_r$. The shape of the spikes evolves along the pulse because the radiation sideband modes are not phase locked. To lock the modes a technique analogous to that used in conventional lasers cavity is adopted—a modulation is added to the system with a frequency equal to the mode spacing, or equivalently a period of s. In the FEL this is done by adding a modulation of period s to the electron beam energy. In the time domain the FEL pulse is then seen to comprise a series of cleanly separated, similar radiation spikes where the length of each spike is approximately equal to the slippage $N_w\lambda_r$ in each undulator module.

The mode-locked amplifier FEL is thus a method for producing a train of separated ultrashort radiation pulses. In addition, because the bandwidth is inversely proportional to the module length when the modules are shorter than a gain length it is possible, by using very short undulators, to produce radiation output pulses with a bandwidth significantly broader than that of a SASE FEL.

The High Brightness SASE FEL

The High Brightness SASE (HB-SASE) FEL utilises the same hardware. The SASE radiation coherence length is artificially extended by using electron beam delays to increase the relative slippage between radiation and electrons. For equal delays s a modal structure is created in the radiation spectrum, as in the Mode-Locked FEL. In the time domain this gives a pulse strongly modulated with period s. It has been found that in this case the increase in radiation coherence length is limited. However, because the mode spacing depends on the delay s then by making all the delays different it can be arranged that the sideband modes are unique for every delay s_i so that there are no modes which are continually amplified. Only the central resonant mode reaches saturation, giving a narrow bandwidth pulse with a smooth temporal structure. For the simulations in this paper the delays are based on prime number sequences [4], but good results have been observed in other studies using delays which are random [2] or steadily increasing by a common factor [3]. Studies of the evolution of the radiation coherence length l_{coh} through the system show that it grows exponentially for a distance of several gain lengths through the undulator and at saturation, for both prime number and

ISBN 978-3-95450-133-5

FEL PROPOSAL BASED ON CLIC X-BAND STRUCTURE

A. Aksoy*, Ö. Yavaş, Institute of Accelerator Technologies, Ankara, Turkey
D. Schulte, A. Latina, W. Wuensch, A. Grudiev, I. Syratchev, CERN, Geneva, Switzerland
Z. Nergiz, Nigde University Physics Department, Nigde, Turkey
M. Jacewicz, R. Ruber, V. Ziemann, Uppsala University, Uppsala, Sweden
G. D'auria, S. Di Mitri, Elettra, Trieste, Italy
M. J. Boland, T. Charles, R. Dowd, G. LeBlanc, Australian Synchrotron, Clayton, Australia
Q. Gu, W. Fang, Shangai Institute of Applied Physics, Shanghai, China
J. Clarke, D. Angal-Kalinin, STFC, Daresbury Laboratory Cockcroft Institute, Daresbury, UK
E. Gazis, A. Charitonidis, National Technical University of Athens, Greece
E. Adli, University of Oslo Department of Physics, Oslo, Norway

Abstract

A linear accelerating structure with an average loaded gradient of 100 MV/m at X-Band frequencies has been demonstrated in the CLIC study. Recently, it has been proposed to use this structure to drive an FEL linac. In contrast to CLIC the linac would be powered by klystrons not by an RF source created by a drive beam. The main advantage of this proposal is achieving the required energies in a very short distance, thus the facility would be rather compact. In this study, we present the structure choice and conceptual design parameters of a facility which could generate laser photon pulses below Angstrom. Shorter wavelengths can also be reached with slightly increasing the energy.

INTRODUCTION

X-band accelerator development has gained improvement within last ten years, motivated by the need for high-gradient accelerators for the future linear colliders in high-energy physics research [1]. Studies on accelerating structures operating at 11.4 GHz were made at SLAC and KEK, in the last two decades of the nineteen (up to 2004), for the development of a TeV-scale high energy Linear Collider, and led to achieve 65-70 MV/m accelerating gradients [2]. Design of accelerator cells [3], manufacturing [4], and characterization technique [5] have been developed. Later, significant progress have been achieved by the CERN CLIC (Compact Linear Collider) Collaboration, that has recently demonstrated the possibility to operate 12 GHz accelerating structures with an average loaded gradient higher than 100 MV/m [6], values far beyond those reached with the present S and C band technology. The development of power sources for x-band structures [7] gives opportunity this technology may represent an useful solution to get very compact and cost effective linacs for multi-GeV electron beams. More recently, after the successful operation of the new FEL light sources like LCLS, SACLA, FERMI, a stronger and more vigorous interest in X-band technology has arose. The demand for new FEL facilities is worldwide continuously increasing, spurring plans for new dedicated machines. This led to a general reconsideration of costs and spatial issues, particularly for the hard X-ray sources, driven by long and expensive multi-GeV NC linacs. For these machines the use of X-band technology can greatly reduce costs and capital investment, reducing the linac lengths and the size of buildings. To pursue this objectives, a scientific collaboration has recently been established among several laboratories, interested in FEL developments, aimed at validating the use of X-band technology for FEL based light sources [8]. The specific objectives of the collaboration will include the design, assembly and high power tests of an X-band accelerating module for FEL applications, made up of two accelerating structures, RF pulse compression and a waveguide distribution systems. Special care will be given to the operating gradients, RF breakdown fault rate, alignment issues, wake fields, and operating stabilities. The overall objective of the collaboration is to support the feasibility studies of new research infrastructures and/or the major upgrading of existing ones, using X-band technology. The work program foresees a strong interaction between FEL scientists, FEL designers and accelerator experts. Starting from the FEL output specification, a fully self consistent FEL facility design will be established (in terms of accelerator layout, major hardware choices, and FEL

MACHINE DESCRIPTION

The proposed facility is a two-stage 6 GeV linac, consisting of an S-Band injector and high-gradient X-band linac which can deliver a high-repetition rate low-emittance beam, one or several undulator sections and photon beam lines with a user facility. The proposed layout is given with Fig. 1. Expected facility length is about 550 m and basic parameters of facility is given in Table 1.

Injector

The injector is proposed to be similar to the injector at SwissFEL [9] . It is based on S-band RF gun operating at about 100 MV/m gradient and standard S-band structures operating at about 20 MV/ gradient.

Main Accelerator

The X-band accelerating structures developed for CLIC project [10] are planned to be used in main accelerating sec-

* avniaksoy@ankara.edu.tr

ISBN 978-3-95450-133-5

A NOVEL MODELING APPROACH FOR ELECTRON BEAMS IN SASE FELs

P. Niknejadi and J.M.J. Madey
University of Hawai'i at Manoa, Honolulu, HI 96822, USA

Abstract

We have recently shown that the Wheeler-Feynman analysis of the interaction of a moving charge with distant absorbers provides a perfect match to the energy radiated by two coherently oscillating charged particles (a heretofore unsolved problem in classical electrodynamics). Here we explain the need to include the Wheeler-Feynman coherent radiation reaction force as an integral part of the solution to the boundary value problem for free electron lasers (FELs) that radiate into "free space". We will also discuss how the advanced field of the absorber can interact with the radiating particles at the time of emission. Finally we will introduce and explore the possibility of improving the temporal coherence of self amplified spontaneous emission (SASE) FELs as well as the possibility of optimizing the spectrum of their emitted radiation via altering the structure of their targets by useing the Wheeler-Feynman coherent radiation reaction force in the analysis of FEL operation.

INTRODUCTION

In the past few years the successful operation of x-ray FELs based on the SASE principle has made them a powerful new tool for addressing fundamental questions in biology, chemistry and nano-technology [1]. On the other hand the fundamental principle that the SASE FEL's rely on, the theory of radiation in classical electrodynamics, has a few unresolved questions of its own. For instance, since classical field theory has, for about a century, failed to provide a non-diverging solution and origin for the radiation reaction field, our understanding of the process of coherent radiation in the classical limit with respect to conservation of energy is not complete. The radiation reaction field is the electric field responsible for energy conservation in the process of radiation.

The analysis provided by Wheeler and Feynman, in their 1945 paper "Interaction with the Absorber as the Mechanism of Radiation," for the first time yields an exact match between the radiated power of oscillating particles and the rate of change of the particle's kinetic energy [2]. The conceptual backbone of the Wheeler and Feynman model has been debated for many years and raises a number of questions about the nature of interactions of fields and particles. But it has been shown that the model is consistent with the quantum electrodynamics [3] and Dirac's theory of single particle radiation reaction force [4]. In their paper, Wheeler and Feynman did not consider the coherent radiation emitted by multiple accelerated charges. However, we have shown that the Wheeler-Feynman derivation for a moving charge interacting with the absorber also provides a perfect match to the radiated energy in the case of two or more coherently oscillating charged particles [5].

These developments seem likely to clarify our understanding and contribute to the further advancement of FEL light sources, and possibly improve the temporal coherence of SASE FELs. With the rapid advancement and reliance upon these sources, this is a good time to consider the effect of the Wheeler-Feynman approach on current technology. We also hope that this approach will provide further insight into physics underlying the behavior of the of these powerful devices as well as additional means to control the spectral intensity and bandwidth in addition to the operating wavelength.

The description of advanced interactions as set forth in the Wheeler Feynman paper has led us to explore both the engineering implications for the design of SASE FEL systems and possible new approaches for the investigation of the distribution of distant matter in the universe as well [6].

APPLYING WHEELER FEYNMAN ANALYSIS TO COLLECTION OF COHERENTLY OSCILLATING PARTICLES

Wheeler and Feynman were able to demonstrate that, when formulated in the language of covariant action-at-a-distance, the solution to the boundary value problem corresponding to an oscillating particle within a spherical absorbing shell of arbitrary density is dominated by the interference of the retarded and advanced forces originating in the accelerated and absorbing particles. This leads to a force on the accelerated particle exactly equal to that needed to match the power carried by radiation to the particles in the absorbing shell. In their 1949 paper, their quantitative findings also show that these interactions are only evident in the immediate vicinity of the radiating/absorbing charges, and converge to the conventional retarded electrodynamics at larger distances from the radiating charge [7].

Case of Two Coherently Oscillating Particles

Consider two coherently oscillating charged particles displaced by distance "r" in an arbitrary direction. If the displacement r has an angle α with respect to the direction of motion of the coherently oscillating charged particles, the integral of Poynting vector (the radiated power) is defined Equation 1. When the charges oscillate perpendicular to the direction of their separation vector, $\alpha = \pi/2$, the power radiated is given by Equation 2.

ISBN 978-3-95450-133-5

STATISTICAL PROPERTIES OF THE RADIATION FROM SASE FEL OPERATING IN A POST-SATURATION REGIME WITH AND WITHOUT UNDULATOR TAPERING

E.A. Schneidmiller, M.V. Yurkov, DESY, Hamburg, Germany

Abstract

We describe statistical and coherence properties of the radiation from x-ray free electron lasers (XFEL) operating in the post-saturation regime. We consider practical case of the SASE3 FEL at European XFEL. We perform comparison of the main characteristics of X-ray FEL operating in the post-saturation regime with and without undulator tapering: efficiency, coherence time and degree of transverse coherence.

INTRODUCTION

Radiation from Self Amplified Spontaneous Emission Free Electron Laser (SASE FEL) [1, 2] has limited spatial and temporal coherence. This happens due to start-up of the amplification process from the shot noise in the electron beam. The fluctuations of the electron beam density are uncorrelated in time and space, and many radiation modes are excited at the initial stage of amplification. As a rule, ground spatial TEM_{00} mode with highest gain dominates, and the degree of transverse coherence grows in the exponential amplification stage. Radiation wave slips forward with respect to the electron beam by one wavelength per one undulator period. This relative slippage on the scale of the field gain length gives an estimate for coherence length. Both, degree of transverse coherence and coherence time reach maximum value in the end of the exponential regime of amplification, and then degrade visibly in the nonlinear regime. Maximum degree of transverse coherence of about 0.95 is reached for the values of diffraction parameter about 1. For large values of the diffraction parameter the degree of transverse coherence falls down due to poor mode selection, i.e. mode degeneration takes place. For small values of the diffraction parameter the degree of transverse coherence falls down due to more poor longitudinal coherence [3–6].

Radiation from SASE FEL with planar undulator contains visible contribution of odd harmonics. Parameter range where intensity of higher harmonics is defined mainly by nonlinear beam bunching in the fundamental harmonic has been intensively studied in refs. [7–16]. Comprehensive studies of the nonlinear harmonic generation have been performed in [16] in the framework of the one-dimensional model. General features of harmonic radiation have been determined. It was found that coherence time at saturation falls inversely proportional to harmonic number, and relative spectrum bandwidth remains constant with harmonic number. Comprehensive study of the coherence properties of the odd harmonics in the framework of 3D model have been performed in [17]. We considered parameter range when intensity of higher harmonics is mainly defined by nonlinear harmonics generation mechanism. The case optimized XFEL has been considered. Using similarity techniques we present universal dependencies for the main characteristics of the SASE FEL covering all practical range of optimized X-ray FELs.

Application of the undulator tapering [18] allows to increase conversion efficiency to rather high values [19–27]. New wave of interest to the undulator tapering came with x-ray free electron lasers [28–32] (see [33–36] and references therein). It is used now not only as demonstration tool [37], but as a routine tool at operating x-ray FEL facilities LCLS and SACLA.

There are several reasons why we performed the present study. The first reason is that SASE3 FEL at the European XFEL operating at long wavelengths can not be tuned as optimized FEL [4] due to limitation on minimum value of the focusing beta function, and dedicated study is required for description of coherence properties. Another reason is that in the parameter range of SASE3 FEL linear mechanism of harmonic generation is essential which results in much higher power of higher odd harmonic with respect to the case of nonlinear harmonic generation [33, 38]. Finally, we compare coherence properties for both, fundamental and the third harmonic for the case of untapered undulator and undulator with optimized tapering. We show that the brilliance of the fundamental harmonic of the radiation from SASE FEL with optimized tapering can be increased by a factor of 3 with respect to untapered case.

GENERAL DEFINITIONS AND SIMULATION PROCEDURE

The first-order transverse correlation function is defined as

$$\gamma_1(\vec{r}_\perp, \vec{r}\prime_\perp, z, t) = \frac{\langle \tilde{E}(\vec{r}_\perp, z, t)\tilde{E}^*(\vec{r}\prime_\perp, z, t)\rangle}{\left[\langle|\tilde{E}(\vec{r}_\perp, z, t)|^2\rangle\langle|\tilde{E}(\vec{r}\prime_\perp, z, t)|^2\rangle\right]^{1/2}} ,$$

where $\tilde{E}$ is the slowly varying amplitude of the amplified wave. For a stationary random process γ_1 does not depend on time, and the degree of transverse is:

$$\zeta = \frac{\int |\gamma_1(\vec{r}_\perp, \vec{r}\prime_\perp)|^2 I(\vec{r}_\perp) I(\vec{r}\prime_\perp)\, \mathrm{d}\,\vec{r}_\perp\, \mathrm{d}\,\vec{r}\prime_\perp}{[\int I(\vec{r}_\perp)\, \mathrm{d}\,\vec{r}_\perp]^2} ,$$

where $I(\vec{r}_\perp) = \langle|\tilde{E}(\vec{r}_\perp)|^2\rangle$. The first order time correlation function, $g_1(t, t')$, is calculated in accordance with the definition:

ISBN 978-3-95450-133-5

OPTIMIZATION OF A HIGH EFFICIENCY FEL AMPLIFIER

E.A. Schneidmiller, M.V. Yurkov, DESY, Hamburg, Germany

Abstract

The problem of an efficiency increase of an FEL amplifier is now of great practical importance. Technique of undulator tapering in the post-saturation regime is used at the existing x-ray FELs LCLS and SACLA, and is planned for use at the European XFEL, Swiss FEL, and PAL XFEL. There are also discussions on the future of high peak and average power FELs for scientific and industrial applications. In this paper we perform detailed analysis of the tapering strategies for high power seeded FEL amplifiers. Application of similarity techniques allows us to derive universal law of the undulator tapering.

INTRODUCTION

Efficiency of FEL amplifier with untapered undulator is defined by the value of the FEL parameter ρ. Application of the undulator tapering [1] allows to increase conversion efficiency to rather high values. In the framework of the one-dimensional theory the status of the problem of tapering has been settled, and it is generally accepted that optimum law of the undulator tapering is quadratic with the linear correction for optimization of the particle's capture in the decelerating potential [2–7]. Similar physical situation occurs in the FEL amplifier with waveguide with small waveguide parameter. In this case radiation is confined with the waveguide. Physical parameters of FEL amplifiers operating in infrared, visible, and x-ray wavelength range are such that these devices are described in the framework of three dimensional theory with an "open" electron beam, i.e. physical case of pure diffraction in a free space. In this case diffraction of the radiation is essential physical effect influencing optimization of the tapering process. Discussions and studies on optimum law of the undulator tapering in 3D case are in the progress for more than 20 years. Our previous studies were mainly driven by occasional calculations of perspective FEL systems for high power scientific (for instance, FEL based $\gamma\gamma$ - collider) and industrial applications (for instance, for isotope separation, and lithography [8–10]). New wave of interest to the undulator tapering came with x-ray free electron lasers. It is used now not only as demonstration tool [11], but as a routine tool at operating x-ray FEL facilities LCLS and SACLA.

During an intermediate physical discussion on the subject of tapering we pointed out that asymptotical law of the undulator tapering for FEL amplifier with "open" beam should be linear in terms of the detuning parameter [7]. The origin for this statement is that radiation power of the bunched electron beam grows linearly with the undulator length for very long undulator. However, the problem of optimum matching of the electron beam into the regime of coherent deceleration is still open. Practical calculations of specific systems yielded in several empirical laws using different polynomial dependencies, application of tricks with detuning jumps, etc (see [12, 13] and references therein).

In this paper we perform global analysis of the parameter space of seeded FEL amplifier and derive universal law of the undulator tapering defined by the only diffraction parameter.

BASIC RELATIONS

We consider axisymmetric model of the electron beam. It is assumed that transverse distribution function of the electron beam is Gaussian, so rms transverse size of matched beam is $\sigma = \sqrt{\epsilon\beta}$,where $\epsilon = \epsilon_{\mathrm{n}}/\gamma$ is rms beam emittance, γ is relativistic factor, and β is focusing beta-function. In the following we consider rectified case of the "cold" electron beam and neglect space charge effects. Under this assumptions the FEL amplifier is described by the diffraction parameter B [7], and detuning parameter $\hat{C}$:

$$B = 2\Gamma\sigma^2\omega/c\ , \qquad \hat{C} = C/\Gamma\ , \qquad (1)$$

where $\Gamma = \left[I\omega^2\theta_{\mathrm{s}}^2 A_{\mathrm{JJ}}^2/(I_{\mathrm{A}}c^2\gamma_z^2\gamma)\right]^{1/2}$ is the gain parameter, $C = 2\pi/\lambda_{\mathrm{w}} - \omega/(2c\gamma_z^2)$ is the detuning of the electron with the nominal energy $\mathcal{E}_0$. In the following electron energy is normalized as $\hat{P} = (E - E_0)/(\rho E_0)$, where $\rho = c\gamma_z^2\Gamma/\omega$ is the efficiency parameter[1]. The following notations are used here: I is the beam current, $\omega = 2\pi c/\lambda$ is the frequency of the electromagnetic wave, $\theta_{\mathrm{s}} = K_{\mathrm{rms}}/\gamma$, K_{rms} is the rms undulator parameter, $\gamma_z^{-2} = \gamma^{-2} + \theta_{\mathrm{s}}^2$, $k_{\mathrm{w}} = 2\pi/\lambda_{\mathrm{w}}$ is the undulator wavenumber, $I_{\mathrm{A}} = 17$ kA is the Alfven current, $A_{\mathrm{JJ}} = 1$ for helical undulator and $A_{\mathrm{JJ}} = J_0(K_{\mathrm{rms}}^2/2(1 + K_{\mathrm{rms}}^2)) - J_1(K_{\mathrm{rms}}^2/2(1 + K_{\mathrm{rms}}^2))$ for planar undulator. Here J_0 and J_1 are the Bessel functions of the first kind.

Equations, describing motion of the particles in the ponderomotive potential well of electromagnetic wave and undulator get simple form when written down in normalized form (see, e.g. [7]):

$$\frac{d\Psi}{d\hat{z}} = \hat{C} + \hat{P}, \qquad \frac{d\hat{P}}{d\hat{z}} = U\cos(\phi_U + \Psi)\ , \qquad (2)$$

where $\hat{z} = \Gamma z$, and U and ϕ_U are amplitude and phase of effective potential. Energy change of electrons is small in the exponential stage of amplification, $\hat{P} \ll 1$, and process of electron bunching in phase Ψ lasts for long distance, $\hat{z} \gg 1$. Situation changes drastically when electron energy change $\hat{P}$ approaches to the unity. The change of phase on the scale of $\Delta\hat{z} \simeq 1$ becomes to be fast, particles start to slip in phase Ψ which leads to the debunching of the electron beam modulation, and growth of the radiation power is saturated. operation. Undulator tapering [1], i.e. adjustment of the detuning

[1] Note that it differs from 1-D definition by the factor $B^{1/3}$ [7].

ISBN 978-3-95450-133-5

AN OVERVIEW OF THE RADIATION PROPERTIES OF THE EUROPEAN XFEL

E.A. Schneidmiller, M.V. Yurkov, DESY, Hamburg, Germany

Abstract

We present an overview of the radiation properties of the European XFEL based on recently accepted strategy of operation at the fixed set of electron energies (8.5 GeV, 12 GeV, 14 GeV, and 17.5 GeV), baseline parameters if the electron beam, and new set undulator parameters. We also discuss potential extension of the parameter space which does not require new hardware and can be realized at a very early stage of the European XFEL operation.

INTRODUCTION

Construction of the European XFEL [1] entered final stage: underground tunnels and infrastructure are ready, and first pieces of the equipment has been already installed [2]. Superconducting accelerator will provide energy of electrons up to 17.5 GeV. It operates in the burst mode with 10 Hz repetition rate of 0.6 ms pulse duration. Each pulse brings train of up to 2700 electron bunches (4.5 MHz repetition rate). Three undulators will be installed at the first stage: SASE1, SASE2, and SASE3. SASE3 undulator is placed sequentially after SASE1 undulator in the same electron beamline. All undulators have similar mechanical design. Length of the undulator module is equal to 5 meters. Length of undulator intersection is equal to 1.1 m. undulators SASE1 and SASE2 are identical: period length is 40 mm, number of modules is 35, range of gap variation is 10 to 20 mm. Undulator SASE3 has period of 68 mm, 10 to 25 mm gap tunability range, and consists of 21 module. Most portion of the undulator modules has been manufactured, and magnetic measurements and tuning are going on [3]. Design and construction of user's end station (instruments) is on track as well. Requirements by users are summarized and analyzed in a proper way to provide maximum opportunities for every instrument and experiment [4].

BASELINE PARAMETERS

Baseline parameters of the European XFEL passed two major corrections: in 2006 [1] and 2010 [4–6]. Operating range for bunch charge is from 20 pC to 1 nC, peak current is 5 kA, and normalized rms emittance is between 0.3 mm-mrad and 1 mm-mrad depending on bunch charge [5]. There are two changes in the baseline option since last update in 2010. Tunability range of undulators has been corrected on the base of magnetic measurements [3], and in terms of undulator parameter is 1.65 - 4 and 4 - 9 for SASE1/2 and SASE3, respectively. Tunability range in terms of $\lambda_{\max}/\lambda_{\min}$ is 3.5 for SASE1/2 and 4.6 for SASE3. Reduction of tunability range caused the change of operating energies providing required flexibility for simultaneous operation of different beamlines and instruments. Now four operating points in the electron energy are fixed: 17.5 GeV, 14 GeV, 12 GeV, and 8.5 GeV [7]. Figures 1 and 2 show an overview of the main photon beam properties of the European XFEL for two values of the baseline parameters for the bunch charge of 0.1 nC and 1 nC. Calculations have been performed with FEL simulation code FAST [8]. Left and right columns in these plots correspond SASE1/2 and SASE3 undulator, and allow visual tracing of the operating wavelength bands, pulse energy, and brilliance as function of the electron energy. General tendencies are that operation with higher charges provides higher pulse energy and higher average brilliance. Qualitative difference in the behavior of the brilliance at 0.1 nC and 1 nC for SASE1/2 requires some clarification. It originates from two reasons. The first reason relates to optimization procedure which corresponds to the choice of optimum focusing beta function providing maximum power gain [9, 10]. Optimization procedure suggests smaller values of focusing beta function for smaller emittances. However, there is always technical limitation on the minimum focusing beta function (15 m in our case). As a result, SASE3 and 0.1 nC option of SASE1 operate with beta function defined by technical limit of 15 m, while optimum beta function for high charge (1 nC) option of SASE1 is above 15 m, and its values depend on operating point in the radiation wavelength and in the electron energy. Another factor defining peculiar behavior of brilliance at high charge and small wavelength relates to degradation of coherence properties of the radiation due to large value of the emittance [10]. This effect is responsible for the reduction of the brilliance for 1 nC case at short wavelengths.

Detailed parameters of the radiation together with 3D field maps are being compiled in the photon data base of the European XFEL [11, 12]. Currently this data base is used in the test mode for optimization of the photon beam transport and imaging experiment [13,14]. When user interface will be finally settled, photon data base will be open for free external access, and can be used by users for planning experiments.

Operation of SASE3

Properties of the radiation from SASE3 presented in Figs. 1 and 2 assume that electron beam is not disturbed by FEL interaction in the SASE1 undulator. Decoupling of SASE3 and SASE1 operation can be performed with an application of betatron switcher [6, 15] (see Fig. 3). Feedback kickers can be used to test and operate this option at the initial stage. In case of positive results dedicated kickers need to be installed [5].

Operation of SASE3 as an afterburner of SASE1 is also possible, but with reduced range of accessible wavelengths, and reduced power (see Fig. 4). General problem is that

ISBN 978-3-95450-133-5

PROSPECTS FOR CW OPERATION OF THE EUROPEAN XFEL IN HARD X-RAY REGIME

R. Brinkmann, E.A. Schneidmiller, J. Sekutowicz, M.V. Yurkov, DESY, Hamburg, Germany

Abstract

The European XFEL will operate nominally at 17.5 GeV in SP (short pulse) mode with 0.65 ms long bunch train and 10 Hz repetition rate. A possible upgrade of the linac to CW (continuous wave) or LP (long pulse) modes with a corresponding reduction of electron beam energy is under discussion since many years. Recent successes in the dedicated R&D program allow to forecast a technical feasibility of such an upgrade in the foreseeable future. One of the challenges is to provide sub-Ångstrom FEL operation in CW and LP modes. In this paper we perform a preliminary analysis of a possible operation of the European XFEL in the hard X-ray regime in CW and LP modes with the energies of 7 GeV and 10 GeV, respectively. We show that, with reasonable requirements on electron beam quality, lasing on the fundamental will be possible in sub-Ångstrom regime. As an option for generation of brilliant photon beams at short wavelengths we also consider harmonic lasing that has recently attracted a significant attention.

INTRODUCTION

The European XFEL [1] will be the first hard X-ray FEL user facility based on superconducting accelerator technology, and will provide unprecedented average brilliance of photon beams. The XFEL linac will operate nominally at 17.5 GeV in a burst mode with up to 2700 bunches within a 0.65 ms long bunch train and 10 Hz repetition rate. Even though the RF pulses are much longer than those available at X-ray FEL facilities, based on normal conducting accelerators, in the context of this paper we will call this SP (short pulse) mode of operation.

In order to cope with high repetition rate within a pulse train, special efforts are being made to develop fast X-ray instrumentation [2]. Still, many user experiments would strongly profit from increasing distance between X-ray pulses while lengthening pulse trains and keeping total number of X-ray pulses unchanged (or increased). Such a regime would require an operation of the accelerator with much longer RF pulses (LP, or long pulse mode), or even in CW (continuous wave) mode as a limit. A possible upgrade of the XFEL linac to CW or LP modes with a corresponding reduction of electron beam energy is under discussion since many years [3]. Recent successes in the dedicated R&D program [4] allow to forecast a technical feasibility of such an upgrade in the foreseeable future.

One of the main challenges of CW upgrade is to provide sub-Ångstrom FEL operation which is, obviously, more difficult with lower electron energies. One can consider improving the electron beam quality as well as reducing the undulator period as possible measures. An additional possibility is a harmonic lasing [5–8] that has recently attracted a significant attention [8]. Harmonic lasing can extend operating range of an X-ray FEL facility and provide brilliant photon beams of high energies for user experiments.

CW UPGRADE OF THE LINAC

A possible upgrade of the XFEL linac to CW or LP modes holds a great potential for a further improvement of X-ray FEL user operation, including a more comfortable (for experiments) time structure, higher average brilliance, improved stability etc. The drawbacks are a somewhat smaller peak brilliance and a reduced photon energy range, both due to a lower electron beam energy. Both disadvantages can, however, be minimized by an improvement of the electron beam quality and application of advanced FEL techniques. Moreover, one can keep a possibility to relatively quickly switch between SP and CW modes thus greatly improving the flexibility of the user facility.

For a CW upgrade of the linac, the following main measures will be needed [4]:

i) Upgrade of the cryogenic plant with the aim to approximately double its capacity;

ii) Installation of new RF power sources: compact Inductive Output Tubes (IOTs);

iii) Exchange of the first 17 accelerator modules by the new ones (including a larger diameter 2-phase helium tube, new HOM couplers etc.) designed for operation in CW mode with a relatively high gradient (up to 16 MV/m). This ensures that the beam formation system (up to the last bunch compressor) operates with a similar energy profile as it does in SP mode. Then 12 old accelerating modules are relocated to the end of the linac;

iiii) Installation of a new injector generating a high-brightness electron beam in CW mode.

The first two items can be realized in a straightforward way; the third one is based on the steady progress of the TESLA technology [9] and is not particularly challenging. Until recently the main uncertainty was connected with the absence of CW injectors providing a sufficient quality of electron beams. However, last year there was an experimental demonstration of small emittances (for charges below 100 pC) at a CW photoinjector using a DC gun followed immediately by acceleration with superconducting cavities [10]. The measured parameters are already sufficient for considering this kind of injector as a candidate for CW upgrade of the XFEL linac (although the operation would be limited to low charge scenarios). As an alternative one can consider a superconducting RF gun that can potentially produce also larger charge bunches with low emittances (the progress reports can be found in [11, 12]) or even a normal conducting

ISBN 978-3-95450-133-5

SUPPRESSION OF THE FUNDAMENTAL FREQUENCY FOR A SUCCESSFUL HARMONIC LASING IN SASE FELS

E.A. Schneidmiller, M.V. Yurkov, DESY, Hamburg, Germany

Abstract

Harmonic lasing in X-ray FELs has recently attracted a significant attention and is now seriously considered as a potential method for generation of brilliant photon beams at short wavelengths. It is clear, however, that for a successful harmonic lasing one has to suppress the fundamental. In this paper we discuss different methods for such a suppression: phase shifters, intraundulator spectral filtering, and switching between the 3rd and the 5th harmonics.

INTRODUCTION

Harmonic lasing in single-pass high-gain FELs [1–7] is the radiative instability at an odd harmonic of the planar undulator developing independently from lasing at the fundamental. Contrary to nonlinear harmonic generation (which is driven by the fundamental in the vicinity of saturation), harmonic lasing can provide much more intense, stable, and narrow-band FEL beam if the fundamental is suppressed. The most attractive feature of saturated harmonic lasing is that the brilliance of a harmonic is comparable to that of the fundamental. Indeed, a good estimate for the saturation efficiency is $\lambda_w/(hL_{sat})$, where λ_w is the undulator period, L_{sat} is the saturation length, and h is harmonic number. At the same time, the relative rms bandwidth has the same scaling. If we consider lasing at the same wavelength on the fundamental and on a harmonic (with the retuned undulator parameter K), transverse coherence properties are about the same since they are mainly defined by emittance-to-wavelength ratio. Thus, also the brilliance is about the same in both cases. In many cases, however, the saturation length for harmonics is significantly shorter than that of the fundamental at the same wavelength. As a consequence, for a given undulator length one can reach saturation on harmonics at a shorter wavelength. It was shown in a recent study [6] that the 3rd and even the 5th harmonic lasing in X-ray FELs is much more robust than usually thought, and can be widely used at the present level of accelerator and FEL technology.

For a successful harmonic lasing the fundamental mode must be suppressed. Otherwise it saturates earlier and spoils the longitudinal phase space of the electron beam thus preventing further exponential growth of harmonics. In this paper we discuss and compare different methods of suppression.

PHASE SHIFTERS

An elegant method to disrupt the fundamental without affecting the third harmonic lasing was suggested in [4]: one can use phase shifters between undulator modules. If phase shifters are tuned such that the phase delay is $2\pi/3$ (or $4\pi/3$)

Table 1: Parameters of Electron Beam and Undulator

Electron beam	Value
Energy	1.25 GeV
Charge	150 pC
Peak current	2.5 kA
Rms normalized slice emittance	0.5 µm
Rms slice energy spread	250 keV
Rms pulse duration	24 fs

Undulator	Value
Fundamental wavelength	3.9 nm
Period	2.3 cm
K_{rms}	1
Beta-function	7 m
Net magnetic length	25 m

for the fundamental, then its amplification is disrupted. At the same time the phase shift is equal to 2π for the third harmonic, i.e. it continues to get amplified without being affected by phase shifters. We define phase shift in the same way as it was done in [4] in order to make our results compatible with the previous studies. For example, the shift $2\pi/3$ corresponds to the advance of a modulated electron beam with respect to electromagnetic field by $\lambda/3$.

Since there are two possible phase shifts, one can consider different ways of their distributions along the undulator. Here we compare four strategies studied in the literature [4–6, 8] by performing simulations with the code FAST [9]. For the sake of comparison we take a set of parameters from a proposal for FLASH upgrade for harmonic lasing up to 1 keV [7]. The parameters of the beam and the undulator are summarized in Table 1. The undulator is supposed to be made of 3 m long segments with integrated phase shifters (in addition to phase shifters between the segments) such that the distance between the phase shifters is 0.5 m.

In the following we present the results of simulations with four different ways of distribution of phase shifters.

Consecutive Use of the Same Phase Shifts

This variation of the phase shifters method was considered in [4]. The simulations in [4] were done for the case of a monochromatic seed, and the results cannot be applied for a SASE FEL. The reason is that in the latter case the amplified frequencies are defined self-consistently, i.e. there is frequency shift (red or blue) depending on positions and magnitudes of phase kicks. This leads to a significantly weaker suppression effect. We illustrate this for the SASE FEL with the parameters from Table 1.

ISBN 978-3-95450-133-5

DESIGN STUDY FOR THE PEHG EXPERIMENT AT SDUV-FEL*

C. Feng, H.X. Deng#, M. Zhang, T. Zhang, X.T. Wang, W. Zhang, B. Liu, D. Wang, Z.T. Zhao
Shanghai Institute of Applied Physics, CAS, Shanghai 201800, China

Abstract

In this paper, design studies for the proof-of-principle experiment of the recently proposed phase-merging enhanced harmonic generation (PEHG) mechanism are presented. A dogleg and a new designed transverse gradient undulator should be added in the undulator system of SDUV-FEL to perform the phase-merging effect. With the help of 3D simulation codes, we show the possible performance of PEHG with the realistic parameters of SDUV-FEL.

INTRODUCTION

High-gain seeded FEL schemes have been developed for producing stable and fully temporal coherence laser pulse from deep UV down to the x-ray regime. The most famous frequency up-conversion scheme is so called the high-gain harmonic generation (HGHG) [1], which uses an external laser pulse to interact with the electron bunch for the generation of coherent micro-bunching. The property of HGHG output is a direct map of the seed laser's attributes, which ensures high degree of temporal coherence and small pulse energy fluctuations with respect to self-amplified spontaneous emission (SASE) [2]. However, significant bunching at higher harmonics usually needs to strengthen the energy modulation in HGHG, which will result in a degradation of the amplification process of FEL. Thus the requirement of FEL amplification on the beam energy spread prevents the possibility of reaching short wavelength in a single stage HGHG.

Recently, a novel seeded FEL scheme termed phase-merging enhanced harmonic generation (PEHG) [3, 4], has been proposed for significantly improving the frequency up-conversion efficiency of harmonic generation FELs. Generally, a transversely dispersed electron beam and a transverse gradient undulator (TGU) [5] are needed in PEHG for performing the phase-merging effect purpose: when the transversely dispersed electrons passage through the TGU, around the zero-crossing of the energy modulation, electrons with the same energy will merge into a same longitudinal phase.

Several ways have been proposed [3, 4, 6] for performing the phase-merging effect as shown in Fig. 1, where doglegs are added before modulators for transversely dispersing the electron bunch. Fig. 1(a) shows the initial proposed PEHG scheme, where a short TGU is used for the energy modulation and to precisely manipulate the electrons in the horizontal dimension. It is found later that these two functions of TGU can be separately performed by employing a modified design, as shown in Fig. 1 (b). In this scheme, a normal modulator is used for the energy modulation, and the TGU is responsible only for transverse manipulation of the electrons, a design that will be much more flexible for practical operation. Fig. 1(c) shows a much simpler scheme that adopts a normal modulator and a wave-front tilted seed laser pulse to realize the phase-merging effect. Analytical and numerical investigations indicate that all these three schemes have the potential of generating ultra-high harmonic bunching factor with a relatively small energy modulation. To demonstrate these theoretical predictions, a proof-of-principle experiment for PEHG has been planned at Shanghai deep ultraviolet free-electron laser facility (SDUV-FEL) [7, 8]. In this paper, we present the design studies for this experiment.

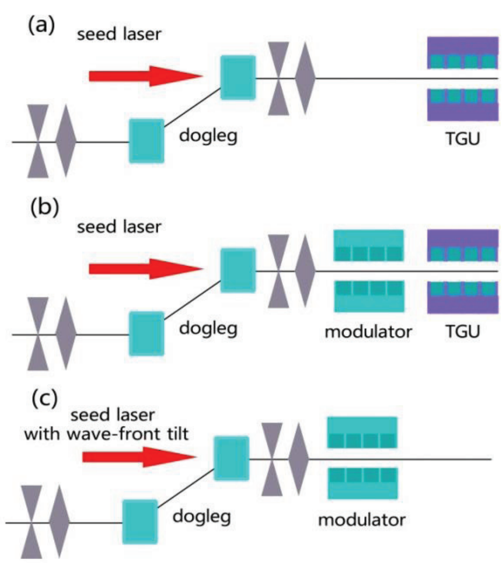

Figure 1: Modulation schemes for PEHG.

LAYOUT AND MAIN PARAMETERS

The SDUV-FEL is an integrated multi-purpose test facility for seeded FEL principles, capable of testing various seeded FEL working modes. A new beam line will be added after the linac of SDUV-FEL for the PEHG and Thomson scattering experiments in this year. The layout of the PEHG experiment is shown in Fig. 2. A dogleg is adopted for switching the electron bunch and introducing a large transverse dispersion into the electron beam. After that, a conventional modulator and a new designed TGU, as shown in Fig. 3, are employed for energy modulation and manipulating the electron beam. The energy modulation will be converted to density modulation by the dispersion section (DS). Then the coherently bunched beam is sent through the radiator for high harmonic radiation.

*Work supported by National Natural Science Foundation of China (11475250, 11175240, 11322550 and 11205234)
#denghaixiao@sinap.ac.cn

ISBN 978-3-95450-133-5

LASER SEEDING SCHEMES FOR SOFT X-RAYS AT LCLS-II

G. Penn, LBNL, Berkeley, CA, USA
P. Emma, E. Hemsing, G. Marcus, T.O. Raubenheimer, L. Wang, SLAC, Menlo Park, CA, USA

Abstract

The initial design for LCLS-II incorporates both SASE and self-seeded configurations. Increased stability and/or coherence than is possible with either configuration may be provided by seeding with external lasers followed by one or more stages of harmonic generation, especially in the soft x-ray regime. External seeding also allows for increased flexibility, for example the ability to quickly vary the pulse duration. Studies of schemes based on high-gain harmonic generation and echo-enabled harmonic generation are presented, including realistic electron distributions based on tracking through the injector and linac.

INTRODUCTION

In addition to SASE [1] and self-seeding [2, 3] schemes, LCLS-II [4] may also incorporate seeding using external lasers. Benefits include more control over the x-ray pulse, better shot-to-shot stability, and possibly a narrower spectrum. The use of external lasers may have an impact on repetition rate and tends to reduce the energy of the final x-ray pulse. In addition, upshifting by very large harmonics from the laser wavelength introduces new challenges. Here we discuss designs for both the two-stage high-gain harmonic generation (HGHG) and single-stage echo-enabled harmonic generation (EEHG) seeding schemes, and compare their performance. Two-stage HGHG with a fresh-bunch delay has been demonstrated at FERMI@Elettra [5] with excellent performance down to the 65th harmonic (4 nm). EEHG has been demonstrated at NLCTA [6] up to the 15th harmonic (160 nm).

ELECTRON BEAM AND UNDULATOR PARAMETERS

The simulations shown below use particles obtained from two start-to-end (S2E) simulations of the linac accelerating the beam to 4 GeV. One simulation uses a 100 pC bunch and the other a 300 pC bunch. Not all aspects of longitudinal dynamics have been modelled, however. The nominal parameters for the electron beam and the main undulator sections for producing radiation are given in Table 1. Local parameters will vary with position along the bunch. The longitudinal phase space of the beams are shown in Fig. 1, and the current profiles are shown in Fig. 2. Compared to the 100 pC bunch, the 300 pC bunch is longer, has a larger emittance and a slightly lower peak current.

The final undulators have a period of 39 mm and cover the desired tuning range from 250 eV to 1.3 keV. Here, we focus on producing radiation at 1 nm, which is the most challenging part of the tuning range. The external laser is fixed at a wavelength of 260 nm. The large overall harmonic jump presents certain challenges which will be noted below.

Table 1: Beam and Undulator Parameters for Soft X-ray Production at LCLS-II

Parameter	Symbol	Value
Electron Beam:		
Bunch charge	Q	100 — 300 pC
Electron energy	E	4 GeV
Peak current	I	1 kA
Emittance	ϵ_N	0.3 — 0.43 µm
Energy spread	σ_E	0.5 MeV
Beta function	β	15 m
Final undulators:		
Undulator period	λ_u	39 mm
Undulator segment length	L_{seg}	3.4 m
Break length	L_b	1.2 m
Min. magnetic gap	g_{min}	7.2 mm
Max. undulator parameter	K_{max}	5.48
Max. resonant wavelength	λ_{max}	5.1 nm

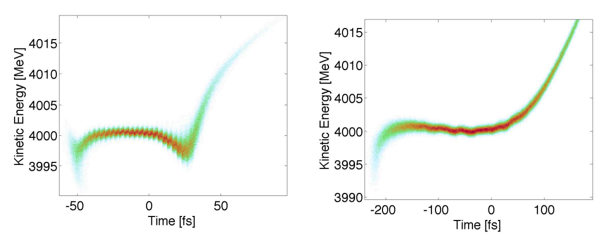

Figure 1: Longitudinal phase space for 100 pC (left) and 300 pC (right) electron bunches.

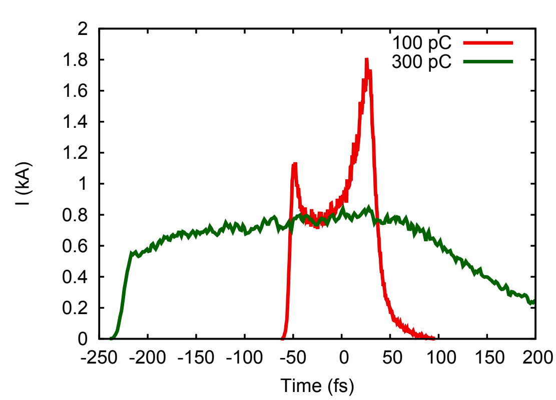

Figure 2: Current profiles for 100 pC and 300 pC electron bunches.

ISBN 978-3-95450-133-5

MEASUREMENTS OF THE FEL-BANDWIDTH SCALING WITH HARMONIC NUMBER IN A HGHG FEL *

Enrico Allaria#, Miltcho B. Danailov, William M. Fawley,
Elettra-Sincrotrone Trieste S.C.p.A., Basovizza, Italy
Luca Giannessi,
Elettra-Sincrotrone Trieste S.C.p.A., Basovizza, Italy and ENEA C.R. Frascati, Frascati (Roma), Italy
Eugenio Ferrari,
Elettra-Sincrotrone Trieste S.C.p.A., Basovizza, Italy and Università degli Studi di Trieste, Trieste, Italy

Abstract

In this work we report recent measurements done at FERMI showing the dependence of the FEL bandwidth with respect to the seed laser harmonic at which the FEL is operated. Comparison of FEL spectra for different Fourier-limit seed and chirp pulses is also reported.

THE HGHG FEL AT FERMI

FERMI is the seeded FEL system in operation at Trieste and running for user's experiment that can use high power pulses in the VUV – soft X-ray spectral range characterized by a high degree of coherence [1,2] and also variable polarization [3]. The two FELs, in operation at FERMI, in order to cover the spectral range that goes from 100 nm down to 4 nm are based on the high gain harmonic generation scheme [4]; this uses an external laser in the UV to initiate the coherent emission at his harmonics that is then amplified by the FEL process. Since the external coherent seed imposes an exact phase relation between various electrons participating to the FEL emission, the seeding is crucial for improving the longitudinal coherence. However, it has been pointed out that the method is affected, like other frequency multiplication processes, by the phase noise amplification [5]. As a consequence of the harmonic conversion, a small residual phase noise in the seeding signal could significantly deteriorate the phase of FEL radiation up to the point to destroy the longitudinal coherence.

Recently a series of numerical simulation have been done for a simplified HGHG FEL showing that as a consequence of the nonlinear process of the bunching creation the time-bandwidth product deterioration due to residual chirp in the seed laser is partially mitigated [6].

By measuring the dependency of the FEL bandwidth as a function of the FEL harmonic and of the seed laser residual chirp, we experimentally investigate the phase noise amplification process in a seeded FEL.

The Seed Laser

Since the FEL process is initiated by the seed laser and the properties of the FEL depend on the quality of the laser a lot of effort has been dedicated at FERMI to guarantee a high performance of the seed laser system, a detailed description can be found in [7]. Depending on the need of the FERMI user to have complete tunability of the FEL or not the seed pulses can be obtained either by using the third harmonic of a Ti:Sapphire laser (THG), or by the use of an Infrared Optical Parametric Amplifier (OPA) with consequent frequency up-conversion to UV. Main parameters for the two possible configurations are reported in Table 1 and Table 2.

Table 1: Seed Laser Parameters for the THG

Parameter	
Pulse length (FWHM)	120 fs
Bandwidth (FWHM)	~0.8 nm
Central Wavelength	261 nm ±1 nm
Energy per pulse	10-100 μJ

It should be noted that in the case of THG seeding the available UV pulse energy allows to use a grating compressor and compensate the linear chirp introduced by the rather complex beam-transport. However, in the case of OPA seeding at present the seed pulses cannot be compressed and contain a residual positive chirp.

Table 2: Seed Laser Parameters for the OPA in the Most Frequently Used 230-262 nm Seed Wavelength Range

Parameter	
Pulse length (FWHM)	120-150 fs
Bandwidth (FWHM)	1-1.1 nm
Central Wavelength	230-262 nm
Energy per pulse	7-50 μJ

The Electron Beam

Because electrons are the medium used in the FEL amplification, it is clear that the quality of the electron beam is another crucial parameter. In particular it has been shown how possible modulation in the longitudinal phase space can deteriorate the FEL bandwidth. For this reason the typical electron beam used for normal operations at FERMI has a moderate compression and a lot of effort is done in order to linearize the longitudinal phase space [8] and suppress the microbunching [9].

*Work partially supported by the Italian Ministry of University and Research under grants FIRB-RBAP045JF2 and FIRB-RBAP06AWK3
#enrico.allaria@elettra.eu

ISBN 978-3-95450-133-5

MEASUREMENTS OF FEL POLARIZATION AT FERMI

Enrico Allaria, Elettra-Sincrotrone Trieste S.C.p.A., Basovizza, Italy

Abstract

We report detailed quantitative characterization of different polarization states of a single-pass, externally-seeded FEL operating with variable polarization undulators in the VUV spectral range. The experiment has been performed at FERMI FEL-1 operated in the 52–26 nm wavelength range. Three different, independent polarimeter setups, installed at the end of experimental beamlines, have been used to characterize the four "pure" polarization states: horizontal, vertical, right-circular and left-circular. The impact of downstream transport optics upon the radiation polarization has been assessed; at longer wavelengths, dichroism effects lead to a non-negligible ellipticity for an originally circularly polarized state. The results from the different polarimeter setups validate each other and allow a cross-calibration of the instruments.

INTRODUCTION

FERMI user facility relies on two different seeded FELs to cover the spectral range from 100 nm down to 4 nm using a common linear accelerator. The first FEL, namely FEL-1, has been designed for the long wavelength spectral range (100 – 20 nm) and is in operation since late 2010 [1]. The second FEL, FEL-2, is based on a double high gain harmonic generation scheme to cover the spectral range from 20 down to 4 nm [2] and user dedicated experiments will start in 2015 [3]. In order to allow the FERMI users to control the radiation polarization, FERMI uses APPLE-II type undulators [4] for the FELs. Because FERMI is the first FEL user facility in the soft-x ray spectral range allowing polarization control through the use of variable polarization undulators it is important the characterization of the degree of polarization produced.

In order to allow a detailed characterization of the degree of polarization, a collaboration has been setup between the FERMI team and other laboratories to perform dedicated experiments. In the framework of this collaboration three different polarimeters have been installed at FERMI and used during one week of dedicated beamtime. The "FERMI polarization measurements" collaboration involved in addition to the FERMI commissioning team; a team from LOA and collaborators responsible for the VUV optical polarimeter [5]; a team from DESY-XFEL and collaborators responsible for the e-TOF polarimeter [6]. In addition to the to aforementioned polarimeters a third polarimeter based on polarized fluorescence has been setup by the LDM team at FERMI and collaborators [7].

In this work we briefly report about the measurement setup. For a discussion about the results of the polarization measurements we refer to the dedicated paper recently published [8].

THE LOA POLARIMETER

The LOA polarimeter is an all-optical device based on the principle described by Schäfers et al. in [9]. The system uses a polarizer followed by an analyser. The polarizer relies on the fact that, at each reflection onto optics, the s and p components of the electric field are characterised by a different delay and a different reflectivity. Both the polarizer and the analyser can be rotated independently around the propagation axis of the input light. A polarization measurement is done by scanning one of the two angles and measuring the detected signal on the analyser.

THE E-TOF POLARIMETER

The e-TOF polarimeter uses angle resolved electron spectroscopy in order to measure the degree of linear polarization of the FEL radiation. It is based on 16 independent electron time-of-flight (e-TOF) spectrometers mounted in a plane perpendicular to the FEL beam. This configuration allows one to accurately determine the angular distribution of the photoelectrons emitted by the ionizing radiation.

THE FLUERESCENCE POLARIMETER

Polarization measurements with the fluorescence polarimeter have been carried out taking advantage of the intrinsic polarization properties of fluorescence light from resonantly excited atoms. This scheme uses the conversion of polarized VUV radiation into longer wavelength radiation that has the same polarization parameters. The scheme has the advantage to allow a polarization measurement in the visible where suitable optics are easily available and has been previously used in an experiment on synchrotron radiation [10].

CONCLUSION

A dedicated experiment has been organized at FERMI for the detailed characterization of the produced radiation. The experiment involved different groups from LOA, DESY, XFEL and SLAC. Results, recently published [8] have shown the FERMI capability of producing high degree and variable polarization.

ACKNOWLEDGMENT

The Author is thankful to all the people involved in the experiment for their effort in allowing the success of the measurement campaign. Author is also indebt with the FERMI team and management for supporting the experiment.

ISBN 978-3-95450-133-5

GENERATION OF MULTIPLE COHERENT PULSES IN A SUPERRADIANT FREE-ELECTRON LASER

X. Yang, S. Seleskiy
National Synchrotron Light Source, Brookhaven National Laboratory, Upton, NY 11973, USA
L. Giannessi, Elettra-Sincrotrone, Trieste, S.C.p.A., Basovizza, and ENEA C.R. Frascati, Italy

Abstract

We analyze the structure of the tail of a superradiant pulse, which is constituted by a train of trailing-pulses with decaying amplitudes. We show how a trailing pulse, with phase advance from the leading pulse, is generated at the falling edge of the leading pulse, where the corresponding phase space is deeply saturated and the electrons become de-trapped by the reduced ponderomotive potential. Once the trailing pulse gains enough energy, it generates a second trailing pulse, and the process takes place again. By performing detailed simulations of the resulting electron phase space distribution and the FEL pulse spectral and temporal structure with PERSEO, we confirm that the deformation and re-bunching of the longitudinal phase space create a sequence of pulses.

INTRODUCTION

The free-electron laser (FEL) is a tunable source of coherent radiation, ranging from terahertz (THz) waves to hard X-rays, with the capability for femtosecond time resolution. Progress was made recently in single-pass FELs in moving toward the X-ray region of the spectrum, such as the self-amplified spontaneous emission (SASE) FEL that successfully lased from soft X-rays down to 1.5Å [1,2], and the high-gain harmonic generation (HGHG) FEL [3] pioneered at Brookhaven [4] and now implemented in a facility at Elettra-Sincrotrone Trieste, where FERMI [5,6] provides radiation for user experiments in the VUV and soft X-ray wavelength range. One of the main advantages of the HGHG and laser-seeded FEL over the SASE FEL is that they produce not only transversely, but also temporally coherent pulses. In contrast, SASE radiation starts from the initial shot-noise of the electron beam, so that the resulting radiation exhibits excellent spatial- , but a rather poor temporal-coherence.

In this report, we present numerical evidence for a slippage-dominant superradiance FEL interaction regime, wherein the emitted main FEL pulse is followed by multiple trailing pulses, which we dubbed a "trailing-pulse regime". This dynamic behavior is guaranteed in the circumstance of an ultra-short seed pulse with the power beyond saturation [7,8]; it may be important for the existing and next-generation short-wavelength-seeded FELs, such as the FERMI, and the LCLS-II [9]. A deep understanding and controlling of these regimes are essential for optimizing the power as well as the quality of FEL sources, features demanded by the user communities. Using the Perseo simulation [10], we investigated the behaviors of the seeded FEL, and obtained new insights on the trailing pulse generation that we interpreted in terms of the fragmentation of the most significantly bunched electrons by the main radiation pulse in the longitudinal phase (LPS) into new buckets, which are responsible for the trailing pulses. Here, the term "bucket" denotes the electric field of a radiation pulse that assures longitudinal focusing, thereby constraining the electron's motion to a stable region in LPS.

The mechanism of FEL amplification commonly is analyzed in three steps: energy modulation, exponential growth, and saturation. In the first step, energy is exchanged between the electrons and the radiation, leading to an energy modulation, and further, to a density modulation (microbunching) of the electrons at the resonant wavelength $\lambda_r = \lambda_w(1+K^2/2)\ /\ (2\gamma_r^2)$, determined by the electron beam's energy $E_r = mc^2\gamma_r$. $K = eB_w/mck_w$ is the dimensionless undulator parameter, and λ_w, k_w, and B_w are, respectively, the undulator's wavelength, wave number, and magnetic field [11]. Initiating the FEL process with a coherent seed allows to lock in the phase of the microbunches and to achieve an improved temporal coherence. Afterwards, the FEL enters the second evolutionary step: radiation power increases exponentially to the detriment of the electron beam's kinetic energy. The strong energy losses, corresponding to a redshift of λ_r, thereafter disable the electron-radiation field's interaction. In the so called steady state regime, the FEL power reaches a maximum and saturates. However, where pulse propagation effects are considered, the radiation pulse is simultaneously dominated by saturation and slippage [12], and its evolution is characterized by the propagation of a solitary wave with the peak power growing quadratically with time and the pulse length decreasing [12,13,14]. In this regime the main pulse propagates at the velocity of light over the electron current leaving highly bunched electrons after its passage. These electrons in the trailing edge coherently radiate into a new trailing pulse. Here, the trailing-pulse regime can be extended over the entire slippage distance along the electron bunch (Fig. 1). Numerical studies reveal that LPS fragmentation and the formation of new buckets are core ingredients of the trailing-pulse dynamics. In these circumstances, an ultra-short seed-pulse induces microbunching when it slips over the electrons at $v_g \sim c$ [14,15]. Microbunching induces coherent emission of the electrons, forming the main radiation pulse and leaving behind those highly bunched electrons with large energy spread. Due to the energy transfer from electrons to the main radiation pulse, the low-energy part ($p < 0$) carries the larger part of charge (≥70%, obtained by counting the

ISBN 978-3-95450-133-5

PERSPECTIVES FOR IMAGING SINGLE PROTEIN MOLECULES WITH THE PRESENT DESIGN OF THE EUROPEAN XFEL

Svitozar Serkez, Vitali Kocharyan, Evgeni Saldin, Igor Zagorodnov
Deutsches Elektronen-Synchrotron (DESY), Hamburg, Germany
Gianluca Geloni
European XFEL GmbH, Hamburg, Germany
Oleksandr Yefanov
Center for Free-Electron Laser Science, Hamburg, Germany

Abstract

European XFEL aims to support imaging and structure determination of biological specimens between less than 0.1 microns and 1 micron size with working photon energies between 3 keV and 16 keV. This wide operation range is a cause for challenges to the focusing optics. A long propagation distance of about 900 m between x-ray source and sample leads to a large lateral photon beam size at the optics. Due to the large divergence of nominal X-ray pulses with durations shorter than 10 fs, one suffers diffraction from mirror apertures, leading to a 100-fold decrease in fluence at photon energies around 4 keV, which seem ideal for imaging of single biomolecules. Moreover, the nominal SASE1 is very far from the level required for single particle imaging. Here we show how it may be possible to optimize the SPB instrument for single biomolecule imaging with minimal additional costs and time, achieving diffraction without destruction at near-atomic resolution with 10^{13} photons in a 4 fs pulse at 4 keV photon energy and in a 100 nm focus, corresponding to a fluence of 10^{23} ph/cm^2. This result is exemplified using the RNA Pol II molecule as a case study.

INTRODUCTION AND REQUIREMENTS

Imaging of single molecules at near-atomic resolution is expected to result in a significant advance in structural biology. One could obtain structural information of large macromolecular assemblies that cannot crystallize, like membrane proteins. In this contribution we study possibilities and opportunities in this field of science, which will be enabled by applying advanced FEL techniques to the SPB (Single Particle and Biomolecule) instrument to be installed in the European XFEL baseline[1] [1, 2]. In order to perform single molecule imaging, a straightforward "diffraction before destruction" method has been proposed [3]- [6]. A great number of single molecules with the same structure are injected into vacuum and interact with ultrashort X-ray pulses, before being completely destroyed. A sufficient number of diffraction patterns is recorded, with unknown orientation. Next, the relative orientations of the different images is determined, so that a 3D diffraction pattern can be assembled in the reciprocal space [7]- [11]. The 3D electron density of the molecule is obtained from the 3D diffraction pattern with the help of a phase retrieval method. An important parameter of the problem is the number of scattered photons per effective Shannon pixel. For biological material, the photon count per shot per pixel of solid angle Ω_p, averaged over shells of wavenumber q is proportional to the wavelength λ^2 [13]. Lower photon energies result in a stronger diffraction signal, but a limit is dictated by the resolution that one needs to achieve, a balance being in the range between 3 keV and 5 keV. The FWHM focal spot size should be roughly between 5 and 10 times larger than the sample size to grant good photon beam quality within the interaction area. For example, a spot size of 100 nm is good for sample sizes of 10 - 20 nm [14]. We find therefore that a biomolecule of around 15 nm diameter, with $N_{\mathrm{atom}} \sim 30000$, requires a pulse fluence of about 10^{13}ph$/(100\ \mathrm{nm})^2$, for an average of $\langle N_p \rangle \sim 1.5$ photons per Shannon pixel at a photon energy of 4 keV. This signal level is higher than what is required by usual methods of pattern orientation determination. Photons have to be delivered in extremely short X-ray pulses to limit radiation-induced changes during the exposure. Estimations indicate that an X-ray pulse duration shorter than about 4 fs is needed [15]- [19]. The key metric for optimizing a photon source for single biomolecule imaging is then the peak power. Ideally, the peak power in our case of interest should be more than 1 TW. For example, we note that 10^{13} photons at 4 keV correspond to an energy of about 6 mJ which yields, in 4 fs, a peak power of about 1.5 TW. It is worthwhile to mention that 1 TW at 4 keV gives the same signal per Shannon pixel as 27 TW at 12 keV (assuming a fixed pulse duration).

[1] A much more fleshed-out report can be found in [12], where the reader is also addressed to for a more complete list of references.

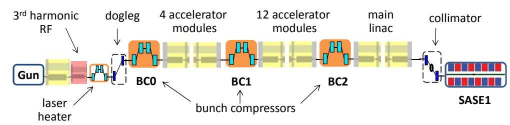

Figure 1: Sketch of the European XFEL, SASE1.

TW SOURCE FOR THE SPB LINE

The SPB instrument at the European XFEL will be located at the SASE1 undulator line [1, 2]. Figure 1 shows this line from the injector up to the SASE1 undulator. Our scheme for an X-ray source suitable for the SPB instrument is heavily based on the use of a slotted spoiler foil in the last bunch compressor chicane, a method devised and ex-

ISBN 978-3-95450-133-5

START-TO-END SIMULATION FOR FLASH2 HGHG OPTION

Guangyao Feng#, Igor Zagorodnov, Martin Dohlus, Torsten Limberg, Winfried Decking,
Jörn Boedewadt, Yauhen Kot, Matthias Scholz, Sven Ackermann, DESY, Hamburg, Germany
Kirsten Hacker, Technische Universität Dortmund, Germany
Tim Plath, University of Hamburg, Germany

Abstract

The Free-electron laser in Hamburg (FLASH) is the first FEL user facility to have produced extreme ultraviolet (XUV) and soft X-ray photons. In order to increase the beam time delivered to users, a major upgrade of FLASH named FLASH II is in progress. The electron beamline of FLASH2 consists of diagnostic and matching sections, a seeding undulator section and a SASE undulator section. In this paper, results from a start-to-end simulation for a FLASH2 High-Gain Harmonic Generation (HGHG) option are presented. For the beam dynamics simulation, space charge, coherent synchrotron radiation (CSR) and longitudinal cavity wake field effects are taken into account. In order to get electron beam bunches with small correlated and uncorrelated energy spread, RF parameters of the accelerating modules have been optimized as well as the parameters of the bunch compressors. Radiation simulations for the modulator and the radiator have been done with code Genesis 1.3 by using the particle distribution generated from the beam dynamics simulation. The results show that for a single stage HGHG, 33.6 nm wavelength FEL radiation can be seeded at FLASH2 with a 235 nm seeding laser.

INTRODUCTION

FLASH has been an FEL user facility since 2005 which can produce XUV and soft X-ray radiation in the wavelength range from 4.1nm to 45nm [1, 2]. In order to increase the beam time, a major upgrade, FLASH II is in progress which will provide seeded FEL radiation as well as SASE FEL radiation [3]. At the exit of the existing linear accelerator, as the extension of FLASH, FLASH2 was built in a separate tunnel. With fast kickers and a DC Lambertson septum, parts of the electron bunch trains generated from the main linac can be extracted into the FLASH2 arc and then pass through the undulator sections. The undulator sections will consist of the seeding undulator section and the SASE undulator section. The layout of the seeding undulator section which will be installed between the extraction arc and the SASE undulator section allows for different seeding schemes, like HHG, HGHG and several combinations of those [4]. The SASE undulator can also be used as the final radiator for the cascaded HGHG scheme and as the amplifier for a direct seeding with HHG. For independent operation of FLASH1 and FLASH2, all FLASH2 undulators will have variable gap to relax the dependency of the radiation wavelength on the electron beam energy.

In this paper, some results of a start-to-end simulation for FLASH2 single stage HGHG option are presented. The injector, the accelerator, the bunch compressors and the extraction arc are studied with help of the codes ASTRA [5] and CSRTrack [6]. Space charge, CSR and longitudinal cavity wake field effects have been taken into account in the beam dynamics simulation. FEL simulations in the modulator and the radiator have been done with Genesis 1.3 [7] by using the particle distribution generated from the beam dynamics simulation. In order to consider the space charge and CSR impacts in the seeding section, the dispersive chicane and the straight beamline between the modulator and the radiator have been simulated with CSRTrack and ASTRA respectively.

LAYOUT OF FLASH

The injector of FLASH consists of a RF gun, an L-band accelerating section and a third-harmonic accelerating section. Electron bunches are generated from a photo cathode by the laser beam and accelerated to 5 MeV by a normal conducting 1.3 GHz RF gun. After the gun, the electron bunches are accelerated in a single TESLA type module named ACC1 [8]. Downstream of ACC1 section a third-harmonic (3.9 GHz) RF system named ACC39 can linearize the RF curvature distortion and minimize the beam tails in the next chicanes [9]. In the L-band superconducting linear accelerator, there are two accelerating sections named L1 and L2 with 1.3 GHz. These two sections are separated by a bunch compressor. L1 has 2 modules (ACC2-3) and L2 has 4 (ACC4-7). There are two bunch compressor chicanes in horizontal plane along the main linac. The first bunch compressor BC2 is located downstream of ACC39. The second bunch compressor BC3 is placed after ACC3 which has an S-type structure (Figure 1).

Behind the main linac of FLASH, three fast vertical kickers and a DC Lambertson-Septum distribute the beam either to the dogleg section of FLASH1 or to the new extraction arc of FLASH2. There are four horizontal bending magnets in the extraction arc of FLASH2 and the arc section is achromatic in horizontal plane. The vertical dispersion caused by the kickers is closed with two vertical bending magnets at the end of the extraction arc. The first order compaction factor (R_{56}) becomes zero at the end of last dipole magnet by using a reverse bending magnet and the proper distribution of dispersion function in the extraction arc section [10]. The undulator

guangyao.feng@desy.de

ISBN 978-3-95450-133-5

ENHANCING COHERENT HARMONIC GENERATION USING TILTED LASER WAVEFRONTS*

S. Khan†, Center for Synchrotron Radiation (DELTA),
TU Dortmund University, 44227 Dortmund, Germany

Abstract

Coherent Harmonic Generation (CHG) to produce ultra-short pulses of synchrotron radiation is based on the interaction of relativistic electrons in a storage ring with femtosecond laser pulses in an undulator. The resulting periodic energy modulation is converted into a density modulation by a dispersive chicane, giving rise to coherent emission at harmonics of the laser wavelength in a second undulator. If the first undulator is in a section with non-zero dispersion, the density modulation can be enhanced using tilted laser wavefronts, thus delaying the phase-space distributions of electrons with different energy with respect to each other. The most simple way to produce a wavefront tilt would be a small crossing angle between the electron and laser beam. Details are discussed for the case of the CHG short-pulse facility at DELTA, a 1.5-GeV synchrotron light source at the TU Dortmund University, but HGHG and EEHG seeding of free-electron lasers could also be enhanced this way.

INTRODUCTION

Synchrotron radiation with short wavelength is the standard tool to study the structure of matter on the atomic level. However, synchrotron radiation pulses with a duration of 30 to 100 ps (FWHM) are insufficient to study dynamic processes such as chemical reactions, phase transitions, fast magnetic changes, lattice vibrations etc. which take place on the sub-picosecond scale. The femtosecond regime, on the other hand, has been made available by mode-locked lasers at wavelengths (e.g. 800 nm in the case of titanium-doped sapphire lasers) which are unsuitable to probe inner atomic shells or to provide spatial resolution on the atomic scale.

The need for radiation with short wavelength *and* short pulse duration has prompted new developments in laser physics, such as high-harmonic generation (HHG), as well as in accelerator physics, notably free-electron lasers (FELs) providing extremely brilliant short-wavelength radiation with femtosecond pulse duration. To date, only four linac-based FEL facilities at short wavelengths are in user operation (in chronological order: FLASH, LCLS, SACLA, and FERMI) while more than 50 synchrotron light sources worldwide [1] provide up to 40 beamlines simultaneously with brilliant and tunable radiation. It is therefore worthwhile to study methods which allow to generate conventional synchrotron radiation with shorter pulse duration.

* Work supported by BMBF (contract 05K13PE3)
† shaukat.khan@tu-dortmund.de

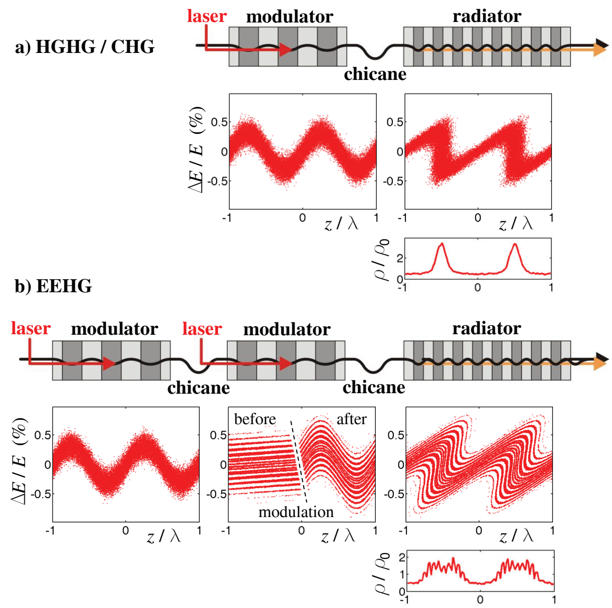

Figure 1: Setup for seeding schemes: a) HGHG or CHG and b) EEHG with respective electron distributions in phase space, i.e. longitudinal coordinate z, here normalized to the laser wavelength λ, versus relative energy deviation $\Delta E/E$.

SHORT-PULSE GENERATION

Some methods to generate sub-ps radiation pulses at storage rings are borrowed from FEL seeding schemes using a femtosecond laser pulse to modulate the energy of electrons at the center of a long electron bunch. FEL seeding aims at assisting a positive feedback loop of exponentially growing microbunching and coherent radiation. In a storage ring, on the other hand, the laser pulse is used to define a short "slice" within the electron bunch. A short radiation pulse is emitted by the energy-modulated electrons together with a long pulse from the rest of the bunch. Off-energy electrons can be transversely displaced by dispersion in order to separate the short and long components of incoherent undulator radiation spatially – this scheme is known as "femtoslicing" [2]. Alternatively, a magnetic chicane may convert the energy modulation into a density modulation giving rise to a short pulse of coherent radiation at harmonics of the laser wavelength, which is brighter than the long incoherent pulse. As long as the signal-to-background ratio

$$\frac{P_{\rm short}}{P_{\rm long}} = \frac{n_{\rm short}^2\, b_h^2}{n_{\rm long}} = f^2\, n_{\rm long}\, b_h^2 \quad \text{with} \quad f \equiv \frac{n_{\rm short}}{n_{\rm long}} \qquad (1)$$

is tolerable, no geometric separation is required. Here, $f \approx 10^{-3}$ is the ratio between the number of electrons in the slice

ISBN 978-3-95450-133-5

BROADLY TUNABLE THZ FEL AMPLIFIER*

Chia-Hsiang Chen#, Yu-Chung Chiu, Kuan-Yan Huang, Institute of Photonics, Technologies/Department of Electrical Engineering, National Tsinghua University, Hsinchu 30013, Taiwan
Yi-Kai Gan, Fu-Han Chao, Yi-Chu Wang, Department of Physics, National Tsing Hua University, Hsinchu 30013, Taiwan
Yen-Chieh Huang, Institute of Photonics Technologies/Department of Electrical Engineering, National Tsinghua University, Hsinchu 30013, Taiwan and Department of Physics, National Tsing Hua University, Hsinchu 30013, Taiwan

Abstract

In this paper we present a broadly tunable high-power THz FEL amplifier driven by a photoinjector with a seed source tunable between 0.7-2.0 THz. A fully synchronized THz seed pulse is provided by an optical parametric amplifier pumped by the very driver laser of the electron injector. The FEL amplification gain is almost 3000 at 2 THz for nominal input beam parameters.

INTRODUCTION

In the THz region, high power radiation sources are scarce. A free electron laser is known to be high-power and tunable over a wide spectral range. In the past, FEL oscillators were often built generate high-repetition-rate [1,2] or quasi-CW [3] THz radiation. With rapid advancement on high-brightness photoinjectors, single-pass FELs are playing a crucial role in generating high-peak-power laser radiation through self-amplified spontaneous emission (SASE) [4]. Unfortunately a low-energy beam is susceptible to the space charge effects and makes a SASE THz FEL more difficult to realize. In addition, it is well known that the noisy spectral and temporal output of a SASE FEL is suitable for applications requiring high spectral and temporal purity. Recently, kW-level tunable THz radiation sources are becoming available from optical technologies. A possible path to realizing a MW-level tunable narrow-line THz source is to seed an FEL amplifier with a fully tunable optical THz source. This idea was studied in the past with a limited wavelength-tunability from a CO_2-laser pumped THz different frequency generator (DFG) using GaAs as its gain material [5]. In this paper, we present a design for a high-power tunable THz FEL seeded by an all-solid-state THz parametric amplifier (TPA) broadly tunable between 0.7 and 2 THz.

SYSTEM LAYOUT

Figure 1 shows the design concept of the proposed FEL amplifier to generate fully tunable, narrow-line, high-power THz radiation. The proposed THz FEL system comprises two major components, the FEL amplifier and the THz seed. The FEL beamline consists of a high-brightness photoinjector and an undulator. The THz seed is a tunable TPA using a lithium niobate ($LiNbO_3$, LN) crystal as its gain material. One unique design that greatly simplifies the operation of the system is to use the driver laser of the photoinjector to pump the TPA and generate a fully synchronized seed THz pulse for the FEL. First, a Nd:YVO_4 mode-locked laser at 1064 nm is sent into a Nd:YAG regenerative amplifier to gain tens of mJ pulse energy. The laser pulse is then divided into two parts; the first part is frequency-quadrupled to ultraviolet to drive the photoinjector and the other is sent to pump the TPA to generate a THz seed pulse to the undulator. As will be shown below, this TPA is capable of generating a kW THz pulse with tunability between 0.7 and 2.0 THz.

Figure 2 shows the hardware arrangement of the proposed single-pass THz FEL amplifier, including a photoinjector, a solenoid, and an undulator. The total length of the setup is about 3.5 m. The accelerator is a 2.856-GHz BNL/SLAC/UCLA type photoinjector [6], generating a 3-5 MeV electron beam with 0.5-nC charge. A solenoid magnet following the gun compensates the emittance growth of electron bunch and focuses the electron beam to the undulator. Installed between the solenoid and the undulator is an input mirror for the THz seed. To keep the whole system compact, the mirror has an aperture to transmit the electrons.

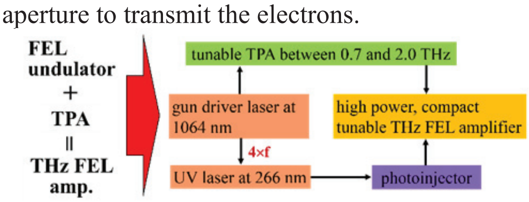

Figure 1: The design concept of the proposed high-power tunable THz FEL amplifier.

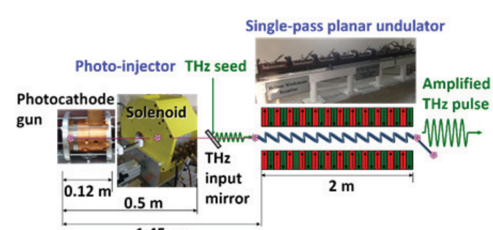

Figure 2: The hardware arrangement of the proposed THz FEL amplifier (planar undulator).

*Work supported by MoST under NSC 102-2112-M-007-002-MY3
#chiahsiang@mx.nthu.edu.tw

ISBN 978-3-95450-133-5

UPGRADE PLANS FOR THE SHORT-PULSE FACILITY AT DELTA*

S. Hilbrich†, M. Höner, H. Huck, M. Huck, S. Khan, C. Mai,
A. Meyer auf der Heide, R. Molo, H. Rast, P. Ungelenk,
Center for Synchrotron Radiation (DELTA), TU Dortmund University, Dortmund, Germany

Abstract

The synchrotron light source DELTA comprises a short-pulse facility based on coherent harmonic generation (CHG) to generate coherent radiation with wavelengths in the VUV regime. Even shorter wavelengths can be produced using the echo-enabled harmonic generation (EEHG) technique. An upgrade of the storage ring is planned to install an EEHG as well as a femtoslicing short-pulse source.

INTRODUCTION

The 1.5-GeV synchrotron light source DELTA, operated by the TU Dortmund University, is shown schematically in Fig. 1. Besides dipole magnets as radiation sources, DELTA comprises two undulators (U55, U250) and a superconducting asymmetric wiggler (SAW). The pulse duration of the synchrotron radiation is about 100 ps (FWHM) given by the bunch length. Shorter radiation pulses with durations in the sub-100-fs range can be generated with commercially available laser systems, but with wavelengths in the near-visible range. In the following, three techniques to combine the advantages of both radiation source types in order to produce radiation with short wavelengths as well as short pulse duration are described.

Coherent Harmonic Generation (CHG)

The CHG technique [1] is based on an interaction between a short laser pulse and an electron bunch. The setup consists of two undulators and a dispersive magnetic chicane between them. A detailed description of the CHG setup at DELTA can be found in [2]. The interaction occurs in the first undulator, the so-called modulator, and leads to a sinusoidal modulation of the electron energy with the periodicity of the

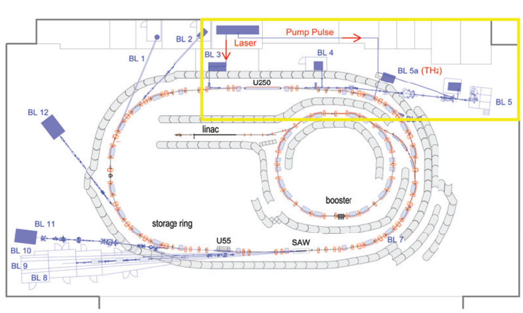

Figure 1: Sketch of the DELTA synchrotron radiation facility. The yellow frame marks the CHG facility in the northern part of the storage ring.

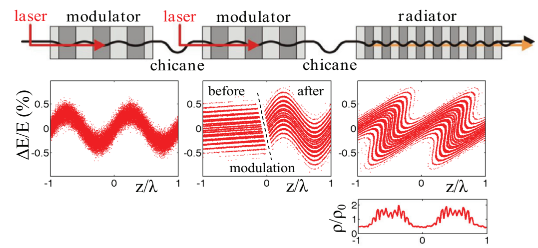

Figure 2: Top: Sketch of the magnetic setup for EEHG. Center: The longitudinal phase space before the first magnetic chicane, before and after the second modulator, and after the second chicane. Bottom: The longitudinal electron density after the second chicane.

laser wavelength within a short "slice" at the center of the bunch. The magnetic chicane converts the energy modulation into a density modulation known as microbunching. In the second undulator, the radiator, the microbunches radiate coherently at the laser wavelength and harmonics thereof with a much higher intensity than the incoherent undulator radiation.
The power of the CHG radiation at the nth harmonic of the laser wavelength is [3]

$$P_n \propto N^2 b_n^2 \tag{1}$$

with N being the number of modulated electrons and the so-called bunching factor

$$b_n \propto e^{-n^2} \tag{2}$$

decreasing exponentially with the harmonic number n.

Echo-enabled Harmonic Generation (EEHG)

The FEL seeding scheme EEHG [4] has been successfully tested at SLAC in Menlo Park (USA) [5] and SINAP in Shanghai (China) [6] and can also be applied at storage rings to generate ultrashort coherent pulses. Compared to CHG, it uses an additional undulator and chicane. As in the case of CHG, the electron energy is sinusoidally modulated in the first modulator, but the first chicane has a larger R_{56} value, such that the electron distribution in the longitudinal phase space is strongly sheared while the density distribution is flat. In the second modulator, the electron energy is modulated by a second laser pulse. In a following magnetic chicane with a moderate R_{56} value, a density modulation with a high content of harmonics is generated (see Fig. 2). The optimized bunching factor for EEHG, i.e., with optimum settings for each harmonic, scales as [7]

$$b_n(\lambda) \propto n^{-\frac{1}{3}} \tag{3}$$

* Work supported by DFG, BMBF, FZ Jülich, and by the Federal State NRW.
† svenja.hilbrich@tu-dortmund.de

ISBN 978-3-95450-133-5

HIGH REPETITION RATE ENERGY MODULATOR SYSTEM UTILIZING A LASER ENHANCEMENT CAVITY *

Y. Honda†, KEK, Tsukuba, Ibaraki, Japan

Abstract

In order to realize a high repetition rate seeded coherent radiation source, it is necessary to develop a seeding system which works in a continuous mode. Utilizing the longitudinal electric field in a higher transverse mode laser stored in an optical cavity, it is possible to introduce an energy modulation in an electron bunch. Through acceleration and dispersion handling, the modulation at laser wavelength can be converted into a finer density structure. It can be used as a seed of coherent radiation. We are developing a laser system to be used in the laser modulator system.

INTRODUCTION

Recent linear accelerators can realize an electron beam of high brightness and small energy spread. Based on such a high quality electron beam, SASE FEL has been realized and it has been provided as an user machine at various laboratories. At the next stage, temporal coherence and high averaged power are expected as additional characteristics to be developed. For temporal coherence, seeding scheme can be used. And for high averaged power, multiple bunch operation and/or energy recovery scheme with a superconducting cw accelerator can be used. But in order to realize the two items at the same time, a seeding system which can work at high repetition rate is necessary. Usually, seeding is done with a high peak power laser system which can work only at a low repetition rate. Here, we propose an optical cavity system which can realize a high enough electric field at ~100 MHz repetition of continuous operation. This can be used to directly modulate electron beam energy in the scale of optical wavelength. Combining the laser modulation with the bunch compression in the following stage, it can seed shorter wavelength radiation.

ACCELERATION BY AN ELECTRIC FIELD OF LASER

We would like to use an electric field of a laser for electron beam acceleration [1] [2]. Usually, it is not possible because the electric field of a plane wave is in transverse direction. Here we think a TM-wave laser beam which transfers in z-direction. The electric field is mainly in x-direction, and the magnetic field is zero in z-direction. Directly from Maxwell's equation, the following relation,

$$ikE_z = \frac{\partial E_x}{\partial x} \tag{1}$$

is obtained. Variation of transverse electric field results in a longitudinal electric field. Transferring an electron beam along with the laser beam, the longitudinal component of the field can accelerate or decelerate the electron beam. It introduces energy modulation in the period of laser wavelength.

A higher order transverse mode, TEM_{10}-mode, is one of such a laser beam. The field profile is shown in Fig. 1. Its transverse field varies and zero-crosses at the center area of the profile. It means there is a longitudinal field at the center.

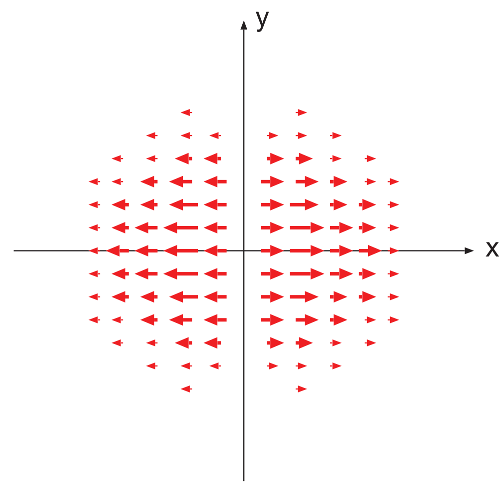

Figure 1: Profile of the higher transverse mode laser.

The x-component of the electric field can be written as,

$$E^x_{10} = A \cdot x \exp(-\frac{x^2}{\omega^2}) \exp(i(\omega t - kz + 2\phi(z))). \tag{2}$$

where $\phi(z)$ is Gouy phase, $\phi(z) = \tan^{-1}(\frac{z}{z_0})$, z_0 is Rayleigh length ($z_0 = \frac{\pi w_0^2}{\lambda}$)). Simplifying this, the transverse electric field E_x is

$$E_x = xe^{-x^2}. \tag{3}$$

And the longitudinal electric field E_z is

$$E_z = \frac{(1-2x^2)e^{-x^2}}{k}. \tag{4}$$

These are shown in Fig. 2.

It can be written using laser power P as,

$$E_z = \frac{1}{2z_0}\sqrt{\frac{P}{c\epsilon_0}}. \tag{5}$$

Laser beam diverges and the phase shifts in the distance of z_0. So, the effective accelerating distance is $2z_0$. Energy gain G is then,

$$G = E_z \times 2z_0 = e\sqrt{\frac{P}{c\epsilon_0}}. \tag{6}$$

* Work supported by KAKENHI
† yosuke@post.kek.jp

ISBN 978-3-95450-133-5

SOFT X-RAY SELF-SEEDING SIMULATION METHODS AND THEIR APPLICATION FOR LCLS

Svitozar Serkez
Deutsches Elektronen-Synchrotron (DESY), Hamburg, Germany
Jacek Krzywinski, Yuantao Ding, Zhirong Huang
SLAC, Menlo Park, California, USA

Abstract

Self-seeding is a promising approach to significantly narrow the Self-Amplified Spontaneous Emission (SASE) bandwidth of XFELs to produce nearly transform-limited pulses. We study radiation propagation through the grating monochromator installed at Linac Coherent Light Source (LCLS). The monochromator design is based on a toroidal Variable Line Spacing (VLS) grating working at a fixed incidence angle mounting without an entrance slit. It covers the spectral range from 500 eV to 1000 eV. The optical system was studied using wave optics method to evaluate the performance of the self-seeding scheme. Our wave optics analysis takes into account the finite size of the coherent source, third-order aberrations and height error of the optical elements. Wave optics is the only method available, in combination with FEL simulations, to simulate performance of the monochromator without exit slit. Two approaches for time-dependent simulations are presented, compared and discussed.

INTRODUCTION

Self-seeding is a promising approach to significantly narrow the SASE bandwidth and to produce a nearly transform-limited pulses [1]- [10]. Recently a soft X-ray Self-seeding setup was installed in LCLS [11]- [15] and is currently under commissioning [16].

In general, a self-seeding setup consists of two undulators separated by a photon monochromator and an electron bypass, normally a four-dipole chicane (see Fig. 1). Both undulators are resonant at the same radiation wavelength. The SASE radiation generated by the first undulator (SASE undulator) passes through the narrow-band monochromator. A monochromatic pulse is created, which is used as a coherent seed in the second undulator (seeded undulator). Chromatic dispersion effect in the bypass chicane smears out the microbunching in the electron bunch produced by the SASE lasing in the SASE undulator. The electrons and the monochromatized photon beam are recombined at the entrance of the seeded undulator, and the radiation is amplified by the electron bunch until saturation is reached. The required seed power at the beginning of the seeded undulator must dominate over the shot noise power within the gain bandpass, which is order of a kW in the soft X-ray range.

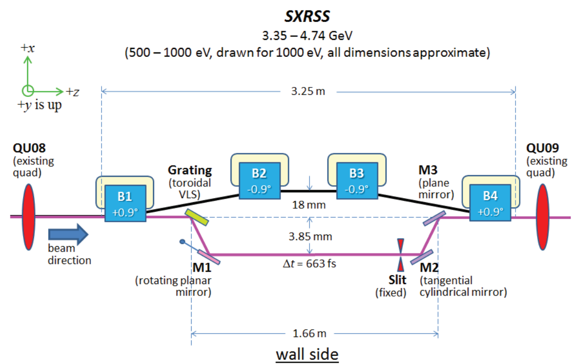

Figure 1: The compact soft x-ray self-seeding system to be located in U9. The grating is a toroidal VLS grating, M1 is a rotating plane mirror, M2 a tangential cylindrical mirror, and M3 a plane mirror used to steer the beam. Adapted from [13].

LCLS SOFT X-RAY SELF-SEEDING SETUP LAYOUT

The overall self-seeding setup consists of three parts: the SASE undulator, the self-seeding grating monochromator and the output seeded undulator in which the monochromatic seed signal is being amplified. The seeded undulator consists of two sections. The first section is composed by an uniform undulator, and the second section - by a tapered undulator. The transform-limited seed pulse is exponentially amplified passing through the first uniform part of the seeded undulator. Finally, in the second part of the seeded undulator the monochromatic FEL output is enhanced after saturation.

The Soft X-ray Self-Seeding (SXRSS) monochromator for LCLS was introduced in [13] and is based on a toroidal variable-line-spacing (VLS) grating, a steering plane mirror, a slit, a spherical mirror and another plane mirror (Fig. 1).

The toroidal VLS grating is illuminated by a SASE FEL radiation produced by the SASE undulator with the source in undulator sections 7 or 8 (depends on set-up). Transverse coherence of a SASE FEL allows one to avoid installation of an entrance slit. The plane mirror M1 is used to steer the certain wavelength of an angularly dispersed radiation to the slit. The spherical mirror M2 re-images the radiation from the slit position to the re-imaging point at the entrance to the seeded undulator. The plane mirror M3 reflects the radiation to the seeded undulator, allowing two additional

ISBN 978-3-95450-133-5

X-RAY MONOCHROMATORS FOR SELF-SEEDING XFELs IN THE PHOTON ENERGY RANGE STARTING FROM 1.5 keV

Yuri Shvyd'ko*
Advanced Photon Source, Argonne National Laboratory, Argonne, Illinois 60439, USA

Abstract

Self-seeding of FELs with photon energies below 1 keV can be performed using grating monochromators [1]. Forward Bragg diffraction (FBD) monochromators [2] were instrumental for achieving self-seeding in hard x-ray FELs in the photon energy range from 5 to 10 keV [3]. Large photo-absorption in the monochromator crystal at lower photon energies makes extension into lower photon energy range difficult. Here an alternative scheme of x-ray monochromatization is introduced which may enable self-seeding in a yet inaccessible spectral range starting from 1.5 keV, and thus to bridge the gap between the soft and hard x-ray self-seeding.

The new scheme uses grazing-incidence Bragg diffraction under specular reflection conditions [4]. Specular reflection mitigates the problem of photo-absorption, as in this case the FBD radiation is reflected from a very thin crystal surface layer. Application of quartz (SiO_2) instead of diamond crystals, makes feasible Bragg diffraction and therefore monochromatization of x-rays starting from 1.457 keV.

INTRODUCTION

A new scheme of x-ray monochromatization is proposed here, which may enable self-seeding in a yet inaccessible spectral range starting from 1.5 keV, and thus to bridge the existing gap between the soft and hard x-ray self-seeding. The scheme uses grazing-incidence Bragg diffraction under specular reflection conditions [4], as shown in Figure 1.

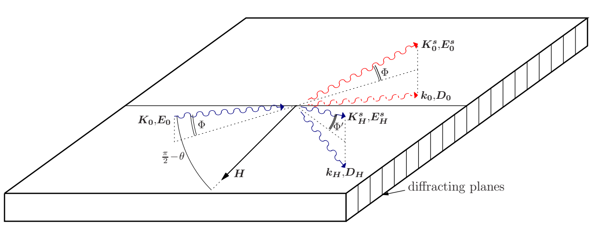

Figure 1: Schematic of grazing incidence x-ray Bragg diffraction in non-coplanar geometry under specular reflection conditions [4].

X-RAY DIFFRACTION UNDER SPECULAR REFLECTION CONDITIONS

Diffracting atomic crystal planes are perpendicular to the crystal surface. Incident x-rays with the wave-vector $\boldsymbol{K}_0$ are at a very small glancing angle of incidence Φ to the crystal surface, and at a Bragg angle θ to the diffracting atomic crystal planes ($\pi/-\theta$ angle with diffraction vector $\boldsymbol{H}$). Under theses conditions, the Bragg diffracted x-rays propagate at a very small glancing angle of reflection to the crystal surface Φ'. $\boldsymbol{K}^s_H$, E^s_H are the wave-vector and the amplitude of the specularly reflected Bragg diffracted beam. Another Bragg diffracted component propagates inside the crystal with the wave-vector $\boldsymbol{k}_H$, and amplitude D_H. Similarly, there are two components of x-rays associated with forward Bragg diffraction (FBD). First, there is an in-crystal component with wave-vector $\boldsymbol{k}_0$ D_0. Second, $\boldsymbol{K}^s_0$, E^s_0 are the in-vacuum wave-vector and the amplitude of the specularly reflected forward Bragg diffracted beam (S-FBD), with the specular reflection angle Φ. Dinamical theory of Bragg diffraction in such scattering geometry has been developed by Afanasev-Melkonyan (1983). For the x-ray monochromator application we will be interested in the S-FBD beam E^s_0.

Specular reflection mitigates the problem of photo-absorption, as in this case the FBD radiation is reflected from a very thin crystal surface layer. Application of quartz (SiO_2) instead of diamond crystals, makes feasible Bragg diffraction and therefore monochromatization of x-rays starting from $\hbar\omega_H = 1.457$ keV, the photon energy for backscattering from the atomic planes with diffraction vector $\boldsymbol{H} = (10\bar{1}0)$. The nominal energy $\hbar\omega_0$ of photons involved in Bragg diffraction is defined as usually by Bragg's angle θ through Bragg's law: $\hbar\omega_0 = \hbar\omega_H / \sin\theta$.

SELF-SEEDING SCHEME

The x-ray FEL self-seeding scheme is shown in Figure 2. X-rays from the first half of the magnetic undulator system

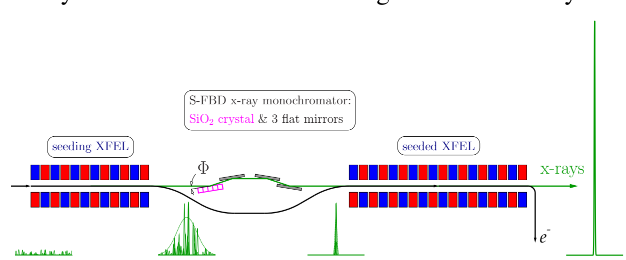

Figure 2: X-ray FEL self-seeding scheme with the S-FBD x-ray monochromator.

(seeding XFEL) are used to seed the electron bunch in the second half (seeded XFEL) via an x-ray monochromator consisting of a SiO_2 crystal and three flat grazing incidence mirrors, used to correct the trajectory of photons. The monochromator produces a delayed monochromatic seed through grazing incidence forward Bragg diffraction under specular reflection (S-FBD) conditions, with a small specular reflection angle $\Phi \lesssim 25$ mrad, see Fig. 1 for details. The

* shvydko@aps.anl.gov

ISBN 978-3-95450-133-5

INDIRECT MEASUREMENTS OF NIR AND UV ULTRASHORT SEED LASER PULSES USING A TRANSVERSE DEFLECTING RF-STRUCTURE

Nagitha Ekanayake, Sven Ackermann, DESY, Hamburg, Germany
Kirsten Elaine Hacker, DELTA, Dortmund, Germany
Christoph Lechner, Theophilos Maltezopoulos, Tim Plath, University of Hamburg, Germany

Abstract

Seeding of free-electron lasers (FELs) using external coherent optical pulses recently became an area of interest as users demand spectrally and temporally coherent FEL radiation which is not achievable in traditional self-amplified spontaneous emission operation mode. Since temporal and spectral properties of the seed laser pulses are directly imprinted on the electron bunch, a proper characterization of these seed pulses is needed. However, the lack of any measurement technique capable of characterizing ultrashort seed laser pulses at the laser-electron interaction region is a primary drawback. In this paper we report indirect measurements of seed laser pulses in an undulator section using a transverse deflecting RF-structure (TDS) at the free-electron laser FLASH at DESY. Temporally chirped and unchirped seed pulse length measurements will be compared with second-harmonic generation frequency-resolved optical gating measurements and theoretical simulations. Using this technique we will demonstrate that pulse artifacts such as pre- and post-pulses in the seed pulse in the femtosecond and picosecond timescales can be identified without any temporal ambiguity.

INTRODUCTION

External seeding techniques such as High Gain Harmonic Generation (HGHG) [1] and Echo-Enabled Harmonic Generation (EEHG) [2] have been demonstrated recently. Proper characterization of seed laser pulses in the interaction region, namely the undulator, is important for successful operation of such seeding schemes. However, to best of our knowledge, currently there is no technique available to directly measure the pulse duration of the seed laser pulses inside the undulator. In this study we provide indirect measurements of ultrashort laser pulses, using a technique which utilizes the energy modulation of an electron bunch due to seed laser beam, observed using a transverse deflecting RF-structure.

EXPERIMENTAL SETUP

Seed Laser System

The seed laser system (Fig. 1) employed in the FLASH1 seeding project is a solid-state, commercial, Ti-sapphire system based on chirped pulse amplification technique (CPA). The 108.3 MHz optical oscillator is synchronized to the master laser oscillator (MLO) via a RF-based link with a 50 fs rms jitter. A two-stage amplifier section is used to amplify the pulse energy up to 50 mJ/pulse at 10 Hz repetition rate and 800 nm centre wavelength. Amplified pulses are then extracted from the cavity and compressed down to 50 fs full width at half maximum (FWHM) duration. Pulse duration is measured using a commercial GRENOUILLE setup [3]. After compression, the pulse energy is 35 mJ/pulse with ± 2% rms stability.

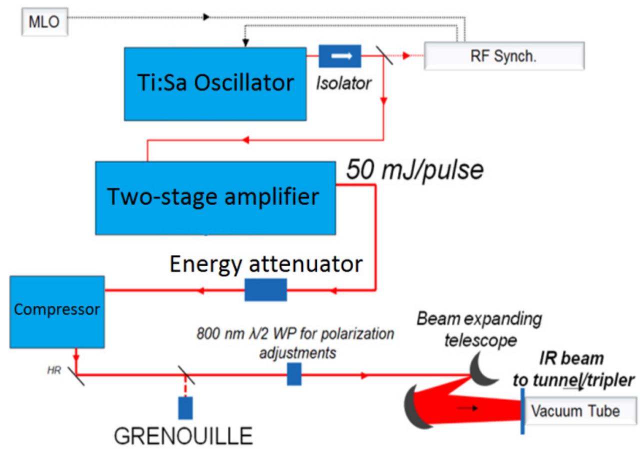

Figure 1: Schematic of the seed laser system at FLASH1.

Beam Delivery

The fundamental 800 nm beam is then delivered to a frequency tripler unit in order to generate the third harmonic of the fundamental beam for seeding. The in-coupling beam line consists of 3 m of air and 1 mm thick fused silica window prior to a high vacuum region of 10^{-6} mbar and 9 m in length. To keep the B-integral below unity the beam diameter is expanded by a factor of 3, from 6 mm FWHM after the amplifier to 18 mm FWHM after the beam expander.

Frequency Upconversion and Injection

Frequency tripling is performed using two β-Barium borate (BBO) crystals. First BBO crystal converts the fundamental frequency to its second harmonic and subsequent α-BBO delay plate adds a temporal delay to the fundamental pulse as both pulses need to be temporally overlapped in the second β-BBO crystal for efficient third harmonic generation. Polarization state of the fundamental beam is adjusted using a quarts waveplate λ/2 @ 800 nm and λ @ 400 nm. The conversion efficiencies for the second and third harmonics are approximately 20 % and 9%, respectively (Fig. 2). Estimated pulse duration of the third harmonics is approximately 150 fs FWHM.

ISBN 978-3-95450-133-5

HGHG AND EEHG MICROBUNCHES WITH CSR AND LSC*

Kirsten Hacker, TU Dortmund, Germany

Abstract

Longitudinal space charge (LSC) forces in a drift and coherent synchrotron radiation (CSR) in a chicane are relevant for high gain harmonic generation (HGHG) and echo enabled harmonic generation (EEHG) seeding designs. These factors determine whether or not the modulator can be located significantly upstream of the radiator. The benefits and dangers of having a drift in between the radiator and the modulator are investigated and a measurement of the LSC enabled reduction of the energy spread of a seeded beam is presented.

INTRODUCTION

The length of a seeded microbunch determines the harmonic content and the harmonic content together with the energy spread determines the shortest wavelength which the system can seed [1-3]. For a given initial uncorrelated energy spread, the length of a microbunch can be reduced by increasing the modulation amplitude, but when the modulation amplitude becomes too great, the energy spread of the microbunches will be too large to lase in the radiator [4]. In addition, microbunches with high peak currents will be subject to significant coherent synchrotron radiation (CSR) in the chicane and longitudinal space charge (LSC) forces in the drift [5,6]. For FLASH2 seeding, a decision about where an HGHG modulator should be placed is determined by how these factors influence the behavior of an HGHG microbunch in a drift. This material was first presented in [7,8]. It represents an initial investigation into this design issue for FLASH2. The full-bunch simulation methods from [9] would be used in a final design study.

Two possible configurations of a FLASH2 seeding installation are drawn in Fig. 1. Option (a.) has the HGHG modulator in the middle of the radiator, minimizing the drift of the microbunched electrons and option (b.) has the modulator at the beginning of the radiator, necessitating a 20 meter drift of an energy modulated electron bunch prior to beginning the radiation process. This drift is required due to the short length of undulator required to achieve saturation in a seeded FEL and due to the necessity of keeping the saturation point at a fixed point in the radiator for longer wavelengths. If the beam saturates too early in the radiator, then the 20-30 nm FEL light cannot be transported to the users.

In order to determine which option is superior, longitudinal dispersion, longitudinal-transverse coupling, coherent synchrotron radiation (CSR), and longitudinal space charge (LSC) all need to be addressed. The conclusion from a study of these issues is that option (a.), with the modulator in the middle of the radiator, suffers

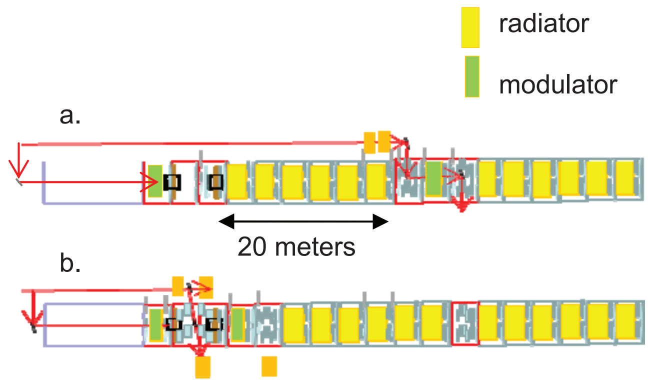

Figure 1: Two possible locations for an HGHG modulator in a FLASH2 seeding installation. Option (a.) shows it in the middle of the radiator in a design which is only suitable for HGHG and option (b.) shows it prior to the radiator in a design which is suitable for a wider range of seeding schemes. The additional, upstream modulator is envisioned for EEHG.

most from CSR, while option (b.), given more ample seed laser intensity, can exploit LSC forces in a beneficial manner, using them to reduce the net energy spread of the microbunches. Measurements and simulations of this LSC enabled increase of the microbunch energy spread concept are presented. Conversely, measurements of the LSC enabled enhancement of a microbunch energy spread are presented in [10] with a different application. Whether or not the LSC force enhances or reduces the microbunch energy spread depends on whether the microbunch is undercompressed or overcompressed at the entrance of a drift.

DISPERSION

The energy modulated beam is affected by dispersion from the chicanes, from the modulator, from mis-aligned magnets or beam trajectories, and from the velocity bunching in the drift itself. Higher order dispersion becomes relevant for large energy modulations in terms of its effect on coupling between longitudinal and horizontal dispersion for non-closed orbit bumps. It will be discussed in the section on 3-D effects. A table summarizing the first-order dispersion (R_{56}=-2Δs) contributions for a 20 meter drift is given below (Table 1).

Table 1: A summary of the contributions to the dispersion over a 20 meter drift for a beam energy of 700 MeV and a trajectory mis-alignment of 100 μm and modulator with 30 periods.

velocity	L_{drift} / γ^2	15 μm
mis-alignment	$L_{drift}\ \theta^2$	5 nm
modulator	$2N_{periods}\lambda_{seed}$	16 μm
chicane	$(L_{chicane}-3L_{bend})\theta^2$	0-200 μm

* work supported by BMBF grant 05K10PE1 and DESY

ISBN 978-3-95450-133-5

ENHANCING THE HARMONIC CONTENT OF AN HGHG MICROBUNCH

Kirsten Hacker, TU, Dortmund, Germany

Abstract

High Gain Harmonic Generation (HGHG) seeding has been demonstrated in the visible and ultraviolet, but it is limited in performance at high harmonics of the seed by the initial uncorrelated energy spread of the electron beam. A recent proposal from SINAP using a chirped electron beam and a canted pole undulator has suggested a new mechanism for reducing the length of the seeded microbunches in order to improve the performance of HGHG seeding at high harmonics. This note reviews the mechanism, the limitation of the concept and extrapolates to some new concepts using analogous mechanisms derived from transverse gradients of the laser properties. The impact of CSR wakes on the vanishingly short microbunches produced by the methods are also investigated.

INTRODUCTION

Seeded electron beams benefit from a small uncorrelated energy spread of the electron beam because it reduces the length of the seeded microbunches. For High Gain Harmonic Generation (HGHG) seeding, the bunching factor as a function of harmonic number n is given in terms of the uncorrelated energy spread, δ, by [1]

$$b_n = e^{-(nD\delta)^2/2} J_n(nD\Delta\gamma) \quad (1)$$

where $\Delta\gamma$ is the energy modulation, n is the harmonic number, $D=2\pi R_{56}/\lambda_s\gamma_0$ where R_{56} is the dispersion of the chicane and J_n is a Bessel function of order n. When the bunching factor is plotted for a range of slice energy spreads, it is apparent that the seeding method could be extended to shorter wavelengths if a technique could reduce or cool the slice energy spread, δ, prior to or during seeding (Fig. 1).

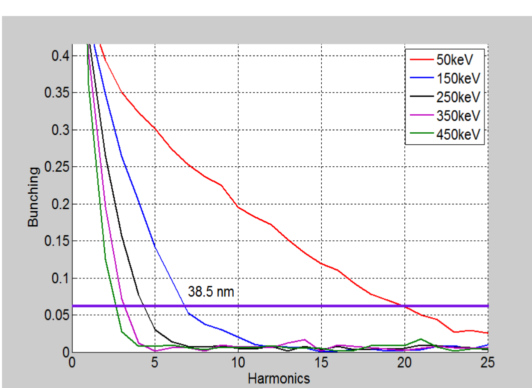

Figure 1: Bunching factor as a function of harmonics for a range of initial uncorrelated energy spreads for a 270 nm HGHG seeded beam.

*work supported by BMBF grant 05K10PE1 and DESY.

Several ideas have been proposed to cool the slice energy spread of an electron beam prior to seeding. The least invasive strategy involves reducing the compression and charge of the electron bunch so that it is easier to transport without suffering from the nonlinearities introduced by various wakefields which scale with the peak current. In simulations, this alone is enough to achieve a 100 keV slice energy spread at FLASH2 [2]. In practice, this is less certain. This strategy also reduces the FEL peak power, since the peak power scales with the peak current.

The next strategy employs a laser heater in the first bunch compressor of the accelerator in order to increase (heat) the uncorrelated energy spread early in the machine and smear out random fine structures in the electron bunch which get amplified as they propagate over large distances [3,4]. The combination of low-charge, weak compression, and laser heating has been shown to reduce the slice energy spread of the Elettra at FERMI beam to ~150 keV for a 500 nC bunch with 500 A of peak current prior to the seeding section [4].

An untried strategy from SINAP uses a canted pole undulator with a transversely chirped electron bunch in order to reduce the effective length of HGHG microbunches [1]. In this note, simulation predictions from seeding with SINAP's canted pole undulator are duplicated and extrapolated to alternatives utilizing novel laser conditions like a transverse intensity gradient, a wavefront rotation, and a transverse chirp as an alternative to the canted undulator pole. The benefits and problems associated with these alternatives are described.

CANTED POLE SEEDING

The SINAP HGHG proposal is to send a transversely chirped electron bunch through an undulator with transversely canted poles (Fig. 2).

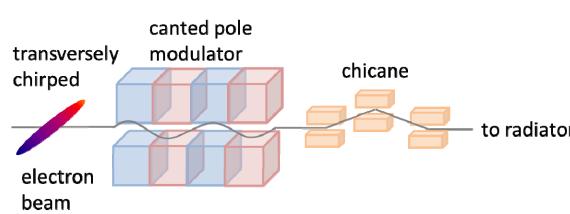

Figure 2: SINAP HGHG proposal sends a transversely chirped electron bunch through an undulator with transversely canted poles.

The mechanism was described by SINAP in the language of off-resonance seed laser modulation for cooling the beam energy spread. This note investigates the mechanism in the language of path length changes and energy transfer from the laser to the electron beam. It then extrapolates to scenarios with transverse variations of

ISBN 978-3-95450-133-5

A CONCEPT FOR SEEDING 4-40 nm FEL RADIATION AT FLASH2

Kirsten Hacker#, TU, Dortmund, Germany

Abstract

This note describes a scheme to seed the FLASH2 FEL over a range of 4-40 nm without impacting SASE capabilities. This scheme combines multiple seeding techniques, builds on current infrastructure and offers a maximized range of performance with higher pulse energies than what are available at lower-peak current facilities. The concept relies on Echo Enabled Harmonic Generation (EEHG), cascaded seeding, and Second Harmonic Afterburners (SHAB) while maintaining the possibility to operate with High Gain Harmonic Generation (HGHG) seeding at >30 nm wavelengths.

INTRODUCTION

High Gain Harmonic Generation (HGHG) and an HGHG cascade have demonstrated seeding at FERMI down to 19 nm with HGHG alone and 4 nm in an HGHG cascaded configuration [1,2]. FERMI operates with low-charge, 400-600 A peak current and weak compression. They have a laser heater and no space for a long, SASE undulator. All of these conditions are the opposite of those presently available at FLASH. In order for FLASH2 to offer a competitive seeding program to users while maintaining SASE capability

- the facility must be compatible with SASE
- first few years of operation without a laser heater
- seeding should work at short, 4 nm wavelengths
- seeding should work over the entire bunch-train
- design must be flexible in order to accommodate different electron beam conditions.

To fulfill these criteria, the seeding methods used at FLASH2 should be High Gain Harmonic Generation (HGHG) down to 40 nm, Echo-Enabled Harmonic Generation (EEHG) down to 7 nm, and an EEHG cascade down to 4 nm and below. Any of these seeding methods can be used with a Second Harmonic After-Burner (SHAB) to reach shorter wavelengths [3]. An HGHG cascade could be attempted, but the tolerances are not generous.

Simulations will show the limitations of each of these radiation (CSR), and laser pulse distortions using 1-D tracking and analytic estimates for 3-D effects. The full-bunch simulation methods from [4] would be used in a final design study.

Each of the seeding concepts, excluding the afterburner, could be tested in FLASH1 in 2014 [5, 6]. The hardware required for these tests has already been commissioned and experts are available for the operation.

Through the FLASH2 configuration shown in Fig. 1, individual commissioning of HGHG, EEHG and an EEHG cascade could be accomplished in a stepwise fashion, allowing for work starting with proven concepts at 40 nm and ending with seeding at 4 nm. 2 nm could potentially be seeded given an afterburner [3]. HHG could also be incorporated into the setup in an EEHG-HHG configuration, but this concept is an add-on of research interest for compact schemes and it is not essential to the design for user operation.

An item which is essential for seeding is the Transverse Deflector Structure (TDS) drawn at the end of the FEL radiator. Aside from providing an unparalleled diagnostic of the overlap of the seed with the electron bunch, this X-band longitudinal beam diagnostic would be shared with the LAOLA plasma wakefield acceleration experiment in FLASH3 [7] and provide information on the FEL pulse length to users.

This paper includes brief descriptions of

- electron beam and laser parameter ranges
- TDS design and resolution
- chicane, modulator and laser injection design
- impacts of electron bunch compression schemes
- impacts of laser parameters
- a simulation of HGHG and EEHG
- the conditions for EEHG cascade and SHAB

The conclusion is that by building a flexible, staged design which has the potential to seed the shortest possible wavelengths for the maximum 1.3 GeV FLASH electron beam energy, a competitive program can be developed for FLASH2 to deliver the benefits of external seeding to the FEL users in terms of longitudinal coherence, increased intensity, direct control over pulse properties and spectral stability.

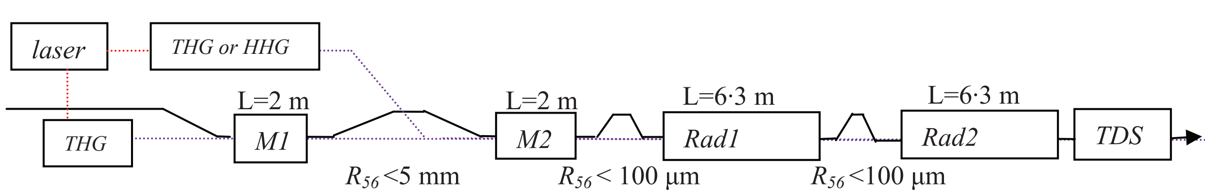

Figure 1: A flexible design for FLASH2 allowing for SASE, HGHG, EEHG, EEHG-HHG, HHG and an EEHG cascade, facilitating seeding between 4 and 40 nm. Harmonics of the Ti:sapphire laser pulse can be generated through Third Harmonic Generation (THG) or High Harmonic Generation (HHG). Two modulators (M1, M2) could be used to facilitate a flexible seeding program, while a Transverse Deflecting Structure (TDS) could diagnose the longitudinal profile and energy spread of the electron beam.

#*kirsten.hacker@cfel.de

ISBN 978-3-95450-133-5

CIRCULAR POLARIZATION CONTROL BY REVERSE UNDULATOR TAPERING

E.A. Schneidmiller, M.V. Yurkov, DESY, Hamburg, Germany

Abstract

Baseline design of a typical X-ray FEL undulator assumes a planar configuration which results in a linear polarization of the FEL radiation. However, many experiments at X-ray FEL user facilities would profit from using a circularly polarized radiation. As a cheap upgrade one can consider an installation of a short helical (or cross-planar) afterburner, but then one should have an efficient method to suppress powerful linearly polarized background from the main undulator. We propose a new method [1] for such a suppression: an application of the reverse taper in the main undulator. The method is free and easy to implement, it can be used at different X-ray FEL facilities, in particular at LCLS after installation of the helical afterburner in the near future. The theoretical background of the method as well as detailed numerical simulations are presented in [1]. In this note we discuss qualitatively the physics of the effect discovered in [1].

METHOD DESCRIPTION

In a short-wavelength SASE FEL the undulator tapering is used for two purposes: to compensate an electron beam energy loss in the undulator due to the wakefields and spontaneous undulator radiation; and to increase FEL power (post-saturation taper). In both cases the undulator parameter K decreases along the undulator length. The essence of our method is that we use the opposite way of tapering: parameter K increases which is usually called reverse (or negative) taper. We discovered [1] that in some range of the taper strength, the bunching factor at saturation is practically the same as in the reference case of the non-tapered undulator, the saturation length increases slightly while the saturation power is suppressed by orders of magnitude. Therefore, our scheme is conceptually very simple (see Fig. 1): in a tapered main (planar) undulator the saturation is achieved with a strong microbunching and a suppressed radiation power, then the modulated beam radiates at full power in a helical afterburner, tuned to the resonance.

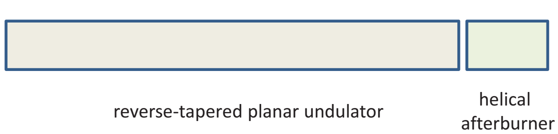

Figure 1: Conceptual scheme for obtaining circular polarization at X-ray FELs.

QUALITATIVE DISCUSSION

The theoretical background of the method as well as detailed numerical simulations are presented in [1]. Here we would like to discuss qualitatively the physics of the considered effect assuming that the reader is familiar with the main results of Ref. [1].

We will characterize the strength and the sign of linear taper by the taper strength parameter:

$$\beta = -\frac{\lambda_{\mathrm{w}}}{4\pi\rho^2} \frac{K(0)}{1+K(0)^2} \frac{dK}{dz} . \qquad (1)$$

Here z is the coordinate along the undulator length, ρ is the well-known FEL parameter, λ_{w} is the undulator period, and K is the undulator parameter with its initial value denoted as $K(0)$.

When the undulator parameter decreases along the undulator length, β is positive and we deal with a standard (positive) taper. In the opposite case the taper is reverse (or negative). Note that there were already two proposals for making use of the reverse taper in FELs: to improve the efficiency of FEL oscillators [2], and to use it in combination with an energy chirp in order to produce attosecond X-ray pulses [3]. Here we discuss a new useful feature of the reverse taper: a possibility to generate a strongly modulated electron beam at a pretty much reduced level of the radiation power.

As for the magnitude of $|\beta|$, one can consider two asymptotes. When $|\beta|$ is small, the undulator tapering leads to a small correction to the FEL gain length which was studied in [4]. Note that the tendency we would like to demonstrate (low power at stron bunching) is not seen in this regime. For this reason we will consider the asymptote of large $|\beta|$ in our qualitative discussion (even though in practical examples we deal with intermediate values of $|\beta|$).

Let us consider the high gain linear regime of the FEL operation and make the following consideration:

i) Consider the evolution of the SASE FEL frequency band which should depend on the sign and the magnitude of β. It was found in [4] that for small $|\beta|$, the central frequency of the amplified band moves half as fast as does the resonance frequency (corresponding to the current value of the undulator parameter K). We have found that situation is quite different in the case of strong taper, i.e. when $|\beta| \gg 1$. In the case of positive β the central frequency completely follows the changes of K, while in the case of a reverse taper, $\beta < 0$, the central frequency remains to be close to the resonance at the beginning of the undulator, i.e. it does not follow the changes of K at all. In other words, in the latter case the detuning from resonance continuously increases along

ISBN 978-3-95450-133-5

RADIATION PROPERTIES OF TAPERED HARD X-RAY FREE ELECTRON LASERS*

C. Emma, C. Pellegrini, UCLA, Los Angeles, CA, USA
J. Wu, K. Fang, S. Chen, SLAC, Menlo Park, CA, USA
S. Serkez, DESY, Hamburg, Germany

Abstract

We perform an analysis of the transverse coherence of the radiation from a TW level tapered hard X-ray Free Electron Laser (FEL). The radiation properties of the FEL are studied for a Gaussian, parabolic and uniform transverse electron beam density profile in a 200 m undulator at a resonant wavelength of 1.5 Å. Simulations performed using the 3-D FEL particle code GENESIS show that diffraction of the radiation occurs due to a reduction in optical guiding in the tapered section of the undulator. This results in an increasing transverse coherence for all three transverse electron beam profiles. We determine that for each case considered the radiation coherence area is much larger than the electron beam spot size, making coherent diffraction imaging experiments possible for TW X-ray FELs.

INTRODUCTION

Self Amplified Spontaneous Emission X-ray Free Electron Lasers (SASE X-FELs) [1–3] have been used to study structures and dynamical processes with spatial resolution of 1 Å and temporal resolution of 1 fs. This has had a particularly significant impact in the field of bio imaging where X-FELs have been used to push the frontiers of what can be done with diffraction based imaging techniques [4–6]. Future research in this field will benefit from a larger number of coherent photons/pulse, a factor of ten to one hundred larger within a pulse duration of 10-20 fs corresponding to a peak output power of 1 TW or more.

Together with high peak power, coherent X-ray diffraction imaging experiments require the radiation to be sufficiently longitudinally and transversely coherent at the sample position [7]. The longitudinal coherence can be improved by seeding or self-seeding the FEL amplifier [8–10]. Tapering the XFEL after self-seeding presents a promising solution to achieving TW power pulses with adequate longitudinal coherence. In this work we examine the transverse coherence properties of the radiation from a seeded and tapered hard X-ray FEL and determine wether the radiation is sufficiently transversely coherent to serve as an adequate source for diffraction based imaging experiments.

RADIATION PROPERTIES

FEL Radiation in a Tapered Undulator

We analyze the case of a hard X-ray tapered FEL with electron beam and undulator parameters similar to those of the LCLS-II upgrade project. The FEL is formed of 3.4 m long undulator sections with 1m breaks for a total length of 200 m. The system is simulated using the fully 3-dmensional FEL particle code GENESIS in both single frequency and time dependent simulations (see table 1 for parameters). The magnetic field and the quadrupole focusing is optimized to yield the maximum output following the work of Ref. [11]. The simulations are performed for three different transverse electron beam distributions: uniform, parabolic and Gaussian. After the initial saturation and exponential gain regime the FEL process is dominated by refractive guiding of the radiation by the electron beam. This can be described by considering the complex refractive index of the electron beam [12]

Table 1: GENESIS Simulation Parameters

Parameter Name	Parameter Value
Beam energy E_0	13.64 GeV
Beam peak current I_{pk}	4000 A
Normalized emittances $\epsilon_{x,n}/\epsilon_{y,n}$	0.3/0.3 µm rad
Electron bunch length l_b	16.4 fs
Peak radiation power input P_{in}	5 MW
Undulator period λ_w	32 mm
Normalised undulator parameter a_w	2.3832
Radiation wavelength λ_r	1.5 Å
FEL parameter ρ	7.361 $\times 10^{-4}$

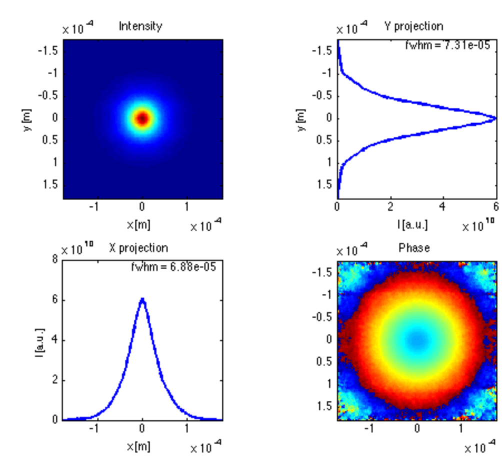

Figure 1: Amplitude and phase of the radiation field at the undulator exit (z=200 m) for a Gaussian transverse electron beam distribution obtained from time independent GENESIS simulation

* Work supported by: DOE Grant Number DE-SC0009983

ISBN 978-3-95450-133-5

CHIRPED AND MODULATED ELECTRON PULSE FREE ELECTRON LASER TECHNIQUES

J. R. Henderson[1], L.T. Campbell[1,2,3,4], and B.W.J. McNeil[1]
[1]SUPA, Department of Physics, University of Strathclyde, Glasgow, UK
[2]ASTeC, STFC Daresbury Laboratory and Cockcroft Institute, Warrington, UK
[3]Center for Free-Electron Laser Science, Notkestrasse 85, Hamburg, Germany
[4]Institut für Experimentalphysik, Universität Hamburg, Hamburg, Germany

ABSTRACT

A potential method to improve the free electron laser's output when the electron pulse has a large energy spread is investigate and results presented. A simplified model is the first given, in which there are a number of linearly chirped beamlets equally separated in energy and time. By using chicanes, radiation from one chirped beamlet is passed to the next, helping to negate the effect of the beamlet chirps and maintaining resonant interactions. Hence the addition of chicane allow the electrons to interact with a smaller range of frequencies ($\Delta\omega < 2\rho\gamma_r$), sustaining the FEL interaction. One method to generate such a beamlet structure is presented and is shown to increase FEL performance by two orders of magnitude.

INTRODUCTION

Free Electron Lasers are already important research tools and have started to unlock many new areas of science in diverse fields such as; Warm-Dense matter studies, short pulse protein diffraction and medicine/surgery. Current Free Electron Lasers rely on linear accelerators to provide the electron bunch, for an x-ray FEL the accelerator can be kilometres long. The potential for plasma-wakefield accelerators to drive the Free Electron Laser has been of theoretical and experimental interest for many years. Plasma accelerators generate accelerating gradients on the order of 10^3 times greater traditional linear accelerators, which offers the potential to reduce the total length of the FEL. Electron pulses used in free electron lasers can exhibit a large energy chirp (greater than 1 % of mean electron beam energy) which can degrade the FEL interaction. Linear energy chirps have been previously studied in [1] the results of this work have been recreated here using Puffin [2] an unaveraged 3D parallel FEL simulator. The results of these chirped pulse simulations are in good agreement with [1] showing the flexibility of Puffin. Electron pulses from plasma accelerators are limited by a large energy spread, this is also issue with older accelerators were energy spread is sacrificed for a larger rho (a measure of FEL efficiency) and higher pulse energies. A method that may allow the free electron laser to operate with a large energy spread is proposed, simulations were performed using Puffin. In this method a chirped electron pulse is split in a number of chirped electron beams or beamlets. To sustain the FEL interaction radiation is passed from beamlet to beamlet by applying a series of chicane slippage sections. By making the slippage in undulator-chicane module equal the beam separation the radiation pulse will continuously interact with electrons within the same energy range. One method to generate a similar beamlet structure, the beamlet method, is presented. In the beamlet method a modulator-chicane section is used to generate a set of beamlets which have a smaller local (slice) energy spread than the initial electron pulse. Radiation is then passed from these areas of reduced energy spreads to sustain the FEL interaction. This method shows an approximate two-fold improvement in the radiation field intensity and a four-fold improvement when the radiation field is filtered around the resonant frequency.

SINGLE CHIRPED PULSE

When an electron pulse is given an energy chirp, the effects can be both beneficial and detrimental to the FEL interaction depending upon the gradient of the chirp [1].

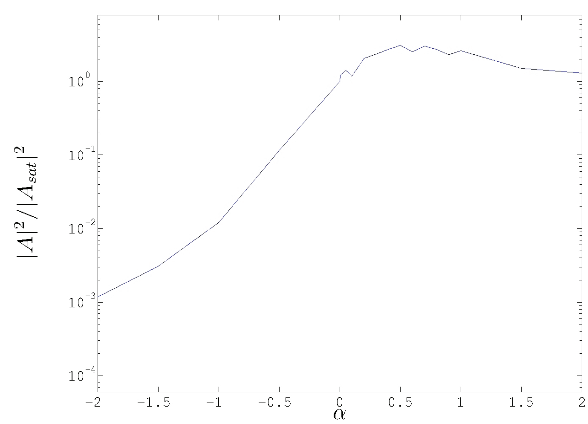

Figure 1: Chirped electron pulse: the scaled saturation power $|A|^2$ is plotted as a function of the energy chirp, the energy chirp parameter [1] is given by $\hat{\alpha} = -\frac{2}{\rho\gamma_r}\frac{d\gamma}{d\bar{z}_2}$, were $|A_{sat}|^2$ is the saturation intensity at $\hat{\alpha} = 0$. This agrees with Figure 2 of [1] where matching parameters parameters have been used. $|A|^2/|A_{sat}|^2$ is equivalent to η from [1].

The results of [1] are reproduced using Puffin. Puffin uses the scaled notation of [3,4],were $\bar{z}_2$ defines a position in the electron bunch and is given by $\bar{z}_2 = (ct - z)/l_c$ where the cooperation length is defined as $l_c = \lambda_r/4\pi\rho$. The scaled radiation is field is given by, $A_\perp = \frac{e u \bar{a}_u l_g}{2\sqrt{2}\gamma_r^2 mc^2\rho} E_\perp$, where u

ISBN 978-3-95450-133-5

A REVIEW OF HIGH POWER OPCPA TECHNOLOGY FOR HIGH REPETITION RATE FREE-ELECTRON LASERS*

M. J. Prandolini†, R. Riedel, Helmholtz-Institut Jena, Fröbelstieg 3, D-07743 Jena, Germany
M. Schulz, Deutsches Elektronen-Synchrotron DESY, Notkestrasse 85, D-22607 Hamburg, Germany
F. Tavella‡, SLAC National Accelerator Laboratory, 2575 Sand Hill Rd., CA 94025, USA

Abstract

High repetition rate free-electron lasers (FEL) require the development of new laser systems that have the ability to operate at high average power. Optical parametric chirped-pulse amplification (OPCPA) is presently the most promising method to fulfill these requirements. This technique has been used to demonstrate amplification up to tens of watts with a repetition rate in the range between tens of kHz to MHz in burst and continuous mode. We review the current OPCPA technology for systems operating around 800 nm; this includes various frontend options, pump amplifier technology and latests results, and we discuss the important requirements for achieving high power lasers in both burst and continuous operation.

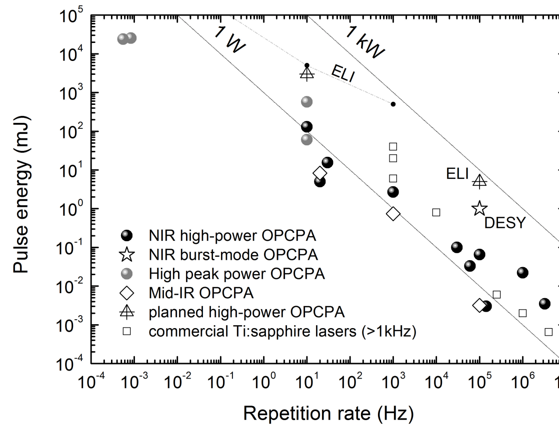

Figure 1: Current and planned high average power laser systems: ELI - Extreme Light Infrastructure; DESY - Deutsches Elektronen-Synchrotron

INTRODUCTION

High repetition rate FELs present some unique challenges for laser developers. Superconducting cavities, developed at DESY [1], allow a much higher repetition rate than conventional accelerator technologies; however, they have a burst mode structure. For example, FLASH at Hamburg has a maximum repetition rate of 1 MHz within a burst structure of 800 μs at 10 Hz [2, 3]. This presents major challenges for the design and operation of FEL seeding and pump-probe lasers operating in burst mode. At lower repetition rates, conventional Ti:sapphire lasers are currently used in FELs [4]. However, in the last years there has been remarkable progress in high average power OPCPA systems (Fig. 1). Currently, the high repetition rate and high power OPCPAs have been demonstrated at an average power of 11.4 W at 3.25 MHz [5] and 22 W at 1 MHz [6], and in a burst operation of 38.5 W at 27.5 kHz within a burst structure similar to FLASH [7]. For the amplification of high power, few-cycle, optical pulses, OPCPA is the leading technology [6, 8–10], due to the inherent bandwidth limitations of Ti:saphire technology [11].

A comparison of a Ti:sapphire amplifier and a non-collinear optical parametric amplifier (OPA) is schematically shown in Fig. 2. In a Ti:sapphire amplifier, the pump pulses are used to create a population inversion, where the pump energy is stored in the gain material itself before being transfered to the signal via stimulated emission. The quantum defect for Ti:sapphire is 34%, the resulting energy difference goes into heating of the gain material, which therefore has to be cooled. In contrast in a noncollinear OPA, the energy of the pump wave (ω_P) is transferred, via a second order nonlinear effect within the gain material, into signal (ω_S) and idler (ω_I) waves. Thereby, energy conservation is maintained between the three waves ($\omega_I = \omega_P - \omega_S$). For certain applications the idler wave can be used, but in general it is discarded. Nevertheless, a small amount of linear absorption from the pump, signal and idler does occur, which starts to become noticeable at around tens of watts of output energy.

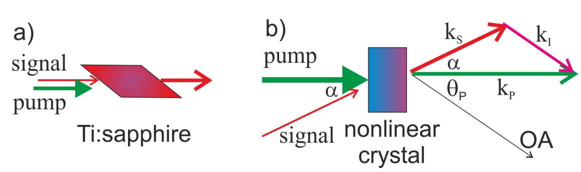

Figure 2: A comparison of laser amplifier technologies: (a) The Ti:sapphire amplifiers operate using the conventional population inversion within the gain material created by a pump pulse. (b) In noncollinear OPA, the energy of the pump is transferred, via a second order nonlinear effect within the gain material, into signal and idler waves: α - non-collinear angle; θ_P - angle between the pump wavevector (k_P) and the optical axis (OA); k_S and k_I - wavevectors of the signal and idler, respectively.

* Work supported by the Helmholtz Institute Jena and the Deutsches Elektronen-Synchrotron DESY in Hamburg. The authors would also like to thank the Helmholtz Association for their support for the spin-off project *Class 5 Photonics*.
† mark.prandolini@desy.de
‡ Formally at DESY

ISBN 978-3-95450-133-5

A GAAS PHOTOEMISSION DC GUN FOR CAEP HIGH-AVERAGE-POWER THz FEL*

Hanbin Wang#, Kai Li, Ming Li, Dai Wu, Dexin Xiao, Xingfan Yang
Institute of Applied Electronics, CAEP, China.

Abstract

FEL-THz plays an important role in THz science and technology research, for high power output and tunable wavelength, which is indispensable to material, biology, medical research. Now, the construction is underway at China Academy of Engineering Physics (CAEP) on high-average-power FEL THz source, and the demonstration of stable, reliable, high brightness, high power electron source operation is one of key issues. The components of the system were constructed and the performance tests are still on. The lifetime of the Negative Electron Affinity (NEA) surface is about 40 hours, which is limitied mainly by vacuum. Up to now, the gun can supply 5mA beam current and has been employed for preliminary experiments. In this paper, the design considerations and present status are given.

INTRODUCTION

FEL-THz source is a strong candidate among THz sources in THz application researches, and now a high-average-power FEL-THz source is under construction in CAEP. The key component of the facility is a high average current, low emittance electron source, which should delivers about 100pC/bunch (the average current of 5mA) . To fulfil the requirements, the DC gun become a leading choice for better technical maturity[1]. Since the gun can offer excellent vacuum, we use a NEA GaAs photocathode, which has a relatively high quantum efficiency (QE) and practical operating wavelength.

The construction of a DC gun is still careful to do, despite its technical maturity and there are two items to consider. One is how to achieve the extra-high vacuum, NEA GaAs is chemically reactive and is degraded by a small fraction of H_2O or CO_2. Photo-cathode's QE can be degraded by ion back bombardment, independent of the gas species forming the ion. the other is how to realize high voltage stable operation, the field emission is a principal challenge[2], which arising from the cathode electrode and its support structure may result in voltage breakdown across the cathode-anode gap, or a punch-through failure of the insulator holding off the cathode potential, and directly affects operation.

The very successful Jlab IR FEL operates based on a photocathode dc gun[3]. The gun design started as a 500 kV gun with a peak electric field of 10 MV/m at the surface of the cathode in the beginning of 1990's[4]. Due to field emission from the electrode structures encountered during the 1kW IR Demo's commissioning, the gun has been modified to a lower gradient at the cathode achieved by lowering the operating voltage to 320kV and by increasing the cathode-anode gap (6 MV/m at 500 kV)[5]. The 500kV operation is realized untill 2011[6]. So, it should be envisioned that the high voltage operation must circumvent many obstacles. We consult the experiences from other lab and ours, and the design incorporates some features of the existing DC gun. In the following sections, the component solutions adopted and the CAEP DC gun status are given.

DESIGN OF CAEP DC GUN

High QE cathode must be prepared and transferred under vacuum. The existing photoemission DC guns can be classified two types; one prepare cathodes in situ in the electron guns, the other transfer cathodes under vacuum from a separate preparation chamber by a load-lock.

As Fig. 1 shows, the CAEP DC gun adopts a load-lock design too, which consists of three components (photocathode load-lock system, main gun chamber and mode lock laser). The following describes a design on the major points of interest about each component.

PHOTOCATHODE LOAD LOCK SYSTEM

The photocathode load lock system includes three chambers as shown in Fig. 1, where the function is realized of cathode puck introduction, preparation and storage.

The beginning part is an introduction chamber, and the primary function is to introduce pucks and store them for succedent processing. The first processing is atomic hydrogen cleaning, which provides a means to clean exotic photocathode materials for which wet chemistry techniques are incapable. A KYKY F700 turbo-pump is used during atomic hydrogen cleaning where typical values for temperature and pressure near the sample are 200 C and 2E-3 Pa respectively. During the process, a ceramic heater is used to raise sample temperature for atomic hydrogen cleaning.

The middle part is a preparation chamber, where the heating and activation processing are completed. A magnet manipulator transfers a puck from introduction chamber to preparation chamber after atomic hydrogen cleaning process. Same to the heating process in the introduction chamber, a ceramic heater is used to heat the wafer to about 450 C at a ramp rate up and down of 1 C per second, and the ramp down control is aided by an active cooler. The preparation chamber is a stainless steel chamber with eighteen ports placed around the circumference, which contains all of the components to produce NEA photocathodes: a channel cesiator, a NF_3 or

*Work supported by the ministry of science and technology
#wanghanbin@caep.cn

ISBN 978-3-95450-133-5

STATUS OF THE SwissFEL C-BAND LINAC

F. Loehl, J. Alex, H. Blumer, M. Bopp, H. Braun, A. Citterio, U. Ellenberger, H. Fitze, H. Joehri, T. Kleeb, L. Paly, J.-Y. Raguin, L. Schulz, R. Zennaro, C. Zumbach,
Paul Scherrer Institut, Villigen PSI, Switzerland

Abstract

The linear accelerator of SwissFEL will be based on C-band technology. This paper summarizes the latest results that were achieved with the first prototype components. Furthermore, the progress and plans of the series production are discussed.

INTRODUCTION

The hard x-ray free-electron laser facility SwissFEL [1] is currently under construction at the Paul Scherrer Institute. In the main linear accelerator (Linac) of SwissFEL, the electron bunches are accelerated from an energy of 350 MeV to a final energy of up to 5.8 GeV. For this, the Linac is divided into three segments (see Fig. 1): Linac 1, Linac 2, and Linac 3. After Linac 1, the electron bunches are compressed in a magnetic bunch compressor chicane BC2 at an intermediate energy of 2.1 GeV - the first bunch compressor BC1 is located within the injector at an energy of ~350MeV. After Linac 2, at an energy of 3.0 GeV, a switch-yard [2] is installed with which electron bunches can be sent either straight into Linac 3 and consequently the hard x-ray Aramis line, or into a future soft x-ray line called Athos. At the end of Linac 3, transversely deflecting structures will be located that will allow for measurements of the longitudinal charge profile with a resolution of a few femtoseconds.

C-BAND MODULE

The C-band modules for SwissFEL consists of four C-band structures that are installed onto two granite girders (see [3] for a schematic). A module is fed by a single RF source with up to 50 MW of RF power. The RF pulse is compressed using a barrel open cavity (BOC) pulse compressor [4], and the compressed pulse is distributed to the four accelerating structures using a wave-guide network that is installed on the side of the girders. That way, the entire linac module can be pre-assembled and complete modules can be brought into the SwissFEL facility, which simplifies the assembly procedure of the 26 modules.

The accelerating modules can be operated in two different modes that are defined by how the pulse compressor is operated. In mode I, a 180° phase jump is applied towards the end of the RF pulse, yielding an RF pulse with more than 300 MW of peak power. The pulse is, however, not flat (see [4]). In mode II, a phase modulation is applied that yields a flat RF pulse at the cost of a significantly reduced RF power.

At an RF power from the klystron of 50 MW, the expected on-crest energy gain of a module is around 220 MeV when a flat RF pulse is applied and 275 MeV with the phase jump mode. In SwissFEL, it is planned to operated the klystrons at up to 40 MW which yields on-crest energy gains of close to 200 MeV and 250 MeV in both modes. When two or more bunches are accelerated within the same RF bunch, as planned for the parallel operation of the hard and soft x-ray lines Aramis and Athos, a flat RF pulse might provide better stability and simplify the operation in Linac 1, where the beam is accelerated off-crest. In Linacs 2 & 3, where the beam is accelerated on-crest, it is planned to operate in the phase jump mode in order to maximize the energy gain.

C-band High Power Test Stand

In order to test RF components, PSI operates a C-band test stand that provides two test benches: a component test bench and a test bench for a complete linac module. All test results that are discussed here are obtained within the component test bench. The second test bench with a complete Linac module is currently being setup and expected to become operational end of this year. The current state of the first prototype module is depicted in Fig. 2. The picture shows the module in beam direction with the accelerating structures and the wave-guide network already in place. On top of the linac module, the water distribution is visible that is also prototyped. The pulse compressor is not yet installed but the support is already visible right at the beginning of the module.

RF Source

The C-band RF pulses with a power of up to 50 MW and a duration of 3 μs are generated by Toshiba klystrons of type E37212 that are driven by solid-state pre-amplifiers and solid-state modulators. In order to save energy, the collectors of the klystrons will be operated at a temperature of 80 °C so that part of the energy can be recovered to heat buildings on the PSI campus. This scheme was successfully tested in the high power test stand. The first klystrons for SwissFEL are already delivered to PSI, and the delivery of the complete set of klystrons will be completed ahead of schedule.

In order to validate their performance, different pre-amplifiers have been characterized in the test stand, showing that the required phase and amplitude stability can be reached. The tender process for the SwissFEL series will start end of this year.

Of major importance for SwissFEL are the modulators that drive the klystrons. The C-band test stand was operated until now with a ScandiNova K2 modulator. Since this modulator does not fulfill the requirements for SwissFEL in terms of reliability and stability, two prototype solid-state modulators were ordered at two companies last year. The first modulator is built by Scandinova, the second one by

ISBN 978-3-95450-133-5

REVIEW OF COHERENT SASE SCHEMES

B.W.J. McNeil[1], L.T. Campbell[1,2], D.J. Dunning[1,2], J.R. Henderson[1] and N.R. Thompson[2]
[1]SUPA, Department of Physics, University of Strathclyde, Glasgow, UK
[2]ASTeC, STFC Daresbury Laboratory, Warrington, UK

Abstract

A review is presented of some of the methods and their origins that have recently been proposed to improve the temporal coherence of SASE output. These methods do not require any external laser seed field, or the use of the so-called self-seeding methods, where the SASE radiation is optically filtered and improved at an early stage of the interaction before re-injection and amplification to saturation. By using methods that introduce an additional relative propagation between the electron beam and the radiation field, the localised collective interaction, which leads to the formation of the 'spiking'associated with normal SASE output, is removed. The result is output pulses which are close to the fourier transform limit without the need for any external seeds or intermediate optics.

INTRODUCTION

This review presents the work of several different authors and closely follows the oral presentation presented at the 36th International Free Electron Laser Conference, Basel, August 25-29, 2014. An historical perspective is given of some methods proposed to improve the temporal coherence properties of SASE output. It is hoped this perspective will demonstrate how some of the quite complex, perhaps non-intuitive, departures from a simple FEL interaction evolved.

SASE

The problem with normal SASE output from a FEL is that it has relatively poor temporal coherence. At shorter wavelengths, the electron pulse length can be significantly greater length than the relative propagation, or slippage, of a light wavefront through the pulse to saturation. As the SASE interaction starts from noise, this itself would limit the temporal coherence length to the slippage length. However, a more fundamental length that limits the temporal coherence length is the cooperation length l_c [1]. This is the length that a light wavefront propagates, or slips, through the electron pulse in one gain length l_g through the undulator. As each region of length $\sim l_c$ starts from noise, this leads to a spiking behaviour in the light intensity with spikes separated by $\sim 2\pi l_c$ [2]. A similar noisy spectrum results which gives a relatively large time-bandwidth product $\Delta\nu\Delta t \gg 1$ with typical simulated output in the X-ray shown in slide 3. A closer look at the phase of the light in slide 4, again from simulations, shows that the phase of each of the radiation 'spikes' is uncorrelated. i.e. each spike appears to have evolved independently from the others from noise.

DIRECT SEEDING

One method to improve this noisy output is to inject a resonant coherent seed light field coincident with the electron pulse at the start of the FEL interaction. If the seed is of sufficient intensity to dominate that due to the spontaneous noise, then the interaction can progress with a well-defined phase imposed by the seed through to saturation. This was first performed at short wavelengths at $\sim$ 53 nm [3] as shown in slide 6. Unfortunately, no such seeds yet exist in the X-ray.

INDIRECT SEEDING

An alternative to direct seeding at the desired wavelength is to first prepare the electron beam by seeding at a longer wavelength where a suitable seed with good temporal coherence properties is available. The bunched electrons will inherit the coherence properties of the seed and will also have strong coherent bunching components at higher harmonic wavelengths. The electrons can subsequently be injected into an undulator resonant at these shorter harmonic wavelengths [4,5] where lasing may continue (slide 8) in a process sometimes called 'High Gain Harmonic Generation'. The electron bunching may be enhanced between undulators by using a dispersive chicane. In principle this process can be 'cascaded' to shorter wavelengths as demonstrated experimentally [6] and shown in slide 9. Unfortunately (slide 10), the phase noise amplification is multiplied by a factor of the square of the frequency increase through the cascaded system, and with current seeds available this method cannot yet be used to reach X-ray wavelengths [7].

An alternative to HGHG is the Echo Enabled Harmonic Generation, first described in [8, 9] and experimentally observed in [10] (slide 13). Interesting variations of the method are also being pursued [11] (slide 14), which may offer scope for further development. The EEHG method is described schematically in slide 15 and involves a preparation of the electron beam by: energy modulation - dispersion - energy modulation - dispersion. This introduces an electron bunching at an harmonic of the energy modulation period which will then emit radiation superradiantly on entering an undulator tuned to the electron bunching period. The limit as to how high the harmonic can be pushed probably remains unresolved, although good progress is being made experimentally with the 15th harmonic emission demonstrated [12]. The work of [13] suggests that the upper harmonic limit will be due to fluctuations in the modulating laser phase and intensity.

It is interesting to note that the final electron bunching spectrum of the EEHG is a comb of modes about the final harmonic with mode separation of the initial modulation

ISBN 978-3-95450-133-5

GENERATION OF INTENSE XVUV PULSES WITH AN OPTICAL KLYSTRON ENHANCED SELF- AMPLIFIED SPONTANEOUS EMISSION FREE ELECTRON LASER

G. Penco # 1, E. Allaria[1], G. De Ninno[1], E. Ferrari[1,2], L. Giannessi[1,3]
[1]Elettra-Sincrotrone Trieste S.C.p.A., Basovizza, Italy
[2]Università Degli Studi di Trieste, Dipartimento di Fisica (Trieste), Italy
[3]ENEA C.R. Frascati, Frascati (Roma), Italy

Abstract

Fermi is a seeded FEL operating in high-gain harmonic generation mode. The FEL layout is constituted by a modulator and six radiators separated by a dispersive section. The modulator and the radiators can be tuned to the same resonant frequency to set up an asymmetric optical klystron configuration where self-amplified spontaneous emission can be generated and studied. This paper presents the experiment consisting in the analysis of the enhancement of the self-amplified spontaneous emission (SASE) radiation by the dispersion in the optical klystron. The FEL pulses produced with the optical klystron configuration are several orders of magnitude more intense than in pure SASE mode with the dispersion set to zero. The experimental observations are in good agreement with simulation results and theoretical expectations. A comparison with the typical high-gain harmonic generation seeded FEL operation is also provided.

INTRODUCTION

The optical klystron (OK) concept was proposed by Vinokurov and Skrinsky in 1977 [1] to enhance the gain of a multi-pass free electron laser (FEL) driven by a storage ring. The basic scheme consists of two undulators separated by a dispersive section, which converts the beam energy modulation produced in the first undulator in density modulation, enhancing the electron bunching at the radiation wavelength and speeding up the FEL process in the second undulator. The first experimental demonstration of the optical klystron FEL was performed in 1979 at the VEPP-3 storage ring of the Budker Institute of Nuclear Physics (BINP, Novosibirsk, Russia) [2], obtaining an initial gain of 0.5% at 630 nm and improving it subsequently up to 2.5% per pass [3]. Afterwards, other FEL oscillator facilities implemented the optical klystron scheme, such as ACO SR FEL (LURE, France), which lased at 635 nm in 1983 [4] and at 463 nm in 1987 [5]. Improvements in the optical cavity mirror coatings made it possible to lase in the ultra-violet at 240 nm in 1989 (OK-4/VEPP-3 storage ring FEL [6]) and step by step down to 193 nm in 1999 (OK-4 Duke SR FEL [7]). In 2000, the ELETTRA storage ring FEL lased at 217.9 nm [8].

The gain of the optical klystron dramatically decreases with decreasing wavelength, while the optical cavity mirrors losses increase, and this has constituted a strong constrain in reaching emission at shorter wavelengths. A distributed optical klystron (DOK) was proposed by Litvinenko [9] to increase the gain and the first successful experiment was conducted in the DOK-1 FEL, at Duke University [10], obtaining a gain of about 48% per pass.

The progress of linac technologies has allowed generating very high brightness electron beams, able to drive single-pass high-gain FELs, providing intense radiation in the XVUV [11-13] and in the X-ray regimes [14,15]. A very common high -gain FEL mode is the self-amplified spontaneous emission (SASE) FEL, that is based on driving a high brightness electron beam through a long undulator tuned at a predetermined wavelength λ_r. The initially incoherent spontaneous radiation emitted by the beam couples with the electron beam itself and is then exponentially amplified, developing energy and density modulation at the wavelength λ_r, and finally emitting intense and coherent radiation. However, to reach the FEL intensity saturation in the extreme VUV and in the X-ray, it is necessary to have a long undulator chain, typically in the order of ~100 m, so alternative schemes have been studied in the past years in order to speed up the amplification process. In the following section we provide a short review of the 1-D theory describing the application of the OK concept to the SASE FEL.

OPTICAL KLYSTRON SASE FEL 1-D THEORY

The possibility to apply the optical klystron concept to high-gain FEL amplifiers has been faced in several papers [16-23]. An important result of these studies is that the klystron high-gain FEL performance is strongly influenced by the electron beam relative uncorrelated energy spread (δ), that is required to be much lower than the FEL Pierce parameter ρ [24,25]. In the following we briefly recall the 1-D theory developed in [20,23] that provides an approximated expression for the gain factor G of the optical klystron relative to the “pure” SASE mode, i.e. dispersive section turned off.

We consider an undulator resonating at the frequency $\omega_r = 2\pi / \lambda_r$. The optical klystron enhancement factor to the radiation electric field E at the scaled frequency $\nu=\omega/\omega_r$ can be written as follows:

$$R(\nu) = \frac{E_\nu^{OK}}{E_\nu^{noOK}} = \frac{1 - \int d\xi \frac{dV(\xi)}{(\mu-\xi)^2 d\xi} e^{-i\rho k_r R_{56}\xi} e^{ik_r \nu R_{56}/2}}{1 + 2\int d\xi \frac{V(\xi)}{(\mu-\xi)^3}} \quad (1)$$

ISBN 978-3-95450-133-5

FEL OVERCOMPRESSION IN THE LCLS*

J.L. Turner, F.-J. Decker, Y. Ding, Z. Huang, R. Iverson, J. Krzywinski, H. Loos, A. Marinelli, T. Maxwell, H.-D. Nuhn, D. Ratner, T. Smith, J. Welch, F. Zhou,
SLAC NAL, Menlo Park, CA 94025, U.S.A.

Abstract

Overcompression of the Linac Coherent Light Source (LCLS) x-ray Free Electron Laser (FEL) at the SLAC National Accelerator Laboratory is studied. The studies and some operational implications are summarized here.

INTRODUCTION

The needs of XFEL users lead to exploring the LCLS parameter space. Some experiments benefit from a broad spectrum x-ray beam. Inducing projected energy spread across the electron bunch leads to a transformation into broader photon spectrum. Overcompression, is where in the second bunch compressor the head of the bunch slips back behind the tail, adding to the wake induced energy spread in subsequent L3 linac. This induces a relatively large energy deviation along the bunch typically leading to broader spectrum at the cost of reduced x-ray intensity. A method is being developed where performance can be improved by lasing using only the core of the electron beam.

DIAGNOSTICS

Two very useful pulse-to-pulse diagnostics are relied upon in these studies: a hard x-ray single-shot spectrometer (HXSSS) [1] (Figure 1), and an x-band transverse deflecting RF cavity (XTCAV) [2].

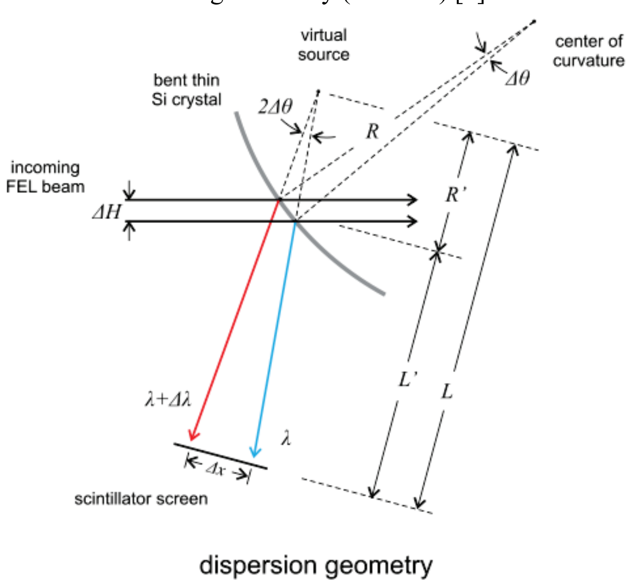

Figure 1: X-ray beam comes in from the left, a small percentage is dispersed by different energies having different Bragg angles from the bent Si crystal. Figure from Ref. [1].

* This work was supported by U.S. Department of Energy, Office of Basic Energy Sciences, under Contract DE-AC02-76SF00515

The cylindrically bent Si(1 1 1) transmissive crystal membrane spectrometer [1] samples different energies across the beam vertical profile, you get amplitude response which is a function of the Gaussian beam profile. To the extent that the beam is larger than the area sampled this makes the response more uniform. In any case, this can be accounted for by nearby beam profile measurement. What you see is the SASE lines in a spectrograph. (Figure 2). The full bandwidth for the data taken was about 120 eV with resolution down to about 1 eV.

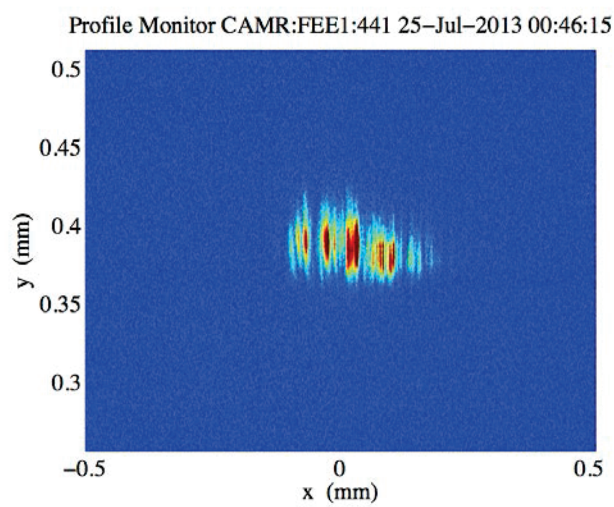

Figure 2: The SASE spikes can be seen dispersed in energy by the spectrometer crystal which in this case is Si(1 1 1). The imaged is rotated, so energy is on the X axis.

The XTCAV

After the electrons exit the undulator, the XTCAV streaks the beam in the horizontal plane, then beam become dispersed in the final bend magnets (Figure 3). The result is an image on a YAG screen which has time for a horizontal axis and energy on the vertical. By taking a non-lasing pulse for reference, images of the electrons during lasing can be used for temporal reconstruction of the x-ray pulse (Figure 3).

REFERENCE DATA

Typical LCLS machine running is undercompressed (see Figure 4) where the LCLS compression scheme leads to the development of high peak current at the head and tail of the beam that are apparent with the temporal reconstruction of the x-rays.

Empirical tuning of the FEL intensity can lead to beta-match and undulator taper match to either the ends or the

ISBN 978-3-95450-133-5

OPERATION OF FLASH WITH SHORT SASE-FEL RADIATION PULSES*

J. Rönsch-Schulenburg#, E. Hass, N.M. Lockmann, T. Plath, M. Rehders, J. Roßbach,
Hamburg University & CFEL, Hamburg, Germany
G. Brenner, S. Dziarzhytski, T. Golz, H. Schlarb, B. Schmidt, E. Schneidmiller, S. Schreiber, B. Steffen, N. Stojanovic, S. Wunderlich, M. Yurkov, DESY, Hamburg, Germany

Abstract

This paper describes the experimental activity on the generation of very short FEL pulses in the soft x-ray range in the SASE-mode at the high-gain free-electron laser FLASH [1, 2]. The key element, a photo-injector laser which is able to generate laser pulses of about 2 ps FWHM has been optimized and commissioned. It allows the generation of shorter bunches with low bunch charge (of up to 200 pC) directly at the photo-cathode. Initially shorter injector laser pulses and thus shorter bunches eases the required bunch compression factor for short pulses below 10 fs duration which makes operation of the electron beam formation system to be more robust with respect to jitters and collective effects. As a result, overall stability of SASE FEL performance is improved. In the optimal case single-spike operation can be achieved. In this paper the experimental results on production of short electron bunches and the SASE performance using the new injector laser will be shown and the measured electron bunch and FEL radiation properties are discussed. In addition, optimizations of bunch diagnostics for low charge and short bunches are discussed.

MOTIVATION

Several user-oriented free-electron laser (FEL) facilities aim for very short vacuum ultraviolet (VUV), extreme ultraviolet (XUV) and X-ray pulses which allow to study ultra-fast processes in different areas of science. In order to achieve such short bunches several schemes have been proposed. The most robust method to generate pulses of a few femtoseconds at FELs is to create a short electron bunch. In the most extreme case the lasing part of the bunch is as short as one longitudinal optical mode and thus the electron bunch length (σ_b) has to fulfill the condition $\sigma_b \leq 2\pi L_{coop}$ [3, 4], with L_{coop} the cooperation length. These so-called single-spike SASE pulses [3, 4] are bandwidth limited, longitudinally coherent and compared to seeding concepts no long background disturbs the signal. At FLASH [1, 2] single-spike operation requires bunches whose lasing part have a duration of a few fs. To mitigate space charge forces, this can only be achieved by applying low bunch charges of about 20 pC.

*The project has been supported by the Federal Ministry of Education and Research of Germany (BMBF) under contract No. 05K10GU2 and FSP301.

#juliane.roensch@desy.de

SHORT PULSE PHOTO INJECTOR LASER

As discussed already in detail in [5] such a short bunch would require a very strong compression (about 2000) in the two bunch compressors at FLASH when applying the standard photo injector laser with an rms laser pulse duration of 6.5 ps, which is optimized for 1 nC. Such a strong compression would lead to strong instabilities in the accelerator caused by small phase fluctuations. Therefore a new photo injector laser with a reduced pulse duration was commissioned [6, 7, 8]. It is optimized for variable pulse length from 0.7 to 1.7. The laser system consists of an oscillator and a Yb:YAG amplifier [9]. In the infrared an average output power of up to 7 W has been achieved, which corresponds to a single pulse energy of about 7 μJ.

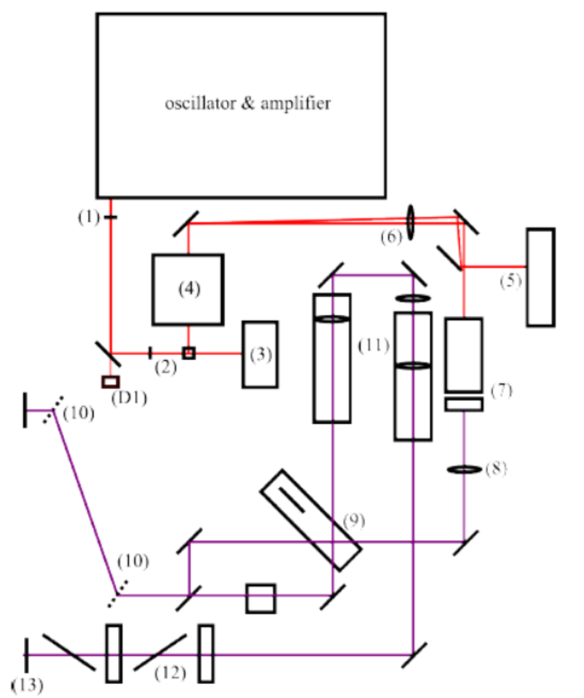

Figure 1: Scheme of the photo injector Laser beamline [8] with the following components: half-wave plate (1); photo diode (D1); beam splitter (2); power meter (3), acusto-optical modulator (AOM) (4); Beam-Dump (5); IR-lens, f = 300 mm (6); LBO-crystal and BBO-crystal (7); collimating UV-lens (8); remote controllable mirror for incoupling into the stretcher (9); pulse-stretcher (10); telescope (11); attenuator (12); aperture (13).

ISBN 978-3-95450-133-5

CHARACTERIZATION OF PARTIALLY COHERENT ULTRASHORT FEL PULSES

C. Bourassin-Bouchet, M.-E. Couprie, Synchrotron SOLEIL, Saint Aubin, France
C. Evain, Laboratoire PhLAM/CERLA, Villeneuve d'Ascq, France

Abstract

The lack of longitudinal coherence, that is shot-to-shot fluctuations, of Free-Electron Lasers (FEL) has prevented so far their full amplitude and phase temporal characterization. To sort out this issue, we propose a solution inspired from attosecond metrology, where XUV pulse measurement techniques already exist, and from coherent diffraction imaging, where numerical solutions have been developed for processing partially coherent diffraction patterns. The experimental protocole implies the measurement of photoelectron spectra obtained through XUV-laser photoionisation. The spectra are then processed with an algorithm in order to retrieve the partially coherent FEL pulse. When applied to SASE FELs, the technique gives access to the full statistics of the emitted pulses. With seeded-FELs, the pulse shape becomes stable from shot-to-shot, but an XUV-laser time jitter remains. In that case, the technique enables the joint measurement of the FEL pulse shape (in amplitude and phase) and of the laser/FEL jitter envelope.

ADAPTING FROG TO FREE-ELECTRON LASERS

Temporal metrology is a major need for emerging ultrashort Extreme Ultraviolet and X-ray (XUV) sources, such as attosecond (1 as = 10^{-18} s) sources based on high-harmonic generation [1, 2] or free electron lasers (FEL) [3, 4]. In attosecond metrology, the most mature technique for temporal characterization is known as the FROG-CRAB technique (*Frequency-Resolved Optical Gating for Complete Reconstruction of Attosecond Bursts*) [5], adapted from the FROG technique used in conventional near-visible ultrafast laser metrology [6]. By sending the XUV pulse through a gas jet in the presence of a laser field, two-color XUV+IR photoionisation is induced. Measuring the spectrum of the produced photoelectrons while varying the IR/XUV delay gives a two dimensional trace called a spectrogram. Such a spectrogram can then be processed with a phase-retrieval algorithm in order to obtain the temporal profile of the XUV pulse.

Ideally, one would like to transpose directly the FROG-CRAB technique to FELs. However, for FELs relying on Self-Amplified Spontaneous Emission (SASE), the XUV pulse changes on a shot-to-shot basis. With seeded FELs, the pulse shape becomes stable from shot to shot, but the synchronization of FEL pulses with an external laser source remains challenging, so that in practice an optical/XUV jitter of a few tens of femtoseconds is often present. For these reasons, FELs have remained incompatible with FROG-CRAB measurements so far. The problem can be understood by considering the XUV pulse as partially coherent, and by seeing the shot-to-shot fluctuations as the source of decoherence in the experiment. As modern ultrafast metrology relies on the hypothesis that the pulse to measure is fully coherent, it fails in the presence of partial coherence.

FEL PULSE MEASUREMENT IN THE PRESENCE OF PARTIAL COHERENCE

To overcome this problem, we propose a solution based on the recent advances in the domain of coherent diffraction imaging (CDI). This microscopy technique consists in reconstructing an object by processing numerically the diffraction patterns that it produces in the far field. The key is to illuminate the object with a fully coherent light beam, and the imaging quality is rapidly degraded as the degree of coherence decreases. However, strong efforts have been made to enable sample reconstructions even with a partially coherent beam [7, 8], simply by adapting the numerical processing used for the inversion of the diffraction patterns.

By adapting algorithms used in CDI, we have developed a numerical treatment for FROG spectrograms that enables the reconstruction of ultrashort pulses even in the presence of partial coherence [9]. In the case of SASE FELs, the statistics of SASE waveforms (temporal intensity and phase) accumulated during the measurement is recovered. Moreover in the case of seeded FELs, this statistics takes a very specific form, since the waveform is constant from shot to shot up to a random arrival time. It is then possible to recover both the XUV pulse shape and the form of the optical/XUV jitter envelope.

CONCLUSION

This work will also benefit to other domains where the FROG technique is used. In attosecond metrology, it will become possible to determine up to which extent the coherence of an optical wave packet, that is the XUV light pulse, is transferred to the electron wave packet during photoionisation [10]. But FROG is mainly used for the metrology of near visible pulses. One can for example expect applications for the coherent control in molecules [11]. This will also enable one to probe the coherence of complex nonlinear processes, such as the generation of supercontinuum pulses from photonics crystal fibers [12].

REFERENCES

[1] P. M. Paul *et al.*, "Observation of a Train of Attosecond Pulses from High Harmonic Generation", Science **292,** 1689-1692 (2001)

[2] M. Hentschel *et al.*, "Attosecond Metrology", Nature **414,** 509-513 (2001).

ISBN 978-3-95450-133-5

QUANTUM FEL II: MANY-ELECTRON THEORY

P. Kling, Helmholtz-Zentrum Dresden-Rossendorf eV, D-01328 Dresden, Germany
and Institut für Quantenphysik, Universität Ulm, D-89069 Ulm, Germany
R. Endrich, E. Giese, Institut für Quantenphysik, Universität Ulm, D-89069 Ulm, Germany
R. Sauerbrey, Helmholtz-Zentrum Dresden-Rossendorf eV, D-01328 Dresden, Germany
W. P. Schleich, Institut für Quantenphysik and Center for Integrated Quantum Science
and Technology $\left(\mathrm{IQ}^{\mathrm{ST}}\right)$, Universität Ulm, D-89069 Ulm, Germany;
Texas A&M University Institute for Advanced Study (TIAS),
Institute for Quantum Science and Engineering (IQSE),
and Department of Physics and Astronomy,
Texas A&M University, College Station, Texas 77843, USA

Abstract

We investigate the emergence of the quantum regime of the FEL when many electrons interact simultaneously with the wiggler and the laser field. We find the Quantum FEL as the limit where only two momentum states are populated by the electrons. Moreover, we obtain exponential gain-per-pass and start-up from vacuum.

INTRODUCTION

The recent years have seen rising interest in a possible novel regime of FEL operation: the so-called Quantum FEL. Bonifacio *et al.* [1] have proposed the implementation of this realm – despite experimental difficulties – because they expect better temporal coherence properties and a narrower linewidth of the radiation in SASE operation. Due to these prospects the Helmholtz-Zentrum Dresden-Rossendorf and Ulm University have started a collaboration to gain deeper insight into the emergence and the properties of the Quantum FEL. In a single-electron model we have identified the quantum regime of the FEL as an effective two-level system for the electron's momentum states [2] and have established a connection to the Jaynes-Cummings model [3].

In this article, we examine a situation where many electrons interact simultaneously with the laser and the wiggler field. Based on collective projection operators we develop a formalism which allows us to identify the two-level behaviour of the Quantum FEL. However, since we are dealing with many electrons, the suitable analogy is the Dicke [4] – describing a collection of two-level atoms interacting with a radiation field – rather than the Jaynes-Cummings model.

In the two-level approximation we find start-up from vacuum and exponential gain-per-pass in the short-time limit which are essential for SASE operation. Moreover, we calculate higher order corrections to this deep quantum regime and thus find analytical expressions which match the numerical results of [1].

MODEL

We start from the one-dimensional, quantized single-mode and many-particle Bambini-Renieri Hamiltonian [5,6]

$$\hat{H} \equiv \sum_{j=1}^{N} \frac{\hat{p}_j^2}{2m} + \hbar g \left(\hat{a}_\mathrm{L} \sum_{j=1}^{N} \mathrm{e}^{\mathrm{i}2k\hat{z}_j} + \mathrm{h.c.} \right) \tag{1}$$

where $\hbar$ and m stand for the reduced Planck constant and for the electron mass, respectively and we already have eliminated the free dynamics of the laser field. The Bambini-Renieri frame – in which a nonrelativistic treatment of the FEL dynamics is possible – is defined by the condition that the wave numbers of the laser (subscript L) and the wiggler field (subscript W) are equal, i.e. $k_\mathrm{L} = k_\mathrm{W} \equiv k$ [5]. The position operator $\hat{z}_j$ for the j-th of the N electrons and its conjugate momentum operator $\hat{p}_j$ fulfill the canonical commutation relation $\left[\hat{z}_j, \hat{p}_j\right] = \mathrm{i}\hbar$. While the laser field is quantized with the bosonic commutation relation $\left[\hat{a}_\mathrm{L}, \hat{a}_\mathrm{L}^\dagger\right] = 1$ for the photon annihilation and creation operators $\hat{a}_\mathrm{L}$ and $\hat{a}_\mathrm{L}^\dagger$, the wiggler is treated as an external classical field due to its high intensity. The coupling constant $g \equiv e^2 \mathcal{A}_\mathrm{L} \tilde{\mathcal{A}}_\mathrm{W}/(\hbar m)$ is given by the product of the amplitudes $\mathcal{A}_\mathrm{L}$ and $\tilde{\mathcal{A}}_\mathrm{W}$ of the vector potentials of the laser and the wiggler field, respectively with e being the elementary charge.

An essential ingredient for recognizing the two-level behaviour of the Quantum FEL in the single-particle case is the occurrence of different time scales in the Schrödinger equation [2]. This feature stands out by expanding the state vector of the system in the scattering basis $|n + \mu, p - \mu q\rangle$ as introduced in [7] which is characterized by the number μ of scattered photons, that is, the number of times the electron experiences the quantum mechanical recoil $q \equiv 2\hbar k$ with n being the initial number of photons in the laser field and p the initial momentum of the electron.

This expansion is not possible in the many-particle case, since complicated entangled states are created by the Hamiltonian Eq. (1) as apparent from the case $N = 2$

$$\left(\mathrm{e}^{2\mathrm{i}k\hat{z}_1} + \mathrm{e}^{2\mathrm{i}k\hat{z}_2}\right) |p_1, p_2\rangle \sim |p_1 + q, p_2\rangle + |p_1, p_2 + q\rangle \ . \tag{2}$$

Therefore, we try to see the occurrence of the relevant time scales directly in the Hamiltonian and not from a particular

ISBN 978-3-95450-133-5

QUANTUM FEL I: MULTI-MODE THEORY

R. Endrich, E. Giese, Institut für Quantenphysik , Universität Ulm, D-89069 Ulm, Germany
P. Kling, Helmholtz-Zentrum Dresden-Rossendorf eV, D-01328 Dresden, Germany
and Institut für Quantenphysik , Universität Ulm, D-89069 Ulm, Germany
R. Sauerbrey, Helmholtz-Zentrum Dresden-Rossendorf eV, D-01328 Dresden, Germany
W.P. Schleich, Institut für Quantenphysik and Center for Integrated Quantum Science
and Technology $\left(\mathrm{IQ}^{\mathrm{ST}}\right)$, Universität Ulm, D-89069 Ulm, Germany;
Texas A&M University Institute for Advanced Study (TIAS),
Institute for Quantum Science and Engineering (IQSE)
and Department of Physics and Astronomy,
Texas A&M University, College Station, Texas 77843-4242 USA

Abstract

The quantum regime of the FEL in a single-mode, single-particle approximation is characterized by a two-level behaviour of the center-of-mass motion of the electrons. We extend this model to include all modes of the radiation field and analyze the effect of spontaneous emission. In particular, we investigate this scattering mechanism to derive experimental conditions for realizing an FEL in the quantum regime.

INTRODUCTION

In [1] the existence of the so-called quantum regime of the FEL was predicted and in [2] a quantum optics approach to the Quantum FEL (QFEL) was developed. Before we extend our model of the QFEL to a multi-mode theory, we briefly recapitulate its essential ingredients.

We start with the Hamiltonian of the FEL, i.e. an electron of mass m and charge e coupled to a single mode of the radiation field of frequency ω by the wiggler of amplitude $\mathcal{A}_W$. This Hamiltonian expressed in the Bambini-Renieri frame [3], which is a comoving non-relativistic frame of reference reads [4] in the interaction picture

$$\hat{H} \equiv \hbar g \hat{a}_L^{\dagger}\, \mathrm{e}^{-2ik\hat{z}}\, \mathrm{e}^{-\mathrm{i}\hat{\Delta}(\hat{p})t} + \mathrm{h.c.}\ . \tag{1}$$

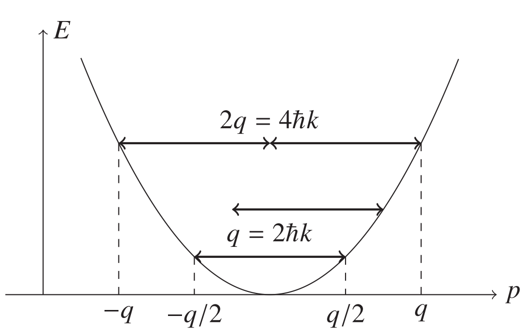

Figure 1: Momentum-energy parabola of the electron, that is $E = E(p)$. Only resonant photon transitions are of interest, the off-resonant ones can be neglected. Higher order photon transitions are on resonance as well, but they are suppressed by the quantum parameter α, defined by Eq. (5).

The coupling constant [2]

$$g \equiv \frac{e^2}{\hbar m}\sqrt{\frac{\hbar}{2\varepsilon_0 V\omega}}\mathcal{A}_W\ , \tag{2}$$

with the quantization volume V, Planck's constant $\hbar$, and the vacuum permittivity ε_0 couples the photon creation operator $\hat{a}_L^{\dagger}$ to the center-of-mass motion of the electron represented by the position and momentum operator, $\hat{z}$ and $\hat{p}$, respectively, where the detuning

$$\hat{\Delta}(\hat{p}) \equiv \hat{p}\,(2k/m) - \omega_r \tag{3}$$

contains the recoil frequency $\omega_r \equiv q^2/2m\hbar$. The operator $\exp[-2ik\hat{z}]$ shifts the electron momentum by the recoil

$$q \equiv 2\hbar k \tag{4}$$

determined by the wave number k.

At this point the Hamiltonian is exact for a strong classical wiggler field. In the classical regime the electron recoil is a negligible quantity, whereas in the quantum domain it enters in a crucial way into the detuning, which suppresses off-resonant photon transitions. This effect is illustrated in Fig. 1 where the initial and final momentum on the energy parabola are on resonance. For a single photon exchange, only the momentum states$|q/2\rangle$ and $|-q/2\rangle$ are on resonance.

Higher-order photon transitions, as seen in Fig. 1, are on resonance for higher momenta as well. However, it has been shown in [2] that a j-photon transition with $j > 1$ is proportional to α^j where

$$\alpha \equiv \frac{g\sqrt{n+1}}{\omega_r} \tag{5}$$

is the quantum parameter and n the photon number.

For $\alpha \ll 1$ only the single-photon transition remains, while higher-order transitions are suppressed. This feature represents the main criterion for the QFEL and the momentum states $|\pm q/2\rangle$ undergo a Rabi oscillation with the frequency

$$\Omega \equiv g\sqrt{n+1}\ . \tag{6}$$

This frequency determines the timescale on which a QFEL is operational, and will play a key role in our considerations.

ISBN 978-3-95450-133-5

TWO-COLOR FREE-ELECTRON LASER VIA TWO ORTHOGONAL UNDULATORS

N. S. Mirian*, School of Particle and Accelerator Physics,
Institute for Research in Fundamental Sciences (IPM), 19395-5531, Tehran, Iran
G. Dattoli, ENEA Centro Ricerche Frascati, via E. Fermi, 45, IT 00044 Frascati, Rome, Italy
V. Petrillo, Università degli Studi di Milano,via Celoria 16, IT 20133 Milano, Italy and
INFN-Mi, via Celoria 16, IT 20133 Milano, Italy

Abstract

An amplifier Free electron Laser (FEL) including two orthogonal polarized undulators with different periods and field intensities is able to emit two color radiations with different frequency and polarization while the total length of device does not change respect to usual single color FELs. The wavelengths of two different colors can be changed by choosing different periods, while variation in the magnetic strengths can be used to modify the gain lengths and saturation powers.

INTRODUCTION

Recently generation of free-electron laser radiation with two or more simultaneous colors opens new promising chapter in applications [1, 2] and in the study of the underlying physics. The packets contain two different spectral lines with adjustable time separation between them. Applications exist over a broad range of wavelengths involving pump-probe experiments, multiple wavelength anomalous scattering, or any process where there is a large change in cross section over a narrow wavelength range [3].

In order to produce this type of radiation several schemes have been proposed, and many promising theoretical proposals have been so far investigated. Some of the initially proposed designs were based on the use of staggered undulator magnets having different values of deflecting parameters to achieve lasing at two distinct wavelengths [4–7]. In this way, the length of the FEL undulator is essentially doubled and a complex scheme is required to reach saturation and power levels comparable with the single color configuration. A different technique involving the use of either a chirped or a two-color seed laser, is recently demonstrated at the FERMI soft X-ray FEL. It initiates the FEL instability at two different wavelengths within the modulator gain bandwidth [8, 9]. Another option is relying on injection of multi-energy electron beam in the FEL undulator [10] resonating at two different wavelength, allowing the control of frequency and time separation ranges of the FEL pulses, while maintaining similar saturated power levels and minimal undulator length [11, 12]. In this configuration, the SASE lasing occurs from separated and nearly independent electron distributions [13].

Recently a new proposal with a further different scheme has been presented in reference [14, 15]. In this case the FEL emission is obtained from two orthogonally polarized undulators with different polarized and field intensities. The two radiations have not only different frequencies, but also different polarizations, while the total length of the device does not change with respect to usual single color FELs. Producing two waves with orthogonal polarizations with comparable intensities is very important because it opens various possibilities to get insights into and to control the internal organization and orientation in space of molecules, taking advantage of the selective excitation of the molecular fluorescence by differently polarized beams.

This paper presents a brief overview over the main theory of the production and properties of two-color radiation generated by two orthogonal undulators.

MODEL EQUATION IN AN AVERAGED AND NON AVERAGED SVEA TREATMENT

The FEL undulator is assumed to be composed by two linear undulators orthogonally polarized with periods given respectively by λ_{01} and λ_{02}. and deflection parameters $K_{1,2} = \left|eB_{1,2}\lambda_{01,02}/mc^2\right|$. The undulator magnetic field, in the paraxial approximation, is described by the following expression

$$\mathbf{B}_w = -B_{w2}\sin(k_{02}z)\hat{e}_x + B_{w1}\sin(k_{01}z)\hat{e}_y, \tag{1}$$

where $k_{01,02} = 2\pi/\lambda_{01,02}$.

Following the Colson's analysis [16], the zero order dimensionless velocity components can be written as

$$\beta_{x,y} = -\frac{K_{1,2}}{\gamma_0}cos(k_{01,02}z) \approx -\frac{K_{1,2}}{\gamma_0}cos(\omega_{01,02}t), \tag{2}$$

$$\beta_z = -\frac{1}{4}\left[\left(\frac{K_1}{\gamma}\right)^2\cos(2k_{01}z) + \left(\frac{K_2}{\gamma}\right)^2\cos(2k_{02}z)\right] + \beta_0 \tag{3}$$

with $\beta_{x(y),j} = v_{x(y),j}/c$ and $\beta_0 = 1/\sqrt{1-\gamma_0^2}$. From Eq (3) the following resonance conditions can be found.

$$\lambda_{1,2} = \frac{\lambda_{01,02}}{2\gamma_0^2}(1 + K_1^2/2 + K_2^2/2). \tag{4}$$

The trajectories of the electrons inside the undulator takes the form:

* najmeh.mirian@ipm.ir

ISBN 978-3-95450-133-5

SPECTRAL LIMITS AND FREQUENCY SUM-RULE OF CURRENT AND RADIATION NOISE MEASUREMENT*

R. Ianconescu, University of Tel-Aviv, Tel-Aviv and Shenkar College, Ramat Gan, Israel
A. Gover, A. Nause, University of Tel-Aviv, Tel-Aviv, Israel

Abstract

The current noise spectrum of an electron beam is generally considered white and expressed by the shot-noise formula (eI_0). It is possible to control the spectral energy of a random electron beam current by longitudinal space charge micro-dynamics and dispersive transport. Both noise suppression (relative to eI_0) and noise enhancement have been demonstrated, exhibiting sub/super-Poissonian particle distribution statistics, respectively. We present a general theory for the current noise of an e-beam and its radiation emission in the entire spectrum. The measurable current noise spectrum is not white. It is cut-off at high frequencies, limited by the measurement length and the beam axial momentum spread (fundamentally limited by quantum uncertainty). We show that under certain conditions the current noise spectrum satisfies a frequency sum-rule: exhibiting noise enhancement in one part of the spectrum when suppressed at another part and vice versa. The spontaneous emission (radiation noise) into a single radiation mode or single direction in any scheme (OTR, Undulator etc.) is sub-radiant when the beam current is sub-Poissonian and vice versa, but the sum-rule does not apply.

INTRODUCTION

Electron beam current-noise is an inherent property of any particulate current resulting from the microscopic discontinuity of charge flow in a charged particles beam. The conventional assumption regarding the current noise in an accelerated electron beam is that it is limited by the Shot-Noise formula:

$$S_{I_{\text{shot}}} = eI_0 \qquad (-\infty < f < \infty), \tag{1}$$

where I_0 is the average current of a continuous coasting electron beam and $S_I(f)$ is the power spectral density (PSD) of the current. This expression is a direct consequence of the assumption that the beam particles positions are random uncorrelated uniform variables, so that the number of particles in each interval satisfies the Poisson statistics.

It has been known [1] that as an electron beam propagates, the Coulomb interaction between the particles results in correlation between the particle positions and therefore, the particles statistics, as well as their current PSD may deviate from the shot-noise formula (1). In particular it has been shown that Eq. (1), is not even a lower limit for random electron beam noise, and taking advantage of the Coulomb interaction effect, or the longitudinal space charge (LSC) interaction of random bunching, it is possible to suppress the current noise below the shot-noise level (current noise suppression) at least in part of the spectrum.

Recently it has been shown theoretically [2–8] and experimentally [9, 10] that shot-noise suppression is possible in high quality e-beams at optical frequencies. This noise suppression process can be achieved by transport of the beam along a drift section of quarter plasma oscillation length [9] or by transport through a drift section and a subsequent dispersive section [10]. In the later case, if the dispersion effect (presented by the parameter R_{56}) is large, the opposite effect - noise gain - is achieved, at least in part of the spectrum (micro-bunching instability [11]).

Current noise is the source of incoherent spontaneous emission of radiation (radiation noise) in all electron-beam radiation sources, and in particular Undulator radiation and SASE (Self Amplified Spontaneous Emission) in FEL [8]. For this reason controlling radiation noise is one of the reasons of interest in controlling electron-beam current noise at short wavelengths. In innovative temporally coherent seed-injected FELs [12] incoherent SASE radiation limits the coherence of the FEL output and imposes stringent demands on the power level of the seed radiation source [8]. Hence current noise suppression of the e-beam before injection into the wiggler is desirable. On the other hand, control over the e-beam current shot-noise can also be useful for the opposite purpose: enhancing SASE radiation [13]. This process has been recently demonstrated by Marinelli et al [14] and may possibly be used to produce high power radiation in SASE FELs with shorter wigglers.

MEASUREMENTS OF CURRENT-NOISE SPECTRUM

Determining the spectral limits of noise-control, and particularly noise-suppression, is a task of prime interest in connection to electron-beam transport in applications of electron beams for emission of coherent radiation (FEL). Of primary importance is the short wavelength limit, as there is significant interest in developing coherent (low noise) X-UV FELs.

The short wavelength limit of current noise suppression by drift over a quarter plasma wavelength is the Debye condition: $\lambda > \lambda_D$, where the Debye wavelength λ_D is determined by the axial velocity spread of the beam due to finite emittance or energy spread [15]. A similar condition applies also to the drift/dispersion noise suppression scheme where the dispersive section enhances the optical phase-spread at short wavelength [15]. The LSC noise-suppression effect is also limited at low frequencies (though this limit is of less interest). The low frequency limitation of LSC interaction

* This research was supported by a grant from the United States-Israel Binational Science Foundation(BSF), Jerusalem, ISRAEL

ISBN 978-3-95450-133-5

AN ANALYSIS OF OPTIMUM OUT-COUPLING FRACTION FOR MAXIMUM OUTPUT POWER IN OSCILLATOR FEL

Jia Qika#, NSRL, University of Sicence and Technology of China, Hefei, 230029, China

Abstract

The effect of the out-coupling fraction on the output power in oscillator FEL is analyzed. The formulas of the optimum out-coupling fraction and the corresponding maximum output power are given. They are dependent on the initial small signal gain and the passive loss rate of the light in the optical cavity. The initial comparison show that the result given by the formula agree well with the results in references.

INTRODUCTION

The basic working modes of free-electron lasers (FELs) include the amplifier, the oscillator and the self-amplified spontaneous emission (SASE). The oscillator FEL work in the low gain regime with the multi-amplifying. For oscillator FEL，one main goal of the design and optimization is to achieve the maximum output power. An important work is to optimize the out-coupling fraction of the light. It has been discussed by several authors [1-3], in this paper we analysis the optimization of the out-coupling fraction for maximum output power, here we don't consider what specific way of the out-coupling is used.

ANALYSIS

By expanding FEL equations and taking some approximation, the optical field gain at the pass n can be given as [4]

$$g_n \approx \frac{e^{g_{ss}}-1}{1+e^{g_{ss}}P_{n-1}/P_c}, \qquad (1)$$

where P_{n-1} is the optical power at the pass n-1,the power of the optical pulse at the undulator exit during the nth passage, g_{ss} is initial small signal gain:

$$g_{ss} = -(2k_u\rho L)^3 \left\langle \frac{\partial}{\partial x}\frac{\sin^2(x/2)}{(x/2)^2} \right\rangle_{\phi_0'}, \qquad (2)$$

where ρ is FEL parameter, k_u and L is the wave vector and length of the undulator, $x=\phi_0' L$, the angular bracket represents the average over the electron's initial phase velocities (i.e. the tuning parameter) ϕ_0'; and

$$P_c = \frac{g_{ss}}{\beta}\rho P_e . \qquad (3)$$

P_e is electron beam power and [4, 5]

$$\beta = (2k_u\rho L)^7 \left\langle \frac{1}{x^7}\{x(6-x^2)\sin x + 4(1-x^2)\cos x + \frac{3}{2}x\sin 2x + \frac{1}{2}(\frac{5}{2}-x^2)\cos 2x - \frac{21}{4}\} \right\rangle_{\phi_0'} . \qquad (4)$$

When the power equal to P_c, i.e. $P_{n-1}=P_c$, from Eq. 1 it has

$$g_n = \frac{e^{g_{ss}}-1}{e^{g_{ss}}+1} = \mathrm{cth}(\frac{g_{ss}}{2}) \approx g_{ss}/2 .$$

Therefore P_c is the value of the intensity halving the small signal gain of the device. The profiles of the angular bracket parts in the expressions of g_{ss} (Eq. 2) and β (Eq. 4) are given in Fig. 1, from which we have $g_{ss}/\beta \sim 100/(2k_u\rho L)^4$. Therefore we can estimate the value of P_c : $P_c \sim 100(\sqrt{3}L_g/L)^4 \rho P_e$, for low gain regime $L<3L_g$, thus we have $P_c >\sim 10\rho P_e$. Notice the saturation power $P_s > P_c$ (Eq. 7), we can know that the saturation power of oscillator FEL is larger than that of SASE FEL(~ρP_e).

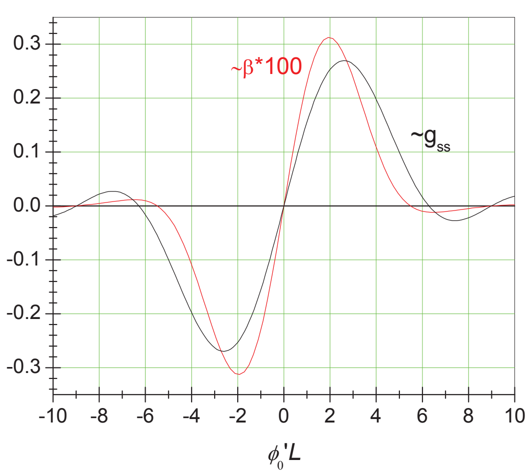

Figure 1: the angular bracket parts of g_{ss} and β in Eq. 2 and 4.

The intra-cavity power at pass n is

$$P_n = P_{n-1}(1+g_n)(1-\alpha) = P_0\prod_{i=1}^{n}(1+g_i)(1-\alpha), \qquad (5)$$

where α is the total loss ratio in optical cavity including the output coupling fraction and the passive loss. P_0 is the initial emission power, i.e. the spontaneous emission power [6]:

#jiaqk@ustc.edu.cn

ISBN 978-3-95450-133-5

A SIMPLE METHOD FOR GENERATING A FEW FEMTOSECOND PULSES IN SEEDED FELS*

Li Heting#, Jia Qika, He Zhigang
NSRL, University of Sicence and Technology of China, Hefei, 230029, China

Abstract

We propose a simple method to generate a few femtosecond pulses in seeded FELs. We use a longitudinal energy-chirped electron beam passing through a dogleg where transverse dispersion will generate a horizontal energy chirp, then in the modulator, a seed laser with narrow beam radius will only modulate the centre part of electron beam and short pulses in high harmonics will be generated in the radiator. Using a representative realistic set of parameters, we show that 30 nm XUV pulse with duration of 8 femtoseconds (FWHM) and peak power of GW level can be generated from a 180 nm UV seed laser with beam waist of 75 μm.

INTRODUCTION

There is a rapidly growing interest in the availability of extremely short pulses, which have facilitated the rapid development of ‘‘ultrafast science’’, including structural studies of single biomolecules, femtosecond chemistry, etc [1]. In recent years, free-electron lasers (FELs) researchers have explored various ways to produce high-power, ultrashort pulses at XUV and shorter wavelengths with a particular emphasis on temporal synchronism with external lasers to facilitate pump-probe experiments [2].

A definition of the ultra-short X-ray pulses in Ref. [3] is the pulse duration of the order of few femtoseconds and shorter. A rather natural way to obtain such pulses is to use ultra-short electron bunches. However, most of short pulse schemes rely upon manipulating one or more properties of an ultrashort temporal portion of a much longer electron bunch, such as transverse emittance, energy or current [4-7]. These manipulations generally use a few-cycle, near-IR laser pulse to energy-modulate the e-beam so that, when combined with other transport elements such as chromatic chicanes, foils, specially tuned undulators, the FEL emission will predominately arise from the modulated portion.

In this paper, we propose a new simple method to generate a few femtosecond pulses in seeded FELs. A both longitudinal and transverse energy-chirped electron beam is obtained from a dogleg section and modulated by a seed laser with a narrow beam radius, thus only the short centre portion of electron bunch is modulated and then generate short pulses emission in the radiator. This is an easy-to-implement scheme for an existed seeded FEL configuration.

*Work supported by Major State Basic Research Development Program of China (2011CB808301) and the Fundamental Research Funds for the Central Universities of China (WK2310000045)
#liheting@ustc.edu.cn

METHODS

Our scheme, as shown in Fig. 1 in which we place a high-gain harmonic generation (HGHG) configuration as an example for seeded FELs, does not require any other hardware or special properties of electron beam. The unique difference is the use of dogleg, however, there usually be one or several doglegs in the transport line between the linac and undulators. This scheme can be combined with other kinds of seeded FELs, such as echo-enabled harmonic generation (EEHG) [8], phase-merging enhanced harmonic generation (PEHG) [9] and so on.

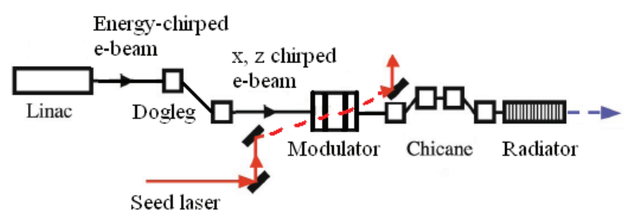

Figure 1: A schematic of the proposed scheme for short pulse production.

We assume an energy-chirped beam at the exit of Linac. The energy chirp parameter

$$h = \frac{d\gamma/\gamma}{dz} \quad (1)$$

is defined such that, for positive sign of h, electrons in the head of the bunch have larger energy than those in the tail, where γ is the relativistic factor and z is the bunch length coordinate. Using the electrons with the average energy γ_0 as the reference particles, for an electron (x_0, z_0), after passing through the dogleg with a momentum compaction R_{56} and a transverse dispersion η, we have its new coordinates (x, z) as

$$z = z_0 + R_{56}(hz_0 + \delta\gamma_0) \approx (1 + hR_{56})z_0 \quad (2)$$

$$x = x_0 + \eta(hz_0 + \delta\gamma_0) \approx \eta hz_0 \quad (3)$$

Here, we use the condition that the initial slice energy spread $\delta\gamma_0$ is much smaller than the chirped energy deviation and the initial beam transverse size is much smaller than that after dogleg. This approximation is reasonable because here the dogleg has a considerable dispersion strength and, to obtain short pulse, we need to extend the transverse size to an enough big level.

In this case, we can give the RMS bunch length and x-plane beam size after dogleg as

$$\sigma_z \approx (1 + hR_{56})\sigma_{z0} \quad (4)$$

ISBN 978-3-95450-133-5

NUMERICAL SIMULATION OF A SUPER-RADIANT THz SOURCE DRIVEN BY FEMTOSECOND ELECTRON BUNCHES*

R. Chulkov, B.I. Stepanov Institute of Physics, NAS, Minsk, Belarus
V. Goryashko, Department of Physics and Astronomy, Uppsala University, Uppsala, Sweden
V. Zhaunerchyk, Department of Physics, University of Gothenburg, Sweden

Abstract

We summarize our studies for a super-radiant source operating in the THz frequency range. In particular, we focus on a single-pass planar undulator comprising no guiding structure. Using a numerical code that supports 3D time-dependent modeling of radiated fields as well as statistical properties of electron bunches, we analyze influence of electron bunch parameters on generated THz radiation and reveal some surprising results. More specifically, for the considered undulator configuration, we predict degradation in the angular divergence and spectral broadening of the generated radiation as the electron bunch emittance decreases. We also demonstrate how electron bunch lengthening associated with the electron energy spread can be suppressed.

INTRODUCTION

Pulsed THz free-electron lasers (FELs) are typically driven by radio-frequency linear accelerators (rf Linacs) able to produce intense electron bunches with a duration in the picosecond or even in the femtosecond range. When the bunch length is much shorter than the resonant wavelength of an excited electromagnetic field in an undulator, the bunch radiates like a point-charge giving rise to the so-called super-radiant regime of an FEL [1]. In this case, output intensity scales as a squared number of all electrons at the FEL start-up while for SASE (self-amplified spontaneous emission) it scales with a number of electrons [2]. The super-radiant regime enables realization of a relatively compact high-power THz FEL facility based on a single-pass undulator configuration. At the same time, the operation efficiency of such a super-radiant source is strongly affected by the quality of a driving electron bunch such that the source design requires a numerical modeling, which should take into account general statistical properties of electron bunches as well as the THz field diffraction. Below, we present results of such a modeling for a single-pass THz super-radiant source comprising a planar undulator.

MODEL DESCRIPTION

Our numerical model describes a single-pass interaction geometry without any guiding structure for generated THz field. A numerical code accounts for a non-zero bunch emittance and an electron energy spread and enables 3D modeling of radiated fields when electron bunches are comparable to or shorter than the FEL resonant wavelength. The key approach of the model is the expansion of a THz field into complete sets of mutually orthogonal Hermite-Gaussian modes. The fast-varying field in a time domain is calculated via inverse Fourier transform of the frequency components. Details of our approach can be found in Refs. [3–8]. The model considers only a single linear polarization of the THz radiation lying in the plane of the wiggling motion of electrons. We also assume that the injected electron bunch is not astigmatic and its waist is located at the undulator center in the ballistic approximation. Then, the initial rms (root-mean-squared) bunch width $\sigma_{x,y}$ can be written as [9]:

$$\sigma_{x,y} = \sqrt{\epsilon\left(\beta_0 + \frac{L_u^2}{4\beta_0}\right)}, \tag{1}$$

where ϵ is the rms bunch emittance, β_0 is the geometrical β-function and L_u is the undulator length. An initial distribution of macroparticles in an electron bunch was simulated using a charge weighted algorithm based on the temporal Poisson statistical properties of electrons [10]. A Gaussian statistics is used to produce an initial energy spread and transverse distribution of the macroparticles. Their initial transverse velocities $[v_{0xj}, v_{0yj}]$ have been taken according to the relations [9, 11]:

$$v_{0xj} = -\vartheta x_{0j} v_{0zj}, \quad v_{0yj} = -\vartheta y_{0j} v_{0zj}, \tag{2}$$

$$\vartheta = \frac{1}{\beta_0}\left(\frac{L_u}{2\beta_0} + \frac{2\beta_0}{L_u}\right)^{-1}, \tag{3}$$

where $[x_{0j}, y_{0j}]$ are the initial transverse coordinates of the macroparticles. The numerical code has been implemented in the double precision arithmetic. The finite-difference integration scheme of the equations for electron motion as well as the equations for the Fourier amplitudes is the 4-th order Bashforth-Moulton predictor-corrector [12] with relative tolerance control on each integration step. Parameters of the simulations are listed in Table 1.

Table 1: Parameters of the Simulation

resonant frequency, THz	0.3	1.0	3.0
bunch charge, nC	1.0	1.0	0.5
mean e-energy, MeV	9.0	9.31	16.5
bunch duration, fs	150	150	100
bunch β_0-function, m	3.0	3.0	3.0
magnetic flux, T	0.31	0.14	0.14
undulator period, cm	11.0	11.0	11.0
number of periods	9	9	9
undulator parameter K_u	2.26	1.0	1.0

* Work supported by the Swedish FEL center

ISBN 978-3-95450-133-5

X-RAY SMITH-PURCELL RADIATION FROM A BEAM SKIMMING A GRATING SURFACE

D.Yu. Sergeeva, A.A. Tishchenko*, NRNU "MEPhI", Moscow, Russia

Abstract

X-Ray Smith-Purcell radiation, i.e. the radiation from a beam of charged particles moving above a periodical target parallel to its surface, is considered for the case when a part of the beam crosses the target. The radiation arising is the superposition of Smith-Purcell radiation and transition radiation (TR) from the grating. The analytical expression for spectral-angular distribution of radiation is obtained. It is shown that characteristics of radiation in this case differ considerably from the characteristics of radiation for the bunch with uniform distribution. The incoherent form-factor of bunch with Gaussian distribution of particles has been obtained; it is proved to provide a considerable increase of the radiation intensity in conditions when bunch skims the grating.

INTRODUCTION

Smith-Purcell radiation as a base of Free Electron Lasers is actively studied experimentally and theoretically in recent years [1]-[3]. Usually the beam is supposed to move at some distance above the target surface. In practice this distance is chosen to be minimal in order to broaden the spectrum of radiation to high frequencies, therefore the beam passes very close to the target surface. Along with that, experimental data contains the information about grating heating, which is apparently caused by interaction of the beam with the grating. For example, authors of article [4] suppose that the beam skims the grating surface. There has been no theory of Smith-Purcell radiation for such conditions yet. We give the analytical description of X-Ray radiation arising when the beam of charged particles moves above the periodical target and a part of the beam crosses the target. The radiation arising is the superposition of Smith-Purcell radiation and transition radiation (TR) from the grating. This radiation determines the process of beam bunching and, consequently, gains of radiation.

Talking of SPR in this article we shall mean that this is the special case of DR – Diffraction radiation for periodical target, i.e. grating. So, sometimes we shall mention DR, meaning that lion share of the bunch goes above the target surface, and sometimes mention TR, when considerable part of the bunch intersects the edges of the target.

FIELD OF RADIATION

We consider Smith-Purcell radiation from the bunch of N particles. The grating consists of N_{st} strips with dielectric permittivity $\varepsilon(\omega)$ and vacuum between the strips. The width of a strip is a, the grating period is d. We assume that each particle has the charge e and moves uniformly with the constant velocity $\mathbf{v}=(v_x, v_y, 0)$, α is the angle between the beam velocity and axis x, see Fig. 1. The center of the bunch is at a distance h above the grating surface $(h>0)$ or under the surface $(h<0)$. The radius-vector of m-th particle is $\mathbf{r}_m=(x_m, y_m, z_m)$. We would like to emphasize that these coordinates can be negative. To find the field of radiation we use the method of polarization, described for single-particle radiation in more detail in monograph [5] and developed for the radiation from the bunch in [6], [7].

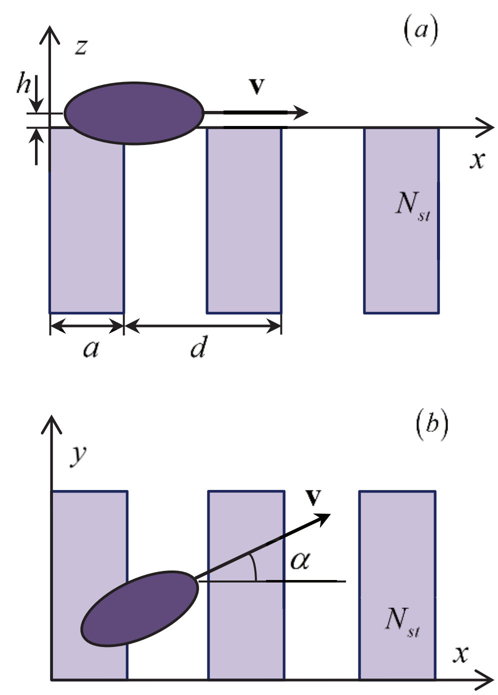

Figure 1: Bunch skimming a grating surface generates radiation (a) side view; (b) top view.

In X-Ray frequency range the dielectric permittivity has the form:

$$\varepsilon = 1 + \chi' + i\chi'', \tag{1}$$

where $\chi' = -\omega_p^2/\omega^2$, $\omega \gg \omega_p$, ω_p is the plasma frequency. Now we consider non-absorbing medium i.e. $\chi'' \ll |\chi'|$.

*tishchenko@mephi.ru

FORWARD X-RAY AND ULTRAVIOLET SMITH-PURCELL RADIATION FOR FEL

A.A. Tishchenko*, D.Yu. Sergeeva, NRNU "MEPhI", Moscow, Russia

Abstract

Smith-Purcell radiation in X-Ray and UV frequency range is investigated. The particle is supposed to move at arbitrary angle to the rulings direction parallel to a grating surface. The radiation going both through the upper and forward target edges is taken into account. Spectral and angular characteristics of the forward radiation are discussed. The influence of oblique incidence of the particle to the grating in on the intensity of radiation is analyzed.

INTRODUCTION

The scheme of Free Electron Lasers based on Smith-Purcell effect is well known to describe the process of interaction between an electron beam and evanescent wave, which bunches this beam. In this work we concentrate on the process of generation of the radiation propagating at small angles. In terms of approach described in detail in [1]-[3], we investigate the Smith-Purcell radiation at oblique incidence of a single charged particle for X-Ray and UV frequency region. This forward radiation propagates through all region of the beam moving, whereas the usual surface waves existing in FELs [4] decrease exponentially with distance from the surface. Therefore, the forward radiation considered in this article is able to provide more close interaction between the beam and the radiation, than the surface waves.

FIELD OF RADIATION

Let the charge e moves with constant velocity $\mathbf{v}=(v_x, v_y, 0)$ at a distance h above the upper edge of a target. The target consists of N strips with dielectric permittivity $\varepsilon(\omega)$ with air between strips. The period of the grating is d. The size of a strip is (a,∞,b) (see Fig. 1). We find the radiation field using the polarization current method. The essence of this method is following. The Coulomb field of a moving particle $\mathbf{E}_0(\mathbf{r},\omega)$ acts upon material of the target and excites dynamically changed polarization currents in it. This leads to arising of the radiation determined by Fourier-image of the current density $\mathbf{j}(\mathbf{r},\omega)$:

$$\mathbf{j}(\mathbf{r},\omega)=\frac{\omega}{4\pi i}\left(\varepsilon(\omega)-1\right)\mathbf{E}_0(\mathbf{r},\omega). \qquad (1)$$

For X-Ray frequency region

$$\omega \gg \omega_p \qquad (2)$$

*tishchenko@mephi.ru

the dielectric function of a medium can be written as:

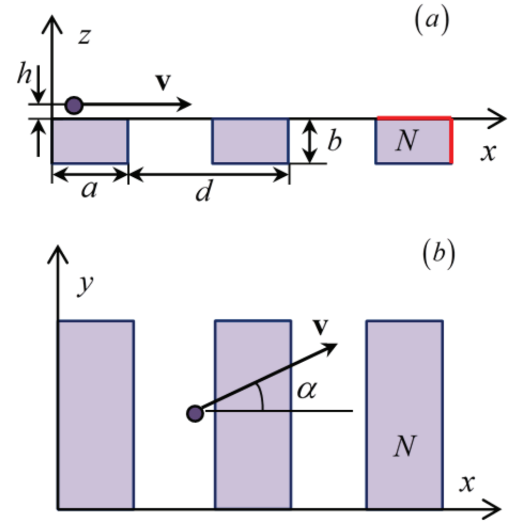

Figure 1: The geometry (a) side view, (b) top view.

$$\varepsilon = 1+\chi'+i\chi'', \qquad (3)$$

where $\chi' = -\omega_p^2/\omega^2$, ω_p is the plasma frequency, which is usually in the range of 15 - 35 eV, in dependence on the target material. The case of absorbing medium can be of interest, for example, to deal with X-ray Cherenkov radiation [5], [6]; now we restrict our consideration to non-absorbing mediums only, i.e. $\chi'' \ll |\chi'|$. However, as the absorption in X-ray region plays a role mainly near narrow lines, our results remain valid in rather wide range of parameters.

The radiation field is determined by current density as

$$\mathbf{E}(\mathbf{r},\omega)=\frac{i\omega}{c^2}\frac{e^{ik'r}}{r}\left[\mathbf{n}\left[\mathbf{n}\int_V d^3r' e^{-i\mathbf{k}'\mathbf{r}'}\mathbf{j}(\mathbf{r}',\omega)\right]\right], \qquad (4)$$

where it is integrated over the region of existence of polarization currents, i.e. over the target volume V; the prime in the designation of wave vector $\mathbf{k}'=\mathbf{n}'\sqrt{\varepsilon(\omega)}\,\omega/c$ stands for the value inside the matter.

To obtain the field of forward radiation we should take into account the refraction of radiation at two target edges: the upper one and the forward one (see the red lines in Fig. 1). Allowing for the law of refraction is important here because of periodicity of the target. The matter is that, despite the weakness of the effect of the refraction in X-ray range, for numerous periodic sources of radiation the effect of refraction is accumulated and becomes prominent.

ISBN 978-3-95450-133-5

RADIATION AND INTERACTION OF LAYERS IN QUASI-PLANE ELECTRON BUNCHES MOVING IN UNDULATORS

N. Balal, Ariel University, Ariel, Israel *, V.L. Bratman, Ariel University, Ariel, Israel and Institute of Applied Physics, Russian Academy of Sciences, Nizhny Novgorod, Russia

Abstract

A simple general 1-D theory of coherent spontaneous undulator radiation from dense bunches allows easily taking into account both Coulomb and radiation interaction of the particles in the bunches with arbitrary densities, velocity distributions and energy chirps. The theory can be applied for estimations of THz radiation sources.

RADIATION OF A MOVING PLANE

Generating powerful coherent THz radiation from dense and relatively low-energy electron bunches formed in compact laser-driven photo-injectors [1-8] is a fairly complicated task because of strong Coulomb repulsion of "insufficiently heavy" particles. To overcome it, one can apply energy chirping [6, 8] or/and formation of quasi-plane bunches with increased transverse size [4, 7]. The main properties of radiation and dynamics for such bunches may be found from the simplest 1-D model representing a bunch as a set of moving charged planes. The field of a plane that consists of electrons moving synchronously along arbitrary identical trajectories $\vec{r}(t)$ can be written in the form [3]

$$E_z = -2\pi\sigma s,\ \vec{E}_\tau = 2\pi\sigma\vec{\beta}_\tau(\tilde{t})[1 - s\beta_z(\tilde{t})]^{-1},\ \vec{H}_\tau = s\,\hat{z}\times\vec{E}_\tau.$$

Here, $-\sigma$ is a surface charge density, $\vec{\beta}=\vec{v}/c$ is the normalized electron velocity, $s=\mathrm{sgn}[z-z(t)]$, $\tilde{t}$ is the retarded time. Unlike the Lienard-Wiechert field of a point charge, the field of the plane is finite at the charges and determine both the self-action of the charged plane and its radiation. If the particles oscillate in the plane and move with a ultrarelativistic translational velocity β_z, the plane generates coherent spontaneous radiation that is contracted/stretched and increased/decreased by amplitude in the passing/counter $\pm z$ directions, respectively.

The motion of electrons in a linearly polarized undulator field $\vec{H}_u = \vec{y}_0 H\cos(2\pi z/d)$ and own field of the charged plane is described by self-consistent equations

$$\frac{dp_x}{d\zeta} = K\cos\zeta - q\frac{p_x}{p_z},\ \frac{dp_z}{d\zeta} = -K\frac{p_x}{p_z}\cos\zeta - q\frac{p_x^2}{1+p_x^2},\ \frac{d\tau}{d\zeta} = \frac{\gamma}{p_z}.$$

Here, $\zeta = 2\pi z/d$, $\tau = 2\pi ct/d$ are the normalized axial coordinate and current time, $\vec{p}=\gamma\vec{\beta}$, γ are the normalized electron momentum and energy, $K = eH/2\pi mc^2$, $q = e\sigma d/mc^2$ are the undulator and space charge parameters, respectively. For particles with the same energy and zero transverse velocities at the entrance into the undulator field the initial conditions are as follows

$$p_x = 0,\ p_z = \sqrt{\gamma_0^2 - 1},\ \tau = 0.$$

For electron with ultrarelativistic axial velocity the transverse electric and magnetic radiation self-forces almost completely compensate each another, and because of it the transverse electron momentum differs from its unperturbed value $p_x = K\sin\zeta$ only on terms of the order of small parameter q/γ_0. In the first approximation both the energy and Doppler up-conversion factor for radiating particles averaged by undulator oscillations linearly decrease along the axial coordinate:

$$\bar{\gamma} = \gamma_0(1-\eta),\ \Gamma = (1-\bar{\beta}_z)^{-1} = \Gamma_0(1-2\eta),$$

where

$$\eta = (\gamma_0 - \bar{\gamma})/(\gamma_0 - 1) = \alpha\zeta$$

is the efficiency of radiation, $\alpha = (q/\gamma_0)(1 - 1/\sqrt{1+K^2})$. The radiation field from the plane presents a signal with duration $\tau_r = 2\pi N\lambda_0/d$ and linear modulation of both amplitude, $E = 1-\alpha\psi$, and frequency, $\omega = \omega_0 E$ (Fig. 1):

$$E_x/2\pi\sigma = (\Gamma_0 K/\gamma_0)E\sin\tilde{\zeta}$$

where $\omega_0 = \Gamma_0(2\pi c/d)$, $\psi = \Gamma_0(\tau - \zeta)$ are the non-perturbed radiation frequency and the phase at the point of observation, $\tilde{\zeta} = \psi(1-\alpha\psi)$ is the retarded coordinate.

The above formulas provide very good coincidence with numerical calculations even for fairly large space charge parameters and undulator lengths. For example, using for the radiating plane the typical parameters of the Israeli THz source (currently under development) [8]: electron energy $E_0 = 5.5\,\mathrm{MeV}$, surface density $\sigma_0 = 0.1\ \mathrm{nC/mm^2}$ and K=0.47 demonstrates coincidence of analytical and numerical results with high precision; in order to show the differences the density in Fig.1a has been increased up to $3\sigma_0$.

*nezahb@ariel.ac.il

ISBN 978-3-95450-133-5

QUASI-OPTICAL THEORY OF TERAHERTZ SUPERRADIANCE FROM AN EXTENDED ELECTRON BUNCH*

N.S. Ginzburg, A.M. Malkin, A.S. Sergeev, I.V. Zotova, V.Yu. Zaslavsky,
Institute of Applied Physics RAS, Nizhny Novgorod, Russia

Abstract

We consider the superradiance of an extended relativistic electron bunch moving over a periodically corrugated surface for the generation of multi-megawatt terahertz pulses. To study the above process we have developed a three-dimensional, self-consistent, quasi-optical theory of Cherenkov stimulated emission which includes a description of the formation of evanescent wave over a corrugated surface and its excitation by RF current induced in the electron bunch.

INTRODUCTION

In recent years, significant progress was gained in the generation of electromagnetic pulses in the centimeter and millimeter wavelength ranges based on the Cherenkov superradiance (SR) of high-current subnanosecond electron bunches with particle energies of 300–400 keV [1–5] propagating in periodically corrugated single-mode waveguides. In these frequency ranges SR pulses of subnanosecond duration with record-breaking gigawatt peak power were obtained by means of compact high-current accelerators. Typical duration of bunches employed in these experiments was, on the one hand, large compared to the wavelength and, on the other hand, it was limited by the so-called coherence length within which coherent emission of a single electromagnetic pulse from the entire bunch volume is possible due to the slippage of radiation relative to the particles. This SR emission includes electron self-bunching, and the peak power of SR pulse is approximately proportional to the square of the total number of particles in the electron pulse.

A natural continuation of this research is a development of Cherenkov SR sources operating at shorter wavelength values, including the terahertz frequency range. Technological advancements in the fabrication of spatially periodic microstructures also encourage such studies. In order to generate powerful single pulses in the THz range, it is necessary to reduce the duration of the electron bunches to several tens of picoseconds with corresponding increase in their densities. In turn, to obtain stable transverse focusing of dense electron bunches, it would be necessary to increase the particle energy up to several MeV. This increase is also a positive factor in view of improving the impedance of coupling to a surface wave. It should be recalled that for the Cherenkov radiation mechanism the spatial scale of the transverse field decay $L_{\perp} \sim \lambda\gamma/2\pi$ (where $\gamma = \left(1-\beta_0^2\right)^{-1/2}$ is the relativistic Lorentz factor) increases with the particle energy due to a decrease in the requirements for the waves deceleration. High brightness electron bunches generated by photoinjectors [6, 7] can satisfy the above conditions.

We should emphasize that the methods used for the theoretical description of stimulated Cherenkov radiation from relativistic electron beams in the short wavelength range must differ significantly from the approach developed previously for the microwave range. The existing theory of relativistic Cherenkov radiation sources operating in the regimes of both long-pulse (quasi-stationary) [8-10] and short-pulse (SR) [1-3] generation was based on an assumption that the transverse size of the microwave system is comparable to the radiation wavelength. Under these conditions, the Cherenkov radiation was described using a formalism according to which the electron beam interacted with a spatial harmonic of the volume waveguide mode possessing a fixed transverse structure.

For wavelengths shorter than one millimeter, the conditions of ensuring the electron beam transport and reducing Ohmic losses imply the use of oversized (or open) slow-wave systems. Accordingly, it is necessary to take into account the diffraction effects and to use a quasi-optical approach for the description of Cherenkov radiation from relativistic electron beams moving over periodically corrugated surfaces. In the case of a quasi-stationary electron beam such an approach was developed in [11] for consideration of surface-wave oscillators. In this letter we demonstrate that a similar method can be effectively used for analysis of stimulated emission of extended electron bunches moving above a corrugated surface. The validity of our consideration is confirmed by direct particle-in-cell (PIC) simulations based on CST STUDIO 3D code.

BASIC MODEL

We consider a three dimensional (3D) model of the Cherenkov SR from an extended electron bunch that moves rectilinearly at a velocity of $v_0 = \beta_0 c$ along guiding magnetic field $\vec{H}_0 = H_0\vec{z}_0$ over a plane with a shallow periodic sinusoidal corrugation

$$b(z) = b_1 \cos\left(\bar{h}z\right), \tag{1}$$

where $b_1 << d$ is the corrugation amplitude, d is the period, and $\bar{h} = 2\pi/d$. We assume that an electron bunch has finite dimensions $l^e_{x,y,z}$ in three space coordinates (Fig. 1a).

Radiation field near the corrugated surface can be presented as a sum of two counter-propagating TM-

ISBN 978-3-95450-133-5

USING LORENTZ TRANSFORMATIONS FOR SIMULATIONS OF WIGGLER SUPERRADIANCE FROM THE PICOSECOND ELECTRON BUNCHES*

A.M. Malkin, I.V. Zotova, Institute of Applied Physics RAS, Nizhny Novgorod, Russia
N.S. Ginzburg, A.A. Golovanov, Institute of Applied Physics RAS, Nizhny Novgorod, Russia
and Nizhny Novgorod State University, Nizhny Novgorod, Russia
V.P. Tarakanov, Joint Institute for High Temperatures RAS, Moscow, Russia

Abstract

In this paper we present a theoretical analysis of superradiance (SR) from picosecond electron bunches wiggling in periodical undulator field based both on the method of averaged ponderomotive force and on a direct numerical PIC (particle-in-cell) simulation. Within both approaches the analysis takes place in the reference frame co-moving with electrons which allows simplifying the procedure of simulation significantly due to the fact that all the spatial scales including the radiation wavelength, the length of the beam and the length of the pump field pacet into which the undulator field is transformed are of the same order. We show that in the reference frame the SR effect can be interpreted as a formation of the distributed Bragg mirror in the bulk of the electron beam which is effectively reflecting (scattering) the pump wave. A possibility of generation of multimegawatt pulses in terahertz and far infrared wave ranges is demonstrated.

INTRODUCTION

Recently, a significant progress has been achieved in generation of ultrashort electromagnetic pulses in centimeter and millimeter waveband based on superradiance (SR) of high-current electron bunches [1]. Generated pulses are characterized by record-breaking (gigawatt) peak powers. As it was shown both theoretically and experimentally at particle energies of ~300 keV, currents ~1 kA and the bunch durations ~ 1 ns the most effective mechanism of SR pulses generation is the Cherenkov one, realized in a periodic slow-wave structure.

The advancement of SR sources further into short wave ranges can be obtained by using the emission of electron bunches moving in the undulator field. In this case the particles energy should be increased up to 4-5 MeV and the bunch duration should be about several picoseconds. The bunches formed by photo-injection guns possess the necessary characteristics [2]. In this paper under assumption that the electron bunch propagates in a planar waveguide a theoretical analysis and KARAT PIC code simulations of above process were performed. In both approaches we analysis SR effects in the co-moving with electrons reference frame K' [3]. In particular, this allows to simplify the numerical simulation procedure significantly, because at relativistic factor values γ ~10 the length of undulator of about several meters according to Lorentz transformations turns into several tens of centimeters, whereas the length of picosecond electron bunch in the rest reference frame stretches up to several centimeters (see Fig. 1). Besides the radiated wavelength transforms from the submillimeter to millimeter range. Proportionality of all scales, including the transverse size of the bunch, allows us to simulate the processes without using significant computational resources, finding then the parameters of radiated pulses in the lab frame using again the relativistic transformations.

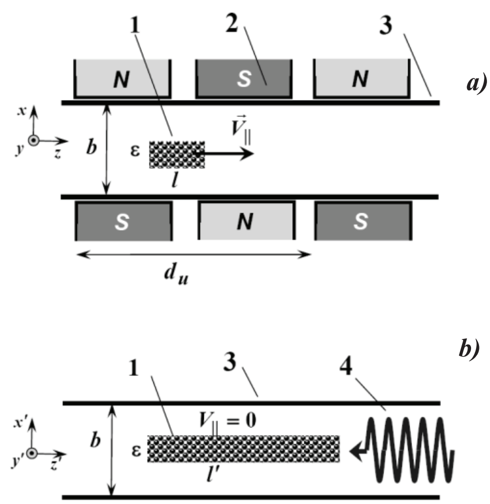

Figure 1: Scheme of generation of superradiance pulse (a) in the lab reference frame and (b) in the co-moving reference frame. (1) - electron beam, (2) - undulator, (3) - planar waveguide, (4) - electromagnetic TE wave, into which the undulator field transforms.

SIMPLIFIED MODEL

We consider here a two-dimensional model assuming that an electron bunch with a length of l moves in a planar waveguide with the gap between plates b_0 (See Fig. 1). Electrons oscillate in a planar undulator field with vector potential:

$$\vec{A}(z,t) = \mathrm{Re}\left(\vec{y}_0 A_u \exp\left[ih_u z\right]\right), \qquad (1)$$

*Work supported by Russian Foundation for Basic Research, grant No.12-02-01152

ISBN 978-3-95450-133-5

SENSITIVITY STUDY OF A TAPERED FREE-ELECTRON LASER

A. Mak*, F. Curbis, S. Werin, MAX IV Laboratory, Lund University, Sweden

Abstract

The output power of a free-electron laser (FEL) can be greatly enhanced by tapering the undulator line. In this work, a sensitivity study of a tapered FEL is presented. The study is conducted using the numerical simulation code GENESIS and a taper optimization method. Starting from a possible case for the future X-ray FEL at the MAX IV Laboratory in Lund, Sweden, a number of parameters are varied systematically and the impact on the FEL power is investigated. These parameters include the electron beam's initial energy, current, emittance, energy spread, as well as the seed radiation power.

INTRODUCTION

In a single-pass free-electron laser (FEL), the technique of undulator tapering involves the decrements in the deflection parameter a_w along the undulator line, thereby maintaining the resonance condition as the electrons lose energy to the radiation. This can increase the output power and the energy extraction efficiency, as has been demonstrated by experiments at the LLNL [1] and the LCLS [2].

The effectiveness of this technique relies on the proper optimization of the tapering profile $a_w(z)$. Two methods are the multidimensional scanning method by Jiao et al. [3] and the GINGER self-design taper algorithm [4] based on the Kroll-Morton-Rosenbluth (KMR) formalism [5]. In a previous work [6], we presented another method based on a modification of the KMR formalism and demonstrated, with numerical simulations, its higher efficiency of energy extraction than the GINGER algorithm.

Utilizing this method of taper optimization, we conduct a sensitivity study to determine the impact of various parameters on the power of a tapered FEL. The results shall provide insights into the development of an X-ray FEL at the MAX IV Laboratory [7], which is part of the laboratory's long-term strategic plan. The plan includes an extension of the MAX IV linear accelerator to 4–6 GeV, enabling the production of hard X-ray.

METHOD

Sensitivity Study

We carry out the sensitivity study using the numerical simulation code GENESIS [8] in the steady-state mode. The starting point is a possible case for the future X-ray FEL at the MAX IV Laboratory, with main parameters as shown in Table 1. We use this as the reference case for the purpose of our sensitivity study.

Table 1: Main Parameters for the Reference Case

Parameter		Value
Electron beam energy	E	4 GeV
Beam current	I	4 kA
Normalized emittance	$\varepsilon_{x,y}$	0.4 mm mrad
Average beta	$\bar{\beta}$	20 m
Energy spread	σ_E/E	1×10^{-4}
Undulator period	λ_w	20 mm
Radiation wavelength	λ	4 Å
Seed radiation power	P_{in}	5 MW

Based on the reference case, we vary five parameters systematically, one at a time. The parameters are the electron beam's energy, current, emittance, energy spread and the seed radiation power. For each parameter value, we apply our taper optimization method, so as to obtain the highest possible FEL power at the end of a 200-metre undulator line. Finally, we examine the impact that the variation of each parameter has on the FEL power.

Taper Optimization

The taper optimization method used in this sensitivity study is the Modified KMR Method, which has been elucidated in a previous work of ours [6]. The method considers a reference particle with phase-space coordinates (ψ_R, γ_R) subject to the following constraints:

$$\gamma_R(z) = \sqrt{\frac{\lambda_w}{2\lambda}[1 + a_w^2(z)]}$$

$$\psi_R(z) = gz \text{ for some } g > 0.$$

The energy γ_R is always on resonance throughout the undulator line, while the phase ψ_R is made to increase linearly with distance z along the undulator line at some desired gradient g. Imposing these constraints on the particle's equation of motion results in a taper profile $a_w(z)$. In numerical simulations, we scan over different values of g to obtain the maximum FEL output power.

RESULTS AND DISCUSSIONS

Sensitivity to Beam Energy

The initial energy of the electron beam is 4 GeV in the reference case. We examine the effects of increasing the energy from 4 GeV to 5, 6 and 7 GeV. For each energy, we apply the taper optimization method to maximize the final FEL power at $z = 200$ m. The resulting FEL power curves and the corresponding taper profiles are shown in Fig. 1. The optimum g-values resulting from the taper optimizations are specified in the figure legend.

The reference case, with initial beam energy 4 GeV, produces a final FEL power of 1.6 TW. Upon increasing the initial beam energy, the FEL power shows a higher growth

* alan.mak@maxlab.lu.se

ISBN 978-3-95450-133-5

UPDATE ON THE FEL CODE GENESIS 1.3

S. Reiche, Paul Scherrer Institut, Villigen, Switzerland

Abstract

The widely used time-dependent code Genesis 1.3 has been modified to address new needs of users worldwide. The existing limitation of tracking isolated slices of the FEL beam has been overcome by keeping the entire electron beam in memory, which is tracked as a whole through the undulator. This modification allows for additional features such as allowing particles to migrate into other slices or applying self-consistent wakefield and space charge models.

INTRODUCTION

Since the first high gain Free-Electron Lasers [1–4] numerical codes have aided the users to understand experimental results and to design future facilities. Several codes are available [5–9] and have been benchmarked against each other and experiments [10]. With the ongoing development of the general computer technology and infrastructures the FEL codes can expand the complexity of the underlying models or operate with more particles for finer resolutions. Currently single-pass FELs at the Angstrom level can be run in a few hours or less.

However new FEL schemes, e.g. self-seeding [11], EEHG [12], high-brightness SASE FELs [13], are rather complex and very difficult to model for users of the FEL codes. The primary obstacle is that most codes have evolved from a single processor platform to a large scale parallel computer platform while preserving the ability to run on a single computer. Nevertheless a new algorithm, where a parallel computer network is deeply embedded, can offer new features beyond the capabilities of existing codes.

In this paper I present the current status of the code Genesis 1.3 [6], which has been modified under the assumption that the computer cluster is large enough to hold the entire electron beam and radiation field in memory. The beam and field is propagated through the undulator as a whole with a resolution down to each individual electron. The core algorithm is still based on the slowly varying envelope approximation (SVEA) [14], where the equations of motion are averaged over one undulator period. It allows one to choose integration step sizes larger than the undulator period to keep the number of integration steps within a reasonable limit even for very long hard-X-ray FELs such as LCLS or SwissFEL. A non-averaged approach is not pursued, but which has been successfully implemented by new codes such as PUFFIN [8].

CURRENT LIMITATION

During the development of Genesis in the late nineties one important factor was the available memory for the calculation. Keeping the entire radiation field and particle distribution was way beyond the practical limit of those days and an extensive bookkeeping has to be done to reduce the required footprint in memory space. This was done by tracking a single electron slice through the undulator interacting with many radiation field slices which are slipping in from behind and then slipping out after a few integration steps, depending on the length of the electron slice. The bookkeeping is storing temporarily the field which slips out to feed it to the next electron slice once the tracking of the current slice has been done. Using this approach the memory needs to store only the data of a single electron slice and the radiation field over one slippage length compared to the entire time window which can be many times longer than a slippage length. However this restricts the algorithm to work sequentially through the electron bunch from the tail to the head. No information can propagate in the backward direction.

Recent ideas to improve longitudinal coherence in SASE FELs [13, 15, 16] are based on an enhancement of slippage to cover the entire bunch. That way the spectral brightness is improved. The consequence is that the record for storing the slippage field needs to be increased by a large factor. In fact, it would use the same memory size if the entire radiation field were kept in memory at all time. The latter approach has the advantage that one could calculate the spectrum during runtime and not, as it is now, as a post-processing step.

A second limitation arises from proposed schemes which are utilizing a large harmonic conversion, either by a multi-staged approach in HGHG cascades or a direct conversion with high efficiency in EEHG schemes [17]. Genesis particle distribution is based on a quiet loading where macro particle are mirrored and evenly distributed in longitudinal position to cancel out completely any Fourier component for a given wavelength. In an explicit step in the beam loading algorithm a controlled random offset is applied to the particle to give the correct statistics in the bunching factor [18]. To include more harmonics more mirror particles are needed, preferably at least twice the number than the highest harmonic considered. For the 100th harmonic this would be at least 200 mirror particles. If one used 1000 particle to generate the remaining 5 D distribution and then apply the mirroring process one slice would be filled with 200k macro particles or if sliced to the final harmonics 2000 particles. For an FEL operating at 1 nm with a 1 kA beam current that is almost of the same order as the real number of electrons to be modeled. With a moderate increase in the particle number then a real one-one simulation could be carried out with the advantage that no mirroring needs to be done and therefore the transverse distribution is much smoother (effectively filled with 200k particles rather than only 1k).

ISBN 978-3-95450-133-5

MINERVA, A NEW CODE TO MODEL FREE-ELECTRON LASERS

H.P. Freund , Department of Electrical and Computer Engineering, Colorado State University, Fort Collins, USA
P.J.M. van der Slot#, Mesa Institute for Nanotechnology, University of Twente, Enschede, the Netherlands
Department of Electrical and Computer Engineering, Colorado State University, Fort Collins, USA

Abstract

Simulation codes modeling the interaction of electrons with an optical field inside an undulator are an essential tool for understanding and designing free-electron lasers (FELs). As there exists a large variety of FELs ranging from long-wavelength oscillators using partial wave guiding to soft and hard x-ray FELs that are either seeded or starting from noise, a simulation code should be capable of modeling this huge variety of FEL configurations. A new code under development, named MINERVA, will be capable of modeling such a large variety of FELs. The code uses a modal expansion for the optical field, e.g., a Gaussian expansion for free-space propagation, and an expansion in waveguide modes for propagation at long wavelengths, or a combination of the two for partial guiding at THz frequencies. MINERVA uses the full Newton-Lorentz force equation to track the particles through the optical and magnetic fields. To allow propagation of the optical field outside the undulator and interact with optical elements, MINERVA interfaces with the optical propagation code OPC. Here we describe the main features of MINERVA and give various examples of its capabilities.

INTRODUCTION

A variety of different free-electron laser (FEL) simulation codes have been developed over the past several decades such as GINGER [1], MEDUSA [2], TDA3D [3], and GENESIS 1.3 [4] among others. Typically, these codes undergo continuous development over their usable lifetimes. As a result, the codes become increasingly complex as new capabilities are added or older capabilities are deleted, and this tends to hobble their performance. It also renders it increasingly more difficult to make further modifications that might be needed. Because of this, we decided to develop a new code using a "clean-slate" approach having the properties and characteristics that we desired. We designate this new code as MINERVA.

The organization of the paper is as follows. The properties of MINERVA are described in the second section. We describe the comparison of MINERVA with the SPARC SASE FEL [5] in the third section, and a comparison with the long wavelength JLAB IR-upgrade FEL oscillator [6] in the fourth section. A summary and discussion follows.

PROPERTIES OF MINERVA

The formulation of MINERVA describes the particles and fields in three spatial dimensions and includes time dependence as well. Electron trajectories are integrated using the complete Newton-Lorentz force equation. No wiggler-averaged-orbit approximation is made. The magnetostatic fields can be specified by analytical functions for a variety of analytic undulator models (such a planar or helical representations), quadrupoles, and dipoles. These magnetic field elements can be placed in arbitrary sequences to specify a variety of different transport lines. As such, MINERVA can set up field configurations for single or multiple wiggler segments with quadrupoles either placed between the undulators or superimposed upon the undulators to create a FODO lattice. Dipole chicanes can also be placed between the undulators to model various high-gain harmonic generation (HGHG) configurations. The fields can also be imported from a field map if desired.

The electromagnetic field is described by a modal expansion. For free-space propagation, MINERVA uses Gaussian optical modes, while waveguide modes are used when the wavelength is comparable to the dimensions of the drift tube. As a result, MINERVA can treat both long and short wavelength FELs. A combination of the Gaussian and waveguide modes is also possible when there is partial guiding at, for example THz frequencies.

The electromagnetic field representations are also used in integrating the electron trajectories, so that harmonic motions and interactions are included in a self-consistent way. Further, the same integration engine is used within the undulator(s) as in the gaps, quadrupoles, and dipoles, so that the phase of the optical field relative to the electrons is determined self-consistently when propagating the particles and fields in the gaps between the undulators.

Particle loading is done in a deterministic way using Gaussian quadrature that preserves a quiet start for both the fundamental and all harmonics. Shot noise is added following the procedure developed for MEDUSA [7], so that MINERVA is capable of simulating SASE FELs.

MINERVA has also been linked to the Optics Propagation Code (OPC) [8,9] for the simulation of FEL oscillators or propagating an optical field beyond the end of the undulator line to a point of interest.

MINERVA is written in Fortran 95 using dynamic memory allocation and supports parallelization using the Message Passing Interface.

#p.j.m.vanderslot@utwente.nl

ISBN 978-3-95450-133-5

RECENT UPDATES TO THE OPTICAL PROPAGATION CODE OPC

P.J.M. van der Slot#
Mesa+ Institute for Nanotechnology, University of Twente, Enschede, The Netherlands
Department of Electrical and Computer Engineering, Colorado State University, Fort Collins, USA
K.-J. Boller
Mesa+ Institute for Nanotechnology, University of Twente, Enschede, The Netherlands

Abstract

In order to understand and design free-electron lasers (FELs), simulation codes modeling the interaction of electrons with a co-propagating optical field in the magnetic field of an undulator are essential. However, propagation of the optical field outside the undulator is equally important for evaluation of the optical field at the location of the application or to model FEL oscillators.

The optical propagation code OPC provides such capabilities and can interface with FEL gain codes like GENESIS 1.3, MEDUSA and MINERVA. Here we present recent additions and modifications to the code that improves the speed of the code and extends the modeling capabilities. These include amongst other, inline diagnostics that results in considerable faster runtimes, the ability to convert from free-space modes to guided modes (currently only cylindrical waveguides), and the possibility to determine the spectrum at each transverse location. The latter opens the possibility to include dispersion in the optical propagation.

INTRODUCTION

Simulation tools play an essential role in the design and understanding of free-electron lasers (FELs). In the last few decades, several codes have been developed to model the interaction of electrons with a co-propagating optical field inside the magnetic field of an undulator, amongst others, GENESIS 1.3 [1], GINGER[2], MEDUSA [3] and MINERVA [4] as a recent addition. These codes are used to calculate the spatio-temporal characteristics of the optical pulse coming out of the undulator. However, self-consistent modelling of an oscillator FEL also requires to model the propagation of the optical pulse outside the gain section, i.e., outside the undulator. Even for single pass systems, a system designer or user is typically interested in the characteristics of the optical pulse in the far field. The optical propagation code (OPC) [5] provides tools for propagating the optical field outside the gain section and interfaces with the FEL gain codes GENESIS 1.3, MEDUSA and MINERVA. The main properties of OPC are described in ref. [5], and we only summarize its main characteristics here. The propagation of the optical field is done using one of three methods, a spectral method, a Fresnel diffraction integral and a modified Fresnel diffraction integral. These methods propagate the complex phasor of the electric field of the optical pulse from an input plane to an output plane, where the modified Fresnel integral allows for an expansion of the grid on which the optical field is defined, but not the number of grid points. OPC allows placement of various optical elements along the propagation path, such as apertures, lenses and mirrors. In this paper we describe the recent additions to the code that enhances its capabilities and increases the speed of the code. The remainder of the paper is organized as follows. We will first describe the addition of inline diagnostics, which is then followed by a description of waveguide modes and finally we discuss the possibility to propagate in the frequency domain, which allows the use of dispersive elements in the optical path. We conclude with a brief summary and outlook for future additions to OPC.

IN-LINE DIAGNOSTICS

In order for the user to analyze the optical properties of the light generated in the FEL, the user has the ability to execute a number diagnostics on the optical pulse, such as obtaining the intensity $I(x,y,s)$ as a function of the position (x,y) in the transverse plane for a specific longitudinal position s, the phase $\Theta(x,y,s)$ as a function of the position (x,y) for a specific s or $\Theta(x=x_0,y=y_0,s)$ as a function of s for a specific transverse location (x_0,y_0), the power $P(s)=\iint I(x,y,s)dxdy$ in the pulse, the fluence $F(x,y)=\int I(x,y,s)ds$, a cross section $I(x,y=y_0,s)$ or $I(x=x_0,y,s)$ through the pulse, the "centre of gravity" (x_c,y_c) of the optical pulse and its rms radius r_{rms} (weighted with the intensity distribution). These diagnostics can be applied at any (intermediate) plane along the optical path where the optical field is evaluated. Until recently, OPC first propagates the optical from start to end of the optical path, while storing the optical field at the locations where diagnostics are requested. After the optical propagation has completed, the user can perform the diagnostic commands to the stored optical field. For this reason, we refer to this as off-line diagnostics.

The stored optical field consists of the complex phasor (amplitude and phase) of a linearly polarized electric field at each grid point for each of the time samples of the optical field, and the amount of data can become very large for large grid sizes ($N_x \times N_y = N_p^2$, for simplicity) and/or number of times samples N_s. For this reason, the optical field is stored on disk and the associated disk I/O can have an impact on the speed of the program when the files become large or a large number of diagnostics are requested.

#p.j.m.vanderslot@utwente.nl

ISBN 978-3-95450-133-5

THE IMPLEMENTATION OF 3D UNDULATOR FIELDS IN THE UNAVERAGED FEL SIMULATION CODE Puffin

J. R. Henderson[1], L.T. Campbell[1,2,3,4], A.R. Maier[3,4] and B.W.J. McNeil[1]
[1]SUPA, Department of Physics, University of Strathclyde, Glasgow, UK
[2]ASTeC, STFC Daresbury Laboratory and Cockcroft Institute, Warrington, UK
[3]Center for Free-Electron Laser Science, Notkestrasse 85, Hamburg, Germany
[4]Institut für Experimentalphysik, Universität Hamburg, Hamburg, Germany

Abstract

The FEL simulation code Puffin is modified to include 3D magnetic undulator fields. Puffin, having previously used a 1D undulator field, is modified to accommodate general 3D magnetic fields. Both plane and curved pole undulators have been implemented. The electron motion for both agrees with analytic predictions.

INTRODUCTION

Puffin [1] is an unaveraged 3D FEL code which does not make the Slowly Varying Envelope Approximation (SVEA) or period averaging in its analytical model. As such, it is capable of modelling the a broad radiation field spectrum, full longitudinal broadband electron beam transport through the undulator, and Coherent Spontaneous Emission (CSE) emerging from current gradients in the beam.

However, although Puffin models a 6D electron beam and 3D radiation field, it does not employ a 3D magnetic undulator field. Instead, it implements a 1D undulator field with no off-axis variation. Superimposed, is an external focusing channel which is an approximation of the natural focusing found in a helical undulator. This focusing channel may be strengthened or weakened through the use of a 'focusing factor' [2] to obtain a desired betatron frequency.

Such a model does not simulate the detuning of the resonance condition in the transverse dimensions. Nor does it allow the focusing to emerge naturally from the off-axis variation of the magnetic fields. The resulting electron motion is an approximation in the case of a helical or curved-pole undulator; it is inaccurate in the case of an undulator with plane poles. Furthermore, the betatron motion as derived in Puffin is only valid when the electron beam is close to mono-energetic.

There is a need to model more realistic undulator fields; in particular, plane pole and curved pole undulators are more common than helical undulators for UV/X-ray FELs. There is therefore a requirement that various 3D planar undulator types be implemented in Puffin.

In the following, the Puffin model is first generalized to include general undulator magnetic fields. This model also allows a helical field description to be developed. Note also that this general magnetic field description need not be limited to undulators, and may allow future alternative applications of the Puffin code, to solve other radiation-electron interactions in static magnetic fields.

This general description is then used to implement both a generic plane pole and curved (canted) pole undulator FEL. Results are presented to demonstrate the correct electron motion and radiation characteristics are being solved.

MODIFIED MATHEMATICAL MODEL

The derivation of the FEL system of equations modelled by Puffin is given in [1], using a magnetic undulator field $\mathbf{B}_u = \frac{B_u}{2}(\mathbf{u}e^{ik_u z} + c.c.)$, where $\mathbf{u} = u_x\hat{\mathbf{x}} + iu_y\hat{\mathbf{y}}$ defines the polarization of the undulator. Following the same derivation, but using a general 3D magnetic field of the form $\mathbf{B} = B_x\hat{\mathbf{x}} + B_y\hat{\mathbf{y}} + B_z\hat{\mathbf{z}}$, one obtains the following system of equations:

$$\Big[\frac{1}{2}\Big(\frac{\partial^2}{\partial\bar{x}^2} + \frac{\partial^2}{\partial\bar{y}^2}\Big) - \frac{\partial^2}{\partial\bar{z}\partial\bar{z}_2}\Big]A_\perp = - \frac{1}{\bar{n}_p}\frac{\partial}{\partial\bar{z}_2}\sum_{j=1}^{N}\bar{p}_{\perp j}L_j\delta^3(\bar{x}_j,\bar{y}_j,\bar{z}_{2j}) \tag{1}$$

$$\frac{d\bar{p}_{\perp j}}{d\bar{z}} = \frac{1}{2\rho}\Big[ib_\perp - \frac{\eta p_{2j}}{\alpha^2}A_\perp\Big] - i\alpha\bar{p}_{\perp j}L_j b_z \tag{2}$$

$$\frac{dp_{2j}}{d\bar{z}} = \frac{\rho}{\eta}L_j^2\Big[\eta p_{2j}(\bar{p}_{\perp j}A^*_{\perp j} + c.c.) - i(1+\eta p_{2j})\alpha^2(\bar{p}_{\perp j}b^*_{\perp j} - c.c.)\Big] \tag{3}$$

$$\frac{d\bar{z}_{2j}}{d\bar{z}} = p_{2j} \tag{4}$$

$$\frac{d\bar{x}_j}{d\bar{z}} = \frac{2\rho\alpha}{\sqrt{\eta}}L_j\Re(\bar{p}_{\perp j}) \tag{5}$$

$$\frac{d\bar{y}_j}{d\bar{z}} = -\frac{2\rho\alpha}{\sqrt{\eta}}L_j\Im(\bar{p}_{\perp j}). \tag{6}$$

where

$$\eta = \frac{1-\bar{\beta}_z}{\bar{\beta}_z} = \frac{\lambda_r}{\lambda_u}, \tag{7}$$

$$\bar{p}_\perp = \frac{p_\perp}{mca_u}, \qquad A_\perp = \frac{eua_u l_g}{2\sqrt{2}\gamma_r^2 mc^2\rho}E_\perp,$$
$$\rho = \frac{1}{\gamma_r}\left(\frac{a_u\omega_p}{4ck_u}\right)^{2/3}, \qquad a_u = \frac{eB_0}{mck_u},$$
$$\alpha = \frac{a_u}{2\rho\gamma_r}, \qquad b_\perp = b_x - ib_y, \tag{8}$$

ISBN 978-3-95450-133-5

MODELING CSR IN A VACUUM CHAMBER BY PARTIAL FOURIER ANALYSIS AND THE DISCONTINUOUS GALERKIN METHOD *

D. A. Bizzozero† [1], R. Warnock [2,1], J. A. Ellison [1]
[1] Department of Mathematics and Statistics, University of New Mexico
Albuquerque, New Mexico 87131, USA
[2] SLAC National Accelerator Laboratory, Stanford University
Menlo Park, California 94025, USA

Abstract

We continue our study [1–3] of CSR from a bunch on an arbitrary curved orbit in a plane. The vacuum chamber has rectangular cross section with possibly varying horizontal width. We make a Fourier transform in $s - ct$ and use the slowly varying amplitude approximation. We invoke a Fourier expansion in the vertical coordinate y, which meets the boundary conditions on the top and bottom plates and makes contact with the Bessel equation of the frequency domain treatment. The fields are defined by a PDE in s and x, first order in s, which is discretized in x by finite differences (FD) or the discontinuous Galerkin method (DG). We compare results of FD and DG, and also compare the computation speeds to our earlier calculations in 3D (paraxial) which did not use the Fourier series in y [4–8]. This approach provides more transparency in the physical description, and when only a few y-modes are needed, provides a large reduction in computation time.

STATEMENT OF THE PROBLEM

Statement of the Physical Problem

We start with the wave equation for the E_y and H_y fields in the Frenet-Serret coordinates (s, x, y, t) :

$$\nabla^2 E_y - \frac{1}{c^2}\frac{\partial^2 E_y}{\partial t^2} = Z_0\Big(\frac{1}{c}\frac{\partial J_y}{\partial t} + c\frac{\partial \rho}{\partial y}\Big), \tag{1a}$$

$$\nabla^2 H_y - \frac{1}{c^2}\frac{\partial^2 H_y}{\partial t^2} = -\frac{R}{x+R}\frac{\partial J_x}{\partial s} + \frac{\partial J_s}{\partial x} + \frac{1}{x+R}J_s. \tag{1b}$$

We shall solve for the fields in a toroidal vacuum chamber with perfectly conducting walls at $x = x_{in}, x_{out}$ and $y = \pm h/2$. The bunch orbit is centered in the chamber and has bending radius R. We next apply a Fourier transform in $s - ct$ and a Fourier series in y. Now the fields and sources are expressed in the form

$$F(s,x,y,t) = \int_{-\infty}^{\infty} dk\, e^{ik(s-ct)} \sum_{p=1}^{\infty} \phi_p(y)\hat{F}_p(s,x,k), \tag{2}$$

$$\phi_p(y) = \begin{bmatrix} \cos \\ \sin \end{bmatrix} \Big(\alpha_p(y+h/2)\Big), \quad \alpha_p = \frac{\pi p}{h}.$$

If the vertical distribution of charge is an even function of y, which we assume, then only odd integers p are involved. For E_y, H_x, H_s, J_y the factor ϕ_p contains only cos terms whereas for H_y, E_x, E_s, ρ, J_x, J_s it contains only sin terms. In the approximation of slowly varying amplitude (paraxial approximation) terms with $\partial^2/\partial s^2$ are neglected and the transformed equations (1) for $\hat{F}_p(s,x,k) = \hat{E}_{yp}$, $\hat{H}_{yp}$ become (with $\gamma_p^2 = k^2 - \alpha_p^2$):

$$\begin{aligned}\frac{2ikR^2}{(x+R)^2}\frac{\partial \hat{F}_p}{\partial s} &= -\frac{\partial^2 \hat{F}_p}{\partial x^2} - \frac{1}{x+R}\frac{\partial \hat{F}_p}{\partial x} \\ &- \Big(\gamma_p^2 - \frac{(kR)^2}{(x+R)^2}\Big)\hat{F}_p + S.\end{aligned} \tag{3}$$

For a charge density of the form $q\lambda(s-ct)H(y)\delta(x)$, where q is the charge, the source terms are:

$$S_{\hat{E}} = \sigma\delta(x), \quad S_{\hat{H}} = \tau\Big(\delta'(x) + \delta(x)/R\Big) \tag{4a}$$

$$\sigma = qZ_0\alpha_p c\hat{\lambda}(k)H_p, \quad \tau = q\beta c\hat{\lambda}(k)H_p\,, \tag{4b}$$

where $\hat{\lambda}$ and H_p are Fourier transforms of λ and H. For a Gaussian H with width $\sigma_y \ll h$ we have $H_p = (-1)^{(p-1)/2}(2/h)\exp(-(\alpha_p\sigma_y)^2/2)$.

The perfectly conducting boundary conditions are guaranteed by:

$$\hat{E}_{yp}|_{x=x_{in},x_{out}} = 0, \quad \frac{\partial \hat{H}_{yp}}{\partial x}|_{x=x_{in},x_{out}} = 0. \tag{5}$$

To construct initial conditions for $\hat{E}_{yp}, \hat{H}_{yp}$, we assume an infinite straight prior to the entrance of the bend and use the steady-state solutions $\hat{F}_{p0} = \hat{E}_{yp0}$, $\hat{H}_{yp0}$ which satisfy:

$$\frac{d^2\hat{F}_{0p}}{dx^2} - \alpha_p^2\hat{F}_{0p} = S \tag{6}$$

With the solutions $\hat{E}_{yp}, \hat{H}_{yp}$ to the initial value problem (3-6) for each p, we construct the remaining fields through additional relations in Eq. (30), then return to the space-time domain by (2).

Statement of the Mathematical Problem

To solve (3) numerically, we first introduce a transformation to treat the singularities of (4a):

$$V = \hat{E}_{yp} - \sigma x\Theta(x), \tag{7a}$$

$$W = \hat{H}_{yp} - \tau\Theta(x), \tag{7b}$$

* Work supported by DOE under DE-FG02-99ER41104 and DE-AC03-76SF00515.

† dbizzoze@math.unm.edu

ISBN 978-3-95450-133-5

TW X-RAY FREE ELECTRON LASER OPTIMIZATION BY TRANSVERSE PULSE SHAPING*

C. Emma, C. Pellegrini, UCLA, Los Angeles, CA 90095 USA
J. Wu, SLAC, Menlo Park, CA 94025, USA

Abstract

We study the dependence of the peak power of a 1.5 Å TW, tapered X-ray free-electron laser on the transverse electron density distribution. Multidimensional optimization schemes for TW hard X-Ray free electron lasers are applied to the cases of transversely uniform and parabolic electron beam distributions and compared to a Gaussian distribution. The optimizations are performed for a 200 m undulator using the fully 3-dimensional FEL particle code GENESIS. The study shows that the flatter transverse electron distributions enhance optical guiding in the tapered section of the undulator and increase the maximum radiation power from a maximum of 1.56 TW for a transversely Gaussian beam to 2.26 TW for the parabolic case and 2.63 TW for the uniform case.

INTRODUCTION

Radiation produced by Self Amplified Spontaneous Emission X-ray Free Electron Lasers (SASE X-FELs) [1] has been used to probe matter at the fastest timescales (fs) and the smallest dimensions (Å). LCLS and SACLA, the world's most powerful existing X-FELs deliver diffraction limited X-ray pulses of a few to a hundred femtoseconds in the energy range of 0.25 to 10 keV with peak power at saturation of 20-30 GW and a line-width on the order of 10^{-3} [2]. Pushing the capabilites of XFELs to TW peak power levels will have a great impact on future scientific endeavours, particularly in the fields of coherent X-ray diffraction imaging and nonlinear science. It is well known that the peak power of an FEL can be increased by tapering the undulator magnetic field to match the electron energy loss while preserving the synchronism condition [3]. The LCLS for example currently boosts its output power by a factor 2-3 using a limited taper capacity $\Delta K/K \sim 0.8\%$. For a SASE FEL this gain is limited due to the spiky nature of the radiation [4]. In a seeded or self-seeded FEL however, recent work has shown that a more flexible taper capacity can lead to much larger output powers, reaching levels of one TW or larger [5,6]. The analytic models developed in previous studies to obtain the optimal tapering profile have included three dimensional effects but only considered electron beams with Gaussian transverse density profile. In this work we examine the effect of using transversely parabolic and transversely uniform electron distributions in a tapered hard X-ray FEL with LCLS-II like parameters. The results are compared to the Gaussian beam case in both single frequency and time dependent simulations using the GENESIS code [7].

* Work supported by: DOE Grant Number DE-SC0009983

Table 1: GENESIS Simulation Parameters

Parameter Name	Parameter Value
Beam energy E_0	13.64 GeV
Beam peak current I_{pk}	4000 A
Normalized emittances $\epsilon_{x,n}/\epsilon_{y,n}$	0.3/0.3 μ m rad
Peak radiation power input P_{in}	5 MW
Undulator period λ_w	32 mm
Normalised undulator parameter a_w	2.3832
Radiation wavelength λ_r	1.5 Å
FEL parameter ρ	7.361 $\times 10^{-4}$

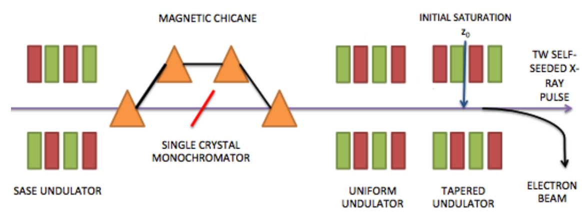

Figure 1: Schematic representation of a tapered X-ray FEL using a self-seeding monochromator and an optimised tapered section.

TAPERING OPTIMIZATION

Transverse Pulse Shaping in a Tapered FEL

In recent work [5] it has been pointed out that diffraction and refraction have an important impact on the peak power of TW X-FELs. Starting from conservation of energy and applying the same assumptions as in Ref. [5] we can write the radiation power as a function of the longitudinal position in the undulator:

$$P(z) = \frac{\pi r_s(z)^2 a_{s0}(z)^2}{4Z_0}\left(\frac{k_s m_e c^2}{e}\right)^2, \quad (1)$$

where $a_{s0}(z) = |e|A_s(z)/\sqrt{2}mc^2$ is the on-axis normalized vector potential of the radiation field for a linearly polarised undulator, $r_s(z)$ is the radiation beam size, k_s is the radiation wavenumber and Z_0 is the free space impedance. We must now optimize the growth of the radiation field inside the undulator in order to maximize the output radiation power. As described first in Ref. [3], this can be achieved by an adiabatic decrease in the resonant energy $\gamma_r(z)mc^2$, which is defined by the now z dependent resonance condition:

$$\gamma_r^2(z) = \frac{k_w}{2k_s}\left(1 + a_w(z)^2\right), \quad (2)$$

where $k_w = 2\pi/\lambda_w$ is the undulator wavenumber and $a_w(z) = |e|B_w(z)/\sqrt{2}k_w mc^2$ is the normalized vector po-

ISBN 978-3-95450-133-5

TRANSVERSE COHERENCE PROPERTIES OF A TGU-BASED FEL

Panagiotis Baxevanis, Zhirong Huang, Ronald Ruth, SLAC National Accelerator Laboratory, Menlo Park, CA 94025, USA
Carl B. Schroeder, Lawrence Berkeley National Laboratory, Berkeley, CA 94720, USA

Abstract

The use of a transverse gradient undulator (TGU) is considered an attractive option for FELs driven by electron beams with a relatively large energy spread. In this scheme, a dispersion is introduced in the beam while the undulator poles are inclined so that the undulator field acquires a linear dependence upon the transverse position in the direction of dispersion. By suitably selecting the dispersion and the field gradient, the energy spread effect can be significantly mitigated, thus avoiding a drastic reduction in the FEL gain. However, adding the dispersion typically leads to electron beams with large aspect ratios. As a result, the presence of higher-order modes in the output FEL radiation can become significant. To investigate this effect, we study the properties of the higher-order eigenmodes of a TGU-based, high-gain FEL, using both a simplified, analytically-solvable model and a variational technique. This formalism is then used to provide an estimate of the degree of transverse coherence for a representative soft X-ray, TGU FEL example.

INTRODUCTION

One of the most crucial parameters which affect the performance of a free electron laser (FEL) is the energy spread in the driving electron beam. A large value of the latter gives rise to a wide spread in the resonant wavelength, resulting in a substantially decreased FEL gain. Using a transverse gradient undulator (TGU) [1]- [2], it is possible to mitigate this problem. By dispersing the electron beam and tilting the undulator poles, both the electron energy and the undulator parameter acquire a linear transverse dependence. A suitable selection of the dispersion and the field gradient minimizes the impact of the energy spread upon the FEL resonance condition, leading to improved performance. This scheme has been shown to be attractive for FEL concepts that utilize the beam from laser-plasma accelerators (LPAs) [3]. However, a drawback of the TGU approach is the increased size of the electron beam in the direction of dispersion (typically the horizontal direction), which can cause the growth of multiple FEL modes in the exponential-gain regime, degrading the transverse coherence of the output radiation. In order to provide a theoretical framework for understanding this effect, we study the properties of the higher-order FEL modes for a TGU-based configuration. Our analysis is based on solving the FEL eigenmode equation for the parallel beam case (negligible emittance and focusing effects) by employing an exactly-solvable, approximate model and a variational approach. When applied to a specific LPA-based example, this formalism yields results which agree with simulation and provide us with insight into the factors which affect transverse coherence in a TGU FEL.

THEORY

As mentioned earlier, our study is based on an analysis of the FEL eigenmodes, i.e. the solutions of the form $A(\mathbf{x})e^{i\mu z}$ for the complex amplitude of the electric field of the radiation - where $\mathbf{x} = (x, y)$ is the transverse position vector and z is the longitudinal coordinate along the undulator. Each eigenmode is thus characterized by a z-invariant transverse profile $A(\mathbf{x})$ and a constant, complex growth rate μ. According to our previous treatment of a TGU-based FEL [4], the equation that is satisfied by the profile and the growth rate of a growing mode (i.e. one with $\mathrm{Im}(\mu) < 0$) in the parallel beam regime is

$$\left(\mu - \frac{\nabla_\perp^2}{2k_r}\right) A(\mathbf{x}) = U(\mathbf{x}, \mu) A(\mathbf{x})\,, \tag{1}$$

where

$$U(\mathbf{x}, \mu) = -8\rho_T^3 k_u^3 \exp\left(-\frac{x^2}{2\sigma_T^2} - \frac{y^2}{2\sigma_y^2}\right) \times \int_{-\infty}^{0} d\xi \xi \mathrm{e}^{i(\mu - \Delta\nu k_u)\xi} e^{-2(\sigma_\delta^{ef})^2 k_u^2 \xi^2} \times \exp\left(-2ik_u C_p \frac{x}{\eta}\xi\right). \tag{2}$$

Here, $\nabla_\perp^2 = \partial^2/\partial\mathbf{x}^2$, $k_r = 2\pi/\lambda_r$ and $k_u = 2\pi/\lambda_u$ - where λ_r is the resonant wavelength and λ_u is the undulator period - $\Delta\nu$ is a dimensionless detuning variable while σ_T and σ_y are the rms electron beam sizes in the x and y directions. The former of the last two parameters includes the contribution of the - constant - dispersion η and is given by $\sigma_T = (\sigma_x^2 + \eta^2\sigma_\delta^2)^{1/2}$, where σ_x is the non-dispersive horizontal beam size and σ_δ is the rms energy spread. Moreover, ρ_T and σ_δ^{ef} are, respectively, the effective Pierce parameter and energy spread of the FEL, quantities that are expressed by $\rho_T = \rho(1 + \eta^2\sigma_\delta^2/\sigma_x^2)^{-1/6}$ and $\sigma_\delta^{ef} = \sigma_\delta(1 + \eta^2\sigma_\delta^2/\sigma_x^2)^{-1/2}$, where ρ is the Pierce parameter for $\eta = 0$. This non-dispersive FEL parameter is in turn given by $\rho = (K_0^2[JJ]^2 I_p/(16 I_A \gamma_0^3 \sigma_x \sigma_y k_u^2))^{1/3}$, where γ_0 is the average electron energy in units of its rest mass m_0c^2, K_0 is the on-axis undulator parameter, $[JJ] = J_0(K_0^2/(4 + 2K_0^2)) - J_1(K_0^2/(4 + 2K_0^2))$, $I_A \approx 17$ kA is the Alfven current and I_p is the peak current of the electron beam. On the other hand, $C_p = \sigma_x^2/\sigma_T^2 + \bar{\alpha}\eta - 1$ with $\bar{\alpha} = K_0^2\alpha/(2 + K_0^2)$, α being the transverse gradient of the

ISBN 978-3-95450-133-5

INITIAL VALUE PROBLEM FOR AN FEL DRIVEN BY AN ASYMMETRIC ELECTRON BEAM

Panagiotis Baxevanis, Ronald Ruth
SLAC National Accelerator Laboratory, Menlo Park, CA 94025, USA

Abstract

FEL configurations in which the driving electron beam is not axially symmetric (round) are important in the study of novel concepts (such as TGU-based FELs, [1]- [2]) but also become relevant when one wishes to explore the degree to which the deviation from symmetry - inevitable in practical cases - affects the performance of more conventional FEL schemes [3]. In this paper, we present a technique for solving the initial value problem of such an asymmetric FEL. Extending an earlier treatment of ours [4], we start from a self-consistent, fully 3D, evolution equation for the complex amplitude of the electric field of the FEL radiation, which is then solved by expanding the radiation amplitude in terms of a set of orthogonal transverse modes. The numerical results from such an analysis are in good agreement with simulation and provide a full description of the radiation in the linear regime. Moreover, when the electron beam sizes are constant, this approach can be used to verify the predictions of the standard eigenmode formalism.

INTRODUCTION

In most theoretical treatments of the free electron laser (FEL), it is assumed that certain characteristics of the electron beam (such as size and angular divergence) and the undulator system (such as focusing strength) are the same in both transverse directions, a premise which defines the so-called round beam case. There exist, however, novel FEL concepts whose treatment requires a definite departure from the round beam scenario. A particularly intriguing example of the latter is an FEL based on a transverse gradient undulator (TGU), where the addition of dispersion may cause the horizontal size of the electron beam to become much larger than its vertical size. Moreover, non-symmetric FEL examples may become relevant even in the context of more conventional configurations since asymmetry is an inherent feature in many key FEL components (we note, for instance, the absence of horizontal focusing in a flat-pole undulator). In this work, we adopt a model that covers both cases and present a semi-analytical method for solving the initial value problem of the FEL in the linear regime.

THEORY

We begin our analysis by presenting a slightly generalized version of an already established analytical result regarding a TGU-based FEL. In particular, using the methods outlined in [4]- [5], one can derive a 3D equation which governs the evolution of the radiation amplitude $E_\nu(\mathbf{x},z)$ throughout the linear regime of the interaction. The result - in its most general form - can be stated as

$$\left(\frac{\partial}{\partial z}+\frac{\nabla_\perp^2}{2ik_r}\right)E_\nu(\mathbf{x},z)+\frac{8i\rho_T^3k_u^3}{2\pi\sigma_x'\sigma_y'}\int_0^z d\zeta\xi e^{-i\Delta\nu k_u\xi}$$
$$\times\exp\left[-2(\sigma_\delta^{ef})^2k_u^2\xi^2\right]\int_{-\infty}^{\infty}dp_xdp_yE_\nu(x_+,y_+,\zeta)$$
$$\times\exp[-2ik_u\xi\left(C_p\frac{x}{\eta}+\left(\bar\alpha\frac{\xi}{2}+\frac{\eta\sigma_\delta^2}{\sigma_T^2}z_x\right)p_x\right)]$$
$$\times\exp\left[-\frac{(x-p_xz_x)^2}{2\sigma_T^2}-\frac{1}{2}\left(\frac{1}{{\sigma_x'}^2}+ik_r\xi\right)p_x^2\right.$$
$$\left.-\frac{1}{2}\left(\frac{1}{{\sigma_y'}^2}+ik_r\xi\right)(p_y^2+k_n^2y^2)\right]\equiv FE_\nu(\mathbf{x},z)=0\,. \quad (1)$$

Here, F is meant as an operator, $\nabla_\perp^2=\partial^2/\partial\mathbf{x}^2$, $\xi=\zeta-z$, $z_x=z-z_0$, $x_+=x+p_x\xi$ and $y_+=y\cos(k_n\xi)+(p_y/k_n)\sin(k_n\xi)$, where z_0 is a constant offset and k_n is the undulator natural focusing strength in the y-direction, $k_r=\omega_r/c=2\pi/\lambda_r$ and $k_u=2\pi/\lambda_u$ - where λ_r is the resonant wavelength, ω_r is the resonant frequency and λ_u is the undulator period - while $\Delta\nu=\nu-1=\omega/\omega_r-1$ is the detuning (ω is a frequency variable). On the other hand, σ_y and σ_y' are the rms values for the vertical size and angular divergence of the electron beam while σ_T and σ_x' are their horizontal counterparts at $z_x=0$. The former of the last two parameters includes the contribution of the - constant - dispersion η and is given by $\sigma_T=(\sigma_x^2+\eta^2\sigma_\delta^2)^{1/2}$, where σ_x is the non-dispersive horizontal beam size (at $z=z_0$) and σ_δ is the rms relative energy spread. It should be emphasized that - unlike the horizontal beam size, which attains a minimum at $z=z_0$ - the vertical beam size is assumed to be constant, so the matching condition $\sigma_y'/\sigma_y=k_n$ holds in the y-direction. Moreover, ρ_T and σ_δ^{ef} are, respectively, the effective Pierce parameter and energy spread of the FEL, quantities that are expressed by $\rho_T=\rho(1+\eta^2\sigma_\delta^2/\sigma_x^2)^{-1/6}$ and $\sigma_\delta^{ef}=\sigma_\delta(1+\eta^2\sigma_\delta^2/\sigma_x^2)^{-1/2}$, where ρ is the Pierce parameter for $\eta=0$. The non-dispersive FEL parameter is in turn given by $\rho=(K_0^2[JJ]^2I_p/(16I_A\gamma_0^3\sigma_x\sigma_yk_u^2))^{1/3}$, where γ_0 is the average electron energy in units of its rest mass m_0c^2, K_0 is the on-axis undulator parameter, $[JJ]=J_0(K_0^2/(4+2K_0^2))-J_1(K_0^2/(4+2K_0^2))$, $I_A\approx17$ kA is the Alfven current and I_p is the peak current of the electron beam. As far as the remaining parameters are concerned, $C_p=\sigma_x^2/\sigma_T^2+\bar\alpha\eta-1$ with $\bar\alpha=K_0^2\alpha/(2+K_0^2)$, α being the transverse gradient of the undulator field. Finally, we should also note that the expression for C_p given above is a generalization of the one contained in [5], which only covered the case with $\bar\alpha=1/\eta$.

ISBN 978-3-95450-133-5

MODE DECOMPOSITION OF A TAPERED FREE ELECTRON LASER

S.D. Chen, K. Fang, X. Huang, C. Pellegrini, J. Wu, SLAC, CA 94025, USA
K. Fang, Indiana University, IN 47405, USA
C. Emma, C. Pellegrini, University of California, Los Angeles, CA 90095, USA
S.D. Chen, C.S. Hwang, NCTU, Hsinchu 30076, Taiwan
C.S. Hwang, NSRRC, Hsinchu 30076, Taiwan
S. Serkez, Deutsches Elektronen-Synchrotron, 22607 Hamburg, Germany

Abstract

For the ultimate use for the scientific experiments, the free electron laser (FEL) will propagate for long distance, much longer than the Rayleigh range, after exiting the undulator. To characterize the FEL for this purpose, we study the electromagnetic field mode components of the FEL photon beam. With the mode decomposition, the transverse coherence can be analyzed all along. The FEL here in this paper is a highly tapered one evolving through the exponential growth and then the post-saturation taper. Modes contents are analyzed for electron bunch with three different types of transverse distribution: flattop, Gaussian, and parabolic. The tapered FEL simulation is performed with Genesis code. The FEL photon beam transverse electric field is decomposed with Gaussian-Laguerre polynomials. The evolutions of spot size, source location, and the portion of the power in the fundamental mode are discussed here. The approach can be applicable to various kind scheme of FEL.

INTRODUCTION

Free electron Laser (FEL) is one of the most powerful tools for frontier scientific research. Many experiments, especially for bioimaging [1, 2], will benefit greatly from the enhanced coherent light peak power at Terawatt (TW) level. To improve the efficiency of an FEL, in recent years, the tapered undulator scheme has gotten renewed attentions [3–5]. More recently, to further improve the taper efficiency, various transverse distributions of the electron bunch are investigated. In this paper, we study this topic by looking into the mode contents of the FEL in the exponential growth regime as well as in the post-saturation tapered regime.

As initiated in Ref. [5], the transverse effect is also an important aspect to be studied for boosting the FEL power into TW level. In this paper, three different types of transverse distributions of the electron beam, the flattop, Gaussian, and parabolic distributions, are analyzed. Different transverse distributions can excite different kinds of high-order modes, which can in principle help trapping the electrons as the FEL interaction develops along the undulator field. Therefore, the FEL power can be further increased. With the mode contents analyzed, the transverse coherence can be studied naturally. The mode decomposition, which is to decompose a field to a set of complete orthonormal modes, is widely used on laser like high directional sources [6].

To compare with the decomposition method, a simple analytical extended "line source" model is developed. The decomposition result and the evolution of the spot size, the source location and the power ratio of fundamental mode to the total power are presented.

LAGUERRE-GAUSSIAN EXPANSION

A complex E-field with the form of $\tilde{E}(x, y)$ can be expanded in a complete orthnormal basis. Here the Laguerre-Gaussian polynomials are chosen as the basis for expansion:

$$E(r) = \sum_{n=0}^{\infty} a_n e^{-\zeta r^2/2} L_n\left(\Re(\zeta) r^2\right), \qquad (1)$$

where we assume that the modes have azimuthal symmetry $r = \sqrt{x^2 + y^2}$ with $\Re(\zeta)$ being the real part of ζ which characterizes the mode size and also the wave-front curvature. With the orthogonality condition, the coefficients a_n can be calculated, and the square of a_n fives the power of each mode.

We get the electric field as a numerical solution from GENESIS [7] simulation. The electric field output is a two-dimensional matrix with complex values, which is in the form of $\tilde{E}(\Delta x m_1, \Delta y m_2)$, where m_1 and m_2 are integers. The a_n should be integrated by discretized form of

$$a_n = \sum_{m_1} \sum_{m_2} \tilde{E}(\Delta x m_1, \Delta y m_2) \exp\left(\frac{-\zeta}{2} r^2\right) * L_n\left(\Re(\zeta) r^2\right) \Re(\zeta) \Delta x \Delta y, \qquad (2)$$

where r^2 should be substituted by $(\Delta x m_1)^2 + (\Delta y m_2)^2$.

We have carefully chosen the grid size and simulation area such that the orthogonality between different Laguerre-Gaussian modes is well preserved. The grid size is small enough to represent the structure in Laguerre-Gaussian modes, while the simulation area is large enough so that the cutoff error is negligible.

Based on the above formalism, an electric field can be decomposed numerically by the mode series of a Laguerre-Gaussian polynomial. However, the set of mode series are not determined until the value ζ is fixed. Although conceptually the basis is complete for an arbitrary complex value of ζ, physics consideration has to be applied to find ζ. The details of our approach is given in next section.

ISBN 978-3-95450-133-5

ISASE STUDY

K. Fang, X. Huang, S.D. Chen, C. Pellegrini, J. Wu, SLAC, CA 94025, USA
K. Fang, Indiana University, IN 47405, USA
C. Emma, C. Pellegrini, University of California, Los Angeles, CA 90095, USA
S.D. Chen NCTU, Hsinchu 30076, Taiwan
S. Reiche Paul Scherrer Institut, 5232 Villigen PSI,Switzerland

Abstract

Improved Self Amplified Spontaneous Emission (iSASE) is a scheme that reduces FEL bandwidth by increasing phase slippage between the electron bunch and radiation field. This is achieved by repeatedly delaying electrons using phase shifters between undulator sections. Genesis 1.3 [1] is modified to facilitate this simulation. With this simulation code, the iSASE bandwidth reduction mechanism is studied in detail. A Temporal correlation function is introduced to describe the similarity between the new grown field from bunching factor and the amplified shifted field. This correlation function indicates the efficiency of iSASE process.

INTRODUCTION

Improved Self Amplified Spontaneous Emission (iSASE) [2, 3]is capable of improving spectrum by increasing cooperation length, and may have the potential to serve as a self-seeding scheme. With several phase shifters installed along the FEL lattice, optical field can be shifted and connection is built up between electrons that separated by several spikes width away. Then with proper interference between new grown field and optical field, bandwidth can be reduced.

Similar idea, known as phase locking of longitudinal spikes in SASE process, is first introduced by A. Gover [4]. Then phase locking FEL amplifier is studied to generate attosecond xray pulse trains by repeatedly delay electron bunch [5]. Similar configuration is then used to improve temporal correlation of SASE FEL [6, 7].

ISASE MECHANISM

SASE mode, radiation field slips one wave length after every undulator period. Slippage field stimulates electrons to radiate in the same phase. Coherent length is built up as electron bunch and radiation field interact through the undulator. One way to improve the temporal coherence is to provide additional slippage to the radiation field. As it's in the SASE mode, slippage field will stimulate electron bunch to generate similar wave package. Therefore it may improves the correlation function and potentially increase coherence length.

Phase shifters are installed after a few gain length. After phase shifters, radiation field is shifted by ϕ, here ϕ is in pondermotive phase. Shifted radiation field stimulates local electron bunch to radiate in similar pattern. Electron bunch, on the other hand, has its own energy and density modulation will also generate radiation field accordingly. iSASE mechanism can be understood by viewing optical field as superposition of new grown field from bunching factor and amplified optical field,

$$E_1(\theta; z) = E_0(\theta; z) + aE_0(\theta + \phi; z). \tag{1}$$

Here θ is the pondermotive phase, z is the location along the undulator, $E_0(\theta; z)$ represents new grown field from electron bunch distribution, and $aE_0(\theta + \phi; z)$ is the amplified shifted radiation field, with a to be complex amplitude describing the amplitude and angle difference between these two field. The phase difference can come from radiation field propagation or electron bunch relative drift.

Then the power spectrum is

$$P(\nu; z) = |\tilde{E}_0(\nu; z)|^2 T(\nu, \phi, a), \tag{2}$$

where $\nu = \omega/\omega_s$ and

$$T(\nu, \phi, a) = 1 + |a|^2 + 2|a|\cos(\nu\phi + \varphi), \tag{3}$$

with φ to be the angle of complex amplitude a. Power spectrum is modulated by $T(\nu, \phi, a)$. Modulation of the original power spectrum $|\tilde{E}_0(\nu)|^2$ has potential to reduce bandwidth. The interference term can be written as $2|a|\cos(\Delta\nu\phi + x + \varphi)$, with $\Delta\nu = \nu - 1$ and x is the fractional phase of ϕ. Modulation function has the period determined by relative shift ϕ in frequency domain. The modulation period in frequency domain is $\frac{2\pi}{\phi}$.

The fractional phase x and complex amplitude phase φ contribute as a detuning factor $(x + \varphi)/\phi$ to the modulation since it shifts the modulation function. In order to maintain FEL power, we can choose $T(\nu, \phi, a)$ peak has to overlap with $|E_0(\nu)|^2$ center where the power is maximal. When the delay ϕ is small, then the modulation function is almost uniform across the FEL spectrum. Therefore the bandwidth is almost unchanged. When the modulation period $\frac{2\pi}{\phi}$ is comparable to the FEL bandwidth, modulation to the FEL spectrum becomes more obvious. Yet if the modulation period is too small, multi harmonics may occur in the spectrum. Choosing $\frac{2\pi}{\phi}$ to be close to the FEL bandwidth, modulated power spectrum may have maximal reduction.

Figure 1,2 shows the power spectrum at two different locations from Genesis simulation. To exclude possible contribution from fractional phase, a unbreaked undulator is used. This guarantees no phase evolution in the radiation field. Slippage is assumed to be multiple number of wavelength. Effect of a phase shifter is like a modulation function to the power spectrum (Eq. 2). At $z = 20m$ (Fig. 1),

ISBN 978-3-95450-133-5

MODE COMPONENT EVOLUTION AND COHERENCE ANALYSIS IN TERAWATT TAPERED FEL

K. Fang, S.D. Chen, X. Huang, C. Pellegrini,J. Wu, SLAC, CA 94025, USA
K. Fang, Indiana University, IN 47405, USA
C. Emma, C. Pellegrini, University of California, Los Angeles, CA 90095, USA
S.D. Chen, C.S. Hwang, NCTU, Hsinchu 30076, Taiwan
S. Serkez, Deutsches Elektronen-Synchrotron, 22607 Hamburg, Germany

Abstract

A fast and robust algorithm is developed to decompose FEL radiation field transverse distribution into a set of orthonormal basis. Laguerre Gaussian and Hermite Gaussian can be used in the analysis. The information of mode components strength and Gaussian beam parameters allows users in downstream better utilize FEL. With this method, physics of mode components evolution from starting stage, to linear regime and post saturation are studied with detail. With these decomposed modes, correlation function can be computed with less complexity. Eigenmodes of the FEL system can be solved using this method.

INTRODUCTION

Free Electron Laser (FEL) is a powerful source that generates high brightness radiation for scientific research. Radiation at TW level may be able to resolve a single molecule image [1,2]. One way to improve brightness is to increase total photon number by tapering the undulator. This scheme has been proposed in [3], Now it is arousing the FEL community's interest [4,5]. Recently the effect different transverse electron distributions on taper efficiency is also studied.

The transverse content for a radiation is an important property of FEL. It may provide useful information in the down stream. Also as it's pointed out in [5], the transverse content plays an important role in tapered FEL. This paper may provide insight into transverse content by decomposing electric field transverse distribution generated from Genesis 1.3 [6] into Hermite Gaussian modes. With this decomposition, correlation function can be computed with less effort. Moreover, this method also provides a tool to study eigenmodes of the FEL system.

MODE DECOMPOSITION METHOD

In this study we decompose electric field into a set of Hermite Gaussian modes. Hermite Gaussian modes is a set of orthonormal basis. Two dimensional Hermite Gaussian modes allows x and y directions to have different distributions. The transverse radiation field along the undulator can be written as

$$E(\mathbf{r};z) = \sum a_{mn}(z) H_m(\frac{\sqrt{2}}{w(z)}x) H_n(\frac{\sqrt{2}}{w(z)}y) \exp(-\zeta r^2). \tag{1}$$

Here $\zeta_r = \frac{1}{w^2}$, $\zeta_i = \frac{k}{2R}$. w is the spot size of fundamental Gaussian mode, while R describes the wave front curvature. In this work, we use orthogonal condition to find amplitude a_{mn} for each Hermite-Gaussian mode. Wavefront curvature need to be eliminated before applying the orthogonal condition. To fit R, a lens with focal length f is applied to electric field. Then beam waist of the modified field is found through propagation. Curvature radius is found when the spot size of modified electric field diverges in both forward and backward propagation. After eliminating wavefront curvature, orthogonal condition is applied to extract mode amplitudes.

$$a_{mn} = \int E(\mathbf{r};z) H_x(\frac{\sqrt{2}}{w}x) H_y(\frac{\sqrt{2}}{w}y) \exp(-\zeta r^2). \tag{2}$$

This integral has to be evaluated in a discrete form with finite cutoff, nevertheless good accuracy can still be achieved when w falls in some range.

To test the orthogonality, we define a matrix elements

$$C_{ij} = \sum_q H_m(\frac{\sqrt{2}x_q}{w}) H_n(\frac{\sqrt{2}y_q}{w}) H_k(\frac{\sqrt{2}x_q}{w}) H_l(\frac{\sqrt{2}y_q}{w}) \exp(-\zeta r_q^2) \frac{2\Delta x \Delta y}{w^2}, \tag{3}$$

where i and j has one to one correspondence with (m,n) and (k,l). Fig. 1 describes how the orthogonality is maintained in this numerical method. In the region where w is small, there is not enough sampling rate to resolve structures in Hermite Gaussian modes. Therefore orthogonality condition is degraded. In large w region, numerical integral is inaccurate because of the cutoff error. Numerical integral could provide accurate expansion for electric field in basis with moderate w. To expand electric field in w where orthogonality condition is not preserved, we could first expand electric field with moderate w. Then expansion in other parameter w' can be computed by transformation method. The amplitudes in w' basis are connected with amplitudes in w basis with

$$a_{mn}(w') = \sum_{k,j} T_{m,k}(w'|w) T_{n,j}(w'|w) a_{kj}(w). \tag{4}$$

Here $T_{m,k}(w'|w) = \int H_m(\frac{\sqrt{2}}{w'}x) H_k(\frac{\sqrt{2}}{w}x) \exp(-\frac{x^2}{w^2} - \frac{x^2}{w'^2}) dx$.

Electric field can be decomposed into Hermite-Gaussian modes along the undulator in a tapered FEL. Yet, there

ISBN 978-3-95450-133-5

FEL CODE COMPARISON FOR THE PRODUCTION OF HARMONICS VIA HARMONIC LASING*

G. Marcus†, W. M. Fawley, SLAC, Menlo Park, CA, USA
E. A. Schneidmiller, M. V. Yurkov, DESY, Hamburg,
Germany S. Reiche, PSI, Villigen, Switzerland

Abstract

Harmonic lasing offers an attractive option to significantly extend the photon energy range of FEL beamlines. Here, the fundamental FEL radiation is suppressed by various combinations of phase shifters, attenuators, and detuned undulators while the radiation at a desired harmonic is allowed to grow linearly. The support of numerical simulations is extensively used in evaluating the performance of this scheme. This paper compares the results of harmonic growth in the harmonic lasing scheme using three FEL codes: FAST, GENESIS, and GINGER.

INTRODUCTION

Numerical simulation has been a critical tool both in the design and the commissioning of short wavelength free-electron lasers based upon the principle of self-amplified spontaneous emission (SASE) such as FLASH and the LCLS. In part due to the complex physics such as the varying exponential growth rates as a function of wavelength, the effective startup noise, and radiation-electron beam slippage effects that help develop longitudinal coherence, accurate numerical modelling for SASE configurations can be more challenging than that required for more simple time-steady FEL amplifiers. Over the past three decades, numerous simulation codes have been developed for FEL modelling purposes, ranging from 1D, time-steady approximations to fully 3D, time-dependent approaches. Some code-to-code benchmarking has been done for high gain FEL's. The study by Biedron *et al.* [1] in the very late 1990's compared results from five different codes for the linear growth rates and saturated power for a time-steady test case based upon parameters corresponding to the Argonne LEUTL FEL. A decade later Giannessi *et al.* [2] compared fundamental and harmonic power vs. z profiles for both single frequency and time-dependent, externally-seeded test cases, finding good agreement between the 1D PERSEO code and the 3D GENESIS and MEDUSA codes. However, apart from a comparison of SASE startup in the GENESIS and GINGER codes with theoretical predictions [3], there appear to be few if any code comparison studies in the literature for full SASE cases.

Here we give the results of a small SASE benchmarking study where we have concentrated upon cases with parameters related to the operating LCLS-1 FEL at SLAC and to the upcoming, soft x-ray LCLS-2 machine. The codes used were FAST, GENESIS, and GINGER, each of which has been used extensively to model SASE-based FELs and each of which has sufficient dimensionality to examine the development of longitudinal and transverse coherence at both the fundamental FEL resonant wavelength and higher odd harmonics. Because of the recent interest in trying to reach higher output photon energies via use of harmonic emission (see, *e.g.*, [4, 5]), we also wanted to look reasonably carefully at the gain and saturation of the third harmonic in "lasing mode", *i.e.*, in situations where the fundamental is suppressed allowing the third harmonic to grow to much higher saturated powers than would be true otherwise. The remainder of this paper is arranged as follows. In §II, we give brief descriptions of each of the three codes concentrating on the features most relevant to SASE and harmonic emission. In §III we present the results of two LCLS-related cases: a) 6-keV fundamental and 18-keV third harmonic emission for a continuous (*i.e.*, non-segmented) LCLS-1 undulator initiated by shot noise b) 1.67-keV fundamental and 5-keV third harmonic emission for a hypothetical, segmented LCLS-II undulator with break sections in which there are special phase shifters tuned to suppress the fundamental via phase shifts of 2/3 and 4/3 wavelengths. We conclude in §IV with a short discussion of our findings.

CODE DESCRIPTIONS

In this section we describe some basic characteristics of the three codes used for this study. They share many common features including a 3D particle mover, an eikonal (*i.e.*, slowly varying envelope approximation) field solver and wiggle-period averaging for calculating the coupling between the radiation and the beam electrons. Each code works in the time domain (*i.e.* spectral decomposition is done only via post-processing) and also subdivides the electron beam into "slices" whose longitudinal centers are spaced uniformly.

FAST

FAST is the generic name for a set of codes developed for analysis of the FEL amplification process in the framework of 1-D and 3-D models using different techniques as described in [6–9]. Analytical techniques implemented in these codes allows analysis of beam radiation modes via an eigenvalue equation and the amplification process during the exponential growth stage (initial-value problem). The simulation codes can simulate the FEL process with both steady-state and time-dependent models and can also treat odd harmonic emission in planar undulator geometries [10]. The three-dimensional version of FAST [11] takes into ac-

* This work was supported at SLAC by the U.S. Department of Energy under Contract No. DE-AC02-76SF00515.
† gmarcus@slac.stanford.edu

ISBN 978-3-95450-133-5

FEL SIMULATION AND PERFORMANCE STUDIES FOR LCLS-II

G. Marcus, Y. Ding, P. Emma, Z. Huang, T. Raubenheimer, L. Wang, J. Wu
SLAC, Menlo Park, CA 94025, USA

Abstract

The design and performance of the LCLS-II free-electron laser beamlines are presented using start-to-end numerical particle simulations. The particular beamline geometries were chosen to cover a large photon energy tuning range with x-ray pulse length and bandwidth flexibility. Results for self-amplified spontaneous emission and self-seeded operational modes are described in detail for both hard and soft x-ray beamlines in the baseline design.

INTRODUCTION

The LCLS-II is envisioned as an advanced x-ray FEL light source that will be fed by both a superconducting accelerator and the existing LCLS copper linac and will be capable of delivering electron beams at a high repetition rate, up to 1 MHz, to a collection of undulators [1–3]. In the initial phase, referred to as the baseline scenario, the CW linac will feed two independently tuned undulators capable of producing radiation covering a large spectral range with each beamline dedicated to either soft or hard x-ray photon energies. The soft x-ray (SXR) beamline will cover photon energies from 0.2 – 1.3 keV while the hard x-ray beamline will cover 1.0 – 5.0 keV. The copper linac will feed the hard x-ray beamline exclusively and will cover photon energies from 1 – 25 keV. Each of the beamlines will be capable of producing radiation in both the self-amplified spontaneous emission (SASE) and self-seeded (SS) operational modes [4, 5]. While various external seeding and other advanced FEL concepts are being explored for LCLS-II [6, 7], this paper reports the results of detailed FEL simulations in the baseline case for multiple start-to-end (S2E) charge distributions coming from the CW superconducting linac at the higher end of the individual undulator beamline tuning ranges. The simulation code `ASTRA` [8] was used to track the electron beams through the injector, `ELEGANT` [9] was used to transport the beams through the linac to the undulators, and `GENESIS` [10] was used for FEL simulations.

ELECTRON BEAM AND UNDULATOR PARAMETERS

The nominal LCLS-II electron beam and undulator design parameters can be found in Table 1. Both the HXR and SXR beamlines will employ a variable gap hybrid permanent magnet undulator broken into individual segments that are interspersed with strong focusing quadrupoles, adjustable phase shifters, and various other diagnostic elements. The vacuum chamber will be made of Aluminum and will have a rectangular cross section with a full height of 5 mm. The relaxation time for Aluminum is $\tau = 8$ fs and can be used to specify not only the DC but also the AC contributions to the resistive wall wakefield (RWW) in the FEL simulations [11].

Table 1: Nominal Electron Beam and Undulator Parameters for the Baseline LCLS-II Scenario

Paramter	Symbol	Value SXR(HXR)	Unit
e-beam energy	E	4.0	GeV
emittance	ϵ	0.45	μm
current	I	1000	A
energy spread	σ_E	500	keV
beta	$\langle\beta\rangle$	12(13)	m
undulator period	λ_u	39(26)	mm
segment length	L_u	3.4	m
break length	L_b	1.0	m
# segments	N_u	21(32)	-
total length	L_{tot}	96(149)	m

The SXR beamline is envisioned to operate with a SASE and SS tuning range of 0.2 – 1.3 keV while the HXR beamline will operate from 1.0 – 5.0 keV in the SASE mode and will use the electron beam from the copper linac for self-seeding from 5.0 – 12.0 keV in the baseline case.

The slice parameters of a S2E 100 pC electron beam are illustrated in Figure 1. The core of the bunch, which is roughly 60 fs long, has a very flat phase space with a current of $I \sim 900$A, slice energy spread of $\sigma_E \sim 450$ keV, and slice emittances of $\epsilon_n \sim 0.27$ μm, all of which satisfy the design requirements. It is also relatively well matched to the lattice where the matching parameter $B_{mag} = 1/2\,(\beta_0\gamma - 2\alpha_0\alpha + \gamma_0\beta) \leq 1.3 - 1.4$ typically does not affect the performance [12, 13].

The slice parameters of a S2E 20 pC electron beam are illustrated in Figure 2. The core of the bunch, which is roughly 30 fs long, has a relatively flat phase space with a current of $I \sim 550$A, slice energy spread of $\sigma_E \sim 280$ keV, and slice emittances of $\epsilon_n \sim 0.1$ μm. The significantly smaller slice emittance and energy spread are extremely beneficial to the performance of the HXR beamline at the high end of the tuning range, as will be illustrated shortly, where the FEL is most sensitive to these parameters. The 20 pC electron beam is also relatively well matched to the lattice with a similar matching parameter in the core of $B_{mag} \leq 1.3 - 1.4$.

The slice energy change over the length of both the HXR and SXR beamlines due to the RWW is illustrated in Figure 3 and Figure 4 for the 100 pC and 20 pC S2E electron beams respectively. It was shown in [14] that the FEL performance could be impacted, due to slowly varying electron beam or undulator parameters, if a slice energy change on the order of $\Delta E \sim 2\rho_{1D}E_0$ occurred before the FEL reached saturation.

ISBN 978-3-95450-133-5

BROADLY TUNABLE FREE-ELECTRON LASER FOR FOUR-WAVE MIXING EXPERIMENTS WITH SOFT X-RAY PULSES

G. Marcus, SLAC, Menlo Park, CA 94025, USA
G. Penn, LBNL, Berkeley, CA 94720, USA
A. A. Zholents, ANL, Argonne, IL 60439, USA

Abstract

This paper examines a FEL design for the production of three soft x-ray pulses from a single electron beam suitable for four-wave mixing experiments. Independent control of the wavelength, timing and angle of incidence of the three ultra-short, ultra-intense pulses with exquisite synchronization is critical. A process of selective amplification where a chirped electron beam and a tapered undulator are used to isolate the gain region to only a short fraction of the electron beam is explored in detail. Numerical particle simulations are used to demonstrate the essential features of this scheme in the context of the LCLS-II design study.

INTRODUCTION

Hard and soft X-ray free-electron lasers (FELs) [1–4] have become essential tools for the investigation of dynamical systems as they have the ability to operate on the time and length scales natural to atomic and electronic motion in matter [5]. Many experiments envisioned for the exploration of the dynamical properties of matter, which leverage the unique capabilities of FEL facilities, will be based on a pump and probe technique. Extending this technique to include a broad variety of four-wave mixing (FWM) spectroscopies, which rely on the use of three fully coherent and independent pulses of light with unique carrier frequencies and wave vectors, is of critical importance.

A pathway for producing FEL pulses suitable for FWM experiments from a single electron beam has recently been proposed [6]. In that study, a process of selective amplification employing a strongly chirped electron beam and a tapered undulator is used to isolate the gain region of a self-amplified spontaneous emission (SASE) FEL allowing for a single longitudinally coherent pulse to amplify to saturation [7–9]. The taper also serves to suppress gain outside the chirped region, leaving the electron beam capable of producing additional radiation in a downstream FEL process. This energy modulation and undulator taper combination can be repeated in multiple stages to produce the three independent FEL pulses necessary for FWM experiments if a broad tuning range is necessary. Alternatively, a grating and mask can be used to split one of these large bandwidth pulses if two nearby frequencies are sufficient. A potential beamline for this scenario is shown in Figure 1.

This paper describes the electron beam energy modulation and undulator taper requirements for the production of longitudinally coherent FEL pulses from the selective amplification process in the context of the LCLS-II design study for photon energies of $E_\gamma = 250-1000$ eV. Numerical

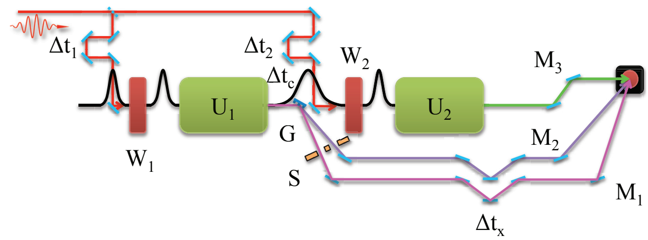

Figure 1: A possible beamline for a FWM FEL [6]: W_1 and W_2 are modulators, U_1 and U_2 are undulators, Δt_1 and Δt_2 are seed laser delay stages, Δt_c is the electron beam chicane delay, Δt_x is the x-ray delay line, G is the grating, S is the slit, and $M_{1,2,3}$ are adjustable x-ray mirrors.

simulations using the FEL code `GENESIS` [10] are used to illustrate the more impressive characteristics of this scheme at $E_\gamma = 1$ keV (see Table 1).

Table 1: Electron Beam, Undulator, and Modulator Laser Parameters for the Nominal LCLS-II Scenario

Paramter	Symbol	Value	Unit
e-beam energy	E	4.0	GeV
emittance	ϵ	0.45	mm-mrad
current	I	1000	A
energy spread	σ_E	500	keV
beta	$\langle\beta\rangle$	12	m
undulator period	λ_u	39	mm
segment length	L_u	3.4	m
break length	L_b	1.0	m
photon energy	E_γ	0.25 – 1	keV
seed wavelength	λ_s	2.1	μm

ELECTRON BEAM ENERGY CHIRP AND UNDULATOR TAPER

In the particular selective amplification scheme employed here, the electron beam is energy modulated by a carrier-envelope-phase-stable, single-cycle, mid-IR laser pulse within a single period modulator. This modulation takes the following idealized form [11]:

$$\gamma = \gamma_0 + \Delta\gamma \sin\left(\frac{2\pi}{\lambda_l}\left[s - s_0\right]\right) e^{-\frac{(s-s_0)^2}{2\sigma_l^2}}. \quad (1)$$

ISBN 978-3-95450-133-5

INVESTIGATION OF REVERSE TAPER TO OPTIMIZE THE DEGREE OF POLARIZATION FOR THE DELTA UNDULATOR AT THE LCLS*

J. MacArthur†, A. Marinelli, A. Lutmann, T. Maxwell, H.-D. Nuhn, D. Ratner, Z. Huang
SLAC, Menlo Park, CA 94025, USA

Abstract

A 3.2 m adjustable phase Delta undulator will soon be installed on the last girder of the LCLS undulator line. The Delta undulator will act as an afterburner terminating the 33 undulator line, providing arbitrary polarization control to users. Two important figures of merit for users will be the degree of polarization and the x-ray yield. In anticipation of this installation, machine development time at the LCLS was devoted to maximizing the final undulator x-ray contrast and yield with a standard canted pole planar undulator acting as a stand in for the Delta undulator. Following the recent suggestion [1] that a reverse taper in the main undulator line could suppress linearly polarized light generated before an afterburner while still producing the requisite microbunching, we report on a reverse taper study at the LCLS wherein a yield contrast of 15 was measured along the afterburner. We also present 1D simulations comparing the reverse taper technique to other schemes.

INTRODUCTION

Circularly polarized soft x-ray radiation is used to probe a variety of material properties, from the electronic structure of magnetic substances [2] to the chirality of biomolecules [3]. Off plane synchrotron radiation [4] and helical undulator radiation [5] have supplied circularly polarized x-rays to synchrotron users for several decades. High quality circularly polarized radiation from FEL facilities is limited to energies at or below the XUV [6], though thin magnetized films have been used to produce circularly polarized soft x-rays at the cost of several orders of magnitude in intensity [7].

A Delta undulator [8] is currently being constructed [9] at the LCLS to address this shortcoming. Unlike canted pole or adjustable gap devices, the Delta is an adjustable phase undulator [10] wherein the longitudinal position of four opposing magnetic arrays is varied to adjust the axial magnetic field strength and helicity. The result is full polarization control – linear, circular, and elliptically polarized light can be produced. The Delta undulator at LCLS will operate in the 300-2000 eV region, extending availability of circularly polarized FEL sources into the soft x-ray. This 3.2 m device will replace the final planar undulator in the 33 undulator-line at LCLS.

The Delta undulator is only 1.5-2 gain LCLS gain lengths long, not nearly long enough reach FEL saturation. Instead, the Delta will act as an afterburner, as seen in Fig. 1. In this configuration, the electron beam is microbunched in a long planar undulator before entering the Delta.

* Work supported by U.S. DOE Office of Basic Energy Sciences under Contract No. DE-AC02-76SF00515.
† jmacart@slac.stanford.edu

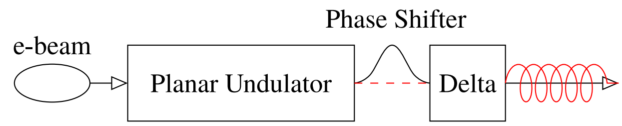

Figure 1: Schematic representation of the Delta undulator in the afterburner configuration. The beam is microbunched in the planar undulator, and a small amount of plane polarized radiation seeds the Delta after an optimum phase shift (red, dashed). The Delta produces circularly polarized x-rays (red, solid).

If the Delta undulator is configured with a helical field, the degree of circular polarization will be dictated by the ratio of the power produced in the Delta and the power produced in the planar undulator. To be more precise, the polarization of light is commonly characterized by the four Stokes parameters. In terms of the complex electric field, these parameters are [11]

$$\begin{aligned} s_0 &= \left\langle E_x E_x^* + E_y E_y^* \right\rangle = I_x + I_y \\ s_1 &= \left\langle E_x E_x^* - E_y E_y^* \right\rangle = I_x - I_y \\ s_2 &= \left\langle E_x E_y^* + E_y E_x^* \right\rangle = I_{45^\circ} - I_{-45^\circ} \\ s_3 &= i\left\langle E_x E_y^* - E_y E_x^* \right\rangle = I_{\mathrm{RCP}} - I_{\mathrm{LCP}}, \end{aligned}$$

where $\langle\rangle$ indicates a time average over the pulse duration. The two figures of merit relevant to circularly polarized light from a helical undulator are the average power $P = \int s_0\, dxdy$, and the degree of circular polarization, s_3/s_0.

Several schemes have been proposed to maximize the average power and $|s_3|/s_0$. A reverse taper can be applied to the planar undulator to suppress background radiation [1], the longer undulator and afterburner may be placed in a crossed-undulator configuration [12, 13], and the resonant frequency of the afterburner may be tuned to the second harmonic of the planar undulator [14]. In this paper we compare the reverse taper scheme to others in a 1D framework and report on an experimental investigation of the reverse taper scheme at LCLS.

1D COMPARISON

The resonant wavelength λ_r in an FEL is given as

$$\lambda_r(z) = \frac{\lambda_u}{2\gamma^2}\left(1 + a_u^2(z)\right), \tag{1}$$

where λ_u is the undulator period and γ is the Lorentz factor. The rms undulator parameter $a_u = e\lambda_u B_{\mathrm{rms}}/2\pi mc$ is given

ISBN 978-3-95450-133-5

OBSERVATION OF SMITH-PURCELL RADIATION AT 32 GHZ FROM A MULTI-CHANNEL GRATING WITH SIDEWALLS

J. T. Donohue, CENBG, CNRS/IN2P3, Université de Bordeaux, France
J. Gardelle, P. Modin, CEA, CESTA, Le Barp, France

Abstract

In a demonstration experiment at 5 GHz, we found copious emission of coherent Smith-Purcell (SP) radiation at the fundamental frequency of the evanescent surface wave, when the grating had sidewalls. Reaching higher frequencies requires a reduction in the size of the grating, which leads to a considerable reduction in power. To partially compensate this, we suggested superposing several copies of the reduced grating in parallel. A test of this concept has been performed with a seven-channel grating, at a frequency near 32 GHz. The SP radiation signals were observed directly with a fast oscilloscope. Power levels were of order 5 kW, in fair agreement with three-dimensional simulations made with the code "MAGIC".

INCREASE FREQUENCY BY REDUCING THE PERIOD AND WIDTH BETWEEN SIDEWALLS

A demonstration experiment in the microwave domain showed that a Smith-Purcell (SP) free electron laser (FEL), with conducting sidewalls placed at the ends of the grating's grooves, emitted intense radiation at the frequency of the surface wave on the grating [1]. In single shot operation, the ratio of emitted power to beam power exceeded 10 %. An earlier experiment, on a grating without sidewalls [2], had demonstrated emission of coherent SP radiation at the second harmonic of the surface wave. That experiment confirmed the scenario proposed in the two-dimensional (2-D) model of Andrews and Brau [3]. But the efficiency was only of order 0.1 %. In the presence of sidewalls the dispersion relation for the grating surface wave is modified [4]. In particular, the intersection of the beam line with the new dispersion relation may occur at an allowed SP frequency, which can't happen in the 2-D theory of Reference [3]. Since the beam bunching at the fundamental frequency is typically must greater than that on harmonics, the emission at the fundamental frequency is much stronger. Thus the use of sidewalls greatly increases the power. Of course, to be of practical interest, it is necessary to reach much higher frequencies, i.e., mm wavelength or less.

The well-known SP relation is [5],

$$\lambda = L(1/\beta - \cos\theta_{SP})/|\mathrm{n}|,$$

where λ denotes the wavelength, L the grating period, n the order of diffraction, θ_{SP} the angle with respect to the beam, and β the relative velocity of the electron. In order to reach shorter wavelengths, it suffices to reduce the grating period. However, the component of the evanescent surface wave in resonance with the beam only extends to a height proportional to the wavelength. In order to reach high frequencies, the beam must closely approach the grating surface. If the grating profile is preserved (groove-depth/period and groove-width/period constant), the 2D dispersion relation of Andrews and Brau in the dimensionless variables is unchanged. The scale reduction doesn't require a reduction in the overall size of the grating, although the task of propagating an intense and wide sheet beam at tiny distances above the grating would certainly be difficult. For the grating with sidewalls, the distance between sidewalls, w, must undergo the same reduction in scale as the period L.. This rapidly leads to long thin gratings when the frequency is increased. Furthermore, our experiment requires an intense (0.5 T) longitudinal magnetic field to control the beam. At the portion of the beam nearest the grating, the image charges produce a moderately strong vertical electric field (a few kV/cm), which, combined with the magnetic field, generates a transverse $\vec{E}\times\vec{B}$ drift. If the number of periods is too great, most of the electrons will drift into the sidewalls. If the radiated intensity is proportional to the total surface of the grating, a grating with sidewalls will suffer a power reduction proportional to the square of the scale factor.

At FEL 2013 two of the authors suggested that it might be possible to superpose laterally N copies of the N-fold reduced gratings [6]. The beam used in the full-scale experiment would continue in use, except that it would be positioned to be flush with the grating top, and of 1 mm thickness. The hope was that the overall power reduction would be only $1/N$, instead of $1/N^2$. In support of this hypothesis, several simulations of multi-channel gratings were performed with the three-dimensional (3D) particle-in-cell code "MAGIC" [7]. These simulations, made with 2, 4, 6, 8 and 10 channels, indicated that the radiation at the bunching frequency (N times the original bunching frequency) occurred at the same SP angle, which was approximately 140°. On the upstream wall of the simulation volume, the azimuthal distribution grew more concentrated around the vertical direction with increasing N. A simple analysis using the theory of antenna arrays was proposed to explain this tendency. It indicated that the width of the azimuthal distribution would decrease as $1/N$, as would the radiated power in the principal lobe

These results depend crucially on the existence of some coherence among the various channels. In the antenna theory this is assumed, but in the simulations, it is seen to be only a fair approximation. Although the simulated fields from each channel merge smoothly into the observed radiation pattern, there is no reason to expect this to occur in practice. It then becomes necessary to

ISBN 978-3-95450-133-5

"FLYING" RF UNDULATOR *

I. V. Bandurkin, S. V. Kuzikov, A. V. Savilov#, A. A. Vikharev,
Institute of Applied Physics, Nizhny Novgorod, Russian Federation

Abstract

A concept for the room-temperature rf undulator, designed to produce coherent X-ray radiation by means of a relatively low-energy electron beam and pulsed mm-wavelength radiation, is proposed. The "flying" undulator is a high-power short rf pulse co-propagating together with a relativistic electron bunch in a helically corrugated waveguide. The electrons wiggle in the rf field of the -1st spatial harmonic with the phase velocity directed in the opposite direction in respect to the bunch velocity, so that particles can irradiate high-frequency Compton's photons. A high group velocity (close to the speed of light) ensures long cooperative motion of the particles and the co-propagating rf pulse.

INTRODUCTION

Typically, the undulator of an X-FEL is a periodic system of DC magnets with a magnetic field ~1 T and a period of several centimeters, where a wiggling relativistic electron bunch produces short wavelength radiation in the self-amplified spontaneous emission (SASE) regime [1-3]. In comparison with this traditional undulator, the so-called rf undulator, where an electron bunch flies toward a counter-propagating rf wave, introduces a strong appeal to use less energetic electron beam in order to produce the same wavelength of Compton's scattered radiation [4-7]. In the case of weak electron wiggling, the wavelength of Compton's photons produced by electrons with the same energy $W = mc^2(\gamma - 1)$, is determined by $\lambda \approx \lambda_{\rm rf}/4\gamma^2$ for the rf undulator (in contrast to $\lambda \approx \lambda_{\rm u}/2\gamma^2$ for the conventional undulator), where $\lambda_{\rm rf}$ and $\lambda_{\rm u}$ are the wavelength of microwaves for the rf undulator and the period of DC magnets for the conventional undulator, respectively. In order to reach the nanometer wavelength scale, one can use an electron bunch with an energy of several hundreds MeV in the rf undulator with a period of about ~1 cm instead of the 1-2 GeV beam in the conventional undulator with a period of several centimeters [8]. The effective undulator period can be as short as the wavelength of the used rf radiation, i.e., $\lambda_{\rm u} = 2\pi/(h+k)$ (here, $k = \omega/c$ is the vacuum wavenumber, and h is the wave propagation constant). That is why millimeter and sub-millimeter radiation is preferable for the rf undulator.

The inevitable cost of these evident advantages is a necessity to provide a high power level of microwaves in order to ensure that an acceptable value of the undulator parameter K is competitive with conventional undulators with $K \sim 1$. In the Ka-band, the necessary power of a wave (for it to be counter-propagating to electrons) in the waveguide with a radius of ~1 cm reaches a GW level. In order to provide such a power level, modern projects of rf undulators employ cavities with high Q-factors powered by existing high-power rf sources like klystrons or gyroklystrons, which are able to provide tens of megawatts. According to such a concept, the whole rf-undulator system should consist of many relatively short (~1 m) and mutually phased sections. As each section should be fed by its own rf source, the X-FEL consisting of tens of sections is very expensive.

Note that high-Q cavities bring a threat of destructive phenomena like rf breakdown and pulsed heating [9,10]. In order to avoid these undesirable phenomena, a short pulse of rf radiation of a high (GW) power level is preferable. In particular, experiments with particle accelerators show that nanosecond rf pulses of the GW level can travel through an electrodynamic structure without a breakdown [11].

There are necessary rf sources of the GW power level. In particular, these sources can be based on moderately-relativistic (hundreds of keV) BWOs [12-14]. Existing sources can deliver more than a 1 GW power in the X-band and about 1 GW in the Ka-band with a repetition rate as high as several kHz. It was proven experimentally that phases of these separate sources can be mutually locked [13]. The mentioned BWOs are able to produce rf radiation in short pulses only (usually shorter than 20 ns). If such a short rf pulse with the duration τ and the group velocity $v_{\rm gr}$ propagates counter to electrons in a waveguide, moving with a velocity close to the light velocity c then the effective undulator length for wiggling (the length of the intersection of electron path and rf pulse) is determined as follows

$$L_{\rm eff}^{\rm count} = \frac{v_{\rm gr}\tau}{1 + v_{\rm gr}/c}. \qquad (1)$$

If τ=10 ns, $v_{\rm gr} \approx c$, then $L_{\rm eff} \approx 1.5\,\rm m$. This is too short for the SASE XFEL, so that a lot of sections and rf sources are required to reach the saturation level.

CONCEPT OF THE FLYING UNDULATOR

We suggest an rf undulator based on co-propagation of an electron bunch and a short high-power rf pulse without a loss in Doppler's up-conversion of the frequency [15]. This "flying" undulator has the following effective undulator length:

*Work supported by the Russian Foundation for Basic Research (Projects 14-08-00803 and 14-02-00691).
#savilov@appl.sci-nnov.ru

HIGH EFFICIENCY LASING WITH A STRONGLY TAPERED UNDULATOR

J. Duris and P. Musumeci
Department of Physics and Astronomy, UCLA, Los Angeles, CA 90095, USA

Abstract

Typical electrical to optical energy conversion efficiencies for FELs are limited by the Pierce parameter to 10^{-3} or smaller. Undulator tapering schemes have enabled extraction of as much as 1 or 2% of the electron energy. Recently, the UCLA BNL helical inverse free electron laser (IFEL) experiment at ATF demonstrated energy doubling and acceleration of 30% of an electron beam from 52 to 93 MeV with a modest 10^{11} W power CO_2 laser pulse. By reversing and retuning the undulator, the electrons may be violently decelerated, thereby transferring energy from the beam to the laser pulse. Simulations show that by sending a 1 kA, 70 MeV electron beam and 100 GW laser into a prebuncher and the reversed undulator, 41% of the electron beam energy should be converted to radiation, allowing the laser pulse power to grow to 127 GW.

INTRODUCTION

Recent results of the UCLA BNL helical IFEL experiment demonstrated the possibility of doubling the energy of an electron beam with a high-power laser. Reversing the process, one could imagine the possibility of extracting half of the e-beam power and converting it into coherent radiation. The essence of this idea is described in another paper in these proceedings as the low gain regime of tapering enhanced stimulated superradiant amplification or TESSA [1]. FELs are typically limited by the Pierce parameter ρ to less than 1 percent electro-optical power conversion and even the best lasers don't exceed efficiencies of about 30% so converting nearly half of the e-beam power to coherent radiation would be significant achievement.

Inverse free electron laser acceleration has seen progress in recent years. The STELLA experiment at ATF demonstrated efficient IFEL acceleration with gradients similar to conventional RF-accelerating cavities and captured up to 80% of electrons with the use of a prebunched beam [2]. The UCLA Neptune IFEL experiment first achieved accelerating gradients surpassing that of conventional rf-accelerators [3]. The LLNL-UCLA IFEL experiment at Lawrence Livermore National Lab used a multi-TW Ti:Sa laser and produced significant peak gradients [4].

The UCLA BNL IFEL collaboration at ATF was conceived to improve the average IFEL accelerating gradient with the use of the first strongly period- and field-tapered helical undulator. Whereas electrons propagating through a linear undulator undergo sinusoidal motion thereby reducing to zero twice per period their transverse velocity, the helical trajectories of the electrons propagating through the undulator provide continuous transverse velocity which in turn enables continuous energy transfer. The experiment accelerated electrons from 52 to 106 MeV with a TW class CO_2 laser, averaging a 100 MeV/m accelerating gradient along the 54 cm undulator, and accelerated up to 30% of electrons from 52 MeV to a stable 93 MeV final energy with <1.8% energy spread [5].

EXPERIMENTAL DESIGN

The IFEL decelerator project builds off of the experience of the helical IFEL experiment by retuning the existing helical undulator to decelerate electrons instead of accelerating them. The experimental setup is depicted in Figure 1. In order to further increase the strength of the stimulated radiation, compression and prebunching are necessary. The peak current of the beam will be increased from 100 A to 1 kA with ATF's compressor. Furthermore, a combination prebuncher and chicane phase delay module is currently being built at UCLA with the goal of increasing the fraction of the beam accelerated to full energy. The electron beam acquires an energy modulation at the resonant wavelength while the chicane module delays the modulated beam in order to phase lock to the ponderomotive wave at the entrance of the helical IFEL undulator. 3D simulations show that 70 to 90% of the injected beam should be accelerated to high energy. With a 30 MeV change in energy, 1 kA current, and 80% capture, an estimated 24 GW e-beam power should be transferred to the radiation field.

Helical Undulator Design

The tapering of the helical undulator was previously changed [5], enabling the first demonstration of IFEL resonant energy tuning. Since the undulator period is predetermined by the dimensions of the magnets in the undulator, the gap between magnets was changed in order to manipulate the field and resonant energy along the undulator. In order to reverse the effect of the accelerator, the undulator may be reversed and the gap tapered in order to reduce the resonant energy during the interaction. The highest stable energy electron beam that may be produced at the ATF is 70 MeV, and the final energy of the decelerated electron beam is 42 MeV. The experimental parameters are summarized in Table 1.

The undulator design follows closely the methods described in [1] but differs slightly since the undulator period is fixed (see Figure 2a). Equations 1 and 2 describe the approximate longitudinal dynamics of a particle undergoing helical IFEL interaction. Here, $K_l = \frac{eE_0\lambda}{m_0c^2 2\pi}$ and $K = \frac{eB\lambda_w}{m_0c2\pi}$ are the laser and undulator normalized vector potentials respectively.

ISBN 978-3-95450-133-5

IFEL DRIVEN MICRO-ELECTRO-MECHANICAL SYSTEM FREE ELECTRON LASER

N. Sudar, P. Musumeci, UCLA Particle Beam Physics Laboratory, Los Angeles, Ca 90024, USA

Abstract

The Free Electron Laser has provided modern science with a tunable source of high frequency, high power, coherent radiation. To date, short wavelength FEL's have required large amounts of space in order to achieve the necessary beam energy to drive the FEL process and to reach saturation of the output radiation power. By utilizing new methods for beam acceleration as well as new undulator technology, we can decrease the space required to build these machines. In this paper, we investigate a scheme by which a tabletop XUV FEL might be realized. Utilizing the Rubicon Inverse Free Electron Laser (IFEL) at BNL together with micro-electro-mechanical system (MEMS) undulator technology being developed at UCLA, we propose a design for a compact XUV FEL.

INTRODUCTION

Current short wavelength Free Electron Lasers (FEL) require long and expensive particle accelerators to produce the necessary high energy electron beams, limiting the housing of these machines to large scale national labs. In order to make this technology more readily available, it is necessary to investigate ways in which we can decrease these space and monetary constraints. In this paper, we investigate a compact design for an FEL that is driven by a beam that has been accelerated through the IFEL acceleration scheme. Furthermore, we investigate the use of micro-electromechanical system (MEMS) undulator technology to decrease both size and resonant wavelength of our FEL.

In an IFEL [1,2] a high power laser is copropagated with the electron beam in an undulator magnet. Through interactions with the undulator field, the beam undergoes transverse oscillations, allowing it to exchange energy with the laser. By tapering the undulator magnets, the beam's transverse oscillations will remain resonant with the laser frequency as it gains energy, maximizing the interaction. Utilizing laser intensities of 10-20 TeraWatts, the IFEL is capable of sustaining GeV/m acceleration gradients over meter scale distances, greatly decreasing the distance required to reach high beam energies [3]. The ability to also preserve an excellent output quality [4] makes the IFEL a great candidate for use in compact FEL design.

RUBICON IFEL

As input of our FEL amplifier we consider a beam accelerated by the Rubicon IFEL at Brookhaven National Laboratory. Rubicon utilizes a strongly tapered undulator driven by a high power 10.3 μm CO_2 laser. Utilizing 625 GigaWatt laser intensities we achieve acceleration gradients up to 100 MeV/m, accelerating the beam from 53 MeV to an energy of 98 MeV in about 50 centimeters [3].

Particles in the beam will bunch around the periodic minima of the IFEL ponderomotive potential as they gain energy propagating in the undulator. This process creates periodically spaced, short bunches of electrons with RMS widths ~1/10 of the laser wavelength while increasing the peak current by about a factor of 5, Fig. 1. Simulations and measurements from the Rubicon IFEL[5] indicate that the IFEL process preserves the initial beam quality, keeping the normalized emittance of the accelerated bunch constant throughout the interaction.

To further enhance the Rubicon IFEL's performance, efforts are currently under way to install a pre-buncher before injection into the IFEL. Utilizing an undulator section tuned to the IFEL drive laser wavelength we impart a modulation on the beam, separating the beam into periodically spaced bunches. Utilizing a chicane to tune the resonant phase of the bunches relative to the IFEL ponderomotive potential, we can inject a large fraction of particles on crest of the accelerating wave, Figure 2. Initial simulations show trapping and acceleration of 74% of the injected particles, greatly increasing the peak current while also decreasing the final energy spread to ~0.1%, providing us with a high quality, high brightness, high energy electron beam, ideal for seeding a high gain FEL amplifier.

MEMS UNDULATOR

The FEL process is achieved by sending a high energy electron beam through a magnetic undulator field with a period λu. The electrons wiggle in this field, and therefore radiate. When the wavelength of the radiation, λr slips ahead of the electron beam one period each cycle of transverse

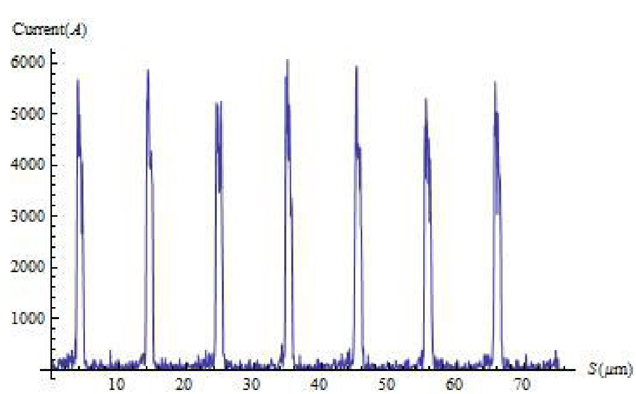

Figure 1: Current profile of Rubicon IFEL output beam.

ISBN 978-3-95450-133-5

TERAHERTZ FEL BASED ON PHOTOINJECTOR BEAM IN RF UNDULATOR

I.V. Bandurkin, S.V. Kuzikov#, M.E. Plotkin, A.V. Savilov, A.A. Vikharev, Institute of Applied Physics, Russian Academy of Sciences, Nizhny Novgorod, Russia

Abstract

Photoinjectors, which can produce picosecond electron bunches of MeV-level, are attractive for THz generation. Fortunately, a long distance to reach scattering power saturation in FEL is not necessary, if bunch length is shorter than the produced THz half-wavelength. However, the energy of several MeVs does not allow providing long traveling of the flying bunch without longitudinal divergence. That is why, we suggest using specific rf undulator in a form of the normal wave in the helical waveguide at 3 GHz frequency. The mentioned wave has the -1st space harmonic with transverse fields and negative phase velocity (responsible for particle wiggling). This wave has also the 0th harmonic with longitudinal field and positive phase velocity equal to bunch velocity. Due to the synchronous 0th harmonic one can effectively channel low-energy bunches (due to longitudinal focusing field) as far as several meters distance. One might also inject electron bunches in slightly accelerating field, in this case the output THz pulse obtain nearly linear frequency modulation. Such long THz pulses with the mentioned modulation of the frequency can be efficiently compressed by pair of diffraction gratings.

CONCEPTS OF THZ FEL BASED ON PHOTOINJECTOR ELECTRON BEAM

In order to produce THz radiation, we suggest to use short bunches of electrons with bunch length less than a half of THz wavelength. Such bunches can be easily produced by means of the existing rf photoinjectors which are driven by high-power picoseconds lasers [1]. Typically rf gun might release bunches of 5-10 MeV and charge up to 1 nC. In order to produce 1 THz radiation, bunch length should not exceed 0.15 mm. This bunch length means that all electrons radiate THz wave in the phased condition (coherently). Unfortunately, the desirable short bunches cannot keep longitudinal size at long distance because Coulomb force causes strong divergence of particles. That is why, one should provide longitudinal focusing of electron bunches at whole length of THz FEL. To solve this problem, we suggest to escort each bunch by slow TM_{01} wave which, being in Cerenkov synchronism with electrons, executes longitudinal focusing in proper phase (at zero longitudinal electric field) like it happens in accelerators (autophasing). Of course, longitudinal focusing inevitably makes whole FEL more complicated and expensive, because it assumes exact injection in proper rf phase. However, in rf photoinjectors particles already are assumed to be synchronized with rf field. In our case we consider THz FEL as a prolonged rf gun. Second, due to focusing one might build long FEL and to produce long THz pulses. In order to multiply power of these long THz pulses, its are appealing to be compressed by means of special pulse compressor consisted of two gratings. Principles of the mentioned pulse compressor were elaborated for high power laser systems [2, 3]. In accordance with these principles, the pulse with the chirped frequency modulation is compressed in a system with frequency dispersion shaped by two gratings operated in non-mirror regime of the reflection [4]. In case of THz FEL the necessary frequency modulation can be provided by using non-equidistant periodicity of undulator's periods. There are two opportunities. The first concept (Fig. 1) can be based on DC-magnet undulator with slow focusing TM_{01} waveguide and pulse compressor.

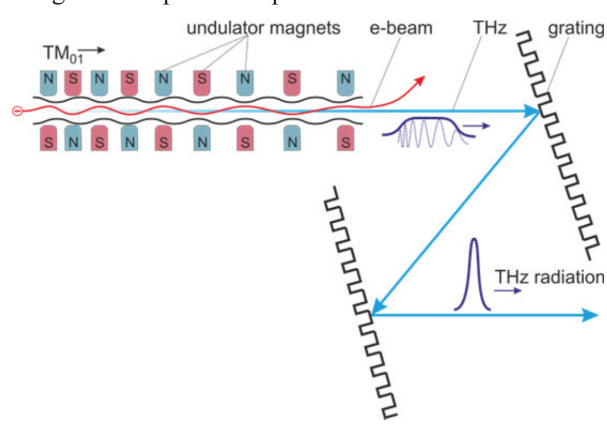

Figure 1: Concept of THz FEL with DC-magnet undulator, focusing TM_{01} waveguide, and built-in pulse compressor.

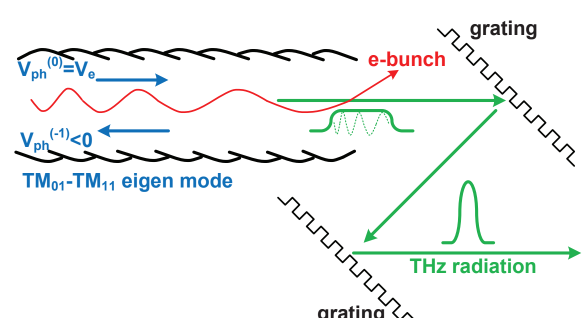

Figure 2: Concept of THz FEL with helical rf undulator and built-in pulse compressor.

In the second scheme (Fig. 2) the helical waveguide supports slow eigen mode consisted of two main space harmonics. The 0-th harmonic is represented by focusing

#kuzikov@appl.sci-nnov.ru

ISBN 978-3-95450-133-5

CHIRPED PULSE SUPERRADIANT FREE-ELECTRON LASER*

Yen-Chieh Huang# and Chia-Hsiang Chen, Institute of Photonics, National Tsinghua University, Hsinchu, Taiwan
Zhen Zhang and Juhao Wu, SLAC, Menlo Park, USA

Abstract

When a short electron bunch traverses an undulator to radiate a wavelength longer than the bunch length, intense superradiance from the electrons can quickly deplete the electron's kinetic energy and lead to generation of an isolated chirped radiation pulse. Here, we develop a theory to describe this chirped pulse radiation in such a superradiant FEL and show the opportunity to generate isolated few-cycle high-power radiation through chirped-pulse compression after the FEL.

INTRODUCTION

High power radiation is useful for applications requiring high energy density. In view of the high-power laser successfully demonstrated by optical chirped pulse amplification, a chirped-pulse FEL followed by a pulse compressor could be an ideal candidate to generate extremely high power radiation in the spectrum no readily accessible by a conventional laser source. It has been suggested previously the use of an energy-chirped electron beam to amplify a frequency-chirped seed laser in an FEL amplifier to obtain temporally compressed high-power radiation at one of the harmonics of the seed laser [1]. It was also suggested the use of an energy-chirped electron pulse to generate self-amplified chirped radiation, which is then filtered to seed a downstream self-amplified-spontaneous-emission (SASE) FEL [2]. Wu *et al.* [3,4] pointed out that manipulating chirps in seed radiation and electron beam to an FEL allows generation of attosecond few-cycle pulses. In this paper we propose a scheme to generate a chirped pulse radiation directly from fast energy depletion of a short electron bunch in an undulator. An external compressor is then used to compress the chirped pulse to achieve few-cycle radiation.

THEORY

From energy conservation, the loss rate of the total electron kinetic energy is equal to the radiation power. To take into account all radiation energy at the expense of the electron kinetic energy, we started from the expression of the coherent synchrotron radiation power of a tightly bunched charge. Given initial electron energy $\gamma = \gamma_0$ at the retarded time $t' = 0$, one can derive the Lorentz factor γ as a function of t' in the relativistic limit $\gamma >> 1$

$$\gamma = \frac{\gamma_0}{1 + t'/\tau_d}, \tag{1}$$

where the pump depletion time τ_d is defined as

$$\tau_d = \frac{W_0}{P_{r,0}}, \tag{2}$$

with W_0 being the initial energy of the electron bunch and $P_{r,0}$ being the initial radiation power of the electrons.

The radiation power is proportional to the square of γ and can thus be expressed as

$$P_{r,N_e}(t') = \frac{P_{r,0}}{(1 + t'/\tau_d)^2}. \tag{3}$$

Furthermore, the wavelength of the dominant radiation mode at t' satisfies

$$\lambda_r = \lambda_u \frac{1 + a_u^2}{2\gamma^2(t')}, \tag{4}$$

where λ_u is the undulator period and $a_u = eB_{\mathrm{rms}}/m_0ck_{\mathrm{u}}$ is the undulator parameter with $k_{\mathrm{u}} = 2\pi/\lambda_u$, m_0 the electron rest mass, e the electron charge, c the vacuum speed of light, and B_{rms} the rms undulator field. Given a known relationship between the retarded time t' and observation time t, the radiation power in (3) and wavelength in (4) can be expressed in terms of the observation time.

By using Eqs. (3,4), one can write the temporal-dependent radiation field as

$$E(t_n) = \frac{E_0}{(3r_\tau t_n + 1)^{2/3}} \exp[j\phi(t_n)] \tag{5}$$

where E_0 is the maximum or the initial radiation field, $r_\tau = \tau_u/\tau_d$ is the ratio of the electron transit time through the undulator τ_u to the electron energy depletion time τ_d, and $\phi(t_{\mathrm{n}})$ is the radiation phase as a function of time. The time variable $t_{\mathrm{n}} = t/(N_{\mathrm{u}}\lambda_{r0}/c)$ is the observation time normalized to the unperturbed slippage time $N_{\mathrm{u}}\lambda_{r0}/c$ with N_u being the number of undulator periods, and λ_{r0} being the initial radiation wavelength. The time duration $t_{\mathrm{n}} = 1$ is the radiation pulse width or the electron slippage length in the undulator without pump depletion. With pump depletion, the electron slows down when traversing the undulator and the time duration $t_{\mathrm{n}} - 1$ gives the amount of thus increased radiation pulse width. Physically r_τ is a figure indicating the degree of pump depletion in a given undulator. The frequency chirp of the radiation is embedded in the radiation phase

$$\phi(t_n) = 2\pi \frac{N_u}{r_\tau}(3r_\tau t_n + 1)^{1/3} + \phi_0 \tag{6}$$

where ϕ_0 is an arbitrary initial phase.

Figure 1 plots the chirped radiation field as a function of the normalized observation time for $r_\tau = 1$ from a 20-peirod undulator. There are two important features in the plot; the field amplitude reduces and the radiation wavelength increases over time, both due to energy loss of electrons to superradiance in the undulator.

*Work supported by MoST of Taiwan under NSC 102-2112-M-007-002 -MY3. #ychuang@ee.nthu.edu.tw

ISBN 978-3-95450-133-5

STORAGE RING XFEL WITH LONGITUDINAL FOCUSING

I. Agapov*, G. Geloni, European XFEL GmbH, Hamburg, Germany

Abstract

In present work we investigate the possibility of running a high gain FEL on a storage ring using a longitudinally focusing insertion to compress bunches passing an undulator. If integrated into a storage ring similar to PETRA III such device could potentially produce continuous ps pulses of photons in the nm range with peak pulse powers of tens of GW. Even without operating in FEL saturation mode the longitudinal focusing can provide means to increase the brightness and shorten the photon pulse length

INTRODUCTION

Low gain FELs with wavelength down to ~ 200 nm (6 eV) have been in operation at storage rings using optical cavities. Short wavelength FELs presently use linacs as drivers since they provide necessary electron beam quality. X-ray FELs such as LCLS, European XFEL or SwissFEL are now in operation or under construction worldwide. They use linacs as drivers to assure beam qualities necessary for a SASE process at those wavelengthes. For a typical wavelength (1 keV-30 keV) the European XFEL requires emittances below 10^6, energy spreads ~ 1 MeV and peak currents ov several kA at electron beam energies up to 17.5 GeV. The saturation length (for basic definitions in the FEL theory see e.g. [1]) roughly defines the minimum practically sensible undulator length. At European XFEL, for the shortest wavelength, achieved with the maximum electron beam energy, the saturation length can be a hundred meters, but for soft X-rays it can be as short as 30 meters depending on the wavelength and electron beam parameters. This makes it in principle possible to fit such an undulator into a storage ring. Beam parameters in latest generation light sources such as PETRA III (see Table 1) are such that for UV photons the beam quality is not far removed from that required for an FEL. For shorter wavelength saturation length becomes larger and the possibility of using the stored beam for SASE FEL directly becomes limited. The interest in shorter wavelength storage-ring based FELs has recently been growing since they could combine extreme peak brightness and coherence of an FEL with continuous operation and lower power consumption of a storage ring (see e.g. [2] and references therein). An insertion device with longitudinal focusing would consist of a compression section, SASE undulator, and a decompression section. The rest of the ring could be passed with the usual bunch length. A design sketch is presented in Fig. 1. It could be used as an insertion or as a bypass subject to space availability. This scheme is in principle similar to a crab cavity type, discussed e.g. in [3], however longitudinal phase space only is manipulated. In the following some simulation studies for the possibility of integrating such an insertion into PETRA III are presented. All calculations are performed with *Ocelot* [4].

Table 1: PETRA III Beam Parameters [5], assuming high bunch charge operation mode with 40 bunches

Parameter	Value
Beam energy	6 GeV
Circumference	2304 m
Emittance $\varepsilon_x, \varepsilon_y$	10^{-9}, 10^{-11}
Energy spread	10^{-3} (6 MeV)
Bunch charge	20 nC
Bunch length	44 ps or 13 mm
Peak current	170 A
Longitudinal damping time	10 msec

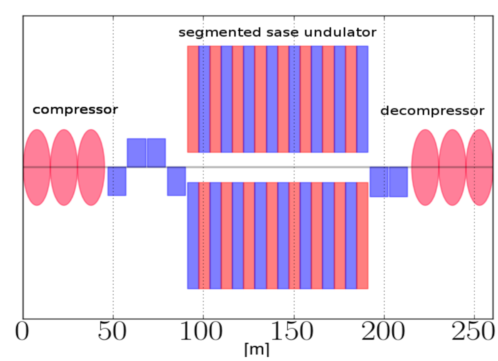

Figure 1: Insertion device layout. Going from left to right, the beam passes an RF module, a dispersive section (chicane or arc), a number of undulators, a disperive section and finally another RF module.

POSSIBILITY OF AN FEL INSERTION DEVICE AT PETRA III

Longitudinal Phase Space Focusing

In a linac-based FEL bunch compression is a key factor, but can allow for certain beam distortion as long as it preserves the lasing bunch core. For a multiturn operation the margin for such distortions is much thinner. Space charge and Coherent Synchrotron Radiation (CSR) [6] effects play much smaller role for longer bunches and higher energies, so cleaner compression and decompression can be in principle expected than for a typical linac FEL. The requirement is that no beam instabilities and distortions should appear on the time scale faster than the longitudinal damping time which is about 1000 turns for PETRA III. Neglecting collective interactions, the longitudinal phase space map for the insertion is

* ilya.agapov@xfel.eu

STATUS OF ELECTRON BEAM SLICING PROJECT AT NSLS-II, BNL*

A. He, F. Willeke, L.H. Yu, BNL, Upton, NY 11973, USA

Abstract

The Electron Beam Slicing (e-beam slicing) at NSLS-II, Brookhaven National Laboratory, supported by the Laboratory Directed Research and Development (LDRD) Program, is focused on the development of the new method to generate ultra-short x-ray pulses using focused short low energy (~20 MeV) electron bunches to create short slices of electrons from the circulating electron bunches in a storage ring. The e-beam slicing activities are staged in 3 main phases. In Phases 0, the theory of e-beam slicing is developed, the low energy linac compressor is simulation designed, the radiation separation between the satellite and core is analyzed by simulation and the properties of the e-beam slicing system are discussed and compared with other ultra-short x-ray sources. In Phase I, the crucial parts of the e-beam slicing scheme will be tested experimentally which include the micro-focusing test of low energy electron beam in space charge dominated regime and the electron beam slicing test using the Accelerate Test Facility (ATF) electron beam as the high energy beam. The kick back system will be simulation designed to increase the repetition rate of e-beam slicing system. At Phase II, the design of e-beam slicing project at NSLS-II will be proposed. Phase 0 has completed successfully, Phase 1 is under way. This paper presents an update on the status of Phase 0.

INTRODUCTION

The community interested in science using sub-pic-second x-ray pulses is growing rapidly. Laser slicing is one of the approaches to generate ultra-short x-ray pulse [1–6]. Typically, for laser slicing the x-ray pulses are of the order of 100 fs with repetition rate of order of 1 kHz and the number of photons per 0.1% bandwidth per pulse is of the order of 1000. To generate ultra-short x-ray pulses with many orders of magnitude higher repetition rate, another method is proposed by Zholents [7, 8] using a crab cavity which provides pulse length of order of a pic-second. It provides a continuous stream of x-ray pulses [9] with a much higher average flux. A new source of ultra-short x-ray pulses is x-ray free electron laser, with the pulse energy many orders of magnitude higher than storage ring and pulse width of 100 fs or less [10]. However, compared with the storage ring sources, the fluctuation of the intensity and wavelength from a SASE FEL is large, and, the repetition rate is low. For example, the repetition rate of LCLS SASE FEL is 120 Hz [11]. Hence, even though the single pulse energy is much lower than the SASE FEL pulse, the high repetition rate and high pulse to pulse stability of storage ring sources continue to attract a wide range of user interests.

The electron beam slicing method [12, 13] is a different approach to generate ultra-short x-ray pulses of the order of 100 fs pulse length. As shown in Fig. 1, when a short electron bunch from a low energy linac (for example, 20 MeV, 200 pC, 150 fs) passes 35 μm above a storage ring bunch (30 ps) at a right angle, it kicks a short slice (~160 fs) of electron bunch vertically. The radiation from the short slice is separated from the core bunch. This method has many advantages, i.e., small space in storage ring for interaction, very short radiation pulse length (~160 fs), high pulse flux, high repetition rate and high stability. We expect the new method may provide a complimentary approach to other ultra-short x-ray pulse sources.

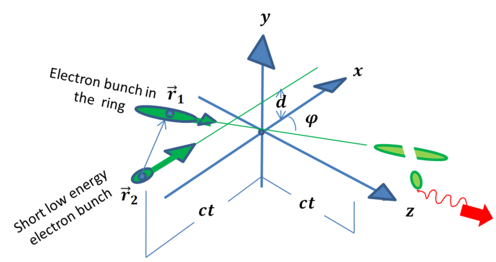

Figure 1: Illustration of electron beam slicing.

THEORY OF E-BEAM SLICING

We explored the new method by calculating the angular kick received by a high energy electron (labeled as bunch 1), generated by a point charge in the low energy linac electron bunch (labeled as bunch 2) and integrated over the 3-D electron distribution of the low energy bunch. The result gives the angular kick as a function of the 3-D position of an electron in the storage ring bunch:

$$\Delta\theta_y = \frac{eq_2 Z_0 c}{2\pi E_1} \frac{\gamma_2(1-\beta_1\beta_2\cos\varphi)}{\sqrt{\gamma_2^2(1-\cos\varphi)^2+\sin^2\varphi}} \frac{1}{\sqrt{2}\sigma_y}, \quad (1)$$
$$\times f_y(\rho, \bar{u}_1, \bar{y}_1)$$

where f_y gives the profile as a function of the high energy electron's position

$$f_y(\rho, \bar{u}_1, \bar{y}_1) =$$
$$\int_0^\infty Re[W(\bar{u}_1 + iy)][e^{-(\rho y - \bar{y}_1)^2} - e^{-(\rho y + \bar{y}_1)^2}]dy \quad (2)$$

* Work supported by DOE under contract LDRD12-023 and LDRD14-022

ISBN 978-3-95450-133-5

DEVELOPMENT OF COMPACT THZ-FEL SYSTEM AT KYOTO UNIVERSITY

Suphakul Sikharin, Yusuke Tsugamura , Heishun Zen, Toshiteru Kii, and Hideaki Ohgaki,
Institute of Advanced Energy Kyoto University, Gokasho, Uji, Kyoto 611-0011, Japan
Qika Jia, University of Science and Technology China, Hefei, 230029, China

Abstract

We are developing a compact accelerator based terahertz (THz) radiation source by free-electron laser (FEL) at the Institute of Advanced Energy, Kyoto University. The system consists of a 1.6-cell S-band BNL-type photocathode RF-gun, a focusing solenoid magnet, a magnetic bunch compressor, focusing quadrupoles and an undulator. The system will generates an ultra-short electron pulse in a few hundred femtoseconds shorter than radiation wavelength, expecting for a super-radiant emission from the undulator. The target radiation wavelength is 100 to 300 µm. A tracking simulation and optimization are performed by using PARMELA and General Particle Tracer (GPT) code. The FEL radiations are analyzed by a 1 dimensional FEL theory. The design parameters, simulation results and status are reported and discussed in this paper.

INTRODUCTION

A new compact terahertz radiation source is under the development at the Institute of Advanced Energy, Kyoto University. The system was designed to be simple, compact and economical aimed using for scientific researches or industrial applications. The system consist of a 1.6-cell S-band BNL-type photocathode RF-gun, a focusing solenoid magnet, a 4-dipole magnetic chicane bunch compressor, quadrupole magnets, a planar halbach undulator and a photocathode drive laser system. Currently, the RF-gun, the undulator and the laser system have been prepared. The magnetic chicane and the quadrupoles are newly designed components. The system is located in the same accelerator room with Kyoto University Free-Electron Lasers (KU-FEL) [1]. The schematic view of the proposed system is shown in Fig. 1.

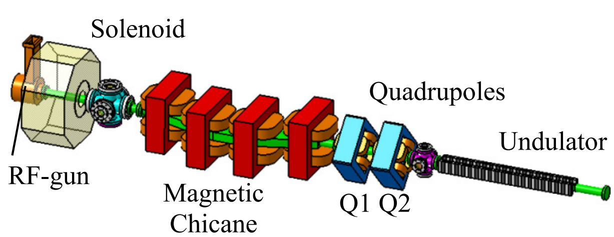

Figure 1: Schematic view of the compact THz-FEL system at Institute of Advanced Energy, Kyoto University.

BEAM DYNAMIC STUDY

The multi-particle beam dynamics was investigated by numerical simulation using PARMELA [2] and GPT [3]. Both codes track particles in the 6-dimensional phase space including the space-charge effect. The simulation of the RF-gun was performed by PARMELA. Then the results are converted to GPT file format and used as the input for the beam dynamics simulations from the RF-gun exit to the end of the undulator by GPT. The parameters of the system was optimized to provide the electron beam with a high peak current, a small beam size and a low energy spread suitable for the FEL radiation generation inside the undulator.

For the simulation of multi-particle beam dynamics, 10,000 macro particles per 2,856 MHz with the total charge of 100 pC are assume to be emitted from photocathode plug illuminated by the lasers.

Photocathode RF-gun

The 1.6-cell S-band BNL-type photocathode RF-gun, which was manufactured by KEK since 2008, is a new adoption component of the laboratory. The RF-gun performances have been studied by numerical simulations in [4]. In this study, this RF-gun numerical model is used.

The photocathode RF-gun is illuminated by a pico-seconds mode-locked Nd:YVO_4 UV laser system [5]. The laser system consists of an acousto-optic modulator, beam position stabilizer, two of double pass amplifiers, SHG and FHG crystals. The cathode plug was made from copper and loaded to the RF-gun by a load-lock system. The quantum efficiency (QE) of the cathode plans to be improved by coating the cathode surface with Cs and Te.

For the simulation, the RF-gun operates at a high accelerating condition with average accelerating voltage of 80 MV/m in order to reduce the space-charge effect. The accelerating field ratio between half-cell and full-cell are assumed to be 1:1. We made several calculations and concluded that the lasers are injected at a low accelerating phase which provides a lower energy spread and a better linearization of an energy chirp. The laser profiles are Gaussian distribution in both transverse and longitudinal with specified cut-off limits. The simulation parameters of the RF-gun are listed in Table.1.

ISBN 978-3-95450-133-5

POTENTIAL PHOTOCHEMICAL APPLICATIONS OF THE FREE ELECTRON LASER IRRADIATION TECHNIQUE IN LIVING ORGANISMS

F. Shishikura[#], K. Hayakawa, Y. Hayakawa, K. Nakao, M. Inagaki, K. Nogami, T. Sakai, T. Tanaka, Laboratory for Electron Beam Research and Application, Nihon University, Chiba, Japan
H. Zen, T. Kii, H. Ohgaki, Institute of Advanced Energy, Kyoto University, Kyoto, Japan
T. Sakae, Nihon University School of Dentistry at Matsudo, Chiba, Japan

Abstract

The free electron lasers (FELs) of the Laboratory for Electron Beam Research and Application (LEBRA), Nihon University and of Kyoto University (KU) were combined to produce tunable FEL wavelengths from the visible to the mid-infrared region (0.4–20.0 μm). We have previously verified that visible light from the LEBRA-FEL can control the germination of lettuce seeds, a well-known photochemical reaction in plants. We found that red light (660 nm FEL) promotes the germination and far-red light (740 nm FEL) inhibits it. In this article, we further examine the photochemical effects on lettuce seed germination of various wavelengths from visible to mid-infrared generated by combining the two FELs. The red spectra of FEL ranging from 600 to 680 nm (activity peak: 660 nm) promoted germination at an activity level of over 40%, whereas the far-red spectra of FEL from 700 to 760 nm (activity peak: 740 nm) inhibited germination at a similar activity level. For the other wavelengths examined, we did not observe the promotion or inhibition of seed germination at an activity level of more than 40%. However, the unique characteristics of the combination of two FELs may prove to be a useful tool because of its high pulse radiation energy, narrow spectral half-bandwidths, and tunable wavelengths from visible to mid-infrared. It may allow the identification of novel photochemical reactions in living organisms.

INTRODUCTION

In 2001, the Laboratory for Electron Beam Research and Application (LEBRA) achieved the first lasing of 0.9–6.5 μm, in the near- and a small part of the mid-infrared regions of free electron lasers (FELs), in which higher harmonics were generated by using nonlinear optical crystals. Now, the FELs cover a wide range of wavelengths from visible to mid-infrared regions from 400 nm to 6.5 μm [1]. In 2012, the Institute of Advanced Energy in Kyoto University (KU), succeeded in producing a FEL (KU-FEL) that covered a large part of the mid-infrared region, and its high-energy and tunable wavelengths have recently been extended from 5 to 20 μm [2]. Following these breakthroughs, we have focused on using both these FELs for investigating photochemical reactions in living organisms. In 2013, we verified that the visible LEBRA-FELs can control the germination of lettuce seeds, a well-known photochemical reaction in plants [3, 4], and showed that red light (660 nm FEL) promotes germination, whereas far-red light (740 nm FEL) inhibits it [5]. We also found that the FEL treatment was still effective when using neutral density filters to reduce radiation energy at 660 nm and 740 nm to as low as about 0.05 μJ/pulse (10 min irradiation) and about 0.63 μJ/pulse (10 min irradiation), respectively [5].

The aim of this study is to determine the photochemical efficiency in lettuce seed germination tests of the tunable wavelengths of FEL from 400 nm to 20 μm, generated by combining the two FEL facilities at LEBRA and KU [1, 2]. The results showed that lettuce seed germination was promoted when the seeds were irradiated by the red FEL spectra from 600 to 680 nm and inhibited by the far-red FEL spectra from 700 to 760 nm. The activity levels that corresponded to the photochemical efficiency were more than 40% for the promotion and inhibition. For the more than 25 other FEL wavelengths examined, ranging from visible to mid-infrared regions, photochemical efficiencies of less than 40% activity was observed for promoting and inhibiting lettuce seed germination.

MATERIALS AND METHODS

Lettuce Seeds and Imbibition

Lettuce seeds (Lactuca sativa L.) from the Red Wave cultivar (a leaf lettuce) were obtained from a commercial supplier (Lot Nos. 546427 and 546430; Sakata Seed Co., Yokohama, Japan) and were used within the recommended period. Prior to irradiation experiments, the seeds were imbibed, as described in our previous report [5].

Setup of FEL Irradiation Systems

The setups of the LEBRA-FEL and KU-FEL irradiation systems are shown in Figure 1 (A-1 and B-1). The sample stages for the FEL irradiation experiments are shown in the magnified views (A-2 and B-2). In the sample stage, 5 or 6 lettuce seeds can be irradiated at once. A set of typical germination results at a wavelength of 690 nm is shown in Figure 2 (A and B).

Radiation Sources

We use the definitions in the Photonics Spectrum Reference Chart (Laurin Publishing, Pittsfield, MA) relating to ranges for the visible (400–750 nm), near-infrared (750 nm to 3 μm), and mid-infrared spectra (3-30

#shishikura@lebra.nihon-u.ac.jp

ISBN 978-3-95450-133-5

NARROW LINEWIDTH, CHIRP-CONTROL AND RADIATION EXTRACTION OPTIMIZATION IN AN ELECTROSTATIC ACCELERATOR FEL OSCILLATOR

H. Marks*, A. Gover, H. Kleinman, J. Wolowolsky, Tel Aviv University, Israel
D. Borodin, M. Einat, M. Kanter, Y. Lasser, Yu. Lurie, Ariel University, Israel

Abstract

In recent years the electrostatic accelerator FEL based in Ariel has undergone many upgrades. By varying the accelerating potential the resonator allows lasing between 95-110 GHz. It is now possible to remotely control the output reflectivity of the resonator and thereby vary both the power built up in the resonator and that emitted. This has allowed fine control over the power for different user experiments. A voltage ramping device has been installed at the resonator/wiggler to correct drops in voltage which occur due to electrons striking the walls of the beam line. This has allowed stable pulses of just over 50 µs with a chirp rate of ~80 kHz/µs.

INTRODUCTION

The Israeli Electrostatic Accelerator FEL (EA-FEL) is one of the few FEL oscillators besides the UCSB FEL [1] that can operate quasi-CW. The Dutch FOM operated along similar principles and at higher power but has since been dismantled [2]. It is most fitting for studying the physics of single mode laser oscillation and developing narrow line-width high power applications in the mm-wave/THz regime, it has in an earlier configuration displayed particularly narrow line-width for an FEL [3].

The EA-FEL is a straight-line Van-de-Graaff ion accelerator. It was converted into an energy-retrieving electron accelerator. The electron beam is injected from a 50 keV electron-gun into the accelerator from ground potential. The beam is accelerated up to the positively charged high-voltage (HV) terminal in the center of the pressurised gas tank. An FEL wiggler/resonator assembly is installed in the HV terminal. After passing through the wiggler in the terminal, the beam is decelerated and transported in a straight line up to the collector. The mm-wave radiation, coupled out of the FEL resonator in the terminal, is guided through an optical transmission line

The laser was upgraded and is now providing longer higher power pulses (up to 50 µs) to a user room. A variable cavity radiation out-coupler was installed as the front mirror of the laser cavity. It is useful for realizing the concept of radiation power extraction maximization of an FEL oscillator [4]. A voltage ramp generator that was installed in the accelerator terminal made it possible to stabilize the voltage of the resonator/wiggler assembly during the laser pulse, and in this way to attain longer laser pulse operation. It also makes it possible to attain narrow laser line-width and controlled frequency chirp that may be used for spectroscopy.

*harry_s_marks@hotmail.com

METHOD

In order to improve the parameters of FEL operation beyond those reported [3] a number of steps were taken. The wiggler was removed from the system and errors in the magnetic field were corrected [5]. Next a new resonator was installed that operates using the Talbot effect to separate the electron beam from the radiation (see Fig. 1). Section 1 is a Talbot (interference) wave splitter composed of a straight rectangular waveguide 10.7X25 mm^2. It allows passage of the electrons whilst fully reflecting the split radiation pattern.

Section 2 is a waveguide with two corrugated walls 10.7X15 mm^2. The third section begins with a section of smooth walled waveguide identical to that in the first section. After 145 mm there is a transition from a rectangular waveguide to a parallel plate waveguide. In one dimension the radiation is guided, in the other free diffraction occurs. The electron beam leaves this section via a hole in an inclined parabolic mirror, whilst the radiation which is split either side of the hole is reflected upwards to a second off-axis mirror. The second off-axis mirror reflects the radiation to an outcoupling element whose reflection and transmission properties can be remotely controlled. The outcoupling element consists of 3 polarisers, the wires of the first and third of which are held vertical, perpendicular to the electric field of the radiation excited in the resonator, whilst the middle polariser is free to rotate.

The accelerator is based on the build-up of positive static charge within the tank, electrons which hit the walls of the beam line cause the accelerating voltage to drop. To correct for this a remotely controlled voltage ramp generator was developed for stabilizing the resonator/wiggler potential during the laser pulse and for controlling laser frequency chirp. The ramp generator is connected between the resonator/wiggler assembly and the high voltage terminal (that are isolated from each other). The ramp voltage generator can produce a voltage ramp of up to 25 kV during the electron beam pulse duration.

Table 1: EA-FEL Parameters

Beam Energy:	1.34-1.44 MeV
Wiggler Period:	44.4 mm
Number of Periods (N_w):	26
Radiation Frequency:	95-110 GHz
Resonator Internal Loss:	30%
Cathode Current:	0.5-3 A

ISBN 978-3-95450-133-5

FACILITY FOR COHERENT THZ AND FIR RADIATION

A. Meseck, Helmholtz-Zentrum, Berlin, Germany
V. Ziemann, Uppsala University, Uppsala, Sweden

Abstract

Linac based THz sources are increasingly becoming the method of choice for a variety of research fields, justifying the increasing demand for high repetition rate THz FEL facilities world wide. In particular, pump and probe experiments with THz and FIR radiation are of major interest for the user community. In this paper, we propose a facility which accommodates an SRF-linac driven cw THz-FEL in combination with an FIR undulator which utilizes the micro-bunched beam. The layout permits almost perfect synchronization between pump and probe pulse as well as nearly independently tunable THz and FIR radiation.

INTRODUCTION

In recent years several accelerator based facilities for THz radiation started to operate. In order to extend the capability of these facilities toward pump-probe experiments a second radiation source synchronized on the femto-second level to the THz source is desirable. The second source could be an external conventional laser system. This option, however, requires complex synchronization of the accelerator based source and the laser. In this report we discuss a way to generate two frequencies from the same electron-beam, such that the synchronization is inherently given.

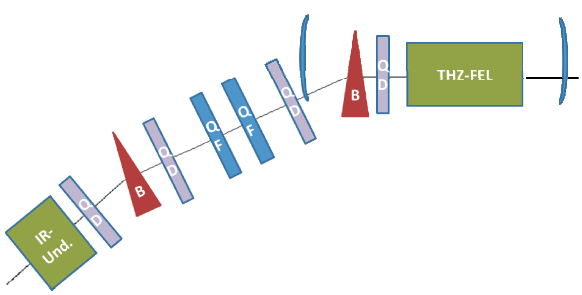

Figure 1: The geometry.

We base our proposal on a 10 MeV electron beam with a typical charge on the order of 300 pC that drives a conventional FEL in oscillator configuration with a frequency of 1 THz. The micro-bunching introduced in the oscillator is converted in a short beam line to a comb-like bunch with a spiked longitudinal distribution capable of generating high harmonics in a second undulator. In the remainder of the report we discuss first the conceptual design, followed by a numerical simulations and concluding remarks.

CONCEPTUAL

Initially we intended to consider an electron beam that had acquired a longitudinal correlation in a buncher cavity, bunch it in an oscillator with a transverse-gradient undulator and then compress it in order to up-convert the micro-bunching to higher frequencies. This proved to be impossible, because the typical momentum spreads generated in THz oscillator destroyed the delicate structures in phase-space. In the process, however, we developed methods to analyze the propagation of distribution functions that proved useful in the analysis of even the simpler setup, we eventually had to settle for.

We started by considering a distribution in longitudinal phase space z_b, δ_b after the initial buncher given by

$$\Psi_b(z_b,\delta_b) = \frac{1}{2\pi\sigma_z\sigma_\delta} \times \exp\left[-\frac{1}{2}\left\{\left(\frac{1}{\sigma_z^2}+\frac{h^2}{\sigma_\delta^2}\right)z_b^2 - 2\frac{h}{\sigma_\delta^2}z_b\delta_b + \frac{\delta_b^2}{\sigma_\delta^2}\right\}\right] \tag{1}$$

where σ_z is the initial bunch length and σ_δ the initial relative momentum spread. The parameter h is the conventional chirp parameter $(dE/dz)/E_0$ of a buncher system, where dE/dz denotes the energy gain per unit length and E_0 the average energy of the beam, 10 MeV in our case.

After modulating the energy in the THz oscillator $\delta_u = \delta_b + a\cos(k_t z_b)$ with amplitude a and wavenumber k_t corresponding to 1 THz we get the distribution function

$$\Psi_u(z_u,\delta_u) = \int d\delta_b \int dz_b \Psi_b(z_b,\delta_b)\, \delta(z_u - z_b)\delta\left(\delta_u - \delta_b - a\cos(k_t z_u)\right) \tag{2}$$

and after ensuring that the Jacobian is unity and doing the integrals we obtain $\Psi_u(z_u,\delta_u)$. We can apply the same method for the propagation through the beam line with a given R_{56} and finally get the distribution function immediately upstream of the second undulator $\Psi_f(z_f,\delta_f)$ as

$$\begin{aligned}\Psi_f(z_f,\delta_f) = &\frac{1}{2\pi\sigma_z\sigma_\delta} \\ &\exp\left[-\frac{1}{2}\left\{\left(\frac{1}{\sigma_z^2}+\frac{h^2}{\sigma_\delta^2}\right)[z_f - R_{56}\delta_f]^2\right.\right. \\ &-2\frac{h}{\sigma_\delta^2}[z_f - R_{56}\delta_f](\delta_f - a\cos(k_t[z_f - R_{56}\delta_f])) \\ &\left.\left.+\frac{(\delta_f - a\cos(k_t[z_f-R_{56}\delta_f]))^2}{\sigma_\delta^2}\right\}\right].\end{aligned} \tag{3}$$

This expression is easily coded in Matlab to produce contour plots of phase space and projections onto the longitudinal axis. The algorithm is extremely rapid. Each run only takes a few second and allows convenient parameter variations.

Playing with the parameters for chirp h, bunching amplitude a and R_{56} of the beam line resulted in the comb-like

CAVITY LENGTH CHANGE VS. MIRROR STEERING IN A RING CONFOCAL RESONATOR*

S. Benson#, Jefferson Lab, Newport News, VA 23606, USA

Abstract

In principle, a ring confocal resonator allows for the use of a short Rayleigh length without the extreme sensitivity to mirror steering typical in a near-concentric resonator [1]. One possible weakness of such a resonator is that the cavity length is no longer independent of the mirror steering. This is one of the strengths of a linear resonator. In this presentation, it is shown that, in a simple 2-dimensional corner cube type ring confocal resonator, the cavity length is, in fact, not dependent on the mirror steering to first order in the mirror angles. Thus the ring-confocal resonator might be a very easy-to-operate and stable resonator for short Rayleigh range operation in FEL oscillators.

INTRODUCTION

It is well known that the optical mode in a confocal resonator has much lower sensitivity to mirror steering than a near-concentric design. Since the mode size in the return path of the confocal resonator is rather large it is more practical to make the confocal resonator for an FEL in a ring configuration so that the mode does not have to pass through a narrow wiggler gap on the return leg. This may lead to a couple of problems. The first is astigmatism, which may be addressed using cylindrical or toroidal optics. The second is a potential coupling of mirror steering to cavity length changes. Decoupling of cavity length and mirror steering, a given in linear resonators, makes laser optimization very straightforward. A dependence of cavity length on mirror steering would greatly complicate operation of the FEL. This note will derive the change in cavity length as each mirror is steered in a ring confocal resonator. As will be seen, the properties of the ring resonator tend to make the cavity length extremely insensitive to mirror steering.

DEFINITION OF VARIABLES

Let us first describe the ring confocal resonator and define our variables. The resonator is shown in Fig. 1. The two flat mirrors that deflect the beam away from the electron beam axis are called the flat deflecting optics or FDOs. The curved mirrors that bring the beam back towards the wiggler are called the fold mirrors or FMs. The angle that the FDOs deflect the beam (twice the angle of incidence on the FMs) will be referred to as θ. The transverse separation between the forward and reverse legs of the resonator will be represented by B. The distance between the FDO and the FM is equal to $B/\sin\theta = C$. The distance from the cavity center (assumed also to be the wiggler center) to the FDO is A. The FMs are concave mirrors that collimate the beam that emerges from the wiggler. The radius of curvature for a ring confocal resonator should be $R_{\rm eff} = 2(A+C)$. The actual radius of curvature will be longer by $\sec(\theta/2)$. It is useful to know the effective radius of curvature as a function of the round trip distance in the resonator. Since the distance in the backleg between the FDO and the FM is $C\cdot\cos(\theta)$, the round trip cavity length $L_{\rm rt}=2(2A+C(1+\cos(\theta)))$. Using this we have $R_{\rm eff} = L_{\rm rt}/2 + C(1-\cos(\theta))$.

NORMAL VIBRATION MODES

To calculate the change in cavity length for a given mirror angle tilt it is useful to define normal modes of the resonator that are linear combinations of all four mirrors. Since the angular shifts are all linear one can represent a change in the angle of any one mirror as a linear combination of these four modes. Since there are four mirrors, it is possible to define four normal modes related to the four angles via a non-singular matrix to be derived below. There is a default beam path that goes through the center of the wiggler, hits the centers of each mirror, and returns a distance B away from the wiggler in the backleg. The default beam path is parallel in the forward and backwards directions in the resonator. Define the following four modes of the beam path with respect to the default beam path. Assume that the mirrors rotate about the point that the default beam path intersects the mirror surface:

- Mode 1 – In this mode the light paths are still parallel in the forward and backward directions but they move either towards the center of the ring or away from the center.
- Mode 2 – In this mode the light path is parallel in the forward and backward directions but the two paths both move in the same direction with respect to the default beam path.
- Mode 3 – In this mode the light path goes through the center of the wiggler and is a distance B away in the backleg at that point. The path goes through the wiggler at an angle and returns with the opposite angle so the mode looks wedged from above.
- Mode 4 – In this mode the light path again goes through the center of the wiggler at an angle but the angle in the backleg is the same as in the forward leg. The mode as a whole is tilted.

*Authored by Jefferson Science Associates, LLC under U.S. DOE Contract No. DE-AC05-84-ER40150, the Office of Naval Research, and the Joint Technology Office. The U.S. Government retains a non-exclusive, paid-up, irrevocable, world-wide license to publish or reproduce this manuscript for U.S. Government purposes
#felman@jlab.org

ISBN 978-3-95450-133-5

NUMERICAL CALCULATION OF DIFFRACTION LOSS FOR CHARACTERISATION OF A PARTIAL WAVEGUIDE FEL RESONATOR*

Q. Fu#, K. Xiong, P. Tan, B. Qin, Y. Q. Xiong
State Key Laboratory of Advanced Electromagnetic Engineering and Technology(AEET)
School of Electrical and Electronic Engineering
Huazhong University of Science and Technology (HUST), Wuhan 430074, China

Abstract

Waveguide is widely used in long wavelength Free-Electron Lasers to reduce diffraction losses. In this paper the amplitude and phase transverse distribution of light emission produced in a partial-waveguide FEL resonator is calculated by Fresnel principle. To acquire high power out-coupled and optimize resonator structure of HUST THz-FEL, the characterisation of reflecting mirror is discussed to reduce diffraction loss.

OPTICAL MODES OF WAVEGUIDE FEL

The geometry of HUST THz-FEL waveguide resonator is shown in Fig. 1. A rectangular waveguide made of good conductor is located at the middle of two reflecting mirrors. The cross section of the waveguide is a×b and the length is L. Two mirrors are at a distance from waveguide entrance, therefore the optical beam propagates in free space during waveguide and mirrors.

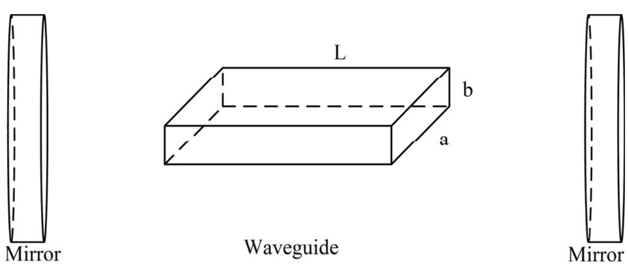

Figure 1: Layout of waveguide resonator.

To simplify this problem, the resistance of the metallic waveguide walls is neglected and the optical modes in the waveguide can be expressed as the solutions of a homogeneous Helmholtz equation [1]:

$$(\nabla^2 + k^2)\varphi(x,y,z) = 0 \tag{1}$$

where k is the wavenumber of radiation.

Since this waveguide is adopted to a planar undulator with vertical periodic magnetic field, the eigenmodes in the waveguide is the pi modes with horizontal polarization, and it can be expressed as a combination of TE and Hermite-Gaussian mode:

$$E(x,y,z) = \cos\left(\frac{ny\pi}{b}\right)\exp\left(\frac{-x^2}{\omega^2(z)} + i\left(\frac{k_n}{2R(z)} - \frac{1}{2}\tan^{-1}\frac{z}{z_R}\right)\right) \tag{2}$$

where $k_n = \sqrt{k^2 - \frac{n^2\pi^2}{b^2}}$, $\omega(z)$, $R(z)$ and z_R are the Gaussian beam x-radius, the x-radius of curvature of wave-fronts and the Rayleigh range. The distance z is measured with respect to the beam waist, in this case, the center of waveguide, then:

$$\omega(z) = \omega_0\sqrt{1 + \frac{z^2}{z_r}}$$
$$R(z) = z\left(1 + \frac{z_r^2}{z^2}\right) \tag{3}$$
$$z_r = \frac{\pi\omega_o^2}{\lambda}$$

The solution describes an optical beam with a Gaussian amplitude distribution in horizontal direction and a cosine amplitude distribution in vertical.

DIFFRACTION LOSS

Optical beam is guided in waveguide so diffraction loss mainly occurs between waveguide and mirrors. In our case, the process starts from a given radiation field distribution out of waveguide, spreading to mirror and back to waveguide in free space. The shape of mirror work as diaphragm and the concave geometry will modulate the phase of optical wavefronts to focus the beam back into waveguide.

Propagation in Free Space

The Fresnel diffraction integral shows the electric field of diffraction pattern is given as a convolutional type function.

*Work supported by the Fundamental Research Funds for the Central Universities : 2014TS146
#qfu@hust.edu.cn

ISBN 978-3-95450-133-5

PRESENT STATUS OF COHERENT ELECTRON COOLING PROOF-OF-PRINCIPLE EXPERIMENT*

I. Pinayev #, F.Z. Altinbas, D.R. Beavis, S. Belomestnykh, I. Ben-Zvi, K.A. Brown, J.C. Brutus, A.L. Curcio, L. DeSanto, A. Elizarov, C.M. Folz, D.M. Gassner, H. Hahn, Y. Hao, C. Ho, Y. Huang, R. Hulsart, M. Ilardo, J. Jamilkowski, Y. Jing, F.X. Karl, D. Kayran, R. Kellermann, N.D. Laloudakis, R. Lambiase, V.N. Litvinenko, G. Mahler, M. Mapes, W. Meng, R. Michnoff, T.A. Miller, M. Minty, P. Orfin, A. Pendzick, F. Randazzo, T. Rao, J. Reich, T. Roser, J. Sandberg, B. Sheehy, J. Skaritka, K. Smith, L. Snydstrup, A. Steszyn, R. Than, C. Theisen, R.J. Todd, J. Tuozzolo, E. Wang, G. Wang, D. Weiss, M. Wilinski, T. Xin, W. Xu, A. Zaltsman, BNL, Upton, New York, USA

M.A. Kholopov, P. Vobly, BINP, Novosibirsk, Russia

G.I. Bell, J.R. Cary, K. Paul, I.V. Pogorelov, B.T. Schwartz, A. Sobol, S.D. Webb, Tech-X, Boulder, Colorado, USA

C. Boulware, T. Grimm, R. Jecks, N. Miller, Niowave Inc., Lansing, Michigan, USA

P. McIntosh, A. Wheelhouse, STFC, Daresbury Lab, Warrington, UK

Abstract

The status of FEL-based Coherent Electron Cooling Proof-of-principle Experiment at BNL is presented. The experimental set-up is comprised of a 2 MeV CW SRF electron gun and 20 MeV CW SRF linac and 8-m long helical FEL amplifier. The status of the accelerator commissioning, and progress in the construction of the helical undulator at Budker INP, is also reported.

PROJECT OVERVIEW

Figure 1 shows the overall layout of our experiment [1, 2]. A CsSb photocathode inside a 2 MeV 112 MHz SRF gun will generate the electron beam when illuminated with a 532 nm laser. Two 500 MHz copper cavities will provide energy chirp for the ballistic compression of the electron beam. The compressed bunches will be accelerated further to 22 MeV by a 704 MHz 5-cell superconducting RF linac.

After passing through a dogleg the electron beam will merge with 40 GeV/u gold ion beam. The ions will "imprint" their distribution on to the electron beam by modulating its density. This modulation will be amplified in a high-gain FEL comprising of three 2.5-m-long helical undulators.

The ions will co-propagate with electron beam through the FEL. Therein, the ion's average velocity is matched to that of the group velocity, e.g., to the propagation speed of the wave-packet of the electron beam's density modulation. A phase shifter, a system of four dipoles forming a chicane structure, follows each undulator. The phase shifters between the undulators will match the phase advance of the optical packet with electron density. The one at the exit of the FEL provides the means to tune the phase of the wave-packet such that the ions with the nominal energy experience zero longitudinal electric field.

The dependence of time-of-flight on the ion's energy will insure that the off-energy ions will be accelerated or decelerated, depending on the sign of their energy error. Such interaction will lessen the energy spread in the ion beam [1]. The used electron beam will be bent away from the ions' path and then dumped.

RF SYSTEM

112 MHz RF Gun

The 112 MHz SRF cavity [3, 4], modified by Niowave, was installed into the RHIC tunnel. Modifications included cavity incorporation into a new cryomodule, addition of the two manual tuners for coarse adjusting of the cavity's resonant frequency. After the installation the cathode launching mechanism manufactured by Transfer Engineering was attached and after several attempts was aligned with cavity (see Fig.2). This mechanism will allow in place exchange of the multialkaline photocathodes planned for usage. The 112 MHz gun was equipped with a water-cooled fundamental power coupler, as shown in Fig. 3. It will be used to fine-tuning of the cavity's frequency. The cathode stalk, situated inside the cavity, is maintained at room temperature by circulating water. Both parts can freeze and piping can be damage if water flow stops. To protect the cavity we developed an emergency blow out system which we expel water with gaseous helium if water block is sensed.

Although its design accelerating voltage is 2 MV, during the test we were limited the maximal voltage to 1 MV by the increasing radiation levels in the semi-open test environment. The SRF gun will be tested at its full accelerating voltage during September 2012. The 112 MHz 2 kW amplifier for the gun is already in place.

After the cavity conditioning and reaching the design voltage we will test photocathode operation in the SRF environment

* Work supported by Stony Brook University and by Brookhaven Science Associates, LLC under Contract No. DE-AC02-98CH10886 with the U.S. Department of Energy.
#pinayev@bnl.gov

HIGH POWER OPERATION OF THE THz FEL AT ISIR, OSAKA UNIVERSITY

K. Kawase#, S. Suemine, R. Kato, A. Irizawa, M. Fujimoto, M. Yaguchi, S. Funakoshi, R. Tsutsumi, K. Miyazaki, K. Furukawa, K. Kubo, A. Tokuchi, G. Isoyama,
ISIR, Osaka University, Osaka, Japan

Abstract

To enhance the power of the THz FEL, we have developed a 27 MHz grid pulser for the thermionic electron gun. It makes the bunch intervals 4 times longer and increases charge of the bunch 4 times higher than the dc-beam injection scheme whereas the beam loading is the same as that in the dc scheme. In this new operation mode, where a single FEL pulse lases in the cavity, we have succeeded in obtaining the micropulse energy exceeding 200 μJ at a wavelength of 67 μm.

INTRODUCTION

The THz FEL has been developed using the L-band electron linac system at the Institute of Scientific and Industrial Research (ISIR), Osaka University. The first lasing was demonstrated at wavelengths from 32 to 40 μm in 1994 [1]. Some years later, the linac system was substantially upgraded for higher stability and reproducibility of its operation. In addition, the pulse duration of the klystron modulator was expanded from 5 to 10 μs for FEL, so that the THz-FEL reached the power saturation first time at a wavelength of 70 μm [2]. The FEL currently operates over the wavelength range from 25 to 150 μm [3].

We pursue research on the upgrade of the FEL to expand the wavelength range and to increase the FEL power. One of the key factors to achieve such objectives is a higher beam current, which is expected to increase FEL gain and the saturation power of the FEL [4]. We are, therefore, developing a new operation mode of the linac system for higher bunch charge.

In the present scheme of the linac operation for the FEL, an electron pulse with a current of 0.6 A and a duration of 8 μs is extracted from the electron gun, and pre-bunched at the rf frequency of 108 MHz using the sub-harmonic buncher system. The electron beam that is a train of bunches at 9.2 ns intervals for the 8 μs duration is accelerated using the 1.3 GHz rf structures consisting of a pre-buncher, a buncher, and a 3 m long acceleration tube of the travelling wave type. The electron beam with the charge of 1 nC/bunch is transported via the FEL beamline to the THz-FEL. In this operation, the rf power measured at the exit of the traveling-wave acceleration tube is reduced to 24% of that without the electron beam. Therefore, the beam loading is too high to further increase the beam current [5].

On the other hand, the optical cavity of the FEL is 5.531 m long, and accordingly, the round-trip time of a light pulse is 36.9 ns, meaning that four FEL pulses independently arise and develop in the cavity. Because a single FEL pulse is sufficient to lase, we can increase the bunch charge four times higher by expanding the bunch interval to 36.9 ns whereas the beam loading in the acceleration tube is kept at the same level. Therefore, we have developed a simple and compact grid pulser system for the electron gun to generate a train of electron pulses with a peak current of 2.4 A and a duration of 5 ns at intervals of 36.9 ns, which corresponds to the repetition frequency of 27 MHz, continuing for 8 μs.

In this paper, we will report recent results of the THz-FEL in high power operation using the electron beam of 4 nC/bunch.

EXPERIMENTAL SETUP

The schematic drawing of the L-band linac and FEL system at ISIR is shown in Figure 1. The electron beam is extracted from the electron gun with the thermionic cathode operating at -100 kV DC and pre-bunched using the three-stage sub-harmonic buncher (SHB) system. The SHB system consists of two 108 MHz 1/4 wavelength resonators and one 216 MHz resonator. The electron beam is bunched and accelerated with 1.3 GHz travelling-wave RF structures, including a pre-buncher, a buncher, and a 3 m long acceleration tube. The accelerated electron beam is tuned using the diagnostic beamline with the analysing magnet and the Faraday cup so that the electron energy is constant over the pulse and the instantaneous energy spread is small. After beam tuning, the electron beam is transported via the FEL beamline to the FEL that consists of a planar type permanent magnet wiggler and an optical cavity. The THz-FEL beam is transported from the accelerator room through the shielding wall to the experimental station in the measurement room.

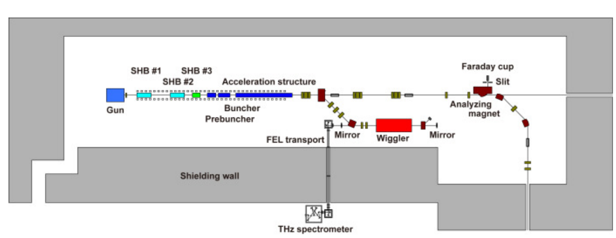

Figure 1: Schematic diagram of the L-band linac and the FEL system at the ISIR, Osaka University.

#kawase@sanken.osaka-u.ac.jp

ISBN 978-3-95450-133-5

HIGH POWER COUPLED FEL OSCILLATORS FOR THE GENERATION OF HIGH REPETITION RATE ULTRASHORT MID-IR PULSES

M. Tecimer, THz-FEL Group, UHM, Honolulu, HI 96822, USA

Abstract

100-200 MeV range ERL driven high gain FEL oscillators generating few cycle short, high intensity mid-IR pulses with tens of MHz repetition rates might become attractive tools in various strong field applications. In a recent study a mode-locked, coupled FEL oscillator scheme has been presented to generate multi-mJ level, ultra-short (<10 cycles) output pulses tunable within the entire IR region. The current work elaborates on an improved FEL oscillator scheme that can cope with the high power levels accumulated within the coupled cavity while operating unidirectionally, eliminating the feedback in the reverse direction. The various operational regimes of the coupled laser system are discussed.

INTRODUCTION

The objective of the study is to draw on the potential of the ERL based FEL devices to produce multi tens of mJ level, ultra-short (≤10 cycles) output pulses tunable within the entire IR region (and beyond) with at least several tens of MHz repetition rates. The latter would be a major step in overcoming the performance limitations of the current ultra-short laser technology in the high-field applications, a domain that is being dominated by conventional NIR/MIR sources. The achieving of the goal relies on taking advantage of the high powers deposited in the beam (average as well as per bunch) by a 100-200 MeV range superconducting ERL system operating at high repetition rates and elaborating on schemes with high extraction efficiency that would enable the generation of few cycle long intense radiation pulses.

In a recent study a high gain FEL oscillator scheme is investigated that encompasses two coupled oscillator cavities [1]. In general terms the system operates as an injection locked laser system whereby the first FEL cavity (master oscillator) provides a strong ultrashort, wide-bandwidth seed signal that is transmitted through the coupler mirror (less than a few percentage coupling ratio) into the amplifier cavity. The latter can be driven in different operational regimes. The most straightforward manner is using the second cavity as a passive pulse stacker cavity. In this mode its finesse is set to optimize the outcoupled pulse energy (unless an intracavity application is considered). On the other hand injecting the spent beam into the second FEL oscillator cavity where it further interacts with the optical pulse that is coupled in and building up within this cavity leads to the injection locked operation. In this operational modus the resultant radiation field circulating in the amplifier cavity can be approximated in the first order by summing up the coupled fields that are coherently accumulating and boosting up the intracavity power in an enhancement cavity (EC) and the field build up resulting from the injection locked FEL interaction. The extent of the latter contribution can be defined by adjusting the undulator and resonator parameters of the two cavities. In the studied cases the amplification effect based on the coherent pulse stacking of an EC turns out to be superior to the growth of the intracavity fields due to the FEL process. Note that unlike the latter, coherent pulse stacking does not suffer from a saturation mechanism that limits the amplification and the associated field build up over many roundtrips. (Reaching the *steady-state* in an EC is a different process than the FEL saturation.) It should also be emphasized here that prior to its injection into the amplifier cavity the beam already starts acquiring a relatively large energy spread since the master FEL oscillator is driven at zero cavity detuning and saturation is attained. Nevertheless, at the presence of the accumulating fields within the amplifier cavity and the broad band interaction with it, the spent beam's energy transfer into the radiation fields exceeds significantly the one due to the fresh injected beam's FEL interaction in the master oscillator, increasing accordingly the final beam energy spread.

In realizing the above mentioned operational regimes a nearly 100% percent coupling efficiency (in coupling the seed) is ensured while a decoupled, virtually reverse feedback free configuration is implemented. Our simulations that allow reverse feedback (bidirectional coupling) indicate a limit value for the coupling ratio back into the master oscillator at around 10^{-8} [2] in order to recover nearly the same performance that results from the fully decoupled case.

On the other hand the high intracavity power levels circulating particularly within the amplifier cavity necessitate designs that can cope with thermal related effects on the mirrors (distortion of the fields, damage at the mirror surfaces) by adopting proper measures in time and space. Whereas the average power can be controlled over the duty cycle (macropulses at lower duty cycle) it is also essential to increase the mode waist on the mirrors. In addition cryocooled laser optics developed for high power applications can be utilized to alleviate the thermally induced adverse effects.

COUPLED FEL OSCILLATORS

The composite resonator shown in Fig.1 is a special case of two coupled lasers in the weak coupling limit [1] (transmission of mirror B << 1.0). In order to incorporate the features that are briefly addressed in the introduction a hybrid cavity design is adopted. While the first cavity supports the Gaussian (fundamental) mode the second (amplifier) cavity is a Bessel-Gauss (BG) type cavity [3-5]. Here we take advantage of two salient features of the

ISBN 978-3-95450-133-5

COMMISSIONING STATUS OF THE ASTA FACILITY AT FERMILAB*

A.H. Lumpkin#, J. Ruan, D. Broemmelsiek, D. Crawford, D. Edstrom, N. Eddy, E. Harms, J. Hocker, J. Leibfritz, J. Santucci, G. Stancari, D. Sun, J. Thangaraj, R. Thurman-Keup, A. Warner, and J. Zhu
Fermi National Accelerator Laboratory, Batavia, IL 60510 USA

Abstract

Early commissioning results and status of the Advanced Superconducting Test Accelerator (ASTA) at Fermilab will be described. The ASTA facility will consist of an L-band rf photocathode (PC) gun, two superconducting L-band rf booster cavities, transport lines, and an 8-cavity TESLA style cryomodule. Early results include first photoelectrons from the Cs_2Te photocathode and operations at 3-5 MeV from the rf PC gun. Measurements of beam size, position, energy, and charge have been obtained with the beam profile station and Faraday cup at that low energy location. Diagnostics for the 20-50 MeV energy beam are also described as well as the first conditioning results for the cryomodule cavities.

INTRODUCTION

The Advanced Superconducting Test Accelerator (ASTA) facility [1] is currently being constructed at Fermilab with initial commissioning steps already in progress. The electron beam has been generated in a photoinjector based on a UV drive laser and the L-band rf photocathode (PC) gun cavity which is shown in Fig. 1. Low energy results at 3-5 MeV sampled after the gun are described. Initial commissioning of beam to the low energy beam dump will be done with one booster cavity. The beam line with one 4-dipole chicane, extensive diagnostics, and spectrometer has been installed in the linac for 20-50 MeV operations in the coming months. Downstream of this location is the 8-cavity cryomodule in which all cavities have been operated individually. Updated cryomodule results will be presented. The feasibility of using the commissioned linac and cryomodule to provide 300-MeV beams to drive EUV FEL oscillator tests at 120 nm was described previously [2].

EXPERIMENTAL ASPECTS

The injector portion of the facility, the first cryomodule, and the proposed FEL oscillator configuration are shown in Fig. 2. After the L-band rf pC gun, two L-band superconducting booster cavities will provide up to 50 MeV acceleration capability. At this time, the first cavity has been temporarily replaced by a spool piece, and the second cavity has been installed and conditioned to 20 MV/m. Only results from the diagnostics after the rf gun and cryomodule conditioning will be presented.

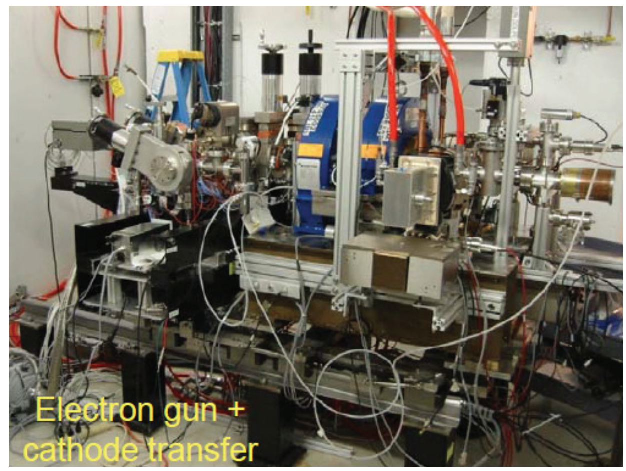

Figure 1: The L-band photoinjector with photocathode transfer hardware, and with two solenoid magnets.

The Drive Laser

The drive laser is based on an Yb fiber laser oscillator running at 1.3 GHz that is then divided down to 81.25 MHz and amplified. The four-stage origination and amplification is a set of commercial components from Calmar collectively referred to as the seed laser in the context of ASTA. The 81.25 MHz packets of IR laser, at a wavelength of 1053 nm is directed into a multi-pass amplifier (MPA), which provides amplified pulses at a 3 MHz rate that are then pulse cleaned with two sets of Pockels cells. The MPA has recently been replaced by a preamp composed of three single pass stages. A third Pockels cell, referred to as the pulse picker is not currently being used. Three YLF-based single-pass amplifiers (SPA) and a Northrup-Grumman SPA (NGA) boost the energy to several μJ per pulse before the two doubling crystal stages that generate the green and then the UV components at 3 MHz [3]. The UV is transported out of the laser lab through the UV transport line to the photocathode of the gun for generation of the photoelectron beams for the SC rf accelerator [1].

Base Electron Beam Diagnostics

The base beam profile imaging stations have been equipped with both YAG:Ce scintillators and optical transition radiation (OTR) screens, optical transport, and digital CCD cameras. The Gig-E vision protocol has been supported by selection of the Prosilica 5 Mpix cameras for

*Work supported under Contract No. DE-AC02-07CH11359 with the United States Department of Energy.
#lumpkin@fnal.gov

ISBN 978-3-95450-133-5

CHARACTERISTICS OF TRANSPORTED TERAHERTZ-WAVE COHERENT SYNCHROTRON RADIATION AT LEBRA

N. Sei, H. Ogawa, Research Institute of Instrumentation Frontier, National Institute of Advanced Industrial Science and Technology (AIST), 1-1-1 Umezono, Tsukuba, Ibaraki 305-8568, Japan
K. Hayakawa, T. Tanaka, Y. Hayakawa, K. Nakao, T. Sakai, K. Nogami, M. Inagaki, Laboratory for Electron Beam Research and Application (LEBRA), Nihon University, 7-24-1 Narashinodai, Funabashi, 274-8501, Japan

Abstract

Nihon University and National Institute of Advanced Industrial Science and Technology have jointly developed terahertz-wave coherent synchrotron radiation (CSR) at Laboratory for Electron Beam Research and Application (LEBRA) in Nihon University since 2011. We have already observed intense terahertz-wave radiation from a bending magnet located above an undulator dedicated for an infrared free-electron laser (FEL), and confirmed it to be CSR. We have transported the CSR to an experimental room, which is next to the accelerator room across a shield wall, using an infrared FEL beamline. The power of the transported CSR was 50 nJ per macropulse, and it was available at frequencies of 0.1–0.3 THz. The transported CSR beam can be applied to two-dimensional imaging and spectroscopy experiments. From two-dimensional imaging performed with the THz-wave CSR, metallic structures concealed by plastic in a smart card were nondestructively detected at a spatial resolution of 1.4 mm.

INTRODUCTION

In order to obtain an FEL with high gain, the electron beam in FEL facilities has a short bunch length and a high charge. The electron beam in the FEL facilities can also generate intense terahertz waves by coherent radiation. Since 2011, then, Nihon University and National Institute of Advanced Industrial Science and Technology have jointly developed intense THz-wave CSR at Laboratory for Electron Beam Research and Application (LEBRA) in Nihon University. We have already observed intense coherent synchrotron radiation (CSR) in the THz-wave region using an S-band linac at LEBRA [1]. Because the CSR does not influence a process of infrared FEL oscillations, it is possible to use the THz-wave CSR and infrared FELs simultaneously. If a complex light source composed from the CSR and FEL are developed, we can conduct highly reliable material identifications.

Then, we transported the CSR to the experimental room, which was next to the accelerator room across a shield wall, using an infrared FEL beamline. We could obtain a CSR beam whose intensity was approximately 50 nJ per macropulse. The CSR beam could be used for spectroscopy experiments at frequencies of 0.1-0.3 THz [2]. In this article, characteristics of the CSR transported to the experimental room are reported in detail.

THZ WAVE SOURCE BY CSR

The S-band linac at LEBRA consists of a 100 keV DC electron gun, prebuncher, buncher, and three 4 m long traveling wave accelerator tubes [3]. The electron beam accelerated by the linac is guided to an FEL undulator line by two 45° bending magnets. The electron-beam energy can be adjusted from 30 to 125 MeV, and the charge in a micropulse is up to 30 pC in full-bunch mode, where the electron beam is bunched in 350-ps intervals. The electron-beam energy was set to 100 MeV in the CSR observations. The macropulse duration determined by the flat-top pulse width of the 20 MW klystron output power is approximately 20 μs. The bunch length is compressed from 3 to less than 1 ps by a magnetic compressor using two 45° bending magnets that guide the electron beam to an FEL undulator line [4]. However, there is no optical beam window to extract the CSR in the FEL undulator line. Thus, we developed the CSR emitted at the entrance of the second 45° bending magnet, where the calculated bunch length was approximately 2 ps in full-bunch mode. Although the CSR is emitted along the electron-beam orbit in a bending magnet chamber (internal height, 24 mm), its solid angle which was incident on an entrance of a transfer pipe (diameter, 20 mm; length, 265 mm) was 0.065 radians.

We observed intense sub-THz-wave radiation emitted from the second 45° bending magnet by using a Schottky D-band diode detector (Millitech Inc., DXP-06) [1]. The measured power of the intense sub-THz-wave radiation was proportional to the second power of the electron-bunch charge in full-bunch mode. The vertically polarized component of the intense sub-THz-wave radiation had roughly the same vertical distribution as the synchrotron radiation. Thus, the radiation was identified as CSR. The measured CSR power per macropulse was approximately 0.4 μJ in the D-band region.

ISBN 978-3-95450-133-5

A SWEDISH COMPACT LINAC-BASED THz/X-RAY SOURCE AT FREIA

V.A. Goryashko*, Uppsala University, Uppsala, Sweden
A. Opanasenko, NSC/KIPT, Kharkiv, Ukraine
V. Zhaunerchyk, University of Gothenburg, Gothenburg, Sweden

Abstract

THz radiation enables probing and controlling low-energy excitations in matter such as molecular rotations, DNA dynamics, spin waves and Cooper pairs. In view of growing interest to the THz radiation, the Swedish FEL Center and FREIA Laboratory are working on the conceptual design of a compact multicolor photon source for multidisciplinary research. We present the preliminary design of such a source driven by high-brightness electron bunches produced by a superconducting linear accelerator. A THz source is envisioned as an FEL oscillator since this enables not only generation of THz pulses with a bandwidth down to 0.01% (with inter-pulse locking technique) but also generation of short pulses with several cycles in duration by detuning the resonator. For pump-probe experiments, the THz source will be complemented with an X-ray source. One of the most promising options is the inverse Compton scattering of quantum laser pulses from electron bunches. Such an X-ray source will operate from 1 to 4 keV with output intensity comparable to a second generation synchrotron. The envisioned THz/X-ray source is compact with a cost comparable to the cost of one beamline at a synchrotron.

INTRODUCTION

The energy of photons from the THz spectrum range corresponds to the energy of many types of excitations in matter such as low-frequency vibrations in large molecules, molecular rotations, lattice vibrations, spin waves, internal excitations of bound electron-hole pairs. A recent workshop *"The Science and Technology of Accelerator-Based THz Light Sources," Uppsala, November 18-19, 2013* clearly demonstrated a tremendous increase in applications of THz radiation in physics, material science and biomedicine. The analysis of literature and the presentations given at the workshop show that apart from a well-established time-domain THz spectroscopy [1], THz radiation allows coherent control of quantum transport in semiconductor superlattices [2], spin waves in antiferromagnets [3], quantum bits in semiconductors [4], high-Tc superconductivity [5]. The control was demonstrated experimentally.

THz radiation also finds a lot of applications in biophysics. In particular, it was reported that irradiation of mammalian stem cells with a THz field results in heterogenic changes in gene expression [6]. The proposed resonant mechanism of interaction of THz fields with stem cells predicts a creation of new open states in the double helix of DNA [7]. One more exciting application of THz radiation is connected to the study of chiral molecules, which are widely found in biology, for example, amino acids. Chirality plays an important role in medicine since drugs containing different enantiomers have different biological activity [8] because receptors, enzymes, antibodies and other elements of the human organism also exhibit chirality. Fingerprints of biological molecules belong to the THz region and it is foreseen that circularly polarized THz radiation can be used for studying chirality of bio-molecules.

In view of growing interest to the THz radiation, the Swedish FEL Center together with the FREIA Laboratory is studying the national user interest in THz physics and working on the conceptual design of a versatile photon source. The ultimate goal is to build a versatile THz/X-ray source for a multidisciplinary national user facility at the FREIA laboratory of Uppsala University. The photon source will be driven by high-brightness electron bunches produced by a superconducting linear accelerator (SC linac). In particular, we aim to combine an envisioned THz FEL with a soft X-ray source and such a combination will provide an opportunity for the time-resolved pump(THz)−probe(X-ray) measurements. Implementation of superconducting technology would greatly enhance flexibility of the envisioned multi-color photon source. Specifically, a photon source based on a SC linac enables the best flexibility in terms of bandwidth and wavelength tunability as well as scalability both in repetition rate and pulse energy [9]. Superconducting linacs enable operation in continuous wave (CW) or quasi-CW mode, which implies higher average brightness of the source. With a high duty factor operation, a SC linac also reduces the overall size of the facility and is economically more efficient than its normal conducting counterpart.

THE COMBINED THZ/X-RAY SOURCE

The conceptual layout of the combined THz/X-ray source is schematically shown in Fig. 1. A SC linac is followed by an X-ray source and a THz FEL oscillator.

One of the main challenges of the project is an electron source since high-brightness low-emittance electron bunches are needed for an efficient inverse Compton scattering process. Currently, only a SC photocathode RF gun can deliver bunches with the required parameters. However, this gun is complicated for fabrication and operation as well as expensive for a university facility. The search for an alternative lead us to a gun design, which is similar to the design proposed at Argonne [10]. The proposed gun utilizes a normal conducting (NC) 176 MHz re-entrant resonant cavity with an acceleration gradient of 20 MV/m. Note that an RF gun cavity of such geometry has been developed at the Lawrence Berkeley National Laboratory (USA) [11, 12] for the NGLS project. This cavity has a high thermal handling capabil-

* vitaliy.goryashko@physics.uu.se; vitgor06@gmail.com

ISBN 978-3-95450-133-5

TOWARDS AN X-RAY FEL AT THE MAX IV LABORATORY

Francesca Curbis, Sverker Werin*, MAX IV Laboratory & MAX Nfak, Lund University, Lund, Sweden
Mikael Eriksson, Christoph Quitmann, Sara Thorin, MAX IV Laboratory, Lund, Sweden
Per Johnsson, Department of Physics, Lund University, Sweden

Abstract

The design of the 3 GeV linac for the MAX IV facility was done to provide the ability to host a future FEL in the hard X-ray as well as in the soft X-ray range. The linear accelerator, with its two bunch compressors, is now under commissioning. Through the years increasing details for the actual FEL have been discussed and presented. In parallel a steering group for the science case for a Swedish FEL has worked and engaged a large number of Swedish user groups. These two paths are now converging into a joint project to develop the concept of an FEL at MAX IV.

We will report on the paths to FEL performance based on the 3 GeV injector, FEL design considerations, the scientific preparation of the project, the linac commissioning and the strategy and priorities.

INTRODUCTION

The MAX IV Laboratory is in a strong phase of development with the completely new MAX IV facility which includes two ultra low emittance storage rings (3 and 1.5 GeV) [1] (Fig. 1). These rings are to be injected from a full energy (3 GeV) linac. The linac will from the start also drive the Short Pulse Facility (SPF) with the FemtoMAX beamline [2] for experiments using short (<100 fs) incoherent X-ray pulses. Currently the linac system is completely installed and under commissioning while the storage ring building is being finalized and magnet delivery has commenced.

From the very start of the MAX IV design around year 2000, it was envisaged that the future development would most likely be in the field of Free Electron Lasers. Thus the facility is prepared to be expanded into an X-ray FEL.

In the strategy of the MAX IV laboratory for the period 2013-2026 the two main goals after completing the MAX IV storage rings are a) the build-up of all 25 experimental stations at the storage rings and b) a FEL. Thus the work has been initialized both on the scientific applications of a FEL and the design of such a source. The first assumed opportunity to apply for funding is after the inauguration of the MAX IV facility (June 21st, 2016).

A FEL AT THE MAX IV LABORATORY

The design of a FEL at the MAX IV Laboratory has so far been driven by accelerator considerations. To realize the project the input from the scientific community in Sweden is being collected, leading to a science case for a FEL in Sweden (see below).

* corresponding author: sverker.werin@maxlab.lu.se

Figure 1: The MAX IV Facility in June 2014 with the Area for FEL Expansion to the Left. (photo P. Nordeng)

The 3 GeV linac at the MAX IV will be the base for a FEL project. It is in its base line design equipped with a photo cathode RF-gun [3], emittance compensating injection and two bunch compressors [4]. The performance is more or less on the level of a soft FEL driver, while expansion towards a hard X-ray FEL is well prepared. We foresee an expansion of the linac by approximately 3 GeV, total 6 GeV, following the second bunch compressor to reach a photon energy of about 9 keV (1.3 Å). The relatively low final electron energy indicates a FEL design with a low normalized emittance which is basically achieved by low charge, < 100 pC, operation.

General Layout

The general layout of the proposed facility is found in Fig. 2, where the necessary expansion is marked by the yellow field. Two FELs share the photon energy range 1.2-9 keV (1.3-10Å) and 0.25-1.2 keV (10-50 Å) respectively. Table 1 summarizes the “Start-of-design” parameters for the FEL which represent a picture of the possible machine performance and a first match to the user requirements. We believe that the final design will come close to these performances but a full design analysis is not done yet, and we expect additional user input.

ISBN 978-3-95450-133-5

CONFIGURATION AND STATUS OF THE ISRAELI THz FREE ELECTRON LASER*

A. Friedman, N. Balal, V. Bratman, E. Dyunin, Y. Lurie, E. Magory, Ariel University, Ariel, Israel
A. Gover, Tel Aviv University, Tel Aviv, Israel

Abstract

A THz FEL is being built in Ariel University. This project is a collaboration between Ariel University, and Tel Aviv University. Upon completion it is intended to become a user facility. The FEL is based on a compact photo cathode gun (60 cm) that will generate an electron beam at energies of 4.5 - 6.5 MeV. The pulses are planned to be of 300 pico Coulomb for a single pulse, and of up to 1.5 nano Coulomb for a train of pulses. The FEL is designed to emit radiation between 1 and 4 THz. It is planned to operate in the super radiance regime. The configuration of the entire system will be presented, as well as theoretical and numerical results for the anticipated output of the FEL, which is in excess of 150 KW instantaneous power. The bunching of the electron bean will be achieved by mixing two laser beams on the photo-cathode. The compression of the beam will be achieved be introducing an energy chirp to the beam and passing it through a helical chicane.

We plan on compressing the single pulse to less than 150 femto seconds. The status of the project at the time of the conference will be presented.

INTRODUCTION

At present there is an operating FEL in Ariel University, operated in collaboration with Tel Aviv University. We are in the process of building a new Tera Hertz Super Radiance FEL[1,2]. Figure 1 depicts the general layout of the system.

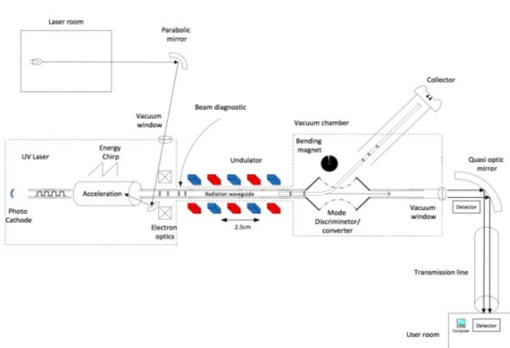

Figure 1: General layout of the Tera Hertz FEL.

The main components of the system are:

1. RF Structure.
2. Photo Cathode.
3. Laser for photo cathode.
4. Helical Chicane.
5. Wiggler.
6. Tera Hertz transmission line.

RF STRUCTURE

The RF structure is an integration of two sections: a standing wave section in which the electrons gain most of their energy, and a traveling wave section in which the energy is set to an energy chirp that would cause the pulse to shrink in time[3,4]. Figure 2 shows a simulation of the field inside the structure; the strong field is in the standing wave section, while the weaker field is in the traveling wave section.

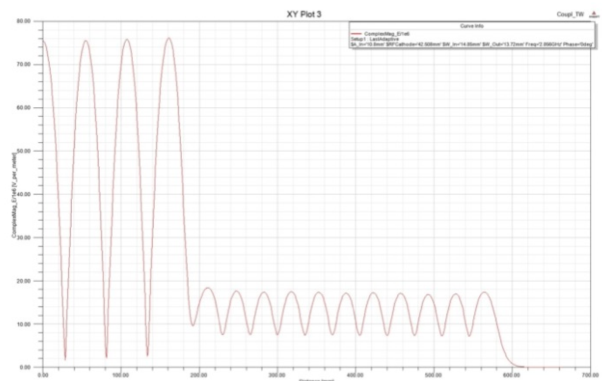

Figure 2: The electric field inside the RF structure

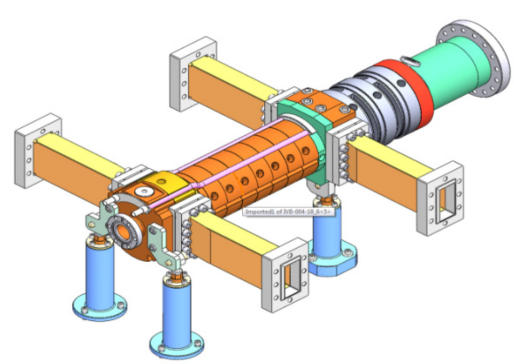

Figure 3: The mechanical design of the RF structure.

Figure 3 shows the 3D mechanical design of the RF structure including the photo cathode to the right of the picture and the input on output ports for the 3 GHz driving field.

LASER

The laser for the THz FEL is a Coherent Laser capable of producing 100 pulses per second with a width of 35 femto seconds. The energy per pulse is about 6 mJ. Currently, the laser has been ordered.

ISBN 978-3-95450-133-5

COHERENT HARMONIC GENERATION AT THE DELTA STORAGE RING: TOWARDS USER OPERATION*

A. Meyer auf der Heide†, S. Hilbrich, M. Höner, H. Huck, M. Huck,
S. Khan, C. Mai, R. Molo, H. Rast, A. Schick, P. Ungelenk,
Center for Synchrotron Radiation (DELTA), TU Dortmund University, Dortmund, Germany

Abstract

At DELTA, a 1.5-GeV synchrotron light source at the TU Dortmund University, a short-pulse facility based on Coherent Harmonic Generation (CHG) is in operation and shall soon be used for pump-probe experiments. Due to the interaction of ultrashort laser pulses with electron bunches in an undulator, CHG provides short and coherent pulses at harmonics of the laser wavelength. In this paper, recent progress towards user operation, pulse characterization studies such as transverse and longitudinal coherence measurements as well as CHG in the presence of an RF phase modulation are presented.

INTRODUCTION

High-gain free-electron lasers (FELs) are almost ideal radiation sources to study the structure and function of matter, combining short wavelength with femtosecond pulse duration and extremely high peak brilliance. However, to date only four of these machines are in user operation (FLASH, LCLS, SACLA, and FERMI), and being based on linear accelerators, their pulse repetition rate is low and they serve only one experiment at a time. In contrast to that, the pulse duration at synchrotron light sources based on storage rings is 30 to 100 ps, given by the bunch length, but there are about 50 of these facilities in operation [1], each providing up to 40 beamlines simultaneously with soft and hard x-rays at a rate of up to 500 MHz. For experiments that do not require or cannot even tolerate the high peak intensity delivered by high-gain FELs, methods to reduce the pulse length can significantly extend the scientific opportunities of conventional synchrotron light sources.

At synchrotron light sources, pulses in the femtosecond regime can be obtained by separating radiation from a small longitudinal part of the electrons from the rest. Such a 'slice' is defined by the interaction of electrons with a co-propagating ultrashort laser pulse in an undulator (the 'modulator') leading to a periodic modulation of the electron energy within the slice. In the case of incoherent radiation from a subsequent undulator (the 'radiator'), a spatial separation of the short radiation component is required, a method known as femtoslicing [2–5].

Coherent Harmonic Generation

Another method based on the interaction of an ultrashort laser pulse with an electron bunch is called coherent harmonic generation (CHG) [6–9]. Here, the energy modulation

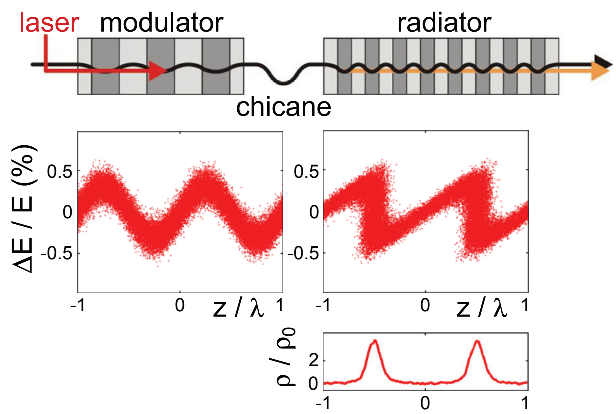

Figure 1: Sketch of the magnetic setup for CHG (top), the longitudinal phase space before and after the magnetic chicane (center), and the longitudinal electron density after the chicane (bottom).

is converted into a density modulation ('micro-bunching') using a magnetic chicane. This leads to the emission of a short coherent pulse in the radiator at harmonics of the laser wavelength. A sketch of this technique is depicted in Fig. 1.

Due to the coherent nature of this radiation mechanism, the CHG pulse can be more intense than the incoherent radiation from the rest of the bunch, such that no spatial separation is required. The radiated power is given by

$$P_{\text{inc}} = N_e \cdot P_e, \quad (1)$$

$$P_{\text{coh}} = \left(\frac{\tau_L}{\tau_b} \cdot N_e\right)^2 \cdot b_n^2 \cdot P_e, \quad (2)$$

where P_{inc} is the incoherent power emitted by an electron bunch with N_e electrons, P_e is the power emitted by a single electron, and P_{coh} is the CHG power emitted by the laser-modulated slice. The number of electrons contributing to the coherent emission is given by N_e times the ratio of laser pulse length τ_L and electron bunch length τ_b. The so-called bunching factor b_n is a measure for the degree of micro-bunching with a value between 0 and 1. It is given by [10]

$$b_n = e^{-\frac{1}{2}n^2 \cdot B^2} \cdot J_n(n \cdot A \cdot B), \quad (3)$$

with

$$A = \frac{\Delta E}{\sigma_E} \quad \text{and} \quad B = r_{56} \cdot \frac{2\pi}{\lambda_L} \cdot \frac{\sigma_E}{E},$$

and the harmonic number n of the laser wavelength λ_L to which the radiator is tuned. Here, J_n is the Bessel function

* Work supported by the DFG, the BMBF, and the state of NRW.
† arne.meyeraufderheide@udo.edu

ALPHA – THE THZ RADIATION SOURCE BASED ON AREAL*

T. Vardanyan#, G. Amatuni, V. Avagyan, A. Grigoryan, B. Grigoryan, M. Ivanyan, V. Khachatryan, V. Petrosyan, V. Sahakyan, A. Sargsyan, A. Tsakanian, V. Tsakanov, A. Vardanyan, G. Zanyan, CANDLE SRI, Yerevan, Armenia

Abstract

Advanced Research Electron Accelerator Laboratory (AREAL) based on photo cathode RF gun is under construction at the CANDLE. The basic aim of this new facility is to generate sub-picosecond duration electron bunches with an extremely small beam emittance and energies up to 50 MeV. One of the promising directions of the facility development is the creation of ALPHA (Amplified Light Pulse for High-end Applications) experimental stations with coherent radiation source in THz region based on the concept of both conventional undulator and novel radiation sources. The status of the AREAL facility, the main features and outlooks for the ALPHA station are presented in this work.

INTRODUCTION

The generation and acceleration of low emittance ultrashort electron bunches present the origin for the development of new coherent radiation sources. The AREAL RF photogun electron linear accelerator is currently under construction at the CANDLE Synchrotron Research Institute [1]. The basic aim of this new facility is to generate electron bunches with extremely small beam emittance and with sub-picosecond pulse duration for advanced experimental study in the field of accelerator technology, new radiation sources and dynamics of ultrafast processes.

The first phase of the AREAL facility with the beam energy of about 5 MeV at the gun exit is completed recently [2]. The second phase foresees 20 MeV design energy with possible upgrade of up to 50 MeV.

After successful realization of AREAL phase 1 which was demonstrated during the machine run shifts in May 2014 [3], the second phase of the project implementation being in progress implies installation of two accelerating S-band modules with corresponding diagnostic equipment.

In the past decade the THz radiation has been of great scientific interest with a wide range of potential application in the field of life, material and environmental sciences, development of bio and nano-technologies [4]. One of the promising directions of the AREAL facility development is the creation of ALPHA experimental station with coherent radiation source in THz region. The project will focus on the development of THz coherent radiation sources based on 1) conventional periodic magnetic (undulator) system, 2) novel single mode slowly travelling waveguide concept and 3) modulated beam plasma interaction. In this paper we present the main features of ALPHA THz Free Electron Laser option based on the planar undulator.

* Work supported by State Committee of Science MES RA in frame of the research project № SCS 13YR-1C0007.
#tvardanyan@asls.candle.am

AREAL FACILITY

The schematic layout of the AREAL laser driven electron linear accelerator is presented in Fig. 1. The facility contains cupper photocathode illuminated by 285 nm wavelength UV laser, 1.6 cell S-band cavity and two 1.5 m long S-Band accelerating sections.

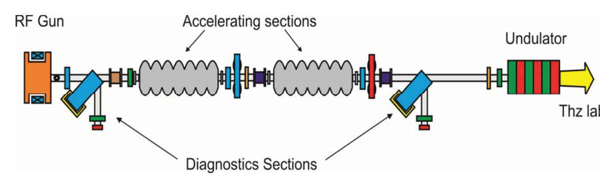

Figure 1: Layout of AREAL gun section with diagnostics.

The main design parameters of the AREAL facility electron beam are given in Table 1.

Table 1: AREAL Beam Parameters List

Energy	20-50 MeV
Bunch charge	10-200 pC
Transv. norm emit.	<0.3 mm-mrad
RMS bunch duration	0.5-8 ps
Energy spread at 20 MeV	0.2%

The ASTRA start-to-end tracking simulations are performed to optimize the acceleration phase and gradients to obtain minimum beam emittance and the energy spread. The results of the beam transverse size and normalized emittance for the beam energy of about 20 MeV is shown in Fig. 2 [5].

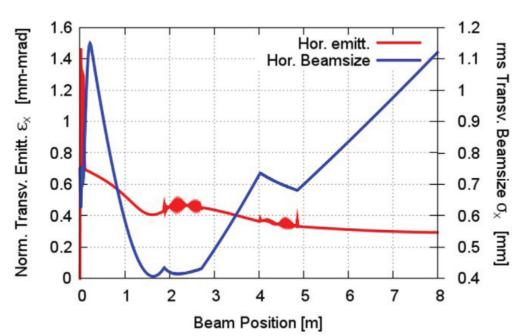

Figure 2: Transverse normalized emittance and beam size along the linac.

ISBN 978-3-95450-133-5

FERMI STATUS REPORT

M. Svandrlik#, E. Allaria, F. Bencivenga, C. Callegari, F. Capotondi, D. Castronovo, P. Cinquegrana, M. Coreno, R. Cucini, I. Cudin, M.B. Danailov, G. D'Auria, R. De Monte, G. De Ninno, P. Delgiusto, A. Demidovich, S. Di Mitri, B. Diviacco, A. Fabris, R. Fabris, W. M. Fawley, M. Ferianis, E. Ferrari, P. Finetti, L. Fröhlich, P. Furlan Radivo, G. Gaio, D. Gauthier, F. Gelmetti, L. Giannessi, M. Kiskinova, S. Krecic, M. Lonza, N. Mahne, C. Masciovecchio, M. Milloch, F. Parmigiani, G. Penco, L. Pivetta, O. Plekan, M. Predonzani, E. Principi, L. Raimondi, P. Rebernik Ribic, F. Rossi, L. Rumiz, C. Scafuri, C. Serpico, P. Sigalotti, C. Spezzani, C. Svetina, M. Trovò, A. Vascotto, M. Veronese, R. Visintini, D. Zangrando, M. Zangrando, Elettra, Trieste, Italy

Abstract

FERMI, the seeded FEL located at the Elettra laboratory in Trieste, Italy, is now in regular operation for users with its first FEL line, FEL-1, which covers the wavelength range between 100 and 20 nm. We will give an overview of the typical operating modes of the facility for users and we will report on the status of beamlines and experimental stations. Three beamlines are now opened for users, three more are in construction. Meanwhile, the second FEL line of FERMI, FEL-2, a HGHG double stage cascade covering the wavelength range 20 to 4 nm is still under commissioning; we will report on the latest results in particular at the shortest wavelength, 4 nm in the fundamental.

INTRODUCTION

The facility covers the photon energy range between 12 and 310 eV thanks to two seeded FEL lines. The low energy FEL line, FEL-1 reaching up to 62 eV, is made by a single stage HGHG scheme, with a modulator undulator and a radiator with six undulator elements [1]. The high energy FEL line, FEL-2 which generates photons down to 4 nm wavelength in the fundamental and 1.3 nm in the third harmonic, is made by a double stage HGHG cascade, in which the first stage is presently made by a modulator undulator and two radiator modules, and the second stage by a modulator undulator and six radiator modules; the "fresh bunch injection" mode is used [2].

FEL-1 started operation for users in December 2012 and since then welcomed scientists from Italy and from all over the world to perform experiments on the three experimental stations so far available, namely the Diffraction Projection Imaging (DiProI) station, the Elastic Inelastic Scattering TIMEX (EIS-TIMEX) station and the Low Density Matter (LDM) station.

FEL-2 produced the first coherent photons at 14.4 nm in October 2012; that was the first experimental demonstration of a high gain seeded free electron laser configured as a two stages cascade operating in the "fresh bunch injection" mode [3]. Since then FEL-2 commissioning runs were performed in-between user operation runs on FEL-1. They allowed to gradually extend the wavelength reach of FEL-2, as can be seen for instance in Fig. 1 that shows the spectrum at 10 nm, until the nominal performance at 4 nm was attained last June.

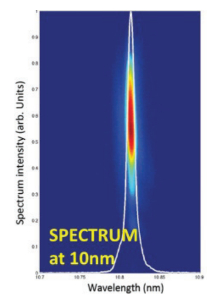

Figure 1: FEL-2 spectrum at 10 nm.

USERS OPERATION REPORT

Three calls for proposal of experiment on FERMI have been opened between 2012 and 2013. A total number of 125 proposals were received and 50 have been ranked by the FERMI Review Panel (FRP) for beamtime. In the 3rd call, 50 proposals have been submitted and 16 have been short listed in the FRP meeting of January 2014 for beamtime, that is, with an oversubscription rate of 3.13. Table 1 shows the standard parameters offered for experiments on FEL-1.

Table 1: FEL-1 Standard Parameters for User Operation

Parameter	FEL-1
Electron beam energy	1.0 - 1.4 GeV
Bunch charge	500 pC
Bunch Peak Current	400 – 600 A
Wavelength	100 – 20 nm
Energy per pulse*	30 – 200 μJ
Photons per pulse**	10^{13} at 20 nm
Intensity stability, rms	10%
Relative bandwidth	10^{-4}
Central wavelength stability	10^{-4} rms

**average, depending on wavelength and spectral purity.*
***up to 10^{14} at longer wavelengths.*

#michele.svandrlik@elettra.eu

ISBN 978-3-95450-133-5

EXPERIMENT PREPARATION TOWARDS A DEMONSTRATION OF LASER PLASMA BASED FREE ELECTRON LASER AMPLIFICIATION

M.-E. Couprie, C. Benabderrahmane, P. Berteaud, C. Bourassin-Bouchet, F. Bouvet, F. Briquez, L. Cassinari, L. Chapuis, M. El Ajjouri, C. Herbeaux, N. Hubert, M. Labat, A. Lestrade, A. Loulergue, J. Luning, O. Marcouillé, J.-L. Marlats, F. Marteau, C. Miron, P. Morin, F. Polack, K. Tavakoli, M. Valléau, D. Zerbib, SOLEIL, Gif-sur-Yvette, France
X. Davoine, CEA/DAM/DIF, Arpajon, France
I. Andriyash, G. Lambert, V. Malka, C. Thaury, LOA, Palaiseau, France
S. Bielawski, C. Evain, C. Szwaj, PhLAM/CERCLA, Villeneuve d'Ascq Cedex, France

Abstract

One direction towards compact Free Electron Laser is to replace the conventional linac by a laser plasma driven beam, provided proper electron beam manipulation to handle the value of the energy spread and of the divergence. Applying seeding techniques also enables to reduce the required undulator length. Rapidly developing Laser Wakefield Accelerators (LWFA) are already able to generate synchrotron radiation. With the presently achieved electron divergence and energy spread an adequate beam manipulation through the transport to the undulator is needed for FEL amplification. A test experiment for the demonstration of FEL amplification with a LWFA is under preparation in the frame of the COXINEL ERC contract in the more general context of LUNEX5. Electron beam transport follows different steps with strong focusing thanks to variable strength permanent magnet quadrupoles, demixing chicane with conventional dipoles, and a second set of quadrupoles for further focusing in the undulator. Progress on the equipment preparation and expected performance are described.

INTRODUCTION

More than 30 years after the first Free Electron Laser (FEL) [1], FEL based fourth generation light sources [2] presently offer femtosecond tuneable radiation in the X – ray domain with LCLS in USA [3], SACLA in Japan [4] and in the VUV- soft X-ray with FLASH in Germany [5] and FERMI in Italy [6]. FEL oscillators being limited to VUV [7], single optical pass FEL devices are preferred for short wavelength operation. After the first coherent harmonic generation experiments [8], seeding has demonstrated major advantages in terms of spectral purity [9-12]. Besides the preparation of additional FEL light sources for users around the world, new schemes are also under investigation. In view of the fifth generation light sources [13], several approaches are considered. One direction goes towards the improvement of FEL performance in a wide spectral range and with versatile properties and flexibility for users. Another one aims at reducing the size either by exploring further seeding and / or by replacing the conventional linear accelerator by a compact alternative one. Indeed, the rapidly developing Laser WakeField Accelerator (LWFA) [14, 15] are now able to generate synchrotron radiation [16]. With an electron divergence of typically 1 mrad and an energy spread of the order of 1 %, an adequate beam manipulation through the transport to the undulator is required for FEL amplification. Different strategies have been proposed, such as a decompression chicane [17], or a transverse gradient undulator [18].

The studies presented here take place in the context of the LUNEX5 (free electron Laser Using a New accelerator for the Exploitation of X-ray radiation of 5th generation) collaboration, aiming at investigating the production of short, intense, coherent pulses in the 40-4 nm spectral range [19] with a 400 MeV superconducting linac and a LWFA both connected to a single FEL for advanced seeding configurations. Both accelerators are complementary: The conventional linac will enable studies of advanced FEL schemes, future upgrade towards high repetition rate and multi-user operation. The LWFA has first to be qualified by the FEL application. LUNEX5, after the completion of a Conceptual Design Report [20], is presently in a phase of R&D and complementary studies. In this frame, after transport calculation of longitudinal and transverse manipulation of a LWFA electron beam showing that theoretical amplification is possible, a test experiment is under preparation, with the support of different grants.

GENERAL DESCRIPTION

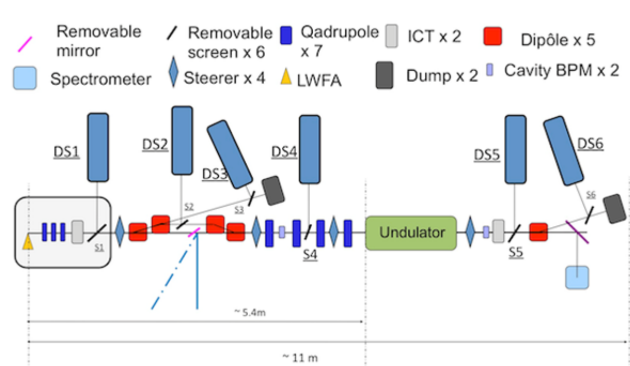

Figure 1: Scheme of the main components.

COXINEL grant aims at demonstrating FEL amplification with a LWFA. First, it intends to provide an appropriate electron beam transport from the source to the

ISBN 978-3-95450-133-5

THE STATUS OF LUNEX5 PROJECT

M. E. Couprie, C. Benabderrahmane, P. Berteaud, C. Bourassin-Bouchet, F. Bouvet, F. Briquez, L. Cassinari,L. Chapuis, M. Diop, J. Daillant, M. El Ajjouri, C. Herbeaux, N. Hubert, M. Labat, P. Lebasque, A. Lestrade,A. Loulergue, P. Marchand, O. Marcouillé, J. L. Marlats, C. Miron, P. Morin, A. Nadji, F. Polack, F. Ribeiro,J. P. Ricaud, P. Roy, K. Tavakoli, M. Valléau, D. Zerbib, Synchrotron SOLEIL, France
S. Bielawski, C. Evain, E. Roussel, C. Szwaj, PhLAM/ CERLA, Lille, France
G. Lambert, V. Malka, R. Lehe, A. Rousse, C. Thaury, Laboratoire d'Optique Appliquée, Palaiseau, France
G. Devanz, C. Madec, A. Mosnier, CEA/DSM/IRFU/SACM, Saclay, France
D. Garzella, B. Carré, CEA/DSM/IRAMIS/ LIDyL, Saclay, France
N. Delerue, Laboratoire de l'Accélérateur Linéaire, Orsay, France
X. Davoine, CEA/DAM/DIF, Bruyère-Le-Châtel, France
A. Dubois, J. Lüning, LCPMR, Paris-VI, France

Abstract

LUNEX5 (free electron Laser Using a New accelerator for the Exploitation of X-ray radiation of 5th generation) aims at investigating the production of short, intense, coherent Free Electron Laser (FEL) pulses in the 40-4 nm spectral range. It comprises a 400 MeV superconducting Linear Accelerator for high repetition rate operation (10 kHz), multi-FEL lines and adapted for studies of advanced FEL schemes, a 0.4 - 1 GeV Laser Wake Field Accelerator (LWFA) for its qualification by a FEL application, a single undulator line enabling seeding with High order Harmonic in Gas and echo configurations and pilot user applications. Concerning the superconducting linac, the electron beam dynamics has been modified from a scheme using a third harmonic linearizer and a compression chicane to a dog-leg coupled to sextupoles. Besides, the choice of the gun is under revision for achieving 10 kHz repetition rate. A test experiment is under preparation in collaboration with the Laboratoire d'Optique Appliquée, aimed at validating the computed transport performance of longitudinal and transverse manipulation on a LWFA electron beam enabling to provide theoretical amplification.

INTRODUCTION

France has a long history in Free Electron laser, and has obtained the second worldwide FEL on ACO (first visible radiation) in 1983 [1] and first FEL based short wavelength harmonic generation [2]. The Super-ACO FEL, commissioned in 1989 [3], delivered in 1993 the first UV FEL beam [4] to users [5, 6, 7, 8, 9] with first pump-probe two colour experiments. Extensive studies aiming at further understanding the FEL dynamics and at improving its own performance were performed, such as temporal structure [10], short pulse operation [11, 12, 13], interplay with the electron beam [14, 15]. Mirror performance and degradation have been also extensively analysed [16].

An infra-red FEL user facility, CLIO is in operation since 1992 [17].

Considering short wavelength single pass FEL, there have been active collaborations for seeding studies, in particular with high harmonics in gas (HHG) using a 160 nm seed providing radiation down to 27 nm [18] and recently with a 60 nm seed [19] at SCSS Test Accelerator and at SPARC [20]. Short wavelength FEL user facilities (LCLS [21], SACLA [22], FLASH [23] and FERMI [24]) are providing new tools for the investigation of matter.

New researches are going towards exploring how to approach closer the diffraction and Fourier limits in a wide spectral range and with versatile properties. Besides, some other trends are investigating how FEL can become more compact, by seeding schemes and replacing the conventional accelerator by LWFA [25].

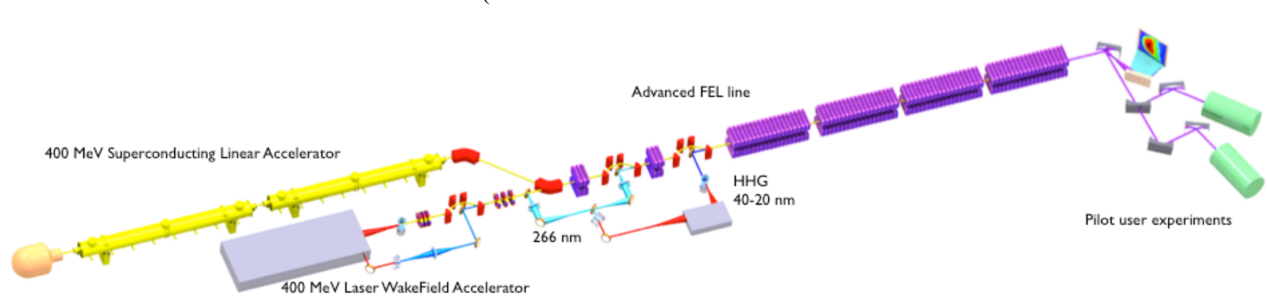

Figure 1: LUNEX5 sketch with two cryomodules (yellow), laser hutch for LWFA (grey), undulators (four radiators and two ECHO modulators) (purple), pilot user experimental sections (green).

ISBN 978-3-95450-133-5

FREE ELECTRON LASERS IN 2014

J. Blau[#], K. Cohn, W. B. Colson, and W. Tomlinson
Physics Department, Naval Postgraduate School, Monterey CA 93943, USA

Abstract

Thirty-eight years after the first operation of the free electron laser (FEL) at Stanford University, there continue to be many important experiments, proposed experiments, and user facilities around the world. Properties of FELs operating in the infrared, visible, UV, and X-ray wavelength regimes are tabulated and discussed.

LIST OF FELS IN 2014

The following tables list existing (Table 1) and proposed (Tables 2, 3) relativistic free electron lasers (FELs) in 2014. The 1st column lists a location or institution, and the FEL's name in parentheses. References are listed in Tables 4 and 5; another useful reference is:
http://sbfel3.ucsb.edu/www/vl_fel.html.

The 2nd column of each table lists the operating wavelength λ, or wavelength range. The longer wavelength FELs are listed at the top and the shorter wavelength FELs at the bottom of each table. The large range of operating wavelengths, seven orders of magnitude, indicates the flexible design characteristics of the FEL mechanism.

In the 3rd column, t_b is the electron bunch duration (FWHM) at the beginning of the undulator, and ranges from almost CW to short sub-picosecond time scales. The expected optical pulse length in an FEL oscillator can be several times shorter or longer than the electron bunch depending on the optical cavity Q, the FEL desynchronism and gain. The optical pulse can be many times shorter in a high-gain FEL amplifier, or one based on self-amplified spontaneous emission (SASE). Also, if the FEL is in an electron storage-ring, the optical pulse is typically much shorter than the electron bunch. Most FEL oscillators produce an optical spectrum that is Fourier transform limited by the optical pulse length.

The electron beam kinetic energy E and peak current I are listed in the 4th and 5th columns, respectively. The next three columns list the number of undulator periods N, the undulator wavelength λ_0, and the rms undulator parameter $K = eB\lambda_0/2\pi mc^2$ (cgs units), where e is the electron charge magnitude, B is the rms undulator field strength, m is the electron mass, and c is the speed of light. For an FEL klystron undulator, there are multiple undulator sections as listed in the N-column; for example 2x7. Some undulators used for harmonic generation have multiple sections with varying N, λ_0, and K values as shown. Some FELs operate at a range of wavelengths by varying the undulator gap as indicated in the table by a range of values for K. The FEL resonance condition, $\lambda = \lambda_0(1+K^2)/2\gamma^2$, relates the fundamental wavelength λ to K, λ_0, and the electron beam energy $E = (\gamma-1)mc^2$, where γ is the relativistic Lorentz factor. Some FELs achieve shorter wavelengths by using coherent harmonic generation (CHG), high-gain harmonic generation (HGHG), or echo-enabled harmonic generation (EEHG).

The last column lists the accelerator types and FEL types, using the abbreviations listed after Table 3.

The FEL optical power is determined by the fraction of the electron beam energy extracted and the pulse repetition frequency. For a conventional FEL oscillator in steady state, the extraction can be estimated as 1/(2N); for a high-gain FEL amplifier, the extraction at saturation can be substantially greater. In a storage-ring FEL, the extraction at saturation is substantially less than this estimate and depends on ring properties.

In an FEL oscillator, the optical mode that best couples to the electron beam in an undulator of length $L = N\lambda_0$ has a Rayleigh length $z_0 \approx L/12^{1/2}$ and has a fundamental mode waist radius $w_0 \approx (z_0\lambda/\pi)^{1/2}$. An FEL typically has more than 90% of its power in the fundamental mode.

At the 2014 FEL Conference, there were two new lasings reported: FLASH2 at DESY and a SASE FEL at the SwissFEL Test Facility at PSI. Progress continues on many other existing and proposed FELs around the world, from small terahertz FELs to large X-ray FEL facilities.

ACKNOWLEDGMENTS

The authors are grateful for support from the HEL-JTO.

[#]blau@nps.edu

THE TURKISH ACCELERATOR AND RADIATION LABORATORY IN ANKARA (TARLA) PROJECT*

A. Aksoy†, Ö. Karslı, Ç. Kaya, Ö. Yavaş, Institute of Accelerator Technologies, Ankara, Turkey
S. Ozkorucuklu, Istanbul University, Istanbul, Turkey
P. Arıkan, Gazi University, Ankara, Turkey

Abstract

The Turkish Accelerator and Radiation Laboratory in Ankara (TARLA) which is proposed as a first facility of Turkish Accelerator Center (TAC) Project will operate two Infra-Red Free Electron Lasers (IR-FEL) covering the range of 3–250 microns. The facility will consist of an injector fed by a thermionic triode gun with two-stage RF bunch compression, two superconducting accelerating modules operating at continuous wave (CW) mode and two independent optical resonator systems with different undulator period lengths. The electron beam will also be used to generate Bremsstrahlung radiation. The facility aims to be first user laboratory in the region of Turkey in which both electromagnetic radiation and particles will be used. In this paper, we discuss design goals of the project,present status and road map of the project.

INTRODUCTION

TARLA, also called the Turkish Accelerator Center (TAC) IR FEL Oscillator facility, has been proposed as a sub-project of TAC in Turkey. TAC is an accelerator based research center project which consists of the conceptual design studies of a third generation synchrotron radiation facility based on 3.56 GeV positron ring, a SASE/X FEL facility based on multi GeV electron linac and a 1–3 GeV proton accelerator,a linac-ring type charm factory, since 2006 [1–3]. The construction phase of TARLA has been supported by Ministry Development (MD) of Turkey since 2010 and the laboratory has been still under construction [4, 5].

The main goal of TARLA is to provide FEL radiation between the ranges of 3–250 µm in the infrared region by using two undulator-resonator system. The facility will also have a bremsstrahlung production target and some fixed target applications using the available electron beam which is in the energy range of 15–40 MeV. The electron beam will be obtained by a thermionic triode electron source operating at 250 kV in continuous wave (CW) mode. And the beam will further be accelerated up to 40 MeV by two super conducting RF modules that are designed for ELBE project [6]. The electron beam will be transported to two independent optical resonator systems housing undulators with the different period lengths of 25 mm and 90 mm. The schematic view of the facility is given in Fig. 1 and the main electron beam parameters as well as some FEL parameters of TARLA are given in Tables 1 and 2 respectively.

* Work supported by Ministry of Development of Turkey
† avniaksoy@ankara.edu.tr

TARLA laboratory building completed in May 2011 under Ankara University Institute of Accelerator Technologies in Golbasi Campus which is about 15 km south of the center of Turkey, Ankara.

Table 1: Electron Beam Parameters of TARLA

Parameter	Unit	Value
Beam energy	MeV	15–40
Max. average beam current	mA	1
Max. bunch charge	pC	77
Horizontal emittance	mm.mrad	<15
Vertical emittance	mm.mrad	<12
Longitudinal emittance	keV.ps	<85
Bunch length	ps	0.4–6
Bunch repetition rate	MHz	13
Macro pulse duration	µs	50 - CW
Macro pulse repetition rate	Hz	1 - CW

TARLA ACCELERATOR

TARLA will consists of three main parts: the injector, the main accelerator and the transport lines to the U25 and U90 undulators (Fig. 1). The high current (1 mA) CW electron beam from injector which provides the energy of 250 keV will be transported to two superconducting modules including two TESLA RF cavities that are separated by a bunch compressor. The maximum available energy of the electron beam with these accelerator modules will be between the range of 15–40 MeV and two independent optical resonator systems will support the generation of FEL radiation.

Injector

TARLA injector will have a thermionic triode DC electron gun, two buncher cavities operating at 260 MHz and 1.3 GHz, five solenoid lenses, one dipole magnet and several steerer magnets. The total length of the injector is about 5.75 m. Although the designs of electron gun and buncher cavities are the same with the ELBE Radiation Source [7], there will be a small difference with the beam line of ELBE by using a bend about 15° just after the gun, in order to avoid the field emission current from the SC cavities to back-bombard the cathode.

Main Accelerator

TARLA main accelerator will include two ELBE cryomodules (Linac-1, Linac-2) and a magnetic bunch compressor (BC) between them (see Fig. 1). Each cyromodule

ISBN 978-3-95450-133-5

DEVELOPMENTS IN THE CLARA FEL TEST FACILITY ACCELERATOR DESIGN AND SIMULATIONS

P. H. Williams#, D. Angal-Kalinin, A. D. Brynes, J. K. Jones, B. P. M. Liggins, J. W. McKenzie, B. L. Militsyn, ASTeC, STFC Daresbury Laboratory, Cheshire, U.K
S. Spampinati, University of Liverpool & The Cockcroft Institute, Cheshire, U.K

Abstract

We present recent developments in the accelerator design of CLARA (Compact Linear Accelerator for Research and Applications), the proposed UK FEL test facility at Daresbury Laboratory. These comprise a revised front-end to ensure integration with the existing VELA (Versatile Electron Linear Accelerator) line, simulations of a magnetically compressed ultra-short mode and a post-FEL diagnostics section. We also present first considerations on the inclusion of final acceleration using X-band structures.

THE CLARA ACCELERATOR

CLARA (Compact Linear Accelerator for Research and Applications) is a proposed 250 MeV, 100-400 nm FEL test facility at Daresbury Laboratory [1]. The purpose of CLARA is to test and validate new FEL schemes in areas such as ultra-short pulse generation, temporal coherence and pulse-tailoring. The accelerator will comprise 4 S-Band, normal-conducting linacs with a medium-energy, variable bunch-compression scheme, feeding into a flexible arrangement of FEL modulators and radiators.

For seeding the accelerator includes a pre-FEL dogleg where laser light can be introduced. The accelerator will be driven by a high rep-rate RF photocathode S-Band (2998.5 MHz) gun, operating in single bunch mode at up to 400 Hz, and with bunch charges up to 250 pC. The accelerator is intended to be flexible, with seeded, ultra-short and multi-bunch train modes provided. Compression can be achieved via a variable magnetic bunch compressor between linacs 2 and 3 or velocity bunching in the injector. Linearisation can be provided by a harmonic X-band structure immediately prior to the magnetic compressor.

FRONT END

The VELA user facility, based on the ALPHA-X photocathode gun, has been commissioned and successfully delivered beam to users in 2013 [2]. The proposed FEL test facility, CLARA, is intimately linked to VELA with much common infrastructure. The design of the CLARA Front End (CLARA-FE) has been optimised to meet the requirements of the CLARA injector as well as to transport higher repetition rate, higher energy bunches to the presently operating VELA facility.

The proposed layout shown in Fig. 1 has been designed to use a common RF and drive laser infrastructure to feed two photo-injector RF guns. This will allow the flexibility of sending ~5 MeV high repetition rate bunches to existing VELA user areas, and up to 50 MeV bunches transported through the S-bend placed after the first linac on the CLARA line to the VELA user areas at lower rep-rate. The layout assumes that the present VELA gun moves to CLARA when the front end is ready and installed. The ~55 MeV bunches after linac-1 can either be transported to (1) the CLARA line, (2) around the first dipole in the S-bend, then straight ahead to a diagnostic spectrometer line for characterising high energy bunches and (3) around the second dipole in the S-bend to the VELA user areas (the quadrupole triplet can be energised to eliminate dispersion in the VELA line). When the new High Repetition Rate Gun (HRRG) [3] is ready for commissioning and characterisation, it will be installed in the present VELA gun position. This is attractive as it provides a full set of dedicated diagnostics including the Transverse Deflecting Cavity (TDC). After this characterisation the HRRG will be moved to the CLARA line. Depending on the experimental programme either the original VELA gun or another new gun will be installed on the VELA line. This option will make low energy, short bunches available to proposed electron diffraction experiments on the VELA line [4]. At present, all simulations for the CLARA machine have been performed using a model of the existing VELA low rep-rate gun as it is assumed this will be installed before the HRRG.

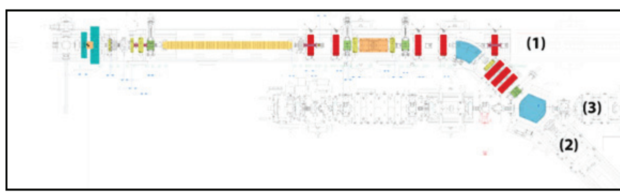

Figure 1: CLARA Front End Layout. The beam can be directed to (1) the rest of CLARA, (2) a diagnostic spectrometer line and (3) the existing VELA line with two user areas. The second “lozenge” dipole also admits beam from the existing VELA gun line allowing to be diverted to (2) or continue to (3).

ULTRA-SHORT MODE

One of the required modes of CLARA operation is transport of a medium charge (100 pC) bunch with length less than 25 fs RMS and corresponding high peak current in excess of 1 kA. This should have transverse normalised emittance of < 1 mm mrad and energy spread of <150 keV RMS. This parameter set is specified for research into FEL schemes where the bunch length must be shorter than the typical SASE spike separation of $2\pi l_c$, with l_c the cooperation length. Previously, accelerator simulations

ISBN 978-3-95450-133-5

A BEAM TEST OF CORRUGATED STRUCTURE FOR PASSIVE LINEARIZER

Heung-Sik Kang, Juho Hong, PAL, Pohang, Kyungbuk, Korea

Abstract

A dechirper which is a vacuum chamber of two corrugated, metallic plates with adjustable gap was successfully tested at Pohang, in August 2013. Another beam test was carried out to test the same structure to see if the flat geometry corrugated structure may work as a passive linearizer. The test result will be presented together with the simulation result.

PASSIVE LINEARIZER TO CORRECT QUADRATIC CHIRP

In August 2013, LBNL and SLAC experts were onsite at PAL-ITF to test a ***dechirper***, an interesting instrument consisting of a vacuum chamber of two corrugated, metallic plates with an adjustable gap. One-meter long proto-type of dechirper was tested successfully to accurately measure the longitudinal, dipole, and quadrupole wakes [1]. And the linear chirp is well corrected by the linear longitudinal wake of dechirper.

An idea to use the same structure came up to see if the flat geometry corrugated structure may work as a passive linearizer replacing an expensive X-band linearizer system which consists of an X-band linearizer cavity and an X-band RF system. The total cost of that system is over 3 MUSD, and if including one spare of klystron and others, it goes to 5 MUSD. However, the passive wake structure is very cheap, below 200 kUSD even though the gap control system of two plates is included.

Figure 1 shows the flat geometry corrugated structure. The dimensions of the structure used at the experiment in August 2013 at PAL-ITF are: the corrugation period (p) is 0.5 mm, the corrugation depth (h) is 0.6 mm, the wall distance (t) is 0.3 mm, and the width of plate (w) 50 mm. Figure 2 shows the longitudinal wake of flat geometry corrugated structure.

For the passive wake structure to act like an X-band linearizer, quadratic part of longitudinal wake needs to be involved in the beam-wake interaction to correct quadratic chirp. So, the longitudinal wakefield wavelength, $\lambda = 2\pi\sqrt{aht/p}$, needs to be comparable to bunch length. Dechirper has two independent motors: jaws are always parallel and move vertically. The gap is adjustable from 1 to 30 mm. As the gap of the two plates goes close, the wavelength is decreased. With the corrugated structure parameters (p=0.5 mm, h=0.6 mm, t=0.3 mm), the calculated wakefield wavelengths are 7.5 mm, 5.3 mm, 3.8 mm for the gaps of 8 mm, 4 mm, 2 mm, respectively. To have the electron beam interact with the quadratic part of longitudinal wake, the electron beam bunch needs to be longer than one fourth of the wake wavelength. But there is a limitation in the gap distance because the quadrupole wake of the flat geometry becomes very strong as the gap goes close.

Instead, we may increase the bunch length from 3 ps to 5 ps in rms in order to have the electron beam interact with the quadratic part of longitudinal wake. The simulation shows that the longitudinal wake at the gap of 6 mm can correct the quadratic chirp.

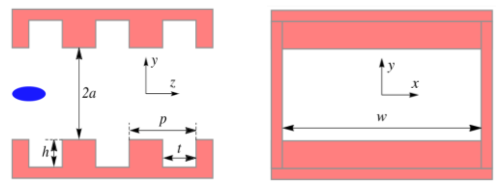

Figure 1: A flat geometry corrugated structure.

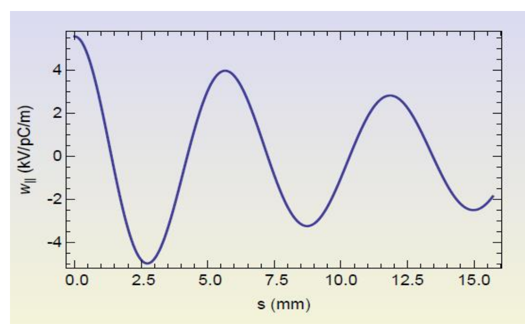

Figure 2: Longitudinal wake.

SIMULATION OF PASSIVE LINEARIZER AND BEAM TEST AT ITF

Figure 3 shows the layout of the PAL-ITF which consists of a PC RF-gun, two S-band Accelerating structures (L0a, L0b), a 1-m long S-band RF deflector, a 30-degree spectrometer, and three quads. A 1-m long corrugated chamber is located between L0b and the deflector. Six YAG screens are available, but Screen-6 is used for the analysis of the simulation and the experiment. In the simulation and measurement, all quads are turned OFF while the deflector is turned ON to allow the time-resolved measurement.

The beam energy is set at 80 MeV and the beam charge is 200 pC, and the pulse repetition rate is 10 Hz. Beam size and centroids measured on YAG screens, Spectrometer bend allows energy loss and energy spread measurements, and Dechirper offset is varied to guide the

ISBN 978-3-95450-133-5

DESIGN OF A COMPACT LIGHT SOURCE ACCELERATOR FACILITY AT IUAC, DELHI

S. Ghosh, B. K. Sahu, A. Rai, G. K. Chaudhari, P. Patra, J. Karmakar, A. Pandey, N. Kumar, R. K. Bhandari, D. Kanjilal, Inter University Accelerator Centre, New Delhi, India
J. Urakawa, A. Aryshev, High Energy Accelerator Research Organization, KEK, Tsukuba, Japan
V. Naik, A. Roy, Variable Energy Cyclotron Center, Kolkata, India
A. Deshpande, T. Dixit, Society for Applied Microwave Electronics Engineering & Research, Mumbai, India

Abstract

There is a growing demand for a high brightness light source with short pulse length among the researchers in the field of physical, chemical, biological and medical sciences in India. To cater to the experimental needs of multidisciplinary sciences, a project to develop a compact Light Source has been initiated at Inter University Accelerator Centre (IUAC). In the first phase of the project, pre-bunched electron beam of ~ 7 MeV energy will be generated by a photocathode RF gun and coherent THz radiation will be produced by a short undulator magnet. In the next phase, the energy of the electron beam will be increased up to 40 MeV by a pair of superconducting niobium resonators. The coherent IR radiation will be produced by using an undulator magnet (conventional method) and X-rays by Inverse Compton Scattering. To increase the average brightness of the electromagnetic radiation, fabrication of superconducting RF gun is going to be started in a parallel development. In this paper, the design of the accelerator system and the plan of producing THz radiation will be discussed.

INTRODUCTION

Inter University Accelerator Centre (IUAC), New Delhi, is a national accelerator facility equipped with many ion accelerators notably a 15UD Pelletron accelerator, a superconducting Linac booster [1], a 1.7 MV Pelletron and various low energy ion beam facilities. These accelerators are used to carry out research in the field of nuclear physics, materials science and radiation biology. Recently, to address the growing needs of the researchers from multidisciplinary fields like biological, chemical, medical and physical sciences, a project to develop a Free Electron Laser (FEL) facility named as Delhi Light Source (DLS) has been initiated at IUAC.

The development of the DLS project is being started with a room temperature (RT) photocathode RF electron gun which will produce a high quality electron beam of energy ~ 7 MeV. The beam will be then injected into a short undulator magnet to produce radiation in the THz range.

Simultaneously, to operate the RF gun in cw or quasi-cw mode, development of the superconducting (SC) RF photocathode electron gun is being explored. The SC RF gun will be either a three and half-cell niobium resonator similar to the structure being used at Rossendorf, Dresden [2] or a Quarter Wave Resonator (QWR) similar to the design adopted by Brookhaven National Laboratory (BNL) [3]. Experience of IUAC in the fields of fabricating niobium resonators, cryostats and cryogenic systems will be useful in this development. The energy obtained from the 3.5 cell elliptical structure is estimated to be ~ 10 MeV. This beam will then be injected into an undulator magnet to produce THz radiation. However, if the QWR structure is adopted as RF gun, then the energy gain from the gun will be only a few MeV, so another 5 cell TESLA type SC resonator will be required to increase the energy upto ~ 10 MeV. Both the options of SC RF gun is shown in Fig. 1.

In the next phase of the development, two 9 cell TESLA type cavities will be installed to boost the energy from ~ 7 MeV (from RT RF gun) or 10 MeV (from SC RF gun) to ~ 40 MeV. This beam will be switched to three different beam lines. One beam line will be dedicated to produce infrared (IR) radiation with the help of a long undulator magnet. The second beam line will be for X-rays produced by the technique of Inverse Compton Scattering whereas the third one will be dedicated for experiments with THz/Far-IR and/or with 40 MeV electron beam. The layout of the complete project plan is shown in Fig. 1.

THE PROJECT – DELHI LIGHT SOURCE (DLS)

The compact light source project will make IUAC a unique national facility with the potential to deliver THz, IR, X-rays and electron beams as well as the energetic ion beams from different ion accelerators. The schematic of the layout of the Delhi Light Source is shown in Fig. 1. The project will be executed in three phases, namely:

(a) Phase-I: to produce THz radiation from a RT photocathode RF gun.
(b) Phase-II: to produce THz radiation from the SC photocathode RF gun
(c) Phase-III: to increase the energy of the electron beam up to 40 MeV with the help of TESLA type resonators and to use this beam to produce THz, IR and X-rays.

The different phases are described in detail in the following sections:

ISBN 978-3-95450-133-5

FAST, MULTI-BAND PHOTON DETECTORS BASED ON QUANTUM WELL DEVICES FOR BEAM-MONITORING IN NEW GENERATION LIGHT SOURCES

T. Ganbold, School of Nanotechnology, University of Trieste, P. le Europa 1, 34127, Trieste, Italy
M. Antonelli, G. Cautero, R. Cucini, D. M. Eichert, W. H. Jark, R. H. Menk, Elettra – Sincrotrone Trieste S.C.p.A., S.S. 14 - km 163,5, 34149 Bazovizza, Trieste, Italy
G. Biasiol, CNR-IOM, S.S. 14 - km 163,5, 34149 Bazovizza, Trieste, Italy

Abstract

In order to monitor the photon-beam position for both diagnostics and calibration purposes, we have investigated the possibility to use InGaAs/InAlAs Quantum Well (QW) devices as position-sensitive photon detectors for Free-Electron Laser (FEL) or Synchrotron Radiation (SR).

Owing to their direct, low-energy band gap and high electron mobility, such QW devices may be used also at Room Temperature (RT) as fast multi-band sensors for photons ranging from visible light to hard X-rays. Moreover, internal charge-amplification mechanism can be applied for very low signal levels, while the high carrier mobility allows the design of very fast photon detectors with sub-nanosecond response times.

Segmented QW sensors have been preliminary tested with 100-fs-wide 400 nm laser pulses and X-ray SR. The reported results indicate that these devices respond with 100 ps rise-times to such ultra-fast laser pulses. Besides, linear scan on the back-pixelated device has shown that these detectors are sensitive to the position of each ultra-short beam bunch.

INTRODUCTION

Several Free-Electron Lasers (FEL) and Synchrotron Radiation (SR) applications require radiation-hard and fast *in-situ* detectors for diagnostics and calibration purposes [1].

The opportunity to use QW devices for photon detection has been proposed in infrared region [2]. Recently, we have reported on QW detectors working in the ultraviolet (UV) and X-ray regions for FEL and SR sources [3, 4]. These QW devices give the possibility to detect a broad energy range of incoming photons, due to the low and direct band gap of the active layers. Furthermore, high carrier mobility at room temperature (RT) makes it possible to detect ultra-fast light pulses operating in either air or vacuum without cooling equipment. Therefore, epitaxially grown metamorphic InGaAs/InAlAs QW devices are here proposed as fast, solid-state detectors for beam monitoring applications.

These novel detectors are good candidates to sense the position and the intensity of a beam meeting the demanding time-resolution requirements posed by recent SR and FEL sources. To this aim, the performances of these detectors have been assessed by measuring their response to ultra-fast laser pulses.

Preliminary experiments have been carried out through a table-top Ti-sapphire laser delivering 100-fs-wide pulses with a 400 nm wavelength. The structure of the aforementioned QW devices and the main results of these the tests are reported.

QUANTUM-WELL DEVICES

Device Structure and Characterization

These devices have been grown by Molecular Beam Epitaxy (MBE) at the CNR-IOM TASC Laboratory, Trieste. The starting material is a 500 µm thick epi-ready semi-insulating GaAs substrate. As shown in Fig. 1, in order to smooth the substrate surface a 200 nm thick GaAs layer was grown on its top, followed by a 200 nm thick GaAs/AlGaAs superlattice, which blocks the impurities from the bulk. Another 200 nm thick GaAs layer was introduced before an $In_xAl_{1-x}As$ step-graded buffer layer (BL) with increasing x from 0.15 to 0.75; this allows the lattice constant to be tuned in order to reduce the residual strain due to the lattice mismatch [5]. A 25 nm thick $In_{0.75}Ga_{0.25}As$ QW containing a 2D Electron Gas (2DEG) was placed in between 50 nm thick $In_{0.75}Al_{0.25}As$ barrier layers and a delta Si-doping was introduced in the upper barrier.

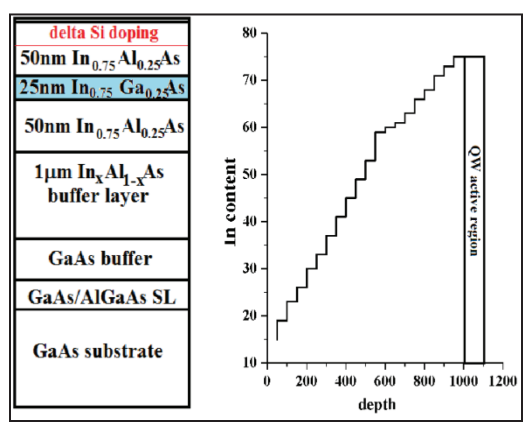

Figure 1: Layered structure of the samples and nominal profile of the In content in the step-graded buffer layer.

Hall-bar measurements were performed to characterize the charge density and the carrier mobility in the QW at room temperature, resulting in $n=7.7\times10^{11}$ cm^{-2} and $\mu=1.1\times10^4$ $cm^2V^{-1}s^{-1}$, respectively. Top-to-bottom resistance was found to be of the order of 100 MΩ at

ISBN 978-3-95450-133-5

HARD X-RAY SELF-SEEDING SETUP AND RESULTS AT SACLA

T. Inagaki#, T. Tanaka, N. Adumi, T. Hara, R. Kinjo, H. Maesaka, Y. Otake, K. Togawa, M. Yabashi, H. Tanaka, T. Ishikawa, RIKEN SPring-8 Center, Sayo, Hyogo, Japan
Y. Inubushi, T. Kameshima, H. Kimura, A. Miura, H. Ohashi, T. Ohata, K. Tono, H. Yamazaki, S. Goto, Japan Synchrotron Radiation Research Insititute, Sayo, Hyogo, Japan
T. Hasegawa, S. Tanaka, SPring-8 service Co. Ltd., Sayo, Hyogo, Japan

Abstract

A self-seeded XFEL system using a Bragg transmission scheme has been implemented at the compact XFEL facility SACLA, in order to generate a single-mode XFEL. The setup is composed of a small magnetic chicane that can delay the electron beam by up to 50 fs, and a diamond single crystal with the thickness of 180 μm. In the beam commissioning, intensity enhancement at 10 keV X-rays due to the self-seeding was observed with a single-shot spectrometer. A spectral bandwidth of the seeded FEL was reduced to 3 eV, being approximately 1/10 of that of SASE. After partial optimizations of the number of undulator segments, a temporal delay of the electron beam, and an rf phase of the pre-buncher cavity, the peak intensity of the seeded FEL signal in the averaged spectrum was 4 times higher than the SASE. Observation probability of the seeded FEL signal in the single-shot spectra was 42%. Although further optimization and improvement are still necessary to keep long-term stability, the initial step was successful to open up the routine operation in a near future.

INTRODUCTION

Self-seeding in the X-ray free electron laser (XFEL) is an important method to improve the temporal coherence of the self-amplified spontaneous emission (SASE) and to obtain high peak brilliance with narrow spectral band width. In order to generate brilliant X-ray laser and supply to user experiments, the self-seeding system has been implemented in the Japanese XFEL facility, SPring-8 Angstrom Compact free electron LAser (SACLA) [1]. The scheme proposed at DESY [2] and firstly demonstrated in LCLS [3] was adopted, which uses a single diamond crystal in a forward Bragg diffraction (FBD) geometry to the initial SASE radiation from the first half of the undulators. It produces monochromatic tail components of transmitted X-ray pulses at a small time delay of several 10 fs. A compact magnetic chicane gives the delay to overlap the electron bunches and the monochromatic tail for seeding in the following undulators.

The hardware components were installed in parallel to the user operation from 2012. In August 2013, a vacuum chamber for housing a diamond single crystal was installed in the middle of the magnetic chicane. The commissioning started in October. After a number of tuning processes, significant spectral narrowing due to the self-seeding was confirmed at 10 keV. In the following sections, the configuration, the tuning process and the experimental results are described.

#inagaki@spring8.or.jp

SETUP

Figure 1 shows the configuration of SACLA and the self-seeding system. The electron beam from the thermionic cathode-type electron gun is sequentially accelerated and compressed at the accelerator section, to obtain high-density electron beam with the peak current of over several kA and the bunch length of several 10 fs. Then, the electron beam is led to the long undulator section composed of 21 segments of the in-vacuum undulators with the small periodic length of λ_u=18 mm and the maximum K-value (the magnetic deflection parameter) of 2.2.

Between the 8th undulator and the 9th undulator, the small magnetic chicane composed of 4 dipole magnets was inserted, in order to detour the electron beam from the diamond crystal and to provide a tunable time delay of maximum 50 fs. In the middle of the chicane, the diamond crystal chamber was installed, in order to generate the FBD of the SASE radiation from the upstream undulators. Figure 2 shows the schematic of the chamber. A diamond single crystal with the thickness of 180 μm is mounted on a holder in the vacuum chamber. The holder is attached on a multi-axis mechanical stage. The crystal is retracted from the beam axis during the usual SASE operation, while it is inserted for the self-seeding. The rotation of the crystal tuned the Bragg angle θ. The diffracted photon is measured by a photo-diode and a CCD detectors, attached on the 2θ-rotational arm. Since the photon energy for our commissioning was 10 keV, the Bragg angle θ was set at about 44 degrees for 400 reflection of the diamond crystal. Under these configurations, monochromatic tail components in the transmitted radiation arise around 10 fs and 24 fs after the initial radiation, according to the theoretical calculation of FBD [3, 4]. The electron beam delaying at the chicane was overlapped to the radiation in the downstream undulators.

Properties of the FEL radiation were measured at the experimental hall. Thin-foil beam monitors in the optics hutch were used as the in-line monitors of the intensity and the center-of-mass position of the radiation [5]. The energy spectrum of the radiation was measured by the single-shot spectrometer [6]. The spectral resolution and the range are selected by changing the diffraction plane of the silicon crystal. The configuration using (220) plane has a wide measuring range of 100 eV, which was used

ISBN 978-3-95450-133-5

GENERATION OF OPTICAL ORBITAL ANGULAR MOMENTUM USING A SEEDED FREE ELECTRON LASER*

P. Rebernik Ribič, D. Gauthier, Elettra, Trieste, Italy
G. De Ninno, Elettra, Trieste, Italy and University of Nova Gorica, Slovenia

Abstract

We propose an effective scheme for the generation of intense extreme-ultraviolet (XUV) light beams carrying orbital angular momentum (OAM). The light is produced by a high-gain harmonic-generation free-electron laser (HGHG FEL), seeded using a laser pulse with a transverse staircase-like phase pattern. The transverse phase modulation in the seed laser is obtained by putting a phase-mask in front of the focusing lens, before the modulator. The staircase-like phase pattern is effectively transferred onto the electron beam in the modulator and the microbunching structure is preserved after frequency up-conversion in the radiator. During light amplification in the radiator, diffraction and mode selection drive the radiation profile towards a dominant OAM mode at saturation. With a seed laser at 260 nm, gigawatt power levels are obtained at wavelengths approaching those of soft x-rays. Compared to other proposed schemes to generate OAM with FELs, our approach is robust, easier to implement, and can be integrated into already existing FEL facilities without extensive modifications of the machine layout.

INTRODUCTION

At present, the radiation modes of modern free-electron lasers (FELs) working at saturation are limited to a fundamental Gaussian-like mode with no azimuthal phase variation. This is true for FELs based on self-amplified spontaneous emission (SASE), where the amplification starts from electron shot-noise [1–6], as well as for seeded FELs, such as those based on high-gain harmonic-generation (HGHG), where the amplification process is triggered by a coherent input seed [7–9].

Generation of high-order radiation modes, however, is a subject of strong interest, not only from the fundamental point of view but also in practical applications. In particular, helically phased light beams or optical vortices with a field dependence of $\exp(il\phi)$, where ϕ is the azimuthal coordinate and l an integer referred to as the topological charge, are currently among intensively studied topics in optics. These light beams, which carry orbital angular momentum (OAM) [10] that can be transferred to atoms, molecules, and nanostructures [11–16], have already been utilized at visible and infrared wavelengths in a wide variety of applications, ranging from micromanipulation [17], detection of spinning objects [18], microscopy [19], and optical data transmission [20–22]. Perhaps the most promising applications of vortex beams at short wavelengths are in x-ray magnetic circular dichroism, where different OAM states allow the separation of quadrupolar and dipolar transitions [23], photoionization experiments, where the dipolar selection rules are violated giving rise to new phenomena beyond the standard effect [24], and in resonant inelastic x-ray scattering, where vortex-beam-mediated coupling to vibrational degrees of freedom could provide important information on a wide range of molecular materials [25].

Hemsing and coworkers proposed two clever approaches to generate intense vortex beams at short wavelengths using FELs. The first one exploits the interaction of an electron beam (e-beam) with a seed laser in a helical undulator [26], while the second one is based on the echo-enabled harmonic generation (EEHG) scheme [27], where two seed lasers and two magnetic chicanes are used to produce harmonic microbunching of an e-beam with a corkscrew distribution [28]. A proof-of-principle experiment has recently been performed to demonstrate the first scheme using a single undulator section, generating optical vortices at 800 nm [29] . In this approach, however, OAM beams are produced at the fundamental frequency of the seed. Reaching short wavelengths would therefore require a coherent XUV or x-ray input signal, which is not trivial to obtain. On the other hand, the technique based on EEHG uses a relatively complex setup, which has yet to be thoroughly tested in experiments.

THE SCHEME TO GENERATE OAM WITH A SEEDED FEL

The scheme is shown in Fig. 1. The main difference with respect to the standard HGHG setup [30] is the use of an optical phase mask in order to create a transverse phase modulation in the seed laser profile. Naively, the simplest way to produce an XUV/x-ray optical vortex with this setup would be to seed the FEL directly with an OAM beam, by using a spiral phase plate as the phase mask. However, this approach fails at short wavelengths. The reason is that the topological charge l_n of higher harmonics is multiplied with the harmonic number n [28]; i.e., $l_n = ln$, where l is the topological charge of the seed. This results in a high-order OAM mode at the entrance of the radiator, which is tuned to $\lambda = \lambda_s/n$, where λ_s is the seed laser wavelength. Due to a lower coupling with the e-beam and stronger diffraction, this high-order OAM mode is not amplified in the radiator [28], leading to a dominant fundamental (non-OAM) mode at saturation.

The idea behind our approach is the following: instead of a helical transverse phase profile, a four quadrant staircase-like phase structure is imprinted onto an axially symmetric e-

* The research was in part funded by the TALENTS UP Programme (7th FP, Specific Programme PEOPLE, Marie Curie Actions - COFUND) G.A. 600204

ISBN 978-3-95450-133-5

FIRST LASING FROM A HIGH POWER CYLINDRICAL GRATING SMITH-PURCELL DEVICE*

H.P. Bluem#, R.H. Jackson, J.D. Jarvis, A.M.M. Todd, Advanced Energy Systems, Princeton, NJ, USA
J. Gardelle, P. Modin, CEA-CESTA, Le Barp cedex, France
J. T. Donohue, CENBG, Gradignan, France

Abstract

Many applications of THz radiation remain impractical or impossible due to an absence of compact sources with sufficient power. A source where the interaction occurs between an annular electron beam and a cylindrical grating is capable of generating high THz power in a very compact package. The strong beam bunching generates significant power at the fundamental frequency and harmonics. A collaboration between Advanced Energy Systems and CEA/CESTA has been ongoing in performing proof-of-principle tests on cylindrical grating configurations producing millimeter wave radiation. First lasing was achieved in such a device. Further experiments performed with a 6 mm period grating produced fundamental power at 15 GHz, second harmonic power at 30 GHz and, although not measured, simulations show meaningful third harmonic power at 45 GHz. Comparison with simulations shows very good agreement and high conversion efficiency. Planned experiments will increase the frequency of operation to 100 GHz and beyond. Ongoing simulations indicate excellent performance for a device operating at a fundamental frequency of 220 GHz with realistic beam parameters at 10 kV and simple extraction of the mode.

BACKGROUND & INTRODUCTION

The generation of tunable, narrowband, coherent, terahertz (THz) radiation is a topic of great interest across a wide variety of disciplines and applications. Although significant scientific and industrial opportunities exist, progress in the development of high-power compact sources has been frustrated by various technical and engineering challenges. AES is developing a flexible, compact, THz source architecture that addresses many of these historical challenges and aims to deliver high average power from 0.2 to 2 THz. The AES concept is a cylindrical extension of the so-called Smith-Purcell free-electron laser (SPFEL). The SPFEL is a type of backward-wave oscillator (BWO) that lases on an evanescent wave (surface wave) supported by an open slow-wave structure (SWS) [1].

When an electron passes in close proximity to an open, periodic, metallic grating, energy is transferred from the electron to radiative modes of the grating. This so-called Smith-Purcell radiation (SPR) is emitted over a broad spectrum with the wavelength of the emitted photons being correlated to the angle of emission by the Smith-Purcell relation:

$$\lambda_{SP} = \frac{L}{|p|}\left(\frac{1}{\beta} - \cos\theta\right),$$

where L is the grating period, p is the diffraction order of the grating, β is the electron velocity normalized to the speed of light, and θ is the emission angle relative to the beam axis [2]. The SPR radiation is always at a higher frequency than the backward surface wave, except when the fundamental is confined laterally on a scale comparable to its wavelength [3]. When the electron beam is bunched by the backward wave interaction the SPR power is dramatically enhanced and is strongly peaked at angles corresponding to harmonics of the bunching frequency [4]. Under these conditions the SPR is said to be superradiant and significant power output can be generated at high frequencies.

The radiation output of a SPFEL is then a combination of the fundamental and the superradiant SPR at its harmonics. The power in the backward wave is much higher than the SPR power; however, because the backward wave is nonradiative, some form of outcoupling is required. Simple, although suboptimal, outcoupling is provided by scattering off of the discontinuities at the ends of the grating. Optimized structures can deliver efficient outcoupling in the forward or backward directions.

The SPFEL can easily be designed for a specific frequency by adjusting the grating geometry and the beam energy. A limited active-tuning range is possible via adjustment of the beam energy. Ultimately, the highest frequency achievable will be determined by current density, energy spread, and ohmic losses in the grating, and fabrication tolerances. This is highly dependent on the specifics of the system design. Higher frequency output, albeit at lower power, may be provided by the coherently enhanced SPR.

The AES concept, which utilizes a cylindrical SWS and a high-power annular electron beam, is compatible with established transport and compression techniques from the microwave-tube industry. Furthermore, the cylindrical geometry provides for maximum grating surface area in a compact package. The open grating design provides significant flexibility in the generation and extraction of fundamental and harmonic radiation; this is a major point of contrast with other e-beam driven sources.

The AES system is a significant departure from previous designs. As such, it was determined that the demonstration of key concepts at microwave frequencies

*Work supported by the Office of Naval Research and the Office of Naval Research Global
#bluem@aesprin.com

ISBN 978-3-95450-133-5

BEAM OPERATION OF THE PAL-XFEL INJECTOR TEST FACILITY*

J.-H. Han†, J. Hong, J. H. Lee, M. S. Chae, S. Y. Baek, H. J. Choi, T. Ha, J. Hu, W. H. Hwang, S. H. Jung, C. B. Kim, C. H. Kim, I. Y. Kim, J. M. Kim, S. H. Kim, H. S. Lee, S.-J. Lee, Y. Y. Lee, C.-K. Min, G. Y. Mun, D. H. Na, S.-J. Park, S.-S. Park, Y. J. Park, Y. K. Son, H. R. Yang, H.-S. Kang, I. S. Ko, Pohang Accelerator Laboratory (PAL), Pohang, 790-834, Republic of Korea

Abstract

The Pohang Accelerator Laboratory X-ray Free electron Laser (PAL-XFEL) project was launched in 2011. This project aims at the generation of X-ray FEL radiation in a range of 0.06 to 6 nm for photon users with a bunch repetition rate of 60 Hz. The machine consists of a 10 GeV normal conducting S-band linear accelerator and five undulator beamlines. The linac and two undulator beamlines will be constructed by the end of 2015 and first FEL radiation is expected in 2016. As a part of preparation for the project, an Injector Test Facility was constructed in 2012. Since December 2012, beam commissioning is being carried out to find optimum operating conditions and to test accelerator components including RF, laser, diagnostics, magnet, vacuum and control. We present the status of beam commissioning and components tests at the test facility.

INTRODUCTION

The Pohang Accelerator Laboratory X-ray Free-Electron Laser (PAL-XFEL) project was started in 2011 [1–3]. This project aims at the generation of X-ray FEL radiation in a range of 0.06 to 6 nm for users. The machine consists of a 10 GeV electron linac and five undulator beamlines. The linac is based on the normal-conducting S-band technology, which has been used for the 3 GeV full energy injector linac of PLS-II, the 3rd generation light source at PAL, over 20 years [4]. As Phase-I of PAL-XFEL, one hard X-ray undulator beamline with two experiment stations and one soft X-ray undulator beamline with one experiment station are under preparation. Both hard and soft X-ray undulator systems are variable-gap, out-vacuum type.

This new machine is being built on the northern hill of the PAL campus (see Fig. 1). The building construction was started in autumn 2012. The building will be ready by December 2014. Accelerator components will be installed from January 2015 during the year. The machine is capable of 60 Hz operation with a single bunch initially. Upgrade to 120 Hz as well as two micro-bunch is foreseen as next phase in a few years. A fast kicker to divide electron pulses into the two undulator beamlines is considered as future upgrade as well. PAL-XFEL commissioning will be started from winter 2015. Beam commissioning will be carried out at a repetition rate of 10 Hz for the first year of operation mainly due to the operation budget. First FEL is foreseen in early summer 2016.

At the beginning of the project in 2011, the construction of the Injector Test Facility (ITF) was started [5]. The facility was built in the extended building of the PLS-II full energy injection linac as shown in Fig. 1. The concrete tunnel, RF gallery, laser clean room and control room were prepared.

The RF system, accelerator components, laser system and control system were installed from summer to autumn 2012. The first beam was generated and transported to the beamline end in December 2012. Emittance measurement was started in spring 2013. Since then, beam test of diagnostics has been carried out.

In this paper, we describe the construction, component installation, beam test of diagnostics and beam property measurement. Some experiment results are shown even though empirical optimization is ongoing.

BUILDING

At the northwestern end of the PLS-II linac building, there has been a multi-purpose test area. This test area is now utilized as the Accelerator Test Facility (ATF) of PAL-XFEL. At ATF, high power modulators, klystrons, low level RF modules, accelerator structures, RF power douplers (SLAC energy doubler, SLED) and SiC loads are tested.

This test area was extended in 2012 for ITF. The extended floor area is about 30 m long and 14 m wide. A concrete tunnel with 1.5 m thickness was built in ITF. The inner area of the tunnel is 19.2 m long and 3.5 m wide. The view of the ITF tunnel and gallery is shown in Fig. 2. The roof of the tunnel is removed for installation work in the photograph. During the operation, the roof is covered with the concrete plates for radiation safety.

A laser clean room was constructed on the same floor of the tunnel and gallery. Temperature and humidity is controlled in the room. On top of the laser room, a control room was constructed.

ACCELERATOR DESIGN

The ITF accelerator was designed for the test of the first 9 m of the PAL-XFEL linac. An S-band (2.856 GHz) photocathode gun and two 3 m long S-band (2.856 GHz) constant-gradient traveling-wave structures are used for electron beam generation and acceleration. The layout is shown in Fig. 3.

Even though the PAL-XFEL injector will have three S-band accelerating structures, the design using two structures was adopted at ITF. After the two structures beam energy is

* Work supported by The Ministry of Science, ICT and Future Planning of the Korean Government

† janghui_han@postech.ac.kr

ISBN 978-3-95450-133-5

EUROPEAN XFEL CONSTRUCTION STATUS

W. Decking*, DESY, Hamburg, Germany
F. Le Pimpec, European XFEL GmbH, Hamburg, Germany
for the European XFEL Project Team

Abstract

The European XFEL is presently being constructed in the Hamburg region, Germany. It aims at producing X-rays in the range from 260 eV up to 24 keV out of three undulators that can be operated simultaneously with up to 27000 pulses/second. The FEL is driven by a 17.5 GeV linear accelerator based on TESLA-type superconducting accelerator modules. This paper presents the status of major components, the project schedule and a summary of beam parameters that are adapted to the evolving needs of the users.

INTRODUCTION

The European XFEL [1] construction has started in 2009 with the ground-breaking for the underground buildings - about 5.5 km of tunnels, six access shafts, two underground dump halls, the injector building and the 4500 m^2 experimental hall. The underground construction is finished and the erection of the above ground buildings on three different sites is well underway. The series production of components is in full swing with many parts already being ready for installation. The completion of the construction phase was planned for end of 2015. Due to the delayed delivery of several components, a new schedule was adopted with the completion date shifted to end of 2016.

Encouraged by the successful operation of LCLS and SACLA and based on the small emittances measured for the XFEL photo-cathode RF-gun at PITZ (DESY/Zeuthen) [2], the European XFEL has adjusted its target parameters in 2011, see Table 1. The new parameter set enlarges the performance range of the facility [3], but puts a strain on different sub-systems, especially for operation at very low charge (20 pC). All beam diagnostics are affected as well as the RF stabilization and the beam-stabilizing feedback systems. As a rule, the original 1 nC-case specifications could be extended down to 0.1 nC and a limit to the deterioration in performance for even lower charges was set.

Table 1: European XFEL Electron Beam Properties

Quantity	Target Parameters
Electron Energy	8/12/14/17.5 GeV
Bunch Charge	0.02 - 1 nC
Norm. Slice Emittance at Und.	0.4 - 1.0 mm mrad
Slice Energy Spread at Und.	4 - 2 MeV
Peak Current	5 kA

* winfried.decking@desy.de

Figure 1 summarizes the photon energy reach of the European XFEL for different accelerator energies and undulator gap settings. The facility covers the photon energy range from the Carbon K-edge up to above 25 keV in the first SASE harmonic.

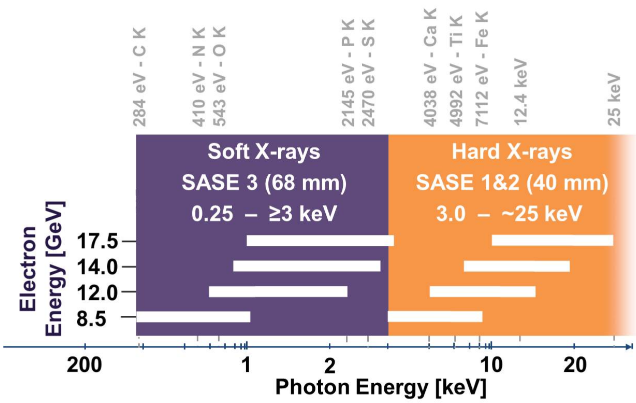

Figure 1: Photon energy reach of the two undulator types of the European XFEL at different electron energies.

ACCELERATOR

Injector and Bunch Compression

The XFEL RF gun is similar to the operating gun at FLASH, DESY. It has been conditioned at PITZ [4]. RF operation in the design configuration in the XFEL injector tunnel took place in December 2013 [5]. The photo-cathode laser - a Nd:YLF laser operating at 1047 nm converted to UV wavelength in two stages - has been delivered by the Max Born Institute, Berlin [6]. The RF gun should produce its first beam after the completion of the laser beam line in October 2014. The injector tunnel will host, in addition to the gun, one standard XFEL superconducting 1.3 GHz module, a superconducting 3.9 GHz module with an accelerating voltage of up to 40 MV, a laser heater and a diagnostic section. The final installation of all components is scheduled for mid 2015. The complete injector can be commissioned and operated independently from the ongoing installation work in the main accelerator tunnel.

The European XFEL employs a three-stage bunch compression scheme to reduce both micro-bunching and the required 3.9 GHz voltage. All magnetic chicanes are tunable within a wide range of R_{56} to allow for flexible compression scenarios, for instance balancing peak current and arrival time stability with LLRF performance. The tuning is achieved by means of large pole width dipole magnets and accordingly wide (400 mm) vacuum chambers. All

ISBN 978-3-95450-133-5

THE NEW IR FEL FACILITY AT THE FRITZ-HABER-INSTITUT IN BERLIN

Wieland Schöllkopf, Sandy Gewinner, Wolfgang Erlebach, Heinz Junkes, Andreas Liedke, Gerard Meijer, Alexander Paarmann, Gert von Helden, Fritz-Haber-Institut der Max-Planck-Gesellschaft, Faradayweg 4-6, 14195 Berlin, Germany
Hans Bluem, David Dowell*, Ralph Lange*, John Rathke, Alan M.M. Todd, Lloyd M. Young*, Advanced Energy Systems, Inc., 27 Industrial Blvd., Medford, NY 11763, USA
Ulf Lehnert, Peter Michel, Wolfgang Seidel, Rudi Wünsch, Helmholtz-Zentrum Dresden-Rossendorf, Bautzner Landstraße 400, 01328 Dresden, Germany
Stephen C. Gottschalk, STI Optronics, Inc., 2755 Northup Way, Bellevue, WA 98004, USA

Abstract

A mid-infrared oscillator FEL has been commissioned at the Fritz-Haber-Institut. The accelerator consists of a thermionic gridded gun, a subharmonic buncher and two S-band standing-wave copper structures. It provides a final electron energy adjustable from 15 to 50 MeV, low longitudinal (<50 keV-ps) and transverse emittance (<20 π mm-mrad), at more than 200 pC bunch charge with a micro-pulse repetition rate of 1 GHz and a macro-pulse length of up to 15 µs. Pulsed radiation with up to 50 mJ macro-pulse energy at about 0.5% FWHM bandwidth is routinely produced in the wavelength range from 4 to 48 µm. Regular user operation started in Nov. 2013 with 6 user stations. The user experiments include nonlinear spectroscopy of solids, spectroscopy of bio-molecules (peptides and small proteins), which are conformer selected in the gas-phase or embedded in superfluid helium nano-droplets at 0.4 K, as well as vibrational spectroscopy of mass-selected metal-oxide clusters and protonated water clusters in the gas phase.

INTRODUCTION

In 2008 the Fritz-Haber-Institut (FHI) embarked on setting up an infrared FEL facility. The aim was to set up an FEL that is capable of providing intense, pulsed laser radiation, continuously tunable from a few micron in the near to mid-infrared (MIR) all the way to several hundred micron in the far-infrared (FIR), or Tera-Hertz (THz) regime. Installation of the FEL started in mid 2011 in a new, dedicated FEL building on the FHI campus in Berlin. We observed first lasing in 2012 [1–3] and started user operation in November 2013.

IR radiation in the spectral region from 3 to 100 µm is often referred to as the molecular fingerprint region, because it is the region in which the fundamental vibrational modes of molecules, clusters or solid materials are located. The vibrational IR spectrum is intimately connected to the molecular structure and dynamics, which is why IR spectroscopy is one of the basic methods for molecular structure characterization. The highest energy vibrations, involving stretching motions of light atoms, are found around a wavelength of 3 µm. Lower energy vibrations are found throughout the IR region, down to the FIR region beyond 100 µm. The vibrational frequencies in the FIR result from heavy atoms and/or weak bonds, or from soft modes that involve large amplitude motions and global geometry changes. Thus, FIR spectroscopy also allows to study the folding dynamics of (bio)molecules.

FIR radiation can also be used to directly probe surface-adsorbate vibrations. This allows to study the structure and dynamics of adsorbates on surfaces, to measure the properties of deposited or gas-phase cluster materials, or to investigate real-world catalysts in action. In addition, the intense FEL radiation can readily induce multiple photon excitation processes and is well suited for double-resonance experiments with other, table-top laser systems.

DESIGN OF THE FHI FEL

To cover the full wavelength range of interest from about 4 to 500 µm the basic design of the FHI FEL includes two different undulator lines as outlined in Fig. 1 [1–5]. The MIR branch works for wavelengths up to about 50 µm and the FIR branch covers the wavelength range from about 40 to 500 µm. A normal-conducting linear accelerator provides electrons of up to 50 MeV energy with a beam transport system feeding either of the FEL branches or the diagnostics beamline (Fig. 1).

Electron Accelerator and Beamline

The electron accelerator and beamline system, designed, built, and installed by Advanced Energy Systems, Inc. (AES), has been described before [4–7]. In brief, the accelerator system is comprised of a gridded thermionic gun, a subharmonic buncher cavity and two standing-wave, $\pi/2$ copper linacs. The first of the two S-band (2.99 GHz) linacs accelerates the electron bunches to a nominal energy of 20 MeV, while the second one accelerates or decelerates the electrons to deliver any final energy between 15 and 50 MeV. A chicane between the linacs allows for adjustment of the electron bunch length as required.

Key performance parameters of the accelerator are low longitudinal (<50 keV-psec) and transverse emittance (<20 π mm-mrad) at more than 200 pC bunch charge with a micro-bunch repetition rate of 1 GHz. The maximum

* Consultants to Advanced Energy Systems, Inc.

ISBN 978-3-95450-133-5

FLASH: FIRST SOFT X-RAY FEL OPERATING TWO UNDULATOR BEAMLINES SIMULTANEOUSLY

K. Honkavaara*, B. Faatz, J. Feldhaus, S. Schreiber, R. Treusch, M. Vogt,
DESY, Hamburg, Germany†

Abstract

FLASH, the free-electron laser user facility at DESY (Hamburg, Germany), has been upgraded with a second undulator beamline FLASH2. After a shutdown to connect FLASH2 to the FLASH linac, FLASH1 is back in user operation since February 2014. Installation of the FLASH2 electron beamline has been completed early 2014, and the first electron beam was transported into the new beamline in March 2014. The commissioning of FLASH2 takes place in 2014 parallel to FLASH1 user operation. This paper reports the status of the FLASH facility, and the first experience of operating two FEL beamlines.

INTRODUCTION

FLASH [1–4], the free-electron laser (FEL) user facility at DESY (Hamburg), delivers high brilliance XUV and soft X-ray FEL radiation for photon experiments.

The TESLA Test Facility (TTF) Linac [5], constructed at DESY in mid 1990's and operated until end of 2002, was originally dedicated to test the feasibility of high gradient superconducting accelerator technology in the framework of the TESLA linear collider project [6]. In addition, it was used to drive a SASE (Self Amplified Spontaneous Emission) free-electron laser pilot facility TTF-FEL [7, 8] at photon wavelengths from 80 nm to 120 nm [9, 10] to demonstrate the feasibility of SASE FELs in the VUV range. Based on the experience gathered from the TTF-FEL operation, FLASH – originally called VUV-FEL at TTF2 – was constructed in 2003-04.

The first lasing of FLASH at 32 nm was achieved in January 2005 [11]. Since summer 2005 FLASH has been operated as an FEL user facility, being the first facility in the world delivering VUV and XUV FEL radiation for photon experiments. During 2005-2007, FLASH delivered FEL radiation in wavelengths from 13 nm to 47 nm (fundamental), entering the water window with the 3rd and 5th harmonics [1]. An energy upgrade to 1 GeV in summer 2007 extended the range to the soft X-rays with wavelengths down to 6.5 nm [12, 13]. The next upgrade [14], accomplished in 2009/10, led to major modifications of the facility, including, for example, the installation of third harmonic RF cavities to linearize the longitudinal phase space and an energy upgrade to 1.25 GeV. This allowed lasing with wavelengths down to 4.1 nm [15], entering thus the water window also with fundamental wavelengths.

The most recent upgrade to include a second undulator beamline has been carried out in 2011-14, mostly parallel to the FLASH user operation. After a shutdown in 2013 to connect the new beamline to the FLASH linac, the operation re-started in August 2013. Since February 2014, FLASH is back in user operation. The beam commissioning of the second undulator beamline (FLASH2) has started in March 2014.

* katja.honkavaara@desy.de
† for the FLASH team

Table 1: FLASH Parameters 2014

Electron beam		
Energy	MeV	380 - 1250
Bunch charge	nC	0.08 - 1
Bunches / train		1 - 500
Bunch spacing	μs	1 - 25
Repetition rate	Hz	10
FEL radiation		
Wavelength (fundamental)	nm	4.2 - 45
Average single pulse energy	μJ	10 - 500
Pulse duration (fwhm)	fs	< 50 - 200
Spectral width (fwhm)	%	0.7 - 2
Peak power	GW	1 - 3
Photons per pulse		10^{11} - 10^{13}
Peak brilliance	*	10^{29} - 10^{31}
Average brilliance	*	10^{17} - 10^{21}

* photons / (s mrad^2 mm^2 0.1 % bw)

This paper reports the status of the FLASH facility, and the first experience of operating two undulator beamlines. Part of the material discussed here has been presented in previous conferences, most recently in [4].

FLASH FACILITY

The layout of the FLASH facility is shown in Fig. 1. The first undulator beamline, being in operation since 2004, is referred to FLASH1, the new one to FLASH2. Table 1 shows typical FLASH operating parameters. These parameters are not all achieved simultaneously, but indicate the overall span of the performance.

A superconducting linac driven by an RF-gun based photoinjector provides a train of electron bunches: the maximum bunch train length is 800 μs, and it can be shared between the two undulator beamlines. Several discrete bunch spacings between 1 μs (1 MHz) and 25 μs (40 kHz) are possible. The bunch train repetition rate is 10 Hz. The typical bunch charge ranges from 80 pC to 1 nC.

The photocathode laser system has two independent lasers, both based on an actively mode-locked pulse train oscillator with a linear chain of fully diode pumped Nd:YLF ampli-

ISBN 978-3-95450-133-5

THz STREAK CAMERA FOR FEL TEMPORAL DIAGNOSTICS: CONCEPTS AND CONSIDERATIONS

Pavle Juranić, Rafael Abela, Rasmus Ischebeck, Luc Patthey, Claude Pradervand, Milan Radović, Volker Schlott, Andrey Stepanov, PSI, Villigen PSI, Switzerland
Ishkhan Gorgisyan, Christoph P. Hauri, Leonid Rivkin,
PSI, Villigen PSI, Switzerland, and EPFL, Lausanne, Switzerland
Balazs Monoszlai, PSI, Villigen PSI, Switzerland, and University of Pécs, Hungary
Rosen Ivanov, Peter Peier, DESY, Hamburg, Germany
Jia Liu, XFEL.EU, Hamburg, Germany
Kanade Ogawa, Shigeki Owada, Tadashi Togashi, Makina Yabashi,
RIKEN SPring-8 Center, Sayo-cho, Sayo-gun, Hyogo, Japan

Abstract

The accurate measurement of the arrival time of a hard x-ray free electron laser (FEL) pulse with respect to a laser is of utmost importance for pump-probe experiments proposed or carried out at FEL facilities around the world. This paper presents the latest device to meet this challenge, a THz streak camera, and discusses the challenges in its design, use, and analysis of results.

INTRODUCTION

Laser pump, x-ray probe experiments performed at FEL facilities around the world [1, 2, 3, 4, 5] typically want to use short pulse length and intense coherent x-ray radiation to perform experiments with sub-picosecond time resolution. As they go towards improved temporal resolutions, the experiments require accurate measurements of the arrival times of the FEL pulses relative to a laser pump on the sample they are probing. This measurement must also be non-invasive, allowing the experimenters the maximum use of the X-ray beam for their work rather than for diagnostics.

Several methods have been proposed and implemented in the past to meet this diagnostics challenge: transmission/reflectivity spatial and spectral encoding used for soft and hard x-rays at FLASH, SACLA, and LCLS [6, 7, 8, 9], the THz streak camera for soft x-rays at FLASH [10, 11] and other methods [12, 13, 14]. These methods all have their advantages and drawbacks, and the only one that has been attempted for hard x-ray arrival time measurement is the spatial/spectral encoding setup, which has an arrival time accuracy of on the order of 10 fs RMS [6, 9]. The potentially more accurate THz streak camera has not been attempted for use at hard x-ray sources due to the small photoionization cross-section of the gas target and the difficulties in differentiating jitters in the photon energy of the FEL beam from an arrival time signal of the FEL beam by electron spectroscopy. The Photon Arrival and Length Monitor (PALM) prototype chamber [15] developed at the Paul Scherrer Institute (PSI) for the future SwissFEL facility mitigates both of these problems, measuring the pulse length, and the arrival times of hard x-ray FEL pulses relative to a THz pulse and the laser it is generated from.

CONCEPTS

The concept of the THz streak camera has been explained in the past in literature [16, 17, 18], and has shown itself capable of measuring pulse lengths of high-harmonic-generation (HHG) soft x-rays in table-top laser laboratories. The device can also be used to measure the arrival time of the x-ray relative to the THz pulse.

The THz streak camera uses a gas that is photoionized by the x-ray light as an electron emitter. The electrons are then subject to a time-varying vector potential generated by co-propagating THz radiation, the duration of which is longer than the pulse length of the x-ray pulse. A shift in the arrival time of the x-ray pulse translates to a shift in the kinetic energy gained by the electrons in the vector potential. The final kinetic energy of the photoelectrons K_f streaked by the vector potential U_p is

$$K_f = K_0 + 2U_p sin^2(\varphi_0) \pm \sqrt{8K_0U_p}\sin(\varphi_0) \quad (1)$$

where K_0 is the initial kinetic energy of the electrons at the time of ionization, φ_0 is the phase of the vector potential at the time of the ionization, and

$$U_p = \frac{e^2E_{THz}^2(t)}{4m_e\omega_{THz}^2} \quad (2)$$

$E_{THz}(t)$ is the (sinusoidal) THz electric field, e is the electron charge, m_e is the mass of the electron, and ω_{THz} is the frequency of the THz f in radians/s.

The time delay between the external THz field and the FEL pulse was controlled by a translation stage, and time of flight of the electrons under different time delays were recorded, forming a two dimensional (2D) streaked spectrogram. As shown in Eq. 1, the shape of the spectrogram is determined by the THz frequency, initial electron kinetic energy and the vector potential. The time-to-energy map can be extracted by recording the center of mass (COM) kinetic energy of each time delay and shot-to-shot arrival time of the FEL pulses related to the THz pulse are retrieved by recording the single-shot electron kinetic energy when the stage is set at the middle of the time-to-energy slope. The pulse lengths are measured by looking at the change in spectral width of

ISBN 978-3-95450-133-5

EXPERIMENTAL CHARACTERIZATION OF FEL POLARIZATION CONTROL WITH CROSS POLARIZED UNDULATORS

E. Ferrari[1,2], E. Allaria[1], J. Buck[3], G. De Ninno[1,4], B. Diviacco[1], D. Gauthier[1,4], L. Giannessi[1,5], Z. Huang[6], M. Ilchen[3,7], G. Lambert[8], A.A. Lutman[6], B. Mahieu[8], G. Penco[1], C. Spezzani[1], J. Viefhaus[9]
[1]Elettra – Sincrotrone Trieste S.C.p.A, Basovizza, Italy
[2]Università degli Studi di Trieste, Dipartimento di Fisica, Trieste, Italy
[3]European XFEL, Hamburg, Germany
[4]Laboratory of Quantum Optics, University of Nova Gorica, Ajdovscina, Slovenia
[5]ENEA C.R. Frascati, Frascati (Roma), Italy
[6]SLAC National Accelerator Laboratory, Menlo Park, CA, USA
[7]Stanford PULSE Institute, Menlo Park, CA, USA
[8]Laboratoire d'Optique Appliqueé, ENSTA, Palaiseau, France
[9]DESY, FS-PE, Hamburg, Germany

Abstract

Polarization control of the coherent radiation is becoming an important feature of recent and future short wavelength free electron laser facilities. While polarization tuning can be achieved taking advantage of specially designed undulators, a scheme based on two consecutive undulators emitting orthogonally polarized fields has also been proposed. Developed initially in synchrotron radiation sources, crossed polarized undulator schemes could benefit from the coherent emission that characterizes FELs. In this work we report the first detailed experimental characterization of the polarization properties of an FEL operated with crossed polarized undulators in the Soft-X-Rays. Aspects concerning the average degree of polarization and the shot to shot stability are investigated together with a comparison of the performance of various schemes to control and switch the polarization.

INTRODUCTION

FEL sources naturally produce radiation with precise polarization states as they use undulators. The polarization of light is in fact directly correlated to the symmetry of the electron trajectory in the magnetic device where radiation and electrons couple in the FEL process. Self Amplified Spontaneous Emission (SASE) FELs, which require several tens of meters of undulators, normally use linearly polarized undulators. The choice was mainly driven by the users' request. Moreover, linear undulators ensure high field quality and reduced cost. Otherwise, if different states of polarization are to be provided, elliptical polarized undulators [1,2] have been demonstrated to be suitable for both low and high gain FELs in the VUV and XUV wavelength range [3]. These devices implement a variable arrangement of the magnetic poles such that the magnetic field can assume a circular, elliptical or planar symmetry and so does the emitted radiation. Unfortunately they are not capable of fast variations of the polarization state as requested, for example, by circular dichroism experiments [4].

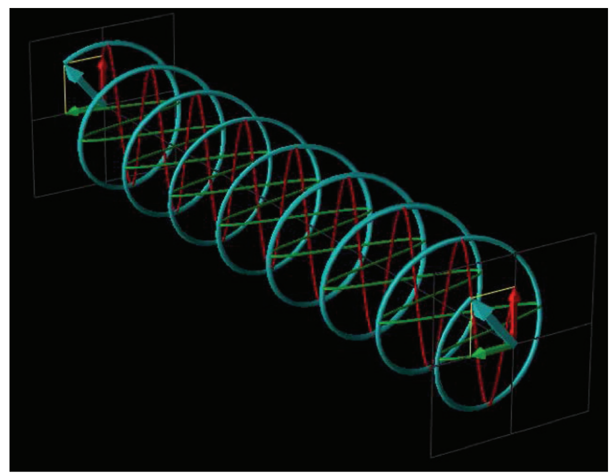

Figure 1: Crossed undulator scheme. One undulator is emitting horizontal polarization (green curve) while the other vertical polarization (red curve) to produce circularly polarized light (blue curve). Image obtained with [5].

CROSSED POLARIZED UNDULATORS

Other possible approaches for fully controlling the output polarization of the emitted radiation have been studied. One is the crossed undulator scheme [6,7].

Synchrotron Sources

Originally demonstrated on synchrotron light sources, the scheme relies on two undulators emitting orthogonally polarized light, e.g., one linear horizontal and one linear vertical undulator, see Figure 1. A suitable phase shifter separates the undulators in order to carefully control the relative phase between the two emitted waves. In this way the scheme is capable of producing linearly polarized light with an arbitrary direction as well as elliptically and circularly polarized light with arbitrary chirality.

ISBN 978-3-95450-133-5

A PLAN FOR THE DEVELOPMENT OF SUPERCONDUCTING UNDULATOR PROTOTYPES FOR LCLS-II AND FUTURE FELS

P. Emma, N. Holtkamp, H.-D. Nuhn, SLAC, Stanford, CA 94309, USA
D. Arbelaez, J. Corlett, S. Myers, S. Prestemon, R. Schlueter, LBNL, Berkeley, CA 94720, USA
C. Doose, J. Fuerst, Q. Hasse, Y. Ivanyushenkov, M. Kasa, G. Pile, E. Trakhtenberg, E. Gluskin, ANL, Argonne, IL 60439, USA

Abstract

Undulators serve as the primary source of radiation for modern storage rings, and more recently for the advent of Free-Electron Lasers (FELs). The performance of future FELs can be greatly enhanced using the much higher magnetic fields of superconducting undulators (SCU) [1]. For example, the LCLS-II hard x-ray undulator can be shortened by up to 70 m using an SCU in place of a PMU (permanent magnet undulator), or its spectral performance can be critically improved when using a similar length. In addition, SCUs are expected to be orders of magnitude less sensitive to radiation dose; a major issue at LCLS-II with its 1-MHz electron bunch rate. We present a funded R&D collaboration between SLAC, ANL, and LBNL, which aims to demonstrate the viability of superconducting undulators for FELs by building, testing, measuring, and tuning two 1.5-m long planar SCU prototypes using two different technologies: *NbTi* at ANL and Nb_3Sn at LBNL. Our goal is to review and reassess the LCLS-II HXR baseline plans (PMU) in July of 2015, after the development and evaluation of both prototypes, possibly in favor of an SCU for LCLS-II.

INTRODUCTION

The LCLS-II [2] FEL project at SLAC aims to construct a new continuous wave (CW), 4-GeV superconducting linac (SC-linac) [3], to feed either of two new undulators: 1) the Soft X-ray Undulator (SXU), or 2) the Hard X-ray Undulator (HXU). The HXU replaces the existing LCLS-I fixed-gap undulator and can be optionally fed by the existing 3-15-GeV copper (Cu) linac (120 Hz), presently used to drive the LCLS-I FEL. The spectral requirements for the SXU are 0.2-1.3 keV (SASE and self-seeded), while the HXU requires 1 keV to ≥ 5 keV (SASE, and self-seeded where possible) when driven by the SC-linac. The HXU spectral range, when driven by the Cu-linac (3-15 GeV), requires 1-25 keV.

The present (2014) baseline design uses two adjustable-gap, planar PMUs (NdFeB) with 39-mm (SXU) and 26-mm (HXU) periods and a 7.2-mm full magnetic gap, g_m. At 4 GeV (limited by SC-linac costs) the PMUs reach these requirements, but with little margin, especially in the HXU which barely produces 5 keV SASE, and cannot exceed 4 keV when self-seeded (limited hall length).

To remove these performance limitations, we propose an SCU undulator, at least for the HXU system, which significantly extends the spectral range when driven by the SC-linac, outperforms the presently foreseen PMU, and can even provide > 1 TW peak power when self-seeded, tapered, and driven by the Cu-linac. It also offers much less magnetic field sensitivity to radiation dose, an issue greatly magnified by the high-rate, high power linac.

Unresolved technical risk issues for SCU systems, such as field correction, and limited experience with SCUs in operating machines [4], [5], have led to an R&D plan with a goal of building, testing, and correcting two 1.5-m long prototype FEL undulators by July 2015 which meet LCLS-II HXU specifications using two different conductors: *NbTi* (21 mm period), and Nb_3Sn (19 mm period), each with an 8-mm magnet gap.

FEL PERFORMANCE MOTIVATION

The motivations for SCUs, especially in comparison to PMUs ("in" or "out" of vacuum), are listed below.

- Higher magnetic fields allow superior FEL performance, or reduced undulator length.
- No permanent magnetic material to be damaged by radiation, allowing long life and smaller gaps.
- Reduced resistive wakefield with a cold bore? [6].
- Much lower vacuum pressure limits gas scattering.
- Smaller footprint and simpler *K*-control than the typical massive adjustable-gap PMU.
- Easily oriented for vertical polarization, if desired.

Figure 1 shows LCLS-II (HXU, SC-linac) calculations [7] of the full undulator system length (2-m magnet segments and 0.7-m breaks; each with a BPM, quadrupole, and phase shifter) versus the upper-limit SASE photon energy that saturates within 80% of that undulator length at 4 GeV (beam parameters in Table 1).

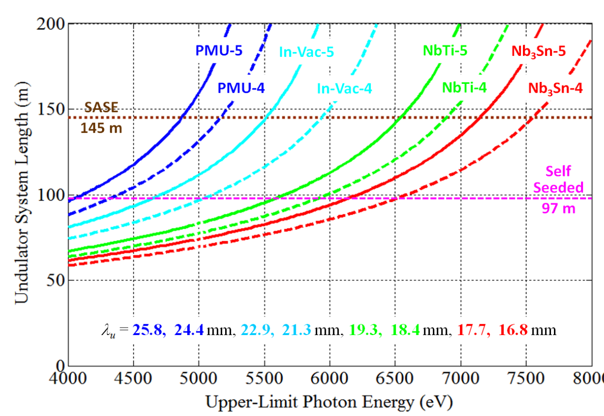

Figure 1: Undulator system length (with breaks) versus upper-limit SASE photon energy saturating in 80% of that undulator length at 4 GeV. Existing 145-m und. hall length is indicated.

ISBN 978-3-95450-133-5

SIMULTANEOUS MEASUREMENT OF ELECTRON AND PHOTON PULSE DURATION AT FLASH

S. Düsterer, DESY, Hamburg, Germany

Abstract

One of the most challenging tasks for extreme ultraviolet, soft and hard X-ray free-electron laser photon diagnostics is the precise determination of the photon pulse duration, which is typically in the sub 100 fs range. In a larger campaign nine different methods, which are able to determine such ultrashort photon pulse durations were compared at FLASH [1]. Radiation pulses at a wavelength of 13.5 nm and 24.0 nm together with the corresponding electron bunch duration were measured by indirect methods like analyzing spectral correlations, statistical fluctuations and energy modulations of the electron bunch, and also direct methods like autocorrelation techniques, THz streaking or reflectivity changes of solid state samples.A detailed description of the measurement campaign can be found in Ref. [2].

THE IDEA

One of the main characteristics of the new generation XUV to X-ray free-electron lasers is their ultrashort pulse duration in the femtosecond range. With these new sources ultra-fast reaction dynamics on the femtosecond time scale [3–5] can be investigated. It also allows the investigation of multi-photon processes in the XUV [6] to the X-ray range [7] which has not been possible before. The accurate knowledge of the FEL key parameters such as pulse peak power, radiance, and on-target irradiance for example is crucial for the analysis of experimental data. It turns out that the number of photons, the focal spot size and the spectral content in such short pulses can be measured reliably [8–11], while the pulse duration is still the most difficult parameter to be determined.

At FLASH [1] the duration of the generated photon pulses can be varied over a range of few tens of femtoseconds up to several 100s of fs. Still, a reliable method to measure pulse durations for the entire parameter range is not yet available. Although a variety of methods have been proposed, they all need to be set-up and tested experimentally to find out the best suited technique. In a campaign nine different techniques – three electron bunch duration measurements and six photon based methods – have been used to determine the photon pulse duration. They are either performed in a *direct* way by measuring the photon pulse duration at the experimental end stations or on the other hand by *indirect* methods measuring only parameters which are linked – by theoretical models – to the actual pulse duration. From the measured information the actual XUV pulse duration can be calculated using these models. From the experimental point of view, indirect methods are typically simpler to realize as compared to the direct approaches. However, they have to be verified and calibrated by direct methods. So far only photon pulse duration measurement campaigns using one (or two) measurement technique have been undertaken at FLASH in the last years [12–17]. Up to now there were no studies at FLASH or at any other XUV/X-ray FEL where many different methods were compared within one dedicated pulse duration measurement campaign as shown in Fig. 1.

The main motivation for this study was three-fold. Firstly, we wanted to address the question how well the results measured by the indirect methods agree with the direct ones. What are the error bars when comparing the different methods? How much information about the photon pulse duration can we deduce from the electron beam parameters in contrast to the photon based methods? Secondly, the realization of all nine techniques together under the same beam conditions allows a direct comparison of advantages and disadvantages of the individual techniques. Thirdly, the aim of the campaign was to identify sensitive parameters of the electron bunch compression and to develop recipes for routine operation to reliably establish a specific user requested XUV pulse duration at FLASH, especially for ultrashort pulses below 50 fs. The detailed description of all methods and the comparison of the various approaches can be found in the extended paper Ref. [2].

CONCLUSION

The FEL was tuned such that all pulses in the bunch train had roughly the same electron bunch and XUV pulse parameters for the measurements that were performed at 13.5 nm. For this case a remarkably good agreement between all methods was found. Most of all it was shown that all used indirect methods reveal the same results as the direct methods and thus the assumptions made for the analysis of the indirect methods seem to be valid for this case. On the other hand, when the electron pulse and thus the XUV parameters were significantly changing within the bunch train, as in the case when the FEL was running at 24 nm, a strong deviation between different methods was observed. Here it is difficult to judge which method can be trusted to what extend.

While in SASE mode of operation the photon pulse is shorter than the total length of the electron bunch from which it is generated, the assumption of a factor 0.6 [2, 17] between the two can only be used as a very simple rule of thumb for first estimations. The measurements as well as start-to-end simulations showed, the factor can be substantially smaller depending on the accelerator settings. Due to the complicated beam dynamics in the energy range FLASH is working in, parameters like slice emittance and energy spread also have to be taken into account as well. Up

ISBN 978-3-95450-133-5

EXPERIMENTAL RESULTS OF DIAGNOSTICS RESPONSE FOR LONGITUDINAL PHASE SPACE

F. Frei*, V. Arsov, H. Brands, A. Saa Hernandez, R. Ischebeck, F. Löhl, B. Kalantari, R. Kalt, B. Keil, W. Koprek, G.L. Orlandi, T. Schilcher, V. Schlott, PSI, Villigen, Switzerland

Abstract

At SwissFEL, electron bunches will be accelerated, shaped, and longitudinally compressed by different radio frequency (RF) structures (S-, C-, and X-band) in combination with magnetic chicanes. In order to meet the envisaged performance, it is planned to regulate the different RF parameters based on the signals from numerous electron beam diagnostics. Here we will present experimental results of the diagnostics response on RF phase and field amplitude variations that were obtained at the SwissFEL Injector Test Facility.

INTRODUCTION

The SwissFEL free electron laser [1] is currently under construction at the Paul Scherrer Institut. To obtain a proper and stable bunching process, certain stability requirements of different sub-systems (Laser, RF, magnets etc...) have to be reached. Diagnostics should be available to measure the related beam parameters and possibly provide this information to feedback systems, which then can be used to stabilize the beam.

In order to develop and optimize different components and procedures for SwissFEL, the 250 MeV SwissFEL Injector Test Facility (SITF) [2] is currently in operation.

To investigate the current status of the systems, a diagnostics response measurement was performed at SITF. Each RF parameter was varied separately around previously chosen initial settings. The measured responses of the diagnostics then allow conclusions on the achievable sensitivities at these initial settings. Additionally, corresponding simulations performed using the code LiTrack are presented in a separate contribution [3]. The post analysis has been done following the concept already described in detail in [4].

It is worth emphasizing that the present paper provides a snapshot of the work presently done at SITF. The systems are under continuous development and optimization to reach the ultimate goals for SwissFEL.

After a first brief overview of the systems installed at SITF, the initial settings of the RF and the diagnostic elements will be described in more detail. Based on this information, the diagnostic response measurement is described in a third section followed by a section discussing the analysis of the deduced response matrix.

SWISSFEL INJECTOR TEST FACILITY

As depicted in Fig. 1, SITF is based on an S-band radio frequency (RF) photoinjector (FINSS). A booster LINAC consisting of normal conducting S-band RF structures (FINSB01-FINSB02-FINSB03/04) is simultaneously generating the acceleration up to 250 MeV and the necessary energy chirp for the magnetic compression in the bunch compressor (BC). To linearize the longitudinal phase space for optimal bunch compression, a fourth harmonic X-band cavity (FINXB) phased for deceleration is located in front of the bunch compressor.

Jitter and drift of field amplitude and phase of each of these accelerating cavities (subsequently referred to as actuators) affect the longitudinal phase space of the electron bunches. To measure the effect on the electron beam, SITF is equipped with longitudinal instrumentation (subsequently referred to as diagnostics) which is illustrated in Fig. 1.

For the present measurements, the bunch charge is measured with stripline beam position monitors (BPMs) that were previously calibrated against a Faraday cup and a wall-current monitor [5]. Two of these stripline BPMs (BPM-E_1, BPM-E_2) are located between the first and the second dipole of the bunch compressor, where the horizontal beam position is a measure of the mean particle energy. Furthermore, a synchrotron radiation monitor (SRM) [6] after the third dipole of the bunch compressor provides the energy distribution by imaging the incoherent synchrotron radiation onto a camera. While the position of the centroid is also a measure of the mean particle energy, the width is related to the relative energy spread.

After the bunch compressor, relative bunch length changes are measured by the bunch compression monitor (BCM). This monitor is based on coherent diffraction radiation (CDR) generated as the electron bunch passes through a hole of radius 3 mm in a 1 μm thick titanium foil. The CDR is thereafter filtered by two different "thick grid" high pass THz filters. The two different spectral bands are individually detected by two Schottky diodes. Additionally, the absolute bunch length can be measured destructively using an S-band transverse deflecting cavity (TDC). Thereby, the longitudinal profile gets vertically deflected. The bunch profile is then measured by imaging the electron distribution onto a subsequent screen.

A bunch arrival time monitor (BAM) after the bunch compressor is based on a Mach-Zehnder type modulator [7]. A high bandwidth pickup signal [8] is sampled at the zero crossing by a laser pulse. This laser pulse provides the timing reference. It is delivered in the accelerator tunnel through single-mode fiber links stabilized in length with femto second precision. The arrival time change results in deviation from the zero crossing, thus creating a modulation voltage for the electro optical modulator, which encodes the arrival time into the amplitude of the reference laser pulse.

* franziska.frei@psi.ch

ISBN 978-3-95450-133-5

FEMTOSECOND-STABILITY DELIVERY OF SYNCHRONIZED RF-SIGNALS TO THE KLYSTRON GALLERY OVER 1-km OPTICAL FIBERS

Kwangyun Jung, Jungwon Kim#, Jiseok Lim, Junho Shin, Heewon Yang,
KAIST, Daejeon, South Korea
Heung-Sik Kang, Chang-Ki Min, PAL, Pohang, South Korea

Abstract

We present our recent progress in optical frequency comb-based remote optical and RF distribution system at PAL-XFEL. A 238 MHz mode-locked Er-laser is used as an optical master oscillator (OMO), which is stabilized to a 2.856 GHz RF master oscillator (RMO) using a fiber-loop optical-microwave phase detector (FLOM-PD). We partly installed a pair of 1.15 km long fiber links through a cable duct to connect and OMO room to a klystron gallery in the PAL-XFEL Injector Test Facility (ITF). The fiber links are stabilized using balanced optical cross-correlators (BOC). A voltage controlled RF oscillator (VCO) is locked to the delivered optical pulse train using the second FLOM-PD. Residual timing jitter and drift between the two independently distributed optical pulse train and RF signal is measured at the klystron gallery. The results are 6.6 fs rms and 31 fs rms over 7 hours and 62 hours, respectively. This is the first comb-based optical/RF distribution and phase comparison in the klystron gallery environment.

INTRODUCTION

Time-resolved X-ray-optical pulse pump-probe experiments with femtosecond time resolution and sub-nm spatial resolution can reveal molecular dynamics and accelerate natural and medical science. Therefore, the future most advanced X-ray Free Electron Lasers (XFELs) require femtosecond-precision synchronization of several lasers and RF signals in tens of accelerator units over km length scale [1]. In the last decade, optical timing and synchronization techniques, based on CW lasers or pulsed mode-locked lasers, have been intensively investigated.

Optical pulsed fiber link stabilization technique based on a balanced optical cross-correlator (BOC) resulted in unprecedented performance. Sub-10 fs in rms long-term stability and short-term jitter were achieved for standard single mode fiber link stabilization in well-controlled laboratory environment [2]. This technique has been already installed in operating FEL facilities (such as FERMI and FLASH), and currently shows <100 fs in peak-to-peak long-term stability over several hours [3,4]. This amount of drift is caused by the polarization mode dispersion (PMD) of the fiber link. Recently, in order to deal with the PMD problem, a polarization maintaining (PM) fiber link was used, and sub-femtosecond long-term timing link stability [5] and remote optical-to-optical synchronization [6] in the laboratory environment was reported.

Synchronization techniques of local RF signals to a mode-locked laser have been also developed in the last decade. A balanced optical-microwave phase detector (BOM-PD) with sub-10 fs long-term stability and short-term jitter was demonstrated [2]. It detects timing error between optical pulse trains and RF signals directly in the optical domains based on electro-optic sampling in the fiber Sagnac-loop interferometer. The BOM-PD is being used in FEL facility (FERMI) for the mode-locked laser stabilization to the RF master oscillator in the well-controlled laser room [3]. In 2012, a fiber-loop optical-microwave phase detector (FLOM-PD) was developed with both sub-femtosecond short-term jitter and long-term stability [7]. It showed ultra-low short-term residual phase noise floor (-158 dBc/Hz) between two 10 GHz microwave oscillators which were locked to a common mode-locked laser locally [8]. The basic principle of the FLOM-PD is very similar with the BOM-PD, but the FLOM-PD is based on balanced photodetection instead of synchronous detection, and it is much simpler and easy to build.

The combination of these two modular methods (BOC + BOM-PD or BOC + FLOM-PD) may lead to a great performance in remote RF transfer or remote synchronization between a mode-locked laser and a RF oscillator. However, the full implementation of such remote laser-RF synchronization has not been demonstrated so far.

In this paper, we show remote synchronization between a 238 MHz mode-locked laser and a 2.856 GHz RF source by combining FLOM-PD-based local laser-RF synchronization units and BOC-based stabilized fiber links in the real accelerator klystron gallery environment [9]. We installed a pair of 1.15 km long fiber links in an accelerator building and measured the relative phase drift between the optical pulse train and the RF signal at the link outputs in a klystron gallery, which resulted in 6.6 fs and 31 fs rms timing drift maintained over 7 hours and 62 hours, respectively [9]. To our knowledge, this is the first demonstration of maintaining few-fs-level drift over hours of operation in the remote synchronization between a femtosecond mode-locked laser and a RF source over a kilometer in distance. This shows the possibility to distribute RF signals, all tightly locked to a master mode-locked laser, to remote locations with femtosecond stability, not only in the well-controlled laboratory but also in the accelerator environment.

#Jungwon.kim@kaist.ac.kr

ISBN 978-3-95450-133-5

ELECTRON BEAM DIAGNOSTICS AND FEEDBACK FOR THE LCLS-II*

Josef Frisch, Paul Emma, Alan Fisher, Patrick Krejcik, Henrik Loos, Timothy Maxwell, Tor Raubenheimer, Stephen Smith, SLAC, Menlo Park CA 94305, USA

Abstract

The LCLS-II is a CW superconducting accelerator driven, hard and soft X-ray Free Electron Laser which is planned to be constructed at SLAC. It will operate with a variety of beam modes from single shot to approximately 1 MHz CW at bunch charges from 10 to 300 pC with average beam powers up to 1.2 MW. A variety of types of beam instrumentation will be used, including stripline and cavity BPMs, fluorescent and OTR based beam profile monitors, fast wire scanners and transverse deflection cavities. The beam diagnostics system is designed to allow tuning and continuous measurement of beam parameters, and to provide signals for fast beam feedbacks.

LCLS-II

The LCLS-II uses a 4 GeV, CW superconducting LINAC to drive two variable gap undulators to generate soft and hard X-rays (see Fig. 1). The hard X-ray undulator and some of the electron beam line are shared with the LCLS-I room temperature LINAC in order to allow operation with either accelerator. The SC LINAC will operate at bunch rates up to approximately 1MHz, and uses fast kickers ("beam spreader") to direct selected bunches to each undulator, or to the beam dump.

The LCLS-II includes a low rate (120Hz) diagnostic line at an energy of 100 MeV. A kicker can select single bunches for diagnostics without interfering with the rest of the bunch train.

The LCLS-II can operate in a variety of modes with varying bunch charge and pulse structure, a representative operating mode is shown in Table 1.

Table 1: LCLS--II Electron Beam Parameters (Nominal)

Beam energy	4 GeV
Bunch Charge	10 – 300 pC
Bunch rate	< 0.93 MHz
Average beam power	<1.2 MW
Peak current	500-1500 A
Bunch length (RMS)	0.6 – 52 μm
Energy spread	125-1500 keV
Energy stability RMS	<0.01%
Emittance (at 100pC, normalized)	~0.3 μm

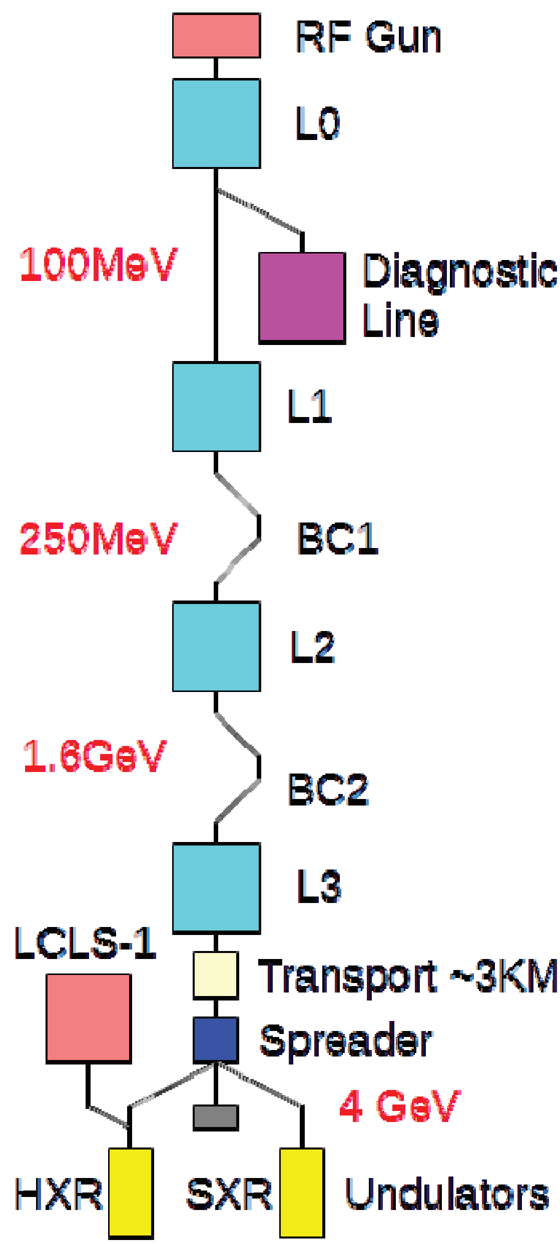

Figure 1: LCLS-II Layout.

DIFFERENCES FROM LCLS-I

Beam Rate / Average Power

The single bunch properties for LCLS-II are similar to those for the existing LCLS-I; however the high average bunch rate and beam power result in new requirements for

*Work Supported by DOE contract DE-AC-02-76-SF00515

ISBN 978-3-95450-133-5

BEAM ENERGY MANAGEMENT AND RF FAILURE COMPENSATION SCENARIOS FOR THE EUROPEAN XFEL

Bolko Beutner, DESY, Hamburg, Germany

Abstract

Total beam delivery time to user stations is a key parameter for FEL user facilities. Therefore downtime due to RF issues, among other things, should be minimized. Specifically in case of a RF failure machine operation and beam delivery should be maintained as long as the next scheduled maintainance day. This is achieved by increasing the power in all remaining klystrons to recover the lost beam energy. These modification of the beam energy profile along the machine induces an optics perturbation which is typically compensated by a rescaling of the quadrupole magnet gradients to maintain a constant focusing strength. However, we would like to resume operation at the next macro-pulse after a RF event. While, in general, the RF systems can handle such changes the magnets can not. In this paper we will explore optics perturbations for the case that we do not change the magnets at all, to estimate the feasibility of fast beam recovery after klystron failure. In addition corrections to the RF setup are calculated with the goal of avoiding changes in the bunch compression dynamics of the machine.

BEAM ENERGY MANAGEMENT FOR THE EUROPEAN XFEL

Superconducting technology used at the European XFEL allows for RF pulses as long as 600 μs supporting bunch trains with an internal repetition rate of up to 4.5 MHz. These pulses are, which are refereed to as *macro-pulses* are triggered with 10 Hz. The European XFEL is driven in total by 26 1.3 GHz multi-beam klystrons [1] [2]. These RF stations are distributed along European XFEL as shown in Fig. 1.

The energy gain ΔE, number of RF stations N, and individual voltages per klystron $\Delta E/N$ and cavity V are summarized in Table 1. Each klystron in the Linac 1-3 sections drives four accelerator cryo-modules consisting of eight cavities with a total energy gain up to 755 MeV. Design gradient of the niobium cavities is 23.6 MV/m. Since the assembly of the cryo-modules is work in progress we do not have final numbers on the actual available gradient. After final testing and should the situation arise re-treatment of all modules we assume an available gradient of 23.6 MV/m with an average overhead of 10% [3]. Linac 3 is configured to achieve nominal final beam energy of 17.5 GeV at the nominal gradient of 23.6 MV/m using 20 instead of 21 RF stations as beam energy reserve.

In the following the name *klystron* refers to the full RF station including modulator, pulse cables, pulse transformers, klystrons, waveguides, down to the cavities, and failures in each of these components are refereed to as *klystron failure*.

From the point-of-view of electron beam energy management the machine is conveniently separated into three parts. First the Injector and Linac 1 section. In this region of the machine each section is essentially driven by one klystron. Klystron failures in this part are fatal and can not be compensated, immediate repair is required to resume operation. The second part is Linac 2. A reduction of acceleration voltage can be recovered by reserves in Linac 3. This Linac 2 however is upstream of the last bunch compressor chicane. Voltage changes effectively modify the energy chirp at BC2 and therefore the final longitudinal beam profile. In addition to energy profile reorganization the off-crest phases needs modification to maintain the final current profile. Linac 3, the main linac, is the last part. Here the majority of the beam energy is generated and here beam energy variations are corrected. The nominal energy gain of Linac 3 is 15.1 GeV. Since we only rely on 20 instead of 21 klystron stations and assume an 10% energy overhead the total voltage capacity of Linac 3 is 17.4 GeV . This additional energy reserve of about 2.3 GeV can be used to compensate the outage of about three klystron stations.

Table 1: XFEL Energy Gain Configuration

Linac Section	ΔE [GeV]	N	$\Delta E/N$ [MeV]	V [MV/m]
Injector	0.13	1	130	16.5
Linac 1	0.57	1	570	17.8
Linac 2	1.7	3	567	17.7
Linac 3	15.1	21/20	719/755	22.5/23.6

MAIN LINAC ENERGY MANAGEMENT

To redistribute the energy gain along we propose an iterative procedure. We start with an index set I which includes all klystrons used for energy correction. Typically I contains all stations except the failed one. The voltages of modules not in I $\Delta V_{j\notin I}$ are not necessarily set to zero, to allow modeling of reduced gradients in individual stations, e.g. detuned cavities within a module or reduced voltage operations as quench prevention. The voltage of each module in operation is modified according to:

$$\Delta V_i' = \frac{E_{\text{nominal}} - \sum_{j\notin I} \Delta V_j}{|I|} \frac{w_i}{\langle w_i \rangle}, i \in I. \qquad (1)$$

The positive weight factors w_i are chosen to set priorities according to the performance and reliability of the individual RF stations. After voltage scaling according to Eq. 1 each ΔV_i is compared with the individual maximum. If the maximum is exceeded it is set to this maximum and the station

ISBN 978-3-95450-133-5

TWO CHARGES IN THE SAME BUNCH TRAIN AT THE EUROPEAN XFEL

Y. Kot, T. Limberg, I. Zagorodnov, DESY, Hamburg, Germany

Abstract

The European XFEL has been initially designed for the operation with bunch charge of 1 nC [1] which was later extended down to 20 pC [2]. An important upgrade of this extension might be the ability to operate different bunch charges in the same RF pulse. In this paper we assume the nominal design of the XFEL injector which means in particular that both charges in the same RF pulse experience the same solenoid field and are generated by the laser of the same rms size. We discuss the requirements which the combined working points of the injector have to fulfil and show the results of the complete start to end (S2E) and SASE simulations for the simultaneous operation of 250 pC and 500 pC bunch charges.

INTRODUCTION

We report about the simulations on the operation of two different bunch charges at the European XFEL. From the beam dynamics point of view the most essential issue there is to achieve the similarity of the beam optical functions keeping emittance growth of the bunches reasonably low. In the next section we give an overview about the XFEL injector with respect to the beam optical functions which is followed by the presentation of the combined working points for the solenoid field and laser beam profile if the injector is operated with two charges in the same RF pulse. Finally we discuss the results of the S2E and SASE simulations for the bunch pair of 250/500 pC.

BEAM OPTICS ISSUES OF THE XFEL INJECTOR

The injector of the European XFEL may be divided into three sections from the beam optical functions point of view. The first section begins at the cathode and is 14.48 m long. Since it doesn't contain quadrupole magnets manipulation of the beam optical functions is achieved here indirectly by the choice of the solenoid field strength as well as gun gradient, RF focussing effects in ACC1 or laser beam size at the cathode.

The next (matching) section begins right after the first accelerating module which is followed by the first quadrupole. It contains six quadrupoles which are used for the matching of the beam optical functions.

The third part of the injector begins after the matching point at 29.51 m where the beam optics is expected to be the same for any bunch charge and any initial settings of the gun.

Since both bunches in the train experience the same magnetic field in the quadrupoles one has to guarantee that they arrive the matching section with similar twiss functions in order to avoid effects of the beam optics distortion like beta beat downstream the matching point.

The ability of the XFEL injector to obtain two different charges in the same RF train with similar beam optical functions has been discussed in [3]. It was shown that it is possible on cost of emittance growth of lower charge if the difference between charges is not too large. Once the suitable value of the peak solenoid field has been found the choice of the laser beam size should be then on the ascending branch for higher charge and on the descending branch for lower charge (see Fig. 1).

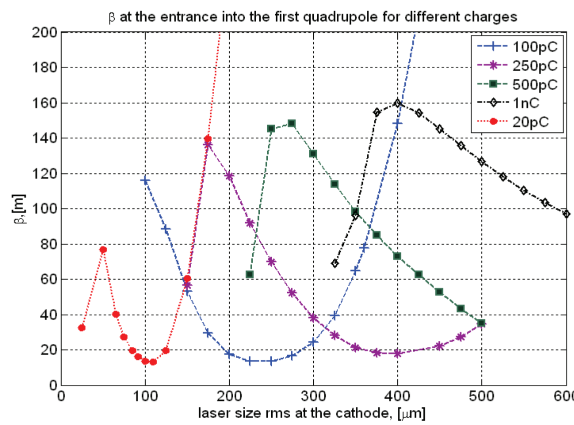

Figure 1: Dependence of the β-function at the beginning of the matching section on laser beam rms size for different bunch charges. Simulations are done for the peak solenoid field of 0.2220 T.

COMBINED WORKING POINTS FOR TWO CHARGES IN THE SAME TRAIN

Under combined working points we define the choice of the settings of the solenoid peak field and rms laser beam size at the cathode. These settings are valid for each particular RF pulse so that they can't be adjusted separately for any bunch in the same RF pulse.

The determination of the combined working points has been also performed under the assumption of the same parameters of the gun and longitudinal gun laser profile for both bunches. These parameters are summarized in the Table 1. The energy of the beam has been fixed to 150 MeV at the exit of the first accelerating module ACC1 and to 130 MeV after the third harmonic module

Table 1: Gun Parameters

Peak Gun Gradient, [MV/m]	Gun Phase	Laser Pulse and Form
60	-1.9	Flat Top 20 ps, rise and fall time 2 ps

ISBN 978-3-95450-133-5

START-TO-END ERROR STUDIES FOR FLUTE

M. Weber*, A.-S. Müller, S. Naknaimueang, M. Schuh, M. Schwarz, P. Wesolowski
KIT, Karlsruhe, Germany

Abstract

FLUTE, a new linac based test facility and THz source, is currently under construction at the Karlsruhe Institute of Technology (KIT) in collaboration with DESY and PSI. With a repetition rate of 10 Hz, electron bunches with charges from 1 pC to 3 nC will be accelerated up to 40-50 MeV and then compressed longitudinally in a magnetic chicane to generate intense coherent THz radiation. Since the stability and repeatability of longitudinal bunch profiles are essential for optimum compression and THz radiation properties, simulation-based start-to-end error studies using the tracking code ASTRA have been performed to determine the influence of the machine elements on the bunches. Thus, critical parameters are identified and their respective tolerance ranges defined. In this contribution a summary of the error studies will be given.

INTRODUCTION

The "Ferninfrarot Linac- Und Test-Experiment" (FLUTE) [1], [2] is a new compact linear accelerator facility, aimed at the generation of coherent THz radiation with fs electron bunches. Additionally, it will serve as a test stand for the study of different generation mechanisms of THz radiation (CSR, CTR and CER) as well as for the development of diagnostics for the ultra-short bunches.

Figure 1 shows the baseline design of FLUTE. In a 3 GHz RF photo gun the initial bunches with charges from 1 pC to 3 nC are generated and accelerated to about 7 MeV. In order to compensate the strong space charge forces acting within the bunches at low energy, a solenoid is used for transverse focusing right after the gun. A travelling wave linac accelerates the bunches to their final energy of 40-50 MeV. In addition, a negative correlated energy spread is induced to longitudinally compress the bunches in the D-shaped bunch compressor (chicane). To control and optimize the transverse bunch size, a focusing quadrupole doublet is used before the chicane.

BEAM DYNAMICS SIMULATIONS

For the design of FLUTE and the optimization of the machine parameters, different simulation tools including the tracking code ASTRA [3] have been used [4] in order to get a minimum RMS bunch length after compression. For the error studies the tracking has been done with ASTRA for the entire machine. Table 1 shows the current design values for the machine parameters applied in the simulations. Depending on the bunch charge, RMS bunch lengths between 220 fs (3 nC) and 5 fs (1 pC) after compression can be achieved. CSR effects inside the chicane are neglected in this case. Simulations including CSR effects result in bunch lengths of about 270 fs for the 3 nC bunches, while for 1 pC CSR leads to about 5% longer bunches. Especially in this highly sensitive low charge regime further optimization is ongoing.

* manuel.weber@partner.kit.edu

Table 1: Design Values for the FLUTE Machine Parameters used in the ASTRA Simulations

Parameter	Unit	Value
Bunch charge	nC	0.001 - 3
Laser spot size (RMS)	mm	0.5 - 2.25
Laser pulse length (RMS)	ps	0.5 - 4
Gun peak field	MV/m	120
Solenoid peak field	T	0.14 - 0.18
Linac peak field	MV/m	10
Quadrupole strength	m^{-2}	11.88 - 12
Dipole bending radius	m	1.12 - 1.006

ERROR STUDIES

A solid understanding of the influence of the machine parameters on the 3D bunch shape is a prerequisite for a stable operation with ultra-short bunches. These parameters include the ones shown in Table 1, as well as the alignment of the different machine components. Two simulation procedures have been applied. On the one hand, systematic scans of individual machine parameters have been performed. On the other hand, randomly generated deviations have been added on the design values of these parameters. This has been done for each machine component separately, as well as for the whole machine at once. The errors follow a Gaussian distribution and each entry in the distribution corresponds to one simulation run. For that purpose an internal routine included in ASTRA has been used. Observing the distribution of the output bunch parameters (such as RMS bunch length and transverse bunch size) after multiple simulation runs then gives information about the average influence of the errors on the bunch. Table 2 shows the RMS values for the error distributions on the considered machine parameter values. A cut-off after three sigma has been made, meaning that deviations of the input values do not exceed this range. So values that are too far off from the design value of the respective machine parameter (with probabilities below 0.3%) are avoided within the random distributions.

Regarding the laser, errors have been added on the laser pulse length, timing offset (jitter), spot size and position at the cathode, as well as on the bunch charge (laser amplitude). Out of these, the timing offset has the strongest influence on the bunch profiles. Figure 2 shows a systematic scan of the laser timing between ±500 fs and the impact on the bunch

ISBN 978-3-95450-133-5

OPTIMIZATION OF THE PITZ PHOTO INJECTOR TOWARDS THE BEST ACHIEVABLE BEAM QUALITY*

M. Khojoyan #, M. Krasilnikov, F. Stephan, G. Vashchenko, DESY Zeuthen, Zeuthen, Germany

Abstract

Uniform 3D ellipsoids are proven to be the best distributions for high brightness charged particle beam applications due to the linear dependence of the space charge fields on the position within the distribution [1]. Such electron bunches have lower emittance and are less sensitive to the machine settings and, therefore, should allow more reliable operation, which is one of the key requirements for single-pass free-electron lasers (FELs). The Photo Injector test facility at DESY, Zeuthen site (PITZ) is optimizing high brightness electron sources for linac based FELs such as the European XFEL. Recent measurements at PITZ using a photocathode laser with a flat-top temporal profile have revealed record low transverse emittance values at different bunch charges [2]. As a next step towards the further improvement of the high quality beams, a cathode laser system, capable of producing quasi-3D ellipsoidal bunches is intended to be used at PITZ. In this work the beam dynamics optimization results for various bunch charges and for flat-top and 3D ellipsoidal cathode laser shapes are presented. For each working point the relative emittance growth is estimated due to possible deviations of the machine parameters.

INTRODUCTION

The Photo Injector test facility at DESY, Zeuthen site (PITZ) is one of the leading laboratories on generation and optimization of high brightness electron bunches of different charges for free-electron laser (FEL) machines such as FLASH [3] and the European XFEL [4]. At PITZ electron beams of excellent quality are created utilizing the photo effect and are accelerated in an L-band RF gun up to several MeV energies. A pair of solenoid coils surrounding the gun is used for beam transverse focusing meanwhile providing zero remnant magnetic fields at the cathode. The final as high as 25 MeV beam energy is reached after passing through a second accelerating structure. The electron beam transverse properties are usually measured with the help of the emittance measurement systems (EMSY), where a single slit scan technique [5] is used to measure the electron beam emittance. Additionally, there are many diagnostics available for full characterization of high brightness electron beams. A more detailed description of the PITZ setup can be found elsewhere [6].

*Work supported by the German Federal Ministry of education and Research, project 05K10CHE "Development and experimental test of a laser system for producing quasi 3D ellipsoidal laser pulses" and RFBR grant 13-02-91323.
#martin.khojoyan@desy.de

Optimization of the photocathode laser shape is one of the key issues on generating high quality bunches. Recent measurements performed at PITZ by applying a nominal flat-top longitudinal laser shape have revealed unprecedented transverse emittance values for different bunch charges [2]. To further improve the achievable beam quality a laser system capable of producing quasi-3D ellipsoidal laser pulses is under development at the Institute of Applied Physics (IAP, Nizhny Novgorod). The project is being realized in the frame of a joint German-Russian research activity including the Joint Institute of Nuclear Research (JINR, Dubna) and PITZ (DESY).

In this contribution, an optimization of the transverse beam emittance is performed for different bunch charges comparing a cylindrical (flat-top temporal profile) and 3D ellipsoidal cathode laser distributions. A new linac setup with shifted (optimized) positions of the second accelerating cavity and the first emittance measurement system (EMSY1) is used in the simulations. The tolerance studies are performed for each optimized machine setup to predict the transverse emittance dilution due to possible mismatch of the machine parameters during the experiments. Finally, the influence of possible imperfections coming from the 3D laser shape on the electron beam emittance is estimated for different bunch charges.

SIMULATION SETUP FOR EMITTTANCE OPTIMIZATION

The ASTRA [7] simulation code has been used to optimize the electron beam quality at various bunch charges assuming flat-top and 3D ellipsoidal cathode laser pulse shapes. Previously performed studies have revealed a much better injector performance of a 1 nC electron beam for the 3D ellipsoidal laser profile with a shifted position (40 cm closer to the gun) of the second accelerating cavity as compared to the current setup [8]. In this work the position of the first emittance measurement system (EMSY1) is shifted accordingly by ~ 45 cm upstream towards the cathode. The simulation setup is shown in Fig. 1. The following values of machine parameters were used during the optimization. A flat-top temporal laser shape with fixed FWHM length of 21.5 ps and 2 ps rise and fall times was considered in simulations for different charges. The transverse laser profile was assumed to be homogeneous. For each bunch charge the longitudinal size of the 3D ellipsoidal laser was tuned accordingly to get the same electron bunch rms length at EMSY1 (Z=5.28 m) as it is for the flat-top case. The gun

ISBN 978-3-95450-133-5

RECENT ELECTRON BEAM OPTIMIZATION AT PITZ

G. Vashchenko*, G. Asova†, P. Boonpornprasert, J. D. Good, M. Gross, I. Isaev, D. Kalantaryan, M. Khojoyan, G. Kourkafas, M. Krasilnikov, D. Malyutin, D. Melkumyan, A. Oppelt, M. Otevrel, T. Rublack, F. Stephan, Deutsches Elektronen-Synchrotron, Zeuthen site, Zeuthen, Germany
G. Pathak, Hamburg University, Hamburg, Germany
D. Richter, Helmholtz-Zentrum Berlin, Berlin, Germany

Abstract

High brightness electron sources for linac based free-electron lasers operating at short wavelength such as FLASH and the European XFEL are characterized and optimized at the Photo Injector Test Facility at DESY, Zeuthen site (PITZ). In the last few years PITZ mainly was used to condition RF guns for their later operation at FLASH and the European XFEL. Only limited time could be spent for beam characterization. However, recently we have performed emittance measurements and optimization for a reduced gun accelerating gradient which is similar to the usual operation conditions at FLASH. The results of these measurements are presented in this paper.

INTRODUCTION

The Photo Injector Test facility at DESY, Zeuthen site (PITZ) is developing, characterizing and optimizing high brightness electron sources for free-electron lasers like FLASH [1] and the European XFEL [2]. One of the most important parameters, influencing the FEL process, is the normalized transverse projected emittance, hereinafter called emittance, of the electron beam. A normal conducting 1.6-cell L-band RF gun cavity with a Cs_2Te photocathode, which is illuminated by cylindrically shaped UV laser pulses, is used to produce high quality electron beams of different charges. The produced electron beam is focused with a pair of solenoids installed around the gun and accelerated further by the cut disc structure booster, hereinafter called CDS booster, after which numerous diagnostic devices are installed. The emittance of the electron beam is measured using the conventional slit scan method based on a direct measurement of the electron beam size and angular spread [3]. As the energy of the electron beam after the final acceleration is not sufficient to prevent a space-charge induced emittance growth, several emittance measurement stations are installed along the beamline to monitor the emittance evolution. More details about the PITZ setup can be found elsewhere [3–5]. All the data presented in this work were obtained using the first emittance measurement station installed just downstream the CDS booster.

In the last few years PITZ was mainly focused on conditioning of electron guns required by FLASH and the European XFEL without the possibility to perform comprehensive electron beam characterization and optimization due to the tight time schedule. However, recently we got the possibility to partially perform electron beam characterization with an RF gun which was conditioned at PITZ and will be delivered for further usage at the European XFEL. Due to lack of time, the measurements were performed only for 1 nC and 100 pC electron beam charges. Only emittance dependencies on the most sensitive machine parameters were measured. In the following section, measured data compared to the results of numerical simulations using the ASTRA code [6] are presented.

EMITTANCE SIMULATIONS AND MEASUREMENT RESULTS

Emittance dependencies on the main solenoid current, gun launching phase and rms laser spot size on the cathode were measured for electron beams with 100 pC and 1 nC charges. A flat-top temporal UV laser profile with a FWHM of about 21 ps was used and is presented together with the transverse laser profile in Fig. 1. The gun on-axis peak field on the cathode was reduced to about 53 MV/m, as compared to the nominal 60 MV/m which is planned for the European XFEL, in order to combine the electron beam characterization with gun stability tests at long RF pulses. This yields an accordingly reduced electron beam momentum after the gun of about $p_z \sim 5.9$ MeV/c as compared to about $p_z \sim 6.8$ MeV/c at 60 MV/m. Further acceleration by the CDS booster operated at the maximum allowed accelerating gradient and tuned to the maximum mean momentum gain phase, hereinafter called MMMG phase, resulted in a final electron beam momentum of about $p_z \sim 21.2$ MeV/c. The emittance of the electron beam was measured using the first emittance measurement station installed 5.74 m from the cathode [3]. For both probed electron bunch charges emittance dependencies on the main solenoid current were measured for various rms laser spot sizes on the cathode and an MMMG gun launching phase (an optimum gun phase according to the simulations, see e.g. [3, 4]). Additionally, for the electron beam with 1 nC bunch charge, the emittance dependence on the gun launching phase was measured for the rms laser spot size on the cathode delivering the minimum emittance at the MMMG phase.

Emittance Data for 1 nC Electron Bunch Charge

As it was mentioned, emittance dependencies on the rms laser spot size on the cathode and gun launching phase were measured for electron beams with a bunch charge of 1 nC.

* Grygorii.Vashchenko@desy.de
† BAS INRNE,1784 Sofia, Bulgaria.

ISBN 978-3-95450-133-5

EVOLUTION OF A WARM BUNCHED BEAM IN A FREE DRIFT REGION

B. Maly, A. Friedman, Ariel University - Schlesinger Family Center for Compact Accelerators, Radiation Sources, and Applications, Ariel, Israel

Abstract

The state of the art of FELs development at present is "Table-Top X Ray Free Electron Lasers". Many such schemes involves a pre-bunched electron beam [1]. In this paper we will analyze the evolution and "survivability" of bunching introduced into the beam in the free drift region prior to the wiggler [2-6]. We examined analytically the first order degradation in beam bunching due to space charge effect. It will be shown that there is a limited interaction region, characterized by an exponential decay of the bunching factor, having a length inversely proportional to the square of the electron beam normalized temperature, followed by a stable bunch region. We will present examples of the effect for several schemes of X Ray and Tera Hertz FELs considered or being constructed presently.

INTRODUCTION

First, we present a solution for the evolution of a cold bunched continuous electron beam in a free drift region, based on a one-dimensional first order Vlasov equations including space charge effects [3-5]. Based on the first order cold beam solution, we expand the analysis for the evolution of a warm bunched electron beam in a free drift region, by assuming normal distributions for both transversal and longitudinal components of the momentum, independently [2,6]. Analytical solution is achieved by using a second order two-dimensional Taylor expansion of the exponent argument in the previously derived cold beam solution.

EVOLUTION OF A COLD BUNCHED ELECTRON BEAM IN A FREE DRIFT REGION

The analysis for cold electron beam is based on relativistic Vlasov equation for plasma:

$$\frac{\partial f}{\partial t}+\vec{v}\cdot\nabla f+\frac{d\vec{p}}{dt}\cdot\nabla_p f=0 \tag{1}$$

where $f(\vec{r},\vec{p},t)$ is the distribution function of the plasma, $\vec{p}$ and $\vec{v}$ are the momentum and velocity vectors, respectively.
The time derivative of the momentum can be replaced by Lorentz force in the absence of an external magnetic field:

$$\frac{d\vec{p}}{dt}=-e\vec{E} \tag{2}$$

where e is the absolute value of the electron charge, and $\vec{E}$ is the electric field vector. In the current model there is no external electric field and no radiation field (since there is no external acceleration/deceleration, this is a good assumption). Therefore only the self-induced Coulomb field is considered (space charge). Thus the electric field can be derived out of the electric scalar potential:

$$\vec{E}=-\nabla\psi \tag{3}$$

where ψ is the electric scalar potential.
Substituting (2) and (3) into (1) results in:

$$\frac{\partial f}{\partial t}+\vec{v}\cdot\nabla f+e\nabla\psi\cdot\nabla_p f=0 \tag{4}$$

where

$$\nabla_p\triangleq\hat{x}\frac{\partial}{\partial p_x}+\hat{y}\frac{\partial}{\partial p_y}+\hat{z}\frac{\partial}{\partial p_z} \tag{5}$$

In this formulation we restrict ourselves to a single (longitudinal) dimension. Hence, equation (4) becomes:

$$\frac{\partial f}{\partial t}+v_z\frac{\partial f}{\partial z}+e\frac{\partial\psi}{\partial z}\frac{\partial f}{\partial p_z}=0 \tag{6}$$

p_z and v_z are the longitudinal components of the momentum and velocity, respectively.
Space charge effects are derived from the Poisson equation:

$$\nabla^2\psi=-\frac{\rho}{\varepsilon_0} \tag{7}$$

ρ is the charge density (per unit volume), and ε_0 is the permittivity of free space.
The charge density can be integrated out of the distribution function:

$$\rho(z,t)=-e\int_{-\infty}^{\infty}f(p_z,z,t)\,dp_z \tag{8}$$

Substituting (8) into (7) results in:

$$\frac{\partial^2\psi}{\partial z^2}=\frac{e}{\varepsilon_0}\int_{-\infty}^{\infty}f(p_z,z,t)\,dp_z \tag{9}$$

The charge density of the electron beam is modulated at the origin ($z=0$), hence the distribution function at the origin can be expressed as:

$$f(z=0)=n_0(1+\alpha e^{j\omega t})\delta(p_z-\bar{p}_z) \tag{10}$$

where n_0 is the electrons density per unit volume, ∝ is the modulation factor, ω is the angular frequency of the modulation, δ is the Dirac delta function, and $\bar{p}_z$ is the average longitudinal momentum; since the electron beam is cold, the spread in longitudinal momentum is described by a Dirac delta function.

Using perturbation theory, we assume that both the distribution function and the electrical scalar potential can be expressed as an infinite series of terms, each proportional to a higher power of the modulation factor, ∝:

$$f=f_0+\propto f_1+\propto^2 f_2+\cdots\ ,\qquad \psi=\propto\psi_1+\propto^2\psi_2+\cdots \tag{11}$$

ANALYSIS OF BEAM STABILITY IN THE KAERI ULTRASHORT PULSE ACCELERATOR

H. W. Kim#, S. Bae, B. Gudkov, K. H. Jang, Y. U. Jeong, Y. Kim. K. Lee, J. Mun, S. H. Park, S. J. Park,
KAERI, Daejon, Republic of Korea, UST Acceleartor and Beam Nano Engineering, Daejon, Republic of Korea
N. Vinokurov, S. V. Miginsky, Budker INP SB RAS, Novosibirsk, Russia and KAERI, Daejon, Republic of Korea, and UST Acceleartor and Beam Nano Engineering, Daejon, Republic of Korea

Abstract

An RF-photogun-based linear accelerator for the Korea Atomic Energy Research Institute (KAERI) ultra-short pulse facility is under construction [1]. It has a symmetry structure with four different beamlines. The UED beamlines will generate ultra-short electron pulses with over 10^6 electrons per pulse for the single-shot measurements on femtosecond dynamics of atomic or molecular structures. Electron bunches with an energy of ~3 MeV from the RF photogun can be compressed up to less than 50 fs by achromatic and isochronous bends. The intrinsic r.m.s. timing jitter of the pulses through the bends is estimated to be less than 30 fs with the r.m.s. energy fluctuation of 0.1%. In the THz pump and X-ray probe beamline, two successive laser pulses with a time interval of ~10 ns are used to generate two electron bunches having more than 100 pC bunch charges. Two electron bunches are accelerated by a linac up to ~25 MeV and separated into individual beamlines by a fast kicker.

INTRODUCTION

The KAERI ultra-short pulse accelerator consists of a 1.5-cell S-band (2856 MHz) RF photogun and a 3-m-long travelling-wave-type linac. The scheme of the facility is shown in Fig. 1.

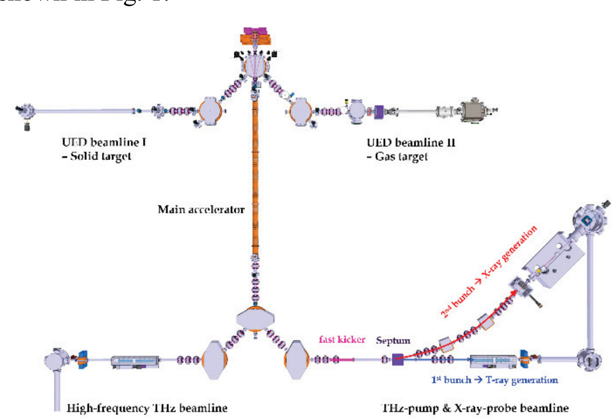

Figure 1: Scheme of the facility.

This facility can be operated in high repetition rate (maximum 500 Hz) and it will provide the ultrafast electron diffraction (UED) and pump-probe experiments to various users. The beam dynamics in the KAERI ultra-short pulse accelerator have been calculated with code ASTRA [2] and ELEGANT [3].

*This work was supported by the World Class Institute (WCI) Program of the National Research Foundation of Korea (NRF) funded by the Ministry of Science, ICT and Future Planning. (NRF Grant Number: WCI 2011-001) #khw8412@kaeri.re.kr

UED BEAMLINE

A third harmonic of a Ti:sapphire femtosecond laser, with a 200-fs-pulse full width at half maximum (FWHM) and the RF photogun are used to generate femtosecond electron bunches. The simulated beam parameters are listed in Table 1.

Table 1: Simulated UED Beam Parameters

Bunch charge	1 pC
Beam energy	2.6 MeV
Bunch length (FWHM)	< 50 fs
Norm. Emittance	0.3 mm mrad
Energy spread (r.m.s.)	0.3%

The power supply usually have overall stability about 10~100 ppm. It is causative of magnet errors. Two bending magnets and six quadrupole magnets comprise the UED beamline. The effects of the magnet errors estimated with an accuracy of the power supply of 0.1% (r.m.s.), are shown in Fig. 2 and Fig 3.

The time resolution of UED depends on the bunch length and timing jitter. The timing jitter depends mostly on the time of flight of the electron bunches from the RF photogun to the sample. MeV UEDs [4-7] are built in all over the world. All they have straight beamline. By comparison, KAERI facility is longer than the other facility but it is expected to have low timing jitter because of the 90-degree achromatic and isochronous bend. We estimate the timing jitter, which is caused by the energy fluctuation at the sample when the electron beam has 0.1% of the energy fluctuation, are shown in Fig. 4. The calculated r.m.s. timing jitter with the isochronous bend (red) is 16 fs, and that with the straight beamline (green) is 54 fs.

BEAM SEPARATION

Two bunches of electron generated at about 10 ns intervals by the RF photogun are accelerated to 25 MeV in the same linac. After that, two bunches are separated into individual beamlines by a fast kicker.

Two bunches are vertically deflected by the steering coil. The first bunch is deflected downward about 10 mm after traveling 0.92 m of drift space. It goes straight for generating intense terahertz pulse.

BEAM MEASUREMENT OF PHOTOCATHODE RF-GUN FOR PAL-XFEL

J. Hong*, J.-H. Han, C.-K. Min, M.S. Chae, Y.-J. Park, S.-J. Park, H.-S. Kang, PAL, Pohang, Korea
I. S. Ko, POSTECH, Pohang, Korea

Abstract

The Injector Test Facility (ITF) at Pohang Accelerator Laboratory (PAL) was constructed to develop an injector for the PAL X-ray free-electron laser (PAL-XFEL) project. The PAL-XFEL design requires the injector to produce an electron beam with a slice emittance of 0.4 mm-mrad at the charge of 200 pC. A 4-hole type RF-gun has been successfully fabricated and tested at ITF. In this paper we report the recent beam-measurement results using the RF-gun at ITF. Emittance measurements have been carried out by changing laser and RF parameters.

INTRODUCTION

Pohang Accelerator Laboratory X-ray Free Electron Laser (PAL XFEL) is now under construction [1].This construction will be finished at the end of 2015. There will be a hard X-ray (0.1nm) beamline with self-seeding scheme with 10 GeV electron beam. There is a 3 GeV branch also to make 1 nm soft X-ray radiation. As part of the PAL-XFEL project, the Pohang Accelerator Laboratory (PAL) constructed the Injector Test Facility (ITF) [2].

The schematic diagram of the ITF beam-line is shown in Fig. 1. The ITF beam-line consists of the RF-devices, magnets and several diagnostic devices. In the 4-hole type RF-gun ('GUN') an electron beam is generated [3]. Downstream of the 'GUN', the emittance compensation solenoid ('S1') which enables the correction of space charge emittance growth is mounted. Downstream of the solenoid, the Turbo Integrating Current Transformer ('ICT1') is installed to measure electron bunch charge. YAG screen #1 ('Y1') is located at the downstream of 'ICT1' to measure the transverse beam profile. Then the electron beam is accelerated by two 3-meter J-type S-band linacs ('ACC1' and 'ACC2') for which enough to accelerate the beam up to 140 MeV. After acceleration the emittance will be measured using the quadrupole #3 ('Q3') and screen #5 ('Y5'). Finally the electron beam will be dumped at the end of the beam-line or after screen #6 ('Y6'). All diagnostic devices are synchronized to the electron beam. The important divice for each measurements is described in Table 1. The control system of ITF is based on the Experimental Physics and Industrial Control System (EPICS).

Table 1: Electron Beam Diagnostics

Measurement	Main Divice	Additional Divice
Size	Y1 to Y5	-
Position	B1 to B5	Y1 to Y5
Charge	ICT1	B1
Energy	D2 + Y6	D1 + Y7
Bunch Length	T-CAV + Y5	-
Arrival Time	BA	-
Emittance	Q3 + Y5	-

EXPERIMENTAL RESULT

Image

The beam size, position and profile are measured using YAG crystals imaged with CCD cameras for image processing. The screen system is manufactured form RADIA BEAM. The images were acquired with an 14-bit CCD camera synched to the electron beam. The lens was set to give a calibration of 8 μm per pixel to allow a compromise between capturing the full variation of the beam size and maximizing the resolution of smallest spot size. Typically five images of the beam are taken at each processing. Typical image of the each screens as shown in Fig. 2.

Charge

Bunch charge is measured using the Tubo Integrating Current Transformer ('ICT1') which is made by BERGOZ. The quantum efficiency (QE) of the photocathode is defined by the ratio of photons hitting the cathode surface and generated electrons. This ratio is expressed as

$$QE = 4.47 \times 10^{-6} \frac{Q_{\text{e-beam}}(\text{pC})}{U_{\text{laser}}(\mu\text{J})}, \tag{1}$$

where $Q_{e-\text{beam}}$ is the photoelectron charge, and U_{laser} is the laser pulse energy. In this case the wavelength of laser is 256 nm. Measurement of bunch charge versus laser energy is shown in Fig. 3. The slope of fitting line gives the quantum efficiency of the copper cathode, which is 1.26×10^{-4}. We also measure bunch charge as a function of laser injection phase as shown in Fig. 4.

Energy

Beam energy and energy spread are measured using the dipole spectrometer. In ITF, there are two types of spectrometers. One is the 90° dipole spectrometer ('D1'+'Y7') for low-energy measurement. The other is the 30° dipole spectrometer ('D2'+'Y6') for high-energy measurement. The electron energy, U and the energy spread, $\frac{\Delta U}{U}$ at the exit of the RF-gun can be written as [4, 5]

$$U = m_e c^2 \left[1 + \frac{\alpha}{2}\left(kL\sin(\phi_f) + \sin(kL)\sin(\phi_f + kL)\right)\right], \tag{2}$$

$$\frac{\Delta U}{U} = \frac{1}{U}\frac{dU}{d\phi_0}\Delta\phi_0, \tag{3}$$

* npwinner@postech.ac.kr

ISBN 978-3-95450-133-5

ERROR ANALYSIS FOR LINAC LATTICE OF HARD X-RAY FEL LINE IN PAL-XFEL*

H. Yang#, J. H. Han, H. -S. Kang, and I. S. Ko
Pohang Accelerator Laboratory, Pohang 790-784, Korea

Abstract

PAL-XFEL consists of the hard x-ray line for 0.06 – 1-nm FEL and the soft x-ray line for 1 – 10-nm FEL. The linac of hard x-ray line is designed to generate 10-GeV, 200-pC, and 3-kA electron beam. It consists of S-band accelerating columns, an X-band linearizer, three bunch compressors (BC). We conduct error simulation in order to evaluate the tolerances of machine parameters and alignments. First, the machine tolerances and beam jitter levels are calculated in the simulations with dynamic errors and we find out the optimized lattice to satisfy the target tolerance of machine. Second, we conduct simulations with misalignment. We quantify the emittance dilution by misalignments, especially those of BCs. In order to compensate the misalignments, the methods of beam correction like Beam Based Alignment (BBA) are presented and the effects of emittance improvements are calculated.

INTRODUCTION

PAL-XFEL is designed to provide the hard x-ray (HX) FEL and the soft x-ray (SX) FEL with the branch line on the middle of the linac lattice, as shown in Fig. 1 [1]. The linac for HX generates 10-GeV, 200-pC, and 3-kA electron beam for 0.06 – 1-nm FEL, as shown in Table 1. The HX linac lattice consists of four sections of accelerating columns, three bunch compressors (BC), an X-band linearizer, and dog-leg line, as shown in Fig. 1. The linac lattice is optimized by the Multi-Objective Genetic Algorithm (MOGA) optimizer whose objectives are the FEL saturation power and length [2]. The parameters of optimized linac lattice are presented in Fig. 2 and the optimized beam parameters are summarized in Table 2. The performance of FEL deteriorates by the dynamic and static errors of the system. The instability of FEL operation is arisen by the dynamic errors of machine like the jitter of the RF phase and voltage. Also, the emittance dilution by static errors should be compensated to achieve the target of FEL performance.

We conducted error simulations for dynamic and static errors with ELEGANT. Two methods were used in the dynamic error simulations, which are the linear interpolation method and the random error simulation with machine parameters. In the first method, not only the machine tolerances were calculated, but also the significant parameters for the stable operation were identified. In the random error simulations, machine tolerances obtained by the previous method were confirmed and beam jittering levels were calculated. The misalignments were applied in the linac lattice for the static error simulations. First, the emittance dilution by the misalignments of bending magnets in BCs was obtained and alignment tolerances of these magnets were calculated. Second, we obtained the emittance dilution by misalignments of all elements in the linac lattice. It was identified that the emittance with best alignment by the developed technology is not enough for FEL operation. In order to suppress the emittance dilution, we conducted two types of the beam correction which are the one-to-one beam correction and the local Beam Based Alignment (BBA) in simulations. In this paper, we present the details of the setting and results in error simulations. Also, we discuss the improvement of the emittance with various beam correction methods.

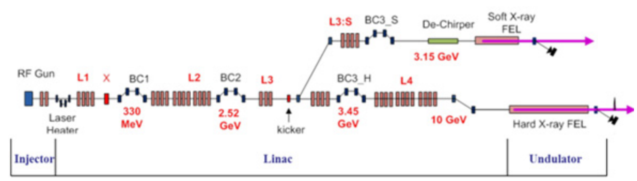

Figure 1: Schematic diagram of PAL-XFEL. The SX branch line is on the middle of the linac lattice.

Table 1: Parameters for HX FEL

Parameters (unit)	Values
Beam energy (GeV)	10
Beam charge (nC)	0.2
Slice emittance (mm-mrad)	0.4
Injector gun	Photocathode RF-gun
Peak current at undulator (kA)	3.0
Repetition rate (Hz)	60
Linac structure	S-band
Hard x-ray wavelength (nm)	0.06 ~ 1

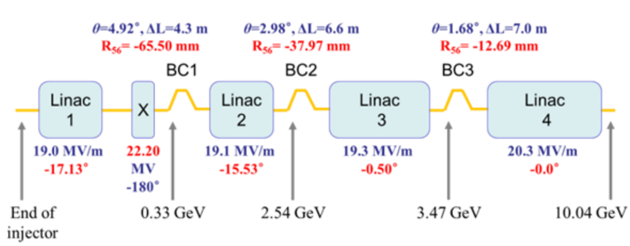

Figure 2: The optimized parameters of the linac lattice for HX line.

*Work supported by MSIP, Korea.
#highlong@postech.ac.kr

ISBN 978-3-95450-133-5

SLICE EMITTANCE MEASUREMENT USING RF DEFLECTING CAVITY AT PAL-XFEL ITF

Jae Hyun Lee, Jang-Hui Han, Juho Hong, Sung-Ju Park, In Soo Ko,
Pohang Accelerator Laboratory, Pohang, 790-834, Korea

Abstract

One of key characteristic for operating PAL-XFEL is the time-dependent transverse properties of a bunch, slice emittance. To achieve the design FEL performance of PAL-XFEL a slice emittance of 0.4 mm mrad at 0.2 nC is required. An Injector Test Facility (ITF) was constructed to study beam properties. In addition to projected emittance measurement, slice emittance measurement is being done using a transverse RF deflecting cavity. We presents results of slice emittance measurement at ITF and future plan for the optimization of operating condition.

INTRODUCTION

The aim of ITF is to study beam dynamics and to produce low emittance electron beams for required future operating condition of PAL-XFEL. The required slice emittance for PAL-XFEL at the exit of injector is 0.4 mm-mrad at 0.2 nC and the acceptable emittance is 0.6 mm-mrad [1]. ITF has been operated to measure emittance and to optimize the elements of injector required for designed condition of PAL-XFEL. Maintaining a low emittance is necessary and one of the principal challenges. The ITF accelerator consists of an S-band 1.6-cell photocathode RF gun, two S-band accelerating columns, solenoids and diagnostic components including quadrupoles and transverse RF deflector [2]. The laser heater is planned to be installed in September 2014. A schematic layout of current ITF elements map is shown in Fig. 2. The Quadrupole for quad scan and YAG screen are located at 13.22 m and 15.86 m from the cathode, respectively. Using the transverse RF deflecting cavity, we can observe an image of the streaked beam at the YAG screen and then measure the slice emittance by the technique of quad scan. The details of the transverse RF deflecting cacity is introduced in the next section. Recently slice emittance has been measured at ITF. In this paper, the results of the slice emittance measurement are described.

EXPERIMENTAL SETUP

The measurements of slice emittance have been performed at the end of ITF with 81.7 MeV of the beam energy at 0.2 nC. The phase of RF photocathode gun is set to 34 ± 0.05 degree. The acceleration phase of two S-band accelerating columns located at 2.14, 5.72 m from cathode is set to on crest. Using the transverse RF deflecting cavity the beam can be streaked at YAG screen. The measurement is carried out by quad scan. The calculation of the slice emittance is fulfilled by using MATLAB code.

Transverse RF Deflecting Cavity

The RF deflecting cavities have been widely studied and used in the accelerator field for the high energy physics research and beam diagnostics of Free Electron Laser and many others. In RF deflecting cavity, as the transverse kick varies sinusoidally in time, each part of the bunch receives a different kick due to finite bunch width. Generally the phase of transverse RF deflecting cavity is chosen to have a zero crossing of RF phase at the middle of the bunch. According to this principle, the bunch gets no net deflection but is streaked vertically at a zero crossing phase of RF field [3]. Therefore we can observe a longitudinal image of the beam. The S-band transverse RF deflecting cavity is described in Fig. 1 and the specifications of it is in Table 1.

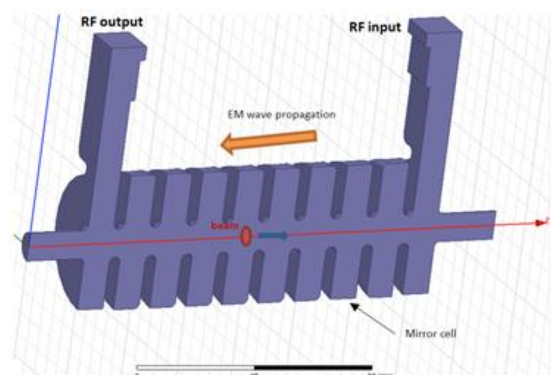

Figure 1: Schematic diagram of Transverse RF Deflecting Cavity.

Table 1: Specifications of Transverse RF Deflecting Cavity

RF parameter	Value	Unit
Frequency f	2.856	GHz
Transverse shunt impedance	28.7	MΩ/m
Unloaded Q	13,400	
Number of cells N	28 (L~1m)	
Attenuation constant α	0.158 (m^{-1})	
Group velocity v_g	0.014 c	
Kick/√power	2.7	MV/√MW

ISBN 978-3-95450-133-5

CYCLOTRON-UNDULATOR COOLING OF A FREE-ELECTRON-LASER BEAM*

I.V. Bandurkin, S.V. Kuzikov, A.V. Savilov#, Institute of Applied Physics, Nizhny Novgorod, Russian Federation

Abstract

We propose methods of fast cooling of an electron beam, which are based on wiggling of particles in an undulator in the presence of an axial magnetic field. We use a strong dependence of the axial electron velocity on the oscillatory velocity, when the electron cyclotron frequency is close to the frequency of electron wiggling in the undulator field. The abnormal character of this dependence (when the oscillatory velocity increases with the increase of the input axial velocity) can be a basis of various methods for fast cooling of moderately-relativistic (several MeV) electron beams. Such cooling may open a way for creating a compact X-ray free-electron laser based on the stimulated scattering of a powerful laser pulse on a moderately-relativistic (several MeV) electron beam.

INTRODUCTION

Fast development of the technique of photo-cathode electron photoinjectors has resulted in creation of compact and accessible sources of moderately-relativistic (several MeV) dense (~1 nC in a ps pulse) bunches [1-3]. Methods for decrease of the energy spread (cooling) are actual from the point of view of various applications of such beams, including free-electron lasers (FELs). However, cooling methods are developed now basically for electron beams of significantly higher energies [4,5]. As for a moderately-relativistic high-dense short e-bunches, the strong Coulomb interaction of the particles results in a requirement for a short (~ 1 m and even less) length of a cooling system. In this situation, the cooling system should possess resonant properties, namely, a strong dependence of parameters of the particles inside the cooling system on their input energies.

We propose to provide cooling by the use of electron wiggling in a circular polarized "cooling" undulator in the presence of an axial magnetostatic field zB_0 (Fig. 1). If the bounce-frequency of electron oscillations in the undulator, $\Omega_u = V_{||} h_u$ is comparable with the electron cyclotron frequency, $\Omega_c = eB_0 / \gamma mc$ (here $V_{||}$ is the electron axial velocity, h_u is the undulator wavenumber, and γ is the relativistic electron mass factor). In this situation, the velocity of undulator oscillations V_u depends strongly on the initial axial velocity.

*Work supported by the Russian Scientific Foundation (grant # 14-19-01723).

#savilov@appl.sci-nnov.ru

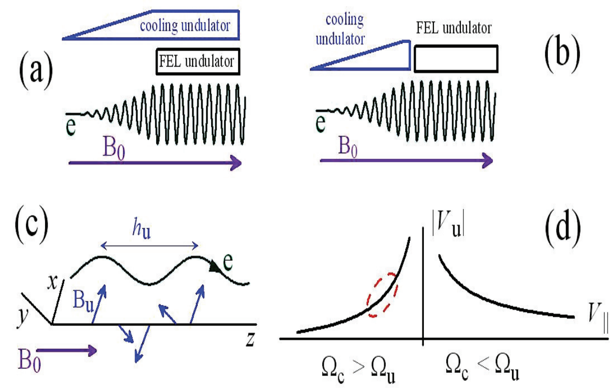

Figure 1: (a) and (b): Schematics of non-radiative cyclotron-undulator cooling systems with the operating FEL undulator placed inside and outside of the cooling system. (c): Electron motion in the circular polarized undulator with the uniform axial field. (d): Characteristic dependence of the undulator velocity on the axial electron velocity (the optimal range is shown schematically).

NON-RADIATIVE "AXIAL" COOLING

Non-radiative "axial" cooling is based on the fact that the axial velocity spread is the only factor important for the FEL operation. This spread can be decreased due to its "transformation" into the spread in the velocity of electron rotation in the cooling system. Electrons move along axial magnetic field and enter the cooling undulator with the adiabatically growing field in the input section, where each electron gets its own rotatory velocity (Fig. 1a). If at the input of the system every particle possesses only the axial velocity $V_0 = \overline{V} + \delta V$, then the axial velocity in the regular region of the undulator is determined by the energy conservation law: $V_{||}^2 \approx V_0^2 - V_u^2$. Thus,

$$V_{||}^2 \approx \overline{V}^2 + 2\overline{V}\delta V - V_u^2(\overline{V}) - \alpha\delta V \quad , \quad \alpha = \partial V_u^2 / \partial V_{||} .$$

If $\alpha = 2\overline{V}$, then the spread in $V_{||}$ disappears. This condition is independent of the initial spread, δV. Evidently, we should use the range of parameters, where $\partial |V_u| / \partial V_{||} > 0$ (Fig. 1d), so that the initial axial velocity excess, δV, is compensated by the greater rotatory velocity, V_u.

If such a cooling system is used in a FEL, then the operating FEL undulator designed to produce optical radiation can be placed inside the regular section of the cooling undulator (Fig. 1a). Another way is to "switch off" the field of the cooling "undulator" sharply (Fig. 1

ISBN 978-3-95450-133-5

OPTIMIZATION OF FEL PERFORMANCE BY DISPERSION-BASED BEAM-TILT CORRECTION

Marc W. Guetg*, Sven Reiche
Paul Scherrer Institut, CH-5232 Villigen PSI, Switzerland

Abstract

In Free Electron Lasers (FEL) the beam quality is of crucial importance for the radiation power. A transverse centroid misalignment of longitudinal slices in an electron bunch reduces the effective overlap between radiation field and electron bunch. This leads to a reduced bunching and decreased FEL performance.

The dominant sources of slice misalignments in FELs are the coherent synchrotron radiation within bunch compressors as well as transverse wake fields in the accelerating cavities. This is of particular importance for over-compression, which is required for one of the key operation modes for the SwissFEL under construction at the Paul Scherrer Institute in Switzerland.

The slice centroid shift can be corrected using multi-pole magnets in dispersive sections, e.g. the bunch compressors. First and second order corrections are achieved by pairs of sextupole and quadrupole magnets in the horizontal plane while skew quadrupoles correct to first order in the vertical plane.

INTRODUCTION

An FEL strives to have a relative bandwidth of the photon energies of the order of 10^{-4}. For specific applications like powder diffraction, Bragg imaging, or single-shot absorption spectroscopy much larger bandwidths are desirable to increase the chance of hitting resonances [1, 2]. A special configuration of the FEL under construction at PSI Switzerland, SwissFEL [3], will yield a bandwidth of up to 3% at 1 Å to fulfill these needs. In the following we refer to it as the large-bandwidth mode of SwissFEL.

This mode uses a high energy chirp along the bunch to increase the photon bandwidth. The longitudinal wakefields [4] originating in the cavities of the last linac and an over-compression in the final bunch compressor (BC) to revert the sign of the incoming energy correlation create the needed chirp. Because of over-compression coherent synchrotron radiation (CSR) considerably deteriorates the transverse profile by introducing beam distortion in the bending plane.

A beam slice misalignment reduces the overlap between the electron beam and its radiation field. This leads to a reduction of SASE performance in the offset regions. CSR, being a major contributor to the beam tilt, is of concern at small bunch lengths within the bending magnets. Therefore correction of the tilt is of special importance for the large-bandwidth mode of SwissFEL utilizing over-compression.

* marc.guetg@psi.ch

This work implements an alternative description of the beam tilt [5] and quantifies its effect on the lasing through genesis [6] simulations. In addition we address the induced orbit and bunch length jitter.

THEORY

This section describes the beam tilt and how to manipulate it. In this work x stands for both transverse planes and z the longitudinal direction. The Taylor approximation of the beam tilt μ is:

$$\tilde{x}(z) = x + \sum_{i=1}^{n} \mu_i \left(z^i - \langle z^i \rangle \right), \tag{1}$$

$$\tilde{x}'(z) = x' + \sum_{i=1}^{n} \mu_i' \left(z^i - \langle z^i \rangle \right), \tag{2}$$

where n corresponds to the highest order to be considered. Misaligned beam parameters are denoted by a tilde. This description has the benefit of adjustable abstraction without losing analytical correctness if n reaches infinity.

This work uses the statistical emittance (ε) defined as:

$$\varepsilon_x^2 = \langle x^2 \rangle \langle x'^2 \rangle - \langle x x' \rangle^2 . \tag{3}$$

The parameter x' denotes the momentum normalized by the total momentum. The beam tilt μ alters the emittance as follows:

$$\tilde{\varepsilon} = \varepsilon \sqrt{1 + M_n + M_n^*} , \tag{4}$$

where M corresponds to the pure and M^* to the mixing term. They are both expressed through

$$M_n = \frac{1}{\varepsilon_x} \sum_{i,j=1}^{n} \left(\beta_x \mu_i' \mu_j' + \gamma_x \mu_i \mu_j - 2\alpha_x \mu_i \mu_j' \right) Z_{i,j} , \tag{5}$$

$$M_n^* = \frac{1}{\varepsilon_x^2} \sum_{i,j,k,l=1}^{n} \left(\mu_i \mu_j \mu_k' \mu_l' - \mu_i \mu_j' \mu_k \mu_l' \right) Z_{i,j} Z_{k,l} , \tag{6}$$

where α,β,γ are the Twiss parameters and $Z_{i,j}$ is the reduced mean, defined as:

$$Z_{i,j} = \langle z^{i+j} \rangle - \langle z^i \rangle \langle z^j \rangle . \tag{7}$$

For a linear longitudinal phase-space correlation, considering μ up to only first-order ($n = 1$), M^* vanishes and M simplifies to

$$M_1 = \frac{\varepsilon_z \beta_z}{\varepsilon_x} \left(\mu_1'^2 \beta_x + \mu_1^2 \gamma_x + 2\mu_1 \mu_1' \alpha_x \right), \tag{8}$$

where ε_z corresponds to the longitudinal emittance and β_z to the longitudinal beta function.

ISBN 978-3-95450-133-5

THE SEED LASER SYSTEM FOR THE PROPOSED VUV FEL FACILITY AT NSRRC

M.C. Chou#, N.Y. Huang, A.P. Lee, W.K. Lau, NSRRC, Hsinchu, Taiwan

Abstract

The possibility of establishing a free electron laser (FEL) facility in Taiwan has been a continuing effort at National Synchrotron Radiation Research Center (NSRRC) in the past several years. The Baseline design of the envisioned NSRRC FEL is a high gain harmonic generation (HGHG) FEL seeded by a 266 nm laser. The seed laser is produced by adding an optical parametric amplification (OPA) system pumped by upgrading the existing IR laser system. To provide broad tunability of the FEL radiation, the seed laser will be tunable. The spectrum considered for seeding the FEL is between 266 - 800 nm with peak power of 200 MW. The spatial and temporal overlap between the sub-100 fs electron bunch and the 100 fs UV seed laser is under study.

INTRODUCTION

An FEL facility aimed for VUV and THz radiation is being studied at NSRRC in Taiwan [1]. To fulfil the user needs, this facility is designed to be operated in two modes, one for VUV applications and the other for THz applications. Recently, there are growing interests in applications like spectroscopy, elementary excitations, and NMR spectroscopy, etc., requiring high power THz radiation from the accelerator-based devices. The non-invasive and non-ionizing nature of THz spectroscopy is vital for medicine and biology applications from the safety point of view. On the other hand, this proposed facility will provide intense, fully coherent ultrafast light sources up to the extreme VUV region. Direct VUV photoionization is a key approach to probe properties of valence electrons of molecules and materials, which mostly lie at about 6 - 20 eV below the ionization limit. The Baseline FEL lies in this exact energy region and is therefore most suitable to study the transformation of molecules and materials that are important in many research fields. This proposed VUV FEL light source will provide scientists a promising tool to develop more sensitive experimental methods to prove important chemical and physical processes in energy, biological and environmental sciences.

Strong consideration has been given to minimize the cost by making maximum use of existing hardware at NSRRC. One unique consideration is to use an existing undulator for the dual functions of the THz radiator and the modulator of an HGHG section. Design emphasizes versatility of operation and beam quality control and compensation of nonlinearities, with an envision that it will allow as much as possible future upgrades as well as later R&D of FEL physics. The possibility of establishing a free electron laser facility in Taiwan has been a continuing effort at NSRRC in the past several years. With the installation of a new 3-GeV storage ring, the Taiwan Photon Source (TPS), it is a good time to renew this effort on the feasibility of an FEL facility. We consider it to serve two purposes:

1. To develop a technology platform for FEL researches in Taiwan. This FEL platform will provide a technology base to pursue a wide range of future possibilities beyond TPS, including industrial applications such as high brightness electron gun technology, and lithography manufacturing.
2. To initiate an FEL science research, and to provide a training ground for FEL researchers in Taiwan. This facility will allow the researchers to gain experience and accumulate credentials, and prepare to compete in the FEL world stage.

In the beginning of 2013, the first operation of the 2998 MHz photoinjector at NSRRC has been successfully preformed after high power microwave processing of the photoinjector cavity up to 60 MV/m. A 266-nm, 300-μJ ultra-violet (UV) laser system has been installed as the drive laser for the photocathode RF gun. A stable electron beam with energy of 2.6 MeV at 250 pC bunch charge has been achieved. Beam transverse emittance of ~3 mm mrad is measured at 250 pC with Gaussian laser pulse [2]. A new photo-cathode rf gun cavity is in fabrication for higher field gradient operation. Laser shaping technique can be employed to further reduce the beam emittance.

THE PROPOSED FEL FACILITY

The System Layout

The Baseline design of the envisioned NSRRC FEL is an HGHG FEL seeded by a 266 nm laser. With the existing linac sections and the high power klystron systems, an accelerated beam with beam energy of ~ 325 MeV at the linac end can be expected. With the existing hardware and the possible upgrades in the limited space, we consider the Baseline design of the envisioned NSRRC FEL as an HGHG FEL seeded by a 266 nm laser to generate the VUV radiation at 66.5 nm which is 4th harmonic of laser wavelength. The resonant condition is satisfied when the radiator strength is tuned as K = 1.98. The performance of HGHG FELs has been discussed widely in recent 10 years [3]. In addition to being much stable and tunable with narrow bandwidth, the HGHG source also offers fully temporally coherent radiation pulse. A schematic of the overall layout is shown in Fig. 1. The length of the accelerator system from the gun to L_3 exit is 27 m. The length of the diagnostics and FEL stations is 6 m. Including a 4 m × 5 m experimental area for users, the whole facility tightly fits into the existing 38 m × 5 m long tunnel in the TPS Linac Test Laboratory.

#chou.mc@nsrrc.org.tw

ISBN 978-3-95450-133-5

HIGHER-ORDER MOMENT MODELS OF LONGITUDINAL PULSE SHAPE EVOLUTION IN PHOTOINJECTORS*

C. Mitchell†, J. Qiang, F. Sannibale, M. Venturini, C. Papadopoulos, D. Filippetto, H. Qian, R. Huang
LBNL, Berkeley, CA 94720, USA

Abstract

The presence of longitudinal asymmetry, sometimes in the form of a one-sided tail, in the current profile emerging from low-energy photoinjectors can strongly impact the beam quality downstream of the compression region of an FEL beam delivery system. To understand the origin of this feature, an approximate model for the evolution of higher-order longitudinal beam moments is developed in the presence of nonlinear kinematic effects and longitudinal space-charge. This model is applied to investigate the evolution of beam skewness in injector systems with parameters similar to the APEX Injector under investigation at Lawrence Berkeley National Laboratory.

INTRODUCTION

Careful control of the longitudinal phase space distribution of each electron bunch exiting an FEL beam delivery system is critical to optimizing the FEL radiation brightness and coherence. Previous studies have shown that, in some cases, an asymmetric tail may appear in the beam current profile out of the injector [1], limiting the portion of charge that contributes to the lasing process. To understand this feature, we attempted to develop a simple model of the longitudinal pulse shape evolution in low-energy photoinjectors using a moment description.

The utility of the second-order rms beam envelope equations [2] has led to the study of systems of such equations for higher-order beam moments [3,4]. Our approach is based on the Hamiltonian formulation of the Vlasov-Poisson equation as described in [5], which provides a systematic framework for constructing moment equations through a given order [6]. The resulting system of equations describes the longitudinal beam moments through fourth order, using a 1D wakefield model of the longitudinal space-charge interaction.

This model was applied to an LCLS-II type injector system based on the design of the Advanced Photoinjector Experiment (APEX) at Lawrence Berkeley National Laboratory [7], whose layout is shown in Fig. 1. After photoemission from a 186 MHz RF gun, each bunch passes through a 1.3 GHz buncher cavity operated near 90° off-crest, which introduces an energy-bunch length correlation. The bunch then undergoes ballistic compression in a drift before entering the first of several 9-cell 1.3 GHz TESLA accelerating cavities.

In the following section, we characterize the longitudinal pulse shape in the injector using a moment description. In the remainder of the paper, this characterization is used to investigate the origin and evolution of longitudinal beam asymmetry in the presence of ballistic compression.

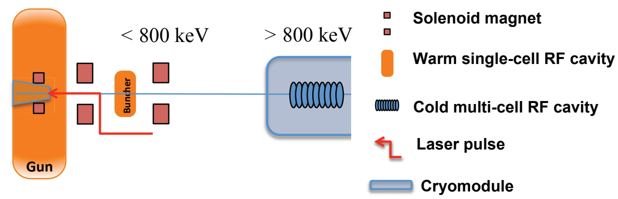

Figure 1: The low-energy portion of the photoinjector for an FEL beam delivery system based on the APEX design.

PULSE SHAPE CHARACTERIZATION

It is useful to characterize the shape of the electron bunch current profile in terms of the sequence of standardized moments:

$$\mu_n = \left\langle \left(\frac{z - \langle z \rangle}{\sigma_z} \right)^n \right\rangle, \quad n = 0, 1, 2, \ldots, \tag{1}$$

where z denotes the longitudinal coordinate within the bunch and σ_z the rms bunch length. The quantities μ_3 and μ_4 define the beam skewness and kurtosis, respectively, which must satisfy the inequality [8]:

$$\mu_4 \geq \mu_3^2 + 1. \tag{2}$$

The skewness is a measure of bunch asymmetry: for a bunch with a unimodal density profile, a value $\mu_3 > 0$ denotes that a low-density tail appears for $z > \langle z \rangle$, while $\mu_3 < 0$ denotes that a low-density tail appears for $z < \langle z \rangle$. The kurtosis is often described as a measure of "peakedness", and for a Gaussian profile takes the value $\mu_4 = 3$. Note that many authors use the excess kurtosis, defined by $\mu_4 - 3$.

An approximation to the shape of the beam current profile can be obtained by matching the centroid location, rms bunch length, and the moments (μ_3, μ_4) to a corresponding probability distribution from the Pearson family [9]- [12]. Figure 2 illustrates the current profile of a 300 pC, 99 MeV electron bunch at the exit of a proposed LCLS-II injector system based on the APEX design (Fig. 1), together with a Pearson distribution of matching skewness and kurtosis. Note the asymmetry of the current profile, with a slight tail appearing for $z < 0$.

Figure 3 illustrates the evolution of the skewness and kurtosis of this bunch during the first 3.5 m of the injector system of Fig. 1 as simulated using IMPACT-T [13]. The beam is nearly symmetric at the exit of the buncher, with

* Work supported by the U.S. Department of Energy under Contract No. DE-AC02-05CH11231.
† ChadMitchell@lbl.gov

ISBN 978-3-95450-133-5

ELECTRON BEAM DYNAMICS OPTIMIZATION USING A UNIFIED DIFFERENTIAL EVOLUTION ALGORITHM*

J. Qiang† and C. E. Mitchell, LBNL, Berkeley, CA 94720, USA

Abstract

Accelerator beam dynamics design depends heavily on the use of control parameter optimization to achieve the best performance. In this paper, we report on electron beam dynamics optimization of a model photoinjector using a new unified differential evolution algorithm. We present the new unified differential evolution algorithm and benchmark its performance using several test examples. We also discuss the application of the algorithm in the multi-objective optimization of the photoinjector.

INTRODUCTION

The photoinjector is a key component in the accelerator beam delivery system of next generation light sources, generating a high brightness electron beam into the accelerator. The goal of photoinjector beam dynamics design is to achieve a high peak current while maintaining low transverse emittances at the same time. This requires optimizing a number of physical control parameters such as accelerating RF cavity amplitudes and phases, focusing solenoid strengths and locations, and the initial distribution of the electron beam. In previous studies, multi-objective optimization based on genetic algorithms has been used in the photoinjector beam dynamics optimization [1–3]. In this paper, we apply a new unified differential evolution algorithm for multi-objective beam dynamics optimization.

The differential evolution algorithm is a relatively new method in evolutionary algorithms [4]. It is a simple but powerful population-based, stochastic, direct-search algorithm with self-adaptive step size to generate next-generation offspring for global optimization. In a number of comparison studies, it has been shown to be efficient in comparison to simulated annealing method, controlled random search, evolutionary programming, and genetic algorithms [4–6]. However, the standard differential evolution algorithm includes multiple strategies during the mutation stage. This could complicate the use of the algorithm. In this paper, we have adopted a unified differential algorithm recently proposed by the authors [7] in a newly developed variable population multi-objective differential evolution algorithm [8] in a photoinjector beam dynamics optimization.

STANDARD DIFFERENTIAL EVOLUTION

In the standard differential evolution algorithm, a population with size NP in control parameter space is randomly generated at the beginning. This population defines the first generation of the control parameters. After this initialization, the differential evolution algorithm consists of three stages to produce a new generation: mutation, crossover, and selection. Dur the mutation stage, for each parameter vector $\vec{x}_{i,G}, i = 0, 1, 2, \cdots, NP-1$ in a population of size NP at generation G, a perturbed vector $\vec{v}_i$ is generated using one of the following mutation strategies [4, 9]:

$$\text{DE/rand/1}: \quad \vec{v}_i = \vec{x}_{r_1} + F_{xc}(\vec{x}_{r_2} - \vec{x}_{r_3}) \tag{1}$$

$$\begin{aligned}\text{DE/rand/2}: \quad \vec{v}_i &= \vec{x}_{r_1} + F_{xc}(\vec{x}_{r_2} - \vec{x}_{r_3}) \\ &+ F_{xc}(\vec{x}_{r_4} - \vec{x}_{r_5})\end{aligned} \tag{2}$$

$$\text{DE/best/1}: \quad \vec{v}_i = \vec{x}_b + F_{xc}(\vec{x}_{r_1} - \vec{x}_{r_2}) \tag{3}$$

$$\begin{aligned}\text{DE/best/2}: \quad \vec{v}_i &= \vec{x}_b + F_{xc}(\vec{x}_{r_1} - \vec{x}_{r_2}) \\ &+ F_{xc}(\vec{x}_{r_3} - \vec{x}_{r_4})\end{aligned} \tag{4}$$

$$\begin{aligned}\text{DE/current-to-best/1}: \quad \vec{v}_i &= \vec{x}_i + F_{cr}(\vec{x}_b - \vec{x}_i) \\ &+ F_{xc}(\vec{x}_{r_1} - \vec{x}_{r_2})\end{aligned} \tag{5}$$

$$\begin{aligned}\text{DE/current-to-best/2}: \quad \vec{v}_i &= \vec{x}_i + F_{cr}(\vec{x}_b - \vec{x}_i) \\ &+ F_{xc}(\vec{x}_{r_1} - \vec{x}_{r_2}) + F_{xc}(\vec{x}_{r_3} - \vec{x}_{r_4})\end{aligned} \tag{6}$$

$$\begin{aligned}\text{DE/current-to-rand/1}: \quad \vec{v}_i &= \vec{x}_i + F_{cr}(\vec{x}_{r_1} - \vec{x}_i) \\ &+ F_{xc}(\vec{x}_{r_2} - \vec{x}_{r_3})\end{aligned} \tag{7}$$

$$\begin{aligned}\text{DE/current-to-rand/2}: \quad \vec{v}_i &= \vec{x}_i + F_{cr}(\vec{x}_{r_1} - \vec{x}_i) \\ &+ F_{xc}(\vec{x}_{r_2} - \vec{x}_{r_3}) + F_{xc}(\vec{x}_{r_4} - \vec{x}_{r_5})\end{aligned} \tag{8}$$

$$\begin{aligned}\text{DE/rand-to-best/1}: \quad \vec{v}_i &= \vec{x}_{r_1} + F_{cr}(\vec{x}_b - \vec{x}_i) \\ &+ F_{xc}(\vec{x}_{r_2} - \vec{x}_{r_3})\end{aligned} \tag{9}$$

$$\begin{aligned}\text{DE/rand-to-best/2}: \quad \vec{v}_i &= \vec{x}_{r_1} + F_{cr}(\vec{x}_b - \vec{x}_i) \\ &+ F_{xc}(\vec{x}_{r_2} - \vec{x}_{r_3}) + F_{xc}(\vec{x}_{r_4} - \vec{x}_{r_5})\end{aligned} \tag{10}$$

where the integers r_1, r_2, r_3, r_4 and r_5 are chosen randomly from the interval $[1, NP]$ and are different from the current index i, F_{xc} is a real scaling factor that controls the amplification of the differential variation, $\vec{x}_b$ is the best solution among the NP population members at the generation G, and F_{cr} is a weight for the combination between the original target vector and the best parent vector or the random parent vector. In order to increase the diversity of the parameter vectors, crossover between the parameter vector $\vec{x}_{i,G}$ and the perturbed vector $\vec{v}_i$ is introduced with an externally supplied crossover probability Cr to generate a new trial vector $U_{i,G+1}, i = 0, 1, 2, \cdots, NP-1$. For a D dimensional control parameter space, the new trial parameter vector $U_{i,G+1}, i = 0, 1, 2, \cdots, NP-1$ is generated using the following rule:

$$\vec{U}_i = (u_{i1}, u_{i2}, \cdots, u_{iD}) \tag{11}$$

$$u_{ij} = \begin{cases} v_{ij}, & \text{if } \text{rand}_j \le CR \text{ or } j = \text{mbr}_i \\ x_{ij}, & \text{otherwise} \end{cases} \tag{12}$$

where $rand_j$ is a randomly chosen real number in the interval $[0, 1]$, and the index mbr_i is a randomly chosen in-

* Work supported by the U.S. Department of Energy under Contract No. DE-AC02-05CH11231.

† jqiang@lbl.gov

ISBN 978-3-95450-133-5

THEORETICAL INVESTIGATION OF COHERENT SYNCHROTRON RADIATION INDUCED MICROBUNCHING INSTABILITY IN TRANSPORT AND RECIRCULATION ARCS*

C. -Y. Tsai#, Department of Physics, Virginia Tech, Blacksburg, VA 24061, USA
D. Douglas, R. Li, and C. Tennant, Jefferson Lab, Newport News, VA 23606, USA

Abstract

The coherent synchrotron radiation (CSR) of a high brightness electron beam traversing a series of dipoles, such as recirculation or transport arcs, may lead to the microbunching instability. We extend and develop a semi-analytical approach of the CSR-induced microbunching instability for a general lattice, based on the previous formulation with 1-D CSR model [1] and apply it to investigate the physical processes of microbunching amplification for two example transport arc lattices. We find that the microbunching instability in transport arcs has a distinguishing feature of multistage amplification (e.g, up to 6th stage for our example arcs in contrast to two stage amplification for a 3-dipole chicane [2]). By further extending the concept of stage gain as proposed by Huang and Kim [2], we developed a method to quantitatively characterize the microbunching amplification in terms of iterative or staged orders that allows the comparison of optics impacts on microbunching gain for different lattices. The parametric dependencies and Landau damping for our example lattices are also studied. Excellent agreement of the gain functions and spectra from Vlasov analysis with results from ELEGANT is achieved which helps to validate our analyses.

INTRODUCTION

As is well known, CSR effects have been one of the most challenging issues associated with the design of magnetic bunch compressor chicanes for X-ray FELs and linear colliders. Typically, CSR is emitted not only for a wavelength range comparable or longer than the bunch length duration but also for shorter wavelengths if the bunch charge density is modulated at such wavelength range (so called microbunching). Such coherent radiation effects, which have been confirmed both in numerical simulation and experiments, can result in undesirable beam quality degradation. The aforementioned works were, however, mostly focused on studies of magnetic bunch compressor chicanes. Recently the superconducting radio frequency recirculation linac facilities (e.g., free-electron laser facility or electron cooler for collider machine) have been brought to attention [3-5]. The recirculation or transport arcs are necessary elements in such facilities. However, similar studies on such systems with multiple modular dipoles as in a transport or recirculation arc were mostly focused on transverse beam dynamics while longitudinal phase space degradation has very limited discussions. In this paper, we pay attention to the CSR effects on the longitudinal beam dynamics as beam traversing around the recirculation arcs, particularly on the CSR-induced microbunching issues. The reasons to be concerned about the microbunching instability are based on the two facts: first, such system is characteristic of long transport lines with many dipole magnets whether in a single or multiple pass operation; the other, the system typically delivers the beam which features high beam quality, i.e. high brightness, for the use in next-generation light sources or hadron cooling in high-energy electron recirculating cooling rings. Thus, the seeds that cause density modulation, derived from either the density ripples from upstream injector or longitudinal space charge especially for low energy beam, would be extremely possible to lead to microbunching instability. Therefore further investigation of CSR-induced microbunching effects and its detailed physical processes are of critical importance and may shed light on how to improve designs for future lattices.

* Authored by Jefferson Science Associates, LLC under U.S. DOE Contract No. DE-AC05-06OR23177.
# jcytsai@vt.edu

METHODS

The CSR-induced microbunching instability can be formulated with the linearized Vlasov equation in typical bunch compressors [1]. This model makes coasting-beam approximation and assumes steady-state 1-D CSR [6] with negligible shielding (boundary) effects. By the method of characteristics, the linearized Vlasov equation can be rewritten as the general form of Volterra integral equation below [1]:

$$g_k(s) = g_k^{(0)}(s) + \int_0^s K(s,s')g_k(s')ds' \tag{1}$$

$$K(s,s') = \frac{ikr_e n_b}{\gamma} C(s)C(s')R_{56}(s'\to s)Z(kC(s'),s')$$

$$\times\ [\text{Landau damping}]$$

where the [Landau damping] term can be expressed as

$$\exp\left\{\frac{-k^2}{2}\left[\begin{array}{l}\varepsilon_{x0}\left(\beta_{x0}R_{51}^2(s,s')+\dfrac{R_{52}^2(s,s')}{\beta_{x0}}\right)\\ +\sigma_\delta^2 R_{56}^2(s,s')\end{array}\right]\right\} \tag{2}$$

Here the kernel function $K(s,s')$ describes the CSR interaction, $g_k(s)$ the resultant bunching factor as a function of the longitudinal position given the wavenumber k, and $g_k^{(0)}(s)$ is the bunching factor without CSR.

ISBN 978-3-95450-133-5

SIMULATION OF ALPHA MAGNET ELEMENTS IN DIPOLE-ONLY TRACKING CODES*,†

J.W. Lewellen# and F. Krawczyk, AOT-AE, LANL, Los Alamos, NM 87544 USA

Abstract

Alpha magnets [1] are useful in a variety of ion-beam and low-energy (< 5 MeV) electron-beam transport systems as both "switchyard" elements and as bunch compressors [2,3]. A unique feature of the alpha-magnet is its broad-band achromatic transport. Particles of different energies, injected at a specific location and angle, will exit at the same location and (symmetry-reflected) angle but with a different time-of-flight.

Despite the general usefulness of alpha magnets in low-energy beam transport and compression schemes, few simulation codes support them as native elements. The (arguably) most-commonly-used codes used for injector design, PARMELA [4], ASTRA [5] and GPT [6] (listed in order of their release) support tracking of space-charge-dominated beams through dipole magnets, but do not support alpha magnets. As a result, these codes are unable to directly model a useful and interesting beam transport device.

We present an approximate method for simulating an alpha magnet in a tracking code using dipole elements. As the simulation code **elegant** [7] supports alpha magnets as well as multiple dipole models, it is used to provide a basic check of the approximation and a means of estimating the induced errors.

INTRODUCTION

Alpha magnets refer to a general class of achromatic bending magnets [1]. They are so-named because a particle beam traversing a properly aligned alpha magnet follows a trajectory reminiscent of the Greek letter α as shown in Figure 1. While alpha magnets in general can have a field dependence $B_z \sim G\, x^n$, $n \geq 1$, quadrupolar alpha magnets (n=1) are the most practical to construct. Unless explicitly stated otherwise, the rest of this paper refers only to quadrupolar alpha magnets.

Figure 1 illustrates the achromatic nature of the alpha magnet: over a ±20% energy spread, electrons injected at the proper angle exit at the same point and angle; the trajectories are self-similar but have different overall length, facilitating the alpha magnet's use as a bunch compressor or stretcher, depending upon the chirp of the incoming beam. All particles cross the midplane, or x=0, line three times: at injection, at their maximum depth Δy within the alpha magnet, and at exit.

Using Borland's notation [8], the included half-angle of the alpha magnet θ_α is 40.71°. The general scaling factor for particle trajectories in an alpha magnet is

$$\alpha^2 = 5.867 \cdot 10^{-4}\text{cm}^{-2}\,\frac{g[\text{G/cm}]}{\beta\gamma}\ , \tag{1}$$

where g is the magnetic field gradient in Gauss cm^{-1}, γ is the particle's Lorentz factor, β is the particle's normalized velocity, and the product βγ is the normalized momentum. The total path length of the particle's trajectory is

$$s_\alpha = \frac{\Lambda_\alpha}{\alpha} = 191.655\ \text{cm} \cdot \sqrt{\frac{\beta\gamma}{g[\text{G/cm}]}}\,, \tag{2}$$

the maximum depth the particle reaches is

$$\Delta y = \frac{\Delta Q_1}{\alpha} = 75.0513\ \text{cm} \cdot \sqrt{\frac{\beta\gamma}{g[\text{G/cm}]}}\,, \tag{3}$$

and the trajectory width is

$$\Delta x = \frac{\Delta Q_2}{\alpha} = 49.212\ \text{cm} \cdot \sqrt{\frac{\beta\gamma}{g[\text{G/cm}]}}\,. \tag{4}$$

Λ_α=4.642, ΔQ_1 = 1.818 and ΔQ_2 = 1.192 are the normalized path length, path depth and path width, respectively, and along with θ_α are invariants for quadrupole-type alpha magnets.

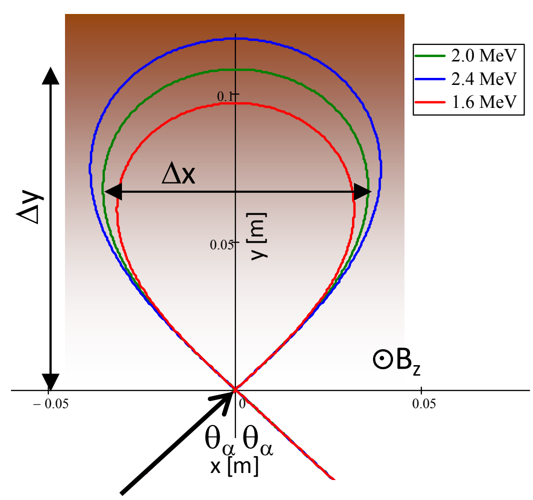

Figure 1: Three electron beam trajectories in an ideal quadrupolar alpha magnet: 2 MeV (green), 2.4 MeV (blue) and 1.6 MeV (red), all injected at the ideal injection angle along the line indicated by the black arrow. Background shading indicates relative magnetic field strength. The magnetic field gradient is 2.32 T/m.

The trajectory is self-similar for all choices of gradient and momentum, providing broadband achromaticity. For a fixed magnetic field gradient g and small variations of normalized momentum βγ around a central value, the path

* Work supported by the Los Alamos Accelerator Code Group
† Approved for public release: LA-UR-14-26276
# jwlewellen@lanl.gov

ISBN 978-3-95450-133-5

HIGH-GRADIENT CATHODE TESTING FOR MaRIE*,†

J.W. Lewellen#, N.A. Moody and F.L. Krawczyk, AOT-AE, LANL, Los Alamos, NM 87544 USA

Abstract

X-ray free-electron lasers (X-FELs) provide unprecedented capabilities for characterizing and controlling matter at temporal, spatial and energetic regimes which have been previously inaccessible. The quality of the electron beam is critical to X-FEL performance; a degradation of beam quality by a factor of two, for instance, can prevent the X-FEL from lasing at all, rather than yielding a simple reduction in output power.

The beam source for the world's first X-FEL, the LCLS at SLAC [1], defines the current state-of-the-art. Next-generation X-FELs such as MaRIE [2], intended to lase at 40 kV and beyond, will demand much higher quality electron beams, delivered at higher repetition rates, than present-generation injectors can deliver.

While conceptual designs for new beam sources exist [3], they incorporate assumptions about the behavior of the photocathode under extreme operating conditions. The combined requirements for high bunch charge, short bunch duration, and small emission area, dictate the use of high-efficiency photocathodes operating at electric field gradients of ~140 MV/m and durations of > 10 µs. No suitable cathode has been operated under these conditions, however, so the success of next-generation X-FELs rests on a series of untested assumptions. We present our plans to address these knowledge gaps, including the design of a high-gradient RF cavity specifically designed for testing cathodes under MaRIE-relevant conditions.

INTRODUCTION

The MaRIE X-ray free-electron laser is intended to produce coherent X-ray photons at energies of 40 kV and higher. MaRIE requires a 12-GeV electron beam at the undulator with a normalized emittance of ~ 0.1 µm RMS, a duration of 12 fs, an energy spread of < 0.015%, and a bunch charge of 100 pC. Further, the MaRIE linac must deliver a pulse train to the undulator, with RF macropulse-average currents up to ~ 100 mA. These requirements, in turn, place extreme demands upon the MaRIE beam source and, in particular, the cathode.

Cathode-Related Considerations

The beam emission radius on the cathode must be small, on the order of a fraction of a millimeter, to satisfy the transverse beam quality requirements; an emission time on the order of a few ps is also required. This combination generally precludes the use of a metallic photocathode because the low quantum efficiency would require a drive laser pulse with power densities approximating the ablation threshold.

The high emission current density requires extremely high electric field gradients at the cathode's surface to overcome the bunch's self-fields, which would otherwise limit the emitted current density or otherwise degrade the beam quality.

Gun-Related Considerations

The cathode must be removable from the injector to allow introduction, replacement and refurbishment of the selected cathode. This means the cathode-to-gun RF joint must also withstand RF fields up to 140 MV/m for durations of at least 10 µs, and potentially much longer if the MaRIE baseline linac design is made superconducting. [4]

DESIGN REQUIREMENTS

Our initial experiments will characterize the effects of a MaRIE-relevant operating environment upon cathode dark current emission and quantum efficiency.

In broad terms, our research will address two questions: What will operating at the high gradients required over long RF pulses do to a semiconductor or multi-alkali cathode; and What will the cathode, operating at high gradient, do to the linac?

The former question relates primarily to the potential damage to the cathode from field-emission electrons and ions within the gun cavity, and to the nature and extent of changes to the surface and emission properties of the emitting surface from exposure to high gradients, both instantaneous and long-term.

The latter question relates to characterization of dark current from the cathode (and candidate RF joint designs), and to the potential for the cathode constituent elements to degrade the gun's ability to generate and sustain the required electric field gradients.

The cathode test cell design, therefore, must meet several primary design objectives:

- It must provide MaRIE-relevant RF gradients (140 MV/m) and pulse durations (10 µs or longer);
- It must provide multiple viewports to both image and direct a photocathode drive laser onto candidate cathodes; and
- It must facilitate ready removal and replacement of candidate photocathodes.

Secondary design objectives include:

- It must be modular, to allow rapid and inexpensive modifications, upgrades or repairs; and
- It must demonstrate successful, low-field-emission operation of the cathode-to-gun RF joint.

* Work supported by the US Department of Energy
† Approved for public release: LA-UR-14-26438
# jwlewellen@lanl.gov

ISBN 978-3-95450-133-5

LINEAR ACCELERATOR DESIGN FOR THE LCLS-II FEL FACILITY

P. Emma, J. Frisch, Z. Huang, A. Marinelli, T. Maxwell, H. Loos, Y. Nosochkov, T. Raubenheimer, J. Welch, L. Wang, M. Woodley, SLAC, Stanford, CA 94309, USA
A. Saini, N. Solyak, FNAL, Batavia, IL 60510, USA
J. Qiang, M. Venturini, LBNL, Berkeley, CA 94720, USA

Abstract

The *LCLS-II* is an FEL facility proposed in response to the July 2013 BESAC advisory committee, which recommended the construction of a new FEL light source with a high-repetition rate and a broad photon energy range from 0.2 keV to at least 5 keV. A new CW 4-GeV electron linac is being designed to meet this need, using a superconducting (SC) L-band (1.3 GHz) linear accelerator capable of operating with a continuous bunch repetition rate up to 1 MHz at ~16 MV/m. This new 700-m linac is to be built at SLAC in the existing tunnel, making use of existing facilities and providing two separate FELs, preserving the operation of the existing FEL, which can be fed from either the existing copper or the new SC linac. We briefly describe the acceleration, bunch compression, beam transport, beam switching, and electron beam diagnostics. The high-power and low-level RF, and cryogenic systems are described elsewhere.

INTRODUCTION

The LCLS-II [1] high-repetition rate FEL project at SLAC aims to construct a new superconducting linac composed of TESLA-like RF cavities in continuous wave (CW) operation, in order to accelerate a 1-MHz electron beam to 4 GeV. This new superconducting linac (SC-linac), driven by a new high-rate injector [2], will replace the existing SLAC copper linac in sectors 1-7 (101.6 m/sector), while the remaining Cu RF structures in sectors 7-10 will be removed and replaced with a simple beam pipe and focusing lattice (the "linac extension"). The existing 2-km PEP-II bypass line (suspended from the tunnel ceiling) will be modified to transport electrons from the linac extension in sector 10 through more than 2.5 km and into either of two undulators in the existing LCLS undulator hall. The layout is shown in Figure 1 with the SC-linac in blue at far left and the SXU and HXU undulators at far right. The "linac extension" and "bypass line" are also shown.

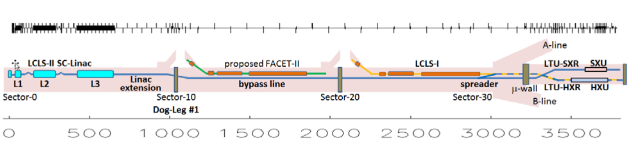

Figure 1: LCLS-II layout in existing SLAC tunnels (3.8 km).

LINAC AND RF LAYOUT

The *nominal* requirements of this new high-power linac are to accelerate a continuous rate of electron bunches, with 100 pC per bunch, at a 0.6-MHz repetition rate (or higher with a reduced bunch charge to 10 pC, or lower with 300-pC, maintaining <120 kW in each of two electron dump lines). This new linac makes use of the 'Tesla-Technology' accelerating module, with thirty-five 13-m long cryomodules (CM), each including eight 9-cell L-band RF cavities (1.038 m/cavity) cooled to 2.0 K using liquid Helium. In addition, a short 3.9-GHz third-harmonic linac (HL) section is used to linearize the bunch compression process in two short cryomodules, each including eight special 9-cell, 3.9-GHz cavities (0.346 m/cavity) with up to 80 MV of on-crest voltage (decelerating). The linac design includes bunch compressors to nominally produce a 1-kA peak current at 100 pC/bunch without significantly increasing the transverse emittance. Finally, the design must reduce the final correlated energy spread to <0.03% rms and stabilize the beam against the microbunching instability by adding a small intrinsic energy spread (5-6 keV rms) at the injector, using a laser heater (LH) system [3] at 100 MeV.

The linac is segmented into several sections in order to include two magnetic chicanes to compress the bunch to a 1-kA peak current (8.6 micron rms bunch length at 100 pC). The linac segments and their various parameters are summarized in Figure 2, including the beam energy, rms bunch length, rms relative energy spread, chicane strength (R_{56}), RF phases, crest voltage, and cryomodule number. The RF parameters are in Table 1.

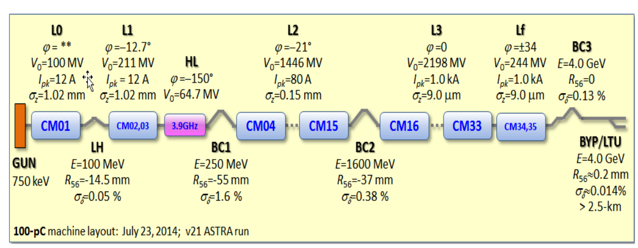

Figure 2: Linac layout with RF and compression parameters.

Table 1: SC-linac RF Parameters at 100 pC/bunch

Linac section	Phase (deg)	Gradient (MV/m)	No. of CM's	Avail. cavities	Powered cavities
L0	~0	16.3	1	8	7
L1	-12.7	13.6	2	16	15
HL	-150	12.5	2	16	15
L2	-21	15.5	12	96	90
L3	0	15.7	18	144	135
Lf	±34	15.7	2	16	15

ISBN 978-3-95450-133-5

DESIGN STUDY OF LCLS CHIRP-CONTROL WITH A CORRUGATED STRUCTURE

Z. Zhang, K. Bane, Y. Ding, Z. Huang, R. Iverson, T. Maxwell, G. Stupakov, L. Wang
SLAC National Accelerator Laboratory, Menlo Park, CA 94025, USA
M. Ruelas, M. Harrison, P. Frigola
Radiabeam Systems, Santa Monica, CA 90404, USA

Abstract

The purpose of this paper is to investigate the use of flat metallic plates with small corrugations as a passive dechirper, studying its effects on beam dynamics. Similar systems have been tested in Pohang and Brookhaven at relatively low energies (100 MeV) and with relatively long bunches (>1ps) [1,2]. Four meters of such a structure are being machined by Radiabeam Systems for use in the LCLS with a high energy and femtosecond electron beam. In this paper we use a field matching program to obtain the longitudinal and transverse wakes for the purpose of the LCLS dechirper design. In addition, we fit the longitudinal wake to simple functions, so that one can obtain the wake without resorting to the field matching program. Since the transverse wakes–both dipole and quadrupole wakes–are strong, we include beam dynamics simulations to find the tolerances for injection jitter and misalignment in the LCLS.

INTRODUCTION

In a linac-based X-ray free electron laser (FEL) there is often a need for energy chirp control of the beam as the magnetic compression employed in such FELs typically leaves an undesired time-energy correlation in the bunch, which can broaden the FEL bandwidth. While the chirp can be removed by the off-crest acceleration in a following linac section, this solution can be costly or impractical, particularly for a superconducting linac-based FEL. For such cases, a dedicated structure that can intentionally generate a strong longitudinal wakefield was recently proposed to dechirp the beam. In Ref. [3], a round metallic structure with corrugated walls was suggested and analyzed as a passive dechirper. Compared to round geometry, the flat geometry of corrugated plates has the advantage of allowing the dechirper strength to be adjusted by changing the separation of the plates [4].

In both round and flat structures, the transverse wakes can be strong, with amplitude scaling as the -4th power of aperture (vs. the -2nd power for the longitudinal wake). In a flat structure, however, in addition to the usual dipole wakefield that is excited when the beam passes through the structure off axis, there is also a quadrupole wake excited, even when the structure and beam are perfectly aligned. These transverse wakes will, if not properly controlled, increase the projected transverse emittance and lead to a deterioration of FEL performance.

Similar dechirper systems have been tested in Pohang and Brookhaven at relatively low energies (100 MeV) [1,2] and a new one is being machined for use at the LCLS [5,6]. However, when this structure is used for high energy beam, such as found in the LCLS, in order to generate a significant dechirping effect, the gap between the two plates needs to be set very small (< 1 mm). And to relax the manufacture tolerance, the size of corrugations are chosen at 0.5 mm, which is comparable to the gap size. In this case, the analytical formulas of wakefields are not applicable. In this paper the longitudinal and transverse wakes of the flat corrugation structure are calculated by the field matching method [7] and a simplified fitting formula with corrugation parameters is obtained for the longitudinal wakefield. A detailed tolerance study including beam offset, alignment error and structure imperfection is also conducted for the designed device.

FIELD MATCHING AND FITTING FORMULA

Figure 1 gives a sketch of the dechirper, showing the parameters half-gap a, corrugation period p, corrugation slit t, corrugation depth h, and width w. The wakefields of the structure are characterized by these parameters.

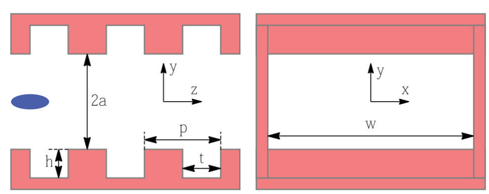

Figure 1: Geometry of dechirper structure parameters.

The analytical theory of wakefields in Ref. [3,7,8] is based on the assumption that all dimensions of the corrugations are much smaller than the gap size and the structures are deeply corrugated

$$p, h \ll a \quad \text{and} \quad h \gtrsim p \tag{1}$$

and also assuming large aspect ratio $w/2a$. The point charge wakefield for the flat pipe with small corrugations can be written as

$$W(z) = \frac{\pi^2}{16}\frac{Z_0 c}{\pi a^2}\cos(kz), \qquad z > 0 \tag{2}$$

where $Z_0 = 377\Omega$ is the characteristic impedance of vacuum and c is the speed of light. The wave number, k, is well approximated by

$$k = \sqrt{\frac{p}{aht}} \tag{3}$$

ISBN 978-3-95450-133-5

LCLS-II BUNCH COMPRESSOR STUDY: 5-BEND CHICANE*

D.Z. Khan[#], T.O. Raubenheimer, SLAC, Menlo Park, CA 94025, USA

Abstract

In this paper, we present a potential design for a bunch compressor consisting of 5 bend magnets which is designed to compensate the transverse emittance growth due to Coherent Synchrotron Radiation (CSR). A specific implementation for the second bunch compressor in the LCLS-II is considered. The design has been optimized using the particle tracking code, ELEGANT [1]. Comparisons of the 5-bend chicane's performance with that of a symmetric 4-bend chicane are shown for various compression ratios and bunch charges. Additionally, a one-dimensional, longitudinal CSR model for the 5-bend design is developed and its accuracy compared against ELEGANT simulations.

INTRODUCTION

The Linac Coherent Light Source (LCLS) at SLAC has shown tremendous success in its scientific capabilities in the biological, chemical, atomic and material sciences [2, 3, 4]. To build upon the success of the LCLS, a myriad of upgrades will be made to push the limits of current x-ray free-electron laser (X-FEL) design and technology to meet the ever growing demands of the scientific community. LCLS-II is an upgrade of the LCLS based on a 4 GeV superconducting RF linac [5]. Among the many upgrades being researched, one of particular interest is the bunch compression system.

Compression of electron beams is important in FELs to minimize the gain length [6]. A successful compression system is one that compresses the bunch longitudinally while preserving the beam's transverse emittance. The currently planned compression system of LCLS-II, and many current X-FEL facilities such as FLASH (DESY) [7] and SACLA (RIKEN) [8], uses a sequence of magnetic chicanes to compress the bunch length by orders of magnitude [5]. LCLS-II's two-stage compression (Fig. 1) is simple and effective but poses problems towards the end of its compression cycle via CSR's dilution of horizontal emittance.

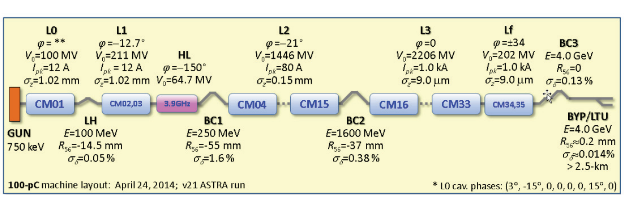

Figure 1: A diagram of the LCLS-II beamline with relevant component details. LCLS-II plans to utilize a two-stage magnetic chicane compression system; BC1 and BC2. The topic of this paper focuses on the self-radiative effects of the electron beam experienced in BC2.

*Work supported by Department of Energy Contract No. DE-AC02-76SF00515.

#donish@SLAC.stanford.edu

On the curved sections of an FEL beamline the electron beam can interact with itself. The synchrotron radiation from the electrons in the tail of the bunch can interact with the electrons in the head under the right conditions. The phenomenon becomes highly disruptive when the phase difference between the radiating electrons is small i.e. when the bunch length becomes comparable to the radiation wavelength. Under this regime, the synchrotron radiation becomes coherent and its power scales as N^2, where N is the electron population of the bunch. In the coherent regime, the radiation causes a strong non-linear longitudinal energy chirp. This chirp can be estimated using a simple 1-D model [9]:

$$\frac{dE}{ds}(z) = \int_{-\infty}^{z} \frac{d\lambda(z')}{dz\prime} \left(\frac{1}{(z-z')^{\frac{1}{3}}} \right) dz' \qquad (1)$$

$$\sigma_{RMS-\delta} = 0.22 \frac{r_e N L_B}{\gamma \rho^{2/3} \sigma_z^{4/3}} \propto [L_B^{\frac{1}{3}}][\theta^{\frac{2}{3}}][\sigma_z^{-\frac{4}{3}}] \qquad (2)$$

where z is the longitudinal position along the bunch, λ is the normalized electron distribution, L_B is the magnet length, ρ is the bending radius and σ_z is the RMS bunch length. Equations 1 and 2 are derived from a 1-D model of the steady-state CSR wakefield. The CSR effect can create a number of unwanted effects on the electron beam [10, 11]. In this paper, we concern ourselves namely on CSR's influence on the bend plane's projected emittance growth.

Novel techniques have been developed to mitigate and nullify the CSR effect. Adjusting the linac optics to provide a $-I_{2x2}$ transfer matrix between two sequential bends (such as in doglegs) has shown to provide excellent cancellation of CSR induced emittance growth [12]. A main assumption of this method is that the bunch length of the beam is constant between successive bends and therefore, the CSR RMS energy spread can be assumed to be identical at each location. The matter becomes highly complicated when the bunch length between the two successive bends is evolving, such as that of the bunch compressor. For an evolving bunch length, studies have shown that a minimization of the $\mathscr{H}$-function in CSR significant bends results in significant reduction of emittance growth [13]. Compressor designs based on matched chicanes or large period wigglers can also reduce the emittance growth [14, 15]. Utilizing asymmetry in a chicane design (allocating more R_{56} in the first half of a, for example, 4-bend chicane) has shown success in partial nullification of emittance dilution when compared to the standard symmetric designs [16, 17]. Additionally, it has been shown that, in multi-stage compression systems, allocating more R_{56} to the initial bunch compressors, while maintaining final compression, dampens the CSR effect in the final compressor where CSR is most detrimental [13]. Though the techniques cited

ISBN 978-3-95450-133-5

MOGA OPTIMIZATION DESIGN OF LCLS-II LINAC CONFIGURATIONS*

L. Wang#, P. Emma, Y. Nosochkov, T. Raubenheimer, M. Woodley and F. Zhou,
SLAC, Stanford, CA 94309, USA
C. Papadopoulos, J. Qiang and M. Venturini, LBNL, Berkeley, CA 94720, USA

Abstract

This paper briefly summarizes the preliminary optimization study on the configurations of LCLSII with superconducting cavity. The setup of each configuration is first optimized using Multi-Objective Genetic Algorithm (MOGA) with LiTrack which includes the longitudinal phase space only. For each operation mode, MOGA is applied to optimize the machine parameters in order to get flat top current profile and zero energy chirp at the beginning of the undulator. The geometric wake of the RF cavities and resistive wall wake of the beam pipe are included, but the coherent synchrotron radiation (CSR) wake is not included. Finally, ELEGANT code is used to do full 3-dimension particle simulation, which includes the CSR and ISR effect. Therefore, the emittance growth due to CSR can be checked. A new code has been recently developed to integrate all the wake field and CSR in the MOGA optimization.

INTRODUCTION

The new LCLS-II high-repetition rate FEL project at SLAC [1] will use a new superconducting linac composed of TESLA-like RF cavities in continuous wave (CW) operation, in order to accelerate a 1-MHz electron beam to 4 GeV. Figure 1 shows the optics (top) of the hard x-ray beam and the layout of LCLS-II linac(bottom). The new superconducting linac is driven by a new high-rate injector [2], will replace the existing SLAC copper linac in sectors 1-7 (101.6 m/sector), while the remaining Cu RF structures in sectors 7-10 will be removed and replaced with a simple beam pipe and focusing lattice (the "linac extension"). The existing 2-km PEP-II bypass line (large β section in Fig.1) will be modified to transport electrons from the linac extension in sector 10 through more than 2.5 km and into either of two undulators in the existing LCLS undulator hall. The overall design of the linac can be found in [3]. The resistive wall wake field along this long bypass beam line play an important role in the linac design as discussed later. The current design has two bunch compressors (BCs), which are located at the 2nd and 3rd non-zero horizontal dispersion sections in Fig. 1. The 1st dispersion section is laser heater. The injector beam is optimized at beam energy of 98MeV [4] to give a small transverse emittance and certain peak current. This paper describes the optimizations afterwards to the beginning of the FEL undulator.

The main parameters to be optimized include the phase and voltage of linac 1 (L1), linearizer (before BC1), linac 2 (L2) (between BC1 and BC2) and the R56 of BC1/BC2. The beam energies at BC1 and BC2 are 250MeV and 1.6GeV, respectively. The beam is accelerated to 4.0 GeV by linac 3 (L3).

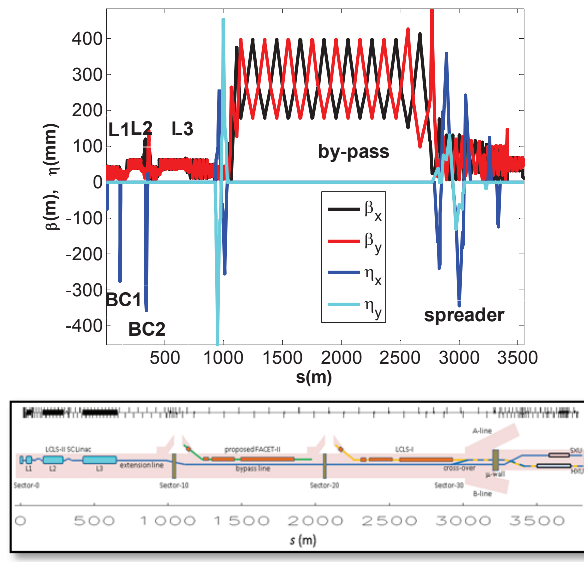

Figure 1: Optics (HXR)(top) and Layout (bottom) of the LCLS-II linac. The BC1 and BC2 are located at the 2nd and 3rd non-zero horizontal dispersion section, respectively.

NONLINEAR BEAM FROM INJECTOR

In the current design, the injector of LCLS-II uses CW normal conducting RF gun [2]. The strong space charge effect at the injector induces large nonlinearity in the longitudinal phase space. The dominant one is cubic term, which is the fundamental term of the longitudinal space charge effect. The high order terms also have large contributions to the linac beam dynamics. These nonlinear effects are amplified throughout the linac when the bunch is compressed. The strong space charge effect makes LCLS-II beam largely different from the existing LCLS beam where the nonlinear term (cubic term dominant) is mainly induced by the strong geometric wake in the normal conducting RF structures. As a result, the design of LCLS-II beam has strong dependence on the injector.

The longitudinal phase space, current profile and $Bmag = 0.5\left(\frac{\beta_0}{\beta} + \frac{\beta}{\beta_0} + \left(\alpha\sqrt{\frac{\beta_0}{\beta}} + \alpha_0\sqrt{\frac{\beta}{\beta_0}}\right)^2\right)$ along the bunch at linac with 98MeV beam are shown in Fig. 2 for three bunch charges: 20pC, 100pC and 300pC. The overall bunch profile is similar: there is a long bunch tail. The nonlinearity can be clearly seen after extracting the linear chirp and RF curvature as shown in Fig. 3. The high order terms are comparable to the cubic term. The

*Work supported by Department of Energy Contract No. DE-AC02-76SF00515
#wanglf@SLAC.stanford.edu

ISBN 978-3-95450-133-5

RECENT PHOTOCATHODE R&D FOR THE LCLS INJECTOR*

F. Zhou, J. C. Sheppard, T. Vecchione, E. Jongewaard, A. Brachmann,
J. Corbett, M. Ferreira, S. Gilevich, J. Lewandowski, S. Vetter, S. Weathersby,
SLAC, Menlo Park, CA 94025, USA

Abstract

The Linac Coherent Light Source (LCLS) has used three copper photocathodes since its commissioning in 2007. Two of three copper cathodes had low initial quantum efficiency (QE) ($<1\times10^{-5}$) in the LCLS radio frequency (RF) gun. The two cathodes were exposed to the plasma cleaning in the cathode test chamber before installation in the RF gun. Recent studies at the SLAC RF gun test bed at the Accelerator Structure Test Area (ASTA) reveals that the pre-cleaning in the test chamber followed by cathode exposure to air for installation in the gun is the major factor leading to the low initial QE. All four cathodes, without the plasma pre-cleaning prior to the installation in the gun, have demonstrated initial QE$>4\times10^{-5}$ at the ASTA. Systematic studies also demonstrate that high-power RF gun operation provides an initial QE boost. In-situ laser cleaning for three new cathodes in the RF gun is extensively investigated, and a robust laser cleaning procedure is established at the ASTA with improvements of previous cleaning recipe for the LCLS cathode. The QE was shown to reproducibly evolved to $>1\times10^{-4}$ from about 4×10^{-5} immediately following the laser cleaning over ~3 weeks, a time much shorter than a few months for the previous laser cleaning for the present LCLS cathode. The intrinsic emittance of copper cathodes is recovered to the normal value within 1-2 days following the laser cleaning, much shorter than 3 weeks for previous laser cleaning for the present LCLS cathode. The experimental results at the ASTA, including comparison with the previous cleaning for the present LCLS cathode, are presented in the paper. Physics of the laser cleaning process and the evolution of the QE is discussed.

INITIAL QE WITHOUT IN-SITU CLEANING IN THE RF GUN

An RF gun test bed located at the SLAC's Accelerator Structure Test Area (ASTA) has been constructed [1] to study photocathodes for the Linac Coherent Light Source (LCLS) injector cathode operations. The beamline of the ASTA gun test bed duplicates the existing LCLS injector gun system [2], consisting of a chirp-pulse-amplifier laser tripled to 253 nm wavelength, LCLS-type RF gun, a solenoid for emittance compensation, one pair of magnet correctors, a Faraday cup to measure the bunch charge, and a YAG screen to measure beam size and intrinsic emittance. Similar to the LCLS injector, the drive laser is configured for normal incident injection to the photo-cathode surface using a 45° in-vacuum mirror. The final electron beam energy from the RF gun is about 5.5 MeV.

*The work is supported by DOE under grant No. DE-AC02-76SF00515.

The Cause for Low Initial QE in the RF Gun

The LCLS located at the SLAC National Accelerator Laboratory has been successfully operated for users for about 5 years. Its copper-based photo-injector has produced an ultra-low emitance and ultra-fast electron beam for the x-ray free electron laser (XFEL). Since its commissioning in 2007, three identical copper cathodes have been used for the LCLS injector operations with different initial quantum efficiency (QE) values. As illustrated in Fig.1, the first and third (present) LCLS cathodes had unexpectedly very low initial QE [3], about 5×10^{-6}, while the second one had 6.5×10^{-5} of initial QE as expected. Lately, it is realized that both the first and third LCLS cathodes were exposed to the plasma cleaning in the test chamber before cathode exposure to air for installation in the RF gun, while the second one did not have this cleaning process. Very low QE measured in the test chamber drives to proceed to plasma cleaning for the cathode prior to the installation in the gun. During the cathode installation in the LCLS RF gun, the cathodes have to be exposed to air for about 3 minutes for the cathode change due to the lack of loadlock system. The recent observations at the ASTA RF gun reveal that the laser-cleaned areas are much more susceptible to the air exposure than the non-cleaned areas do. The ASTA RF gun is vented to nitrogen and then exposed to air for about 3 minutes to mimic the LCLS cathode change before its vacuum starts to be pumped down. Figure 2 (left) and (right) shows the QE maps before and after the RF gun vacuum venting to air, respectively. Before the RF gun vacuum venting, areas A, B, C, D, E, F, G and H on the cathode have been cleaned by the intensive laser, while the circled center area is not exposed to any laser cleaning. In Fig. 2 (left), bunch charge from areas A, B and C have been evolved to about 7500 units for a given laser energy, equivalent to 1×10^{-4} of QE, while the cathode center area has about 3500 units of the bunch charge for the same laser energy, equivalent to about 4×10^{-5} of QE. After gun vacuum venting, bunch charge productions from the previously cleaned areas A, B, C, D, E, F, G, and H were dropped to 1500-2000 units shown in Fig. 2 (right), equivalent to about $1\text{-}2\times10^{-5}$ of QE, but the QE of the cathode center area still remains unchanged, at 4×10^{-5}. The observations indicate that the cleaned or activated surface is susceptible to the air-exposure, revealing the pre-cleaning is the cause for low initial QE measured in the RF gun.

Total four cathodes are characterized, which are not exposed to the pre-cleaning prior to the installation in the ASTA RF gun. All four ASTA cathodes have good initial QE in the RF gun ranging from 4×10^{-5} to 8×10^{-5}, as illustrated in Fig. 1. We conclude that the pre-cleaning

ISBN 978-3-95450-133-5

FURTHER UNDERSTANDING THE LCLS INJECTOR EMITTANCE*

F. Zhou, K. Bane, Y. Ding, Z. Huang, and H. Loos, SLAC, Menlo Park, CA 94025, USA

Abstract

Coherent optical transition radiation (COTR) from the laser heater chicane is recently observed at the OTR screen used for the injector emittance measurements at the Linac Coherent Light Source (LCLS). The injector emittance measured at the OTR screen is under-estimated by 30% due to the COTR effect. Slice emittance upstream of the first LCLS magnetic bunch compressor (BC1) is measured, 0.45 µm for a central slice beam, using a traditional transverse s-band radio frequency deflector. Slice x- and y-emittances downstream of the BC1 are measured using a recently developed technique. It makes use of a collimator in the BC1 center to select a small portion of beam as a time-sliced beam. The measured projected emittance for the slice beam is considered as the slice emittance. With the technique, the measured central slice y-emittance is 0.45 µm after the BC1, similar to the injector emittance before the BC1, but the measured so-called central slice x-emittance has about 20% of increase after the BC1. Further measurements and analyses reveal that the parasitic effects, including collimator wakes, longitudinal space charge and dispersion due to the introduction of the beam collimation, do not impact the measured slice x- and y-emittance but coherent synchrotron radiation (CSR) deteriorates the projected x-emittance of the slice beam. The measured projected x-emittance of a slice beam under the CSR condition cannot be considered as a slice x-emittance. The technique is capable of reliable measurements of a slice emittance in non-bending plane instead of the bending plane, when a beam transports through magnetic bunch compressors.

EMITTANCE AT 135 MEV, PRIOR TO THE BC1

The Linac Coherent Light Source (LCLS), located at the SLAC National Accelerator Laboratory, has been successfully operated for users for more than five years [1]. Accurately characterizing emittance particularly the injector emittance is of importance for the x-ray Free Electron Laser (FEL) operations. Figure 1 shows the major components of the LCLS injector and its first magnetic bunch compressor (BC1) [2]. It begins with a copper cathode s-band RF gun and two s-band linac sections producing an electron beam with energy of 135 MeV. The 135-MeV beam then passes through a small laser heater (LH) chicane, followed by an s-band transverse RF deflector for time-resolved beam measurements. The 135-MeV beam is measured by the emittance station consisting of three optical transition radiation (OTR) screens or wire scanners. Then the beam is transported into the main linac and accelerated to 240 MeV through the L1S before entering the BC1. Located between these two structures is the x-band RF structure to linearize the longitudinal phase space before the bunch compression. There are three wire scanners downstream of the BC1 for emittance measurements. The quadrupole scan is used to measure emittance for a 135 MeV beam with one OTR screen or wire-scanner, and for a 220 MeV compressed beam after the BC1 with one wire scanner. The bunch charge is 150 pC for all emittance measurement discussed in the context.

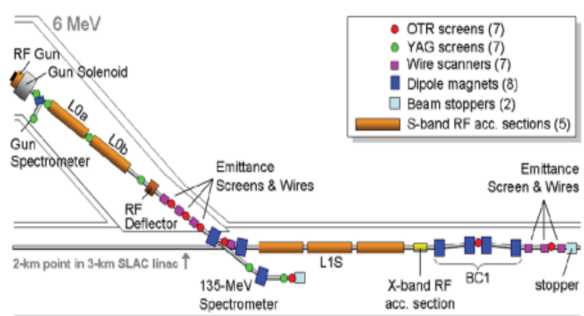

Figure1: Schematic layout of the LCLS injector including the BC1. The laser heater chicane is located in between the L0B and the RF deflector.

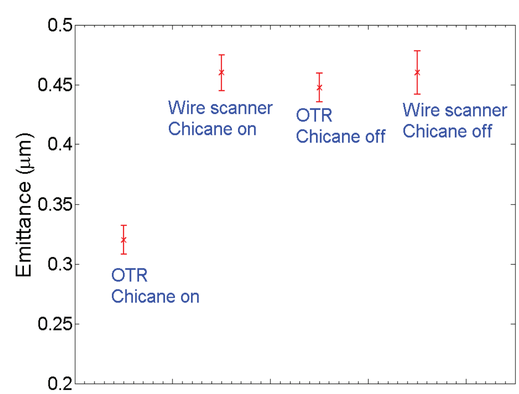

Figure 2: Projected emittance with the OTR screen and the wire-scanner for the LH chicane on and off at 135 MeV for 150 pC.

The LH chicane is to accommodate a short undulator for interaction of the laser beam with the electron beam to introduce an uncorrelated energy modulation of the electron beam to suppress the micro-bunching instability. The interaction of the electron beam with the laser beam in the LH chicane also induces micro-bunching at the laser wavelength and its harmonics, leading to coherent optical transition radiation (COTR) effects on the OTR screen [3] thereby impacting the accuracy of the emittance measurement. Therefore, the laser beam for the LH was always turned off but the LH chicane is normally

* The work is supported by U.S. DOE under grant No. DE-AC02-76SF00515.

ISBN 978-3-95450-133-5

EFFECTS OF POTENTIAL ENERGY SPREAD ON PARTICLE DYNAMICS IN MAGNETIC BENDING SYSTEMS *

R. Li , Jefferson Lab, Newport News, VA 23606, USA

Abstract

Understanding CSR effects for the generation and transport of high brightness electron beams is crucial for designs of modern FELs. Most studies of CSR effects focus on the impacts of the longitudinal CSR wakefield. In this study, we investigate the impact of the initial retarded potential energy of particles, due to bunch collective interaction, on the transverse dynamics of particles on a curved orbit. It is shown that as part of the remnants of the CSR cancellation effect when both the longitudinal and transverse CSR forces are taken into account, this initial potential energy at the entrance of a bending system acts as a pseudo kinetic energy, or pseudo energy in short, because its effect on particle optics through dispersion and momentum compaction is indistinguishable from effect of the usual kinetic energy offset from the design energy. Our estimation indicates that the resulting effect of pseudo energy spread can be measurable only when the peak current of the bunch is high enough such that the slice pseudo energy spread is appreciable compared to the slice kinetic energy spread. The implication of this study on simulations and experiments of CSR effects will be discussed.

INTRODUCTION

When a high brightness electron beam is transported through a curved orbit in a bending system, the particle dynamics is perturbed by the coherent synchrotron radiation (CSR) forces, or the collective Lorentz force as a result of the Lienard-Wiechert fields generated by particles in the bunch. The longitudinal CSR interaction takes place when the fields generated by source particles at bunch tail overtake the motion of the test particles [1] at bunch head and cause changes of kinetic energy for the head particles. For parameters currently used in most machine designs and operations, the approximation of the longitudinal CSR force by that calculated using 1D rigid-line bunch model [2] often gives good description of the observed CSR effects [3].

In addition to the longitudinal CSR force, the transverse CSR force [4] can directly perturb transverse particle dynamics. This force features energy independence and, due to divergent contribution from nearby-particle interaction, has strong nonlinear dependence on the transverse (and longitudinal) positions of particles inside the bunch. Meanwhile, the potential energy change, as a result of both longitudinal and radial CSR or Coulomb forces, can cause change of kinetic energy of the particles and impact transverse particle dynamics via dispersion. The joint effects of both the transverse CSR force and the kinetic energy change on bunch transverse dynamics have been analyzed earlier [5–7], and it is found that their harmful effects related to the potent feature of strong transverse dependence are cancelled. After the cancellation, the transverse dynamics of particles is perturbed by the remaining driving factors such as the effective longitudinal CSR force and the centrifugal force related to particles' initial potential energy.

In this study, we present the role of potential energy in the particle transverse dynamics after the cancellation effect is taken into account. We will show that the initial slice potential energy spread of a bunch, which we call pseudo slice energy spread, is indistinguishable from the usual slice kinetic energy spread in its perturbation to the transverse particle optics via both dispersion and momentum compaction. This effect is measurable only when the peak current of the bunch is high enough such that the pseudo slice energy spread is appreciable compared to the slice kinetic energy spread. The implication of this study on simulations and experiments of CSR effects will be discussed.

.

ROLE OF POTENTIAL ENERGY IN BUNCH TRANSVERSE DYNAMICS

In this section the CSR cancellation effect is briefly reviewed. We show how a centrifugal force term, which is related to the initial potential energy of particles, emerges as one of the remnant of the cancellation. We also discuss the role of initial potential energy in transverse particle dynamics.

Consider an ultrarelativistic electron bunch moving on a circular orbit with design radius R and design energy $E_0 = \gamma_0 mc^2$. Let $x = r - R$ be the radial offset of particles from the design orbit. The single particle optics is determined by the configuration of the external magnetic fields, while for a bunch with high peak current, this design optics will be perturbed by the Lorentz force $\mathbf{F}^{\rm col}$ resulting from the collective electromagnetic interaction amongst particles within the bunch. For transverse dynamics, such perturbation is expressed in terms of the first order equation

$$\frac{d^2x}{c^2dt^2} + \frac{x}{R^2} = \frac{\Delta E}{RE_0} + \frac{F_x^{\rm col}}{E_0}, \qquad (1)$$

with $F_x^{\rm col}$ being the radial component of the collective Lorentz force $\mathbf{F}^{\rm col} = F_s^{\rm col}\mathbf{e}_s + F_x^{\rm col}\mathbf{e}_r$, and $\Delta E = E - E_0$ being the deviation of the kinetic energy from the design energy. The existence and effect of transverse CSR force $F_x^{\rm col}$ were first pointed out by Talman [4] when he analyzed $F_x^{\rm col}$ for space charge interaction of a bunch on a circular orbit using Lienard-Wiechert fields. His study shows that

* Work supported by Jefferson Science Associates, LLC under U.S. DOE Contract No. DE-AC05-06OR23177.

ISBN 978-3-95450-133-5

MECHANICAL DESIGN FOR A CORRUGATED PLATE DECHIRPER SYSTEM FOR LCLS

M. Harrison*, P. Frigola, D.W. Martin, A. Murokh,
M. Ruelas, RadiaBeam Systems, Santa Monica, California, USA
Z. Huang, R. Iverson, T. J. Maxwell, Z. Zhang, SLAC, Menlo Park, California, USA

Abstract

RadiaBeam Systems is developing a novel passive chirp removal system using corrugated plates as studied by Bane and Stupakov [1]. Following on from low-energy experiments at BNL-ATF [2], RBS will install a much larger and powerful system for removing the chirp from the 3 GeV beams in the LTU section at LCLS. The larger plates will present new challenges in the areas of manufacturing and mechanical control. In this paper we review the requirements for the dimensions of the corrugated plates for proper operation and the infrastructure necessary for precisely placing the plates so as not to adversely disrupt the beam.

INTRODUCTION

Following the successful proof-of-concept dechirper experiment at Brookhaven National Laboratory [2], RadiaBeam Systems presents here plans for a scaled-up corrugated plate dechirper system for use in the 3 GeV Linac-To-Undulator (LTU) section at Linac Coherent Light Source (LCLS). The system will be designed to completely remove the residual chirp left over from the earlier compression sections. Prior beamlines required up to hundreds of meters of accelerating cavities running off-crest in order to lower the energy spread of the beam bunch enough for use in undulator light sources. The system described in this study will completely remove the chirp from the LCLS beamline with only two two-meter sections

CORRUGATED PLATES

The wakefield of a single electron is approximated by

$$W(z) = \left(\frac{\pi^2}{16}\right)\frac{Z_0 c}{\pi a^2} cos\left(\frac{2\pi z}{\lambda}\right), \qquad (1)$$

where Z_0 is the impedance of free space (377 Ω), c is the speed of light, and z is the bunch longitudinal coordinate. The wavelength of the wakefield, λ, given by

$$\lambda = 2\pi\sqrt{\frac{a\delta g}{p}}. \qquad (2)$$

The rest of the dimensions (a, δ, g, and p) refer to dimensions of the corrugations, detailed in Table 1 and Fig. 1.

The total wakefield of the bunch forms a linear region over the bunch. The slope of this region determines the dechirping strength, h, is given by

$$h = \left(\frac{\pi^2}{16}\right)\frac{Z_0 cQL}{\pi a^2 l}, \qquad (3)$$

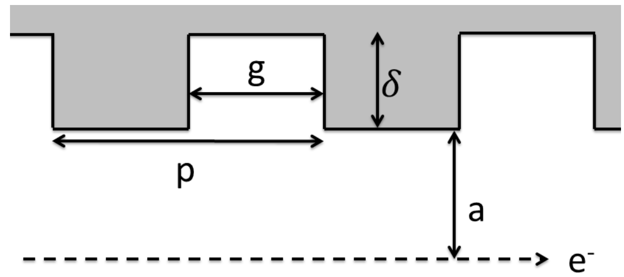

Figure 1: Dimensions of corrugated plates. See Table 1.

Table 1: Corrugated Plate Dimensions

Length	L	4.0	m
Width		12.7	mm
Period	p	0.51	mm
Depth	δ	0.51	mm
Gap	g	0.25	mm
Plate separation	a	1–30	mm
Material		Aluminum	

where Q is the bunch charge, L is the length of the dechirper, and l is the bunch length. More accurate simulations of the wakefield ([3, 4]) show this to be an overestimation by factor of about 1.5, but Equation 3 serves to motivate the dimensions of the corrugated plates.

From Equation 3, the most important dimension in the corrugated plate dechirper is the gap between the plates and the total length. Dechirping power scales proportionally with L and $1/a^2$. Balancing beamline space and the minimum size of the beam determines the overall size constraints. The other dimensions—period, depth, and gap—are only constrained by the wakefield equations to being much smaller than a [1]. Specifically,

$$\delta, p \ll a \qquad h \geq 0.8p \qquad t = p/2. \qquad (4)$$

For the LCLS dechirper, a total length of four meters (split into two equal length sections) was chosen to have a design gap ($2a$) of 1.4 mm [3]. A two-section dechirper also allows for cancellation of unwanted transverse quadrupole effects (to be discussed in the Other Considerations section.

The material of the corrugated plates was chosen to be aluminum because of its light weight and easy machinability. As long as the fundamental mode of the wakefield is dominant, the conductivity of the metal is unimportant [5]. To ease manufacturing and installation, the corrugated plates will be made in several sections each 0.5 meters long. Numerous simulations have been run to determine the tolerances

* harrison@radiabeam.com

ISBN 978-3-95450-133-5

FURTHER ANALYSIS OF CORRUGATED PLATE DECHIRPER EXPERIMENT AT BNL-ATF

M. Harrison*, G. Andonian, P. Frigola, M. Ruelas, A. Murokh,
A. V. Smirnov, RadiaBeam Systems, Santa Monica, California, USA
M. Fedurin, BNL, Upton, Long Island, New York, USA

Abstract

RadiaBeam Systems successfully completed testing of a proof-of-concept corrugated plate dechirper at the Brookhaven National Laboratory Accelerator Test Facility. [1] Such passive devices should prove indispensable for the efficient operation of future XFEL facilities. These experiments demonstrated a narrowing of the energy spectrum in chirped beam bunches at 57.6 MeV. In this paper, we compare these results with results from Elegant simulations of the BNL-ATF beam. We also compare GdfidL simulations of the wakefield with the analytic results of Bane and Stupakov. [2]

GdfidL WAKEFIELD SIMULATION

The analytic equation for the wakefield [2] used to determine the dimensions of the corrugated plates is given by convolving the bunch charge density with the single electron wakefield:

$$W(z) = \frac{\pi^2}{16}\frac{Z_0 c}{\pi a^2} cos\left(\frac{2\pi z}{\lambda}\right), \qquad (1)$$

where Z_0 is the impedance of free space (377 Ω), c is the speed of light, z is the bunch longitudinal coordinate, λ is the wavelength of the wakefield given by

$$\lambda = 2\pi\sqrt{\frac{a\delta g}{p}}. \qquad (2)$$

The other variables describe the dimensions of the corrugated plates and are listed in Table 1.

To check the accuracy of the analytic equations used in designing the plates, a numerical simulation of the wakefield was run using the program GdfidL. A 500-pC, 1-ps beam bunch with Gaussian longitudinal profile was simulated passing through the corrugated structure defined in Table 1 and the resulting wakefield calculated. A comparison between these two calculations is seen in Fig. 1. The GdfidL simulation reports a wakefield about 64% the magnitude of the analytic equations inside the electron bunch. This factor will be used in simulating the effect of the bunch's wakefield as it passes through the corrugated structure. Note that this factor matches field-matching simulations performed by SLAC with $F\left(\frac{h}{a} = 1, \frac{p}{a} = 1\right)$. [3]

ELEGANT SIMULATION

Using the beam simulation software package Elegant, a bunch was propagated through ATF's beamline to the chamber housing the dechirper. Bane and Stupakov's analytic

* harrison@radiabeam.com

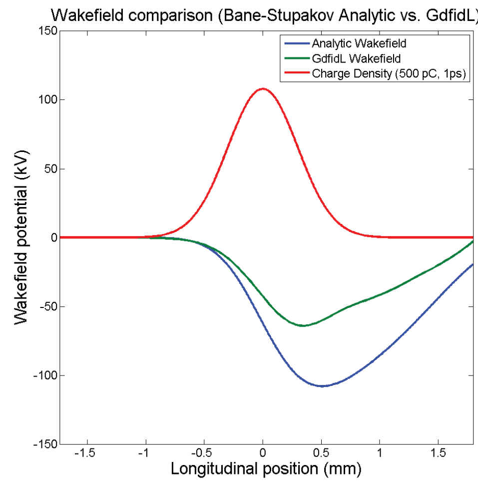

Figure 1: Comparison of the wakefield given by the analytic equations [2] and GdfidL simulations. The bunch charge density is also plotted for longitudinal position reference.

expression of the wakefield with the correction factor determined by the GdfidL simulation was directly applied to the bunch to determine the total dechirping power. Representative phase space plots at various plate gaps are shown in Fig. 2.

Table 1: Corrugated Plate Dimensions

Length	L	181	mm
Width		38.1	mm
Period	p	1.15	mm
Depth	δ	1.15	mm
Gap	g	0.77	mm
Plate separation	a	1–30	mm
Material		Aluminum	

Table 2: BNL ATF Beam Parameters

Beam energy	E	57.6	MeV
Bunch charge	Q	340	pC
Initial chirp		400	keV/mm
Transverse beam size		100	microns
Pulse length (full width)	l	3.4	ps
Longitudinal profile		Rectangular	

ISBN 978-3-95450-133-5

RELATIVISTIC EFFECTS IN MICRO-BUNCHING

Vladimir N. Litvinenko, Stony Brook University, Stony Brook, USA
Gang Wang, Brookhaven National Laboratory, Upton, USA

Abstract

In this paper we present our theoretical studies of limits on bunching using magnetic systems. We discuss the connection of this limit with plasma oscillations in electron beams and present simple formulae for an additional limit of micro-bunching amplification.

INTRODUCTION

Bunching and microbunching are very popular beam manipulation techniques. They are used (or planed to be used) for creating high peak current beams for X-ray FELs [1-4], for controlling or amplifying the shot noise in electron beams [5-12], or even using it for cooling of hadron beams [13-14].

Majority of these applications rely on magnetic bunchers providing time-of-flight dependence on particle energy, which is usually described by the R_{56} coefficient of the transport matrix. One underlying assumption in many of these papers is that the bunching parameters are limited by kinematics of the motion, e.g. by R_{56} and the beam energy spread. For example, there is no assumed limit on the maximum amplification of the shot noise (micro-bunching) in electron beam.

On other hand, it is known from plasma physics that in ballistic compression case the energy oscillates between the space charge and the kinetic energy of the particles. Specifically, it is shown in [15,16], placing an external point charge q into a cold plasma (an electron beam) or warm plasma with κ-2 velocity distribution [16] will cause oscillations of the screening charge with maximum value not exceed $-2q$. This limit does not depend on the value of R_{56} or beam energy spread. It also means that in such system the shot noise can not be amplified. Nevertheless, the micro-bunching using magnetic chicanes with gain exceeding unity was both predicted theoretically and demonstrated experimentally [5-12].

Hence, there are fundamental questions about the attainable bunching in electron beam:

(a) what energy is available to compensate for the space charge energy acquired during the process?
(b) what is the maximum attainable microbunching gain?

In this paper we show that this is purely relativistic effect and are given a simple answer on the maxim amplification for micro-bunching.

We are not considering here any dynamic issues related to bunching such as coherent synchrotron radiation and focus only on the fundamental limit.

STANDARD APPROACH

Standard approach used on modern theory of micro-bunch (see for example [11]) uses the bunching and energy modulation factors, defined as follows:

$$b_k = \frac{1}{N}\sum_{n=1}^{N} e^{-ikz_n}; \mu_k = \frac{i}{N}\sum_{n=1}^{N}\eta_n e^{-ikz_n}; \eta_n = \frac{\delta\gamma_n}{\gamma_o}, \quad (1)$$

to describe the microbunching process using matrix formalism [7]:

$$\begin{bmatrix} b_k(s_2) \\ \mu_k(s_2) \end{bmatrix} = R\left(s_1 | s_2\right)\begin{bmatrix} b_k(s_1) \\ \mu_k(s_1) \end{bmatrix} \quad (2)$$

Propagation through a straight section is described as a simple (plasma) oscillation between the bunching and the energy modulation, which is a good approximation:

$$R\left(s_1 | s_2\right) = \begin{bmatrix} \cos\varphi_p & -\alpha\sin\varphi_p \\ \alpha\sin\varphi_p & \cos\varphi_p \end{bmatrix}; \quad (3)$$
$$\varphi_p = k_p\left(s_2 - s_1\right);\ k_p = \sqrt{4\pi r_e n_e / \gamma^3};\ \alpha = k/\gamma^2 k_p.$$

The other, and much stronger approximation, is used for propagating the beam through a chicane (buncher) with longitudinal compaction factor, R_{56}, yielding in case of longitudinally cold e-beam [7]:

$$R_b = \begin{bmatrix} 1 & -kR_{56} \\ 0 & 1 \end{bmatrix}. \quad (4)$$

Taking into account Gaussian energy spread, yields an exponential suppression factor, which is well know from theory of optical klystron [17,18]:

$$R_b = \begin{bmatrix} 1 & -kR_{56}\cdot e^{-\frac{1}{2}\left(\frac{kR_{56}\sigma_\gamma}{\gamma}\right)^2} \\ 0 & 1 \end{bmatrix}. \quad (5)$$

formally limiting amplification to $g_{mn} \le \gamma / \sqrt{e}\sigma_\gamma$. With high quality e-beam having $\sigma_\gamma / \gamma \sim 10^{-3} \div 10^{-4}$, Eq. (5) predicts a possibility if very high microbunching gain. Hence, standards treatment assumes that the bunching amplification in a chicane is determined by the values of R_{56} and is limited by the relative energy spread in the

ISBN 978-3-95450-133-5

BENCHMARK AND SIMULATION DESIGN OF A LOW ENERGY BUNCH COMPRESSOR

A. He, F. Willeke, L.H. Yu, L. Yang BNL, Upton, NY 11973, USA
J. Qiang LBNL, Berkeley, CA 94720, USA

Abstract

In the electron beam slicing method [1], a low energy bunch with very short and focused beam size is required to interact with the storage ring bunch. We have designed a low energy bunch compressor with BNL photo-cathode electron RF-gun [2] by applying simulation code PARMELA [3].

In this paper, in order to confirm the simulation result, we benchmark the simulation result from PARMELA with that from IMPACT-T [4] for our compressor with BNL RF-gun. In order to increase the repetition rate of the electron beam slicing system, and change the compressor's RF gun from BNL RF-gun to LBNL's VHF gun [5] to redesign the compressor by applying IMPACT-T with both space charge effects and CSR effects considered. The benchmark between PARMELA and IMPACT-T has produced excellent agreement. The comparison of the CSR effects also shows the bunch can be compressed and focused to our desired size after optimization using code IMPACT-T with CSR effects turned on. The new compressor with high repetition rate still works in space charge dominated domain and the bunch with a negative energy chirp at the entrance of the chicane is compressed by a chicane with positive R_{56}. After the optimization, we have achieved a low energy bunch with the 128 fs RMS bunch length, 42 μm and 25 μm RMS beam size in the vertical and horizontal directions respectively, at 22 MeV with 200 pC charge.

INTRODUCTION

The electron beam slicing method [1] generates ultra-short x-ray pulses using focused short low energy (~20 MeV) electron bunches to create short slices of electrons from the circulating electron bunches in a synchrotron radiation storage ring. When a low energy electron bunch crosses from top of a high energy storage ring electron bunch, its Coulomb force will kick a short slice from the core of the storage ring electron bunch. The separated slices, when passing through an undulator, will radiate ultra-short x-ray pulses at about 100 fs. In order to minimize the cost of the electron beam slicing system and to explore the lower limit of the compressor's bunch energy, a low energy bunch compressor [2] without acceleration after the RF-gun exit has been designed to achieve the desired bunch compression and focusing. The RF gun used in this compressor is BNL RF-gun and the simulation code applied is PARMELA with space charge effects considered. Some optimized results for the BNL RF-gun compressor are given in Table 1.

In this paper, to verify the simulation results, we benchmark the simulation results from PARMELA with the results from IMPACT-T for the low energy compressor with BNL RF-gun. To study the coherent synchrotron radiation (CSR) effects, we compare the simulation results when CSR effects is turned on with those when CSR is turned off in IMPACT-T. In order to increase the repetition rate of the electron beam slicing system, we change the compressor's RF gun from BNL RF-gun to LBNL's VHF gun [5] and redesign the compressor by applying IMPACT-T with both space charge effects and CSR effects considered.

BENCHMARK AND CSR EFFECTS

Both Linac tracking codes PARMELA [3] and IMPACT-T [4] can track relativistic particles taking into account space charge effects in the 6D space, whereas the space-charge solver is 2D r-z or 3D depending on the code. IMPACT-T also considers the coherent synchrotron radiation (CSR) effects which are not included in PARMELA.

To verify our simulation results from PARMELA, taking the compressor of case 3 in Table 1 as an example we benchmark the results with PARMELA against those with IMPACT-T. By applying IMPACT-T, we also discuss CSR effect which is not considered in code PARMELA. The CSR effects are related to the bunch energy, bunch charge and bunch length. To check the CSR effects, we compare the simulation results when CSR effects being turned on with the results when CSR effects being turned off in IMPACT-T. The results of the benchmark and comparison is shown in Table 2, Fig. 1 and Fig. 2.

Data in Table 2 show the RMS bunch length difference between PARMELA and IMPACT-T with CSR off is less than 6%. The difference of the transverse RMS beam size between the two codes is larger than 20% when all the results are calculated for 90% particles, with 10% longitudinal tails cut-off. If the transverse RMS beam size are calculated for 100% particles as shown in Fig. 1, the difference of those between the two codes decrease to ~10%. Fig. 1 show the 6-D phase space at the final focus point for the three simulation results: PARMELA (the 1st row), IMPACT-T with CSR effects off (the 2nd row) and IMPACT-T with CSR effects on (the 3rd row). The color bar indicates the particle density.

Due to the space charge forces the particle energy is no longer constant, and the dispersion function and beta functions both lose their original meaning. We redefine the equivalent dispersion and the equivalent beta functions as described in [1]. To show the agreement between the two codes and the difference of the calculations with and without the CSR effects considered, we plot the evolution of the newly defined beta functions and the dispersion function along the dispersive chicane section of the compressor for the three simulation results in Fig. 2. Although the exact

ISBN 978-3-95450-133-5

BEAM PERFORMANCE OF THE PHOTOCATHODE GUN FOR THE MAX IV LINAC

J. Andersson*, F. Curbis, D. Kumbaro, F. Lindau, S. Werin
MAX IV Laboratory, Lund University, Lund, Sweden

Abstract

The MAX IV facility in Lund (Sweden) is under construction and conditioning of the electron guns for the injector is ongoing. There are two guns in the injector, one thermionic gun for storage ring injection and one photocathode gun for the Short Pulse Facility. In this paper we report on the beam performance tests of the photocathode gun. The measurements were performed at the MAX IV electron gun test stand [1] during spring 2014. Parameters that were studied includes quantum efficiency, emittance and emittance compensation. Results from the measurements are also compared to particle simulations done with ASTRA.

INTRODUCTION

The MAX IV facility [2] is under construction in Lund, Sweden and includes two storage rings for production of synchrotron radiation and a short pulse facility (SPF) [3]. Both storage rings and the SPF are injected from a full energy LINAC and the injector for the LINAC has two different guns, a thermionic gun and a photocathode gun. The thermionic gun is used for ring injection but due to the requirements of short bunches and the long tail of low energy electrons, the thermionic gun is unsuitable for injection to the SPF. A 1.6 cell photocathode gun will be used instead, based on the FERMI@Elettra [4] gun operating at a frequency of 2.9985 GHz.

One part of the commissioning of the facility is conditioning of the photocathode gun and measurement of basic beam properties to find the performance of the gun. The gun was conditioned during last part of 2013 and the measurements of beam parameters were done during the first half of 2014. In this article the results from these measurements will be presented and we compare some of them to simulated values. The goal of these measurements is to verify that the gun can perform well enough for the commissioning of the LINAC and the SPF operations. The requirement of the SPF is a beam energy of 3 GeV and a transverse normalised rms emittance of 1 mm mrad at the undulator entrance.

GUN TEST STAND

The photocathode gun was operated in the gun test stand at MAX IV. Measurements of beam energy were performed using a magnetic energy filter installed at the end of the test stand. The magnetic energy filter consists of two dipoles that bend the beam 120°. The setup in the gun test stand used for measurements of spot size, emittance and phase-charge curves is displayed in Fig. 1. The pepperpot used for the emittance measurements is installed between the beam viewers YAG1 and YAG2, at a distance of 1.45 m from the cathode.

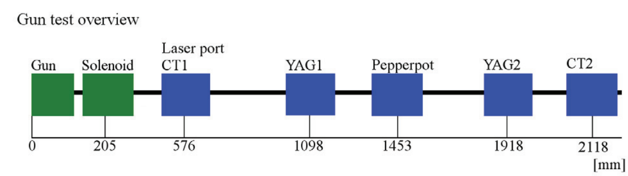

Figure 1: Schematic overview of the gun test stand.

The gun is powered by a klystron with a connected SLED cavity at 2.9985 GHz. The laser system is based on a Ti:Sapphire laser and the pulses are stretched, split and tripled to give a FWHM laser pulse length of 8 ps at 263 nm wavelength. The laser oscillator is locked to the 3 GHz signal of the RF system and the energy of the laser pulse can be changed during operation. The transport of the laser beam from the laser hutch to the cathode is done through air, the beam is then focused on the cathode through an aperture of 2 mm diameter. The laser is triggered to hit the cathode when the RF pulse has lasted long enough for the cavity to be filled, the precise injection phase is then controlled using a motorized optical delay stage.

SIMULATIONS

Simulations were made using ASTRA [5] with 10 000 particles, and the fields used to describe the gun and the solenoid are based on measured fields. The beam properties depend on the laser phase, the spot size, the electric field in the gun, as well as other parameters, so a number of different simulations were run for different settings to understand the behavior of the gun. The results for simulations of beam energy as function of the electric field for an injection phase of 10°, corresponding to the setting for the energy measurement, can be seen in Fig. 2.

To understand the phase-charge relation for the gun, simulations were made with a maximum electric field strength at the cathode of 90 MV/m to determine the charge as a function of the injection phase. ASTRA was used to determine the number of accelerated electrons as a function of the injection phase and this result combined with a field dependent charge curve gives an estimate of the phase-charge relation. These simulations do not fully account for the Schottky effect and shielding effects, so the amount of charge is

* joel.andersson@maxlab.lu.se

ISBN 978-3-95450-133-5

COMISSIONING OF THE PHOTO-CATHODE RF GUN AT APS*

Y. Sun#, J. Dooling, R. Lindberg, A. Nassiri, S. Pasky, H. Shang, T. Smith, A. Zholents
Advanced Photon Source, ANL, Argonne, IL 60439, USA

Abstract

A new S-band Photo-Cathode (PC) gun is recently commissioned at the Advanced Photo Source (APS), Argonne. In this paper we report the high-power RF conditioning process of the gun. Dark current is monitored during the RF conditioning. Following the RF conditioning, photo-electron beams are generated from the gun. The quantum efficiency of the copper cathode is monitored. Normalized beam emittance at different drive-laser sizes is measured as a function of solenoid strength, RF gradient and phase. Beam energy is also measured in a spectrometer.

THE APS PC GUN

The APS PC gun is a LCLS type gun [1-3] fabricated by SLAC. The gun is delivered to APS Oct. 2013 and installed at the Injector Test Stand (ITS) Dec. 2013.

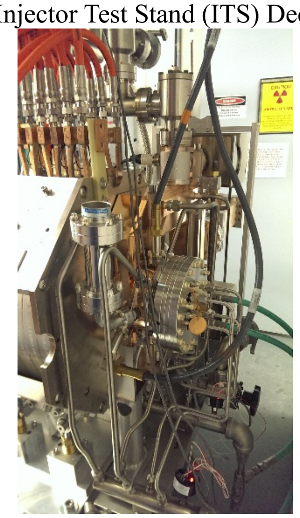

Figure 1: The S-band photo-cathode RF gun and solenoid as installed at the ITS.

HIGH POWER RF CONDITIONING

High power RF conditioning of the PC gun started on March 5, 2014. Forward RF power of 12 MW, pulse length 2.5 μs and 30 Hz repetition rate were successfully achieved on March 20, 2014.

To protect the gun from damaging during RF conditioning, three types of interlocks are implemented: reflected RF power, vacuum pressure and arc detector installed on the view port of the cathode cell.

The waveforms of the forward and reflected RF at the gun waveguide are saved at different RF power levels. An example is shown in Figure 2. Furthermore, waveforms of the field probes of the half-cell and full-cell are also collected, see Figure 3.

*Work supported by U.S. Department of Energy, Office of Science, under Contract No. DE-AC02-06CH11357.
#yinesun@aps.anl.gov

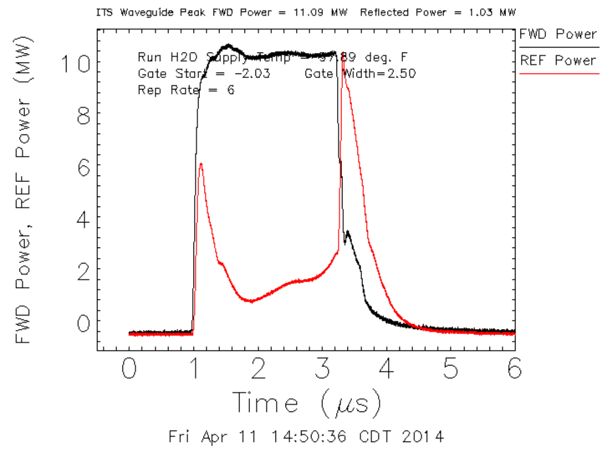

Figure 2: The forward and reflected RF waveforms at the gun waveguide.

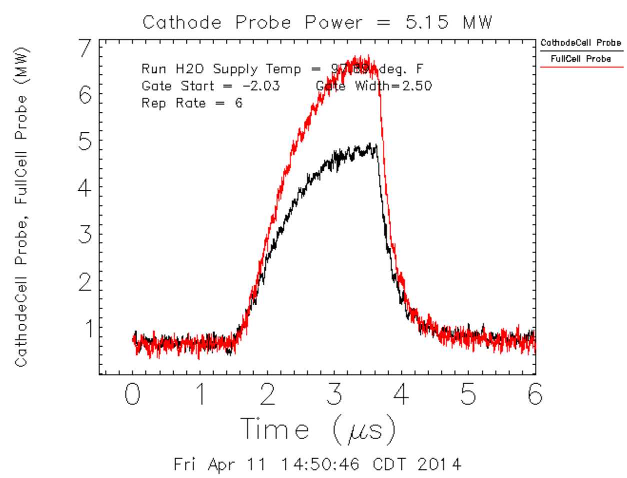

Figure 3: The cathode half-cell and the full cell field probe waveforms.

Dark currents are measured using the ICT at different solenoid strengths and RF power levels. A set of ICT measurements at 12 MW forward RF power, solenoid current ranging [20 ~ 240] A are plotted in Figure 4.

The total charge is calculated from integrating the current monitor waveforms. At different RF repetition rate, the dark current collected by the ICT varies as the solenoid current is changed, see Figure 5. The maximum dark current per RF pulse observed during the RF conditioning is less than 150 pC.

ISBN 978-3-95450-133-5

STATUS OF PUMP-PROBE LASER DEVELOPMENT FOR THE EUROPEAN XFEL

L. Wißmann#, M. Emons, M. Kellert, K. Kruse, G. Palmer, M. Pergament, G. Priebe, J. Wang, U. Wegner, and M. J. Lederer, European XFEL GmbH, Notkestrasse 85, 22607 Hamburg, Germany

Abstract

The European XFEL is under construction and is designed to become a multi-user facility. Three SASE beam lines with two experimental areas each are foreseen to guarantee a high user throughput. In order to enable the full scientific potential of the facility, optical laser pulses for either pumping or probing samples will be deployed regularly.

We are presenting the pump-probe laser concept and the current status of the development, showing some experimental results of the prototype laser, achieved to date. The main emphasis of the presentation lies on the integration of the laser system into Karabo, the emerging control system of the European XFEL.

INTRODUCTION

The requirements for the pump-probe laser system (In the following: 'PP laser') are given by the XFEL accelerator (burst repetition rate 10 Hz, intra-burst pulse repetition rate 4.5 MHz, burst length 600 µs, high arrival time stability) and the needs of experimentalists (pulse energy, pulse length, arbitrary pulse picking, wavelength tunability). Machine operation demands a high uptime while long-time planning and different experimentalists' needs require high flexibility of the design. The general concept relies on a burst-mode, ps-pumped non-collinear optical parametric amplifier (NOPA), which draws on commercially available components where possible, and utilizes collaborative or in-house developments where needed.

The most important subsystems of the PP laser are described first, as depicted in Fig. 1. In the second half of this paper the integration of the laser into the control system is outlined, covering the necessary hardware, software, and machine timing issues.

PP LASER SUBSYSTEMS

A stable seed oscillator (OneFive Origami10), which is locked to the XFEL laser master oscillator via the optical synchronization system, emits a 54 MHz pulse train at 1030 nm. The timing jitter of the oscillator itself is specified to be <20 fs (rms, [1kHz-10Mhz]). The endpoint-to-endpoint stability of the synchronization systems is envisioned to reach 20 fs after XFEL commissioning [1]. Passive and active measures are taken to maintain this arrival time stability unto the exit of the PP laser.

For laser/x-ray overlap search, a long delay stage is implemented (Feinmess PMT 240). It supports a travel range of 400 mm (5 ns, quadruple pass) with an encoder resolution of 100 nm (stable 200 nm or 2.5 fs steps shown). Coupling the laser pulses into a single mode fiber for front end seeding has been successfully tested and yields less than 3% deviation over the full travel range.

The All-Fibre Front-End has multiple tasks [2]. It consists of several fibre amplifier stages, pulse picking devices, chirped fiber bragg gratings for dispersion management and extensive timing and control electronics. The laser pulse train from the seeder is split after pre-amplification and pre-stretching into two paths, XF1 (for power amplification and NOPA pumping) and XF2 (for supercontinuum generation and NOPA seeding). The output of the XF2 path is a 5 ms long burst with 4.5 MHz intra-burst repetition rate and a burst power of 20 W. An acousto-optic modulator (AOM) enables the selection of arbitrary pulse patterns inside the burst, before the pulses are compressed to 300 fs for supercontinuum generation.

In the XF1 path, the front-end output pulse train can be chosen to have different intra-burst repetition rates at constant burst power (of 4 W). This constant power mode enables different working points of the whole PP laser (incl. burst mode pump-pulse amplifiers). The tested repetition rates are 4.5 MHz, 1 MHz, and 0.2 MHz. The output burst length is again 5 ms, the pulse duration being 1.3 ns, and the spectral properties are optimized for the subsequent power amplifiers.

Further down the XF1 path, an InnoSlab multi-pass amplifier enhances the burst power to 400 W [3]. Two double-pass booster stages are planned to sequentially reach power levels of 7 kW and 20 kW. The currently achieved performance includes burst powers of 600 W (400 W specified), and with settable intra-burst frequencies of 0.2 MHz to 4.5 MHz this corresponds to 0.09 mJ to 2.1 mJ at 400W. The spectral width of the output pulses is measured to be $\Delta\lambda = 2.5$ nm, the beam quality factor M^2 equals 1.5, and the constancy of the pulse energy over the burst (in a 600 µs window) is better than 1%. Intra-burst variations of beam shape and pointing have been measured to be negligible.

A Pockels cell arrangement, suited for high laser energies, is used to enable arbitrary pulse picking also in the pump path. Alternative, user selectable, beam exits before the XF1 compressor (pulse length ~ns) and after the XF1

#laurens.wissmann@xfel.eu

ISBN 978-3-95450-133-5

DEVELOPMENT OF ALL-METAL STACKED-DOUBLE GATE FIELD EMITTER ARRAY CATHODES FOR X-RAY FREE ELECTRON LASER APPLICATIONS *

P. Das Kanungo, Y. Oh, C. Lee, M. Paraliev, V. Guzenko, H.-H. Braun, S. Tsujino[#]
Paul Scherrer Institut, Villigen, Switzerland
T. Feurer, University of Bern, Bern, Switzerland

Abstract

Design, fabrication, and characterization of all-metal double-gate field emitter array cathodes at the Paul Scherrer Institute are reported. The beam characterization at low beam energies, combined with the neon gas conditioning for improving the beam uniformity indicated more than an order of magnitude reduction of the emittance. A combination of the proposed double-gate structure with the surface-plasmon-enhanced near infrared laser-induced field emission for ultrafast, high charge bunch generation is discussed.

INTRODUCTION

Realization of a high current and high brightness cathode using field emission has been proposed based on an array of metal nanotip emitters [1,2]. Comparing with conventional etched-wire needle-shaped field emitters, field emitter arrays (FEAs) produced by micro- and nanofabrication methods with an on-chip electron extraction electrode are advantageous for high acceleration gradient operation since the switching of the electron emission can be controlled independently from the acceleration gradient by applying a electron extraction potential in the order of 100 V to the electron extraction gate electrode G_{ex}. Using the all-metal single-gate FEAs developed at PSI, stable operation of FEAs in a combined diode-RF cavity electron gun with gradient up to 30 MV/m [3,4], and electrical pulsing of the FEAs down to ~200 ps [5] were demonstrated. Generation of 5 ps electron bunches was also demonstrated by exciting the FEAs by 50 fs near infrared laser pulses [6]. Although the curved shape of the emitter tip apex leads to a relatively large angular beam spread [7], the transverse emittance of array beam can be reduced by collimating the individual beamlet with a second beam collimation electrode G_{col} fabricated on top of G_{ex} [1,2]. One of the challenges to use double-gate FEAs for practical applications has been the large reduction of the emission current with the application of the beam collimation potential [8]. This was however in part solved with the recently reported double-gate structures with large collimation gate aperture diameters [9,10]. Such double-gate FEAs are promising for advanced accelerator applications including the compact X-ray free-electron lasers (FELs) when an extremely low emittance below 0.1 mm-mrad is required [11] or by utilizing the spatial beam structure combined with the emittance exchange [12]. Double-gate FEAs with low emittance can also be key to realize compact THz vacuum electronic oscillators and amplifiers [13]. Our recent report showed the fabrication of up to 4×10^4 tip stacked-double-gate FEAs and their excellent beam collimation characteristics at low current level [14]. Here we report recent progress of the double-gate FEAs and the numerical study of the emission characteristics for a high density FEAs excited by near infrared laser pulses for X-ray free electron laser applications [15,16].

*Work partially supported by the Swiss National Science Foundation, No. 200020_143428 and 2000021_147101.
[#]E-mail: soichiro.tsujino@psi.ch

BEAM CHARACTERISTICS OF SINGLE- AND DOUBLE-GATE FIELD EMITTER ARRAYS

The FEAs used in the experiments consist of pyramidal shaped molybdenum nanotip emitters with the height of ~1 μm and the tip apex radius of curvatures of 5-10 nm. The emitter pitches are equal to 5 μm or 10 μm. The emitters are supported on metal substrates and equipped with G_{ex} and G_{col} electrodes. The gate electrodes and emitters are insulated each other by 1.2 μm-thick SiON layers [14,17,18]. Electron emission characteristics of the all-metal single-gate FEAs have been studied previously [3-6,15,17] including the intrinsic transverse emittance. In Figure 1, we summarize the experimentally observed emittance of *single-gate* FEAs with the FEA diameters between 0.2 and 2.3 mm. The upper boundary of the target emittance with the double-gate FEAs equal to 0.1 mm-mrad with the FEA diameter of 1 mm is also indicated in Figure 1.

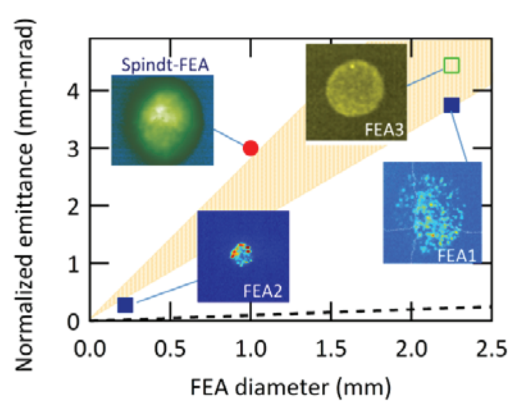

Figure 1: Normalized rms emittance of *single-gate* FEAs. The shaded area corresponds to the rms beam divergence of 20-30°. The broken line is the upper boundary of the target emittance with double-gate FEAs equal to 0.1 mm-mrad with the FEA diameter of 1 mm.

ISBN 978-3-95450-133-5

THE LCLS-II INJECTOR DESIGN*

J.F. Schmerge#, A. Brachmann, D. Dowell, A. Fry, R.K. Li, Z. Li, T. Raubenheimer, T. Vecchione, F. Zhou, SLAC, Menlo Park, CA 94025, USA
A. Bartnik, I. Bazarov, B. Dunham, C. Gulliford, C. Mayes, Cornell University, Ithaca, NY 14853, USA
A. Lunin, N. Solyak and A. Vivoli, FNAL, Batavia, IL 60510, USA
D. Filippetto, R. Huang, C. Papadopoulos, G. Portmann, J. Qiang, F. Sannibale, S. Virostek, R. Wells, LBNL, Berkeley, CA 94720, USA

Abstract

The new LCLS-II project will construct a 4 GeV continuous wave (CW) superconducting linear accelerator to simultaneously feed two undulators which will cover the spectral ranges 0.2-1.2 keV and 1-5 keV, respectively. The injector must provide up to 300 pC/bunch with a normalized emittance < 0.6 μm and peak current > 30 A at up to 1 MHz repetition rate. An electron gun with the required brightness at such high repetition rate has not yet been demonstrated. However, several different options have been explored with results that meet or exceed the performance requirements of LCLS-II.

The available technologies for high repetition-rate guns, and the need to keep dark current within acceptable values, limit the accelerating gradient in the electron gun. We propose a CW normal conducting low frequency RF gun for the electron source due to a combination of the simplicity of operation and the highest achieved gradient in a CW gun, potentially allowing for lower beam emittances. The high gradient is especially significant at the 300 pC/bunch charge where beam quality can suffer due to space charge. This paper describes the design challenges and presents our solutions for the LCLS-II injector.

INTRODUCTION

LCLS-II [1] is a proposed FEL user facility driven by a 4 GeV CW superconducting linac under construction at SLAC. The injector must simultaneously deliver high repetition rate up to 1 MHz and high beam brightness with normalized emittance of < 0.6 μm at 300 pC/bunch and peak current > 30 A. An injector capable of delivering the desired parameters has not yet been demonstrated. This paper describes one possible design for the LCLS-II injector.

The preferred LCLS-II electron gun is a normal conducting, CW, rf gun operating at 186 MHz (7$^{\text{th}}$ sub-harmonic of 1.3 GHz) like the APEX gun at LBNL [2]. Multiple gun technologies with different advantages and disadvantages were considered and the APEX gun was ultimately adopted for LCLS-II largely due to the high achieved gradient of 20 MV/m and the demonstrated reliable CW operation. The gradient is especially important at 300 pC/bunch where beam quality can suffer due to space charge. The nominal values as well as the range of all the injector parameters are listed in Table 1. Parameters are specified at the injector exit unless otherwise indicated. The layout of the full injector is shown in Figure 1 including the gun, buncher, superconducting accelerator, laser heater for microbunching instability suppression and diagnostics. The accelerator is comprised of a single standard TESLA cryo-module with eight 9-cell SRF cavities which accelerates the beam from < 1 to approximately 100 MeV.

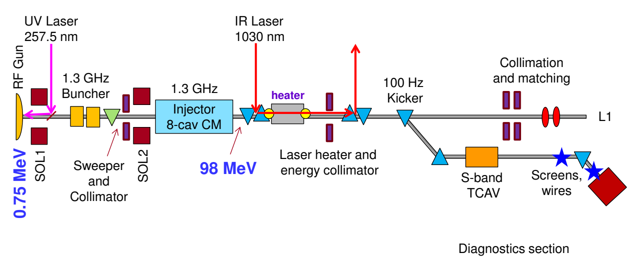

Figure 1: Injector layout.

GUN TECHNOLOGY

Three gun technologies, each with distinct advantages and disadvantages, were considered for LCLS-II.

1. DC guns
2. VHF rf gun at linac sub-harmonic
3. Superconducting high gradient multi-cell gun

The DC gun at Cornell has nearly demonstrated the nominal LCLS-II parameters as shown in Figure 2 [3]. These results were obtained with the DC gun operating at 350 kV corresponding to about 4 MV/m at the cathode but the gun will need to be operated at closer to 500 kV to meet the LCLS-II emittance requirements at 300 pC. The Cornell DC gun has recently been operated at 400 kV but no DC gun has yet demonstrated reliable e-beam operation at 500 kV including guns with segmented insulators. One advantage of the DC gun is to allow for arbitrary pulse separation which can fill adjacent linac buckets and is desired for multi-bunch operation. However, LCLS-II is currently designed to operate with only a single bunch.

*Work supported by U.S. Department of Energy under Contract DEAC03-76SF00515
#schmerge@slac.stanford.edu

ISBN 978-3-95450-133-5

MODEL-BASED KLYSTRON LINEARIZATION IN THE SwissFEL TEST FACILITY

Amin Rezaeizadeh*, Paul Scherrer Institut, Villigen, Switzerland
and Automatic Control Laboratory, ETH, Zürich, Switzerland
Roger Kalt, Thomas Schilcher, Paul Scherrer Institut, Villigen, Switzerland
Roy Smith, Automatic Control Laboratory, ETH, Zürich, Switzerland

Abstract

An automatic procedure is developed to provide the optimal operating point of a klystron. Since klystrons are nonlinear with respect to the input amplitude, a model-based amplitude controller is introduced which uses the klystron characteristic curves to obtain the appropriate high voltage power supply setting and amplitude, such that the operating point is close to the saturation. An advantage of the proposed design is that the overall open-loop system (from the input to the RF station to the klystron output amplitude) is linearized. The method has been successfully tested on a full scale RF system running at nominal power.

INTRODUCTION

The Swiss Free Electron Laser is currently being constructed at PSI [1]. The SwissFEL injector and the Linac Radio Frequency drives operate in a pulsed mode at the rate of 100 Hz. The pulse-to-pulse stability of the electron beam characteristics, such as beam energy, are crucial for the quality of laser pulses. As the RF phase and amplitude stability plays a significant role in this goal, an automatic procedure is developed to obtain the operating point of a klystron such that the output amplitude is close to its saturation level so that the pulse-to-pulse amplitude jitter is minimized. The procedure is model-based, using the klystron (AM/AM) characteristic curves. The major advantage of the design is that the overall system from the Low Level RF input to the vector modulator to the output of the klystron is linearized. Moreover, from the system dynamics standpoint, the closed-loop system can be treated as a linear system. A recent contribution [2], uses a third order polynomial function to correct the nonlinearity of the klystron. The method is open-loop and for constant high voltage.

Throughout this paper, the klystron and the upstream RF and LLRF subsystems such as the pre-amplifier and the vector modulator are referred to as the "drive chain". The high voltage power supply setting and the input amplitude to the klystron are automatically determined according to the desired output power and the predefined headroom to the saturation. For the case where the demand power is obtainable via slight change in the input amplitude, the high voltage is kept unchanged. For precise control, a pulse-to-pulse feedback loop is closed around the operating point.

* aminre@ee.ethz.ch

In the following section, we discuss the klystron amplitude-to-amplitude (AM/AM) modeling, followed by a pulse-to-pulse amplitude feedback scheme.

KLYSTRON MODELING

For fixed and constant high voltage, the klystron can be characterized by Rapp's model used for solid-state power amplifiers (SSPA) [3] (which was initially introduced by Cann in 1980 [4]). The model is suitable for systems that are approximately linear with gradual saturation. We generalize the formulation of the model as follows,

$$y(a_{in}) = \frac{p_1\, a_{in} + p_2}{\sqrt{1 + (\frac{a_{in}}{p_0})^2}} + p_3, \qquad (1)$$

where, y denotes the output amplitude of the klystron, a_{in} is the input amplitude and p_i's are constant parameters. This model describes the saturation and over-saturation characteristics of a klystron for constant high voltage.

Figure 1 illustrates the data of a klystron in the SwissFEL test facility and the fitted model from (1). In the original form [3, 4], the p_2 term is zero which does not capture the power drop in the over-saturation region.

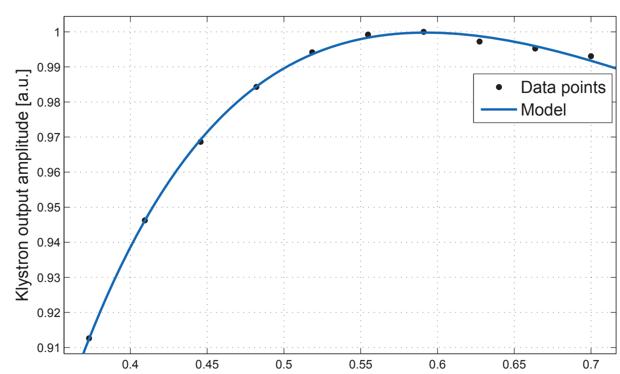

Figure 1: The klystron input-amplitude to output-amplitude (AM/AM) conversion curve. The output amplitude is normalized to the maximum amplitude. The regression of fitting is $R^2 = 0.999$.

According to the experiments, the output amplitude change is approximately linear with respect to high voltage changes. Therefore, the following formulation is introduced, connecting the input, output amplitude and the high voltage

ISBN 978-3-95450-133-5

RF PULSE FLATTENING IN THE SWISSFEL TEST FACILITY BASED ON MODEL-FREE ITERATIVE LEARNING CONTROL*

Amin Rezaeizadeh†, Paul Scherrer Institut, Villigen, Switzerland
and Automatic Control Laboratory, ETH, Zürich, Switzerland
Thomas Schilcher, Paul Scherrer Institut, Villigen, Switzerland
Roy Smith, Automatic Control Laboratory, ETH, Zürich, Switzerland

Abstract

This paper introduces an iterative approach to producing flat-topped radio frequency (RF) pulses for driving the pulsed linear accelerators in the Swiss free electron laser (SwissFEL). The method is based on model-free iterative learning control which iteratively updates the input pulse shape in order to generate the desired amplitude and phase pulses at the output of the RF system. The method has been successfully applied to the klystron output to improve the flatness of the amplitude and phase pulse profiles.

INTRODUCTION

The SwissFEL project at PSI will develop a Free Electron Laser capable of generating extremely bright and short X-ray pulses [1]. The SwissFEL injector and linac RF drives operate in a pulsed mode at the rate of 100 Hz, using normal conducting RF accelerating structures. The input RF pulse length is relatively short (in the order of 1-3μs) and there is no RF digital feedback running within a pulse. In the two-bunch operating mode of the SwissFEL, each electron bunch is separated by 28 ns, and it is often required that the two bunches see the same amplitude and phase in the accelerating structure. To achieve this goal, an Iterative Learning Control (ILC) technique is introduced to generate a flat-topped (or generally any desired shape) RF pulse.

Iterative Learning Control is a method for controlling systems that operate in a repetitive, or trial-to-trial mode [2,3]. In this method, the measured trajectory is compared to the desired trajectory to give an error estimate which is then used to update the input for the next trial. A model-based ILC algorithm has been previously introduced in [4] which uses an intra-pulse state feedback and it has been implemented in several systems [5] including accelerators [6]. However, this approach is not applicable in the SwissFEL since no intra pulse digital feedback is feasible. A new version of ILC has been recently developed which is not based on the model of the system and thus the usual system identification procedure is not required [7]. The recent method has been modified and successfully tested on a C-band RF station in the SwissFEL test facility.

RF STATION LAYOUT

The RF and low-level RF layout of the SwissFEL C-band station is illustrated in Fig. 1. The discrete waveforms of the in-phase, I, and quadrature, Q, components of the RF signal are fed into the vector modulator to be up-converted to the carrier frequency (5.712GHz). Each waveform contains 2048 samples with the sampling time of $T_s = 4.2$ ns. The RF signal drives the klystron which delivers high power RF at the output. In C-band stations, an RF pulse compressor (Barrel Open Cavity) is placed after the klystron, followed by four accelerating structures.

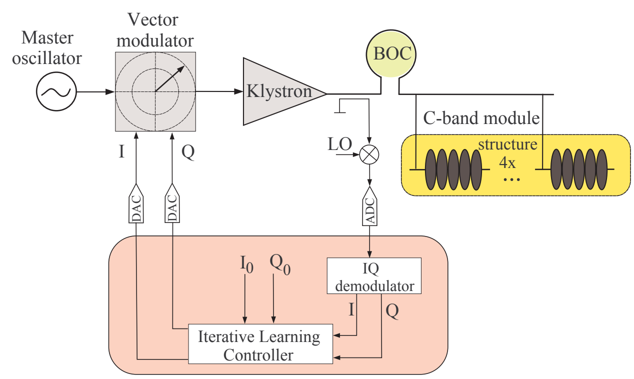

Figure 1: The RF layout of the SwissFEL C-band station.

For our experiment, we take the output of the klystron as the measured pulse whose shape is to be controlled. The signal is measured by a directional coupler and then down converted to the intermediate frequency (IF) of 39.67 MHz. The resulting signal is then sampled at the rate of 238 MHz, followed by a demodulation algorithm to obtain discrete waveforms of I and Q. The measured waveforms are compared to the desired ones and the ILC controller generates the next I and Q inputs to the DAC.

ITERATIVE LEARNING CONTROL SCHEME

The ILC is a technique to manipulate the input pulse shape iteratively until the output pulse shape fulfills the requirement. Model-free ILC methods are rarely investigated in literature, in contrast to a variety of model-based methods. Model-free ILC algorithms have the advantage that no system identification experiments are required. The idea behind our approach was developed by Janssens *et al.* [7].

Figure 2 illustrates the initial output signals of the klystron as a response to a rectangular input pulse. The colored area which is after filling time of the structures, denotes the region in which the electron bunches are fired. We refer to it as

* Work supported by Paul Scherrer Institut.
† aminre@ee.ethz.ch

ISBN 978-3-95450-133-5

DEVELOPMENT OF PHOTOCACHODE DRIVE LASER SYSTEM FOR RF GUNS IN KU-FEL*

H. Zen#, S. Suphakul, T. Kii, H. Ohgaki, Institute of Advanced Energy, Kyoto University, Gokasho, Uji, Kyoto, 611-0011, Japan
R. Kuroda, Y. Taira, National Institute of Advanced Industrial Science and Technology (AIST), 1-1-1 Umezono, Tsukuba, Ibaraki 305-8568, Japan

Abstract

A photocathode drive laser system has been developed for RF guns in Institute of Advanced Energy, Kyoto University. Those RF guns require single-bunch and multi-bunch operation. Therefore, single-pulse and multi-pulse performances of the drive laser system have been examined for our laser system. As the result of test experiment, we have succeeded in generating UV laser pulses with micro-pulse energy of 205 μJ/micro-pulse in the single-pulse condition. On the other hand, in the multi-pulse condition, UV pulse lasers having flat macro-pulse shape with micro-pulse energy of 3.9 μJ and macro-pulse duration of 5 μs were successfully generated. Those values satisfy our target value required for the photocathode drive laser system and developed drive laser system will be used for electron beam generation.

INTRODUCTION

We have been developing an oscillator type mid-Infrared free electron laser (MIR-FEL) to contribute energy related sciences in Kyoto University [1]. The facility utilizes a 4.5-cell thermionic RF gun for its electron source. The gun can provide us high energy (~9 MeV) and multi-bunch electron beam with relatively long macro-pulse duration (~7 μs). However, the bunch charge is limited to less than 40 pC because of serious backbombardment effect [2]. Even with the limited bunch charge, we could provide MIR-FEL beam in the wavelength region from 5 to 20 μm. In addition to the MIR-FEL, development of THz-FEL has been started [3].

Two upgrade projects of MIR-FEL by modifying the thermionic RF gun have been carried out as well. One is a triode RF gun project [4] and the other is a photocathode project [5]. The triode RF gun uses a thermionic cathode and additional small cavity around the cathode. A numerical simulation predicted that the backbombardment effect could be solved by the proposed triode configuration [4]. The photocathode project is much simpler than the triode one. The photocathode RF gun driven by pico-second laser is completely free from the backbombardment effect and can produce electron beams with higher bunch charge and longer macro-pulse duration than the thermionic one. Initially we planned to install a modified BNL-type 1.6-cell RF gun to upgrade the MIR-FEL [6]. The gun cavity was manufactured in 2008. However, because of growing scientific interest in THz region, we changed our plan and decided to use the manufactured 1.6-cell gun as an electron source of compact single pass THz-FEL [3].

For the photocathode upgrade project of existing MIR-FEL device, we need to develop multi-pulse laser for oscillator FEL. On the other hand, single-pulse laser is enough for single pass THz-FEL. Our early work on the multi-pulse laser system was reported in the proceedings of FEL2012 [7]. At that time, we tried to develop a four-pass amplifier using a laser diode (LD) pumped amplifier module. In this scheme, however, we suffered from a self-oscillation of the amplifier module. Therefore we modified the amplifier configuration to have two double-pass amplifiers and installed nonlinear crystals for second harmonic generation and fourth harmonic generation. In this paper we will report the performance of our photocathode drive laser system.

PHOTOCATHODE DRIVE LASER SYSTEM

In this section, target values of our photocathode drive laser system and system configuration are described.

Target Values

There are so many choices for photocathode material and then the required performance of its drive laser strongly depends on the quantum efficiency (QE) of the photocathode. In this work, we assume usage of high QE photocathode (e.g. Cs-Te: QE > 1×10^{-2}) for the RF gun of multi-bunch operation and copper photocathode (QE ~ 1×10^{-4}) for the RF gun of single-bunch operation. Then we set the target bunch charge as 1 nC for both cases. Therefore the target micro-pulse energy of drive laser can be calculated as 0.47 μJ for the multi-bunch case and 47 μJ for the single-bunch case at the laser wavelength of 266 nm. The main parameters are shown in Table 1.

The maximum repetition rate of macro-pulse is given by the maximum repetition rate of RF power source used to drive the RF gun, which is 10 Hz in KU-FEL. The repetition rate of micro-pulse must be harmonics of 29.75 MHz which is a roundtrip frequency of optical cavity used for MIR-FEL. The number of micro-pulse determines the number of FEL amplification in the FEL optical cavity. A numerical simulation predicted that very high FEL gain (~ 300%) could be achieved with photocathode operation of 4.5-cell RF gun [5]. Therefore, not so large number of amplification is required but here we set the target number of micro-pulse to have more

*Work supported by the "ZE Research Program, IAE (ZE26A-22)."
#zen@iae.kyoto-u.ac.jp

ISBN 978-3-95450-133-5

Cu AND Cs_2Te CATHODES PREPARATION AND QE HISTORY AT THE SwissFEL INJECTOR TEST FACILITY

J. Bossert, R. Ganter, M. Schaer, T. Schietinger, PSI, Villigen, Switzerland

Abstract

The installation of a load-lock chamber attached to the RF photoinjector gives the possibility to carefully prepare the metallic cathodes under vacuum and also to use semiconductor cathodes like Cs_2Te cathodes which cannot be transported through air. An annealing procedure of copper cathodes to desorb water guarantees a good reproducibility of the initial quantum efficiency (QE) above 10^{-4}. Cs_2Te cathodes were tested in the same gun and showed that they also fulfill the emittance requirements of SwissFEL but with a much higher QE (1-2%). In order to better understand and improve the deposition procedure at PSI (based on a CERN recipe), surface analysis were performed and are discussed in the paper (SEM, EDX, interferometry, microscopy).

INTRODUCTION

The main advantage of semi-conductor cathodes (like Cs2Te) over metallic cathodes (copper) is the increase in quantum efficiency by several orders of magnitudes (QE). The laser energy required for photoemission can then be reduced and invested elsewhere like in a better shaping (which always consumes laser power) or in multi bunch operation. The main drawbacks of Cs_2Te cathodes is however the increase in slice emittance and the short lifetime (rapid decrease of QE). At SwissFEL we would like to have both cathode options (Cu and Cs2Te) ready for the future operation. In this paper we present the preparation procedures for both cathode materials together with their QE performances.

EXPERIENCE WITH COPPER CATHODES AT THE SITF

The SwissFEL Injector Test Facility (SITF) is a 250 MeV accelerator to test components and beam quality for SwissFEL. SITF produces beam since 2009 using copper cathode plugs installed in a RF photo-injector [1]. Cathodes are illuminated with laser pulses at 262 nm with a duration of σ_t=4 ps rms (Gaussian), a nominal diameter of σ_r=250µm (flat top transverse profile) and a repetition rate of 10 Hz. The electric field at the cathode surface during illumination is about 52 MV/m.

Until 2013, SITF was operated without any load-lock system and the QE directly after cathode installation was not reproducible and sometimes below the specification threshold of QE_{min} ~ 7.e-5, see for example Cu_7 and Cu_8 in Fig. 1. Only cathode Cu_3 has behaved exceptionally well for a very long period. After the installation of the load-lock chamber in july 2013, we have established a cleaning and annealing procedure with temperature as high as 250°C [1] which guarantees a starting QE always above 10^{-4}. This could be demonstrated on more than 5 cathodes. The duration until the QE decreases below $7.0 \cdot 10^{-5}$, is between 50 and 150 days (see Cu_19 and Cu_17 in Fig. 1).

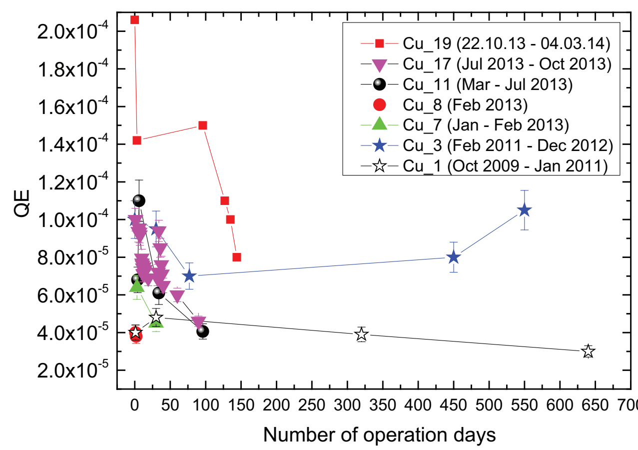

Figure 1: Evolution of the QE of copper cathodes installed in the injector since 2009. The load-lock chamber has been installed in July 2013.

The future laser system of SwissFEL (Yb:CaF_2 crystal) will be more powerful so that the minimum required QE will be as low as 4.10^{-5}. In view of Fig. 1, this would mean that the duration between two consecutive cathode exchanges should exceed 100 days. This would correspond to one shift shutdown every 100 days. Indeed, the exchange of cathodes with the load-lock takes only a few minutes but the RF conditioning of a new cathode still takes several hours.

Cs_2Te PREPARATION AND PERFORMANCES AT THE SITF

Cs2Te Cathode Preparation

The deposition procedure used at PSI is copied from a CERN [2,3] recipe where 15 nm of tellurium and 25 nm of caesium are successively evaporated directly on the copper cathodes [4]. The copper cathodes undergo beforehand the same annealing procedure as for operation with pure copper cathode. An aperture mask limits the deposition area to a disc of 1cm diameter (Fig. 2). The cathodes can then be transferred from the evaporation chamber to the gun load-lock via a vacuum suitcase. The initial pressure in the evaporation chamber is around 3.10^{-10} mbar going up to 1.10^{-8} mbar during evaporation. The base pressure in the gun during operation is around 1.10^{-9} mbar when RF is powered.

ISBN 978-3-95450-133-5

PHOTOEMISSION STUDIES OF NIOBIUM AND LEAD PHOTOCATHODES USING PICOSECOND UV LASER*

R. Xiang #, A. Arnold, P. Lu, P. Murcek, J. Teichert, H. Vennekate, HZDR, Dresden, Germany
R. Barday, HZB, Berlin, Germany

Abstract

We present the results of our investigations on superconducting photocathodes for supercondcuting rf injectors. Bulk niobium and lead film on niobium have been considered as the best candidates. The quantum efficiency (QE) at room temperature has been measured with 258 nm UV laser pulses of 14 ps duration. A QE of 10^{-4} has been obtained for the lead film. In order to improve the photoemission yield of niobium, new treatment methods, like Cs-activation and implantation with alkali metals, have been applied and the results are reported.

INTRODUCTION

In the past two decades, superconducting RF photoinjectors (SRF gun) have drawn a lot of attention because of their continuous-wave (CW), low emittance and high bunch charge operation. Different research projects have been launched at a growing number of accelerator laboratories [1-3]. A lot of efforts have been spent on solving the conflict between the normal conducting photocathodes and the superconducting cavity. The most direct and easiest way is to use superconducting materials as photocathodes. Previous experimental results showed that lead and niobium are the most promising candidates [4,5].

At HZDR, Cs_2Te is the standard photocathode material, and the drive laser has the wavelength of 258 nm in CW mode with adjustable repetition rate 100-500 kHz, and the pulse length is 14 ps FWHM. In this work, we used the present drive laser to investigate the photoemission properties of lead layer and bulk niobium, and tried to find a new recipe to improve the QE for niobium photocathode.

THIN LEAD LAYER

Lead is an attractive option for a low to moderate average current source. Arc deposition technique has been proved to be the best choice for coating [5]. QE investigation was done with the SRF gun drive laser for the lead layer produced at National Centre for Nuclear Research (NCBJ) of Poland [6].

Experimental Setup

The vacuum chamber used to measure the QE of cathodes is shown in Fig. 1. It consists of an anode ring and a cathode in a parallel geometry with a spacing of 10 mm. The anode ring can be biased up to 400 V. The cathode is connected to a picoammeter Keithley6485 for the photocurrent measurement. The laser used for photoemission was focused on the cathode surface with a diameter of 1 mm, illuminating at normal incidence through the anode ring. A turbo-pump was used to keep the vacuum inside the chamber at a level of 10^{-7} mbar.

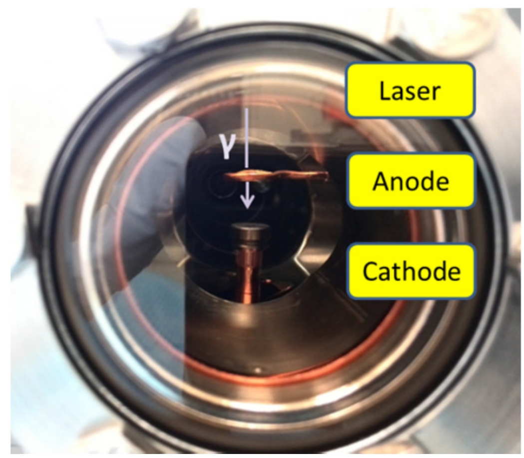

Figure 1: The experimental setup for QE measurement.

Preparation Progress

The 2 µm thick lead layer was coated on polycrystal niobium plugs. The mirror-like Ø 10 mm Nb plugs were mechanically polished with diamond suspension, resulting in a mean roughness of 25 nm.

The lead layer deposition was done at NCBJ (Swierk) using an UHV arc device equipped with a 30° bent plasma duct for droplets filtering at a deposition rate of 200 nm/min. Sample #C2 was additionally treated with three Ar plasma pulses in the IBIS rod plasma injector at NCBJ. Energy-dispersive X-ray spectroscopy (EDX) measurement showed 86 – 93 % lead in the 2 µm layer [6].

For all samples, the lead layers were briefly exposed to air between deposition, post-processing, SEM studies and QE measurement.

QE Measurement and Laser Cleaning

The QE of the layer was determined by measuring the laser power on the cathode and the current leaving the cathode. The bias on anode was adjustable from 30 V to 400 V.

*Work supported by the European Community under the FP7 programme (EuCARD-2, contract number 312453, and LA3NET, contract number 289191), and by the German Federal Ministry of Education and Research (BMBF) grant 05K12CR1.

#r.xiang@hzdr.de

ISBN 978-3-95450-133-5

FORMATION OF THE ELECTRON BUNCH LONGITUDINAL PROFILE FOR COHERENT ELECTRON COOLING EXPERIMENT*

I. Pinayev#, D. Kayran, V.L. Litvinenko, BNL, Upton, NY 11973, USA

Abstract

Proof-of-principle experiment of the coherent electron cooling (CeC) is ongoing at Brookhaven National Lab. CeC mechanism utilizes amplification of density modulation, induced by hadrons, by an FEL structure. To fully utilize electron beam cooling capacity we need uniform longitudinal beam profile. In this paper we present two frequency injector system tuned for this requirement.

INTRODUCTION

The principle of the coherent electron cooling is the following [1]. The hadrons imprint their distribution onto the co-propagating electron beam thus creating a density modulation of the electron bunch. This modulation is amplified by a FEL structure and electric field is significantly increased. Due to the longitudinal dispersion a hadron arrives into the accelerating or decelerating phase of the field depending on its energy. With properly tuned system a net reduction of energy spread is obtained.

The cooling rate depends on the strength of the longitudinal space charge field, i.e. on the FEL gain, which depends exponentially on the peak current distribution of the electron bunch. Therefore it is desirable to have as much gain as possible. However, reaching saturation regime leads to the loss of the phase coherence and hence cooling. For this reason the FEL should operate under the saturation threshold but as close as possible. To fully utilize the electron beam cooling capacity we need to have flat longitudinal profile.

SYSTEM DESCRIPTION

The electron accelerator for the CeC proof of principle experiment [2] comprises a 112 MHZ superconducting RF gun [3, 4], two normal conducting 500 MHz buncher cavities and 20 MeV five-cell 704 MHz accelerating cavity. In order to reduce project cost the RF equipment was chosen from the available hardware and no optimization of the frequencies values was available. The design voltage of the gun cavity is 2 MV, and each copper cavity is capable of the producing 300 kV voltage.

The electrons will be generated by a multialkaline cathode, illuminated by a fiber laser with frequency doubling to 530 nm wavelength. Laser, manufactured by NuPhoton, is capable to produce 78 kHz pulses (RHIC revolution frequency) with regulated pulse width from 100 to 550 picoseconds. The rise/fall time is around 50 picoseconds. The peak power is not less 1 kW. With 1% quantum efficiency the extracted photocurrent is 4 Amperes, which is much less below of the required 80 A. Due to the low energy of electron beam we chose ballistic bunching of the beam, when compression is obtained in the drift space due to the velocity modulation. The energy chirp is eliminated in the 704 MHz cavity with slightly off-crest accelerating.

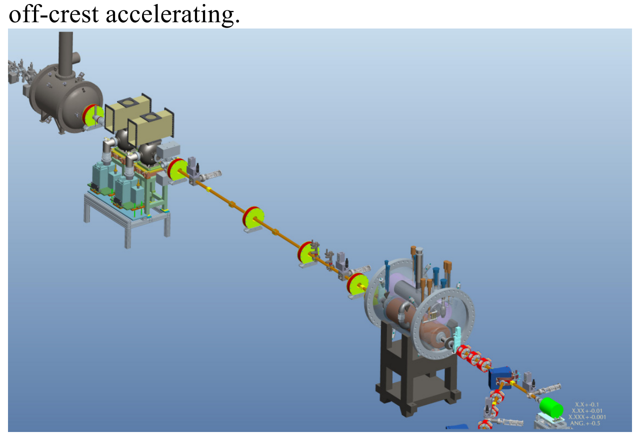

Figure 1: General layout of the electron accelerator for the coherent electron cooling proof-of-principle experiment. Electrons are generated in the 112 MH SRF gun shown in the upper-left corner, proper velocity modulation is provide by the two copper cavities, the electron bunch is compressed in the drift section and further accelerated in the superconducting 704 MHz cavity shown in the lower-right corner.

The high degree of the desired compression makes significant high order terms such as δ_{566}, which causes unevenness of compression. Such effect is well known [5, 6] and there are two approaches to overcome it. The first approach, utilized in [5], is two modulate the initial beam current and non-linear compression will provide a flat top pulse. The second approach utilizes the second order (parabolic) energy chirp, which cancels the non-linearity. We have chosen the second approach in order fully utilize the available laser power and have ability with ease adjust the pulse length. In our set-up the electron beam will be generated off-crest of the gun voltage to have the compressing chirp. The normal conducting cavities along with additional chirp will provide a parabolic compensation term.

SIMULATIONS RESULTS

The simulations were performed using code ASTRA. The initial electron beam has 2 nC charge distributed in plateau with 0.4 ns FWHM and 80 ps rise/fall time. The transverse distribution was uniform round beam with 2 mm radius and zero emittance. Total 50000 particles were generated. The gun cavity voltage was to provide 2 MeV

*Work supported by DoE program on Research and Development for Next Generation Nuclear Physics Accelerator Facilities
#pinayev@bnl.gov

ISBN 978-3-95450-133-5

HIGH POWER RF TEST AND ANALYSIS OF DARK CURRENT IN THE SwissFEL-GUN

P. Craievich*, S. Bettoni, M. Bopp, A. Citterio, C. Ozkan. M. Pedrozzi,
J.-Y. Raguin, M. Schaer, A. Scherer, T. Schietinger, L. Stingelin, PSI, Villigen, Switzerland

Abstract

To fulfill the beam quality and operational requirements of the SwissFEL project, currently under construction at the Paul Scherrer Institut, a new RF photocathode gun for the electron source was designed and manufactured in house. A 2.6 cell S-band gun operating with near-perfect rotationally symmetric RF field was designed to operate with a 100 MV/m cathode field at a repetition rate of 100 Hz with average power dissipation of 0.9 kW with pulse duration of 1 µs. The first SwissFEL-gun is now fabricated and installed in the SwissFEL Injector Test Facility (SITF). The frequency spectrum and field balance, through bead-pulling, have been directly verified in-situ and then the gun has been operated with high-power RF. The results of bead-pull measurements and high-power tests are presented and discussed. In addition the emitted dark current was also measured during the high-power tests and the charge within the RF pulse was measured as a function of the peak cathode field. Faraday cup data were taken for cathode peak RF fields up to 100 MV/m for the case of a diamond-milled polycrystalline copper cathode.

INTRODUCTION

The SwissFEL free electron laser project currently under construction at the Paul Scherrer Institut will be composed of a 5.8 GeV accelerator and two undulator beam lines which will cover the photon energy ranges from 12.4 keV to 1.8 keV and from 1.8 keV to 0.18 keV for Aramis and Athos lines, respectively [1]. To fulfill the beam quality and operational requirements a new RF photocathode gun for the electron source was designed [2] and manufactured in house [3]. It is composed of 2.6 cell operating with a near-perfect rotationally symmetric π-mode at the S-band frequency. The middle cell is coupled to two rectangular waveguides symmetrically arranged to cancel the dipolar component of the field. The racetrack interior shape of this coupling cell is optimized to minimize the quadrupolar field component. It is designed to operate with a 100 MV/m cathode field at a repetition rate of 100 Hz with average power dissipation of 0.9 kW and a pulse duration of 1us. The first SwissFEL-gun is now fabricated and installed in the SwissFEL Injector Test Facility (SITF) [4]. In order to have the possibility to exchange cathode without breaking the vacuum the back-plane of the RF gun has a hole where a cathode plug can easily be inserted through a load-lock system [5]. Figure 1 shows a 3-D view of the SwissFEL-gun where the cathode-plug is visible in the back-plane. Measurements at room temperature in the clean room showed that the resonant frequency depends on the force with the cathode-plug is pushed into the gun and thus the frequency spectrum and field balance, through bead-pulling, have been directly verified in SITF before starting with RF conditioning. Table 1 lists a comparison between RF simulations with HFSS [6] and measurements of the SwissFEL-gun RF parameters. In addition the emitted dark current was also measured during the high-power tests. Past measurements on the previous installed CTF3 gun showed quite high value of the dark current [7], thus the charge within the RF pulse of the SwissFEL-gun was measured as a function of the peak cathode field at different pulse durations. Faraday cup data were taken for different cathode peak RF fields for the case of a diamond-milled polycrystalline copper cathode with surface roughness R_a=5 nm.

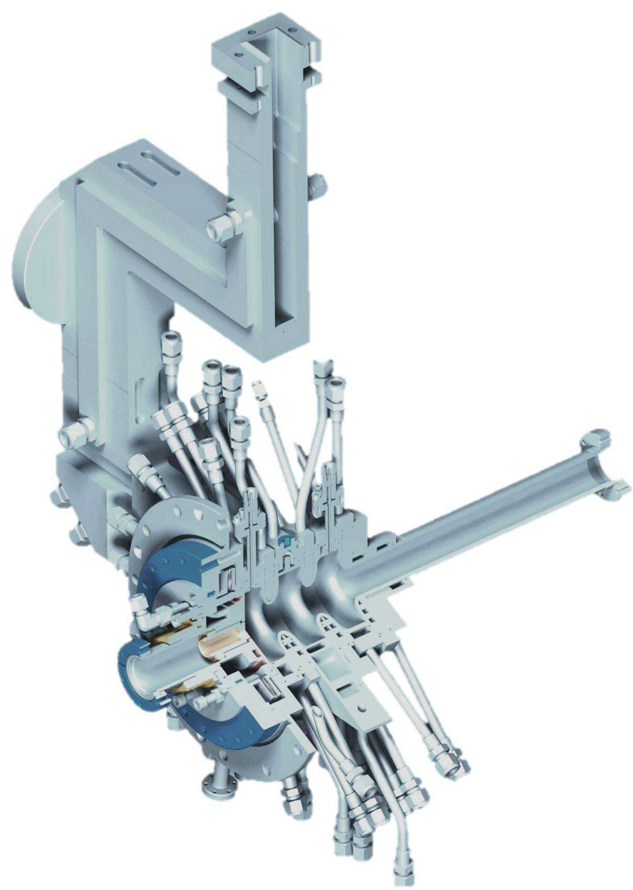

Figure 1: 3-D view of the SwissFEL-gun.

* paolo.craievich@psi.ch

ISBN 978-3-95450-133-5

THYRATRON REPLACEMENT*

Dr. Ian Roth, Dr. Marcel P.J. Gaudreau, PE, Michael Kempkes,
Diversified Technologies, Inc., Bedford, MA 01730, USA

Abstract

Thyratrons in high-power, short-pulse accelerators, have a limited lifetime. It would be desirable to replace the thyratrons with solid-state devices. One possibility, thyristors, are being developed for this application; however, they have not, to date, demonstrated the reliability needed for installation in the short pulse, high peak power RF stations used in many pulsed electron accelerators. An alternate solid-state device, the insulated-gate bipolar transistor (IGBT), can readily operate at the speed needed for accelerators, but commercial IGBTs cannot handle the voltage and current required. It is, however, possible to assemble these devices in arrays to reach the required performance levels without sacrificing their inherent speed. Diversified Technologies, Inc. (DTI) has patented and refined the technology required to build these arrays of series-parallel connected switches. Under a DOE contract, DTI is currently developing an affordable, reliable, form-fit-function replacement for the klystron modulator thyratrons at SLAC.

INTRODUCTION

The Stanford Linear Collider (SLC) has used thyratrons in its klystron modulators since its inception in 1963. While the thyratrons function, they need replacement every 10,000 hours at a cost of $13,000 each, plus labor. Furthermore, periodic maintenance is required to adjust their reservoir heater voltage over the thyratron lifetime. As the Stanford Linear Accelerator Center (SLAC) continues to run its accelerator over the next two decades, replacing the thyratrons with a solid-state switch that would last 25 years or more, and does not need maintenance, would provide significant savings – both in the avoided cost of thyratrons as well as the labor in replacing and adjusting them.

SLAC is presently funding the development of a solid-state switch, based on thyristor technology, to replace the thyratrons (Figure 1). The difficulty is that a fast rising current in a thyristor tends to be carried in a small region, rather than across the whole device, and this localized current concentration can cause a short circuit failure.

APPROACH

An alternate solid-state device, the insulated-gate bipolar transistor (IGBT), can readily operate at the speed needed for the accelerator, but commercial IGBTs cannot handle the voltage and current required. It is, however, possible to assemble these devices in arrays to reach the required performance levels without sacrificing their inherent speed. Diversified Technologies, Inc. (DTI) has patented and refined the technology required to build these arrays of series-parallel connected switches. DTI has shipped more than 500 systems leveraging this technology, which have been operating in facilities around the world for many years.

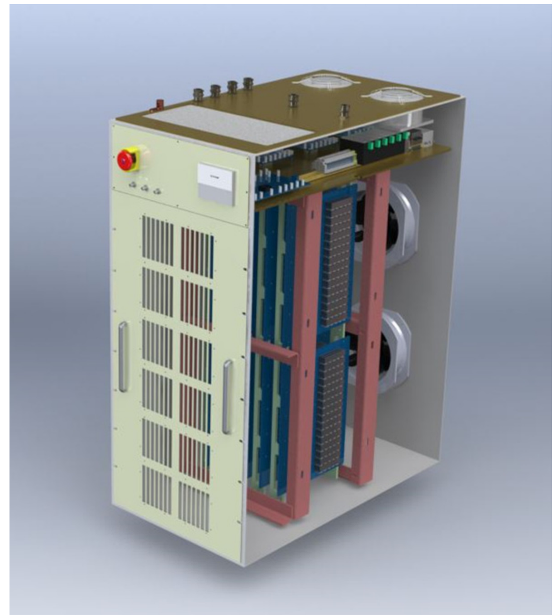

Figure 1: Artist's conception of thyratron-replacement solid-state switch array. Target specifications are detailed in Table 1.

DTI has begun this effort with careful consideration of potential candidate IGBTs, identifying the optimal device based on price and performance in single-device tests, determining the gate drive performance necessary to allow high-current operation, and targeting the development of a multi-device switch plate. In the second Phase of this SBIR, DTI will develop the gate drive for the system, then design, build, and test a complete switch that is small enough to be integrated into the existing cabinet. These switches will be delivered to SLAC, and their performance and reliability will be demonstrated in a SLC modulator.

MOTIVATION

The market for thyratrons is in decline. As newer solid-state modulators are deployed, and older thyratron systems are taken out of service, the demand for thyratrons has diminished significantly. In response, several vendors have either gone out of business or stopped manufacturing thyratrons, further diminishing their availability. It is not clear how long the supply of thyratrons for these legacy systems will continue, making

*Work supported by U.S. Department of Energy SBIR Award DE-SC0011292

ISBN 978-3-95450-133-5

AFFORDABLE SHORT PULSE MARX MODULATOR*

Robert Phillips, Gerard DelPriore, Dr. Marcel P.J. Gaudreau, PE, Michael Kempkes,
Diversified Technologies, Inc., Bedford, MA 01730, USA
Dr. Jeffery Casey, Rockfield Research, Inc., Las Vegas, NV 89135, USA

Abstract

Under a U.S. Department of Energy grant, Diversified Technologies, Inc. (DTI) is developing a short pulse, solid-state Marx modulator. The modulator is designed for high efficiency in the 100 kV to 500 kV range, for currents up to 250 A, pulse lengths of 0.2 to 5.0 µs, and risetimes <300 ns. Key objectives of the development effort are modularity and scalability, combined with low cost and ease of manufacture. For short-pulse modulators, this Marx topology provides a means to achieve fast risetimes and flattop control that are not available with hard switch or transformer-coupled topologies.

INTRODUCTION

Under a DOE SBIR grant and based on research begun under the Next Generation Linear Collider (NLC) program, high energy, short-pulse modulators are being re-examined for the Compact Linear Collider (CLIC) and numerous X-Band accelerator designs. At the very high voltages required for these systems, however (Table 1), all of the existing designs are based on pulse transformers, which significantly limit their performance and efficiency. There is not a fully optimized, transformer-less modulator design capable of meeting the demanding requirements of very high voltage pulses at short pulsewidths.

MARX GENERATOR

A Marx generator is a system with energy storage capacitors which are charged in parallel at low voltage and discharged in series to provide high voltage output (Figure 1). This is a legacy idea, practiced for decades using resistor charging networks and spark-gaps for discharge. Constrained by the limits of closing switches, such systems required pulse forming networks and crowbars, with their attendant limitations.

The Marx topology allows a new degree of freedom unavailable to other architectures – DTI can intentionally underdamp the series snubbing within the pulse circuit. This cannot be done conventionally – the reactive overshoot endangers the load. In a Marx, we can compensate for the overshoot by initially firing only a subset of the switches – thus “sling-shotting” the leading edge faster than otherwise possible. We can tune the number and timing of subsequent module firings to counter the reactive ringing, and hold a flattop pulse to the desired voltage and accuracy.

Similarly, additional modules may be added to fire

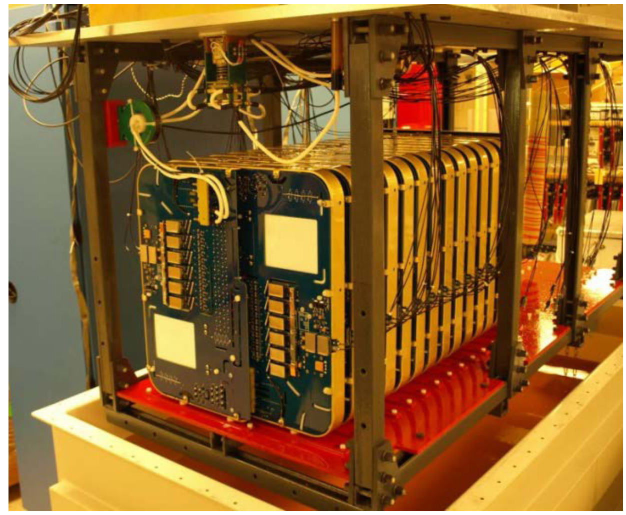

Figure 1: The Yale Marx 500 kV modulator charges many stages in parallel at low voltage, then discharges in series at high voltage. Each 12.5 kV, 250 A “flat pack” module is identical, providing for low fabrication and assembly cost.

sequentially later in the pulse to compensate for capacitor droop. This is a critical enabling technology motivating Marx use for long-pulse accelerators (such as ILC), and yields valuable optimization even for very short-pulse systems. The reduction of capacitor size afforded by this flexibility further reduces parasitic capacitance, and thus reduces equipment size and cost while increasing power efficiency.

DESIGN BENEFITS

Reduced Module Costs

Through the use of PC board trace shielding and RF cans in sensitive areas of the circuit, we were able to co-locate controls directly on the board within reasonable proximity to pulsed current sections of the same board. By exposing the IGBTs directly to the oil, we can cool the devices effectively while eliminating machined parts and hardware, further reducing the module parts count, associated materials, and assemly costs. Since the flat-pack design significantly reduces voltage gradients from module to module within the Marx bank, the only significant need for corona and field reduction geometry is at the interface between the Marx bank stack and the walls of the tank. We anticipate more than a four-fold reduction in module mechanical costs, with the potential for additional reductions in manufacturing costs, compared to earlier designs.

*Work supported by U.S. Department of Energy SBIR Award DE-SC0004251

ISBN 978-3-95450-133-5

STEADY STATE MULTIPACTING IN A MICRO-PLUSE ELECTRON GUN

Zhou Kui*, Lu Xiangyang†, Quan Shengwen, Luo Xing, Yang Ziqin, Zhao Jifei
State Key Laboratory of Nuclear Physics and Technology, Peking University, Beijing 100871, China

Abstract

Multipacting is a resonant electron discharge phenomenon via secondary electron emission, while micropulse electron gun (MPG) utilizes the multipacting current in a radio-frequency (RF) cavity to produce short pulse electron beams. The concept of MPG has been proposed for many years. However, the unstable operating state of MPG vastly obstructs its practical applications. This paper presents a study on the steady state mulitpacting in a MPG. The requirements for steady state multipacting are proposed through the analysis of the interaction between the RF cavity and the beam load. Accordingly, a MPG cavity with the frequency of 2856 MHz has been designed and constructed. Various kinds of grid-anodes are tested in our primary experiments. Both the unstable and stable multipacting current have been observed. Presently, the stable output beam current has been detected at about 12.2 mA. Further experimental study is under way now.

INTRODUCTION

Multipacting is a resonant electron discharge phenomenon via secondary electron emission [1], which is frequently observed in microwave systems. When the multipacting effect occurs, it usually causes some undesirable problems, such as deterirorating the vacuum, absorbing incident power, leading to quenching of superconducting cavity, etc. So, most studies on multipacting focus on how to suppress or eliminate it. Until 1993, Fredrick M. Mako and William Peter proposed the concept of MPG [2], which utilized the multipacting current in a RF cavity to produce pulsed electron beams. Due to its self-bunching property, MPG is capable of providing high current and short pulse electron beams. In addition to that, its simple structure and high tolerance to contamination make it a potential electron source for accelerators and microwave systems.

The main problem in the development of MPG is the stability of the output beam current. To get high beam current and low emittance, previous studies on MPG always tried to feed high power into the cavity to get high surface field [3,4]. The stable multipacting current in the MPG was considered to be formed as the equilibrium result of the self-bunching effect and the space charge effect [1]. However, we believe the beam loading effect also plays an important role in the forming process of stable multipacting current.

This paper presents a study on the steady state mulitpacting in a micro-pluse electron gun with theory and experiments. In the second section, a MPG model is setup to show the basic characteristics of the MPG. The requirements for the steady state multipacting is proposed through the analysis of the interaction of the RF cavity and electron beams. In the third section, a MPG cavity with the frequency of 2856 MHz has been designed and constructed. Different kinds of grid-anodes are tested in our experiments. Both the unstable and stable multipacting current have been observed sucessfully. The detected stable output beam current has reached 12.2 mA. Finally, a conclusion of this paper is given.

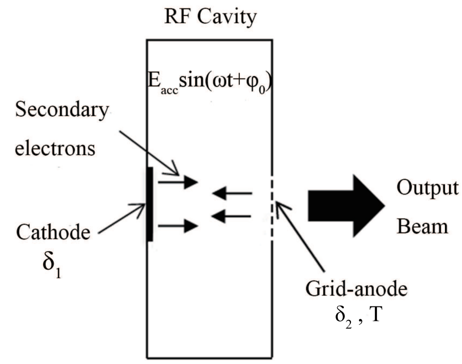

Figure 1: The schematic diagram of the MPG model [3].

ANALYSIS OF STEADY STATE MP

The MPG Model

The MPG model (Fig. 1) consists of three parts: an RF cavity working in the TM_{010} mode, a secondary emission surface and a grid, which is opaque to the microwave electric field but partially transparent to the electrons in order to extract the electron beams [3]. We suppose the secondary emssion surface to be the cathode with secondary emission yield (SEY) δ_1 and the grid to be the grid-anode with SEY δ_2 and transmission coefficient T. Here, we adopt Vaughan′s empirical formula for δ_1 and δ_2 [5].

$$\delta_1(E_i) = \delta_{\max1}(v_1 e^{1-v_1})^k \quad (1a)$$
$$\delta_2(E_i) = \delta_{\max2}(v_2 e^{1-v_2})^k \quad (1b)$$

Where E_i is the electrons impact energy, $\delta_{\max1}$ and $\delta_{\max2}$ is the maximum value of δ_1 and δ_2, $v_1 = (E_{i1} - E_0)/(E_{\max1} - E_0)$, $v_2 = (E_{i2} - E_0)/(E_{\max2} - E_0)$, in which E_{max1} and E_{max2} are the impact energy corresponding to δ_{max1} and δ_{max2}, E_0 being the initial energy of secondary electrons and $k = 0.62$ for $v < 1$; $k = 0.25$ for $v > 1$. For one RF period, the total effective secondary electron emission yield δ is:

* Email: zhoukui@pku.edu.cn
† Corresponding author, email: xylu@pku.edu.cn

ISBN 978-3-95450-133-5

DARK CURRENT STUDIES AT THE APEX PHOTOINJECTOR*

Ruixuan Huang†, NSRL, University of Science and Technology of China
Hefei, Anhui, 230029, China
Daniele Filippetto, Christos Frantzis Papadopoulos, Fernando Sannibale
Lawrence Berkeley National Laboratory, Berkeley, CA 94720, USA

Abstract

The increasing scientific demand for a high repetition rate FEL light source is driving the development of electron sources with high beam quality, delivering electron bunches at rates in the MHz range. An ongoing project to develop such a source is the Advanced Photoinjector Experiment (APEX) at LBNL. High brightness electron beams require high fields at the cathode during the electron emission. Such high fields associated with imperfections on the cathode surface area can induce undesired electron field emission (dark current). Excessive dark current can generate quenching of SRF structures and undesired radiation doses activating accelerator components and damaging undulator structures. In the present paper, we discuss the dark current studies performed at APEX. Field emitters in the cathode area have been localized and characterized, and techniques for minimizing dark current emission and to passively remove it have been investigated.

INTRODUCTION

APEX aims to demonstrate the capability of a new concept RF gun, the CW 186 MHz VHF-Gun [1,2], of delivering electron beams with quality required by X-ray FEL applications at MHz-class repetition rates. Figure 1 shows a cross section of the VHF-Gun. The requirements of CW operation and high accelerating field cause many technical challenges, and dark current control is one of them. Here we report on the dark current studies at APEX, with experimental measurements and simulation results. Based on the specific position of dark current emitters, a scheme for a passive collimation is proposed which could significantly reduce the dark current amount transported downstream.

DARK CURRENT MEASUREMENTS AND SIMULATIONS

Dark current measurements in APEX included the imaging of field emission sources located in the cathode area, and the measurement of dark current versus accelerating field at the cathode (for a single emitter and integrated over all emitters).

Sources of Dark Current in the VHF-Gun

In APEX the photo-emitting material is deposited on a molybdenum plug that can be inserted into the gun by the vacuum loadlock system located in the rear side of the gun.

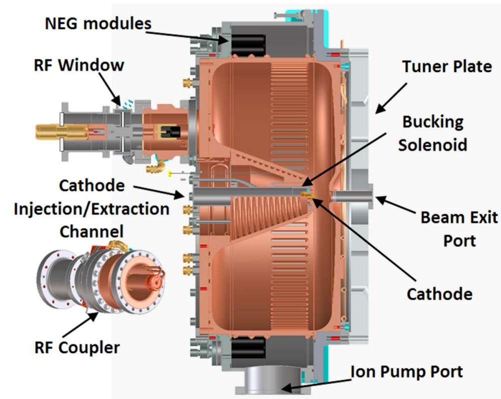

Figure 1: CAD cross-section of the VHF-Gun, with main components in evidence. The gun copper RF cavity resonates at 186 MHz and operates in continuous wave (CW) mode accelerating beams at a nominal energy of 750 keV with a gradient at the cathode of ~ 19.5 MV/m.

When inserted, see Fig. 2, only the tip part of the plug is exposed to the RF fields in the gun. This part has a radius of 5 mm and is surrounded by the copper of the cavity nose.

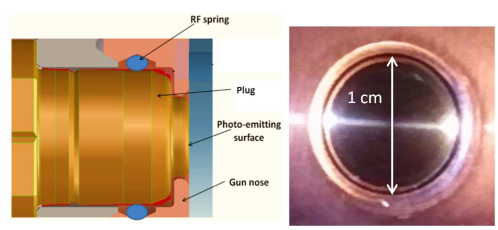

Figure 2: Left: CAD side view of the molybdenum cathode plug inserted in the gun nose. Right: picture showing the plug tip inside the gun viewed from the beam exit pipe.

By properly tuning two solenoids downstream, dark current electrons were used to create an image of the field-emitters at the cathode on a screen located downstream of the second solenoid. In the left side of Fig. 3 one of those images is shown. Several field emitting points are located with good accuracy along a ring are clearly visible. The image magnification was calibrated with the help of ASTRA simulations [3], revealing a ring radius of ~5.3 mm, implying the source to be located just outside the molybdenum plug, on the copper side surrounding the plug itself. The right side of Fig. 3 shows the dark current in the same imaging conditions, but the picture is taken with a much higher dynamic range, unveiling also the weakest sources.

* Work supported by Director of the Office of Science of the US Department of Energy under Contract no. DEAC02-05CH11231
† ruixuanhuang@lbl.gov

ISBN 978-3-95450-133-5

THE SWISSFEL C-BAND RF PULSE COMPRESSOR: MANUFACTURING AND PROOF OF PRECISION BY RF MEASUREMENTS

Urs Ellenberger, Heinrich Blumer, Markus Bopp, Alessandro Citterio, Mathias Heusser, Max Kleeb, Ludwig Paly, Markus Probst, Thomas Stapf, Riccardo Zennaro,
Paul Scherrer Institut, 5232 Villigen PSI, Switzerland

Abstract

A pulse compressor is required to compress the RF power distributed to the four accelerating structures of a single C-band (5.712 GHz) module of the SwissFEL. The pulse compressor is of the barrel open cavity (BOC) type. A total of 26 BOC devices are necessary to operate the linear accelerator (26 modules or 104 C-band structures) of SwissFEL X-ray laser. The C-band BOC combines the advantages of compactness and large RF efficiency i.e. large compression factor. Key features of the BOC are described and how they have been implemented in the manufacturing and tuning processes. RF measurements of the BOC are presented to account for the mechanical precision reached by manufacturing. So far 4 BOCs have been manufactured in-house and one has been high power tested in a RF test stand to simulate the operation in SwissFEL.

INTRODUCTION AND OVERVIEW

The linear accelerator (LINAC) of the SwissFEL consists of 26 C-band modules each of 4 pieces of 2m long C-band structures made of copper discs and supported on two granite girders. The waveguide system of each module is fed through a pulse compressor made of the barrel open cavity (BOC) type [1]. It is mounted on top of one end of the module as depicted in Fig. 1.

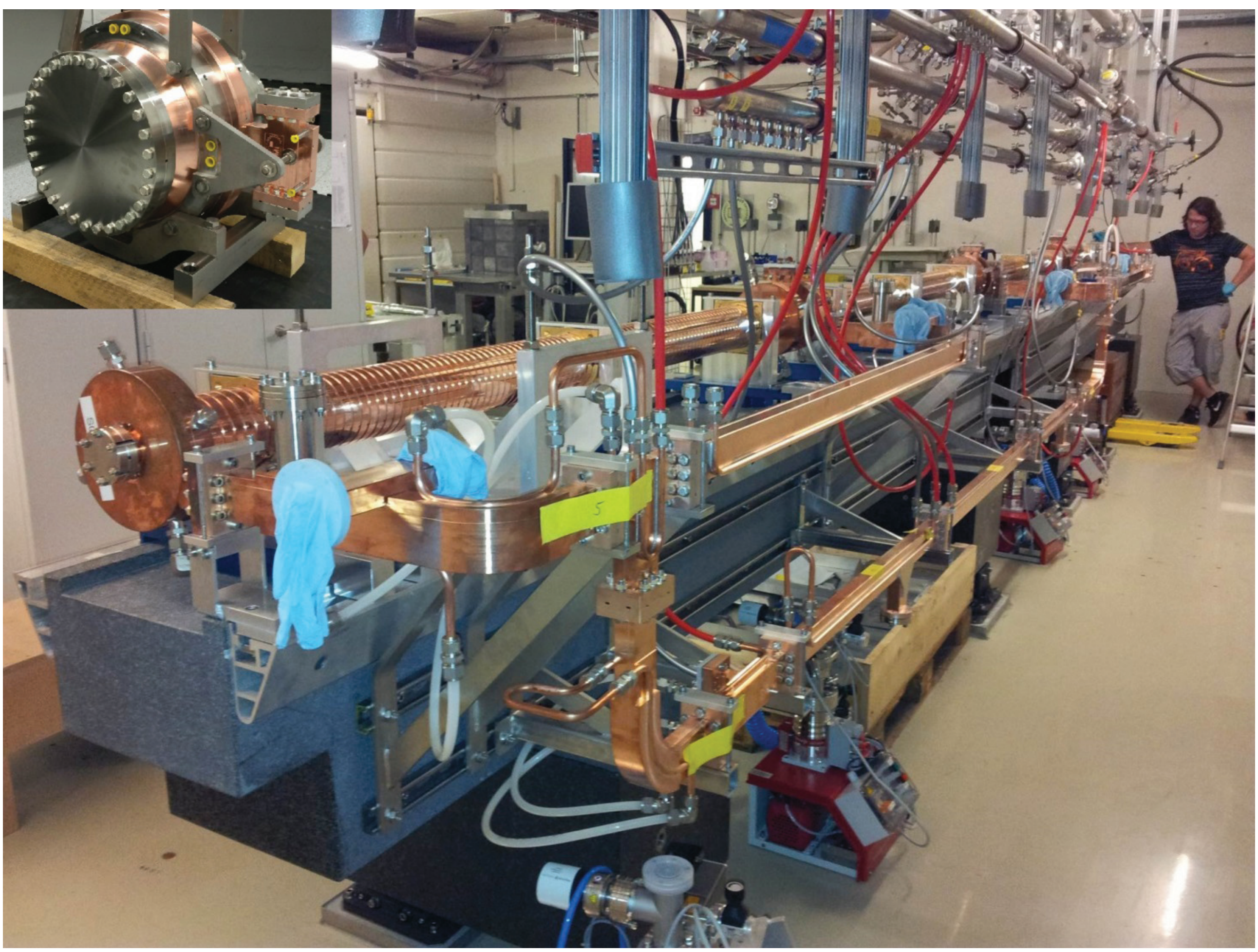

Figure 1: One C-Band module consists of 4 C-band structures made of copper discs and supported on two granite girders. The waveguide system is attached laterally on the girders. On the top left side of the module the pulse compressor BOC will be mounted (note inset photography on top, left).

ISBN 978-3-95450-133-5

LONGITUDINAL AND TRANSVERSE OPTIMIZATION FOR A HIGH REPETITION RATE INJECTOR[1]

C. F. Papadopoulos, D. Filippetto, R. Huang, G. J. Portmann, H. Qian, F. Sannibale, S. Virostek, R. Wells, LBNL, Berkeley, California, USA
A. Bartnik, I. V. Bazarov, B. Dunham, C. Gulliford, C. Mayes, Cornell University (CLASSE), Ithaca, New York, USA
A. Vivoli, Fermilab, Batavia, Illinois, USA
A. Brachmann, D. Dowell, P. J. Emma, Z. Li, T. Raubenheimer, J. Schmerge, T. Vecchione, F. Zhou, SLAC, Menlo Park, California, USA

Abstract

The injector is the low energy part of a linac, where space charge and non relativistic kinematic effects may affect the electron beam quality significantly, and in the case of single pass systems determines the brightness in the downstream components. Following the increasing demand for high repetition rate user facilities, a normal conducting, high repetition rate (1 MHz) RF gun operating at 186 MHz has been constructed at LBNL and is under operation. In the current paper, we report on the status of the beam dynamics studies. For this, a multi-objected approach is used, where both the transverse and the longitudinal phase space quality is optimized, as quantified by the transverse emittance and the bunch length and energy spread respectively. We also report on different bunch charge operating modes, as well as the effect of different gun gradients.

INTRODUCTION

LCLS-II [1] is a proposed user facility based on a superconducting RF linac driving a high repetition rate FEL, at SLAC. One of the important components of the project that have been identified is the injector part, which needs to accommodate the simultaneous objectives of high repetition rate and high beam brightness. For this reason, the Advanced Photoinjector Experiment (APEX) [2], an R&D project, is under way at LBNL, and is currently the baseline for LCLS-II. APEX is based on a normal conducting, continuous wave (CW) VHF electron gun, operating at 186 MHz. Another option being investigated in parallel is a photoinjector based on DC gun technology at Cornell University [3]. In the rest of the paper, the injector beam dynamics based on the VHF gun will be presented.

LCLS-II Injector Requirements

In order to accommodate the scientific requirements of LCLS-II [1], the requirements on the electron beam at the injector exit are given in Table 1.

A number of these requirements have already been demonstrated at APEX [2], specifically the ones related to the operation of the gun only, such as quantum efficiency, bunch charge and electron energy at the gun exit.

Simulations of the APEX and LCLS-II injectors, discussed later in this paper, show that the brightness requirements can be achieved by APEX. For the experimental verification of this, the installation of APEX phase II is required, which will bring the energy of the beam higher (30 MeV) and allow for the demonstration of beam emittance, bunch compression and the conservation of 6D beam brightness.

INJECTOR LAYOUT

A schematic of the baseline design of the LCLS-II injector, based on the NCRF VHG electron gun, is shown in Fig. 1

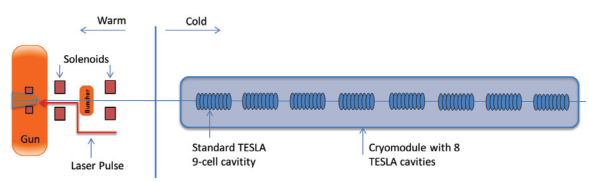

Figure 1: Schematic of LCLS-II injector. The beam energy at the warm-to-cold transition is nominally 750 keV.

The main difference with APEX is the cold part of the injector. In the case of LCLS-II, superconducting TESLA cavities [4] are used, while APEX will be using 3 normal conducting cavities, at 1.3 GHz like the TESLA ones. The final energy of APEX will be lower than 95 MeV, at approximately 30 MeV, enough to demonstrate the main dynamical processes of emittance compensation and bunch compression. The warm part of the LCLS-II injector [5] is essentially identical to the APEX layout.

As discussed below, for some bunch charges and especially the high (300 pC) case, the optimization requires relatively low gradient in the second and third TESLA cavities. This opens the possibility of having a single capture cavity in a stand-alone cryomodule followed by a drift and then a standard, 8 cavity cryomodule. Such a layout has the advantage of allowing more diagnostics as well as easing the maintenance procedure. The implications of using different layouts is discussed in a later section.

[1] This work was supported in part by the Work supported, in part, by the LCLS-II Project and by the Director of the Office of Science of the US Department of Energy under Contract no. DEAC02-05CH11231

ISBN 978-3-95450-133-5

SOLID-STATE SWITCH FOR A KLYSTRON MODULATOR FOR STABLE OPERATION OF A THZ- FEL

G. Isoyama[#], M. Fujimoto, S. Funakoshi, K. Furukawa, A. Irizawa, R. Kato, K. Kawase, K. Miyazaki, A. Tokuchi, R. Tsutsumi, M. Yaguchi, ISIR, Osaka University, Osaka, Japan
F. Kamitsukasa , Graduate School of Science, Osaka University, Osaka, Japan

Abstract

A solid-state switch using static induction (SI) thyristors has been developed for a klystron modulator of the L-band electron linac at Osaka University to enhance stability of a THz-FEL based on the linac. The switch meets the maximum specifications such that the holding voltage is 25 kV with the switching time of 270 ns, that the current is 6 kA for a pulse duration of 10 μs, and that the repetition frequency is 10 Hz. The fluctuations of the klystron voltage are considerably reduced compared to those with a thyratron. The FEL is operated with the solid-state switch and the macropluse energy of the FEL at a wavelength of ~70 μm are measured with an energy meter for infrared lasers. The fractional variation of the macropulse energy measured in successive 500 pulses is 2.4 % for the solid-state switch (standard deviation), which is much smaller than 5.4 % for the thyratron.

INTRODUCTION

We are conducting basic studies on the THz-FEL and its applications using the L-band electron linac at the Institute of Scientific and Industrial Research (ISIR), Osaka University. The FEL has been operated in the wavelength range from 25 to 150 μm (2~12 THz). Performance of the FEL depends strongly on the accelerator providing the electron beam for the FEL. One of the crucial factors affecting such studies is stability of the FEL macrpoulse energy. To obtain a highly intense and stable FEL beam, the energy and the intensity of the electron beam must be constant in an electron pulse of a several microsecond duration, and pulse-to-pulse intensity fluctuations are required to be small. To enhance the stability of the electron beam, the klystron modulator was upgraded, in such a way that the fluctuations of the charging voltage of the PFN are reduced to 0.008% (peak-to-peak). Nevertheless, pulse-to-pulse fluctuations of the height of the high voltage pulse applied to the klystron are measured to be almost ten times larger than those of the charging voltage. Because the source of the instability is considered to be the thyratron, which is a fast high voltage and high current switch for a PFN in the klystron modulator, we have developed a solid-state switch that is expected to be more stable.

The first klystron modulator with a solid state switch for an electron linac was developed, to our knowledge, in the early 1990s at the FOM Institute for Plasma Physics for the FEL facility, FELIX [1]. The switch is made of 32 thyristors that are connected in a series to operate at the maximum voltage of 40 kV and the maximum current of 2.6 kA. The following activities to develop solid-state switches and to use them began increasing at approximately 2000 in Europe, America, and Japan using semiconductor devices, including thyristors, IGBTs, and MOS-FETs. These devices, however, have both advantages and disadvantages for meeting the specifications and requirements for various klystron modulators.

Another candidate for a semiconductor device that is suitable for the solid state switch is the Static Induction Thyristor (SI-thyristor) because it has fast switching characteristics as well as a high holding voltage and a high current [2]. Two types of solid state switches with different types of SI thyristors were developed for the JLC project and were successfully tested at KEK. These switches, however, have not been used in operation of linacs.

In this paper, we will describe the development of the solid-state switch using SI thyristors and the evaluation of its performance in terms of the stability of the klystron voltage, the RF power and phase, and energy of the FEL macrpulses. More detailed report on the solid-state switch will be published elsewhere.

STATIC INDUCTION THYRISTOR

The SI thyristor is a type of PIN diode that is equipped with the gate. The characteristics that are measured from a test sample for pulsed-power applications are reported to be as follows: the hold-on voltage is 5.5 kV, and the turn-on time is 35 ns, with di/dt = 95 kA/μs [2]. Because these values are sufficient for our purpose, we decided to develop a solid-state switch using SI thyristors. Although they are not available on the market, we obtain SI thyristors by courtesy of Shindengen Electric Manufacturing Co., Ltd., which is developing such devices. Figure 1 shows an SI thyristor manufactured by the company.

Two important specifications of the SI thyristors that we use are the maximum blocking voltage of 3.2 kV and the maximum average current of 50 A (root-mean-square), although the details are not available yet from the manufacturer. It is, however, expected that a much higher current can flow if the pulse duration is short and the repetition rate is not so high that the average power consumption in the SI thyristor does not exceed the value in the slow operation. Characteristics of a SI thyristor measured with square pulses of 2 kV, 1 kA, and a 2 μs duration are the switching time of 360 ns (90%-to-10% change) and the turn-on resistance of 0.12 Ω. To evaluate

[#] isoyama@sanken.osaka-u.ac.jp

ISBN 978-3-95450-133-5

THE LASER HEATER SYSTEM OF SWISSFEL

M. Pedrozzi, M. Calvi, R. Ischebeck, S. Reiche, C. Vicario, PSI, Villigen, Switzerland
B. D. Fell, N. Thompson, STFC/DL/ASTeC, Daresbury, UK

Abstract

Short wavelength FELs are generally driven by high-brilliance photo-cathode RF-guns which generate electron beams with an uncorrelated energy spread on the order of 1 keV or less. These extremely cold beams can easily develop micro-bunching instabilities caused by longitudinal space charge forces after the compression process. This can result in a blow up of the energy spread and emittance beyond the tolerable level for SASE emission. It has been demonstrated theoretically and experimentally [1] that a controlled increase of the uncorrelated energy spread to typically a few keV is sufficient to strongly reduce the instability growth. In the laser heater system, one achieves a controlled increase of the beam energy spread by a resonant interaction of the electron beam with a transversally polarized laser beam inside of an undulator magnet. The momentum modulation resulting from the energy exchange within the undulator is consequently smeared out in the transmission line downstream of the laser heater system. In SwissFEL, the laser heater system is located after the first two S-band accelerating structures at a beam energy of 150 MeV. This paper describes the layout and the sub-components of this system.

INTRODUCTION

SwissFEL is the hard X-ray free-electron laser presently under construction at PSI in Switzerland [2-3]. Table 1 summarizes the main beam parameters at the injection in the undulator section specified for SASE operation at 1 Å radiation.

Table 1: Beam Parameters - SASE Hard X-Ray Line

Parameter		units
Energy	5.8	GeV
Charge	200/10	pC
Uncorrelated RMS slice energy spread	350/250	keV
RMS normalized projected emittance	< 0.65/0.25	mm.mrad
RMS normalized slice emittance	<0.43/0.18	mm.mrad
Peak current	2.7/0.7	kA
Bunch length	25/6	fs

The final electron beam energy of roughly 6 GeV was defined according to the state of the art accelerator and undulator technology in order to maximize compactness and minimize costs. The energy is relatively low with respect to other facilities of this class resulting in tighter beam quality requirements. The mitigation of emittance and energy spread growth during the acceleration and compression of the electron beam, caused in particular by micro-bunching instabilities [4-5], are therefore of primary importance for this facility [6]. It should be noted that for efficient self-seeding operation one aims to reach a normalized slice emittance of ~0.3 mm.mrad. The SwissFEL injector complex includes a laser heater (LH) system which will allows a controlled enhancement of the uncorrelated energy spread of the electron beam. Carefully adjusted, the energy spread can drastically reduce the gain of the micro-bunching instability without affecting the FEL performances.

SYSTEM DESCRIPTION

General Layout

Figure 1 shows a schematic of the SwissFEL injector facility. The PSI RF Photo-injector [7] produces 7.1 MeV high brightness electron bunches with an intrinsic emittance of 0.55 mm.mrad/mm [8] and a peak current of 20 A. The normalized slice emittance at the end of the injector with uncompressed beam will be typically around 0.2 mm.mrad for a bunch charge of 200 pC [9]. In Booster 1 two S-band traveling-wave cavities accelerate on crest the electron beam up to 150 MeV. After this first acceleration stage a set of 5 quadrupoles allows matching the optical functions trough the laser heater chicane and 5 additional quadrupoles follow the LH modulator undulator to control the matching in booster 2. This section consists of two S-Band RF modules including each one klystron amplifier and two accelerating cavities. In booster 2 one accelerates off crest (up to 345 MeV) to provide the necessary energy-time correlation needed for the compression. Enough space has been reserved to allow future energy upgrades with a third RF accelerating module. The focusing along booster 2 consists of three FODO cells with 11m period. To suppress the second order energy-time correlation two X-band RF cavities (S-band 4th harmonic) running in decelerating mode precede the 13.5 m long compression chicane which is typically operated at compression factors between 10 and 15. The final nominal energy of the injector is 320 MeV.

Laser Heater Basic Specifications and Layout

As schematically illustrated in Figure 2 the LH consists of 3 main parts:

- A small magnetic chicane required for the laser coupling which corresponds to the first dispersive section of the accelerator complex.

ISBN 978-3-95450-133-5

DESIGN OF A SPATIO-TEMPORAL 3-D ELLIPSOIDAL PHOTOCATHODE LASER SYSTEM FOR THE HIGH BRIGHTNESS PHOTOINJECTOR PITZ*

T. Rublack#, J. Good, M. Khojoyan, M. Krasilnikov, F. Stephan, DESY, Zeuthen, Germany
I. Hartl, S. Schreiber, DESY, Hamburg, Germany
A. Andrianov, E. Gacheva, E. Khazanov, S. Mironov,
A. Poteomkin, V. V. Zelenogorskii, IAP/RAS, Nizhny Novgorod, Russia
E. Syresin, JINR, Dubna, Russia

Abstract

Minimized emittance is crucial for successful operation of linac-based free-electron lasers. Simulations have shown that 3-D ellipsoidal photocathode laser pulses are superior to the standard Gaussian or cylindrical laser pulses in this manner. Therefore, in collaboration with the Joint Institute of Nuclear Research (JINR, Dubna, Russia) and the Photo Injector Test facility at DESY, Zeuthen site (PITZ), a prototype laser system capable of producing spatio-temporal 3-D ellipsoidal pulses has been constructed at the Institute of Applied Physics of the Russian Academy of Science (IAP / RAS, Nizhny Novgorod, Russia). It is expected to receive the finalized prototype at PITZ within this year.

The laser system to create such 3-D ellipsoidal laser pulses will be introduced. Also the procedure of pulse shaping will be described in detail.

INTRODUCTION

The operation of modern free-electron lasers (FELs) necessitates high brightness electron bunches with small energy spread. As the electron beam parameters along the beam line depend strongly on initial conditions at the photocathode, a minimized emittance is crucial for a successful FEL operation. An important parameter crucial for the initial conditions is given by the characteristics of the cathode laser.

In the following paragraphs the influence of different laser pulse parameters on the initial electron beam quality will be briefly discussed. While some of the parameters are well known due to previous experience, others have to be simulated and/or empirically determined.

If the photon energy is below the vacuum energy level (where an electron is free) of the photocathode material, it is impossible to generate emission of free electrons with single photon excitation [1]. The vacuum energy level is defined as the sum of the electron affinity and the band gap energy for semi-conductors, or equivalently as the work function in metals.

Due to scattering processes within the material the (quasi) free electrons can lose enough energy (thermalize) before reaching the cathode surface and therefore produce an electron beam with small mean transverse energy [2]. In contrast, higher incident photon energies lead to increased energy spread and to a reduction of the ablation threshold intensity of the photocathode material [3].

This naturally leads to the second important parameter which has to be considered – the laser pulse energy (or to be more precise the number of photons within a laser pulse). By first approximation the number of generated free electrons is proportional to the number of photons. However, space charge shielding effects and depletion of electrons at the surface of the photocathode as well as electron-hole recombination within the material – only to mention a few processes - reduce the quantum yield defined as the number of generated free electrons at the cathode per number of incident photons. At high laser pulse energies the space-charge shielding effect can even lead to saturation (Fig. 1).

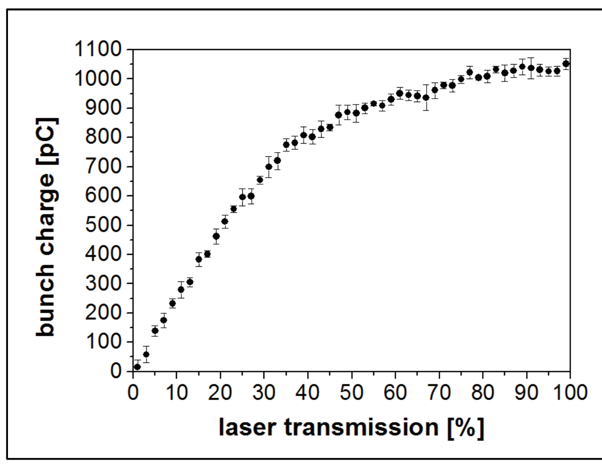

Figure 1: Example of measurement of the electron bunch charge with a Faraday cup as a function of laser energy 80 cm downstream the cathode. The laser energy is given in per cent of the maximum.

High pulse energies combined with high photon energies also risk thermal laser ablation of the photocathode material, which would destroy the characteristics of the photocathode and hence the properties of the electron bunch.

There are two more crucial laser pulse parameters – pulse duration and pulse shape. The latter has to be considered in three dimensions (spatially and temporally).

*Work supported by the German Federal Ministry of education and Research, project 05K10CHE "Development and experimental test of a laser system for producing quasi 3D ellipsoidal laser pulses" and RFBR grant 13-02-91323.
#Tino.Rublack@desy.de

ISBN 978-3-95450-133-5

COMMISSIONING OF AN IMPROVED SUPERCONDUCTING RF PHOTO INJECTOR AT ELBE

J. Teichert#, A. Arnold, M. Freitag, P. Lu, P. Michel, P. Murcek, H. Vennekate, R. Xiang, HZDR, Dresden, Germany
P. Kneisel, JLab, Newport News, USA
I. Will, MBI, Berlin, Germany

Abstract

In order to produce high-brightness electron beams in a superconducting RF photo injector, the most important point is to reach a high acceleration field in the cavity. For this reason two new 3.5-cell niobium cavities were fabricated, chemically treated and cleaned in collaboration with Jlab. The first of these two cavities was shipped to HZDR and assembled in a new cryomodule. This new gun (SRF Gun II) was installed in the ELBE accelerator hall in May 2014 and replaces the previous SRF Gun I. Beside the new cavity the ELBE SRF gun II differs from the previous gun by the integration of a superconducting solenoid. The paper presents the results of the first test run with a Cu photocathode.

INTRODUCTION

At the superconducting (SC) electron linear accelerator of the ELBE radiation facility [1] a new superconducting electron photo injector (SRF gun) has been installed in May 2014. The new gun (SRF Gun II) replaces the previous one which had been in operation from 2007 until April 2014. For the old SRF gun the handicap was the low acceleration gradient. Due to strong field emission of the cavity the maximum gradient (peak field) was only 17.5 MV/m in CW belonging to a kinetic energy of 3.3 MeV of the emitted electrons. Although SRF gun I could not reach the design specifications, it was successfully operated for R&D purposes and also for some dedicated user experiments at ELBE.

Table 1: Design Parameters of the ELBE SRF Guns at HZDR

Operation mode	FEL mode	High charge mode
Laser rep. rate	13 MHz	100-500 kHz
Laser pulse length	3 ps fwhm	12 ps fwhm
Peak field	50 MV/m	50 MV/m
Bunch charge	77 pC	1 nC
CW beam current	1 mA	≤ 0.5 mA
Kinetic energy	9.5 MeV	9.5 MeV
Transv. emittance	1 µm	2.5 µm

#j.teichert@hzdr.de

In a collaboration of HZDR and Jlab two new niobium cavities for the next ELBE SRF gun have been built, treated and tested at JLab. At the same time a new cryomodule has been designed and built at HZDR. One of the two new cavities was shipped to HZDR in November 2013. After arrival the assembly of the cryomodule was completed and the gun was installed in the ELBE accelerator hall in May 2014. The gun has been running since June 2014 for first RF and beam tests

The aim for ELBE SRF gun II is to approach the beam specification as given in Table 1. At ELBE an electron gun with high-brightness beam, high average current, and high bunch charge is needed to fulfill the future user requirements and provide high-flux neutron and positron beams as well as to operate the THz facility and the CBS x-ray source for users.

CAVITY AND CRYOSTAT DESIGN

The design of the new cryomodule for SRF gun II is shown in Fig. 1. The 1.3 GHz Nb cavity consists of three TESLA cells and a specially designed half-cell. Another superconducting cell, called choke filter, prevents the leakage of the RF field towards the cathode support system. The normal conducting (NC) photocathode is installed in this system, which is isolated from the cavity by a vacuum gap and cooled with liquid nitrogen. This design allows the application of NC photocathodes with high quantum efficiency (QE) like Cs_2Te.

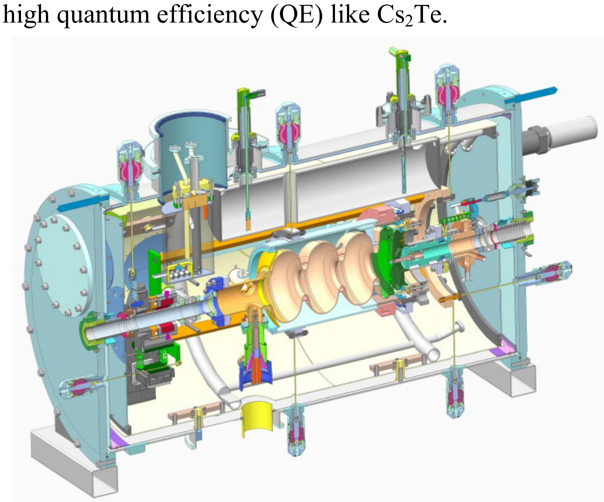

Figure 1: CAD view of the SRF Gun II cryomodule.

Similar to cavity and cathode support system, most of the cryomodule components, the cavity tuners, and the fundamental power coupler are identical in the design

ISBN 978-3-95450-133-5

PRODUCTION OF C-BAND DISK-LOADED TYPE CG ACCELERATING STRUCTURES

N. Shigeoka, D. Suzuki#, S. Miura, Mitsubishi Heavy Industries, Ltd., Mihara, Hiroshima, Japan
T. Sakurai, T. Inagaki, Y. Otake, RIKEN SPring-8 Center, Kouto, Sayo, Hyogo, Japan
H. Ego, T. Asaka, JASRI, Kouto, Sayo, Hyogo, Japan

Abstract

Mitsubishi Heavy Industries, Ltd. manufactured six C-band disk-loaded type and quasi-constant gradient (CG) accelerating structures for the XFEL facility, SACLA (SPring-8 Angstrom Compact free electron LAser). These structures were newly designed by RIKEN for operation at an acceleration gradient of over 45 MeV/m and a repetition rate of 120 pps. We report the production and low-power RF properties of these accelerating structures.

INTRODUCTION

In April 2013, Mitsubishi Heavy Industries, Ltd. contracted with RIKEN to manufacture six C-band disk-loaded type and CG accelerating structures for the XFEL facility, SACLA. The first structure was delivered in August 2013 to RIKEN and the other five were delivered in March 2014.

Devices of the accelerator system operable at a high repetition rate are being developed by RIKEN, as one of the possibilities to grow in the performance of SACLA. The C-band disk-loaded type structures were designed to enable us operation at a high repetition rate of more than 120 pps and a highly acceleration gradient of more than 50 MV/m. We paid attention to reduction in manufacturing cost and compatibility with the C-band choke-mode type accelerating structures in use as the main accelerators of the SACLA [1, 2].

We will report the results of the production and low-power RF test of these newly manufactured six accelerating structures in this paper.

FEATURES OF THE ACCELERATING STRUCTURES

The disk-loaded accelerating structure is a quasi-constant gradient (Quasi-CG) type. Its resonant frequency is 5712 MHz (30 deg. C in vacuum) and its total length is 1.8 m. Figure 1 shows the outline view of the accelerating structure. Table 1 shows required specifications.

The resonant frequency, total cavity length, attenuation constant τ, filling time t_F, and position of cooling pipe are designed to be compatible with the present choke-mode type structure [3, 4] for SACLA. There are two major modifications from the choke-mode type structures. One is that the regular accelerating cells have no choke structure but tuning holes and the other is that the accelerating mode was changed from 3π/4 to 2π/3. As a result of the former, the phase shift can be tuned after the

#daisuke4_suzuki@mhi.co.jp

Table 1: Requirements Specifications of the C-band Disk-Loaded Type Accelerating Structure

Items	Requirements Specifications
Resonance frequency	5172 MHz +/- 0.2 MHz
	30 deg. C in vacuum
Coupler type	J-type double-feed coupler
Number of cells	100 + 2 coupler cell
Total cavity length	1.8 m
Structure type	Quasi-constant gradient
Phase shift	2π/3
Integrated phase error	≤ +/- 3deg.
VSWR	≤ 1.1
Q factor	8000 ≤
Average shunt impedance	55 MΩ/m ≤
Attenuation constant τ	0.56
Filling time t_F	270 ns
Material of cells	OFC-CLASS1 HIP
Brazing process	Vacuum brazing

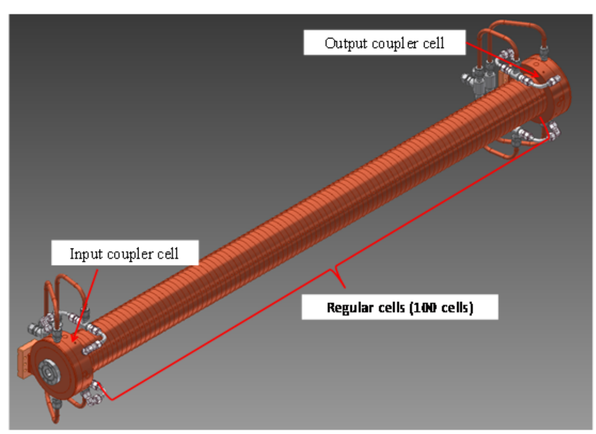

Figure 1: C-band disk-loaded type accelerating structure.

ISBN 978-3-95450-133-5

HIGH REPETITION RATE S-BAND PHOTOINJECTOR DESIGN FOR THE CLARA FEL

J.W. McKenzie, P.A. Goudket, T.J. Jones, B.L. Militsyn, STFC/DL/ASTeC, UK
L.S. Cowie, STFC/DL/ASTeC & Lancaster University, Cockcroft Institute, UK
G. Burt, Lancaster University, Cockcroft Institute, UK
V.V. Paramonov, INR of RAS, Moscow, Russia

Abstract

We present the design of a 1.5cell S-band photoinjector RF gun intended to be operated at repetition rates up to 400 Hz in single bunch mode. This gun is intended for use at the proposed CLARA (Compact Linear Accelerator for Research and Applications) FEL test facility at Daresbury Laboratory in the UK and will first be tested and characterised on VELA (Versatile Electron Linear Accelerator) in 2015. The final cavity design is presented including optimisation for CLARA beam dynamics, and choice of a novel coaxial H-shaped coupler.

INTRODUCTION

CLARA (Compact Linear Accelerator for Research and Applications) is a proposed 250 MeV, 100-400 nm FEL test facility at Daresbury Laboratory in the UK [1]. The electron source for CLARA needs to be able to operate in various regimes to meet the different FEL operational modes. In single bunch modes it needs to deliver bunch charges up to 250 pC at repetition rates of up to 400 Hz. In multi-bunch mode it needs to deliver 16 x 25 pC bunches with a bunch separation of 100 ns.

To meet this requirement, a 1.5 cell, 2.9985 GHz photocathode RF gun, shown in Fig. 1, has been designed. The gun is intended to operate with a peak field of 120 MV/m for the 100 Hz modes, which will be reduced to 100 MV/m for the 400 Hz modes to moderate the average power in the gun and thus heat loads. The gun will initially be tested on VELA [2] which contains a suite of diagnostics to fully characterise the 6D phase space of the emitted electron beam.

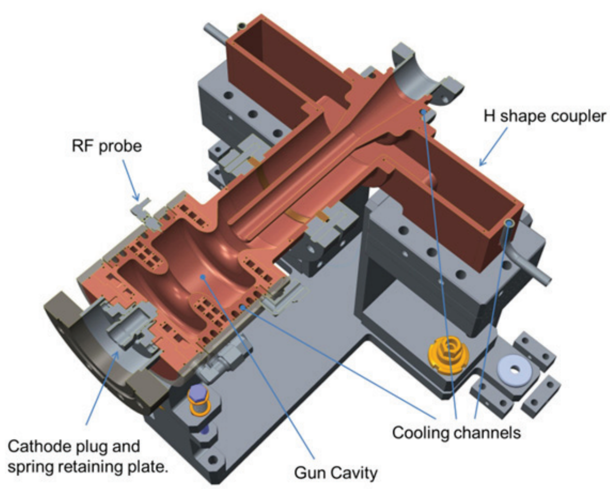

Figure 1: Overview of the gun design.

OVERVIEW AND COOLING

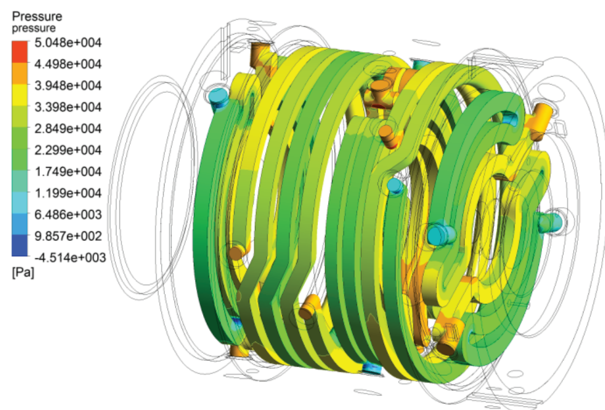

Figure 2: Pressure profiles at the surface of the cooling channels.

A 1.5 cell gun was chosen over 2.5 cells as, although this reduces the final energy of the electron bunch, it reduces the power requirements to the gun. Power fed into the gun manifests as heat deposited into the cavity walls and needs to be extracted by the cooling system. The expected average power for a 2.5 cell gun is almost double that of a 1.5 cell cavity, and for 100 MV/m at 400 Hz was estimated to be 6.8 kW for the 1.5 cell case.

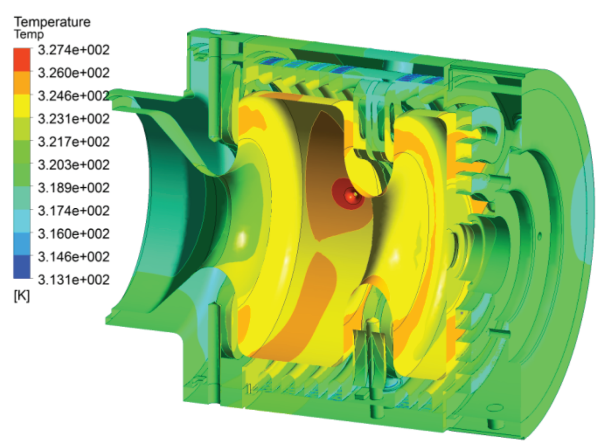

Figure 3: Temperature profile with the proposed cooling system with the gun operating at 100 MV/m at a 400 Hz repetition rate.

The magnetic field distribution of the cavity was converted into a heat flux and computational fluid dynamics simulations carried out in ANSYS. This showed that the proposed cooling, shown in Fig. 2,

ISBN 978-3-95450-133-5

PERFORMANCE STUDY OF HIGH BANDWIDTH PICKUPS INSTALLED AT FLASH AND ELBE FOR FEMTOSECOND-PRECISION ARRIVAL TIME MONITORS

M.K. Czwalinna*, Ch. Gerth, H. Schlarb, C. Sydlo, DESY, Hamburg, Germany
A. Angelovski, R. Jakoby, A. Penirschke, IMP, TU Darmstadt, Darmstadt, Germany
T. Weiland, TEMF, TU Darmstadt, Darmstadt, Germany
M. Kuntzsch, TU Dresden, Dresden, Germany and HZDR, Dresden-Rossendorf, Germany
M. Gensch, HZDR, Dresden-Rossendorf, Germany

Abstract

At today's free-electron lasers, high-resolution electron bunch arrival time measurements have become increasingly more important in fast feedback systems for a timing jitter reduction down to the femtosecond level as well as for time-resolved pump-probe experiments. This is fulfilled by arrival time monitors which employ an electro-optical detection scheme by means of synchronised ultrashort laser pulses. Even more, at FLASH and the European XFEL the measurement has to cover a wide range of bunch charges from 1 nC down to 20 pC with equally sub-10 fs resolution. To meet these requirements, recently a high bandwidth pickup electrode with a cut-off frequency above 40 GHz has been developed. These pickups are installed at the macro-pulsed SRF accelerator of the free-electron laser FLASH and at the macro-pulsed continuous wave SRF accelerator ELBE. In this paper we present an evaluation of the pickup performance by direct signal measurements with high bandwidth oscilloscopes and by use of the electro-optical arrival time monitor.

INTRODUCTION

FLASH at the Deutsches Elektronen-Synchrotron is a free-electron laser with pulsed superconducting RF acceleration. Beam energies of up to 1.25 GeV correspond to FEL wavelengths down to 4.2 nm. THz sources and an optical laser are provided for pump-probe experiments. In addition, with the second FEL beamline, FLASH 2, the facility offers the possibility to apply or test different seeding schemes, i.e. HGHG, EEHG and HHG [1, 2]. Recently, increasingly more often user experiments demand for short FEL pulse lengths down to few 10 fs duration, which is achieved by decreasing the bunch charge well below 100 pC. Thus, the charge operation regime of FLASH now expands from a few 10 pC up to 3 nC.

ELBE at the Helmholtz-Zentrum Dresden-Rossendorf is a superconducting electron accelerator with a quasi-continuous wave (quasi-CW) mode of operation achieving beam energies up to 40 MeV. Bunches with up to 1 nC, after the next upgrade, and durations down to 200 fs are accelerated and transported to different beamlines, where they are used for various purposes, e.g. FEL pump-probe experiments, THz generation or for experiments with Thomson back-scattering, with positron or neutron radiation [3, 4].

At both facilities, all of the diverse applications rely on stable beam conditions, which concerns electron bunch parameters such as charge, energy, compression and arrival time.

Arrival time drift and jitter are imprinted onto the electron bunch from instabilities in the electron source and from RF field fluctuations in the accelerating modules.

Besides delivering information to experiments, bunch arrival time monitors (BAMs) with femtosecond resolution also offer the possibility of feedback systems to actively stabilise the arrival time at different locations of the facility.

At FLASH e.g., such a beam-based feedback system has been implemented and has already proven a jitter reduction within the MHz repetion rate bunch train to below 20 fs (RMS) at a moderate bunch charge of 200 pC [5].

Bunch Arrival Time Monitor

At both facilities, the same basic layout of the arrival time monitor is implemented. Making direct use of timing-stabilised laser pulses, which are provided by an optical synchronisation system [6], the BAM measures the electron bunch timing with an electro-optical detection scheme by means of integrated-optics devices.

For this, a broadband RF pickup delivers a transient beam-induced voltage signal, which is transported through phase-stable cables to the electro-optical modulator (EOM). In this Mach-Zehnder type EOM the voltage magnitude is translated into an amplitude modulation of the laser pulses, depending on the relative timing between optical and electrical signal. The optical, amplitude modulated signal then is detected and processed in high-speed, FPGA-based electronics. The arrival time is derived from an according time calibration showing a sensitivity of the monitor in the range of a few 10 fs per percent of amplitude modulation, which offers the possibility of sub-10 fs resolution [7].

In order to extent this high resolution operation of the BAMs also to low bunch charges, a broadband, cone-shaped pickup has recently been developed in coorperation with the Technical University of Darmstadt [8]. The RF feedthrough part has been produced by Orient Microwave and the mechanical vacuum parts were designed and built by DESY.

At FLASH and at ELBE, these new pickups with a cut-off frequency above 40 GHz have been installed lately.

* marie.kristin.czwalinna@desy.de

ISBN 978-3-95450-133-5

A TOOL FOR REAL TIME ACQUISITIONS AND CORRELATION STUDIES AT FERMI*

Enrico Allaria, William M. Fawley, Elettra-Sincrotrone Trieste S.C.p.A., Basovizza, Italy[#]
Eugenio Ferrari, Elettra-Sincrotrone Trieste S.C.p.A., Basovizza, Italy and Università degli Studi di Trieste, Trieste, Italy

Abstract

In this work we report the recent implementation of a Matlab-based acquisition program that, exploiting the real time capabilities of the TANGO control system, can be used at FERMI for acquiring various machine parameter and electron beam properties together with most FEL signals on a shot-by-shot basis. Analysis of the saved datafiles is performed with a second code that can retrieve correlations and study dependence of FEL properties on machine parameters. An overview of the two codes is reported.

THE REAL TIME CAPABILITIES AT FERMI

The control system of FERMI uses the Tango [1] toolkit to provide an effective integration of technical systems and the software controlling them. A distributed real-time framework is integrated into the control system and provides the capability to measure the seed laser, electron and FEL output photon properties on a pulse-to-pulse basis [2]. With this framework, a unique "bunch number" time-stamp is distributed to all of the low level computers. Most of the measurement system detectors (e.g., electron and photon diagnostics) and actuators (e.g., power supplies) are synchronized with the bunch trigger and can have the "bunch number" associated to their measurements.

Using the Tango bindings, the FERMI control system allows interfacing the accelerator instrumentation to Matlab. This capability has been used to develop various scripting procedures and GUIs to permit user interaction with the machine and has been extensively used for the commissioning of both FEL-1 [3] and FEL-2 [4].

THE ACQUISITION PROGRAM

In this section we describe the MATLAB code implemented at FERMI for real time acquisition of relevant machine and FEL output signals. A brief description of the main features and components of the code will be presented.

Acquisitions are first setup from the RT MATLAB graphical user interface (GUI) (see Fig. 1) that allows the user to define the type of acquisition and select some of the device signals to be acquired. Before the main acquisition begins, a one shot record of the most important machine parameters (e.g., undulator gap settings, dipole and quadrupole magnet currents, lasers intensities, …) is acquired to provide a snapshot of the machine and FEL configuration. This information is stored and saved in the final achival data file. The predefined list of the acquired devices in principle saves all the relevant information that will allow reconstruction of the linac and FEL state during the data analysis phase. When needed, the list of saved signals can be changed on a case-by-case basis via a user-defined configuration file.

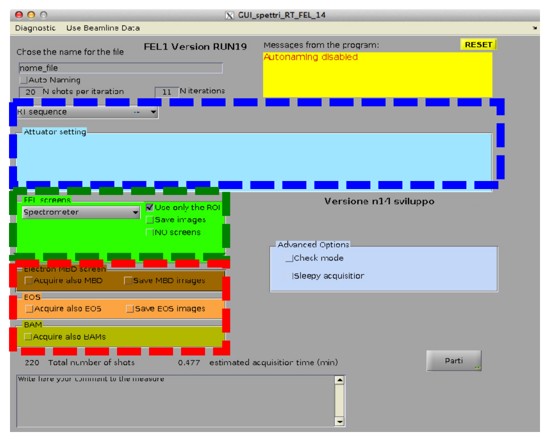

Figure 1: Graphical user interface for RT acquisition of FERMI machine instruments.

Types of Acquisition

The region highlighted in blue in Fig. 1 is used to select the type of acquisition. At present three possible acquisition types are available: "RT sequence" and "actuator scan" and "script scan".

The **RT sequence** is the standard acquisition of the specified list of the machine devices, without any linac or FEL parameter being purposefully changed (i.e., "scanned"). The type of sequence is normally used to collect large quantities of data for statistical studies (e.g. correlations). The user can decide the length of the acquisition by deciding the number of shots acquired.

The **actuator scan** allows the user to actively change a particular machine parameter (e.g., the seed laser power or a dispersion section magnet strength) in order to map the response of the FEL. The parameter is selected from a predefined list as shown in Fig. 2.

*Work partially supported by the Italian Ministry of University and Research under grants FIRB-RBAP045JF2 and FIRB-RBAP06AWK3
#enrico.allaria@elettra.eu

OPTICS MEASUREMENTS AT FLASH2

M. Scholz*, B. Faatz, M. Vogt, J. Zemella, DESY, Hamburg, Germany

Abstract

FLASH2 is a newly build second beam line at FLASH, the soft X-ray FEL at DESY, Hamburg. Unlike the existing beam line FLASH1, it is equipped with variable gap undulators. This beam line is currently being commissioned. Both undulator beam lines of FLASH are driven by a common linear accelerator. Fast kickers and a septum are installed at the end of the linac to distribute the electron bunches of every train between FLASH1 and FLASH2. A specific beam optic in the extraction arc with horizontal beam waists in the bending magnets is mandatory in order to mitigate CSR effects. Here we will show first results of measurements and compare to simulations.

INTRODUCTION

The existing superconducting single-pass high-gain SASE FEL FLASH (Free-electron LASer in Hamburg) at DESY, Hamburg [1] delivers photons in the wavelength range from 4.2 nm to 45 nm. The photons generated in the fixed gap SASE undulators can be delivered to five experimental stations one at a time. A second undulator beam line was attached to the linac during the last three years and is now under commissioning [2]. The FEL will continue to be referred as FLASH and the two beam lines are named FLASH1 and FLASH2. Fast kickers and a DC Lambertson-Septum are installed behind the FLASH linac allow to distribute the beam either to FLASH1 or to the extraction arc leading to FLASH2. The final angle between FLASH1 and FLASH2 is 12°. Strong bending magnets in the extraction arc require specific Twiss functions in order to mitigate emittance growth due to coherent synchrotron radiation (CSR) [2, 3]. The FLASH2 undulator beam line is equipped with variable gab undulators [4] for SASE and reserves space for future seeding options. The extraction to a proposed third beam line hosting a plasma wake field experiment is considered in the beam line layout at the end of the FLASH2 arc.

In this paper, we will describe the first optics and dispersion measurements and the matching of the these functions to the design values in a diagnostic section upstream of the FLASH2 undulators.

DISPERSION MEASUREMENT AND MATCHING

The dispersion describes the dependence of the transverse position on the relative momentum offset.

$$\eta_{x,y} = \frac{\Delta(x,y)}{\Delta p/p_0} \tag{1}$$

With the dispersions $\eta_{x,y}$, the positions x, y and the relative momentum offset p/p_0. The design dispersion functions of FLASH2 can be found in Fig. 2. In order to minimize the distortion of the centroid trajectory through non-linear dispersion, the measurement should be performed using bunches with minimized energy spread. Since the RF systems are capable of splitting their 800 μs long flat tops between FLASH1 and FLASH2, this can be achieved to a large extent for FLASH2 while FLASH1 is in SASE operation [5]. We measured the horizontal beam offset at four different BPMs [6–10] downstream the extraction while changing the beam energy with the accelerating Module ACC45 of the linac. A MATLAB [11] script was used to control the measurement, to change the gradients of the accelerating module and to read the beam positions from the BPMs. The beam energy was changed during the procedure in 10 steps from 551.7 MeV to 554.7 MeV. The dispersion matching was carried out with a linac version of MAD8 [12, 13]. First, a setting of η_x and η'_x upstream the second last quadrupole in the extraction arc was searched fitting the measured dispersions at the four BPMs using the current machine settings. These values where then be used to close the dispersion in an optimization run using the last two quads in the extraction arc. After five iterations the procedure had converged. The data from the last measurement is presented in Fig. 1.

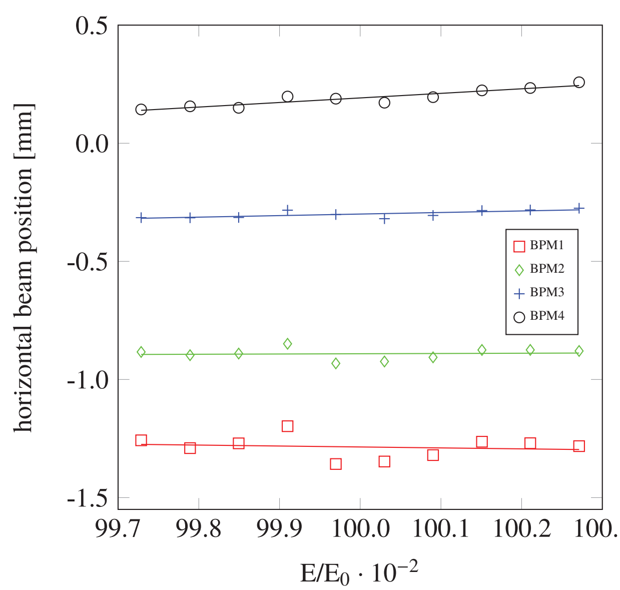

Figure 1: Results of the last dispersion measurement. This plot shows the horizontal beam positions at four different BPMs for different relative beam energies. The energy is normalized to E_0 = 552 MeV.

The final dispersion at the four positions was $\eta_{x,i}$ = [-4, 1, 7, 20] mm and the dispersion prime at the first BPM was calculated as $\eta'_{x,1} = 3.8 \cdot 10^{-4}$.

* matthias.scholz@desy.de

ISBN 978-3-95450-133-5

INFRARED DIAGNOSTICS INSTRUMENTATION DESIGN FOR THE COHERENT ELECTRON COOLING PROOF OF PRINCIPLE EXPERIMENT*

T. Miller#, D. M. Gassner, V. Litvinenko, M. Minty, I. Pinayev, B. Sheehy,
C-AD, BNL, Upton, NY, 11973, U.S.A.

Abstract

The Coherent Electron Cooling Proof-of-Principle experiment [1] based on an FEL is currently under construction in the RHIC tunnel at BNL. Diagnostics for the experimental machine [2] are currently being designed, built and installed. This paper focuses on the design of the infrared diagnostic instrumentation downstream of the three tandem 2.8 m long helical wiggler sections that will act on a 22 MeV 68 uA electron beam co-propagating with the 40GeV/u RHIC gold beam. The 14 um FEL radiation, or wiggler light, will be extracted from RHIC via a viewport in a downstream DX magnet cryostat and analysed by instrumentation on a nearby optics bench. Instruments concentrating on three parameters, namely intensity, spectral content, and transverse profile, will extract information from the wiggler light in an attempt to quantify the overlap of the electron and ion beams and act as an indicator of coherent cooling.

INTRODUCTION

The success of Coherent Electron Cooling (CeC) experiment will depend largely on the effectiveness of the instrumentation available. This paper focuses on those instruments associated with measuring and characterizing the infrared light emitted by the wiggler that functions as an FEL and amplifier [3] in this arrangement of modulator, amplifier, and kicker sections. See reference [4] for an update of CeC beam cooling theory using this three-step process. Presented in this paper are details of the instruments that will be employed to measure the wiggler light. Also presented are low cost alternatives to readily available off the shelf instruments and some other low cost alternative solutions.

The construction of the CeC experiment is underway and has been segmented into three phases, each requiring an increasing number of electron beam instruments. As elaborated on elsewhere at this conference [4], the instrumentation for the wiggler's infrared radiation, or wiggler light, will only be installed as part of phases two and three (see Fig. 1). The wiggler sections will be appended to the injector beamline after the injector is commissioned in Phase 1. Phase 2 allows for the wiggler sections to be tested with the electron beam as a stand alone experiment in the RHIC tunnel, independent of RHIC operations, except for use of the cryogenic system. During this phase, a local optical bench will be installed downstream of the three wiggler sections. The instruments located there will receive the wiggler light through a ZnSe viewport in a downstream auxiliary port of the dipole magnet that brings the electron beam to the beam dump. The optics bench will be located in the RHIC tunnel to avoid the upfront cost of an optical beam transport back to the laser building, approximately 60m away. When the experiment moves into Phase 3, the wigglers will be installed into the RHIC beam path to allow co-propagation of the electron beam and the Yellow ion beam. In this phase, the optical instrumentation table may be relocated to a laser trailer installed outside the RHIC tunnel to avoid further exposure to high radiation levels in the tunnel. A modification of the DX magnet cryostat, responsible for splitting and recombining the RHIC blue & yellow counter circulating beams, will be made so that the wiggler light can propagate straight out between the two emerging (blue & yellow) beam pipes via a viewport. A sealed optical beam transport could be installed to bring the light from the viewport to the laser trailer.

WIGGLER

The three helical permanent magnet wiggler sections are being constructed by the Budker Institute of Nuclear Physics. Table 1 summarizes the parameters of the electron beam and the wigglers.

Table 1: Wiggler & e-beam Parameters

e-Beam	**Value**
Energy	21.8 MeV
Charge per bunch	0.5 – 1 nC
Current (1nC), Avg / Pk	78 µA / 60 – 100 A
Beam Power	1.7 kW
Bunch Length	10 ps
Repetition Rate	78.3 kHz
Wiggler	**Value**
Length (3 sections)	3 x (2.5 + 0.30 m)
Period (λ_u) / poles	4 cm / 60 + 2.5 ea. section
Strength (K)	0.50
Wavelength (λ)	14 µm
Optical Power	250 nW – 250 mW

*Work supported by U.S. DOE under contract No DE-AC02-98CH10886 with the U.S. DOE
#tmiller@bnl.gov

ISBN 978-3-95450-133-5

DESIGN OF TDS-BASED MULTI-SCREEN ELECTRON BEAM DIAGNOSTICS FOR THE EUROPEAN XFEL

J. Wychowaniak*
DMCS, Technical University of Łódź, Łódź, Poland
Ch. Gerth, M. Yan
Deutsches Elektronen-Synchrotron DESY, Hamburg, Germany

Abstract

Dedicated longitudinal electron beam diagnostics is essential for successful operation of modern free-electron lasers. Demand for diagnostic data includes the longitudinal bunch profile, bunch length and slice emittance of the electron bunches. Experimental setups based on transverse deflecting structures (TDS) are excellent candidates for this purpose. At the Free-Electron Laser in Hamburg (FLASH), such a longitudinal bunch profile monitor utilizing a TDS, a fast kicker magnet and an off-axis imaging screen, has been put into operation. It enables the measurement of a single bunch out of a bunch train without affecting the remaining bunches. At the European X-ray Free-Electron Laser (XFEL) multi-screen stations in combination with TDS are planned to be installed. In order to allow for flexible measurements of longitudinal bunch profile and slice emittance, a configurable timing and trigger distribution to the fast kicker magnets and screen stations is required. In this paper, we discuss various operation patterns and the corresponding realization based on MTCA.4 technology.

INTRODUCTION

The performance of a hard X-ray free-electron laser (FEL), such as the European XFEL, depends critically on the transverse emittance of the electron beam [1]. Hence, it is important to generate electron beams with lowest possible emittance [2, 3] and efficiently preserve the emittance through acceleration and longitudinal bunch compression. Measurement and control of the transverse emittance is crucial for the optimisation and operation of the FEL as the beam emittance may be degraded due to non-linear effects, e.g. emission of coherent synchrotron radiation (CSR) or micro-bunching instabilities [4].

As the FEL amplification process takes place locally within longitudinal bunch slices, measurements of time-resolved properties, i.e. slice emittance, rather than time-averaged properties, i.e. projected emittance, are of interest. Excellent candidates for the measurement of the slice emittance with single-bunch resolution are transverse deflecting structures (TDS) [4, 5]. The electron bunch is streaked in transverse direction by the TDS and imaged with an imaging screen. The slice emittance can then be measured in the plane perpendicular to the streak direction by changing the phase advance between the TDS and the imaging screen. This can be achieved by either changing quadrupole currents between the TDS and imaging screen (quad-scan method) or by employing several screens (multi-screen method) [6]. A disadvantage of this direct time-domain method is that the emittance of the diagnosed bunch is drastically degraded due to the scatter process in the imaging screen and the bunch cannot be used for FEL operation.

CONCEPTUAL LAYOUT OF THE SLICE EMITTANCE MONITOR SETUP

The super-conducting accelerator of the European XFEL will operated with RF macro pulses of up to 650 μs at a repetition rate of 10 Hz. Each RF macro pulse can be filled with a train of up to almost 3000 bunches at a maximum repetition rate of 4.5 MHz. This offers the possibility of using several bunches of each bunch train for on-line measurements. A generic layout of a slice emittance monitor, employing a TDS followed by four fast kicker magnets and four screen stations equipped with off-axis screens, is depicted in Fig. 1. Four electron bunches out of the bunch train are streaked by the TDS and then deflected by the fast kicker magnets onto the off-axis screens without disturbing FEL operation of the remaining bunches in the bunch train. A longitudinal bunch profile monitor, comprising one kicker magnet and one off-axis screen, has been commissioned successfully at the Free-Electron Laser in Hamburg (FLASH) [7].

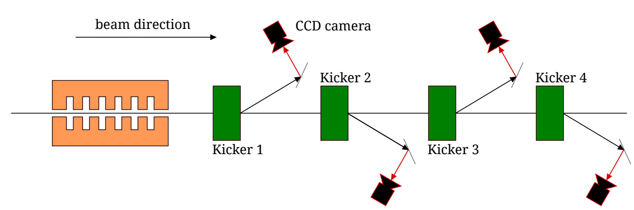

Figure 1: Generic layout of a slice emittance monitor.

At the European XFEL, installation of slice emittance monitors is foreseen at three different locations (see Fig. 2): in the injector and after the second and third bunch compressor chicane. Each TDS is followed by a matching section and a FODO lattice in which four screen stations are incorporated [8]. The screen stations will be equipped with off-axis scintillation screens made of 200 μm thick LYSO:Ce [9]. The scintillation screens will be installed at an angle of 0° with respect to the beam axis and imaged under 45° by a CCD camera in Scheimpflug arrangement. Micro-bunching instabilities can lead to the emission of coherent optical transition radiation (COTR) at the boundary of vacuum and the scintillator [10]. The imaging angle has been chosen to sup-

* jan.wychowaniak@desy.de

ISBN 978-3-95450-133-5

MEASUREMENTS OF THE TIMING STABILITY AT THE FLASH1 SEEDING EXPERIMENT*

C. Lechner†, A. Azima, M. Drescher, L. L. Lazzarino, Th. Maltezopoulos, V. Miltchev, T. Plath, J. Rönsch-Schulenburg, J. Rossbach, M. Wieland, University of Hamburg, Hamburg, Germany
K. E. Hacker, S. Khan, R. Molo, DELTA, TU Dortmund University, Dortmund, Germany
S. Ackermann, J. Bödewadt, H. Dachraoui, N. Ekanayake, B. Faatz, M. Felber, K. Honkavaara, T. Laarmann, J. Müller, H. Schlarb, S. Schreiber, S. Schulz, DESY, Hamburg, Germany
P. Salen, P. van der Meulen, FYSIKUM, AlbaNova, Stockholm, Sweden
G. Angelova Hamberg, Uppsala University, Uppsala, Sweden

Abstract

For seeding of a free-electron laser, the spatial and temporal overlap of the seed laser pulse and the electron bunch in the modulator is critical. To establish the temporal overlap, the time difference between pulses from the seed laser and spontaneous undulator radiation is reduced to a few picoseconds with a combination of a photomultiplier tube and a streak camera. Finally, for the precise overlap the impact of the seed laser pulses on the electron bunches is observed. In this contribution, we describe the current experimental setup, discuss the techniques applied to establish the temporal overlap and analyze its stability.

INTRODUCTION

For the operation of an externally seeded free-electron laser (FEL), relative beam-beam jitter between the electron bunch and the laser pulse initiating the FEL gain process is only acceptable to a certain extent. Inhomogeneities in the electron beam slice parameters will directly translate into fluctuating performance of the seeded FEL. The duration of the region of the bunch with suitable electron beam parameters, such as slice energy spread, beam current, and emittance, is limited, which defines the timing jitter budget. Large jitter will naturally result in poor overlap quality. For instance, a major limitation of the studies of direct seeding with an high-harmonic generation (HHG) source at FLASH was the quality of the temporal overlap [1, 2].

EXPERIMENTAL LAYOUT

Electron Beamline

The seeding experiment is installed at the FLASH1 beamline of FLASH [3], the free-electron laser user facility in Hamburg, delivering high-brilliance SASE FEL radiation in the extreme ultra-violet (XUV) and soft x-ray range wavelength ranges. The superconducting linear accelerator of the FLASH facility generates trains of high-brightness electron bunches at a maximum energy of 1.25 GeV. These bunch trains, accelerated at 10 Hz repetition rate, consist of up to 800 electron bunches at an intra-train repetition rate of 1 MHz.

The seeding experiment is installed between the collimation section of FLASH1 and the FLASH1 main undulator system. The electron beamline, shown schematically in Fig. 1, can be divided into three parts: (i) the modulator section, (ii) the variable-gap undulator system, and (iii) the photon extraction and diagnostics section. Of these, however, only the modulator section was used for the measurements presented in this paper. It comprises two electromagnetic undulators (5 periods of 20 cm, maximum K value 10.8) that originally had been installed for a longitudinal electron bunch diagnostics experiment [4]. At the exit of each electromagnetic undulator, a magnetic chicane is installed.

Downstream of the seeding experiment, a combination of a transverse-deflecting structure (TDS) and a dipole energy spectrometer is installed. First, an arrival-time-dependent transverse kick is applied in the TDS, an RF structure operated at 2856 MHz. After this conversion of longitudinal to spatial position, the contents of the longitudinal phase space of the electron bunch can be measured on the observation screen in the dispersive section downstream of the energy spectrometer.

Laser System

The laser system used for seeding experiments at FLASH1 was originally installed for direct-HHG seeding experiments at FLASH and consists of a 108.3 MHz Ti:sapphire oscillator used as seed in a classical chirped pulse amplification (CPA) scheme with 35 mJ maximum pulse energy at 35 fs FWHM minimal pulse duration. As described in the following section, the oscillator is electronically synchronized to a reference signal derived from an optical reference. The amplifier is pumped by a frequency-doubled Nd:YAG laser operating at 10 Hz allowing to seed one electron bunch per train [5].

For high-gain harmonic generation (HGHG) seeding at short wavelengths, a conversion of the $\lambda = 800$ nm laser pulses to UV wavelengths is required. For this, an in-vacuum arrangement of two non-linear optical crystals in the accelerator tunnel is employed: While the first one converts the laser light into its second harmonic, the second one emits its third harmonic at 267 nm when overlapping the 800 nm and 400 nm pulses [6].

* Work supported by Federal Ministry of Education and Research of Germany under contract No. 05K10PE1, 05K10PE3, 05K13GU4, and 05K13PE3 and the German Research Foundation programme graduate school 1355.

† christoph.lechner@desy.de

ISBN 978-3-95450-133-5

A LOW-COST, HIGH-RELIABILITY FEMTOSECOND LASER TIMING SYSTEM FOR LCLS*

Karl Gumerlock, Josef Frisch, Bruce Hill, Justin May, David Nelson, Stephen Smith,
SLAC National Accelerator Laboratory, Menlo Park, CA, USA

Abstract

LCLS has developed a low-cost, high-reliability radio-frequency-based ("RF") locking system which provides phase locking with sub-25-femtosecond jitter for the injector and experiment laser systems. This system does not add significantly to the X-ray timing jitter from the accelerator RF distribution. The system uses heterodyne RF locking at 3808 MHz with an I/Q vector phase shifter and variable event receiver triggers to control the timing of the emission of the amplified laser pulse. Controls software provides full automation with a single process variable to control the laser timing over a 600 microsecond range with up to 4 femtosecond resolution, as well as online diagnostics and automatic error correction and recovery. The performance of this new locking system is sufficient for experiments with higher-precision timing needs that use an X-ray/optical cross-correlator to record relative photon arrival times.

LASER TIMING REQUIREMENTS

Lasers in the LCLS experiment hutches require sub-picosecond timing relative to the X-ray beam, originating as an electron beam from the SLAC linear particle accelerator ("linac"). The LCLS X-ray beam operates at a maximum repetition rate of 120 Hz and has a pulse-to-pulse timing jitter of approximately 60 fs RMS [1]. The relative timing of the laser and X-rays is measured in the experimental chamber by an X-ray/optical cross-correlator with approximately 10 fs resolution [2]. This cross-correlator is used to order the experimental data based on relative X-ray and laser arrival time. Any laser locking system must not substantially add to the total uncorrected experiment timing jitter. This corresponds to a target timing jitter of less than 75 fs RMS. The need to improve locking system jitter at LCLS was originally identified by Glownia *et al.* [3].

The cross-correlators used at LCLS include an optical delay stage to allow for high resolution timing measurements over a wide range of laser/X-ray time delays. The measurement range of the cross-correlator itself is approximately 1 picosecond. The timing jitter, drift, and the accuracy of laser time delay changes are required to keep the laser timed within that range, so that the cross-correlator is able to return good shot-to-shot timing data.

The range of timing scans required for experiments vary from sub-picosecond to 600 microseconds. The laser system timing needs to be adjustable over that range without additional user intervention or expert knowledge.

TIMING SYSTEM ARCHITECTURE

X-ray pulse timing is determined by the electron beam timing, which is in turn controlled by the RF fields in the accelerator cavities. The accelerator RF sources are locked to a 476 MHz RF coaxial cable phase distribution system ("RF reference"). This reference is re-stabilized to the electron beam with each shot using electron arrival time measured at RF phase cavities (Fig. 1) in the LCLS undulator hall [1]. The RF reference is then transmitted through a stabilized coaxial cable to the experiment hutches, where it is used as a phase reference for the laser locking systems described in this text.

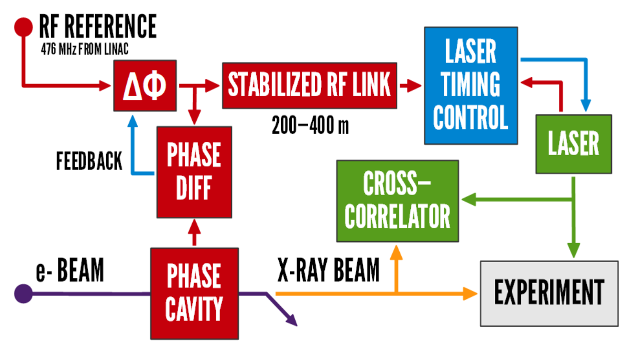

Figure 1: Laser timing system overview.

LASER TIME CONTROL

The experiment laser systems use a mode-locked Ti:sapphire laser oscillator which feeds a regenerative amplifier ("regen"). In some systems, a multipass amplifier is also used, however, the principle of operation remains the same.

The mode-locked laser oscillator (Fig. 2) operates at 68 MHz, 1/7th of the 476 MHz RF reference frequency. A commercial regenerative amplifier just after the oscillator is designed to accept an external trigger input: upon triggering, the regen selects and amplifies the next pulse from the mode-locked laser. A similar system also triggers any multipass amplifiers used downstream of the regen.

A frequency counter continuously measures the mode-locked laser cavity frequency. Controls software moves a stepper motor to coarsely control the cavity length to within 1 Hz of 68 MHz.

*Work supported by DOE Contract DE-AC02-76-SF00515
* Linac Coherent Light Source ("LCLS")

ISBN 978-3-95450-133-5

MEASUREMENTS OF COMPRESSED BUNCH TEMPORAL PROFILE USING ELECTRO-OPTIC MONITOR AT SITF *

Y. Ivanisenko†, V. Schlott, PSI, Villigen, Switzerland
P. Peier, DESY, Hamburg, Germany

Abstract

The SwissFEL Injector Test Facility (SITF) is an electron linear accelerator with a single bunch compression stage at Paul Scherrer Institute (PSI) in Switzerland. Electro-optic monitors (EOM) are available for bunch temporal profile measurements before and after the bunch compressor. The profile reconstruction is based upon spectral decoding technique. This diagnostic method is non-invasive, compact and cost-effective. It does not have high resolution and wide dynamic range of an RF transverse deflecting structure (TDS), but it is free of transverse beam size influence, what makes it a perfect tool for fast compression tuning.

We present results of EOM and TDS measurements with down to 150 fs short bunches after the compression stage at SITF.

INTRODUCTION

Hard X-ray FEL facilities are based upon multi-stage compression of electron bunches. Bunch temporal profile monitoring is normally done after each compression stage. The most common approach is to use an RF transverse deflecting structure (TDS) [1].

Electro-optic monitor (EOM) represents another method for bunch temporal profile measurements [2]. The transverse electric field component of a moving charged particle is enhanced by the Lorentz factor. For an ultra-relativistic particle the field lines are concentrated in a thin disk, approaching zero thickness with Lorentz factor growing to infinity. The disk circumference lies in a plane perpendicular to the propagation direction. An ultra-relativistic bunch of particles will induce an electric field which is localized in the longitudinal extent of the bunch itself. The bunch length can be measured by sampling the distribution of its electric field. In electro-optic monitor a traveling electric field pulse can be converted into a laser pulse modulation of the same duration in a non-linear crystal. A modulation is produced on the top of a chirped laser pulse (with time-to-wavelength correlation) by using the electro-optic spectral decoding (EOSD) method. It is sufficient to know the spectrum of the pulse and its chirp to reconstruct the temporal profile of a bunch.

Although achievable time resolution is limited, an EOM has some advantages when compared to a TDS, since it is an alternative non-invasive technique to measure the longitudinal bunch profile. It requires much less beamline space and it is only sensitive to a longitudinal distribution of charge. Both are time domain measurement approaches with absolute calibration. A TDS allows to measure bunch longitudinal profile in a larger dynamic range by changing the deflecting gradient. TDS has the best resolution achieved to date [3]. But it needs a separate RF system, and destroys the measured bunch.

EOM SETUP AT SITF

The SwissFEL Injector Test Facility (SITF) is a 250 MeV linear accelerator with a single bunch compression stage. There are two EOMs installed at SITF: one in front of and one behind the bunch compressor. A TDS is installed 1 meter downstream of the second EOM.

The EOSD measurement scheme is shown in Fig.1. An in-house developed fiber laser oscillator generates about 1 nJ pulses with the wavelength of 1030 nm and the spectral bandwidth of 25 nm at 40 MHz. A pulse picker lowers repetition rate to 1 MHz in front of an amplifier, that boosts up the pulse energy to 5-10 nJ. A grating compressor pre-compensates dispersion caused broadening of the pulse in the long fiber to the tunnel.

A 2 mm thick GaP crystal is installed in the vacuum beam pipe on a specially designed actuator platform with all other optical elements responsible for laser transport and polarization control. In case the crystal is put in the whole assembly moves not disturbing the internal alignment. The laser enters the vacuum through an optical view port and is directed to the crystal by a mirror. Then it propagates through the crystal, and it is reflected back at the end facet. After this it moves against the direction of the electron bunch and is guided out of the beam pipe to a spectrometer.

The linearly polarized laser beam is almost blocked by nearly crossed polarizers configuration without external electric fields. The laser light polarization is changed due to the electro-optic effect in the crystal in presence of an electron beam. In perfect case laser pulse has to propagate in the crystal synchronously to the electric field envelope of an

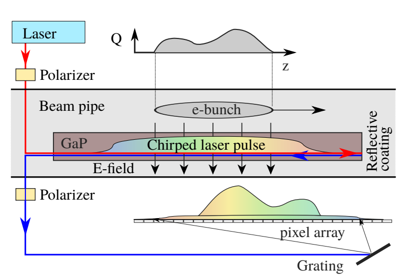

Figure 1: EOM setup scheme.

* The research leading to these results has received funding from the European Community's Seventh Framework Programme (FP7/2007-2013) under grant agreement n.°290605 (PSI-FELLOW/COFUND)
† yevgeniy.ivanisenko@psi.ch

ISBN 978-3-95450-133-5

COHERENT RADIATION DIAGNOSTICS FOR LONGITUDINAL BUNCH CHARACTERIZATION AT EUROPEAN XFEL

P. Peier, H. Dinter, and Ch. Gerth, DESY Hamburg, Germany

Abstract

European XFEL comprises a 17.5 GeV linear accelerator for the generation of hard X-rays. Electron bunches from 20 pC to 1 nC will be produced with a length of a few ps in the RF gun and compressed by three orders of magnitude in three bunch compressor (BC) stages. European XFEL is designed to operate at 10 Hz delivering bunch trains with up to 2700 bunches separated by 222 ns. The high intra-bunch train repetition rate offers the unique possibility of stabilizing the machine with an intra-bunch train feedback, which puts in turn very high demand on fast longitudinal diagnostics. Two different systems will be installed in several positions of the machine. Five bunch compression monitors (BCM) will monitor the compression factor of each BC stage and be used for intra-bunch train feedbacks. A THz spectrometer will be used to measure parasitically the longitudinal bunch profile after the energy collimator at 17.5 GeV beam energy. We will present concepts for fast longitudinal diagnostics for European XFEL based on coherent radiation, newest developments for high repetition rate measurements and simulations for the feedback capability of the system.

INTRODUCTION

European XFEL will be a linac-driven hard X-ray free electron laser operating at wavelength down to 0.1 nm [1]. The machine will produce up to 2700 short (2-100 fs) X-ray pulses per macro pulse (10 Hz) with a repetition rate of up to 4.5 MHz. The X-ray pulse generation requires kA peak current of the electron bunches which will be achieved by three stages of bunch compression (BC0, BC1 and BC2 in Fig. 1). The corresponding bunch lengths are indicated in Table 1 (source: start-to-end simulations [2]). A high power laser

Table 1: RMS electron bunch lengths in European XFEL for three different charges. Highlighted row: used in simulations.

Charge	Gun	BC0	BC1	BC2
20 pC	4.5 ps	1.5 ps	180 fs	5 fs
100 pC	4.8 ps	1.6 ps	200 fs	12 fs
1000 pC	6.8 ps	2.2 ps	300 fs	84 fs

will generate 4 ps - 7 ps rms long electron bunches in the normal conducting photocathode gun. In the subsequent super conducting acceleration module (1.3 GHz) and the longitudinal phase space linearizer (3.9 GHz) the beam gets an energy of 130 MeV. In BC0 the bunches are compressed by a factor of three before they are accelerated to 700 MeV in the first part of the linear accelerator (L1). In the second compression stage (BC1) the length of the bunches is reduced by a factor of eight and they are accelerated to 2.5 GeV in L2. In BC2 the bunches are compressed to their final length (fs level) and in L3 they are accelerated to the maximum energy of 17.5 GeV. The electrons are then transported through an energy collimator to the distribution area and to SASE1 or SASE2 undulator beamlines, respectively.

Stable X-ray SASE output requires among other parameters precise control of the longitudinal shape of the electron bunches. The longitudinal shape is tailored only in the BCs. Bunch compression is achieved with an accelerating module running off-crest to induce an energy chirp in the electron beam and a magnetic chicane. In operation the compression level is mainly defined by the phase setting of the corresponding acceleration module. Five bunch compression monitors (BCM), three independent and two redundant, will measure at full repetition rate a quantity that is directly related to the current profile. The independent BCMs are the monitors of a feedback system controlling the RF phase settings. In addition one broadband infrared spectrometer is used to resolve accurately the final longitudinal bunch profile with single bunch resolution. It will be installed after the energy collimator where the electrons are fully compressed and have their final energy of 17.5 GeV. The spectrometer works best for short bunches producing short wavelength diffraction radiation.

In this paper, we will describe the requirements on the BCMs and feedback system in European XFEL as well as design considerations for the monitors. The performance of the whole system is estimated using simulation tools and operation experiences gained at the VUV Free-electron-LASer-Hamburg (FLASH).

MONITORING THE LONGITUDINAL BUNCH SHAPE

Requirements and Concepts

Table 2: Longitudinal diagnostic requirements overview (numbers in brackets: injector).

Charge	20 - 1000 pC
Energy	(0.005)0.13 - 17.5 GeV
Bunchlength	5 - 2000(7000) fs rms
RF phase stability	0.01 deg
Bunch spacing	min. 222 ns
Repetition rate	10 Hz

ISBN 978-3-95450-133-5

LONGITUDINAL DIAGNOSTICS OF RF ELECTRON GUN USING A 2-CELL RF DEFLECTOR*

M. Nishiyama#, T. Takahashi, T. Toida, K. Sakaue, M. Washio, Waseda University, Tokyo, Japan
T. Takatomi, J. Urakawa, KEK, Ibaraki, Japan

Abstract

We have been studying a compact electron accelerator based on an S-band Cs-Te photocathode rf electron gun at Waseda University. We are using this high quality electron bunch for many application researches. It is necessary to measure the bunch length and temporal distribution for evaluating application researches and for improving an rf gun itself. Thus, we adopted the rf deflector system. It kicks the electron bunch with resonated rf electromagnetic field. Using this technique, the longitudinal distribution is mapped into the transverse space. The rf deflector has a 2-cell standing wave π-mode structure, operating in TM_{210} dipole mode at 2856 MHz. It provides a maximum vertical kick of 1.00MV with 750 kW input rf-power which is equivalent to the temporal resolution of around 58 fs bunch length. In this conference, we report the details of our rf deflector, the latest progress of longitudinal phase space diagnostics and future prospective.

INTRODUCTION

A photocathode rf electron gun is now widely utilized for an accelerator system in many facilities due to its controllability of initial beam profile and ability to generate low emittance beam. In Waseda University, we built a compact electron accelerator system based on an S-band Cs-Te photocathode rf electron gun. The rf gun is an improved BNL type IV 1.6 cell rf gun. It is applied to many researches, such as a pulse radiolysis experiment for tracing rapid initial chemical reactions by ionizing radiation [1], a laser Compton scattering for generating soft X-ray [2] and synchrotron radiation and transition radiation for generating coherent THz wave [3][4]. In these experiments, it is necessary to measure the bunch length and temporal distribution for evaluating temporal resolution, luminosity and coherence, respectively. The measurement of the bunch length is also helpful for studying the effect of rf acceleration. Thus, we adopt the rf deflector system.

THE METHOD OF BUNCH LENGTH MEASUREMENT USING RF DEFLECTOR

Figure 1 shows a principle of measuring the bunch length and temporal profile using an rf deflector. An rf deflector is one of rf cavities. It has been used as a strong tool for bunch length and temporal profile measurements in FELs and other facilities recently. Electromagnetic field of its own resonates in an rf deflector when rf power is supplied. In Waseda University, the rf deflector generates the electromagnetic field of the TM_{210} mode. Lorentz force gives the transverse momentum on the electron beam by the high frequency time variation of the magnetic field and the beam is “kicked” horizontally. The electric field has no effect on the beam in the rf deflector, because it doesn’t exists on the axis of the beam. Thus, the rf deflector can convert the longitudinal information of the electron beam into the transverse one. Using this technique, the temporal profile of an electron beam can be obtained directly as an image on screen.

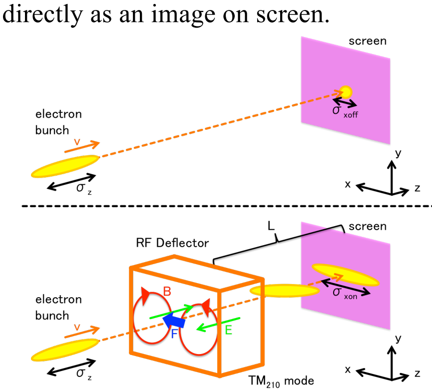

Figure 1: Bunch length measurement using an rf deflector.

Considering the transfer matrix between the rf deflector and the screen, the transverse position of each relativistic electron on the screen, *Δx*, as a function of longitudinal position from the bunch centroid along the bunch, *Δz*, is given approximately by

$$\Delta x = \frac{eV_T}{p_z c} L \sin\left(k\Delta z + \varphi\right) \cong \frac{eV_T}{p_z c} L\left[k\Delta z \cos\varphi + \sin\varphi\right] \quad (1)$$

where c is the light velocity, p_z is the longitudinal momentum, V_T is the deflecting voltage, L is the drift length between the rf deflector and the screen, k is the rf wave number, and φ is the rf phase [5]. The approximation is made that $|\Delta z| \ll 1/k$ because the longitudinal position is much shorter than the rf wavelength of 0.105 m. Operating at the zero-crossing phase like Figure 2, we can substitute $\varphi=0$ to Eq. (1),

$$\Delta x = \frac{eV_T}{p_z c} Lk\Delta z \quad (2)$$

This phase gives the best kicking effect with the horizontal beam size corresponding to the bunch length ($\sigma_x \propto c\sigma_t$).

* Work supported by JSPS Grant-in-Aid for Scientific Research (A) 10001690 and the Quantum Beam Technology Program of MEXT.
#masa.hero@ruri.waseda.jp

ISBN 978-3-95450-133-5

COMMISSIONING AND RESULTS FROM THE BUNCH ARRIVAL-TIME MONITOR DOWNSTREAM THE BUNCH COMPRESSOR AT THE SwissFEL INJECTOR TEST FACILITY

V. Arsov#, M. Aiba, M. Dehler, F. Frei, S. Hunziker, M. Kaiser, A. Romann,V. Schlott,
PSI, Villigen, Switzerland

Abstract

A high bandwidth Bunch Arrival-Time Monitor (BAM) has been commissioned downstream the bunch compressor at the SwissFEL Injector Test Facility (SITF). A new acquisition front end allowing utilization of the ADC full dynamic range was implemented. The resolution was measured as a function of the bunch charge for two different electro-optical intensity modulators (EOM). BAM measurements of machine relevant parameters were made. A comparison with the results from other diagnostics shows good agreement.

INTRODUCTION

SwissFEL is planned to start user operation in 2017 at charges between 10 pC - 200 pC [1]. To secure stable machine operation by applying feedbacks, as well as for decoupling of error sources manifested as bunch arrival time jitter, the latter should be measured non-destructively with resolution of 10 fs. In addition, BAM should have a low drift in the order of 10 fs/day. Such requirements are fulfilled for a scheme based on Mach-Zehnder type electro-optical modulator (EOM) [2], interfaced to a single-mode optical fiber link, through which reference laser pulses from a mode locked laser (few 100 fs pulse duration) are distributed [3]. These fiber links are stabilized in length via optical cross-correlation. A pick-up signal generated from the electron bunch is sampled at zero crossing with one of the reference laser pulses. At zero crossing this pulse is not modulated, but any temporal-offset of the beam produces a modulation voltage, which is converted in the EOM to amplitude modulation. With proper calibration, this amplitude modulation is interpreted in terms of arrival-time. An advantage of the method is that when acquiring the BAM signal with a fast ADC by sampling the amplitude and baseline points of the laser pulse-train, not only the pulse which interacts with the electron bunch is measured, but also multiple pulses preceding it, thus obtaining online information about the instantaneous BAM resolution. The technical difficulty is, that for the low charges foreseen for Swiss FEL, the pick-up response is small, thus limiting the resolution, as demonstrated with the first BAM prototype installed in SITF upstream the bunch compressor [4]. This paper describes the commissioning of a second BAM downstream the bunch compressor, for which several improvements were implemented, aiming for higher resolution at low charge.

#vladimir.arsov@psi.ch

IMPROVEMENTS IN THE BAM SETUP

The general system topology and schematic layout was already described in [4]. The new BAM front-end is located close after the last dipole of the SITF bunch compressor. Among the improvements aiming to increase the resolution is the use of higher bandwidth components. The EOMs are 40 GB/s (33 GHz), PowerBit SD40 (Oclaro) and MXAN-LN40 (Photline) installed in the first and the second BAM channels. All the RF cables are PhaseMaster160 from Teledyne with 40 GHz band width, low-drift at 24°C and with low sensitivity to radiation [5]. The pick-up Type KX00-0258 with cone-shaped buttons and 40 GHz bandwidth was developed by DESY and TU-Darmstadt for the European XFEL and produced by Orient Microwave [6]. The design is for the European XFEL beam pipe diameter of 40.5 mm. The vacuum chamber is adapted on both sides to the 38 mm beam pipe of the SITF with 20 cm long tapers. For SwissFEL the same cone-shaped button pick-up feedthroughs were adapted for 16 mm beam pipe diameter. A prototype KX00-0293 has been ordered at Orient Microwave and is expected to arrive for test at PSI at the beginning of September. It is expected that the smaller beam pipe diameter of SwissFEL will provide for stronger RF signals, thus improving the resolution at low charge.

The only low bandwidth components inherited from the first BAM are the limiters N9356C (25dBm threshold, 26.6 GHz bandwidth, Agilent), which allow higher voltages and full utilization of the EOM half-wave voltage range. A higher bandwidth limiter Type N9355F (50 GHz, 10 dBm) was also tested, but for higher input voltages than the nominal 10 dBm it starts to distort the signal, thus spoiling the resolution.

The next modification aiming the achievement of higher resolution at low charge is the combination of a photoreceiver and an offset-DAC. The photoreceiver accepts higher input optical powers (~2mW) and has 3V pk-pk output at 0.5mW optical input. The amplification stage is externally accessible, allowing optimal adjustment of the RF signal thresholds, thus preventing saturation. The offset-DAC shifts the RF signal by a DC voltage to optimally match it to the acquisition ADC input thus utilize the full resolution (presently 12 bit). The use of this combination showed considerable improvement in the BAM resolution, which otherwise was unsatisfactory despite the high bandwidth components [7]. A 16 bit ADC which is expected to further improve the resolution was recently installed and beam tests are pending.

ISBN 978-3-95450-133-5

ELECTRON BEAM DIAGNOSTICS FOR COXINEL

M. Labat, N. Hubert, M. El Ajjouri, L. Cassinari,
C. Bourrassin-Bouchet, A. Loulergue, M.E. Couprie,
Synchrotron SOLEIL, France

Abstract

On the path towards more compact free electron lasers (FELs), the project COXINEL was recently funded: a transfer line will be installed to adapt a plasma accelerated beam (from LOA) into an in-vacuum undulator built by SOLEIL. This experiment should enable to demonstrate the first FEL based on a plasma accelerator. Because plasma beams are intrinsically very different from RF acceletor beams (much shorter, divergent and smaller with a higher energy spread and energy jitter), their transport and matching in the undulator is critical if willing to obtain a significant amplification. This is why special care has to be taken in the design of the beam diagnostics to be able to measure the transverse beam sizes, energy spread and jitter, emittance and bunch length. For these purposes, several diagnostics will be implemented from the plasma accelerator exit down to the undulator exit. In each station, several screen types will be available and associated to high resolution imaging screens. In this paper, we present the experimental layout and associated simulation of the diagnostics performances.

COXINEL LAYOUT

COXINEL project [1] was recently funded by the European Research Council. This project aims at demonstrating the operation of a plasma accelerator based Free Electron Laser. The key concept relies on an innovative electron beam longitudinal and transverse manipulation in between the plasma accelerator and the undulator. Indeed, typical plasma accelerator beams exhibit percent level energy spread which intrinsicly disables any FEL amplification. The very small transverse dimensions and very large divergence of those beams also tend to dramatically spoil the initial emittance along the transport to the undulator. We proposed to use a "demixing" chicane to sort the electrons in energy and reduce the slice energy spread from 1 % to 0.1 %. Following the chicane, a set of quadrupoles is used to maintain the transverse density seen by the FEL radiation constant all along the undulator.

The COXINEL layout is illustrated in Figure 1. COXINEL will use the plasma accelerator of the Laboratoire d'Optique Appliquée (Palaiseau, France). The downstream equipements are under preparation at Synchrotron SOLEIL. They consist, following the electron beam path, in a triplet of quadrupoles, a demixing four dipoles chicane, a second set of quadrupoles, an undulator and a final beam dump. The expected electron beam and FEL parameters are summarized in Table 1. The targetted wavelength is 200 nm in first phase and 40 nm in second phase. The FEL will be operated in seeded mode.

Table 1: COXINEL Expected Parameters. (*) At the plasma accelerator exit.

Parameter	Value
Electron beam	
Energy	400 MeV
Energy spread (*)	1 %
Charge	10 pC
Peak current (*)	500 A
Electron beam duration in ID	15 fs-FWHM
Undulator	
Period	20 mm
Length	2 m
Peak magnetic field	0.9 T

Since the experiment relies on a refine manipulation of the electron beam phase space, beam diagnostics are vital on this project. Their location is indicated in Figure 1.

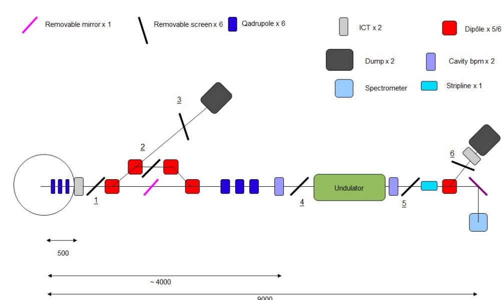

Figure 1: COXINEL layout.

DIAGNOSTICS STATIONS

Six diagnostics stations (DS) will be implemented on COXINEL. They are all designed on the same principle to ease their operation and reduce their cost. The fisrt one will be installed just after the first triplet, the second one in the demixing chicane, the third one on the first beam dump, the fourth and fifth at entrance and exit of the undulator and the last one will be on the final beam dump. They consist in:

- a motorized tree than can position on the beam axis three different targets at 45^o (see Figure 2),
- three targets: OTR screen, YAG:Ce or LYSO:Ce screen and calibration grid,
- an extraction viewport,
- an optical system to image the targets' surface,

ISBN 978-3-95450-133-5

COMPARISON OF QUADRUPOLE SCAN AND MULTI-SCREEN METHOD FOR THE MEASUREMENT OF PROJECTED AND SLICE EMITTANCE AT THE SwissFEL INJECTOR TEST FACILITY

M. Yan*, Ch. Gerth, DESY, Hamburg, Germany
B. Beutner†, R. Ischebeck, E. Prat, PSI, Villigen, Switzerland

Abstract

High-brightness electron bunches with small transverse emittance are required to drive X-ray free-electron lasers (FELs). For the measurement of the transverse emittance, the quadrupole scan and multi-screen methods are the two most common procedures. By employing a transverse deflecting structure, the measurement of the slice emittance becomes feasible. The quadrupole scan is more flexible in freely choosing the data points during the scan, while the multi-screen method allows on-line emittance measurements utilising off-axis screens in combination with fast kicker magnets. The latter is especially the case for high-repetition multi-bunch FELs, such as the European X-ray Free-Electron Laser (XFEL), which offer the possibility of on-line diagnostics. In this paper, we present comparative measurements of projected and slice emittance applying these two methods at the SwissFEL Injector Test Facility and discuss the implementation of on-line diagnostics at the European XFEL.

INTRODUCTION

Control and optimization of the transverse emittance as well as the slice emittance of the driving electron bunch are crucial to the performance of X-ray free-electron lasers (FEL). The principle of emittance measurement is described, for instance, in detail in Ref. [1]. The emittance to be reconstructed at a reference point is based on the second-order beam moments with $\epsilon^2 = \langle x_0^2\rangle \cdot \langle x_0'^2\rangle - \langle x_0 x_0'\rangle^2$. Transportation of the beam moments to a downstream position using the transport matrix R yields the relation

$$\langle x^2\rangle = R_{11}^2\langle x_0^2\rangle + 2R_{11}R_{12}\langle x_0 x_0'\rangle + R_{12}^2\langle x_0'^2\rangle. \quad (1)$$

The squared beam size $\langle x^2\rangle$ can be accessed directly using observation screens. At least three measurements for three different transport matrices R are required to obtain the second-order beam moments at the reference point. Commonly, linear least squares method is employed for the fit to the equation system. The same procedure can be adapted for the y-plane.

Variation of the transport matrices can be achieved with the quadrupole scan or multi-screen method. In the quadrupole scan method, the measurement point is fixed and the strengths of the quadrupoles between the reconstruction and measurement point are changed. In the multi-screen method, the measurement point is chosen at different downstream locations to provide various transport lattices.

The quadrupole scan is more flexible in arranging data points, but cannot be performed in parallel to the FEL operation. The multi-screen method requires more space and diagnostic stations, but provides the possibility of parasitic emittance measurements utilizing off-axis screens. Such online diagnostics are highly demanded at high repetition multi-bunch FEL, such as the European XFEL [2]. A comparison of different aspects of these two methods is studied in Ref. [3].

Combined use of a transverse deflecting structure (TDS) with these two methods allows for measurement of the slice emittance. The longitudinal coordinate of the bunch is translated by the TDS to one transverse direction. The emittance in the other transverse plane perpendicular to the streak direction can then be determined in a time-resolved domain. Careful consideration in the accelerator optics has to be taken into account for the time resolution, which is correlated inversely to the TDS streak parameter [4]

$$S \sim \frac{eV_0 k}{pc}\sqrt{\beta_{y,\mathrm{TDS}}} \cdot \sin(\Delta\mu_y). \quad (2)$$

Comparative measurements of projected and slice emittance using these two methods have been conducted at the SwissFEL Injector Test Facility (SITF) at PSI in Switzerland. In this paper, the experimental setup is described and the results are discussed.

DIAGNOSTIC SECTION

One main purpose of the SITF [5] is to demonstrate the feasibility of the SwissFEL. A schematic layout of the SITF is shown in Fig. 1. The nominal beam energy is 250 MeV and the charge can be varied from 10 pC to 200 pC.

The diagnostic section for the comparative emittance measurement is located downstream of the bunch compressor at a nominal energy of 250 MeV. An S-band TDS streaks the bunch in the vertical direction and enables slice emittance measurement in the horizontal plane. The TDS is followed by several matching quadrupoles, a 3.5-cell FODO section with multiple standard screen stations and a high-resolution transverse profile monitor [6]. The screen stations inside the FODO section are equipped with optical transition radiation (OTR) screens. The high-resolution profile monitor, which employs a scintillator screen, is designed in a special configuration to achieve resolution much smaller than the thickness of the scintillator and more robust than the OTR screen for operation with low charge bunches due to its higher light

* minjie.yan@desy.de
† Now at Deutsches-Elektronen Synchrotron DESY

ISBN 978-3-95450-133-5

FEMTOSECOND TIMING DISTRIBUTION FOR THE EUROPEAN XFEL

C. Sydlo*, F. Zummack, M. K. Czwalinna, M. Felber, T. Lamb,
S. Schulz, Ch. Gerth, H. Schlarb, DESY, Hamburg, Germany
S. Jablonski, Warsaw University of Technology, Warsaw, Poland

Abstract

Accurate timing synchronization on the femtosecond timescale is an essential installation for time-resolved experiments at free-electron lasers (FELs) such as FLASH and the upcoming European XFEL. To date the required precision levels can only be achieved by a laser-based synchronization system. Such a system has been successfully deployed at FLASH and is based on the distribution of femtosecond laser pulses over actively stabilized optical fibers. Albeit its maturity and proven performance this system had to undergo a major redesign for the upcoming European XFEL due to the enlarged number of stabilized optical fibers and an increase by a factor of up to 10 in length. The experience and knowledge gathered from the operation of the optical synchronization system at FLASH has led to an elaborate and modular precision instrument which can stabilize polarization maintaining fibers for highest accuracy as well as economic single mode fibers for shorter lengths. This paper reports on the laser-based synchronization system focusing on the active fiber stabilization units for the European XFEL, discusses the most recent performance results, which already meet the stringent requirements for operation.

INTRODUCTION

The optical synchronization system for the European XFEL will adopt to the greatest possible extent the proven and reliable system from FLASH. The long term experience with the optical synchronization system at FLASH has led to numerous enhancements and deeper understanding of the issues involved in such a complex and sensitive precision arrangement. Consequently, for the European XFEL an inimitable possibility arises to incorporate all the gathered knowledge from the bottom up into a new benchmark setting synchronization system.

A schematic representation of the synchronization system is shown in Figure 1. The master-oscillator (MO) distributes a stabilized 1.3 GHz reference to which the master laser-oscillator (MLO), with a repetition rate of 216.7 MHz (a sixth of the MO frequency), is locked. While this MLO lock still employs a simple homodyne scheme at FLASH, the locking of the MLO at the European XFEL will benefit from a more robust and drift-free approach [1]. The stabilized pulse train from the MLO is split into multiple channels and guided to the individual link stabilization units (LSUs) through the free-space distribution (FSD). Each LSU actively stabilizes the effective length of its assigned optical link fiber, which can be conveniently guided through the entire FEL to stations obliged to femtosecond timing stability.

* cezary.sydlo@desy.de

The optical synchronization supplies 12 stations the stabilization of the RF reference [1], 7 laser-to-laser locking stations (L2L) [2] and 7 stations with direct usage of the pulse train for bunch arrival-time measurement (BAM) [3]. One notable feature in this optical synchronization system is the slave laser-oscillator (SLO) at the end of the FEL. A sub-synchronization will be located in the experimental hall at the end of the beamlines to facilitate all the synchronization needs for the pump-probe lasers on-site. Additionally, it will stabilize all stations between 2.1 km and the end of the experimental hall. Hence, two more links with a length of 3.5 km are provided for SLO to MLO locking. On the one hand this serves as a redundancy improving reliability and robustness. On the other hand these two long links can be cross-correlated in-situ for diagnostics providing numbers for the actual synchronization accuracy. One more LSU is included in this planning to reserve space for later use yielding 24 LSUs in total for the main synchronization.

The latest status of the LSUs deployed at FLASH is described in [4], while a redesigned LSU has been introduced in [5] and is shown in Figure 2.

MEASUREMENTS

Set-up

The set-up for measuring the residual error of the fiber-link stabilization is kept as close as possible to the operation conditions at the European XFEL. A 1.3 GHz signal source is used as the Master-Oscillator (MO) to lock the Laser-Oscillator at its repetition frequency of 216.7 MHz, which is a sixth of the 1.3 GHz. The 200 fs pulses of the MLO centred around an optical wavelength of 1553 nm are distributed to the Link-Stabilization-Unit (LSU) and the out-of-loop (OOL) optical cross-correlator (OXC). The LSU is connected to 3.6 km of polarization maintaining fiber (PMF) with a partly reflecting fiber mirror at its end, which reflects a part of the light back to the LSU for timing detection. The transmitted part is fed into the OOL-OXC for timing error measurement. All components are placed in a climatized laboratory except for the fiber. The fiber is installed in a large hall at the DESY campus next to the laboratory to emulate completely uncontrolled ambient influence. As temperature and humidity do influence optical fibers [6] only such a test environment can guarantee proper test conditions. Identical to the installation in the European XFEL only the 3.6 km PMF is subjected to changes of temperature and humidity. All complementary fibers such as the dispersion compensating fiber, the piezo fiber stretcher, erbium doped fiber amplifier, etc., are left in the climatized laboratory. The deviation between the fiber length of 3.6 km and the European XFEL length of 3.4 km is

ISBN 978-3-95450-133-5

DESIGN AND TEST OF WIRE-SCANNERS FOR SwissFEL

G.L. Orlandi*, M. Baldinger, H. Brands, P. Heimgartner, R. Ischebeck, A. Kammerer, F.Löhl, R. Lüscher, P. Mohanmurthy†, C. Ozkan, B. Rippstein, V. Schlott, L. Schulz, C. Seiler, S. Trovati, P. Valitutti, D. Zimoch, Paul Scherrer Institut, 5232 Villigen PSI, Switzerland

Abstract

The SwissFEL light-facility will provide coherent X-rays in the wavelength region 7-0.7 nm and 0.7-0.1 nm. In SwissFEL, view-screens and wire-scanners will be used to monitor the transverse profile of a 200/10 pC electron beam with a normalized emittance of 0.4/0.2 mm mrad and a final energy of 5.8 GeV. Compared to view screens, wire-scanners offer a quasi-non-destructive monitoring of the beam transverse profile without suffering from possible micro-bunching of the electron beam. The main aspects of the design, laboratory characterization and beam-test of the SwissFEL wire-scanner prototype will be presented.

INTRODUCTION

SwissFEL will provide coherent X-rays light in the wavelength region 7-0.7 nm and 0.7-0.1 nm [1]. Electron bunches with charge 200/10 pC and normalized emittance of 0.4/0.2 mm.mrad will be emitted by a photocathode at a repetition rate of 100 Hz according to a two-bunches train structure with a temporal separation of 28 ns. Thanks to a RF kicker switching the second electron bunch of the beam train into a magnetic switch-yard, the SwissFEL linac will simultaneously supply two distinct undulator chains at a repetition rate of 100 Hz: the hard-Xrays line Aramis and the soft-Xrays line Athos. The electron beam will be accelerated up to 330 MeV by a S-band RF Booster and to the final energy of 5.8 GeV by a C-band RF linac. Thanks to an off-crest acceleration in the RF Booster, the electron beam will experience a two-stages longitudinal compression from an initial bunch length of 3/1 ps (RMS) down to 20/3 fs (RMS) in two magnetic chicanes. Two X-band RF cavities will compensate the quadratic distortion of the longitudinal phase space due to the off-crest accelerating scheme of the beam and the non-linear contribution of the magnetic dispersion. A laser-heater in the Booster section will smooth down possible micro-structures affecting the beam longitudinal profile of the beam. Macro-bunching can be detrimental to the monitoring of the beam profile based on scintillator or OTR screens (Optical Transition Radiator) because of the emission of coherent OTR. As an alternative to view screens, wire-scanners (WSC) can be used to monitor the beam transverse profile. Moreover, the quasi-non-invasive feature of the WSCs - compared to view screens - can be beneficial to monitoring the beam transverse profile during FEL operations of the machine. In the following, results on design, characterization and beam test of wire-scanners for SwissFEL will be presented.

* gianluca.orlandi@psi.ch
† presently at Massachusetts Institute of Technology, MA, USA

WSC DESIGN

Wire-Scanners can be used to measure the transverse profile of the electron beam in a particle accelerator [2–4]. Carbon or metallic wires with different diameter (D) - stretched on a wire-fork - can be vertically inserted at a constant velocity into the vacuum chamber by means of a motorized UHV linear stage to scan the beam transverse profile with an intrinsic resolution D/4 (rms). An encoder mounted on the linear stage allows the relative distance of the wire from the axis of the vacuum chamber to be measured at each machine trigger event. The interaction of the electron beam with the wire produces a "wire-signal" - scattered primary electrons and secondary particles (mainly electrons, positron and bremsstrahlung photons) - which is proportional to the number of the electrons sampled by the wire in the bunch. The Beam Synchronized Acquisition (BS-ACQ) - over a sufficient number of machine trigger shots - of the wire position and the wire-signal - detected by a loss monitors downstream the wire - allows the beam transverse profile along the horizontal or the vertical direction to be reconstructed. In SwissFEL, view screens and WSCs will be used to monitor the transverse profile of the electron beam which varies between 500 μm and 5 μm (rms) along the entire machine. View-screens will be mainly equipped with YAG crystals. In SwissFEL, only WSCs are in principle able to discriminate the 28 ns time structure of the two-bunches emitted at 100 Hz by the photocathode. The SwissFEL WSCs are designed according to the following criteria, see Fig. 1: use a single UHV linear stage to scan the beam profile in the X,Y and X-Y directions; use Tungsten wire with different diameters from 5 to 13 μm to ensure a resolution in the range 1.5-3.5 μm; equip each wire-scanner station with spare/different-resolution wires; detect the wire losses in the bunch charge range 10-200 pC and resolve the 28 ns time two-bunches structure of the electron beam; BS-ACQ of the read-out of both the encoder wire position and the loss-monitor; wire-fork suitably designed for routine scanning of the beam profile during FEL operations (no beam interception with the wire-fork); wire-fork equipped with different pin-slots where the wires can be stretched at different relative distances so that the scanning time can be minimized and optimized according to the WSC position in the machine, see Fig. 1. In SwissFEL the wire losses will be measured by means of scintillator fibers (PMMA, Poly-Methyl-Methyl-Acrylate, Saint Gobain BCF-20, emission in the green) winding up the beam pipe. The fiber are directly connected to a photomultiplier (PMT,Hamamatsu H10720-110). For more information on the detection sys-

ISBN 978-3-95450-133-5

TRANSITION RADIATION OF AN ELECTRON BUNCH AND IMPRINT OF LORENTZ-COVARIANCE AND TEMPORAL-CAUSALITY

Gian Luca Orlandi*,
Paul Scherrer Institut, 5232 Villigen PSI, Switzerland

Abstract

The study of Transition Radiation (TR) of a bunch of N electrons offers a precious insight into the role that Lorentz-covariance and temporal-causality play in an electromagnetic radiative mechanism of a relativistic beam. The contributions of the N single electrons to the radiation field are indeed characterized by emission phases from the metallic surface which are in a causality relation with the temporal sequence of the N particle collisions onto the radiating screen. The Lorentz-covariance characterizing the virtual quanta field of the relativistic charge is also expected to imprint the radiation field and the related energy spectrum. The main aspects of a Lorentz-covariance and temporal-causality consistent formulation of the TR energy spectrum of an electron bunch will be described.

INTRODUCTION

The electromagnetic field of a relativistic charge in a rectilinear and uniform motion can induce the boundary interface between two media with different dielectric properties to emit radiation, the so called Transition Radiation (TR) [1, 2]. Forward and backward radiation is emitted with an angular distribution scaling down with the Lorentz factor γ of the relativistic charge ($\gamma = E/mc^2$) and a frequency bandwidth determined by the plasma frequency and the finite dimension of the radiating surface. TR finds various application in beam diagnostics of a particle accelerator: to monitor the beam transverse profile by imaging the visible light spot (OTR, Optical Transition Radiation) emitted by the charged beam while crossing a metallic foil [3] or to measure the length of the charged beam via spectroscopic analysis of the coherent enhancement of the radiation intensity [4]. For observation condition of the radiation in the visible or in the far infrared, the interface vacuum-metal practically behaves like an ideal conductor. The modelling of the radiator surface as an ideal conductor allows a better comprehension of the dynamics of the charged distributions involved in TR emission and of the attribute as "polarization radiation" that is sometimes given to TR. An ideal conductor surface can be indeed schematized as a double layer of charge. The collision of a bunch of N relativistic electrons with the metallic surface can be modelled as the interaction of an incident relativistic charge with a double layer of charge (a beam collision at a normal angle of incidence onto the radiator surface is supposed in the present paper). At the same time, the radiation emission can be interpreted as the result of the dipolar oscillation of the double layer of charge which is induced by the relativistic electron bunch, see Fig. 1. The observation of a backward emitted component in the TR can be indeed explained as the result of a dipolar oscillation of a double layer of charge. The propagation of the radiation field from the metallic surface can be interpreted in terms of the Huygens-Fresnel principle and formally expressed in terms of the Helmholtz-Kirchhoff integral theorem. Under far-field approximation, the Helmholtz-Kirchhoff integral theorem allows to express the single harmonic component of the radiation field as the Fourier transform - calculated with respect to the coordinates of the radiator surface - of the transverse component of the electric field of the relativistic charge, the so called *virtual quanta* field. The density-like Lorentz-covariance characterizing the electric field of the incident electron bunch is expected to characterize both the TR field and the corresponding energy spectrum. Signature of the Lorentz-covariance is the dependence of the radiation energy spectrum on the Lorentz-invariant distribution of the transverse coordinates of the N electrons. Besides Lorentz-covariance, the TR field and the related energy spectrum of the N electron bunch are also expected to bear the imprint of the temporal-causality constraint: the emission phases of the N single electron amplitudes composing the radiation field must be causality related to the temporal sequence of the N electron collision onto the metallic screen, which only depends on the distribution of the longitudinal coordinates of the N electrons. Lorentz-covariance and temporal-causality are physical constraints an electromagnetic radiative mechanism by a relativistic charged beam must fulfill. Both these two constraints are expected to imprint the TR energy spectrum of a bunch of N electrons. The failure in implementing the one of the two physical constraints in the formula of the TR energy spectrum of a bunch of N electrons implies necessarily also the defect of the other and vice-versa. In the present paper, a Lorentz-covariance and temporal-causality consistent formulation of the TR energy spectrum of a relativistic bunch of N electrons is presented and the agreement of the presented model with well-known results of the TR theory of a single electron is demonstrated [5–7]. The breaking point between a Lorentz-covariance and temporal-causality consistent or inconsistent theoretical model of TR of a bunch of N electrons is discussed.

TR ENERGY SPECTRUM

Causality and Covariance

The case of a bunch of N relativistic electrons at normal incidence onto a metallic screen is considered in the present paper. The N electrons are supposed to move with a common rectilinear and uniform velocity $\vec{w} = (0, 0, w)$ along the z-axis of the laboratory reference frame. The radiator

* gianluca.orlandi@psi.ch

ISBN 978-3-95450-133-5

COHERENT ELECTRON COOLING PROOF OF PRINCIPLE PHASE 1 INSTRUMENTATION STATUS*

D. M. Gassner#, J. C. Brutus, R. Hulsart, V. Litvinenko, R. Michnoff, T. Miller, M. Minty, I. Pinayev, M. Wilinski, Brookhaven National Laboratory, Upton, NY 11973, USA

Abstract

The purpose of the Coherent electron Cooling Proof-of-Principle (CeC PoP) [1] experiment being designed at RHIC is to demonstrate longitudinal (energy spread) cooling before the expected CD-2 for eRHIC. The scope of the experiment is to longitudinally cool a single bunch of 40 GeV/u gold ions in RHIC. The cooling facility will be installed inside the RHIC tunnel in 3 phases. The status of the instrumentation systems planned for phase 1 commissioning efforts will be described. This paper will also describe updates to the instrumentation systems proposed to meet the diagnostics challenges during the final phase of cooling commissioning [2]. These include measurements of beam intensity, emittance, energy spread, bunch length, position, and transverse alignment of electron and ion beams.

INTRODUCTION

Cooling of ion and hadron beams at collision energy is of critical importance for the productivity of present and future Nuclear Physics Colliders, such as RHIC, eRHIC and ELIC. An effective cooling process would allow us to cool the beams beyond their natural emittances and also to either overcome or to significantly mitigate limitations caused by the hour-glass effect and intrabeam scattering. It also would provide for longer and more efficient stores, which would result in significantly higher integrated luminosity. The scaled down economic version called CeC PoP does not offer optimal cooling conditions, but it includes the most critical and untested elements (from modulator to kicker) and is sufficient for demonstration. The diagnostics systems described here are based on the requirements determined by the latest simulations; additional systems may be added as further simulations look more closely at non-ideal conditions. The CeC PoP phase 1 beam line is presently in the construction phase. The primary goals of this first phase are to test the 112 MHz SCRF gun [3] and 500 MHz buncher cavities and to measure low power 2 MeV electron beam characteristics. Initial system commissioning is planned for early FY15.

ELECTRON BEAM DIAGNOSTICS

During the initial commission phase the electron beam diagnostics will provide the necessary measurements to commission the 112 MHz SRF Gun, then transport the 2 MeV beam through the 11m straight beam line to a low power dump as shown in Fig. 1. During the next phase the low power dump will be replaced with a 704 MHz SRF Linac and the wigglers and associated beam lines will be installed. The 21.8 MeV beam will be transported through the Linac and the FEL wigglers to the high power (10 kW) dump as shown in Fig. 2. During the following RHIC run the wigglers will be relocated into the nearby RHIC transport to allow electron co-propagation with the gold ion bunches and allow initial cooling studies as shown in Fig. 3.

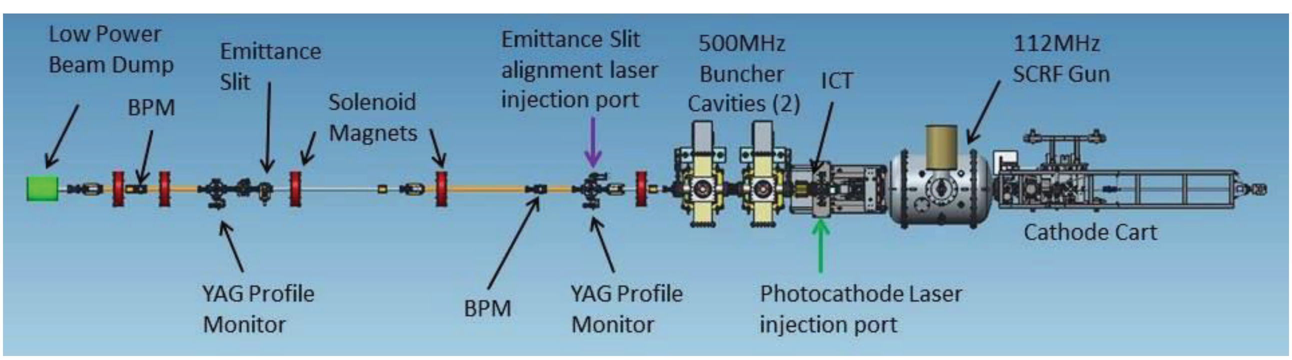

Figure 1: Plan view of the phase 1 electron beam line (2 MeV), the commissioning goals include SCRF gun and buncher testing and beam parameter measurements.

*Work supported by U.S. DOE under contract No DE-AC02 98CH10886 with the U S DOE
#gassner@bnl.gov

ISBN 978-3-95450-133-5

EVOLVEMENT OF THE LASER AND SYNCHRONIZATION SYSTEM FOR THE SHANGHAI DUV-FEL TEST FACILITY*

B. Liu†, X.T. Wang, X.Q. Liu, S.P. Zhong, W.Y. Zhang, T.H. Lan, L. Feng, D. Wang
SINAP, CAS, Shanghai 201800, China

Abstract

Many attractive experiments including HGHG, EEHG, cascaded HGHG, chirped pulse amplification etc. are carried out or planned on the Shanghai Deep- Ultraviolet Free-Electron Laser test facility. These experiments are all utilizing a laser as seed, and need precise synchronization between the electron beam and the laser pulse. We will describe the history and current status of the seeding and synchronization scheme for the SDUV-FEL together with some related measurement results in this paper.

INTRODUCTION

High gain free-electron lasers (FELs) are being developed to serve as high-intensity coherent radiation sources for advanced user applications. One of the most feasible ways for delivering short-wavelength FEL is self-amplified spontaneous emission (SASE) [1, 2]. However, SASE radiation starts from shot noise of the electron beam, and results in a poor temporal coherence. With the growing interest in fully coherent sources, various seeded FEL schemes have been proposed on the basis of harmonic generation and seeding of external lasers. A typical scheme is high-gain harmonic generation (HGHG) [3], which has been demonstrated from the infrared to the soft X-ray spectral region [4–7].

Seeded FEL schemes need precise synchronization of laser and beam. Usually the electron beam duration for FEL is from picosecond down to femtosecond, and pulse length of the seed laser is at the same level. Thus the synchronization precision should be sub-picosecond and sometimes even down to femtosecond level. Such stringent requirement could be fulfilled with various ways, such as high harmonic phase-locked loop (PLL) and optical cross-correlation [8].

FEL experiments of HGHG, echo-enabled harmonic generation (EEHG) [9–11]and cascaded HGHG [12–14] have been carried out, and chirped pulse amplification [15, 16] are underway at Shanghai Deep-Ultraviolet Free-Electron Laser test facility (SDUV-FEL) [17], which is consisting of an injector, a main accelerator, a bunch compressor, two laser modulation stages, and a long undulator section. The seed laser interacts with the electron beam in the two modulator undulators.

All these experiments are externally seeded, and precise synchronization between the seed laser and electron beam is necessary. In this paper, the history and current status of related laser and synchronization systems are reviewed. Some measurement results are also presented.

* work supported by the National Natural Science Foundation of China (Grant No. 11175241)

† liubo@sinap.ac.cn

LASER SYSTEMS

The SDUV-FEL was originally a SASE test facility, and had only one Nd:YLF laser system serving as the drive laser. With some modification on the laser transport system, it had been successfully turned into a HGHG test facility since 2009. One Ti:Sapphire laser system was put into operation as the dedicated seed laser in 2010 and an optical parametric amplifier (OPA) system was added to extend the capability in 2011. Currently, a rather complicated laser transport system has been established to fulfill different requirements, which is shown in Figure 1.

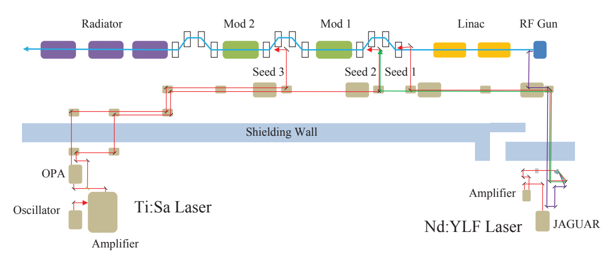

Figure 1: Layout of the laser transport system.

There are three laser injection points and two modulation sections along the beam line. The seed laser could be coming either from the Nd:YLF system or from the Ti:Sa system depending on the requirement of the planned experiment.

Nd:YLF Laser

The basic parameters of the Nd:YLF laser system is shown in Table 1.

Table 1: Parameters of the Nd:YLF Laser System

Parameter	Value	Remark
Wavelength	1047 nm	fundamental
Pulse length	8.7 ps	FWHM
Repetition rate	119 MHz	oscillator
Repetition rate	2 Hz (100 Hz max.)	amplifier
	>5 mJ@1047 nm	amplifier
Pulse energy	>2 mJ@523 nm	2nd harmonic
	>1 mJ@262 nm	4th harmonic

The Nd:YLF laser is mainly used to drive the RF gun at its fourth harmonic through two BBO crystals, while the residual fundamental and second-harmonic light could be used as the seed laser.

ISBN 978-3-95450-133-5

LONGITUDINAL RESPONSE MATRIX SIMULATIONS FOR THE SWISSFEL INJECTOR TEST FACILITY

A. Saa Hernandez*, B. Beutner†, F. Frei, R. Ischebeck, PSI, Villigen, Switzerland

Abstract

The Singular Value Decomposition (SVD) method has been applied to the SwissFEL Injector Test Facility to identify and better expose the various relationships among the possible jitter sources affecting the longitudinal phase space distribution and the longitudinal diagnostic elements that measure them. To this end, several longitudinal tracking simulations have been run using the Litrack code. In these simulations the RF and laser jitter sources are varied one-by-one within a range spanning several times their measured stability. The particle distributions have been dumped close to the diagnostic locations and the measured quantities analyzed. A matrix has been built by linearly fitting the response of each measured quantity to each jitter source. This response matrix is normalized to the stability of the jitter source and the instrumentation accuracy, and it is inverted and analyzed using SVD. From the eigenvalues and eigenvectors the sensitivity of the diagnostics to the jitters can be evaluated.

INTRODUCTION

The SwissFEL free electron laser [1] is currently being constructed at the Paul Scherrer Institute. The SwissFEL Injector Test Facility (SITF) has been operated since 2010 as a platform to develop and test the different components and optimize the procedures necessary to operate later SwissFEL.

Several sources of jitter and drift affect the longitudinal phase space dynamics of the SITF. In order to identify and better expose the various relationships among the error sources and the longitudinal diagnostics that measure them, longitudinal response matrix simulations have been performed for the SITF in a similar manner as previously realized for SwissFEL [2]. These simulations have been used to predict the response matrix later measured at SITF during two shifts. A detailed description and analysis of the experimental results is given on a separate contribution [3].

A scheme of the SITF showing the longitudinally relevant elements is sketched in Figure 1. The electrons emerge from an S-band RF photoinjector and are accelerated by a booster linac based on normal conducting S-band RF technology, which simultaneously generates the necessary energy chirp for the magnetic compression. In front of the magnetic chicane a fourth harmonic X-band cavity, phased for deceleration, linearizes the longitudinal phase space for optimal bunch compression. The last drift section is dedicated to the beam characterisation.

The bunch charge is measured with stripline beam position monitors (BPM), that were calibrated via a Faraday cup and a wall-current monitor [4]. BPMs in dispersive sections measure the horizontal beam position from which the mean particle energy is inferred, while the energy distribution is measured by imaging the incoherent synchrotron radiation with a monitor (SRM) [5]. The bunch arrival time monitor (BAM) samples the deviation of a RF pick-up signal from the electron bunch with a pulsed reference laser [6]. The absolute bunch length is measured in a destructive manner using a transverse deflective cavity (TDC) and imaging the bunch at a screen, while the relative bunch length variations are measured with a bunch compression monitor (BCM) based on coherent diffraction radiation (CDR) generated as the electron bunch passes through a hole in a foil. After passing through THz filters, the emitted CDR is detected by Schottky diodes [3]. An overview of the longitudinal diagnostics relevant for the response matrix studies is also shown in Figure 1.

SIMULATIONS

To analyze the sensitivity of the electron beam to RF-phase, RF-amplitude, and charge errors the entire beamline must be considered. The beamline is modeled in *LiTrack* [7], a one-dimensional tracking code which includes the effect of longitudinal wakefields. The physics model of Litrack is more appropriate for highly-relativistic beams. For this reason the following trick is applied to study the entire beamline; initially a low-energy high space-charge 3D tracking simulation is done with *Astra* [8] and a particle distribution at 130 MeV (after FINSB02) is generated. The energy and longitudinal coordinates of these particles are used as a 1D input distribution for the LiTrack simulation, where it is firstly tracked backwards to the photocathode and afterwards tracked forward including the error sources. A total of 11 error sources have been studied in this work; the phase and amplitude of the photoinjector RF gun (ϕ_{SS}, A_{SS}), the phase and amplitude of the three S-band accelerating cavities (ϕ_{S1}, A_{S1}, ϕ_{S2}, A_{S2}, ϕ_{S3}, A_{S3}), the phase and amplitude of the linearizer X-band cavity (ϕ_X, A_X) and bunch charge (Q) due to laser fluctuations. The nominal settings of the charge and RF parameters in the simulations, presented in Table 1, are taken such to match those of the experiments performed at SITF. Thus, bunches of 20 pC are accelerated to a final energy of 200 MeV and compressed approximately 7 times their original length, from 1.9 ps (570 μm) down to 266 fs (79 μm) in the experiment, and only down to 85 μm, approximately 10% less compression, in the simulations with the same RF settings.

The tracking simulations are run varying the error sources one by one, in five steps, within the range shown in Table 1.

* angela.saa-hernandez@psi.ch
† presently at DESY, Hamburg

ISBN 978-3-95450-133-5

CAMERALINK HIGH-SPEED CAMERA FOR BUNCH PROFILING

Daniel Llorente, Rasmus Ischebeck, Helge Brands, Patrick Pollet, Volker Schlott
Paul Scherrer Institut, Villigen, Switzerland

Abstract

In the context of upcoming SwissFEL linear accelerator, we are working on a high-speed high-resolution instrument capable of delivering good sensitivity even in dark conditions. The camera selected is a PCO.Edge with SCMOS technology and an ultra-low noise sensor with 2560x2160 pixel resolution working at 100Hz. This allows for single bunch monitoring in SwissFEL, allowing eventually for on-the-fly inter-bunch image processing.

The communication between the PCO.Edge camera and a last-generation Kintex7 FPGA has been demonstrated using a prototyping evaluation board and an 850-nm optical link connected to a 10Gbit SFP+ transceiver. Rudimentary packet processing has been implemented to confirm the satisfactory operation of the new link-layer protocol X-CameraLinkHS, specifically development for high-speed image transmission. We aim for online image processing and investigating the feasibility of achieving inter-bunch feedback (< 10 ms).

SYSTEM DESIGN FOR PROCESSING IMAGE AT ON-THE-FLY

The system is designed to monitor bunches of electrons with a high-resolution high-speed camera, capturing frames at 100Hz, the working frequency of the SwissFEL laser gun [1]. A last-generation FPGA will process such frames at a high speed, extracting the relevant parameters, comparing these values to programmable thresholds and eventually allowing for fast feedback to the machine without the intervention of the operator (see Fig. 1).

Frames need to be transmitted from the camera to the processing system over a distance of up to 1km, using for this purpose an 860-nm multimode optic fibber, which comfortably allows for the 10Gbps data rate of the camera. The preference of optic fibber over cooper cabling is advised due to the long distances and noisy environment in which the system will be deployed.

Data is formatted in the camera according to the Camera-Link High Speed (CLHS) Protocol [2], which has been designed to provide low latency and low jitter in real-time signals for high-bandwidth image transmission. This is a proprietary link-layer protocol which can be implemented over commodity Ethernet connectors, thus benefiting in terms of price and availability of hardware. Particularly in our design, we use two Small form-factor pluggable transceivers (SFP+), a widely-spread standard in the communication industry for optic fibbers.

The frame grabber has been implemented on a KC705 Prototyping Platform from Xilinx. This board includes a last-generation Kintex7 FPGA, which is the targeted device for the final design implementation. On this board, DDR3 memory and one PCI connector are available, which are a powerful asset for further expanding the system capabilities. For deploying the instrument in the accelerator tunnel, we will transfer the firmware to a General Purpose Carrier Board v.3.0 (GPAC), which is expected to be the workhorse electronic board for future SwissFEL instruments.

The embedded system includes the Frame Grabber (an Intellectual Property (IP) Core) running along many other modules. For instances, the 10GBASE-KR core from Xilinx conveys the physical signals into CLHS packets (it is actually our PHY layer). The CLHS packets are decoded and transformed into frames by the X-Protocol decoder, provided by PCO, the camera manufacturer [3]. From this point on, the data format is presented as rows and columns of pixels. Together with the corresponding context data, the frame can be rebuilt.

At this point, we have two options. Data can be either processed at wire-speed on the FPGA in order to extract the relevant parameters or it can be alternatively stored on a temporary local buffer, waiting for retrieving from the control system an eventually processed offline. Both options present its advantages and drawbacks. Buffering large amounts of information require of fast big buffers, which can only be implemented with a reasonable cost on DDR memories. Even in this case, only some ms of video streaming can be stored.

A second option consists in processing the frames on-the-fly using a set of Hardware Accelerators specifically designed for this purpose (*Schwerpunkt* Extractor, Gradient Machine…). If fast enough, this early extraction of information from the frames may allow for inter-bunch feedback to the actuators, greatly speeding up the precise calibration of the machine. In this last case, the need for a large buffer would be overcome, though at the price of increasing design effort while flexibility for later modifications becomes more difficult.

SCMOS SENSORS

Many scientific imaging applications demand multi-megapixel focal plane sensors that can operate with very high sensitivity and wide dynamic range. Scientific CMOS technology delivers a very large high field, together with a low noise figure, that can be up to one degree of magnitude smaller [4]. This is especially the case when the number of photons is very low, as it is in our case, when only a handful of photons (~200) excite the sensor.

This high performance is obtained without reducing the fps rate, so the sensor is capable of capturing frames at 100 Hz without the traditional trade-off in CCD cameras that requires reducing resolution to increase frames per

ISBN 978-3-95450-133-5

THERMAL EMITTANCE MEASUREMENTS AT THE SwissFEL INJECTOR TEST FACILITY

E. Prat*, S. Bettoni, H. H. Braun, M. C. Divall, R. Ganter, T. Schietinger, A. Trisorio, C. Vicario
PSI, Villigen, Switzerland
C. P. Hauri, EPFL, Lausanne, Switzerland and PSI, Villigen, Switzerland

Abstract

In a laser-driven RF gun the ultimate limit of the beam emittance is the transverse momentum of the electrons as they exit the cathode, the so-called intrinsic or thermal emittance. In this contribution we present measurements of the thermal emittance at the SwissFEL Injector Test Facility for electron beam charges down to a few tens of fC. We have studied the dependence of thermal emittance and quantum efficiency on the laser wavelength, the RF-gun gradient and the cathode material (copper and cesium telluride).

INTRODUCTION

The electron beam emittance is of great importance for Free-Electron Laser (FEL) facilities. First, transversely coherent FEL radiation is generated if $\varepsilon_n/\gamma \approx \lambda/4\pi$, where ε_n is the normalized beam emittance, γ is the Lorentz factor and λ is the FEL radiation wavelength. This condition entails that by reducing the normalized emittance the final beam energy can be decreased, which translates into a more compact and affordable accelerator. Second, for a given beam energy, a smaller emittance implies a higher radiation power and a shorter undulator beamline to reach FEL saturation.

As accelerator technology advances and the emittance of the electron source is preserved downstream of the injector, the source becomes a significant contributor to the final emittance and brightness of the electron beam. The intrinsic or thermal emittance, which is proportional to the transverse momentum of the electrons exiting the cathode, is related to the initial kinetic energy or effective temperature of the electrons.

The thermal emittance for both metal and semiconductor photo-cathodes can be expressed as [1, 2].

$$\varepsilon_{th} = \sigma_l \sqrt{\frac{\phi_l - \phi_e}{3m_0c^2}}, \qquad (1)$$

where ϕ_l is the laser photon energy, σ_l is the RMS laser beam size, m_0c^2 is the electrons rest mass energy, and ϕ_e is the effective work function. We call $\varepsilon_{th}/\sigma_l$ the normalized thermal emittance, expressed in nm/mm, as it is independent of the laser beam size. We note that the above expression is correct if tilted-surface effects related to the surface roughness of the cathode are negligible [3].

To illustrate the effect of the thermal emittance on the final FEL performance, Fig. 1 shows the dependence of the FEL power on the normalized thermal emittance for the 200 pC charge operation mode of SwissFEL [4]. For each normalized thermal emittance value we performed numerical simulations to optimize the emittance at the end of the injector, from which the FEL power was calculated. For instance, the FEL power increases by about 25% for a normalized thermal emittance reduction from 600 nm/mm to 400 nm/mm.

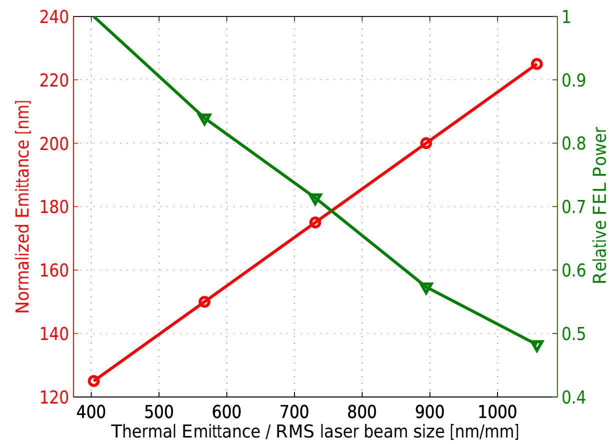

Figure 1: Relative FEL power as function of the normalized thermal emittance. Normalized core slice emittance is simulated for the 200 pC charge operation mode of SwissFEL for different normalized thermal emittance values. The corresponding normalized emittance for optimized laser beam size (red circles) is then used to calculate the relative FEL power (green triangles).

The effective work function is defined as the material work function ϕ_w, reduced by the Schottky effect ϕ_s [5]:

$$\phi_e = \phi_w - \phi_s = \phi_w - \sqrt{\frac{e^3}{4\pi\varepsilon_0}\beta E_c(\varphi)}, \qquad (2)$$

where e is the charge of the electron, ε_0 is the vacuum permittivity, β is the local field enhancement factor that depends on the cathode surface properties, and $E_c(\varphi)$ is the applied field on the cathode at the injection phase φ.

When $E_c(\varphi)$ varies in a small range, the quantum efficiency (QE) of a metal photo-cathode is linked to the laser photon energy and the effective work function as follows [1, 6]:

$$QE \propto (\phi_l - \phi_e)^2. \qquad (3)$$

Equations 2 and 3 allow the determination of the effective work function of the employed cathodes directly from measurements in the RF gun in two independent ways: by measuring the emitted charge as a function of the injection

* eduard.prat@psi.ch

ISBN 978-3-95450-133-5

SUPPRESSION OF THE CSR-INDUCED EMITTANCE GROWTH IN ACRHOMATS USING TWO-DIMENSIONAL POINT-KICK ANALYSIS*

Y. Jiao#, X. Cui, X. Huang, G. Xu, IHEP, Beijing, China

Abstract

Coherent synchrotron radiation (CSR) effect causes transverse emittance dilution in high-brightness light sources and linear colliders. Suppression of the emittance growth induced by CSR is essential and critical to preserve the beam quality and to help improve the machine performance. To evaluate the CSR effect analytically, we propose a novel method, named "two-dimensional point-kick analysis". In this method, the CSR-induced emittance growth in an n-dipole achromat can be evaluated with the analysis of only the motion of particle in (x, x') two-dimensional plane with n-point kicks, which can be, to a large extent, counted separately. To demonstrate the effectiveness of this method, the CSR effect in a two-diople achromat and a symmetric TBA is studied, and generic conditions of suppressing the CSR-induced emittance growth, which are independent of concrete element parameters and are robust against the variation of initial beam distribution, are found. These conditions are verified with the ELEGANT simulations and can be rather easily applied to real machines.

INTRODUCTION

Electron beams with low transverse normalized emittance (at the μm.rad or sub-μm.rad scale), short bunch length (at the sub-picosecond scale), and high peak current (up to thousands of Amperes) are generated or expected in high-brightness light sources and linear colliders. In these machines as beams pass through bending magnets, the emission of the coherent synchrotron radiation (CSR) leads to beam quality degradation, by inducing increased beam energy spread and causing transverse emittance dilution. Suppressing this effect is necessary and important to preserve the expected machine performance that is evaluated without considering the CSR effect. This has stimulated extensive analytical, numerical, and experimental studies [1-20] on the CSR effect in the past few decades. One important topic among these studies is to suppress the CSR-induced emittance growth. It has been shown that the CSR effect can be suppressed through optical balance method [4, 19], CSR-kick matching [12, 13], shielding [17], and pulse shaping [18].

In this paper we present a novel method of analysing the net CSR kick after passage through an achromatic cell, named "two-dimensional (2D) point-kick analysis" [20]. With this method, the CSR-induced emittance growth in a n-dipole achromat can be evaluated with the analysis of only the motion of particle in (x, x') 2D plane with n-point kicks, which can be, to a large extent, counted separately. In addition, the beam line between adjacent dipoles is treated as a whole and is formulated with a 2-by-2 transfer matrix. As a result, general CSR-cancellation (in linear regime) conditions can be obtained with this method. In the following, we will introduce the CSR point-kick model, and then use the 2D point-kick analysis to study the CSR effect in a two-dipole achromat and a symmetric TBA, respectively.

*Work supported by the National Natural Science Foundation of China (No. U1332108)
#jiaoyi@ihep.ac.cn

CSR 2D POINT-KICK MODEL

It has been shown that for an electron bunch of Gaussian temporal distribution, the rms energy spread caused by CSR is [12, 13]

$$\Delta E_{rms} = 0.2459 \frac{eQ\mu_0 c_0^2 L_b}{4\pi\sigma_z^{4/3}\rho^{2/3}}, \tag{1}$$

where Q is the bunch charge, μ_0 is the permeability of vacuum, c_0 is the speed of light, L_b is the particle bending path in a dipole, σ_z is the rms bunch length, and ρ is the bending radius. Note that ΔE_{rms} is proportional to both L_b and $\rho^{-2/3}$, or namely, $\Delta E_{rms} \propto \rho^{1/3}\theta$, with θ being the bending angle. Therefore the CSR effect can be linearized by assuming $\delta(csr) = k\rho^{1/3}\theta$, where $\delta(csr)$ is the CSR-induced particle energy deviation, k depends only on the bunch charge Q and the bunch length σ_z, and is in unit of $m^{-1/3}$. It reveals [20] through ELEGANT simulations that this relation applies well to the cases with θ ranging from 1 to 12 degrees and ρ ranging from 1 to 150 m. With the so-called R-matrix method [12], the coordinate deviations of a particle relative to the ideal path after passage through a sector bending magnet can be evaluated,

$$\Delta X = \begin{pmatrix} D \\ D' \end{pmatrix}\delta_i + \begin{pmatrix} \zeta \\ \zeta' \end{pmatrix}k, \tag{2}$$

where $D = \rho(1\text{-}\cos\theta)$ and $D' = \sin\theta$ are the momentum dispersions, and $\zeta = \rho^{4/3}(\theta\text{–}\sin\theta)$ and $\zeta' = \rho^{1/3}(1\text{–}\cos\theta)$ are the "CSR-dispersions".

Through theoretical derivations, we find that the CSR effect in a dipole can be simplified as a point-kick. This kick occurs at the center of the dipole, and is in the form of [20]

$$X_k = \begin{pmatrix} \rho^{4/3}k[\theta\cos(\theta/2) - 2\sin(\theta/2)] \\ \sin(\theta/2)(2\delta + \rho^{1/3}\theta k) \end{pmatrix}. \tag{3}$$

After each kick, the particle coordinates increase by X_k, and in addition, the particle energy deviation increases by $kL_B/\rho^{2/3}$ (or $k\rho^{1/3}\theta$).

ISBN 978-3-95450-133-5

BEAM SIMULATIONS OF HIGH BRIGHTNESS PHOTOCATHODE DC GUN AND INJECTOR FOR HIGH REPETITION FEL LIGHT SOURCE

T. Miyajima*, Y. Honda, M. Yamamoto, X. Jin, T. Uchiyama,
KEK, Tsukuba, Ibaraki 305-0801, Japan
N. Nishimori, R. Nagai, R. Hajima, JAEA, Tokai-mura, Ibaraki 319-1195, Japan

Abstract

As a next generation FEL light source based on linac, high repetition rate operation to increase average FEL power has been proposed, e.g. LCLS-II project. The injector, which generates high brightness and high average current beam, is one of key components. A photocathode DC gun and superconducting RF cavities, which are developed for ERL light source, can be employed for the high repetition rate injector. For high repetition rate operation of FEL light source, injector simulations were carried out based on ERL injector with demonstrated hardware performance by the cERL beam operation in KEK. The optimization results show that the gun voltage of 500 kV is helpful to achieve low emittance. In addition, to estimate optimum gun voltage and cavity acceleration gradient for the FEL operation, two optimizations with different injector layouts were carried out. The results show that the both different layouts have potential to achieve target emittance for FEL operation. Under the realistic operation condition, the transverse normalized rms emittance of 0.8 mm mrad with the rms bunch length of 3 ps, the bunch charge of 325 pC, and the beam energy of 10 MeV is obtained from the optimizations.

INTRODUCTION

To increase average FEL power, high repetition rate operation of FEL light source based on linac is important for the next generation FELs, e.g. LCLS-II project [1]. In order to achieve the high repetition rate operation, the injector, which generates high brightness and high average current beam, is one of key components. The target emittances of high repetition rate FEL are 0.45 mm mrad and 0.7 mm mrad with the bunch charges of 100 pC and 300 pC, respectively [2]. A photocathode DC gun and superconducting RF cavities, which are developed for ERL light source, can be employed for the high repetition rate injector. The performance of ERL injector has been demonstrated at Cornell University, and 90 % transverse normalized emittance has been reached to 0.51 mm mrad with 77 pC/bunch [3]. In KEK, a high repetition rate and high brightness injector, whose repetition rate is 1.3 GHz, is being operated for compact ERL (cERL), which is a test ERL accelerator [4, 5]. In the beam operation, the hardware performance has been demonstrated. In the cERL operation, although the design gun voltage and the injector acceleration gradient are 500 kV and 15 MV/m, respectively, to keep stable beam operation we reduced them and demonstrated the beam operation with 390 kV and 7 MV/m. Based on the demonstrated performance of the cERL injector, particle tracking simulations and optimizations of it with several hundred pC/bunch for the FEL injector were carried out. In addition, to estimate optimum gun voltage and acceleration gradient of cavity for FEL operation, we carried out two optimizations with different injector layouts.

* tsukasa@post.kek.jp

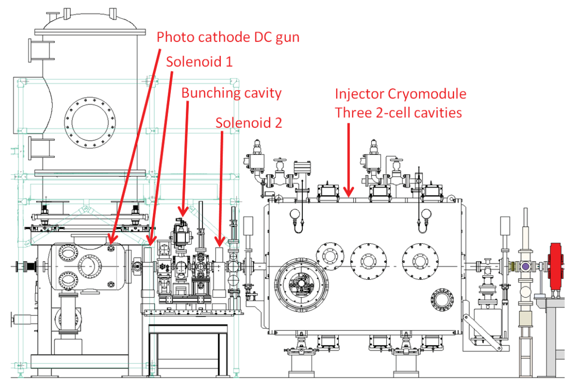

Figure 1: Layout of cERL injector.

Table 1: Center Positions of Injector Elements from Cathode Surface

Element	Original cERL (m)	New layout (m)
SL0	-	0.294
SL1	0.445	0.494
BC	0.809	0.752
SL2	1.218	0.909
SC1	2.221	1.519
SC2	2.781	2.079
SC3	3.341	2.639
SC4	-	4.519
SC5	-	5.079
SC6	-	5.639

PERFORMANCE OF CERL INJECTOR

The cERL injector consists of a photocathode DC gun, two solenoids, a bunching cavity, and three 2-cell superconducting cavities inside an injector cryomodule. Figure 1 shows the layout of the cERL injector. In this paper, SL, BC, SC denote that the solenoid magnet, the bunching cavity, and the 2-cell superconducting cavity, respectively. The element positions of the cERL injector are shown in Table 1. For ERL operation, the target maximum bunch charge is 77 pC, which corresponds to 100 mA average current. The cERL injector layout was optimized for 77 pC operation.

ISBN 978-3-95450-133-5

WAVE-MIXING EXPERIMENTS WITH MULTI-COLOUR SEEDED FEL PULSES

F. Bencivenga#, A. Battistoni, F. Capotondi, R. Cucini, M. B. Danailov, G. De Ninno, M. Kiskinova, C. Masciovecchio, Elettra-Sincrotrone Trieste S.C.p.A., SS 14 km 163,5 in AREA Science Park, 34149 Basovizza, Trieste, Italy

Abstract

The extension of wave-mixing experiments in the extreme ultraviolet (EUV) and x-ray spectral range represents one of the major breakthroughs for ultrafast x-ray science. Essential prerequisites to develop such kind of non-linear coherent methods are the strength of the input fields, comparable with the atomic field one, as well as the high temporal coherence and stability of the photon source(s). These characteristics are easily achievable by optical lasers. Seeded free-electron-lasers (FELs) are similar in many respects to conventional lasers, hence calling for the development of wave-mixing methods. At the FERMI seeded FEL facility this ambitious task is tackled by the TIMER project, which includes the realization of a dedicated experimental end-station. The wave-mixing approach will be initially used to study collective atomic dynamics in disordered systems and nanostructures, through transient grating (TG) experiments. However, the wavelength and polarization tunability of FERMI, as well as the possibility to radiate multi-colour seeded FEL pulses, would allow to expand the range of possible scientific applications.

INTRODUCTION

Non-linear coherent methods based on wave-mixing processes are nowadays used in the optical domain to study a vast array of dynamical processes, taking place over a wide timescale range, with high time resolution as well as energy and wavevector selectivity [1]. In a typical wave-mixing experiment two or more coherent optical fields (input fields) interfere into the sample giving rise to a signal field. The large number of combinations between the parameters of the input fields (wavelength, polarization, bandwidth, arrival time, angle of incidence, etc.) allows to obtain selective information on very different dynamical processes occurring into the sample, some of them non achievable by linear methods [1].

The possibility to extend the wave-mixing approach at wavelengths shorter than the optical ones have attracted the interest of the scientific community and resulted into several theoretical and perspective works and also practical discussions on how to achieve this goal [2-5]. The only experimental report on a wave-mixing process stimulated by EUV/x-ray radiation is an optical/x-ray second order (three-wave-mixing) process, reported in [6]. More recently, we used a specially designed setup [7] to demonstrate the occurrence of a four-wave-mixing (FWM) process stimulated by the EUV coherent photon pulses radiated by FERMI [8].

Some of the major advantages in using EUV/x-ray photons with respect to optical ones are related to the possibility to: (i) achieve element selectivity through the exploitation of core resonances [2,4], (ii) probe high energy collective excitations, as valence band excitons or plasmons [2,4], (iii) exploit a much larger wavevector range, which can compare or even exceed the inverse inter-atomic/molecular distances and may thus allow for atomic/molecular-scale resolution [4,9].

WAVE-MIXING: BASIC CONCEPTS

On formal grounds, non-linear radiation-matter interactions can be described by replacing the basic relation $\mathbf{P}=\varepsilon_0\chi\cdot\mathbf{E}$ (where $\mathbf{P}$, ε_0, χ and $\mathbf{E}$ are the polarization vector, the vacuum permittivity, the linear susceptibility tensor and the electric field vector impinging into the sample, respectively) with a power expansion in $\mathbf{E}$, i.e. [1]:

$$\mathbf{P}=\mathbf{P}^{L}+\mathbf{P}^{NL}=\varepsilon_0\chi\cdot\mathbf{E}+\varepsilon_0\Sigma_{n>2}\chi^{(n)}\cdot\mathbf{E}^{n}, \quad (1)$$

where $\mathbf{P}^{L}$ and $\mathbf{P}^{NL}$ are the linear and non-linear terms of the induced polarization, while $\chi^{(n)}$ is the n^{th}-order susceptibility tensor (of rank n+1), associated to (n+1)-wave-mixing processes. When Eq. 1 is inserted into the Maxwell equations one obtains an inhomogeneous wave equation, in which each "$\chi^{(n)}\cdot\mathbf{E}_1\cdot\mathbf{E}_2\cdot\ldots\cdot\mathbf{E}_n$" term plays the role of a driving force. These can be regarded as radiation sources at frequency $\omega_{nwm,p}=\pm\omega_1\pm\omega_2\ldots\pm\omega_n$, where ω_i (i=1-n) are the frequencies of the n input fields while p labels the possible $\pm\omega_i$ permutations. It is worth noticing that $\omega_{nwm,p}$ are not necessarily equal to any ω_i.

Momentum conservation implies that the radiation emitted at $\omega_{nwm,p}$ (wave-mixing signal) is localized into a well defined region of space, centered around a $k_{nwm,p}$ vector defined by the phase matching condition: $\Delta k=|\mathbf{k}_{nwm,p}-(\pm\mathbf{k}_1\pm\mathbf{k}_2\ldots\pm\mathbf{k}_n)|=0$, where k_i (i=1-n) are the wavevectors of the input fields. In real experiments $\Delta k\neq0$, also in light of the finite bandwidth and divergence of the input beams. However, as long as the coherence length ($L_c=\pi/\Delta k$) of the non-linear process exceeds the size of the illuminated region of the sample (L_{int}), the fields generated at different locations sample interfere constructively, leading to a N^2 increase of the non-linear signal (where N the number of elementary emitters).

#filippo.bencivenga@elettra.eu

ISBN 978-3-95450-133-5

OPTIMIZATION OF HIGH AVERAGE POWER FEL BEAM FOR EUV LITHOGRAPHY APPLICATION *

A.Endo, K.Sakaue, M.Washio, RISE, Waseda University, Tokyo, Japan
H.Mizoguchi, Gigaphoton Inc, Oyama, Japan

Abstract

EUV source community is interested in evaluating an alternative method based on high repetition rate FEL, to avoid a risk of the potential source power limit by the plasma based technology. Present SASE FEL pulse (typically 0.1mJ, 100fs, 1 mm diameter) has higher beam fluence than the resist ablation threshold, and high spatial coherence which results in speckle and interference patterns, and random longitudinal mode spikes of high peak power micro pulses, which is not favourable to resist chemistry. This paper discusses on the required technological assessment and lowest risk approach to construct a prototype, based on superconducting linac and cryogenic undulator, to demonstrate a MHz repetition rate, high average power 13.5nm FEL equipped with specified optical components, for best optimization in EUVL application, including a scaling to 6.7nm wavelength region.

INTRODUCTION

Extreme Ultraviolet Lithography (EUVL) is entering into the high volume manufacturing (HVM) stage, after intensive research and development of various component technologies like Mo/Si high reflectivity mirror, chemically amplified resist, and especially high average power EUV source from laser produced plasma at 13.5nm. Semiconductor industry road map requires a realistic scaling of the source technology to 1kW average power, and further wavelength reduction to 6.7nm. It is recently recognized by the community of the necessity to evaluate an alternative approach based on high repetition rate FEL, to avoid a risk of the source power limit by the plasma based technology.

It is discussed by several papers on the possibility to realize a high repetition rate (superconducting) FEL to generate a multiple kW 13.5nm light [1,2]. We must notice that the present SASE FEL pulse (typically 0.1mJ, 100fs, 1 mm diameter) has higher beam fluence than the resist ablation threshold [3], and high spatial coherence which results in speckle and interference patterns in resist, and random longitudinal mode beat which leads to high peak power micro spikes. The interaction of the SASE pulses with chemically amplified resist is not known, because the typical EUV (13.5nm) pulses from Tin plasma has a characteristics of continuous spectrum of 2% bandwidth with 10ns pulse width. The emission is fully non coherent, and the pulse energy is typically mJ level at 100 kHz repetition rate.

This paper discusses on the scaling of the FEL technology to kW average power level, optical technology to optimize the FEL beam for lithography application, and scaling to 6.7nm wavelength region.

SCALING TO KW AVERAGE POWER

We start to evaluate a general perspective of high average power 13.5nm generation by SASE mode from recent typical operational parameters and future projects like LCLS2 etc. Genesis calculation was performed to estimate available single shot pulse energy by the electron beam and undulator parameters shown in the table 1.Pulse length was assumed as 100fs and 200fs to evaluate the difference of the output pulse energy depending on the pulse lengths. The calculation result is shown in the Figure 1, which indicates the saturation distance is nearly 20m with 0.1mJ pulse energy for short and long pulse lengths. The average power is 100W level with MHz repetition rate, and 1kW is obtained by 10MHz repetition rate with cryogenic superconducting linac and undulator. There are indeed various engineering challenges for this operation ahead.

Table 1: Parameters for Genesis Calculation

Charge	300pC
Emittance	1mm•mrad
Energy Spread	10^{-4}
Bunch Length	100fs/200fs
E-beam Energy	331.13MeV
Undulator Period	9mm
K Value	1
EUV Wavelength	13.5nm

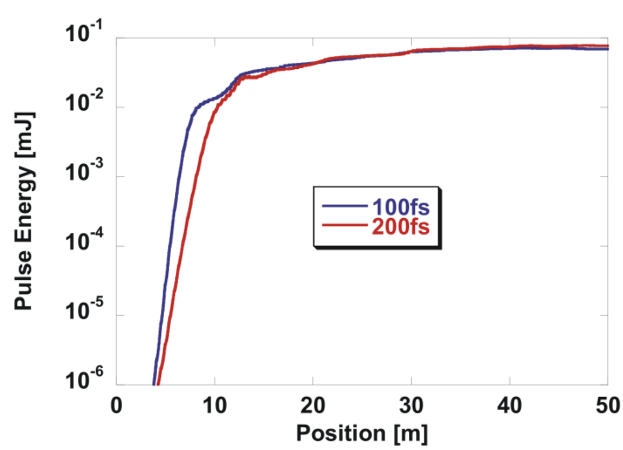

Figure 1: FEL pulse energy growth along Undulator.

*Work supported by NEDO

ISBN 978-3-95450-133-5

A COLLINEAR WAKEFIELD ACCELERATOR FOR A HIGH REPETITION RATE MULTI BEAMLINE SOFT X-RAY FEL FACILITY*

A. Zholents [#], W. Gai, R. Lindberg, J.G. Power, Y. Sun, ANL, Argonne, IL 60439, USA
C. Jing, A. Kanareykin, Euclid Techlabs LLC, Solon, OH 44139, USA
C. Li, C.X. Tang, Tsinghua University, Beijing, China
D. Yu. Shchegolkov, E.I. Simakov, LANL, Los Alamos, NM 87545, USA

Abstract

A concept is presented for a multi beamline soft x-ray free-electron laser (FEL) facility where several FEL undulator lines are driven by an equal number of high repetition rate single-stage collinear wakefield accelerators (CWA). A practical design of the CWA, extending over 30 meters and embedded into a quadrupole wiggler, is considered. The wiggler's structure of alternating focusing and defocusing quadrupoles is used to control single-bunch breakup instability. It is shown that practical restrictions on the maximum attainable quadrupole field limit the maximum attainable charge in the drive bunch whose sole purpose is to produce a high accelerating field in the CWA for the following main bunch. It is also pointed out that the distance between drive and main bunches varies along the accelerator, causing a measurable impact on the energy gain by the main bunch and on the energy spread of electrons in it. Means to mitigate these effects are proposed and results are presented for numerical simulations demonstrating the main bunch with plausible parameters for FEL application including a relatively small energy spread. Finally, results are presented for the expected FEL performance using an appropriately chosen undulator.

INTRODUCTION

A number of FEL facilities are currently in operation [1-4] and more have been planned. While tremendously effective in providing extreme photon fluxes, these machines can only accommodate a small number of users at a time. To address this limitation, multi-user FEL facilities have been recently proposed (see, for example, [5]). The mainstream approach is to accelerate electron bunches in a few GeV cw superconducting rf (SRF) linac and send them to a switchyard of ten or more FELs at a high bunch repetition rate. Here, we consider a different approach where a single cw SRF linac of a much lower energy (~400 MeV) and ten CWAs are used to provide ten FELs with a few GeV electron bunches. It is expected that the construction and operational costs of the facility, which are largely defined by the large SRF linac, can be significantly reduced. A high-gradient room-temperature CWA structure is the key to this proposal. Advanced accelerator studies aimed at a future high-energy collider have shown impressive results, achieving multiple-GV/m energy gradients in various wakefield acceleration schemes [6,7].

A CWA SCHEME FOR FEL

In a collinear wakefield accelerator [8,9], the field generated by a leading, high-charge drive bunch is used to accelerate a trailing low-charge main bunch. The collinear configuration has the two beams traversing the accelerator along the same trajectory so that the energy is directly transferred from the drive bunch to the main bunch. There are two main candidates for a CWA structure. The corrugate pipe wakefield accelerator (CPWA) [10] structure consists of a metallic pipe with wall corrugations where traveling on the pipe's axis relativistic electrons excite a synchronous monopole mode whose amplitude and frequency is defined by the pipe radius and geometry of corrugations. The dielectric wakefield accelerator (DWA) [11] structure consists of a cylindrical dielectric tube with an axial vacuum channel inserted into a copper outer jacket. The dielectric constant and the inner and outer radii of the dielectric tube are chosen to adjust the fundamental monopole mode (TM_{01}) frequency excited by the relativistic electrons. The phase velocity of the mode equals the beam velocity ~c.

The overall facility layout is shown in Figure 1. The scheme consists of 10 parallel FELs and ten parallel CWAs that supply FELs with a ~ 2 GeV electrons. The CWAs share a single 650 MHz cw SRF linac that accelerates 8-nC drive and 250-pC main bunches to ~400-MeV. Because of a need for the tight synchronization between drive and main bunches (of the order of 250 fs), both bunches are obtained from one source bunch as discussed below. The repetition rate of duets of drive and main bunches in the CWA is limited to ~ 50 kHz. This keeps the average wakefield power dissipation in the accelerating structure at a manageable level, as shown later. Thus, the bunch repetition rate in the cw SRF linac is ~500-kHz. A spreader switchyard distributes electron bunches to the ten CWAs on a rotating basis (or as needed). The drive bunch has a special double triangular current profile, shown in Figure 2. The bunch current shape is tailored to maximize the transformer ratio *R*, defined as the ratio of the maximum accelerating field behind the drive bunch over the maximum decelerating field inside the bunch. Obtaining short drive bunch ~ 3.3 ps requires off-crest acceleration of the already pre-shaped bunch in SRF linac producing ~ 10% energy chirp

*Work supported by U.S. Department of Energy, Office of Science, under Contract No. DE-AC02-06CH11357 and by the U.S. Department of Energy through the Laboratory Directed Research and Development (LDRD) program at Los Alamos National Laboratory.
#azholents@aps.anl.gov

DIVERGENCE REDUCTION AND EMITTANCE CONSERVATION IN A LASER PLASMA ACCELERATION STAGE

I. Dornmair, A. R. Maier*,
CFEL, Center for Free-Electron Laser Science, 22607 Hamburg, Germany
University of Hamburg, Institute for Experimental Physics, 22761 Hamburg, Germany
K. Floettmann, DESY, 22607 Hamburg, Germany

Abstract

In laser-plasma accelerators, very high acceleration gradients are reached, which makes them promising candidates for high-energy applications as well as as drivers for next-generation light sources. Yet, conserving the beam quality when coupling the beam into and extracting it from the plasma is very challenging. The concept presented here employs tapered matching sections to increase the matched beamsize at the plasma entrance and to adiabatically reduce the beam divergence at the plasma exit, which suppresses chromatic emittance growth.

INTRODUCTION

The electric fields present in the wakefield of a driver laser or beam in a plasma accelerator [1,2] are far larger than in conventional cavities. Acceleration of electron bunches to GeV energies over cm-scale distances has been shown [3,4,5]. However, the focusing forces provided by the transverse field components are very strong.

An electron bunch whose transverse beam size is not matched to these focusing forces will perform betatron oscillations. The betatron frequency depends on the phase in the wake and on the bunch energy. Finite bunch length and (acquired correlated) energy spread then lead to emittance growth. The bunch size therefore needs to be matched, requiring extremely strong focusing optics both for injection into and extraction out of the plasma [6]. The combination of large divergence and large energy spread also leads to strong emittance growth in the drift following the plasma target [7,8].

ADIABATIC MATCHING IN PLASMA ACCELERATORS

We include adiabatic matching sections at the start and end of a plasma stage to increase the beta function needed to match an external beam into the plasma and to reduce the divergence before the plasma-vacuum transition. Adiabatic profiles are characterized by the changes of focusing strength being slow enough so the bunch envelope can follow its changes and stay matched. Since no betatron oscillations are performed, the emittance is conserved. Here, we derive with simulations ideal profiles for both plasma density and driver laser evolution.

* andreas.maier@desy.de

We use the linear wakefield model with

$$E_z(r,\zeta) \propto a^2 k_p^2 \exp(-k_p^2\sigma_z^2/2 - 2r^2/w^2) \cos\Psi,$$

$$E_r(r,\zeta) \propto -a^2 k_p r/w^2 \exp(-k_p^2\sigma_z^2/2 - 2r^2/w^2) \sin\Psi,$$

that we implemented in the particle tracking code Astra [9] and cross-checked for short plasma targets with the PIC code VSim (formerly Vorpal) [10]. Here, $\Psi = k_p\zeta$ is the phase, $\zeta = z - v_g t$ the co-moving variable, v_g the laser group velocity and $k_p c = \sqrt{ne^2/m_e\varepsilon_0}$ the plasma frequency. The normalized vector potential a of the Gaussian laser pulse is given by $a^2 = a_0^2 \exp(-2r^2/w^2)\exp(-\zeta^2/2\sigma_z^2)$. The model is valid for $a_0 < 1$ and includes changes of bunch phase due to the laser group velocity and due to changes in density. It does not include pump depletion and changes of the wakefield caused by transverse density profiles.

We consider a plasma stage separated into injection, acceleration and extraction section and has a peak density of $n_0 = 1 \cdot 10^{17}\,\mathrm{cm}^{-3}$. An electron beam of 100 MeV kinetic energy, normalized emittance $\varepsilon_{nx} = 1$ mmmrad and $\sigma_z = 1$ µm is injected externally. The laser with $a_0 = 1.3$, fwhm length 130 fs and a spot size of $w_0 = 26$ µm is focused at the start of the acceleration section. In the injection section it follows the Gaussian beam evolution while it is assumed to be guided throughout the acceleration section.

The matching condition reads $\beta_m = 1/\sqrt{K}$ for K the focusing strength of the wakefield given by

$$K = \frac{e}{\gamma m_e c^2} \frac{\partial E_r}{\partial r}\bigg|_{r=0} \propto -\frac{a^2 k_p}{w^2} \exp(-k_p^2\sigma_z^2/2) \sin\Psi. \quad (1)$$

For a sharp plasma edge, i.e. no injection section, the laser focus and the electron focus coincide and a matched beta function of $\beta_m = 0.5$ mm is required.

In an injection section, the bunch experiences slowly increasing focusing forces. This lensing effect leads to a decrease of bunch size till the start of the acceleration section. The bunch therefore can be injected with a virtual focus in the injection section that can be much larger than without this section. The section length is naturally limited by the Gaussian evolution of the laser leading to much weaker fields in the wake away from the focus.

ISBN 978-3-95450-133-5